Thermomechanical behaviour of bituminous materials including RAP and rejuvenator and environmental impact of their fabrication process

A Thesis Submitted for obtaining
the Scientific Title of PhD in Engineering from
Politehnica University Timișoara
in the Field of Civil Engineering and Installations
in international co-supervision with
University of Lyon, ENTPE
by

Eng. Andrei-Roman FORTON

PhD Committee Chair:
Prof. Raul ZAHARIA, Politehnica University Timisoara
PhD Supervisors:
Prof. Adrian CIUTINA, Politehnica University Timisoara
Prof. Hervé DI BENEDETTO, University of Lyon, ENTPE
Scientific Reviewers:
Prof. María del Carmen RUBIO GAMEZ, University of Granada
Prof. Mihai MARASTEANU, University of Minnesota
Prof. Cédric SAUZÉAT, University of Lyon, ENTPE

Date of the PhD Thesis Defense: 24 June 2021

Foreword

This thesis has been elaborated during my activity in the Department of Department of Overland Communication Ways, Foundation and Cadastral Survey of the Politehnica University Timişoara, Romania and in the Université de Lyon/École Nationale des Travaux Publics de l'État (ENTPE), laboratoire de Tribologie et Dynamique des Systèmes (LTDS) from France.

I address my special thanks to my PhD supervisors, Prof. Adrian Ciutina from Politehnca University Timișoara and Prof. Hervé Di Benedetto from ENTPE, for their guidance and support throughout the research project. I would like to thank them for encouraging my research and for allowing me to grow as a research scientist. Their advice on both research as well as on my career have been invaluable. I am thankful for the opportunity of working with them.

I also wish to thank all the other members of my PhD defense committee, Prof. Raul Zaharia from Politehnica University Timişoara, who acted as president of the jury, Prof. María del Carmen Rubio Gamez from University of Granada, Prof. Mihai Marasteanu from University of Minnesota and Prof. Cédric Sauzéat from University of Lyon, ENTPE, who reviewed my dissertation. I am honored for their participation to my defense, and I thank them all for their appreciation.

Sincere thanks to the French Institute in Romania, Campus France for providing me a scholarship for 12 months funded by the French Government. I thank them for providing me a various learning, enriching, networking, and professional and personal development experiences.

I am also pleased to say thank you to Prof. Gheorghe Lucaci, Dr. Paul Marc and Dr. Salvatore Mangiafico for giving me the encouragement and sharing insightful suggestions. It would not have been possible to conduct this research without their precious support. Their endless guidance is hard to forget throughout my life.

The years spent working on the thesis will always be a happy memory and this is also due to all the PhD colleagues, professors, faculty members, technicians, and personnel I met at the Department of Department of Overland Communication Ways, Foundation and Cadastral Survey from Politehnica University Timişoara and also at the ENTPE. Thank you for all your support and for the merry moments spent between science, crosswords, and coffee.

In the end, I wish to thank my family and my friends. They gave me all the moral support, encouragement, and motivation that I needed to accomplish my personal goals. Words cannot express how grateful I am to all of you.

Timişoara, 24 June 2021 Andrei-Roman FORTON

FORTON, Andrei-Roman

Thermomechanical behavior of bituminous materials including RAP and rejuvenator and Environmental impact of their fabrication process

Keywords: Recycling, RAP material, rejuvenator, estimation, prediction, environment.

Abstract: The study presented in this thesis has been carried out within a collaboration between Politehnica University Timisoara/Faculty of Civil Engineering/Department of Overland Communication Ways, Foundations and Cadastral Survey from Romania and Université de Lyon/École Nationale des Travaux Publics de l'État (ENTPE), laboratoire de Tribologie et Dynamique des Systèmes (LTDS) from France. The objectives are, i) the characterization of the thermomechanical performances of binder blends and bituminous mixtures produced with Reclaimed Asphalt Pavement (RAP) and rejuvenator (Rej) and, ii) the investigation of the potential environmental impact related to the production of a mixture containing different amounts of RAP material and Rejuvenator.

Therefore, comprehensive experimental investigations were performed on binders and mixtures. All tests on binders and mixtures were performed in the Road Laboratory from Politehnica University Timisoara, together with the environmental impact assessment. On the other hand, the analyses, estimations and predictions of most parameters/characteristics of binders and mixtures were performed at ENTPE.

The study on binders focused on the investigation of the influence of a RAP extracted binder and the rejuvenator on the properties of different binder blends produced by mixing one type of fresh binder, a straight run 50/70 pen. grade binder, a RAP-extracted binder and a rejuvenator of vegetal origin. The experimental plan includes a total of 17 binders. A new method is proposed to estimate the conventional properties, the LVE properties, the steady shear viscosity and critical temperatures. Stronger correspondence, proved by the statistical analysis, was found between the estimated values of all above-mentioned parameters obtained with the proposed method compared to the classical method, and experimental values.

The study on mixtures focused on the investigation of the effects of the RAP material and the rejuvenator on the thermo-mechanical properties of 13 bituminous mixtures produced with different amounts of RAP material and with or without a mix of vegetal origin used as a rejuvenator. One conventional Hot Mix Asphalt was used as a reference. All materials used in this study are specific for Romania. SHStS transformation was applied. A satisfactory prediction was obtained even by using the limited DSR measurements on binders.

The Environmental Impact Assessment (EIA) proved that the addition of RAP material leads to a net decrease of the energy use and environmental impact. On the other side, when the rejuvenator is used in this process, it can affect the energy balance and reduce the difference in environmental impact.

TABLE OF CONTENTS

Notations, abbreviations, acronyms

RAP	Reclaimed Asphalt Pavement	γ	shear strain amplitude
HMA	Hot-Mix Asphalt	T_{ref}	reference temperature
WMA	Warm-Mix Asphalt	a_T	temperature shift factors
Rej	rejuvenator	E_{00}	static modulus
DSR	Dynamic Shear Rheometer	E_0	glassy modulus
BBR	Bending Beam Rheometer	$\delta, k, h, \beta, \tau$	2S2P1D constants
PG	Performance Grade	η_0	steady shear viscosity
RAS	Reclaimed Asphalt Shingles	$pen.$	penetration at 25°C
LVE	Linear Visco Elastic	$T_{R\&B}$	ring and ball temperature
EIA	Environmental Impact Assessment	PI	penetration index
LCA	Life Cycle Assessment	T_{Fraass}	Fraass temperature
LCC	Life Cycle Cost	$T_{DSR\ high\ critical}$	high critical temperatures
TTSP	Time-Temperature Superposition Principle	$S(t)$	flexural creep stiffness
T	temperature	$m(t)$	m-values
f	frequency	$T_{BBR\ low\ critical}$	low critical temperatures
N	number of cycles	ρ_A	SSD bulk density
ε	strain	ρ_{max}	maximum density
σ	stress	A_V	water absorption
t	time	V_M	void content
ω	angular frequency	VMA	voids in mixing aggregates
E^*	complex modulus	VFB	voids filled with bitumen
G^*	complex shear modulus	S	Marshall stability
φ	phase angle	F	Marshall flow
E_1	real part of E^*	F_t	Marshall tangential flow
E_2	imaginary part of E^*	S/F	ratio between Marshall stability and flow
$\lvert E^* \rvert$	norm of complex modulus	$S_M(T)$	measured stiffness modulus
$\lvert G^* \rvert$	norm of complex shear modulus	$S_A(T)$	adjusted stiffness modulus

List of tables

CHAPTER 1

CHAPTER 2

CHAPTER 3

CHAPTER 4

List of figures

CHAPTER 1

CHAPTER 2

CHAPTER 3

CHAPTER 4

Introduction

For economic and environmental reasons, the use of Reclaimed Asphalt Pavement (RAP) in the production of new bituminous mixtures HMA (hot-mix asphalt) and WMA (warm-mix asphalt) has become a common strategy for the construction and maintenance of roads. The milled material from deteriorated pavement, the so-called Reclaimed Asphalt Pavement (RAP) is 100% recyclable and is considered to be an alternative material for the road industry. The use of RAP material in the production of new bituminous mixtures presents many advantages as conservation of energy, aggregates and binder, cost reduction, etc.

Over the last decades, many transportation agencies implemented different technologies in order to reuse the materials and important research efforts were made in order to increase the use of RAP due to the increasing demand for eco-friendly mixtures and to the increased prices for the raw materials. Several studies showed that a solution that must be taken into consideration is the use of the so-called recycling agents or rejuvenators. However, the recycling rates are still relatively low, rarely passing 60%, therefore substantial work for the improvement of these technologies remains.

The use of RAP materials in the production of new bituminous mixtures should not be considered only from economic and environmental reasons. Several studies highlighted that the use of RAP material can lead to an improvement of the bituminous mixtures performances. Bituminous materials present an extremely complex behaviour and when RAP materials and rejuvenators are used, the characterization of the behaviour of the final products becomes more challenging. Many research efforts were spent in order to better highlight the influence and the effects of RAP and rejuvenators on the mixtures properties and to model or predict their behaviour from binder blends properties of the fresh, RAP binders and rejuvenators.

The recycling technologies and the polices regarding the reuse of materials in road industry are well applied and used in many countries. However, these technologies are not very popular in Romania. A national strategy regarding the reuse of the materials in the idea of producing higher-performance bituminous mixtures, is still missing. A proper strategy will lead in time to other strategies related to the increase of the amounts of RAP materials in the idea of producing higher-performance bituminous mixtures (‘up-cycling’). This up-cycling solution could be a key factor in the sustainable development of Romania’s public road network, and not only.

This thesis has been carried out within the framework of a collaboration between University Politehnica Timisoara/Faculty of Civil Engineering/Department of Overland Communication Ways, Foundations and Cadastral Survey/Infrastructures for Constructions and Transportation Research Centre from Romania and Université de Lyon/École Nationale des Travaux Publics de l'État (ENTPE)/Laboratoire de Tribologie et Dynamique des Systèmes (LTDS) Unité Mixte de Recherche Centre National de la Recherche Scientifique 553 (UMR CNRS 5513) Vaulx-en-Velin Cedex, from France. The objectives are, i) the characterization of the thermomechanical performances of binder blends and bituminous mixtures produced with Reclaimed Asphalt Pavement (RAP) and rejuvenator (Rej) and, ii) the investigation of the potential environmental impact related to the production of a mixture containing different amounts of RAP material and Rejuvenator.

Two comprehensive experimental plans were performed on binders and mixtures. The study on binders focused on the investigation of the influence of a RAP extracted binder and the rejuvenator on the properties of different binder blends produced by mixing one type of fresh binder, a RAP-extracted binder and a rejuvenator of vegetal origin. Different types of tests were performed on binders from classical European tests to more advanced laboratory tests (DSR and BBR tests). The obtained test results were analysed by applying a rheological model. Three estimation methods were proposed in order to estimate values of different parameters of all binder blends. A statistical analysis was performed to highlight the precision of the estimation methods.

The study on mixtures focused on the investigation of the effects of the RAP material and the rejuvenator on the thermomechanical properties of several bituminous mixtures produced with different amounts of RAP material and with or without a mix of vegetal origin used as a rejuvenator. One conventional Hot Mix Asphalt was used as a reference. All materials used in this study are specific for Romania. Particular attention was given to the relation between binder blends and mixture behaviours.

Finally, an Environmental Impact Assessment (EIA) was performed to estimate the potential environmental impact related to the production process of several types of bituminous mixtures, defined by the following three stages: raw material supply, transport, and manufacturing, of one tonne (1 T) of the considered bituminous mixtures while all the other processes were assumed to be similar.

All tests on binders and mixtures were performed in the Infrastructures for Constructions and Transportation Research Centre from University Politehnica Timisoara, together with the environmental impact assessment. On the other hand, the analyses, estimations, and predictions of most parameters/characteristic of binders and mixtures were performed in ENTPE.

The thesis is organized in different sections. After this introduction, a literature review is presented about the context of the research, the recycling process and RAP material characteristics, the bituminous materials properties together with a brief overview about the environmental impact assessment. The two following chapters report obtained experimental results and analysis procedures followed, respectively, for binders and mixtures. Afterwards, the environmental impact assessment results were presented. At the end, general conclusions of the study and perspectives for future research are presented.

1. Literature review

1.1 Romanian context

1.1.1 Current status of national, county and local roads in Romania

The public road network in Romania provides motorized access in most regions, localities of the country and according to the National Institute of Statistics [1] the length of the public road network at the end of 2019 measured 86 391 km from which: 17 873 km (20.69%) highways and national roads, 35 083 km (40.61%) county roads and 33 435 km (38.70%) local roads. The density of the public road network reported to the surface of Romania is 36.24 km public roads/100 km^2.

All roads from Romania can be classified based on the M.T. (Ministry of Transport) order 1297/2017 [2]. Table 1.1 shows the length of the public roads from Romania (highways, national, county and local roads). Also, Figure 1.1 shows the map of the national road network from Romania [3].

Table 1.1. Length of Romanian's public road network at the end of 2019 (data from the National Institute of Statistics website [4]).

	Public roads Total	National roads	County roads	Local roads
Total, km:	86 391	17 873	35 083	33 435
from which:				
Highways	866	866	-	-
European roads	6 176	6 176	-	-
Roads – 3 traffic lanes	298	290	8	
Roads – 4 traffic lanes	1 963	1 923	40	-
Roads – 6 traffic lanes	38	35	3	-

As a function of the type of their viability state, the surface course and their service life the public roads can be classified as:

- modernized roads:
- roads with concrete surface course;
- roads with bituminous (asphalt) surface course;
- paved roads;
- roads with semi-permanent surface course (macadam);
- cobblestone roads;
- dirt roads.

Table 1.2 shows the data presented by the National Institute of Statistics regarding the length of the Romanian's public road network, at the end of 2019, as a function of their surface course for each type of roads (national, county and local). Also, the length of the roads that exceeded their service life is presented in Table 1.2.

Moreover, the percentage distribution of Romanian's public road network based on their territorial administrative importance and the type of their surface course, at the end of 2019 (data from the National Institute of Statistics website [4]) is presented in Table 1.3.

In order to better highlight the viability of the Romanian's public road network, Table 1.4 shows their percentage distribution based on their viability.

Table 1.2. Length of the Romanian's public road network as a function of their surface course at the end of 2019 (data from the National Institute of Statistics website [4]).

	Public roads Total	National roads	County roads	Local roads
Modernized roads, km	**38166**	**16991**	**14840**	**6335**
- concrete surface course	2646	880	956	810
- bituminous surface course	35404	16088	13810	5506
- paved roads	116	23	74	19
Roads that exceeded their service life	13411	9297	3459	655
Roads with semi-permanent surface course, km	**21365**	**720**	**13227**	**7418**
- roads that exceeded their service life	9217	572	6340	2305
Cobblestone roads, km	**17831**	**144**	**5310**	**12377**
Dirt roads, km	**9029**	**18**	**1706**	**7305**

The national roads represent the majority network of the country, approximative 70% of road traffic takes place on them (Figure 1.1). Based on the rehabilitation and modernization program that was performed over the past years in Romania, at the end of 2019 the national roads reached 95.1% roads with modernized surface course, 4% roads with semi-permanent surface course (macadam), 0.8% cobblestone roads and 0.1% dirt roads. More details for the other type of roads (county and local roads) are given in Table 1.3, where it can be observed that only 42.3% of the county roads and 19% of the local roads presents a modernized surface course.

On the other side, only 62% of the total public roads did not exceed their service life. Table 1.4 presents more details regarding the percentages of the roads that exceed their service life as a function of their importance.

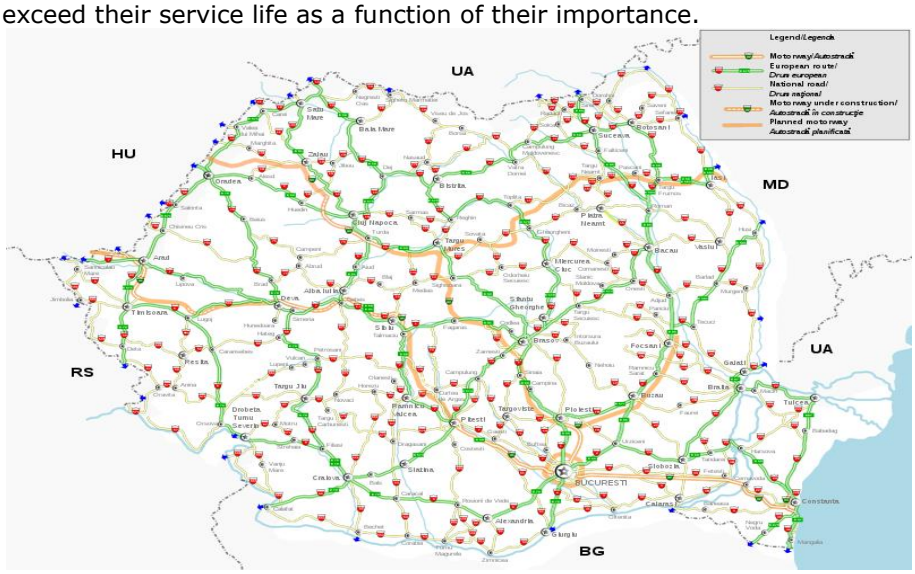

Figure 1.1. Romania's national road network (Wikipedia website) [5].

Table 1.3. Percentage distribution of Romanian's public road network based on their territorial administrative importance and the type of their surface course, at the end of 2019 (data from the National Institute of Statistics website) [4].

Type	Total public roads 100%		
	National roads and highways (20.69%)	County roads (40.61%)	Local roads (38.70%)
Modernized roads	95.07%	42.30%	18.95%
Roads with semi-permanent surface course	4.03%	37.70%	22.18%
Cobblestone roads	0.80%	15.14%	37.02%
Dirt roads	0.10%	4.86%	21.85%

Table 1.4. Percentage distribution of Romanian's public road network based on their viability, at the end of 2019 (data from the National Institute of Statistics website) [4].

Percentage distribution of roads who exceeded their service life (%)			
	National roads and highways	County roads	Local roads
Roads with semi-permanent surface course (15.48%)	6.21%	68.79%	25.01%
Modernized roads - exceeded their service life (22.53%)	69.32%	25.79%	4.88%

*Roads with modern surface course - do not exceeded their service life - 61.99%

Therefore, by analysing all the presented data it can be concluded that a national program of rehabilitation and modernization of the Romanian's public road network is welcome in the near future.

It must be also mentioned that no data were found regarding the recycling technologies and the amounts of Reclaimed Asphalt Pavement (RAP) that are used in road industry in Romania.

1.1.2 Development policies for road network in Romania

The General Transport Master Plan (MPGT) of Romania, adopted by the Romanian Government by H.G. no. 666/2016, is a strategic reference document that defines the financing needs with those of territorial development of roads infrastructure, having as a target the year 2030. The MPGT of Romania aims two consecutive periods, 2014-2020 and 2020-2030. The main benefit of this Master Plan is that it establishes a clear strategy for the development of road infrastructure as a result of a process of analysis, diagnosis and prioritization of projects part of the Trans-European Transport Network (TEN-T) [6].

The first objective of the H.G. no. 666/2016 was related to the implementation of the projects provided in the MPGT which is the task of the National Company for Road Infrastructure Management (C.N.A.I.R.). The main priorities are to continue and to finish the projects for some important parts of the highways network until 2022: A1 Lugoj - Deva (lot 2, 3, 4) and A10 Sebeş - Turda (lot 1, 2, 3, 4) [6]. Other objectives are related to the rehabilitation or modernization of different main national roads, the development of bypasses for the main cities and the construction of new

express roads and highways. An important program which aims to recover the gap in the development of Romania's transport infrastructure, any by ensuring the European carbon reduction targets and the transfer to sustainable and safe mobility is the Transport Operational Program 2021-2027 (POT 2021-2027).

Another national program which is still an on-going program, is the National-Local Development Program (PNDL). This program represents the main source of funding for local infrastructure and is based on the principle that in each locality from Romania, a minimum set of public services must be provided. PNDL program covers the following fields: health, education, water-sewerage, heat and electricity, including public lighting, transport/roads, sanitation, culture, worship, housing and sports [7].

Regarding the road domain, the investment objectives that are financed under this program include works for the construction/rehabilitation/modernization of part of public roads such as county roads, local roads and/or public roads inside the localities.

These two mentioned national programs are the most important policies developed in Romania. However, even if these programs were adopted, some difficulties appeared in their implementation, fact that is proved by the data presented in the Global Competitiveness Report 2019 where Romania ranks 119th place (32.6 score out of 100) out of 141 countries in terms of road infrastructure quality. Also, regarding the road connectivity Romania ranks 55th place (79.3 score out of 100) out of 141 countries [8]. Figure 1.2a shows the index regarding the quality of road infrastructure and Figure 1.2b shows the index regarding the road connectivity obtained for the countries from the Eastern Europe (neighbouring countries of Romania). Also, the values of the two index components obtained for the main poles of the Western Europe (France, Germany and Spain) are reported in Figure 1.2.

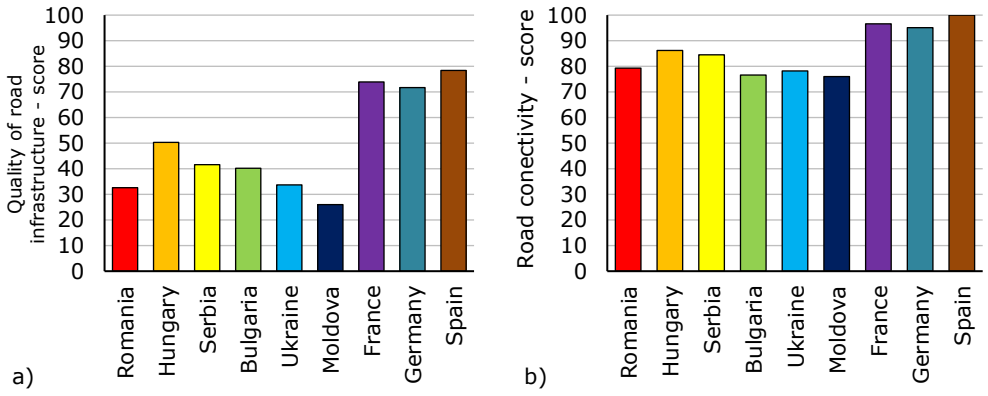

Figure 1.2. (a) Quality of road infrastructure score for different countries [8]; (b) Road connectivity score for different countries [8].

As it can be observed, the roads quality from Romania is deficient proved by the lowest score compared to the other Eastern European countries. A significant difference can be observed between the quality of roads from the Western European countries and the Eastern ones.

Regarding the road connectivity index, it can be observed that a better score was obtained for Romania, compared with the other Eastern countries.

The deficit of road infrastructure is reflected in reduced mobility, insufficient connectivity in some regions with a major impact on regional disparity (for example

the North-East region), high transit traffic in many cities that do not benefit from bypass, etc.

Also, at the end of 2019, Romania ranks last place in Europe in terms of length of highway per 100 000 inhabitants. Unfortunately, in Romania, some parts of the TEN-T road network were not built to proper standards related to the traffic needs and to the connection which must be ensured. This leads to a weak interconnection of the main economic and urban cities and with other nodes of intermodal transport, such as ports and airports. On the other side, some areas have poor accessibility to transport networks, which requires further investments for the national and county roads. Therefore, the lack of an adequate road infrastructure has a negative effect on the economy by increasing the time and costs of transport on that section, by increasing fuel use and by increasing maintenance costs for the vehicles [9].

The importance of highways is well known, and it consists in creating modern infrastructures which implies the regional development of the area, transit traffic deviation, increase of the safety, time saving and reduction of pollution.

It is important to mention that in Romania there are no policies regarding the reuse and/or recycle of materials in road domain even if there are some guidelines and some norms regarding the recycling methods. A national strategy regarding the reuse of the materials obtained by milling the old existing road pavements that exceeded their service life in the idea of producing higher-performance bituminous mixtures, is still missing. A proper strategy could be to impose the use of a minimum percentage of Reclaimed Asphalt Pavement (RAP) in the production of new bituminous mixtures. Such a strategy will lead in time to other strategies related to the increase of the amounts of RAP materials in the idea of producing higher-performance bituminous mixtures ('up-cycling'). This up-cycling solution could be a key factor in the sustainable development of Romania's public road network.

A proper strategy of re-using the RAP materials, based on the experience of other European countries and the European recommendations will become a key tool for Romania. The sustainability principles such as increasing the re-used and recycled content in products by ensuring their performance and safety, enabling remanufacturing, high-quality recycling, reducing environmental footprints, restricting single-use and improving product durability, reusability, upgradability and reparability should be accomplished (European Circular Economy Action Plan, 2020).

1.1.3 Romanian infrastructure integration in the European transport networks

Through its geographical position, its traditions and the open spirit of its good neighbourly policies, Romania, with an area of over 238 397 km^2 and 19.40 million inhabitants, is part of the family of European countries, irreversibly committed to integration into European and Euro-Atlantic structures. The location on the transit corridor between Western Europe and the Middle East and the potential offered by the natural advantages - a country bordering the Black Sea and crossed on a length of 1075 km by the most important waterway in Europe, the Danube river, gave Romania a favourable strategic position in the confluence of transport poles from Europe, the Balkans and the Middle East.

The aim of the Romanian infrastructure integration in the European transport networks is to promote the interconnection and interoperability of the existing networks by focusing on some specific infrastructure arteries which are located along the 10 Pan-European transport corridors that cross geographical areas of several countries and connect the main economic and social centres.

The construction and modernization of infrastructure networks located on Pan-European transport corridors contributes to the gradual integration of Romania into the family of European countries.

The instruments that formed the basis for the definition of Pan-European transport corridors, which also include Romania, are the European agreements developed within the UNECE (AGR, AGC, AGTC, TER and TEM) resulting from the three Pan-European Transport Conferences in Prague (1991), Crete (1994) and Helsinki (1997) and Decision of the European Parliament and of the Council no. 1692/96 / EC of 23 July 1996 on guidelines for the development of the trans-European transport network, as amended by Decision of the European Parliament and of the Council no. 1346/2001/EC of 22 May 2001. The 9 Pan-European transport corridors were established at the Pan-European Transport Conference in Crete (March 1994). At the third Pan-European Transport Conference from Helsinki, it was agreed to adjust the Pan-European transport corridors by adding a new corridor to the 9 already defined. 4 Pan-European Transport Zones were also defined at this conference. Thus, Europe is crossed by 10 Pan - European Transport Corridors and has defined 4 Pan - European Transport Zones. Figure 1.3 shows a map of the Pan-European corridors.

As it can be observed, Romania is crossed by:

- corridor IV (Berlin - Nuremberg - Prague - Budapest - **Arad - Bucharest - Constanta** - Istanbul - Thessaloniki);
- corridor VII (**Danube, with the Sulina arm and Danube Canal - Black Sea**);
- corridor IX (Helsinki - St.Petersburg - Moscow - Pskov - Kiev - Ljubasevka - Chisinau – **Iasi - Bucharest** - Dimitrovgrad - Alexandroupolis).

Starting from the definition of the Pan-European Transport Corridors, the Pan - European Transport Network on the territory of the associated countries was defined within the TINA project (Transport Infrastructure Needs Assessment). This network will ensure the interconnection and interoperability between the transport network (road, rail, inland waterways) at national and European level.

Figure 1.3. Pan-European corridors (Wikipedia website) [10].

1.2 Bituminous mixtures and their components

A bituminous mixture can be defined as a composite material which is produced, by using a specific technology, by mixing a mix of mineral aggregates, generally considered as the 'rock part', and a bitumen that acts as a binder [11]–[13]. Also, the air voids, the voids not filled with binder, represents the third component of a bituminous mixture.

Bituminous mixtures are composite materials whose properties are dependent on the characteristics of the component materials: aggregates, bitumen, filler. In order to know the final product, an in-depth study of each component is needed.

In Romania, all bituminous mixtures (Hot Mix Asphalt) produced only with virgin materials must meet the requirements specified in the Romanian Standard AND 605 [14]. This Standard presents the technical conditions for the design, production, transportation, laying and compaction of different types of bituminous mixtures, together with the quality control provisions of materials, technology and the compacted bituminous layers.

In the following subsections, a short overview of the main mix design parameters of a bituminous mixture produced with virgin materials with a 16 mm maximum aggregate size used for a surface layer, together with the requirements specified in the Romanian Standard AND 605 and the European Standard, is presented.

1.2.1 Aggregates

The properties of the aggregates are fundamental in the design of a bituminous mixture due to the fact that this rock part represents approximatively 95% of the total mass of a bituminous mixture and 80-85% of its total volume [11].

In the production of a bituminous mixture different homogenous aggregates fractions, which constitute the skeleton of a mixture, are used. Usually, in Romania, the aggregates used to produce bituminous mixtures with 16 mm maximum aggregate size are quarry crushed aggregates fractions 0-4; 4-8 and 8-16, natural sand (rounded aggregates) fraction 0-4 and limestone filler.

The requirements that each aggregate fraction must fulfil in order to be used in the production process of asphalt mixtures are well defined in AND 605 [14], which are in accordance with the specifications from SR EN 13043 [15], and they refer to the size and shape of the granules, the nature of the rock, the granularity, etc. All aggregates must be clean, must have a good adhesiveness to the bitumen used, must have adequate mechanical strength and must be resistant to wear.

According to the Romanian Standard AND 605 the following physical-mechanical characteristics of each aggregate fraction must be determined, and the result obtained must respect the limit values specified in Tables 5, 6, 7, 8 from AND 605 [14]:

- grading curve;
- purity-fine particles (63μm);
- shape index;
- flakiness index;
- dry real density;
- water absorption;
- resistance to fragmentation - Los Angeles coefficient (fractions 4-8 and 8-16);
- resistance to wear - micro-Deval coefficient (fractions 4-8 and 8-16);

- freeze/thaw resistance (fractions 4-8 and 8-16);
- sand equivalent index (natural sand 0-4);
- methylene blue value (fraction 0-4);
- affinity between aggregate and bitumen (fractions 4-8 and 8-16);
- adhesivity between binder and aggregate - spectrophotometric method (fractions 4-8 and 8-16).

1.2.2 Bituminous binders

According to Permanent International Association of Road Congresses (PIARC), the term bitumen (binder) is defined as a ''very viscous or nearly solid, virtually involatile, adhesive and waterproofing organic material derived from crude petroleum or present in natural asphalt, which is completely or nearly completely soluble in toluene'' [16].

The main source of the bitumen used in the road industry is crude oil (heavy crude oil) refining. There are various manufacturing processes of bitumen (depending on the equipment and the source of the heavy crude oil) which are based on the separation of the lighter fractions from the residues.

Depending on the refining and manufacturing processes, the most common types of bitumen are:

- straight run bitumen (obtained from atmospheric and vacuum distillation);
- air-rectified bitumen (obtained by increasing the asphaltene concentration);
- cutback bitumen (obtained by decreasing temporarily the viscosity of binders by adding volatile solvents);
- fluxed bitumen (obtained by decreasing the viscosity of binders by adding non-volatile products);
- multi-grade bitumen (obtained by air rectification in order to lower their temperature sensitivity);
- modified bitumen (obtained by adding one or more additives);
- bitumen emulsions.

In the European method (based on semi-empirical tests) the binders are classified according to their penetration value determined at 25°C measured according to SR EN 1426 [17].

The systematization of a road bitumen, according to the European Standard /Romanian Standard SR EN 12591 [18] is the following: AA/BB
where:
AA – the minimum value of the penetration at 25°C of a binder (1/10 mm);
BB – the maximum value of the penetration at 25°C of a binder (1/10 mm).

The Superpave Performance Grade (PG) method is a classification system used and developed in the United States in the framework of the Strategic Highway Research Program (SHRP) [19]. In this method the semi-empirical tests used in the European classification were replaced with some specific test in order to measure the rheological properties of binders. Therefore, in this PG system the binders are characterized by two critical temperatures (high and low) that represents the extreme temperatures.

The systematization of a road bitumen, according to the PG system is the following: PGAA-BB
where:
AA – the high critical temperature in which the binder should resist rutting (°C);
BB – the low critical temperature in which the binder should resist cracking (°C).

In the Romanian Standard AND 605 there are some requirements that must be taken into consideration when the type of binder is chosen. These specifications are related to the technical class of the road (determined as a function of the traffic intensity for an imposed perspective period), the climacteric zone and the minimum binder content in % by mass of the total mixture. As an example, for a road classified as being in the third technical class located in warm area (according to Annex A from AND 605), for a bituminous mixture produced with a 16 mm maximum aggregate size used for a surface layer, the minimum binder content is 5.70% by mass of the mixture. However, this minimal value can be corrected as a function of the real density of the aggregates.

In Romania, the optimal binder content is determined as a function of the specific surface of the aggregates according on the French method that was developed by Duriez [20]. Therefore, for a given grading curve an optimal binder content is defined in order to assure an adequate aggregate coating and by achieving at the same time the greatest compactness and the best homogeneity in normal conditions executed on site.

The specific surface of aggregates S is calculated as follows:

$$100S = 0.17A + 0.32a + 2.30N + 12n + 135f \tag{1.1}$$

where:

S – specific surface, in m^2/kg;

A – percentage of aggregate particles larger than 8 mm;

a – percentage of aggregate particles between 2 mm and 8 mm;

N – percentage of aggregate particles between 0.125 mm and 2 mm;

n – percentage of aggregate particles between 0.063 mm and 0.125 mm;

f – percentage of filler particles smaller than 0.063 mm.

The relation used to establish the optimal binder content reported per 100 parts of aggregates is [20]:

$$b = a \cdot k \cdot \sqrt[5]{S} \tag{1.2}$$

where:

b – percentage of binder reported per 100 parts of aggregates, in %;

a – coefficient depending on the density of the aggregates ($a = 1$ for a density of the aggregates = 2.65 g/cm^3);

k – richness modulus related to the conventional thickness of the bitumen film coating aggregates;

S – specific surface calculated with the equation 1.1, in m^2/kg.

The binder content expressed as the percentage of binder mass of the total mass of the final bituminous mixture is calculated using the equation 1.3.

$$b' = \frac{100 \cdot b}{100 + b} \tag{1.3}$$

where:

b' – the binder content (%) from the mass of the bituminous mixture.

For the same grading curve, depending on the percentages of bitumen b', a series of bituminous mixtures must be produced in order to determine the physical-

mechanical characteristics, following the Marshall mix design. Therefore, as a function of the obtained results and according to the limitations imposed by AND 605 regarding the physical-mechanical parameters of bituminous mixtures, an optimal binder content will be chosen.

1.3 Recycling of bituminous materials

Over the last decades, many research efforts were spent to find better solutions to increase the amounts of recovered/recycled and renewable materials used in the road construction industry.

Roads, as all the other types of constructions require during their lifetime or at the end of it, several interventions such as rehabilitation, modernization, resurfacing, reconstruction, etc. in order to ensure the safety and comfort of the traffic participants. The Reclaimed Asphalt Pavement (RAP) refers to the term used for the material obtained by milling or by full-depth removal of the old asphalt pavement. The RAP material is considered 100% recyclable and its use in the production of new asphalt mixtures leads to important benefits as cost reduction or conservation of energy, virgin aggregates and binders, etc. [21], [22].

According to the Directive 2008/98/EC on waste (Waste Framework Directive) [23] the waste legislation and policy of the European Union countries the waste management hierarchy presented in Figure 1.4 should be applied.

Most of construction materials can be only recyclable. On the other side, the asphalt is one of the few construction materials that is 100% reusable. Therefore, asphalt materials are considered as 100% reusable and recyclable materials. According to the Technical Briefing (2020) of the European Asphalt Pavement Association (EAPA) 'the reuse of the existing road material shall always be the first option and the recycling the second one' [24].

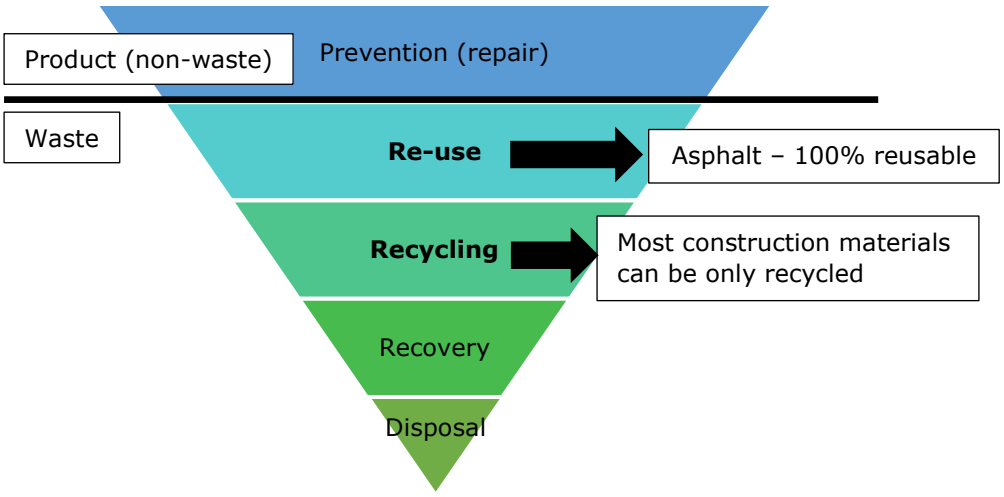

Figure 1.4. Waste hierarchy stablished by the Directive 2008/98/EC on waste [23], [24].

For economic and environmental reasons, the use of Reclaimed Asphalt Pavement (RAP) in the production of new bituminous mixtures HMA (hot-mix asphalt)

[22], [25]–[28] and WMA (warm-mix asphalt) [29], [30] has become a common strategy for the construction and maintenance of roads.

During recent years, many countries have developed various policies based on the sustainability in the road domain, based on the recovery, the reuse, the recycling of materials in order to produce new eco-friendly materials.

According to the Annual Technical Report from 2018 in USA the asphalt industry is considered 'the most diligent recycler', where more than 99% of RAP material is being reused and 82.2 million tons of RAP material are used in new bituminous mixtures [31].

On the European side, according to the European Asphalt Pavement Association (EAPA) the amount of RAP material available in various European countries, at the end on 2018, was 49.50 Mt. Table 1.5 shows the available amounts of RAP materials and the percentages of re-use and recycling of reclaimed asphalt in 2018 in 16 European countries [24].

As it can be observed in Table 1.5 the highest percentages of RAP material correspond to Germany (26% of total available RAP in 2018 in Europe), Italy (18%), France (16%), Great Britain (12%) and 28% for the other countries.

According to these data, in 2018, in Europe, near to 76% of the total available RAP material was reused in the production of a new hot/warm/cold bituminous mixture (71% hot or warm mix asphalt + 5% cold mix asphalt), 20% recycled of total and 4% used in other applications or put to landfill.

However, the reuse of RAP in the production of new bituminous mixtures is not very popular in Romania as there is no reporting data regarding the reuse of such materials.

Table 1.5. Reuse and recycling of reclaimed asphalt in 2018 – Europe [24].

Country	All available Reclaimed Asphalt in 2018 in tonnes	% of available reclaimed asphalt						Applied area in m² of hot reuse of existing asphalt pavement material in-situ / on the road (Remixing, Repaving, Reshaping, Road Train etc.)	The amount of "only" reheated (reused) asphalt material in-situ / on the road (Remixing, Repaving, Reshaping, Road Train etc.) in metric tonnes
		Re-use in Hot and Warm Mix Asphalt Production	Re-use in Half Warm Mix Asphalt Production	Re-use in Cold Recycling**	Recycling in Unbound Road Layers	Use in other Civil Engineering Applications	Put to Landfill /Other Applications/ Unknown		
Austria	1.900.000	70	30					no data	no data
Belgium	1.687.000	100	0	0	0	0	0	no data	no data
Croatia	200.000	no data	no data	no data	no data	no data	no data	no data	no data
Czech Republic	2.700.000	12	0	25	25	10	28	>400000	>420000
Denmark	1.185.000	68	no data	no data	7	0	25	no data	no data
Finland	1.300.000	100	0	0	0	0	0	8200000	no data
France	7.817.000	73	10	no data	no data	no data	no data	1589300	286360
Germany	13.000.000	82	0	0	18	0	0	no data	no data
Great Britain	6.100.000	30	70					no data	no data
Hungary	200.000	70	0	0	10	1	19	no data	no data
Italy	9.000.000	no data	no data	no data	no data	no data	no data	no data	no data
Norway	1.004.000	34	0	0	66	0	0	no data	no data
Slovakia	150.966	82	0	2	12	1	0	135627	16624
Slovenia	106.200	24	0	5	0	0	61	no data	no data
Spain	1.165.000	76	0	9	15	0	1	no data	no data
Turkey	1.965.000	1	0	0	99	0	0	no data	no data

The only data reported for Romania regarding the processes of reusing or treatment of the construction waste were found for the year 2016 according to the European Environment Agency [32].

Figure 1.5 shows the percentages reported for 30 European countries regarding the treatment of the mineral part of construction and demolition, waste

treatment (% of treated waste). For 2016 a total of 374 million tonnes of construction and demolition waste were reporter for all countries presented in Figure 1.5.

A comparison between the data reported for Romania and the average values obtained for all European countries (from Figure 1.5) was made, as shown in Table 1.6.

Table 1.6. Construction waste data reported in 2016 for Romania and the average values obtained for all European countries.

Romania (2016)	**Average European values (2016)**
- recycling: 48.4% - backfilling: 36.4% - energy recovery: 0.2% - incineration: 0% - landfill and other: 15.0%	- recycling: 82.8% - backfilling: 5.6% - energy recovery: 0.6% - incineration: 0% - landfill and other: 11.0%

It can be observed that in Romania the recycling of waste construction materials is a half of the European average value. Unfortunately, these materials are used as backfilling (the value reporter for Romania is six time higher than the European average value). Therefore, these data confirm the need of a national strategy in Romania regarding the reuse of asphalt materials.

In many reports the RAP material is considered as being a waste material. Nevertheless, as this RAP material is considered 100% reusable in the production of new mixtures or in the maintenance of roads and 100% recyclable in other applications, the specialists from EAPA recommends 'to never consider asphalt as waste' [24].

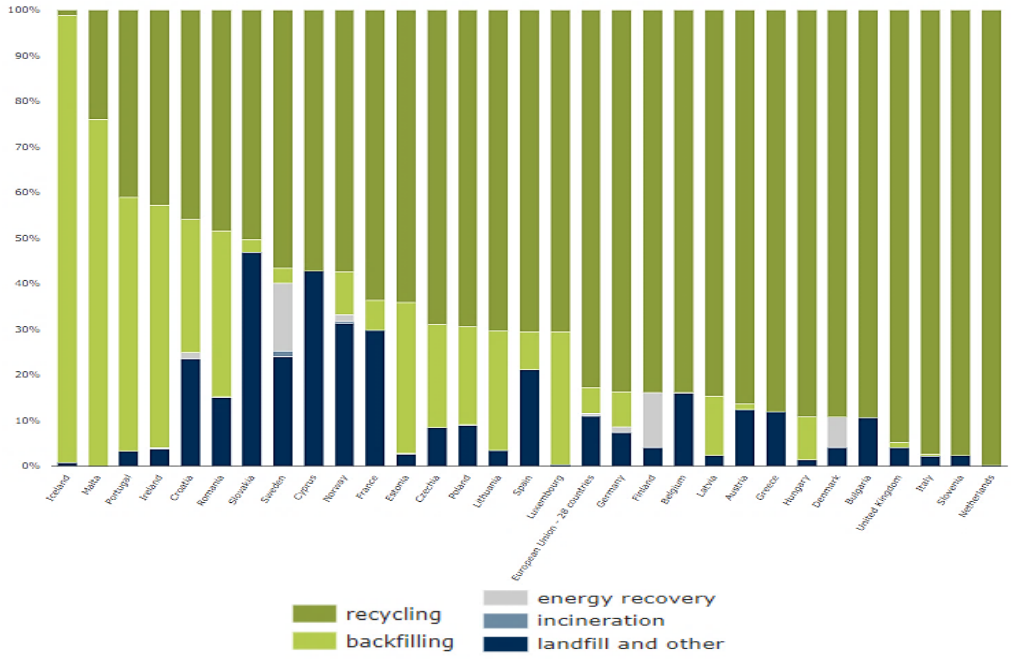

Figure 1.5. Mineral waste from construction and demolition, waste treatment in European countries in 2016. Source: European Environment Agency [32].

In the production process of a bituminous mixture containing RAP material, fresh aggregates must be used depending on the amount of the RAP material and its characteristics in order to obtain the desired grading curve of the final mix. The mix also needs a fresh binder - usually a softer binder is needed - in order to ensure the optimal binder content of the final mix. Regarding the production of an eco-friendlier bituminous mixture containing high amounts of RAP material, many studies showed the potential of renewable materials such as vegetal oils to regenerate the hard-aged RAP binder and finally to improve the mix characteristics [33]–[36].

Due to the long-term aging process, the physical and rheological properties as well as the chemical structure of the RAP-bitumen suffer irreversible changes [37], [38]. For these reasons, in order to achieve an adequate workability and good mechanical performance of a new bituminous mixture containing RAP material, a softer bitumen [39], [40] and when high amounts of RAP (30% or more) some rejuvenators [33], [41]–[45] could be used.

Many studies showed the efficiency of using vegetal oils by evaluating the conventional properties (such as penetration, ductility, Fraass temperature, ring and ball temperature), fatigue or complex modulus of final blends produced with these products, different RAP binders and different base fresh binders [25], [46]–[50].

In the following sections an overview of the requirements and the characterization of RAP material and rejuvenators, together with the normative specifications for the production of bituminous mixtures with RAP material and rejuvenator are presented.

1.3.1 Reclaimed Asphalt Pavement (RAP) material

1.3.1.1 RAP material characterization

As already mentioned, the RAP material is an aged material due to the long-term aging process. Therefore, the physical and rheological properties as well as the chemical structure of the bitumen from the RAP material suffer irreversible changes during the lifetime of the road. On the other side, the aggregates from the RAP material suffer a degradation process due to the traffic combined with the exposure to meteorological phenomena.

In Europe, the RAP material must be classified and characterized by performing the tests required by SR EN 13108-8 [51]. This Standard is also applied in Romania.

A PSD (Particle Size Distribution) analysis must be performed on the reclaimed asphalt. Some requirements must be respected, related to the water content of the RAP material, before drying for PSD analysis, that should be lower than 3% and the grading curve which must be between 0/20 mm and 0/31 mm. Also, the material retained at 25 mm must be lower than 7%. According to the EN 13108-8 the maximum size of the RAP material must be declared.

According to the above-mentioned European Standard, the RAP material is classified and characterized in function of the possible foreign matter incorporated, the type and properties of the binder and the characteristics of the natural aggregates.

Regarding the foreign matter, in EN 13108-8 [51] this term is defined as the other materials incorporated in the RAP material, different from the aggregates, divided in two groups: group 1 (concrete, metal, bricks, etc.) and group 2 (wood, plastics, etc.). By determining the foreign matter content [52], the RAP material can be classified in three categories (F_1, F_5 and F_{dec}) [51].

As already mentioned, a very important step in the characterization of the RAP material is related to the determination of the binder properties. The binder from the RAP material must be extracted and recovered [53], [54] and the penetration [55], softening point [56] and the viscosity [57] of this RAP binder must be evaluated.

Also, it is very important to know the type of the binder that was used (paving grade binder, hard grade binder or modified binder), based on the documentation and the declared information of the road network administrators. Therefore, the reclaimed asphalt shall be declared as a function of its penetration, softening point and viscosity of the RAP binder.

The mean grading curve of the aggregates [58] obtained after the binder extraction from the RAP material must be determined. Some requirements related to the RAP aggregates grading curve must be taken into consideration: grading curve must be between 0/10 mm and 0/14 mm and the filler content must be between 8% and 12%. Other laboratory tests can be performed in order to evaluate the resistance to fragmentation or the resistance to wear of the RAP aggregates.

1.3.1.2 Bituminous mixtures produced with RAP material

Towards the end of the normal duration of exploitation of bituminous coating (10 years), the dynamics of the evolution of the technical condition is a degrading curve, with an increasing slope, which translates into a pronounced degradation of it in the coming years. At this moment it is time to carry out preventive maintenance work, which will have a major impact not only on improving the technical condition of modernized road sectors, but also on future maintenance costs, by significantly reducing them. In Figure 1.6 the evolution curve of the technical condition with the qualitative highlighting of the intervention moments through different types of preventive maintenance works was plotted [59], [60]. These types of works are also provided in the Romanian Guide AND 554-2002 [61].

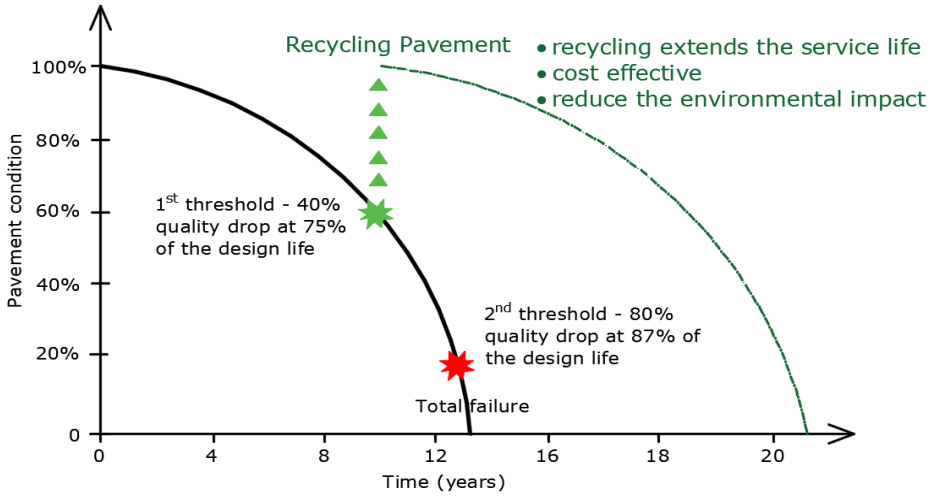

Figure 1.6. Pavement condition versus time [59], [60].

The durability of the road structures during the operation life of the road must also be implicitly linked to the periodicity and quality of the maintenance. Thus, many studies [59], [60] shows that the first periodic maintenance work must be performed before reducing the overall technical index by more than 40% and consuming about

75% of the design operating time. The delay in carrying out the maintenance work leads to a rapid deterioration of the technical condition, reaching a point that practically requires the reconstruction of the road structure (to decrease the technical condition index by about 80% and consuming about 87% of the designed life). The technology adopted for maintenance in this first stage depends on the existing financial resources and the maintenance strategy adopted by each road administration. However, the adoption of a maintenance solution, before reaching the critical threshold of technical condition, leads to the extension of the initial service life.

The use of RAP in new bituminous mixtures is a technique which is more and more used for the construction of new pavements or for maintenance of road structures for sustainable reasons [22], [25], [28], [30], [62]–[70].

The recycling of bituminous materials obtained by milling the old deteriorated layers, RAP materials, can be performed either directly in the place, 'in-situ' recycling or by using this material in an asphalt mix plant and transferred to the field, 'asphalt mix plant' recycling [71].

The following recycling methods are well known among the literature in the road industry [72]–[74]:

- hot in-place recycling;
- hot recycling: Hot Mix Asphalt (HMA) and Warm Mix Asphalt (WMA) containing RAP materials;
- cold recycling: cold in place recycling or cold central plant recycling.

The hot in-place recycling is the recycling method where the existing deteriorated pavement is softened with heat and scarified or milled to a specific depth. The scarified material is then mixed with or without virgin materials and/recycling agents (rejuvenators) and/or other additives in order to produce an HMA or a WMA.

There are three main hot in-place recycling processes: surface recycling, remixing and repaving. The surface recycling method was described above. In the remixing method the scarified material is combined with a new virgin bituminous mixture HMA, mixed in a pugmill and then placed and compacted. The repaving process represents a combination between the surface recycling process with a bituminous mixture (HMA or WMA) overlay placed and compacted at the same time [74].

In Romania the specifications regarding the application, the preliminary determinations, the type of the recycled bituminous mixtures, the materials, the physical-mechanical characteristics of the final product and other requirements regarding the hot in-place recycling are described in the Romanian Standard NE-026-2004 [75]. However, this Standard is considered as obsolete and must be updated due to the fact that many Standards which are referred in this old version, were replaced or cancelled.

HMA and WMA recycling is the method in which the RAP material (milled and crushed) is combined with virgin materials and/or rejuvenators and/or additives in order to produce in an asphalt plant an HMA or WMA. In Romania the specifications regarding the hot in plant recycling are described in the Romanian Standard DD-509-2003 [76]. The same comment is valid for this Standard as for the one regarding the hot in-place recycling, an updated version of this Standard is recommended.

The cold recycling method which does not involve heat processes, can be of two types:

- cold in-place recycling where the deteriorated pavement is milled and manipulated in place, a bitumen or emulsions is added, and the final product is recompacted. This method is usually used.

- cold central plant recycling where the material from the existing pavement is removed and transported to a plant where it is crushed and screened, then an emulsion or a foamed bitumen is added, and the mixing process is performed. The final product is then transported back for paving.

The specifications regarding the application of the cold recycling method in Romania, are described in the Romanian Standard AND 532-1997 [77]. Similar comment can be made here as in the case of the other Romanian Standards for the asphalt recycling, an updated version of this Standard is recommended.

1.3.2 Rejuvenators

1.3.2.1 Types of rejuvenators

Various studies highlighted that when more than 20% of RAP material is used in new asphalt mixtures it lead to an increase of complex modulus and to deteriorations on fatigue life of final mixtures [27], [28], [30], [78]–[80].

In order to increase the amount of RAP material and to improve the mix characteristics, many studies showed the potential of rejuvenating agents to regenerate the hard-aged RAP binder and finally to induce a positive effect on the mechanical characteristics of the final product which can be considered as an eco-friendlier bituminous mixture [33]–[36].

The use of rejuvenators was first introduced in 1960 as preservation treatment of pavement with the primary role to restore the physical and chemical characteristics of the hard-aged RAP binder [81].

In the literature, the term 'rejuvenator' is used as a general term for many products such as softening agents, fluxing agents (flux oil, slurry oil, etc.) with the main scope to decrease the viscosity of the RAP binder. Same term is usually used for another product category which can be called 'real rejuvenators' that must restore the physical-chemical and rheological properties of the aged binder [82], [83].

The difference between these two rejuvenator categories is that the real rejuvenators contain a higher amount of maltene constituents that must restore the balance between asphaltenes and maltenes from the aged RAP binder, compared to the softening agents. Also, they can have a positive effect on the ductility, cohesiveness, adhesivity and relaxation characteristics of the aged binder [84].

Based on the material source, the rejuvenators/recycling additives used for asphalt materials were classified in NCAT (2014) [85], as it is highlighted in Table 1.7.

Table 1.7. Types of rejuvenators according to NCAT (2014) [85].

Category	Description
Paraffinic oils	Refined used lubricating oils.
Aromatic extracts	Refined crude oil products with polar aromatic oil components.
Nathenic oils	Engineered hydrocarbons for asphalt modification.
Triglycerides and fatty acids	Derived from vegetable oils. *has other key chemical elements in addition to triglycerides and fatty acids.
Tall oils	Paper industry by-products. Same chemical family as liquid as liquid antistrip agents and emulsifiers.

It should be mentioned that this classification does not consider the performance differences that could be achieved by using a product that is part of one of the categories presented in Table 1.7, regarding the physical, chemical and rheological properties and the production process of the final mix.

Nowadays, many products including vegetal oils or recycled waste oils have been used as regenerating agents in order to mobilise the RAP bitumen with a double benefit of increasing RAP content and achieving good performances of the new mix [86]–[88].

Shen, Amirkhanian, and Miller (2007) [45] applied the PG binder testing method in order to obtain the optimal rejuvenator content for which the similar properties (in terms of DSR and BBR) were obtained for a binder blend (fresh binder + RAP binder + rejuvenator) as for the used virgin bitumen. On the other side, Karki and Zhou (2016) [89] highlighted that the type of the rejuvenator, the amount and the level of aging of the aged binders play an important role in the determination of the optimum rejuvenator content. The laboratory investigation of various binder blends showed that the effect of rejuvenators on aged binders consists in a reduction of stiffness, oxidation and cracking potential. Moreover, the above-mentioned researchers showed that the investigated rejuvenators had a lower influence on the high PG temperature and a greater influence on the low PG temperature. Therefore, the selection of a rejuvenator and its proper dosage based on only one direction could not meet all the specifications of a fresh virgin bitumen.

Nsengiyumva et al. (2020) [90] investigated the effects of different types, dosages and treatment methods of three rejuvenators on the properties of several binder blends and mixtures. One of the conclusions of this study was that the PG binder testing combined with chemical investigation can be successfully used in order to determine the optimal dosage and the effect of each rejuvenator.

The conclusions of recent studies focusing on conventional properties (penetration, ductility, softening point), rheological properties (complex modulus) and fatigue resistance show the capability of vegetal oils to rejuvenate hard aged binders and to provide a final product with similar properties to fresh binders [47]–[50], [91]–[93].

Also, the potential of bio-oils to be used as rejuvenators in bituminous mixtures containing RAP or RAS by diminishing the effect of the increase in stiffness due to the presence of the aged materials [94]–[96] and also in blends with aged binders by restoring to a significant extend the properties of the aged binder [97], [98].

1.3.2.2 Requirements

In order to use a product as a rejuvenator it must fulfil certain specifications/requirements related to the 'real role' of it, as follows:

- to restore the maltene characteristics;
- to reactivate the hard-aged RAP binder not just to soften or to plasticize the binder;
- it must have a high flash point;
- to reduce cracking of asphalt mixture;
- to maintain or to improve the rut resistance the asphalt mixture;
- the diffusion and dispersion must happen readily, and it must maintain the miscibility with RAP binder;
- it should be non-hazardous;
- it should present a stability over a wide temperature rage;

- it should not present any evaporation or exudation during the lifetime of the asphalt mix;
- other requirements depending on the specifications from the country or the administration agency where this solution is intended to be implemented.

Studies showed that rutting issues (permanent deformation of the pavement at high temperatures) and thermal cracking of bituminous mixtures produced with rejuvenators do not always occur if two essential aspects are considered: the diffusion and dispersion of the rejuvenator into the aged binder within a RAP material (the rejuvenator needs a proper time to establish a stable chemical bond with the bitumen) [99]–[101] and the use of an optimum percentage of the rejuvenator [26], [29], [41], [45], [102]–[104].

The diffusion of the rejuvenator into the hard-aged binder which is influenced by its dispersion rate (viscosity of the maltene), is a process that happens during the mixing and construction stages and it stops after a considerable period [105]. Carpenter and Wolosick (1980) [106] defined the four-step diffusion process of an additive/rejuvenator into the aged asphalt and Zaumanis et al. (2017) [107] illustrated this process in Figure 1.7.

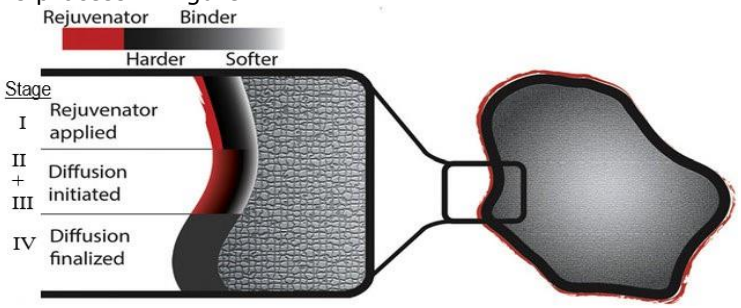

Figure 1.7. Diffusion stages of rejuvenator according to Zaumanis et al. 2017 [107].

The diffusion of the rejuvenator into the RAP binder can be investigated by evaluating the chemical components and the conventional properties of the rejuvenator coated-aged binder and Feng et al. (2011) [108] highlighted that this diffusion process can be improved by increasing the time and temperature.

When renewable materials are used for binders and bituminous mixtures, they must fulfil certain essential requirements related to the health and safety of the users and as well as of the environment, their use must be an economically solution which should give some performance benefits and as well they must be recyclable and available in large quantities without suffering changes during the transport, storage and mixing process [34].

Recent studies highlighted that when a proper dosage of bio-oils, such as waste cooking oils, are used as modifiers/rejuvenators, an improvement of the performances (fatigue cracking resistance, low-temperature cracking resistance, etc.) of the HMA's produced with RAP material, and their corresponding binder blends, was observed. Moreover, it was indicated that the rejuvenator has a positive effect by reducing the effect of the long-term aging of the corresponding binder blends (for an HMA produced with 40% up to 60% RAP material and an optimal percent of rejuvenator) and finally it can lead to a Superpave grade of a fresh binder [109], [110].

Over the last years many methods were developed in order to determine the optimum rejuvenator content starting from the theory that the rejuvenator amount

must be determined from the virgin bitumen with respect to the amount of the hard-aged binder.

Shen et al. (2007) [45] proposed a method in order to obtain the optimum rejuvenator content based on the temperature blending charts determined at high and low temperatures by measurements performed with DSR (Dynamic Shear Rheometer) and BBR (Bending Beam Rheometer). Therefore, the dosage of rejuvenator for which the same properties (in terms of DSR and BBR) were obtained for a binder blend as for the used virgin bitumen was considered the optimum content of rejuvenator.

In 2018, Lee et al. [101] proposed a similar method in which the BBR tests were performed on long term aged binder blends (PAV aging) and the optimum rejuvenator content was considered when a similar PG low temperature of a binder blend was obtained as the one obtained for the fresh binder.

Usually, the rejuvenators are incorporated into an asphalt mixture that contain RAP material based on the producer/manufacturer's recommendations regarding the optimum dosage of the rejuvenator.

Most of the time the recommended optimum amount of rejuvenator is expressed from the percentages of RAP or RAS materials with respect to the total weight of final mixture. Bennert et al. (2015) [111] and Haghshenas et al. (2016) [112] used different additives/rejuvenators in the dosages recommended by the manufacturers and they investigated the behaviour of the final materials in order to verify the effect of the rejuvenator. They concluded that the recommendations given by the manufacturers regarding optimum dosage of rejuvenator can be considered valid but still preliminary investigation is needed in order to know if the rejuvenator is 'compatible' with the aged RAP binder and the fresh binder, if used.

1.3.2.3 Bituminous mixtures produced with RAP material and rejuvenators

Regarding the production of bituminous mixtures containing RAP material and rejuvenator there are different processes related to the type of the chosen recycling method, the type of the rejuvenator (recommendations of the manufacturer) and other requirements depending on the specifications from the country or the administration agency where this solution is intended to be implemented.

As an example, in Romania for bituminous mixtures realized with RAP material, rejuvenator and fresh crushed aggregates, the mixing temperature according to the Romanian Standard AND 605 [14] and DD 509 [76] is 160±10°C. Other requirements are related to the actual production process as follows:

- the virgin aggregates should be preheated at 160±10°C for 12 hours;
- the fresh binder should be preheated at 160±10°C for 4 hours;
- the RAP material should be preheated at a 165±10°C for 2 hours;
- usually the rejuvenator is added at ambient temperature (no heating process needed).

As described in the above sections, it is very important firstly to know the characteristics/properties of each materials separately, and then to investigate the compatibility between them.

By investigating the interaction between a virgin binder and a RAP binder, Noferini et al. (2017) [49] showed that the rheological properties and the viscosity of the binder blends are little influenced when less than 10% of RAP material is used in the asphalt mixtures. Therefore, the effect of the RAP binder is significant on the properties of binder blends when more than 10% RAP material are used in the

production of new asphalt mixture. In this case, recycling agents or rejuvenators are frequently used in order to increase the amounts of RAP and to assure a good workability and satisfactory mechanical properties of the final mix.

The potential of different recycling agents to rejuvenate the aged RAP binder was highlighted in various studies by evaluating the rheological or conventional properties, of various binder blends and also by investigating the effect of rejuvenators on the thermomechanical performances of bituminous mixtures (produced with RAP material). Mogawer et al. (2013) [48] showed that rejuvenators can mitigate the stiffness of the rejuvenated binder blends and the cracking performances of the corresponding bituminous mixtures were improved. However, when the rejuvenator is not used in a proper dosage it can lead to an adversely impact on the moisture susceptibility and the rutting performances of mixtures.

Zaumanis et al. (2014) [113] used the Superpave PG tests in order to determine the optimum dosage of six rejuvenators and highlighted that a proper amount of rejuvenators can reduce the performance grade of a rejuvenated binder blend to the level of a fresh binder, can ensure excellent rutting resistance, good cracking performances and can provide a longer fatigue life of 100% recycled asphalt mixtures. Therefore, the type and the optimum dosage of rejuvenators play an important role on the behaviour of binder blends and bituminous mixtures produced with RAP binder/material.

Nowadays many products of vegetal origin are used as rejuvenators. Mangiafico et al. (2017) [47] showed that the addition of a recycling agent of vegetal origin into recycled bituminous mixtures can reduce the norm of complex modulus and when more than 40% of RAP material were used, an improvement on the fatigue performances was observed.

Menapace et al. (2018) [91] and Oldham et al. (2018) [50] concluded that the reduction of stiffness should not be used as a single indicator of the rejuvenation effect of a recycling agent. A true rejuvenator should lead to a restoration of both stiffness and morphology of the final binder blends. Therefore, the selection of a rejuvenator and its proper dosage based on only one direction could not meet all the specifications of a fresh virgin binder.

The conclusions of several studies and the purposes of several ongoing research programs that are focusing on the investigation of the influence and the effect of various RAP materials and different rejuvenators on the final performances of the mixtures can be summarized as follows:

- rejuvenators can improve the permanent deformation of final bituminous mixtures - conclusions of Haghshenas et al. (2016) [112], Zhou et al. (2015) [114];
- the long-term performance of rejuvenators may not exhibit stability when exposing to high temperature for a long period of time – conclusion NRRA report (2020) [115];
- rejuvenators can reduce the moisture resistance - conclusion of Haghshenas et al. (2016) [112], Tran et al. (2012) [116], Hajj et al. (2013) [44], Im and Zhou (2014) [117];
- rejuvenators can reduce the stiffness of the final mixtures – conclusions from Tran et al. (2012) [116], Hajj et al. (2013) [44], Im et al. (2014) [117];
- rejuvenators may improve the resistance to cracking of the final mixtures – conclusions of Tran et al. (2012) [116], Hajj et al. (2013) [44], Im et al. (2014) [117];

- rejuvenators improved the fatigue resistance and they can provide fatigue resistance even after expended hours of aging – conclusions from NRRA report form 2020 [115];
- low temperature cracking susceptibility of mixtures produced with RAP material is improved when rejuvenators were used. Also, even if the mixtures were subjected hours of aging, this process did not cause an important effect on the low cracking temperature – conclusions from NRRA report form 2020 [115], Lee et al. (2018) [101].

1.4 Thermo-mechanical behaviour of bituminous materials

Flexible and semi-rigid road pavement structures are the most widespread, both in Romania and worldwide. Therefore, complex studies of these structures which involves different combinations of layers of different materials realized by different techniques, subjected to loads from various factors (traffic, climatic conditions), are still needed.

Due to the increase of the intensity of road traffic and the increasing axle loads and tire pressures of vehicles combined with the climate changes, the problem of the structural design of roads was and still is a topic of major importance.

Therefore, these two types of load acting on the pavement are reviewed in the following section (Section 1.4.1) and further the thermo-mechanical behaviour of binders (Section 1.4.2) and bituminous mixtures (Section 1.4.3) are described.

1.4.1 Load acting on flexible and semi-rigid pavement structures

The diversity of the types of vehicles as well as of the temperature variations resulted in the last 20 years, creates a real difficult decision regarding the quantification of these loads when a structural design of a flexible or of a semi-rigid pavement structures is performed.

According to the mechanical models of operation of road structures, as well as the structural design calculation methods developed so far, vehicles with various axle loads are transformed into an equivalent number of standard vehicles, with a certain axle load, based on certain factors obtained from theoretical or experimental criteria. The establishment of these equivalence coefficients involves the grouping by type of vehicle (by axle load) and the determination of the equivalence coefficient for each group of vehicles, based on the characteristics of a representative vehicle. This implies a deviation from the actual demand, given the different characteristics of the vehicles in a given group, as well as the share of each type within that group [118].

According to Di Benedetto and Corte (2005) [12] and Huang (2004) [119], the road pavements can be modelled as multi-layer systems of a certain number of infinite slabs where the interface between two consecutive layers can vary from being full friction (bound) to full slip (unbound).

The effect of traffic on a pavement structure leads to the appearance of horizontal tensile stresses and strains at the bottom of each layer and to vertical compressive stresses and strains in cross section, under the wheel, as shown in Figure 1.8 [12], [120], [71].

After a repeated number of passes (traffic load) at the bottom of layers the fatigue phenomena can occur. On the other side, in vertical section the rutting (permanent deformation) phenomena can appear.

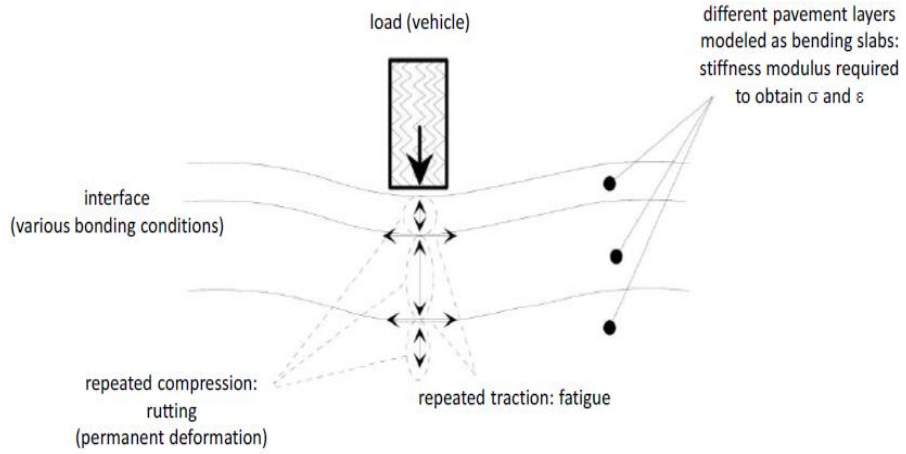

Figure 1.8. Scheme of traffic load and corresponding pavement response [12], [71], [120].

Usually, the pavement response is determined depending on the number of layers and the traffic load, by considering an isotropic linear elastic multilayer model for each layer.

The climatic conditions that can intervene in the structural design and in the characterization of the behaviour of pavement structures are varied. The most important climatic factors can be grouped as follows:

- abundance of precipitation related to drainage;
- the effect of the seasonal temperature cycles – asphalt layers are sensitive to temperature variations;
- freeze-thaw cycles action.

As already mentioned, the characteristics of bituminous materials are very closely related to temperature, its effect leads to stresses and strains within the analysed material due to the expansion and thermal contractions. The scheme of thermal loads and the corresponding response of the pavement is shown in Figure 1.9 (according to Di Benedetto, 1998 [120]).

Therefore, the effects of temperature on the pavement layers made with bituminous materials are the following:

- bituminous materials are thermal susceptible materials – stiffness increase with the decrease of temperature and vice versa;
- temperature variations lead to thermal expansion and contraction into the materials;
- at low temperature variations the restrained thermal contraction of the bituminous layers leads to thermal cracking;
- repeated temperature cycles (variations) can also conduce to 'thermal fatigue';
- in case of a pavement structure where a foundation layer is produced with hydraulic treatment, if a crack appear in this layer and if it is combined with the thermal contraction, this can lead to the propagation of the crack in the bituminous layers (phenomena known as 'reflective cracking');
- the freeze-thaw cycles action combined with certain problems related to ensuring the drainage of the surface water, can lead to a progressive degradation of the bituminous material.

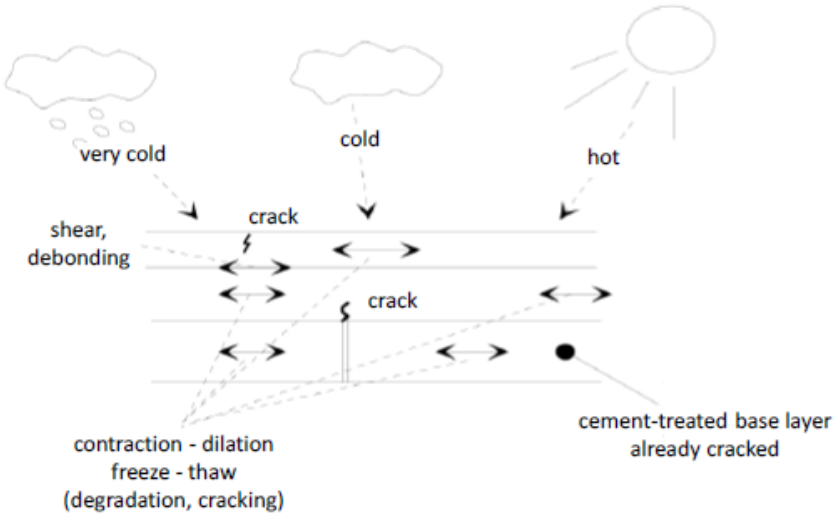

Figure 1.9. Scheme of thermal load and corresponding pavement response [12], [71], [120].

1.4.2 Binders

The binder has a very complex thermomechanical behaviour that is influenced by the temperature, the speed and the load level. In a wide range of loading the behaviour can be considered as linear viscoelastic [11], [12]. The linear viscoelastic response of a binder is commonly analysed in terms of complex shear modulus.

It is well known the behaviour of a bitumen is influenced by four factors:

- the temperature, T ;
- the frequency, f ;
- in case of a cyclic sinusoidal loading - the number of loading cycles, N ;
- the strain amplitude, ε .

Several mechanical behaviour domains can be defined depending on the values of the three above mentioned factors [11], [12], [71], [121], [122].

Di Benedetto and Corté (2005) [11] indicated different behaviours of bituminous materials based on the temperature (T) and the amplitude of the deformation $(|\varepsilon|)$. As it can be observed in Figure 1.10, the following behaviours of binders can be distinguished: the brittle and the ductile domains, the linear elastic behaviour (characterized by E and G), the Linear ViscoElastic (LVE) domain (characterized by E^* and G^*), the purely viscous Newtonian behaviour (characterized by the viscosity η), the fragile rupture (characterized by the toughness K_C) and the non-linear domain which are the typical mechanical domains depending on the strain amplitude and the temperature, at an imposed number of cycles, for a binder.

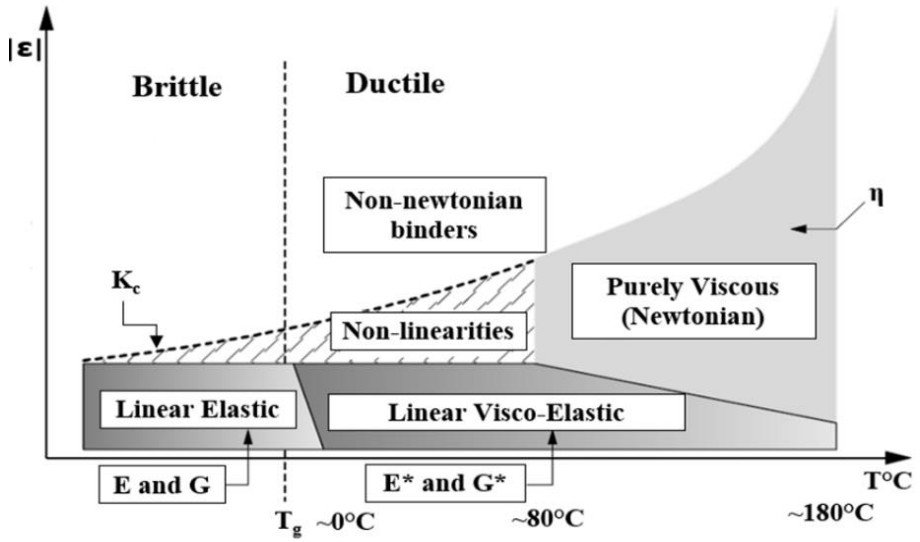

Figure 1.10. Mechanical behaviour domains of a binder as a function of temperature T and strain amplitude ε [11], [71].

On the other side, depending on the strain amplitude and the number of cycles at an imposed temperature, the following mechanical behaviour domains can be defined, as shown in Figure 1.11.

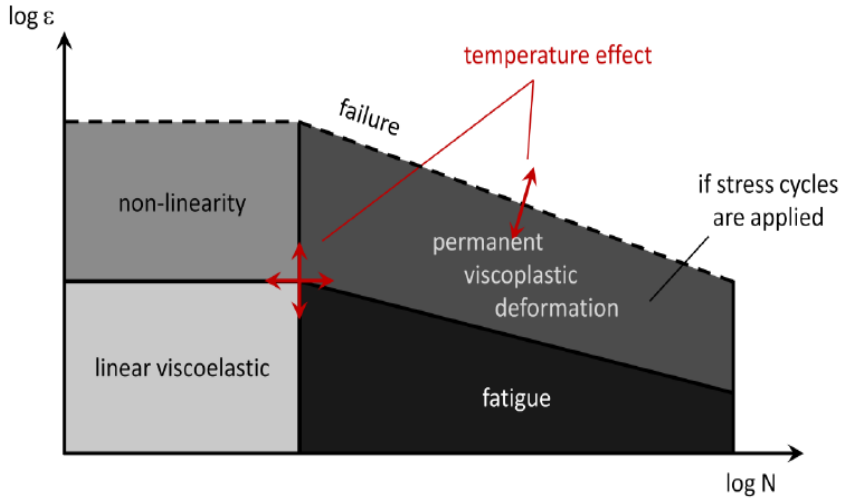

Figure 1.11. Mechanical behaviour domains of a binder at a given temperature as a function of strain amplitude and number of cycles [71].

As it can be observed in Figure 1.11, if a bitumen is subjected, at a given temperature, to a small number of a cycles and to a small amplitude strain, it can be considered as being a linear viscoelastic material. Moreover, from Figure 1.10 it can be observed that for temperatures approximately below T_g (the glass transition

temperature), the viscous aspect of the binder can be neglected, then it can be assumed linear elastic.

On the other side, if a bitumen is subjected to a small number of cycles and to a large amplitude strain, its mechanical behaviour becomes non-linear.

In the small strain domain, fatigue can occur when a high number of cycles is applied. Moreover, in Figure 1.11 it can be observed that for high amplitude strain for relatively high number of cycles and when stress cycles are applied to the bitumen, a permanent viscoplastic deformation occurs.

The relation between temperature and viscosity is very important in the context of determining and evaluating some characteristics such as adhesion, rheology, durability, etc. of binders.

Complex shear modulus together with the steady and complex shear viscosities are the most important rheological properties, used to characterize the linear viscoelastic behaviour of binders. Viscosity is a fundamental characteristic property of binders and rejuvenators and it can be determined by several methods [123]–[125].

Therefore, the characterization and the understanding of the viscoelastic behaviour of binders can be considered essential in the design process of a bituminous mixture due to the fact that the binder has an important influence on the mechanical response of the bituminous mixture [29].

1.4.3 Bituminous mixtures

The mechanical behaviour of bituminous mixtures is complex and it depends on many factors. However, Corté and Benedetto (2005) [11] identified different types of behaviour of bituminous mixtures depending on the strain amplitude and the number of cycles, for a given temperature, as shown in Figure 1.12, where the following domains were highlighted:

- the linear viscoelastic domain – for a low number of cycles and small strains $\left(\varepsilon < 10^{-4} m/m\right)$ – complex modulus tests;
- non-linear domain – for a low number of cycles and more important strain – deformability tests;
- fatigue domain - for a higher number of cycles under low deformations – fatigue tests;
- when stress-deviating cycles are applied from zero stress, non-negligible irreversible deformations occur for deformation amplitudes close to the rupture. Their accumulation creates rutting.

These typical mechanical behaviour domains reflect the behaviour domains that were described in Section 1.4.2 for binders.

Also, it must be specified that the values presented in Figure 1.12 were used only as general indicators.

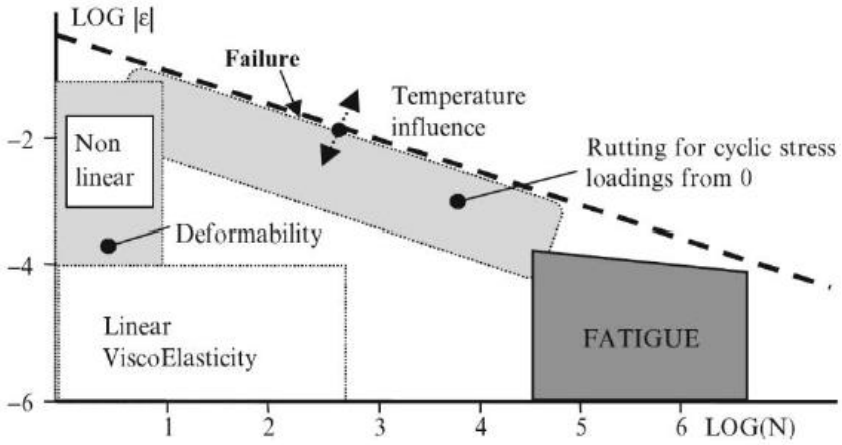

Figure 1.12. Mechanical behaviour domains of a bituminous mixture at a given temperature as a function of strain amplitude (ε) and number of cycles (N) [11], [71].

1.5 LVE behaviour of bituminous materials

1.5.1 Viscoelastic behaviour

1.5.1.1 Definition. Boltzmann superposition principle

A material presents a viscoelastic behaviour if by applying a deformation, its response presents both elastic and viscous characteristics. Therefore, in order to verify if a material can be considered as viscoelastic the cancellation test can be performed on an original non-aged material by loading it in strain-control mode and by highlighting its response where a complete stress recovery is shown $\sigma_\infty = 0$ when $t \to \infty$, as presented in Figure 1.13.

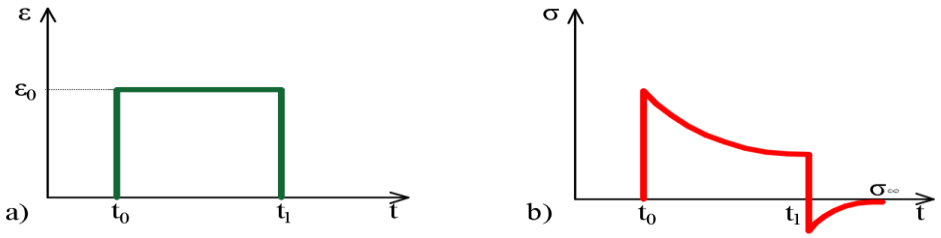

Figure 1.13. Cancellation test: (a) imposed strain history; (b) resulting stress.

Moreover, a material can be considered as Linear ViscoElastic (LVE) if its total response to a superposition of different loads is equal to the superposition of the individual responses to each load (Boltzmann superposition principle [126], [127]). An example is shown in Table 1.8 in order to describe better the Boltzmann superposition principle.

Table 1.8. Boltzmann superposition principle.

Action		Response
$\varepsilon_1(t)$	→	$\sigma_1(t)$
$\varepsilon_2(t)$	→	$\sigma_2(t)$
$\lambda \cdot \varepsilon_1(t) + \mu \cdot \varepsilon_2(t)$	→	$\lambda \cdot \sigma_1(t) + \mu \cdot \sigma_2(t)$

1.5.1.2 Creep

The creep can be defined as the increase in the strain of a material over time, under the action of a constant stress. The creep test for a viscoelastic material consists in imposing a constant stress σ_0, at a constant temperature, from a moment t_0 as shown in Figure 1.14, where the stress $\sigma(t)$ at any t can be determined with the equation 1.4 and its response, the strain $\varepsilon(t)$ can be determined with equation 1.5.

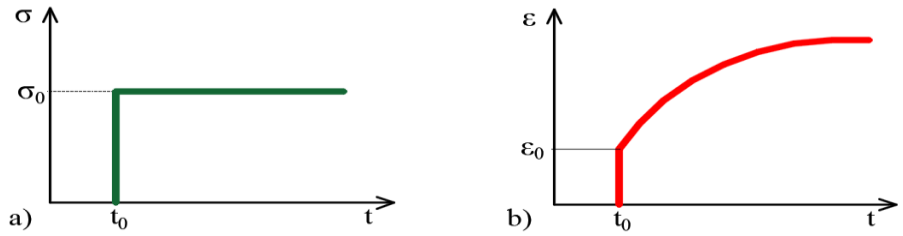

Figure 1.14. Linear viscoelastic material - creep test: (a) imposed stress; (b) resulting strain.

$$\sigma(t) = \sigma_0 H(t - t_0) \tag{1.4}$$

where H is the Heaviside function:

$H(t - t_0) = 0$ if $t < t_0$

$H(t - t_0) = 1$ if $t \geq t_0$

$$\varepsilon(t) = \sigma_0 F(t_0, t) \tag{1.5}$$

where:

$F(t_0, t)$ – creep function of material at any time t for the stress σ_0 applied at t_0.

When the applied stress is not constant, but it consists in a stress history, $d\sigma(t)$, as shown in Figure 1.15, the incremental notation is used, where the corresponding strain variation is equal to:

$$d\varepsilon(t) = d\sigma(\tau) F(\tau, t) \tag{1.6}$$

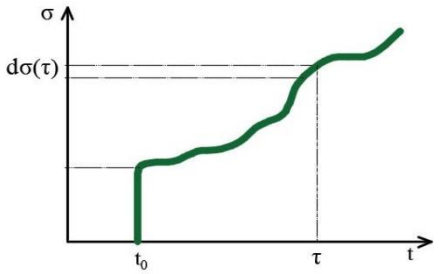

Figure 1.15. Example of stress history.

As already shown in Section 1.5.1.1, for a linear viscoelastic material the Boltzmann superposition principle must be valid, therefore the total response must be equal to the sum of the individual responses to each stress variation (equation 1.7).

$$\varepsilon(t) = \int_{t_0}^{t} F(\tau, t)\, d\sigma(\tau) = \sigma(t_0) F(t_0, t) + \int_{t_0}^{t} F(\tau, t)\, \dot{\sigma}(\tau)\, d\tau \qquad (1.7)$$

1.5.1.3 Relaxation

The relaxation can be defined as the time dependent stress response to a constant strain (inverse of creep). The relaxation test for a viscoelastic material consists in applying a constant strain ε_0, at a constant temperature, from a moment t_0 as shown in Figure 1.16, where the strain $\varepsilon(t)$ at any t can be determined with the equation 1.8 and its response, the resulting stress $\sigma(t)$ as shown in equation 1.9.

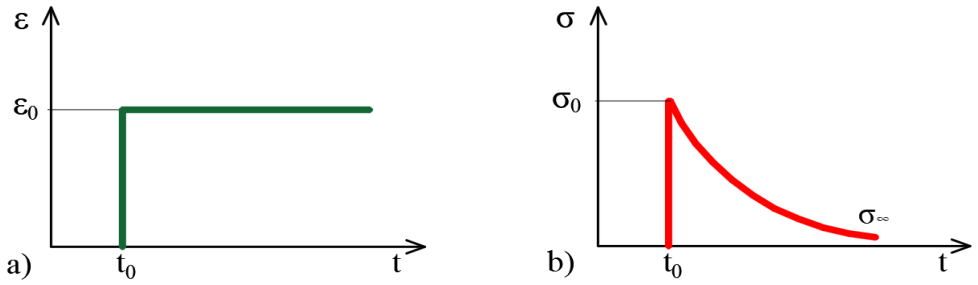

Figure 1.16. Linear viscoelastic material - relaxation test: (a) imposed strain; (b) resulting stress.

$$\varepsilon(t) = \varepsilon_0 H(t - t_0) \qquad (1.8)$$

$$\sigma(t) = \varepsilon_0 R(t - t_0) \qquad (1.9)$$

where:

$R(t-t_0)$ – relaxation function of the material at any time t for the strain ε_0 applied at t_0.

Similar to the creep test (Section 1.5.1.2) by following the same approach, for a generic strain history (Figure 1.17) where the incremental notation is used and where the corresponding stress variation is equal to:

$$\sigma(t) = \varepsilon(t)R(0) + \int_{t_0}^{t} \varepsilon(\tau)\frac{\partial R}{\partial \tau}(t-\tau)d\tau \tag{1.10}$$

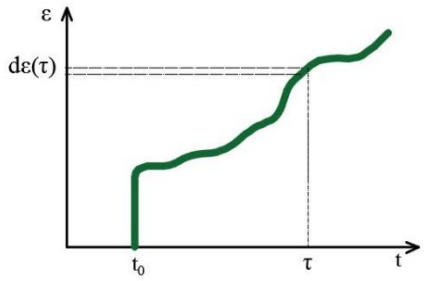

Figure 1.17. Example of strain history.

1.5.1.4 Carson - Laplace transform

In practice, the integral equations for strain (Section 1.5.1.2 – equation 1.7) and stress (Section 1.5.1.3 – equation 1.10) that describe the LVE behaviour, are difficult to apply. Therefore, the Carson-Laplace transform described by Mandel (1995) [71], [126] is used. This transformation consists in transforming $\tilde{f}$ of generic function $f(t)$ depending on time as described in equation 1.11 where p is a complex variable corresponding to time in the transform domain of Laplace.

$$\tilde{f}(p) = p\int_{0}^{\infty} f(t)e^{-pt}dt \tag{1.11}$$

Equations 1.7 and 1.10 can be rewritten as follows:

$$\tilde{\varepsilon}(p) = \tilde{F}(p)\cdot\tilde{\sigma}(p) \tag{1.12}$$

$$\tilde{\sigma}(p) = \tilde{R}(p)\cdot\tilde{\varepsilon}(p) \tag{1.13}$$

where:
$\tilde{\varepsilon},\tilde{F},\tilde{\sigma},\tilde{R}$ – the Carson-Laplace transformations of strain, creep function, stress and relaxation function.

Also, it must be mentioned that the creep function multiplied by the relaxation function is equal to 1 (equation 1.14).

$$\tilde{F}(p)\cdot\tilde{R}(p) = 1 \tag{1.14}$$

1.5.1.5 Complex modulus

When a sinusoidal stress $\sigma(t) = \sigma_0 sin(\omega t)$, with the frequency f (where ω is the angular frequency, $\omega = 2\pi f$) is applied on a linear viscoelastic material, its response (deformation) presents a similar sinusoidal form $\varepsilon(t) = \varepsilon_0 sin(\omega t - \varphi)$ where φ is the phase angle (phase lag between both $\varepsilon(t)$ and $\sigma(t)$ sinusoidal signals). Figure 1.18 shows an example of complex modulus test on a LVE material regarding the sinusoidal signals in stabilized mode.

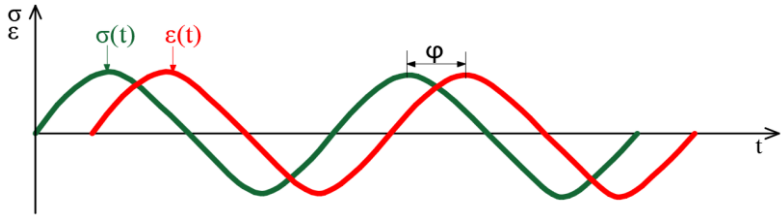

Figure 1.18. LVE material – example of complex modulus test: sinusoidal signals of stress and strain.

In an exponential form by using the complex notation $i^2 = -1$, the stress and strain can be written as follows:

$$\sigma^*(t) = \sigma_0 e^{i\omega t} \tag{1.15}$$

$$\varepsilon^*(t) = \varepsilon_0 e^{i\omega t - \varphi} \tag{1.16}$$

where:

$$\sigma(t) = Im\left[\sigma^*(t)\right] \tag{1.17}$$

$$\varepsilon(t) = Im\left[\varepsilon^*(t)\right] \tag{1.18}$$

where $Im[A]$ represents the imaginary part a complex variable A.

It can be shown that:

$$\sigma^*(t) = \tilde{R}(i\omega) \cdot \varepsilon^*(t) \rightarrow \tilde{R}(i\omega) = \frac{\sigma^*(t)}{\varepsilon^*(t)} = E^*(\omega) \tag{1.19}$$

where $E^*(\omega)$ is called complex modulus and is equal to the Laplace-Carson transform of the relaxation function $\tilde{R}$ determined in $i\omega$.

By applying equations 1.15 and 1.16, the equation 1.19 can be rewritten as follows:

$$E^*(\omega) = \frac{\sigma_0 e^{i\omega t}}{\varepsilon_0 e^{i\omega t - \varphi}} = \left|E^*\right| e^{i\varphi} \tag{1.20}$$

where $\left|E^*\right| = \frac{\sigma_0}{\varepsilon_0}$ is the norm of complex modulus.

Moreover, as E^* is a complex number then it is defined by its real (E_1) and imaginary (E_2) parts, as follows:

$$E^* = E_1 + iE_2 = \left|E^*\right| cos\,\varphi + i\left|E^*\right| sin\,\varphi \tag{1.21}$$

where:

E_1 shows the elastic aspect of the behaviour of the tested material and it is called 'storage modulus';

E_2 represents the viscous aspect of its behaviour and is called 'loss modulus';

φ is the phase angle with $0° < \varphi < 90°$. If $\varphi = 0°$ the material is linear elastic and if $\varphi = 90°$ the material is purely viscous.

The complex shear modulus, in case of a binder, can be defined in a similar way as the complex modulus:

$$G^*(\omega) = \frac{\tau_0 e^{i\omega t}}{\gamma_0 e^{i\omega t - \varphi}} = \left|G^*\right| e^{i\varphi} = \left|G^*\right| cos\,\varphi + i\left|G^*\right| sin\,\varphi \tag{1.22}$$

where:

τ_0 – amplitude of the sinusoidal shear stress $\tau(t)$;

γ_0 - amplitude of the sinusoidal shear strain $\gamma(t)$.

Moreover, if the tested material is isotropic, between E^* and G^*, the following relation is valid:

$$G^* = \frac{E^*}{2\left(1+\nu^*\right)} \tag{1.23}$$

where ν^* is the complex Poisson's ratio which can be defined for the radial strain ε_2^* on the axial deformation ε_1^* (equation 1.24), in case of a uniaxial loading σ_1^*

$$\nu^* = -\frac{\varepsilon_2^*}{\varepsilon_1^*} = \frac{\varepsilon_{02} e^{i\omega t - \varphi + \pi + \varphi_\nu}}{\varepsilon_{01} e^{i\omega t - \varphi}} = \left|\nu^*\right| e^{i\varphi_\nu} = \left|\nu^*\right| cos\,\varphi_\nu + i\left|\nu^*\right| sin\,\varphi_\nu \tag{1.24}$$

where:

$\left|\nu^*\right|$ is the norm of complex Poisson's ratio;

φ_ν is the phase angle of the Poisson's ratio.

The following graphical plots are generally used in order to highlight the variation of complex modulus or complex shear modulus and their components as a function of frequency and temperature:

- **isochronal curves**: plot of norm of complex modulus $|E^*|$ values as a function of test temperatures (t) for each frequency test (f), in a semi-logarithmic scale;
- **isothermal curves**: plot of norm of complex modulus $|E^*|$ values as a function of test frequencies (f) for each test temperature (t), in a logarithmic scale;
- **Black diagram**: plot of norm of complex modulus $|E^*|$ values against phase angle (φ) values, in a semi-logarithmic scale $(log|E^*| \; vs. \; \varphi)$;
- **Cole-Cole plot**: plot of the real part of norm of complex modulus $|E^*|$ values (E_1) against the imaginary part of norm of complex modulus $|E^*|$ values (E_2).

1.5.2 Time-Temperature Superposition Principle

As already mentioned, the complex shear modulus G^* (or complex modulus E^*) is a measure of the total resistance to deformation of a linear viscoelastic material when subjected to cyclic sinusoidal shear. Phase angle φ is an indicator of the relative amount of recoverable and non-recoverable deformation [43].

For a linear viscoelastic material, it was observed that the complex modulus values $(|E^*|, E_1, E_2, \varphi)$ plotted in Black diagram and Cole-Cole plot tend to form a unique curve independent of frequency and temperature [127]. The materials that present this type of behaviour are named 'thermorheologically simple' [12]. This property of a material which equates the effects of the temperature and frequency (time in the time domain) on its behaviour is called Time-Temperature Superposition Principle (TTSP).

This TTSP principle consists in the translation of complex modulus curves among the horizontal axis (frequency) for a chosen reference temperature (T_{ref}) in order to obtain a unique master curve. This translation of the isothermal curves is performed by using some coefficients $a_T(T)$ which are called shift factors. The equation 1.25 is considered.

$$E^*(f,T) = E^*(f \cdot a_T(T), T_{ref}) \tag{1.25}$$

In practice, after choosing the reference temperature, the shifting of all the other isothermal curves is performed by multiplying the frequencies of all the values of each curve by the shift factors which are determined for each isothermal curve.

Master curves of the phase angle (φ) can be built by using the same values of the shift factors as those used for the norm of complex modulus $(|E^*|)$ or the norm

of complex shear modulus $\left(\left|G^*\right|\right)$ master curves. As an example, the master curve of a binder is shown in Figure 1.19 (from Forton et al. 2019) [128].

On the other side, the Time-Temperature Superposition Principle can be applied to isochronal curves by using the same procedure with the difference that a reference frequency must be chosen in order to obtain the isochronal master curves.

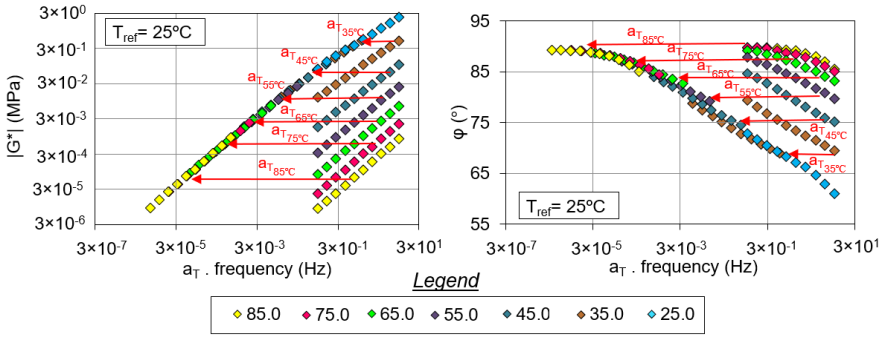

Figure 1.19. Example of master curves of complex modulus $\left(\left|E^*\right| - left, \varphi - right\right)$ for a bitumen [128].

The most common equation that is used in order to fit the shift factors as a function of temperature is the Williams-Landel-Ferry (WLF) equation (equation 1.26).

This WLF equation can be used and applied over the whole range of test temperature. An example is shown in Figure 1.19 for the same material as the one exemplified in Figure 1.20.

$$log\left(a_T\right) = \frac{-C_1\left(T - T_{ref}\right)}{C_2 + \left(T - T_{ref}\right)} \tag{1.26}$$

where C_1 and C_2 are empirical constants depending on the material and T_{ref} .

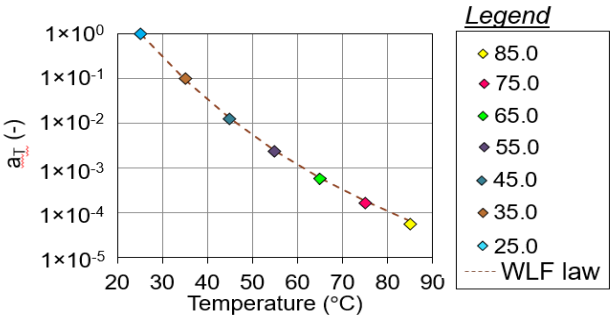

Figure 1.20. Example of shift factors and WLF fit for a bitumen [128].

As already mentioned, the TTSP can successfully be applied for thermorheologically simple materials. Several studies showed that the binders that are modified with different polymers do not show this property of being thermorheologically simple. However, this superposition principle can be partially

applied. Therefore, for this type of materials the Partial Time Temperature Superposition Principle (PTTSP) can be applied [121], [129], [130].

1.5.3 Modelling viscoelastic behaviour – 2S2P1D model

Over the years, many theoretical/analogical LVE models were proposed in order to perform a mathematical approximation of the real behaviour of the tested materials, all of them composed by different combinations of springs (corresponding to the elastic behaviour) and dashpots (corresponding to the Newtonian viscous behaviour) [131].

The main models that are used in case of bituminous materials are the following:

- models with a discrete relaxation spectrum:
  - Maxwell model: a linear spring assembled in series with a linear dashpot [132];
  - Kelvin-Voigt model: same elements as in case of the Maxwell model but assembled in parallel [133]–[137];
  - Burgers model: two Maxwell models assembled in parallel;
  - generalized Maxwell model: a finite number of Maxwell elements assembled in parallel;
  - generalized Kelvin-Voigt model: a finite number of Kelvin-Voigt elements assembled in series;
- models with a continuous relaxation spectrum:
  - Huet model: a linear spring and two parabolic elements assembled in series [138];
  - Huet-Sayegh model: a Huet element assembled in parallel with a second linear spring [139];
  - 2S2P1D model: two springs, two parabolic elements and one dashpot [129], [140];
- analytical expressions:
  - CA model: Christensen-Anderson model expresses the complex shear modulus of binders as a function of frequency [141];
  - CAM model: Christensen-Anderson-Marasteanu model [142];
  - HN model: Havriliak–Negami model [143], [144].

Further, in this section the 2S2P1D (2 Springs, 2 Parabolic, 1 Dashpot) (Figure 1.21) model was described due to the fact that it was the only model which was fitted on the experimental values obtained for the tested bituminous materials (Chapters 2 and 3).

The 2S2P1D model is an analogical adapted version of the Huet-Sayegh model, where a linear dashpot was added in series with the two parabolic elements in order to take into consideration the purely viscous (Newtonian) behaviour of binders in the high temperature-low frequency domain.

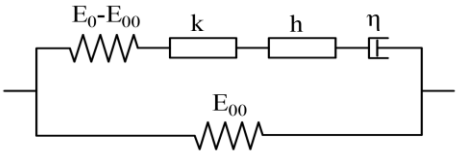

Figure 1.21. 2S2P1D model [129], [140].

The complex modulus is expressed by equation 1.27 where only seven parameters $(E_0, E_{00}, \delta, k, h, \tau, \beta)$ are considered (all 2S2P1D parameters have a physical meaning).

$$E^*(i\omega\tau) = E_{00} + \frac{E_0 - E_{00}}{1 + \delta(i\omega\tau)^{-k} + (i\omega\tau)^{-h} + (i\omega\beta\tau)^{-1}} \tag{1.27}$$

where:
ω is the angular frequency;
E_{00} is the value of the complex modulus when $\omega \to 0$, the static modulus;
E_0 is the value of the complex modulus when $\omega \to \infty$, the glassy modulus;
τ is the characteristic time, a function of temperature and accounting for Time-Temperature Superposition Principle as in equation 1.28;
δ, k *and* h are dimensionless constants, where $0 < k < h < 1$ related to the E_2/E_1 ratio when $\omega \to 0$, respectively when $\omega \to \infty$;
β is a dimensionless parameter related to Newtonian viscosity η, equation 1.29.

$$a_T = \frac{\tau}{\tau_0} \tag{1.28}$$

where τ_0 is the characteristic time at reference temperature T_{ref} and a_T is the shift factor, varying with temperature.

$$\eta = (E_0 - E_{00})\beta\tau \tag{1.29}$$

where η is the Newtonian viscosity.

Figure 1.22 shows the influence of six 2S2P1D parameters on a general Cole-Cole diagram of a bituminous material.

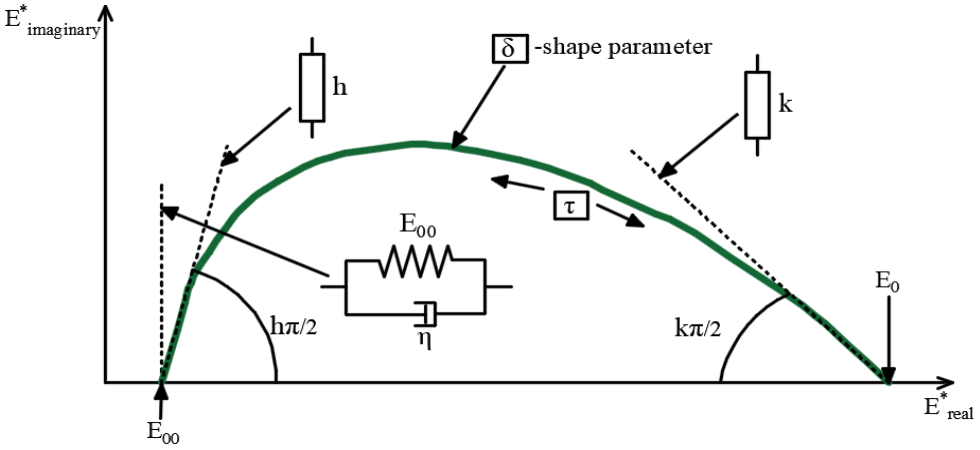

Figure 1.22. Influence of 2S2P1D parameters on a general Cole-Cole diagram of a bituminous material [71].

In a 3D extension other two parameters are used υ_0 - static value of Poisson's ration and υ_{00} - glassy value of Poisson's ration, as shown in equation 1.30 [122], [145]. Therefore, to fully characterized the behaviour of a bituminous material over the entire temperature and frequency domain, a total of nine 2S2P1D parameters $\left(E_0, E_{00}, \delta, k, h, \tau, \beta \text{ for 1D formulation} + \upsilon_0, \upsilon_{00} \text{ for the 3D formulation}\right)$ and the two WLF constants $\left(C_1 \text{ and } C_2\right)$ are needed.

$$\upsilon^*(\omega) = \upsilon_{00} + (\upsilon_0 - \upsilon_{00}) \frac{E^*(\omega) - E_{00}}{E_0 - E_{00}} \tag{1.30}$$

On the other side, Mangiafico (2014) [71] proposed an estimation method in order to predict/estimate the 2S2P1D parameter and the shift factors of binder blends from the 'experimental' values obtained for the two base binders. A linear estimation rule was proposed for the parameters E_0, δ, k, h, β (equation 1.31) and a logarithmic rule for the 2SP1D parameter τ and for the shift factors (equation 1.32).

$$A_{x\%} = A_{0\%} + x\left(A_{RAP\%} - A_{0\%}\right) \tag{1.31}$$

$$log\left(B_{x\%}\right) = log\left(B_{0\%}\right) + x\left[log\left(B_{RAP\%}\right) - log\left(B_{0\%}\right)\right] \tag{1.32}$$

where:

A and B – generic terms that represents 2S2P2D parameters and a_T shift factors;

x – the RAP binder percentage.

Similar rules were proposed in order to estimate the penetration by using a log-log rule shown in equation 1.33 according to SR EN 13108-1 [146], and Corté and Benedetto (2005) [11] and Al-Qadi et al. (2007) [147] proposed a linear rule (equation 1.34) in order to estimate the PG temperatures of binders.

$$log\left(pen_{blend}\right) = a \cdot log\left(pen_A\right) + b \cdot log\left(pen_B\right) \tag{1.33}$$

$$T_{blend} = a \cdot T_A + b \cdot T_B \tag{1.34}$$

where A and B are the two base binders, T_A and T_B are the PG temperatures of the base binders and a and b represent the relative mass concentrations of the base binders.

1.5.4 Prediction of mechanical behaviour of bituminous mixtures from properties of binders

Over the last decades many authors developed different models in order to predict the bituminous mixtures from the experimental values determined for the binders (Ugé et al. model [148], Hirsch model [149], Witczak model [150], SHStS transformation [129], [130]).

Further, in this section the SHStS transformation presented in Figure 1.23 will be described. With this model the LVE behaviour of a bituminous mixture can be predicted from the LVE behaviour of the corresponding binder. Also, the inverse procedure is valid, regardless of the aggregate skeleton.

This transformation is well described in Figure 1.23 where the Cole-Cole diagram of the normalized moduli (expressed by equation 1.35) of a binder is first shifted along the horizontal axis, then a homothetic transformation is performed, then it is shifted of characteristic time and finally a second shift along the horizontal axis was performed. This sequence Shift-Homothety-Shift in time-Shift represents the SHStS transformation [71], [151]–[153].

$$E^*_{norm} = \frac{E^* - E_{00}}{E_0 - E_{00}} \tag{1.35}$$

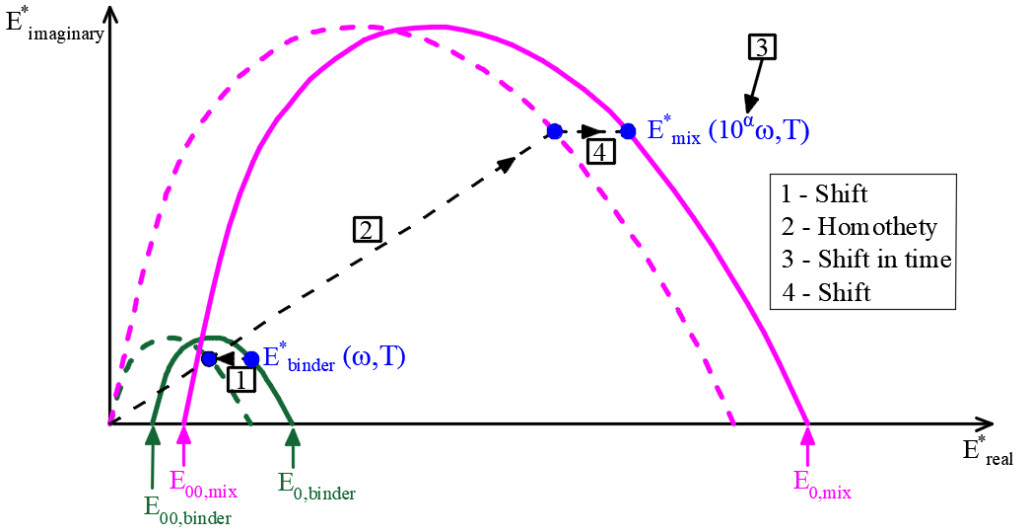

Figure 1.23. SHStS transformation scheme from binder properties to the bituminous mixture properties (source [71], [151]–[153]).

Therefore, the equation 1.36 allows to calculate the complex modulus of a bituminous mixture $\left(E^*_{mix}\right)$ at a temperature T when the complex modulus of the corresponding binder $\left(E^*_{binder}\right)$ is known (or vice-versa) at the same considered temperature. It must be mentioned that this relation is independent of any rheological model that was used.

$$E^*_{mix}(\omega,T) = E_{00,mix} + \left[E^*_{binder}\left(10^{\alpha}\omega,T\right) - E_{00,binder}\right]\frac{E_{0,mix} - E_{00,mix}}{E_{0,binder} - E_{00,binder}} \tag{1.36}$$

where:

ω – the loading frequency;

T – the chosen temperature;

$E_{00,mix}$ and $E_{00,binder}$ – are the static moduli of the bituminous mixture, respectively, the corresponding binder;

$E_{0,mix}$ and $E_{0,binder}$ – are the glassy moduli of the bituminous mixture, respectively, the corresponding binder;

α – parameter depending on the mix design and the binder aging that occurs during the mixing process, determined with equation 1.37.

$$\tau_{0,mix} = 10^{\alpha} \cdot \tau_{0,binder} \tag{1.37}$$

where:

$\tau_{0,mix}$ – value of τ_0 obtained for the bituminous mixture;

$\tau_{0,binder}$ – value of τ_0 obtained for the corresponding binder.

Moreover, when the Time Temperature Superposition Principle is verified, the equations 1.36 and 1.37 can be rewritten as follows:

$$E^*_{mix}\left(\omega a_T(T), T_{ref}\right) = E_{00,mix} + \left[E^*_{binder}\left(10^{\alpha} a_T(T), T_{ref}\right) - E_{00,binder}\right] \frac{E_{0,mix} - E_{00,mix}}{E_{0,binder} - E_{00,binder}} \tag{1.38}$$

$$\tau_{mix} = 10^{\alpha} \cdot \tau_{binder} \tag{1.39}$$

A simplified relation (relation 1.40) can be determined for a bituminous mixture taking into consideration that for pure fresh binders its glassy modulus is nil $\left(E_{00,binder} = 0\right)$.

$$E^*_{mix}\left(\omega a_T(T), T_{ref}\right) = E_{00,mix} + \left[E^*_{binder}\left(10^{\alpha} a_T(T), T_{ref}\right)\right] \frac{E_{0,mix} - E_{00,mix}}{E_{0,binder}} \tag{1.40}$$

1.6 Physical-mechanical characteristics of recycled bituminous mixtures

As already mentioned in Section 1.3.1.2, in Romania the specifications regarding the hot in plant recycling are described in the Romanian Standard DD-509-2003 [76].

According to this Standard, the recycled asphalt mixtures can be used only as base bituminous layer or as an intermediate layer between the base and the surface layers, only for roads classified as having the technical class between II to V. It must be mentioned that the recommendations regarding the types of bituminous mixtures, the maximum aggregate size of the recycled bituminous asphalt, the maximum binder content, the limits of the grading curve, the tests that must be performed in order to verify the characteristics of the recycled bituminous mixtures are not in accordance with the measures specified in the European Standards and with the Romanian Standards which were updated after 2003. Therefore, an update version of this Standard is needed.

Regarding the characteristics that must be determined for a bituminous mixture produced in plant with RAP material with or without rejuvenators, in DD-509-2003 only the Marshall characteristics (Marshall stability, flow and the ratio between them), the bulk density and the water absorption, should be determined. Also, for the virgin materials that are used in this process, their main characteristics must be

known, such as the grading curve, shape index, flakiness index of the virgin aggregates while for the binder is required only the penetration and the ring and ball temperature.

An important observation mentioned in this Standard is related to the use of rejuvenators in the production process of a recycled asphalt mixture: the rejuvenators can be used if the RAP binder presents a high ring and ball temperature (65…80°C) and the amount of RAP material is higher than 10% (11…30%) [76]. Therefore, this Standard is limited for recycled asphalt mixtures containing maximum 30% of RAP material.

According to studies that were performed over the last decades in order to increase the reuse of RAP materials in the production of new bituminous mixtures, it was highlighted that is important to verify the performances of the final product by performing some typical laboratory investigations [22], [25], [28], [30], [62]–[70].

The laboratory tests that are performed on bituminous materials can be classified in three categories according to Bonnot (1984): empirical tests, simulation tests and determination tests [154] and on the other side according to Di Benedetto (1990) the laboratory mechanical tests can be classified in two categories: homogenous and non-homogenous tests [155].

The most used laboratory tests on bituminous mixtures are the following:

- bulk density and water absorption, determination of void content-hydrostatic method (more details regarding the procedure used in this study are given in Section 3.5.1);
- Marshall test (more details regarding the procedure used in this study are given in Section 3.5.2);
- ITSR test (indirect tensile strength ratio);
- rutting test;
- complex modulus tests (more details regarding the procedure used in this study - two-point bending test on trapezoidal specimens - are given in Section 3.5.5);
- indirect tensile test, IT-CY test (more details regarding the procedure used in this study are given in Section 3.5.3);
- permanent deformation resistance-dynamic creep test wit confinement (more details regarding the procedure used in this study are given in Section 3.5.4);
- fatigue test;
- repeated compression test;
- low temperature cracking test, etc.

Also, it is very important to evaluate the characteristics of the corresponding binder blends of the bituminous mixtures produced with RAP material with or without rejuvenators. Many studies highlighted the possibility of predicting the behaviour of mixtures starting from the properties of their corresponding binder blends [33], [35]–[48].

The most used laboratory tests on binders are the following:

- conventional European tests:
  - penetration test (more details regarding the procedure used in this study are given in Section 2.3.1.1);
  - ring and ball test (more details regarding the procedure used in this study are given in Section 2.3.1.2);
  - Fraass test (more details regarding the procedure used in this study are given in Section 2.3.1.4);

- elongation test (more details regarding the procedure used in this study are given in Section 2.3.1.5);
- density test (more details regarding the procedure used in this study are given in Section 2.3.1.6);

– DSR test - complex shear modulus test (more details regarding the procedure used in this study are given in Section 2.3.2);
– BBR test (more details regarding the procedure used in this study are given in Section 2.3.3);
– DTT test;
– adhesivity between binder and aggregates test;
– adherence test;
– aging tests (RTFOT test, PAV test),etc.

1.7 Environmental impact assessment of roads

1.7.1 Sustainable road transport system

The term 'sustainable development' is more and more used in the road industry domain. Over the last decade many polices and strategies were developed all over the world regarding the sustainability in road transport in order to meet the needs of the present generations without compromising the ability of future generations to meet their own needs (sustainable development definition) [156].

It is well known that all the sustainable strategies are based on the balance of the three main pillars (Figure 1.24): environmental sustainability (ecological stability), economic sustainability (economic efficiency) and social sustainability (distributional/social equity). In the road design or in its construction phase ensuring a balance between the three pillars is not an easy task due to the fact that is very difficult to quantify what is truly 'sustainable'.

However, when a sustainable road transport strategy is proposed or pursued, the costs play a central role, where the costs are usually split in two main categories: internal costs (construction, maintenance of roads, transport equipment) and external costs (congestion, accidents, emissions, pollution, noise, etc.) [157].

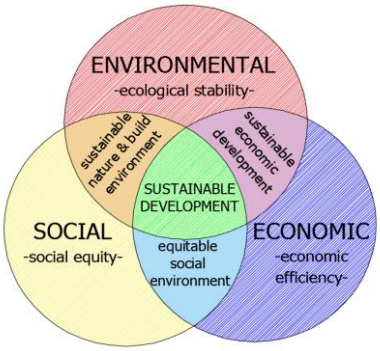

Figure 1.24. Sustainable development pillars [158].

Through the integration of Romania in the European Union (EU), Romania must implement and apply the norms regarding the sustainable development of the construction works. In the framework of the European Committee for Standardization

(CEN) there is a Technical Committee 350 (TC350), which provides the basis for the legislative framework on sustainable development in the construction sector.

The scope of TC 350 is to develop different instruments in order to measure or to parameterize the impact of the construction (or other process) on the environment, economy and its social impact. These instruments must take into consideration the production phase, the construction stage, use and disposal (recycling and disposal of waste) of a final product. The mirror technical committee dealing with this subject in Romania is CT 343, within ASRO.

The main document underlying the sustainable development strategies in Romania is: National Sustainable Development Strategy Romania 2013-2020-2030, where the strategic objectives for the short, medium and long run are the following [159]:

- 2013: to incorporate the strategies and practices of sustainable development of EU in all the programmes and public policies of Romania;
- 2020: to reach the current EU average values for the main indicators of sustainable development;
- 2030: to get significantly close to the EU average performance.

Moreover, the ECMT's members developed in 2000 some sustainable transport policies, the most important policies are related to the following [160]:

- improvement of the decision regarding the best practice in cost benefit analysis and environmental assessment;
- fictionization of costs and the financing of infrastructure;
- reduction of CO_2 emissions from road transport;
- improving road safety;
- promoting the use of low emission trucks;
- improving the competitiveness of road alternatives;
- in urban environments – to resolve the conflicts between transport and sustainable development.

It is well known that the construction of a road requires a lot of energy use (production of bituminous mixtures, the excavating process, the processes used for the maintenance, etc.). As an example, according to the European Asphalt Pavement Association (EAPA) in EU approximatively 240 million tonnes of Hot Mix Asphalt and Warm Mix Asphalt were produced in 2017 [161]. Considering that near 10% of the total mixtures produced in EU corresponds to WMA and approximatively 216 mil. tonnes of HMA. Therefore, as the HMA is produced at temperatures of 160 - 180°C and by considering an average of 275 MJ of energy use is used to produce one tonne of HMA, it can be highlighted that only the production of HMA in EU countries, in 2017, implied a use of approximatively 59 billion MJ. This information proves that the bituminous mixtures production is one of the most energy demanding industry that generates massive quantities of CO_2.

Therefore, to reduce the energy use in order to reach the term 'sustainable road', the following strategies must be taken into consideration:

- replace the HMA with WMA (produced at lower temperatures – conduce to lower energy consumption, reduce the paving costs, etc.);
- reuse the existing bituminous materials and recycle. Example of materials that can be used in recycling process: reclaimed asphalt pavement (RAP), recycled materials components (RMCs), recycled concrete aggregates (RCA), ground tire rubber (GTR), etc. In Figure 1.25 an example is given of how sustainability can be 'introduced' in the road industry.
- use of local materials;
- use of renewable materials and of bio-binders, etc.

Figure 1.25. Road pavement sustainability – recycling/reusing of waste asphalt materials.

By introducing these sustainability measures, some essential benefits for the road design and construction or maintenance will be reached, such as reduction of emissions, water usage, energy consumption, virgin materials, costs and lower impact on environment, etc. Therefore, these measures must be promoted into countries like Romania, where the reuse of materials is not so well known.

1.7.2 Life Cycle Assessment (LCA)

Life Cycle Assessment (LCA) is a technique, a tool that is used to assess the environmental aspects and the potential impact associated with a product, process, or activity by quantifying raw materials, energy and waste it releases into air, water and soil [162].

The principles, the framework together with the requirements and guidelines of an LCA are defined in the ISO 14040 series (Figure 1.26). According to ISO 14040-14044 standards, four main steps (goal and scope definition, life cycle inventory, live cycle impact assessment and life cycle interpretation) must be considered when an LCA is performed. Also, as an example Zheng et al. (2020) [163] highlighted the main life-cycle stages of a road pavement, as it can be observed in Figure 1.27.

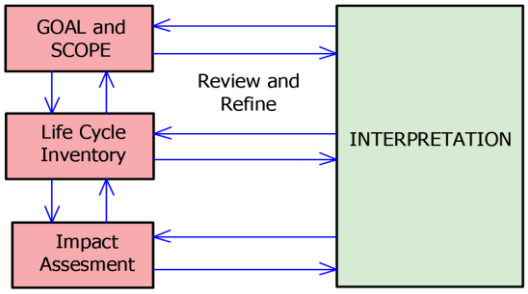

Figure 1.26. LCA framework – source ISO 14040-14044 standards.

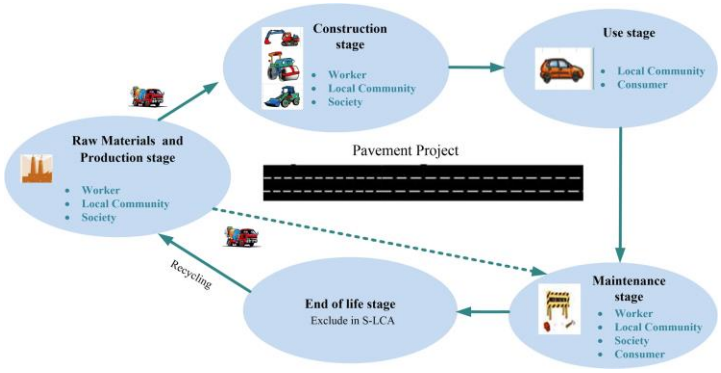

Figure 1.27. Life cycle stages of pavement according to Zheng et al. (2020) [163].

The goal of an LCA defines the aim of the study and the audience of the study and the scope of an LCA defines the unit and the system boundaries of the assessment.

Depending on how the system boundaries are chosen different assessments can be made: cradle to gate (from resource extraction to the factory gate), cradle to grave (from resource extraction to use phase and disposal phase) and cradle to cradle (from resource extraction to use phase and disposal phase=recycling process). Therefore, as an example in Figure 1.28 different system boundaries are shown for an LCA of road pavement.

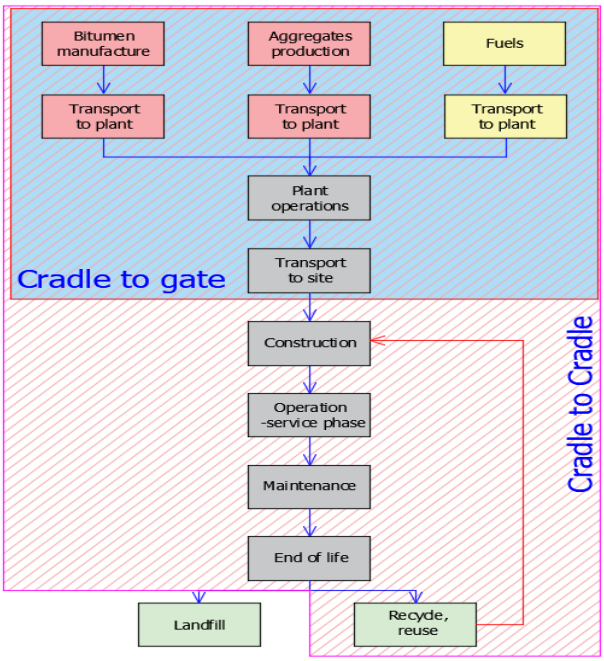

Figure 1.28. System boundaries.

The life cycle stages that can be used in an environmental impact assessment, according to European Standards EN 15804+A1:2013, EN 15804+A2:2019 [164] are the following:

- product stage: A1 (raw material extraction and processing), A2 (transport to manufacturer) and A3 (manufacturing);
- construction process stage: A4 (transport to the building site) and A5 (construction installation);
- use stage: B1 (use or application of the installed product), B2 (maintenance), B3 (repair), B4 (replacement), B5 (refurbishment), B6 (operational energy use) and B7 (operational water use);
- end of life stage: C1 (de-construction, demolition), C2 (transport to waste processing), C3 (waste processing for reuse, recovery or recycling) and C4 (disposal).

In the life cycle inventory for each material, product, activity its quantity (for materials), the use energy and the emissions associated to these processes must be evaluated to quantify relevant inputs and outputs of each activity (Figure 1.29). Preferably, these inputs and outputs (emissions) for each activity should be extracted from the Environmental Product Declaration (EPD) which are the declarations type III according to ISO 14025. Most software that are used to perform an LCA have access to international databases. Therefore, in this step it is very important to take into considerations the specifications indicated in ISO 14044 concerning the quality regarding the temporal, geographical, technological coverage, precision, and representativeness of data, etc.

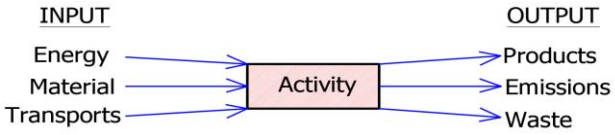

Figure 1.29. Input and output data for each activity.

The aim of the impact assessment is to evaluate the significance of potential environmental impacts by using the results of the life cycle inventory analysis. In this step, to each inventory data are associated environmental impacts. In order to obtain the environmental impact categories characterization factors are used (equation 1.41) [165].

$$Impact_{category} = \sum_{i} m_i \cdot characterization\ factor_{category,i} \tag{1.41}$$

where:

m_i – mass of the inventory flow i;

$characterization\ factor_{category,i}$ – characterization factor of inventory flow i for the impact category.

Usually a normalization is performed on the environmental indicators (impact category) and then a weighting is performed on the normalized indicators in order to assign numerical factors to their relative importance [165]. The most common environmental impact categories used in an LCA are described in the following section according to the EN 15804+A1:2013 and EN 15804+A2:2019 standards.

Regarding the interpretation of the obtained results, when an Environmental Impact Assessment (EIA) is made on roads domain, a comparison between a basic traditional/conventional solution and a new proposed solution is usually performed to highlight the advantages or the disadvantages of the proposed solution regarding its

potential environmental impact. Also, the obtained results can help on the identification of the impact category that has a massive impact on the environment.

The impact of roads construction on the environment is very difficult to control at a macro-component level (global or integrated approach). Therefore, many researchers suggested to perform this analysis at different levels, as follows:

- at the micro-component level (the case of materials analysis with the same destination);
- when a difference cannot be made at the level of the individual elements, the analysis must contain components (assemblies);
- at the macro-components level (analysis performed integrated for the entire construction process).

Frequently, when an LCA is performed, also a Life Cycle Cost (LCC) analysis is performed to evaluate the total cost performance of a product on the duration of a standardized period, including the acquisition, operation, maintenance, and disposal cost. Therefore, LCA and LCC can be used with a common purpose, in a global evaluation, where each process can become the input for the other process.

Both assessments, LCA and LCC can be used to identify the best solution that meet the target environmental impact for the lowest cost or to choose an alternative solution or to recalculate the environmental impact in costs.

1.7.3 Environmental impact categories

According to the EN 15804+A1:2013 the following parameters must be evaluated in order to describe the environmental impact categories:

- Global Warming Potential (GWP) represents the heat that was absorbed by any greenhouse gas (GHGs) in the atmosphere as a multiple of the heat that would be absorbed by the same mass of CO_2 [166]. Therefore, the global warming indicator can be determined by using the relation 1.42.

$$GW = \sum_i m_i \cdot GWP_i \tag{1.42}$$

where:

GW – global warming indicator, in kg CO_2 eq.;

m_i – mass of the released substance i (in kg);

GWP_i – global warming potential, in kg CO_2 eq.

- Ozone Depletion Potential of the stratospheric ozone layer (ODP) is a measure of the potential destructive effects of a substance compared to a reference substance trichlorofluoromethane (R11 also known as CFC-11) [167]. A similar relation to the 1.42 equation is used.

$$OP = \sum_i m_i \cdot ODP_i \tag{1.43}$$

where:

OP – ozone depletion indicator, in kg R11 eq.;

m_i – mass of the released substance i (in kg);

ODP_i – ozone depletion potential, in kg R11 eq.

➢ Acidification Potential of soil and water (AP) represents the acidification potential of any acid forming chemical relative to benchmark compound SO_2 (sulphate) as shown in relation 1.44 [168].

$$A = \sum_i m_i \cdot AP_i \tag{1.44}$$

where:

A – acidification indicator, in kg SO_2 eq. (kg of Sulphur dioxide equivalent);

m_i – mass of the released substance i (in kg);

AP_i – acidification potential, in in kg SO_2 eq.

➢ Eutrophication Potential (EP) represents a measure of the over-enrichment of water courses that can lead to damage of ecosystems (relation 1.45) [167].

$$E = \sum_i m_i \cdot EP_i \tag{1.45}$$

where:

E – eutrophication indicator, in kg Phosphate eq.;

m_i – mass of the released substance i (in kg);

EP_i – eutrophication potential, in kg Phosphate eq.

➢ Photochemical Ozone Creation Potential $(POCP)$ represents a measure of the relative ability of a substance to produce ozone in the presence of nitrogen oxides (NOx) and sunlight (relation 1.46) [165].

$$POC = \sum_i m_i \cdot POCP_i \tag{1.46}$$

where:

POC – photochemical ozone creation indicator, in kg Ethene eq.;

m_i – mass of the released substance i (in kg);

$POCP_i$ – photochemical ozone creation potential, in kg Ethene eq.

➢ Abiotic depletion potential for non-fossil resources $(ADPE)$ which includes all non-renewable, abiotic material resources represents the ratio between the quantity of resource extracted and the recoverable reserves of that resource, expressed in kg of the reference resource [165] in kg Sb eq.;

➢ Abiotic depletion potential for fossil resources $(ADPF)$ based on the energy content of the fossil fuel [169], in MJ, net caloric value.

According to the recent version of the EN 15804+A2:2019 which includes explicitly biogenic carbon uptake and re-emission, the following parameters should be evaluated in order to describe the environmental impacts:

➢ Climate Change, in kg CO_2 eq. (kg of Carbon dioxide equivalent);
  - Climate Change (fossil), in kg CO_2 eq.;
  - Climate Change (biogenic), in kg CO_2 eq.;
  - Climate Change (land use change), in kg CO_2 eq.;

- Ozone Depletion, in kg CFC-11 eq. (kg of ChloroFluoroCarbon-11-equivalents);
- Acidification terrestrial and freshwater, in Mole of H+ eq. (mole of Hydrogen ions equivalent);
- Eutrophication freshwater, in kg P eq. (kg of Phosphorus equivalent);
- Eutrophication marine, in kg N eq. (kg of Nitrogen equivalent);
- Eutrophication terrestrial, in Mole of N eq. (mole of Nitrogen equivalent);
- Photochemical ozone formation - human health, in kg NMVOC eq.;
- Resource use, mineral and metals, in kg Sb eq. (kg of antimony equivalent);
- Resource use, energy carriers, in MJ;
- Water scarcity, in m^3 world equiv.

The above-mentioned environmental indicators are calculated with similar relations as those used in case of the parameters specified in EN 15804+A1.

Moreover, other category of parameters related to the energy can be determined and used to describe the use of renewable and non-renewable material resources, primary energy, and water. Therefore, the following parameters can be investigated:

- use of renewable primary energy (PERE), in MJ;
- total use of renewable primary energy resources (PERT), in MJ;
- use of non-renewable primary energy (PENRE), in MJ;
- total use of non-renewable primary energy resources (PENRT), in MJ;
- use of net fresh water (FW), in MJ.

In order to perform a complete EIA, the parameters that describe the waste categories should be evaluated:

- Hazardous waste disposed (HWD), in kg;
- Non-hazardous waste disposed (NHWD), kg;
- Radioactive waste disposed (RWD), kg.

Depending on the software and available methods of investigation used in these analyses, some optional parameters can be obtained and analysed in order to highlight the potential impact of the analysed process on the human health. Therefore, the following common indicators can be analysed:

- Cancer human health effects (Inorganic), in CTUh (Comparative Toxic Unit for human which expresses the estimated increase in morbidity in the total human population per unit mass of a chemical emitted, cases per kilogramme);
- Cancer human health effects (Metal), in CTUh;
- Cancer human health effects (Organic), in CTUh;
- Ecotoxicity freshwater (Inorganic), in CTUh;
- Ecotoxicity freshwater (Metals), in CTUh;
- Ecotoxicity freshwater (Organic), in CTUh;
- Non-cancer human health effects (Inorganic), in CTUh;
- Non-cancer human health effects (Metals), in CTUh;
- Non-cancer human health effects (Organic), in CTUh;
- Respiratory inorganics, in Disease incidences;
- Ionising radiation - human health, kBq U235 eq. (equivalent uranium radiation measured in kg Becquerel);
- Ecotoxicity freshwater, in CTUh;
- Cancer human health effects, in CTUh;
- Non-cancer human health effects, in CTUh;
- Land Use, in Pt (point - yearly environmental load of one average inhabitant).

More details regarding the Environmental Impact Assessment are given in Chapter 4.

2. Performed tests on binders, analysis and modelling

2.1 Objectives

The main objective of this chapter is to evaluate the influence of the RAP extracted binder and the rejuvenator on the properties of different binder blends produced by mixing one type of fresh binder, a RAP extracted binder and a rejuvenator of vegetal origin. The effects of RAP binder and rejuvenator were analysed in terms of conventional properties of binders (penetration at 25°C, ring and ball temperature, Fraass temperature, density and elongation at 25°C), complex shear modulus at intermediate and high temperatures: 2S2P1D model (presented Section 1.5.3 equation 1.28) parameters, steady shear viscosity and high critical temperatures, and BBR test results at low temperatures (flexural creep stiffness, m-values and low critical temperatures).

Some possible relations were investigated between the conventional parameters *pen.* at 25°C, $T_{R\&B}$ and T_{Fraass} and steady shear viscosity at 25°C η_0 and the critical temperatures $T_{DSR\ high\ critical}$ *and* $T_{BBR\ low\ critical}$ (obtained in agreement with the overall Superpave framework but some minor differences in the analysis of test results were applied).

Two different approaches were proposed in order to estimate the values of several parameters for all binder blends from experimental values of the base constituents (fresh and RAP binders, rejuvenator and blends between RAP binder and rejuvenator). The precision of both estimation methods is analysed by plotting the correlation between the estimated and the experimental results. Also, a statistical evaluation is performed in order to analyse the validity of both estimation approaches.

Details regarding the experimental results obtained for all binders, the relations between these parameters, the obtained estimated results and the statistical evaluation are given in the following sections.

2.2 Materials and experimental plan

In this campaign, three base materials were used: one type of fresh binder (a straight-run 50/70 penetration grade bitumen), one type of RAP-extracted binder and a rejuvenator of vegetal origin.

The RAP binder was extracted from a well-known RAP material classified and described by performing the tests required by SR EN 13108-8 [51]. The RAP material used in this study is characterized in Chapter 3. Its binder content is 4.0% (measured through extraction and recovery). RAP binder was recovered from the RAP material using an extractor called 'asphaltanalysator' according to the European Standard SR EN 12697-1 [55]. Trichloroethylene was used as solvent. The solution of bitumen and trichloroethylene from prior extraction was distilled with a rotary evaporator, according to SR EN 12697-3 [53].

A mixture of vegetal oils (a commercial product) was used as rejuvenator (Rej) in different dosages (0%, 5%, 10% and 15% by mass of RAP binder).

The experimental plan includes a total of 17 binders (Table 2.1): 12 blends of the 50/70 fresh binder with the RAP-extracted binder with and without rejuvenator, three blends of RAP binder with the rejuvenator and pure fresh and RAP binders.

Blending proportions between RAP binder, fresh binder and rejuvenator were calculated in order to reproduce the ratios between these components within the bituminous mixtures studied in Chapter 3. These mixtures were produced with a 5.6% total binder content (rejuvenator not considered as part of it) containing 25%, 50%, and 75% RAP material and 0.00%, 0.20%, 0.40% and 0.60% of rejuvenator by mass of RAP material (corresponding to 0%, 5%, 10% and 15% of rejuvenator by mass of the RAP binder). Three other blends between RAP binder and rejuvenator were considered (RAP + 5% Rej, RAP + 10% Rej, RAP + 15% Rej). These additional blends were produced and tested considering that they were used as 'base materials' in the estimation approaches presented in following sections.

The actual blending percentages of the different components for all blends are reported in Table 2.1.

For simplicity, binder blends were named according to the penetration grade of the fresh bitumen, the percentage of RAP material used for the production of the corresponding bituminous mixture and the dosage of the rejuvenator (Rej) by the mass of RAP bitumen (e.g.: 50/70 + 75% RAP + 5% Rej).

Table 2.1. Proportion of different components in tested binders: pure bitumen (50/70), RAP-extracted binder (RAP) and Rejuvenator (Rej).

Binders	% by weight		
	50/70	RAP	Rej
50/70	100.00	0.00	0.00
RAP	0.00	100.00	0.00
RAP + 5% Rej	0.00	95.24	4.76
RAP + 10% Rej	0.00	90.91	9.09
RAP + 15% Rej	0.00	86.96	13.04
50/70 + 25% RAP	82.14	17.86	0.00
50/70 + 25% RAP + 5% Rej	81.42	17.70	0.88
50/70 + 25% RAP + 10% Rej	80.70	17.54	1.76
50/70 + 25% RAP + 15% Rej	80.00	17.39	2.61
50/70 + 50% RAP	64.29	35.71	0.00
50/70 + 50% RAP + 5% Rej	63.16	35.09	1.75
50/70 + 50% RAP + 10% Rej	62.07	34.48	3.45
50/70 + 50% RAP + 15% Rej	61.02	33.90	5.08
50/70 + 75% RAP	46.43	53.57	0.00
50/70 + 75% RAP + 5% Rej	45.22	52.17	2.61
50/70 + 75% RAP + 10% Rej	44.07	50.85	5.08
50/70 + 75% RAP + 15% Rej	42.97	49.59	7.44

The procedures used to produce the studied binder blends were chosen in order to reproduce in laboratory the actual production process of bituminous mixtures containing RAP material and rejuvenator.

Fresh and RAP binders were heated to 160°C. The rejuvenator was not heated before blending. The rejuvenator was mixed with the fresh binder (manually mixed

for 5 minutes) in order to reproduce the real industrial process of the production of bituminous mixtures in which the rejuvenator is added to the fresh binder tank when all the components (fresh aggregates, RAP material and fresh binder) are heated before mixing. This preliminary blend was then heated for 20 min at 160°C. RAP binder was added, and this final blend was manually mixed for 5 minutes in order to produce a homogenous blend. The 160°C temperature was chosen with respect to the Romanian technical specifications for the production on bituminous mixtures. Figure 2.1 shows the scheme of the binder blends production.

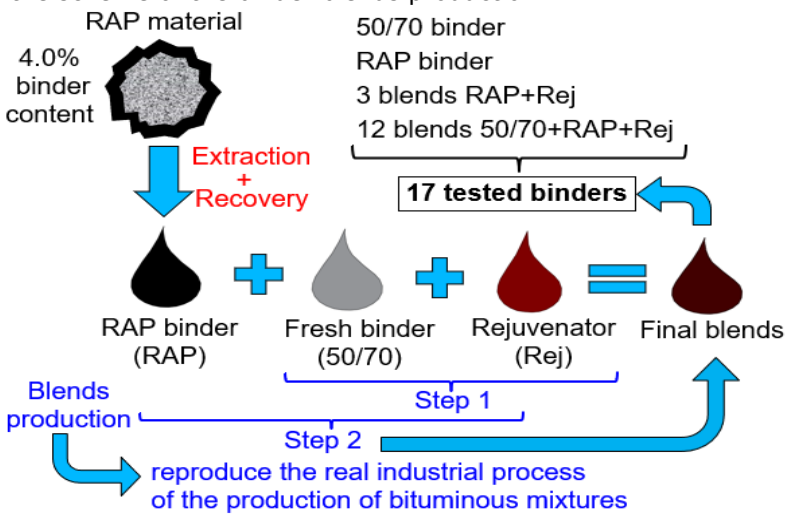

Figure 2.1. Scheme of the production process of binder blends.

Regarding the experimental campaign (shown in Figure 2.2), European conventional tests (penetration at 25°C, softening point, Fraass breaking point, ductility at 25°C, density at 25°C), DSR complex shear modulus and BBR tests were performed for all binders. All test procedures are described in Section 2.3. All tests were performed in the Road Laboratory from University Politehnica Timisoara, Romania.

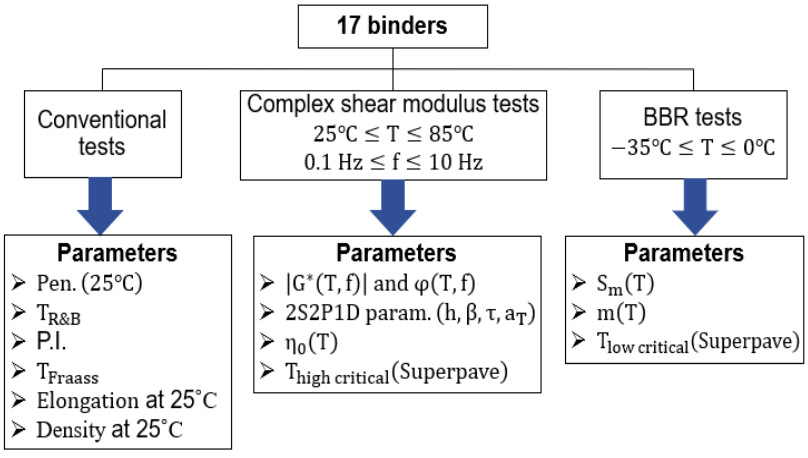

Figure 2.2. Experimental campaign – Binder blends.

European conventional tests were performed in order to determine: penetration at 25°C (*pen.* , SR EN 1426 [17]), softening point (ring and ball temperature, $T_{R\&B}$, SR EN 1427 [56]), penetration index (PI , SR EN 12591 [18]), Fraass breaking point (Fraass breaking point temperature, T_{Fraass}, SR EN 12593 [170]), ductility at 25°C (*elongation* , SR 61 [171]) and density at 25°C (SR EN 15326+A1 [172]). Test procedures are shown in Sections 2.3.1. The results obtained for these conventional parameters are shown in Section 2.5.

Complex shear modulus tests were performed at intermediate and high temperatures (from 25°C to 85°C with a 10°C increment) and at a frequency ranging from 0.1 Hz to 10 Hz (more details given in Section 2.3.2). The linear viscoelastic behaviour of several blends was characterized in terms of complex shear modulus $\left(G^*(T,f)\right)$ by means of Dynamic Shear Rheometer (DSR) tests. Experimental results were analysed by using the 2S2P1D model (presented in Section 1.5.3 equation 1.28) and a specific approach was proposed in order to highlight the effect of the RAP binder and the rejuvenator on the 2S2P1D parameters. The obtained results are presented in Section 2.6.

Another parameter analysed is the steady shear viscosity at different temperatures $\eta_0(T)$ of all binders from complex modulus test results (details given in Section 2.7). Also, high critical temperatures $\left(T_{DSR\ high\ critical}\right)$ were determined when $\left|G^*\right|/\sin\varphi = 1.0\ KPa$, when $\omega = 10\ rad/s$. Results are shown in Section 2.10.1.

Tests at low temperatures (BBR tests) were performed in order to determine the flexural creep stiffness $S(t)$ and m-values $m(t)$ for all binders. Tendencies of these two parameters were analysed as a function of RAP binder and rejuvenator contents and BBR low critical temperatures $\left(T_{BBR\ low\ critical}\right)$ were determined (details given in Section 2.9 and Section 2.10.2).

2.3 Experimental procedures

2.3.1 European conventional tests

2.3.1.1 Penetration at 25°C

Penetration is considered to be the conventional test used to determine the consistency of a bitumen as the penetration depth of a normalized needle (needle load is 100 g) who penetrates a bitumen sample at a set temperature (25°C) for a charging time of 5 seconds (Figure 2.3a) [17].

All penetration tests were performed by using an automated penetrometer (Figure 2.3b), by following the prescriptions from SR EN 1426:2015 [17].

For each binder, three samples were tested (three measurements/sample). The reported value of penetration for a binder is considered the average between the three *pen.* values/sample expressed in tenths of mm rounded to the nearest integer.

If the measurements differ from the average value by more/less than 15% the test must be repeated.

A total of 51 penetration tests were performed in this campaign.

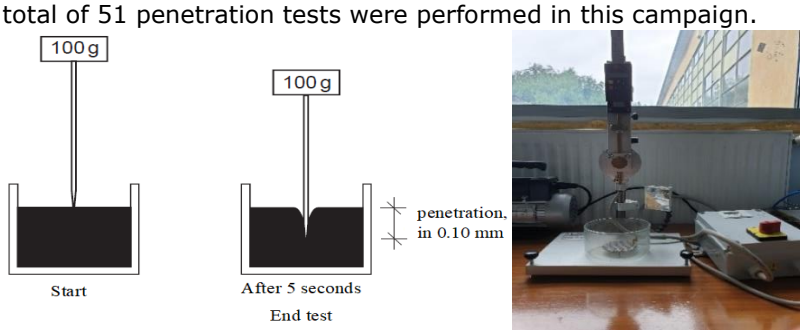

(a) (b)

Figure 2.3. (a) Penetration test principle; (b) Automated penetrometer Matest@ - Road Laboratory, University Politehnica Timisoara.

2.3.1.2 Softening point (ring and ball temperature)

By performing this classical test, the 'conventional temperature', ring and ball temperature $(T_{R\&B})$ of a binder is obtained.

Two bitumen samples placed into metal rings, under certain conditions, are placed on a metal stand, in a Berzelius recipient and heated in a control mode (5°C/minute) in distillate water. Two metal balls (normalized diameter and mass) are placed over the two bitumen samples. The test starts from the temperature of 5°C. The temperature at which the ball pass through the bitumen sample reaching the lower plate (placed at 25 mm under the rings) is reported as the softening point temperature of a binder (Figure 2.4a) [56]. The average value between two measurements/binder expressed to the nearest 0.2°C is reported as $T_{R\&B}$. If the difference between the two measurements/binder is higher than 2°C the test must be repeated.

All tests were performed by using an automated ring and ball test equipment (Figure 2.4b), following the prescriptions from SR EN 1427:2015 [56].

A total of 17 ring and ball tests were performed in this campaign.

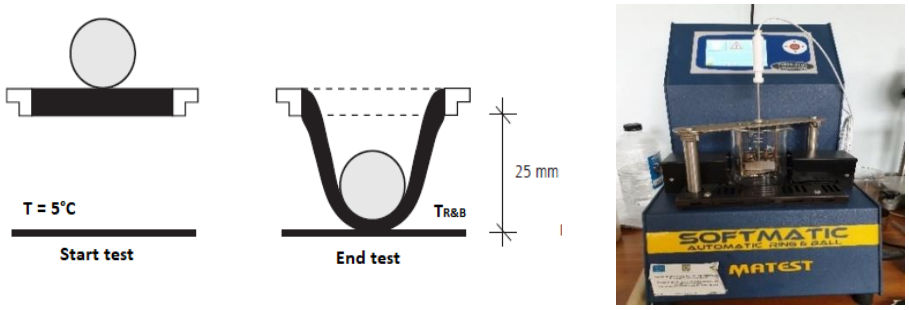

(a) (b)

Figure 2.4. (a) Ring and ball test principle; (b) Automated ring and ball test device Matest@ - Road Laboratory, University Politehnica Timisoara.

2.3.1.3 Penetration Index

Based on the experimental measurements ($pen.$ at 25°C and $T_{R\&B}$) performed for all binders in this campaign, the Penetration Index (PI) was calculated according to the equation 2.1 specified in SR EN 12591:2009 [18].

$$PI = \frac{20 \times T_{R\&B} + 500 \times log\ pen. - 1952}{T_{R\&B} - 50 \times log\ pen. + 120} \quad (2.1)$$

Usually, PI values are used as an indicator of temperature susceptibility of binders.

2.3.1.4 Fraass breaking point temperature

Fraass test consists in determining the temperature at which a bitumen film of 0.50 mm thickness spread on a metal plaque (20 x 41 x 0.15 mm) is cooled and flexed under specific conditions, specified in SR EN 12593:2015 [170], will become first brittle, indicated by the appearance of cracks (Figure 2.5a).

The bending process of the metal plaque is made every 1°C during a uniform decrease of temperature of 1°C/minute. When the first crack appears at the surface of the bitumen layer the test will end by recording the temperature (T_{Fraass}).

All tests were performed by using a classic Fraass apparatus (Figure 2.5b), by following the prescriptions from SR EN 12593:2015 [170].

For each binder, two samples were tested. The reported value of Fraass temperature for a binder was considered the average between the two measurements, rounded to the nearest integer. If the difference between the measurements is higher than 1°C the test must be repeated.

A total of 34 Fraass breaking point tests were performed in this campaign.

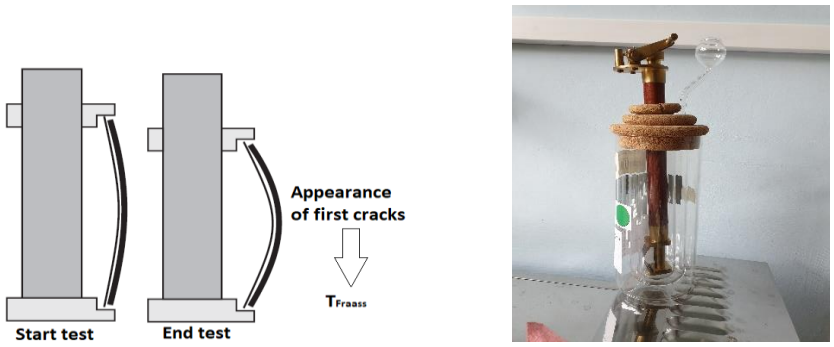

(a) (b)

Figure 2.5. (a) Fraass test principle; (b) Classical Fraass device Matest@ - Road Laboratory, University Politehnica Timisoara.

2.3.1.5 Ductility at 25°C

Ductility at 25°C was determined by performing elongation test, as prescribed in the Romanian Standard SR 61 [171], bitumen samples, prepared under certain conditions, were pulled apart at a constant speed of 50 mm/min in a water bath at a constant temperature of 25°C until rupture (Figure 2.6a). The elongation at rupture (in cm) was used as an indication of ductility.

All tests were performed by using an automated ductilimeter apparatus (Figure 2.6b), by following the prescriptions from SR 61 [171].

For each binder, three samples were tested at the same time. The reported value of elongation for a binder was considered the average between the three measurements, rounded to the nearest integer.

A total of 51 elongation tests were performed in this campaign.

(a) (b)

Figure 2.6. (a) Elongation test principle; (b) Ductilimeter Matest® - Road Laboratory, University Politehnica Timisoara.

2.3.1.6 Density at 25°C

Density at 25°C of all binders was determined by using the capillary stoppered pycnometer method described in SR EN 15326+A1:2009 [172] and Figure 2.7a.

Values of density were obtained as a relation between the weights of the pycnometer as is described in equation 2.2 from SR EN 15326+A1:2009 [172], at a temperature of 25°C.

$$Density = \frac{m_c - m_a}{(m_b - m_a) - (m_d - m_c)} \quad (2.2)$$

where m_a is the weight of empty pycnometer, m_b is the weight of the pycnometer filled with distilled water (measured after conditioning at 25°C for 45 minutes in a water bath), m_c is the weight of the pycnometer half filled with bitumen (measured after conditioning at 25°C for 45 minutes in a water bath) and m_d is the weight of the pycnometer half filled with bitumen + distilled water (measured after conditioning at 25°C for 45 minutes in a water bath).

All tests were performed by using a capillary stoppered pycnometer equipment (Figure 2.7b), following the prescriptions from SR EN 15326+A1:2009 [172]. For each binder, two samples were tested.

A total of 34 density tests were performed in this campaign.

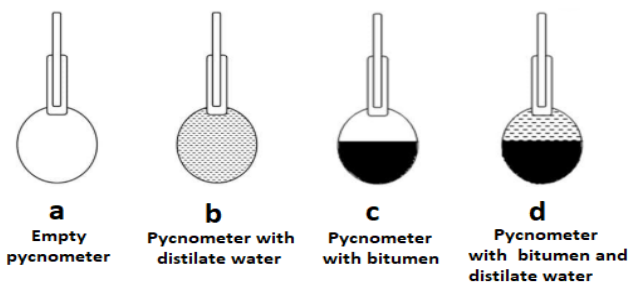

(a)

(b)

Figure 2.7. (a) Density measurement principle; (b) Capillary stoppered pycnometer - Road Laboratory, University Politehnica Timisoara.

2.3.2 Complex shear modulus test

Complex shear modulus tests were performed on all binders. A DSR apparatus with a 25 mm diameter plate-plate configuration with a 1 mm gap was used at temperatures ranging from 25°C to 85°C and at frequencies ranging from 0.1 Hz to 10 Hz (Figure 2.8). Main characteristics of the rheometer are shown in Table 2.2.

Tests were performed at 5% targeted shear strain amplitude (γ), by imposing a sinusoidal shear strain signal and measuring the corresponding shear stress. However, the torque limit of the instrument was reached for strain amplitudes lower than the 5% targeted value during some tests at the lowest temperatures and highest frequencies. Therefore, these tests were performed at strain amplitudes lower than 5%. It must be mentioned that at temperatures higher than 45°C the tests were carried out for sure in the LVE domain. Since the LVE limit was not explicitly studied in this work, maybe at low temperature (< 35°C) the tests were performed at the limit of the LVE domain. A wider temperature and frequency ranges should be considered in a future work and tests should be performed by using both 25 mm / 8 mm plate-plate configurations. Also, a study of the linearity should be performed.

Regarding the preparation of samples, the blends (prepared as described in Section 2.2) were poured into a silicon mould and maintained at ambient temperature for 4 hours until thermal equilibrium was reached. Then, the samples were placed in the DSR test machine where the plates were already preheated at 45°C. The gap between two plates was initially set to 1.10 mm and trimming was performed before setting the final gap to 1 mm.

Table 2.2. Main characteristics of DSR apparatus used in this campaign.

Characteristics	Anton Paar MCR SmartPave 102
Plate diameter	25 mm
Temperature control	Peltier cell
Max. temperature range	-160°C … 1000°C
Angular frequency range	10^{-7} rad/s … 628 rad/s
Normal force range	0.01N … 50N
Normal force resolution	1 mN
Torque range	7.50 nNm … 200 nNm

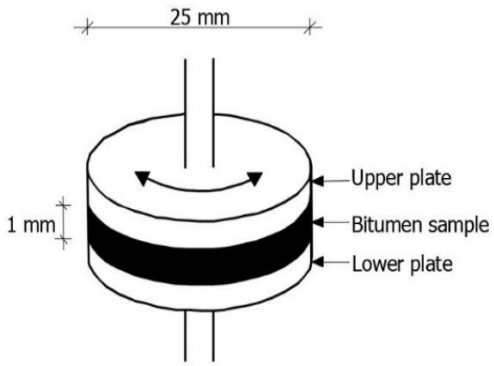

(a)

(b)

Figure 2.8. (a) Scheme of a DSR test and sample size; (b) DSR Anton Paar@ MCR SmartPave 102 device - Road Laboratory, University Politehnica Timisoara.

It must be specified that in this study only the 25 mm configuration as this was the only available configuration in the Road Laboratory – University Politehnica Timisoara.

The norm of complex shear modulus $|G^*|$ and its phase angle φ were calculated from DSR test results. Complex shear modulus G^* is a measure of the total resistance to deformation of a linear viscoelastic material when subjected to cyclic sinusoidal shear. Phase angle φ is an indicator of the relative amount of recoverable and non-recoverable deformation [43].

In this work, for the phase angle the symbol φ was used instead of δ which is usually used for the phase angle obtained from DSR measurements due to the fact that the symbol δ was used for a 2S2P1D parameter.

Complex shear modulus tests were performed at seven temperatures and different frequencies from 0.1 Hz to 10 Hz, as shown in Table 2.3. A total of 17 DSR complex shear modulus tests were carried out in this campaign.

Table 2.3. Temperatures and frequencies used for DSR complex shear modulus tests on all binders from this campaign.

Temperature (°C)	Frequency (Hz)
	0.100
25	0.167
35	0.278
45	0.464
55	0.774
65	1.290
75	2.150
85	3.590
	5.990
	10

2.3.3 Bending Beam Rheometer (BBR) test

BBR test is designed to characterise the low-temperature behaviour of binders. BBR tests were performed in order to determine the flexural creep stiffness, $S(t)$, and the m-value, $m(t)$, (absolute value of the slope of the curve of $log\,S(t)$ vs. $log\,m(t)$) for all the binder blends at different temperatures. The test consists in a three-point bending creep test in which a constant load (0.980 N) is applied to the mid-point of a bitumen beam (125 x 12.5 x 6.4 mm) for a specific loading time (240s) and the evolution of the mid-point deflection is observed as a function of time according to the standard EN 14771:2012. Figure 2.9 shows the scheme of the BBR test (Figure 2.9a) and the equipment used from the Road Laboratory – University Politehnica Timisoara (Figure 2.9b). Main characteristics of the BBR rheometer are shown in Table 2.4. The calibration of the measurement system was carried out before starting the tests provided in this campaign.

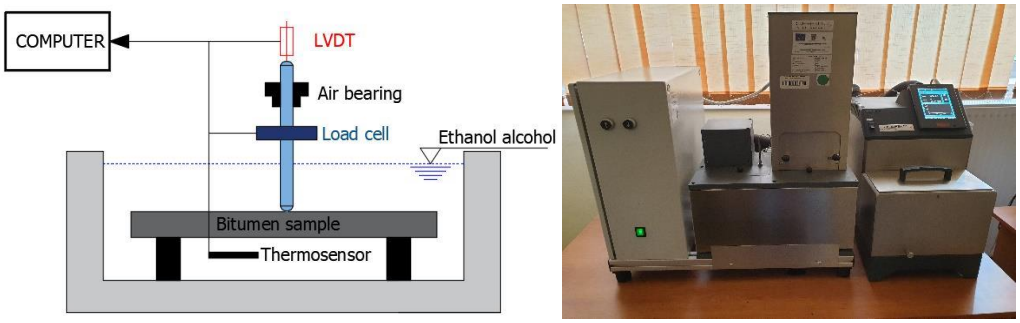

(a) (b)

Figure 2.9. (a) Scheme of a BBR test; (b) BBR apparatus Coesfeld MaterialTest@ and Huber@ thermostat - Road Laboratory, University Politehnica Timisoara.

Table 2.4. Main characteristics of BBR apparatus used in this campaign.

Technical data	Bending Beam Rheometer
Temperature range – Huber@	-45°C … +200°C
Heating power	2kW
Travel	up to 10 mm ± 0.001 mm
Force	up to 2000 mN ± 0.1 mN
Fluid used for cooling	ethanol
Control	through PC, fully automatic

Regarding the preparation of samples, the blends (prepared as described in Section 2.2) were poured into an aluminium mould (protected with plastic strips covering the inside faces). O-rings were used in order to hold the hole assemble.

The filled mould was cooled in the ambient temperature for 60 minutes and trimming was performed. Prior de-moulding, the mould containing the bitumen specimen was cooled for 5 min in a liquid bath at the chosen test temperature.

After de-moulding, the bitumen specimen was placed in the testing bath in order to conditionate it for 60 minutes at the chosen test temperature. The preparation process of beam samples is shown in Figure 2.10.

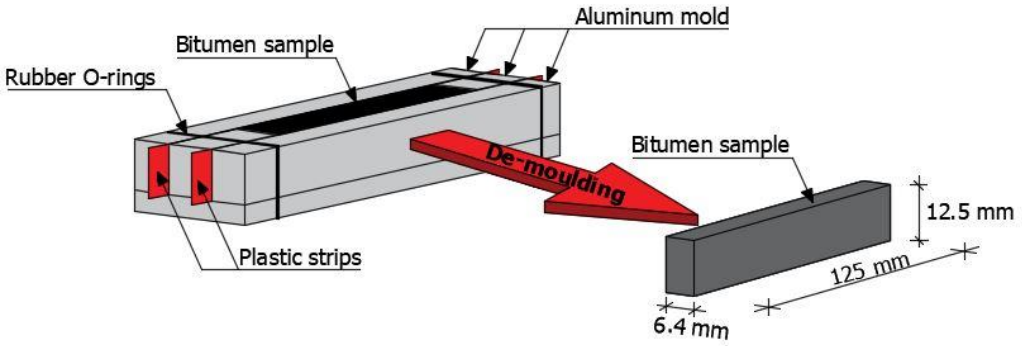

Figure 2.10. BBR bitumen sample preparation: mould and sample size.

BBR test was performed for all binders from this campaign following the method described in SR EN 14771:2012 [173]. Two samples/binder were tested at each test temperature reported in Table 2.5.

Values of flexural creep stiffness $S(t)$ and m-values $m(t)$ at a specific loading time, were determined by using equations 2.3 and 2.4, according to SR EN 14771:2012 [173].

$$S(t) = \frac{PL^3}{4bh^3\delta(t)} \tag{2.3}$$

$$m(t) = \frac{\left|d\log S(t)\right|}{\left|d\log(t)\right|} \tag{2.4}$$

where: $S(t)$ is the flexural creep stiffness at time t, MPa; $P = 0.980\ N$ is the measured test load, N; $L = 125\ mm$ is the span length, mm; $b = 12.5\ mm$ is the width of the test specimen, mm; $h = 6.4\ mm$ is the thickness of the test specimen, mm; $\delta(t)$ is the measured deflection of the test specimen at time t, mm; t is the time of loading, s.

All binder blends were tested at the same temperatures (from 0°C to -35°C, every 5°C). However, some binders were too flexible (the measured deflection was higher than 4 mm), or too stiff (the measured deflection was lower than 0.08 mm / the bitumen sample broke during the test) during the BBR test at the highest and lowest temperatures. Therefore, these test results were neglected. Table 2.5 shows the test temperatures for each type of binder.

A total of 272 BBR tests were performed in this campaign (17 binders x 2 samples/binder x 8 test temperatures).

Table 2.5. Temperatures used for BBR tests on all binders from this campaign.

Binders	Temperature (°C)
RAP	0; -5; -10; -15
RAP + 5% Rej	0; -5; -10; -15; -20
RAP + 10% Rej 50/70 50/70 + 25% RAP + 5% Rej 50/70 + 25% RAP + 10% Rej 50/70 + 25% RAP + 15% Rej 50/70 + 50% RAP + 5% Rej 50/70 + 50% RAP + 10% Rej 50/70 + 50% RAP + 15% Rej 50/70 + 75% RAP + 5% Rej 50/70 + 75% RAP + 10% Rej	 -10 -15 -20 -25 -30 -35
50/70 + 25% RAP 50/70 + 50% RAP 50/70 + 75% RAP	-5; -10; -15; -20; -25
RAP + 15% Rej 50/70 + 75% RAP + 15% Rej	-15; -20; -25; -30; -35

2.4 Definition of the two proposed estimation methods

The values of conventional parameters $(pen.\ at\ 25°C, T_{R\&B}, T_{Fraass})$, steady shear viscosity at different temperatures $\eta_0(T)$, 2S2P1D parameters, norm of complex shear modulus, $|G^*(T,f)|$ and critical temperatures $(T_{DSR\ high\ critical}\ and\ T_{BBR\ low\ critical})$ of the blends of pure fresh binder, RAP binder and rejuvenator were estimated using two different approaches and compared with experimental values.

Both estimation methods are based on the same hypothesis which supposes that the values of different parameters of a binder blend produced by mixing two or more base materials, two binders or two binders and a rejuvenator, can be estimated from experimental values obtained for the base constituents following a linear or a logarithmic relationship (depending on the parameter) as a function of their concentrations. More details are given in the following sections. Due to the fact that the specific parameters for binders cannot be physically evaluated for the rejuvenator some equivalent values must be used in the calculation (more details are given in Section 2.4.2).

The analysis of the correlations between the experimental and estimated results for all the blends is presented in the following sections.

2.4.1 First estimation method

The first approach which is classical two-way blending rule, supposes that values for fresh binder and values for blends of RAP and rejuvenator (RAP + Rej) are

known from experimental tests. The blending rule expressed in equations 2.5, 2.6 and Figure 2.11 is considered.

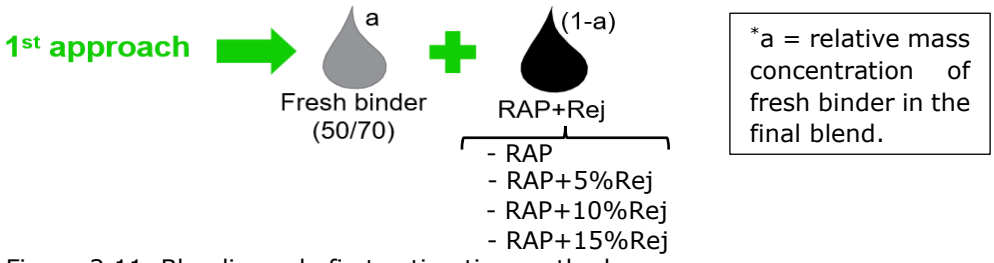

Figure 2.11. Blending rule first estimation method.

In the equations, estimated parameters of the 12 blends, $X_{blend\ est.\,1}$ *and* $Y_{blend\ est.\,1}$ for equations 2.5 and 2.6, respectively, are calculated from experimental values obtained for pure fresh binder, $X_{50/70}$ *and* $Y_{50/70}$ for equations 2.5 and 2.6, respectively, and for blends of RAP binder and rejuvenator, $X_{RAP+Rej}$ *and* $Y_{RAP+Rej}$ for equations 2.5 and 2.6, respectively, as a function of the relative mass concentration of fresh binder in the final blend, a.

$$X_{blend\ est.\,1} = a \cdot X_{50/70} + (1-a) \cdot X_{RAP+Rej} \quad (2.5)$$

$$\log Y_{blend\ est.\,1} = a \cdot \log Y_{50/70} + (1-a) \cdot \log Y_{RAP+Rej} \quad (2.6)$$

Output (estimated parameters for 12 blends)

Input (experimental parameters for 5 blends)

where:

$X = T_{R\&B}$, T_{Fraass}, *2S2P1D parameter* (h), $T_{DSR\ high\ critical}$ *and* $T_{BBR\ low\ critical}$;

$Y = pen.$, $\eta_0(T)$, $\left|G^*(T,f)\right|$, *2S2P1D parameters* (β,τ), a_T;

$a =$ relative mass concentration of fresh binder in the final blend.

Equation 2.5 was used to estimate ring and ball temperature $(T_{R\&B})$, Fraass temperature (T_{Fraass}), 2S2P1D parameter (h) and critical temperatures $(T_{DSR\ high\ critical}$ *and* $T_{BBR\ low\ critical})$ while equation 2.6 (which is identical to equation 2.5 in log-log axes) was used in order to estimate penetration $(pen.)$, steady shear viscosity (η_0) at different temperatures, norm of complex shear modulus $\left|G^*(T,f)\right|$, 2S2P1D parameters (β,τ) and a_T temperature shift factors. Equation 2.6 is usually referred to as log-log rule [173]. Mangiafico et al. (2014) [174] proposed a similar estimation method for the 2S2P1D constants and temperature shift factors for binder blends produced by mixing one type of RAP binder and different types of fresh binders. As values for fresh and RAP + Rej binders are known, only values of 12 produced blends have to be determined.

2.4.2 Second estimation method

The second approach requires only values of concentration and parameters of the three base components (fresh binder, RAP and rejuvenator). The blending rule expressed in equations 2.7, 2.8 and Figure 2.12 is considered.

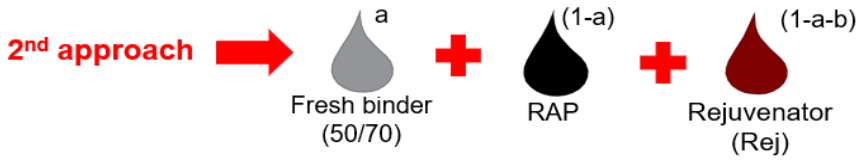

*a = relative mass concentration of fresh binder in the final blend.
*b = relative mass concentration of RAP binder in the final blend.

Figure 2.12. Blending rule second estimation method.

Equation 2.7 was used to estimate values of $T_{R\&B}$, T_{Fraass}, 2S2P1D parameter (h), $T_{DSR\ high\ critical}$ and $T_{BBR\ low\ critical}$ while equation 2.8 was used for values of *pen.*, $\eta_0(T)$ at different temperatures, norm of complex shear modulus $\left|G^*(T,f)\right|$, 2S2P1D parameters (β,τ) and a_T shift factors for the 15 blends.

Estimated values of the blends, $X_{blend\ est.\ 2}$ and $Y_{blend\ est.\ 2}$ for equations 2.7 and 2.8, respectively, were calculated from experimental values obtained for pure fresh binder ($X_{50/70}$ and $Y_{50/70}$ for equations 2.7 and 2.8, respectively) and RAP binder, X_{RAP} and Y_{RAP} for equations 2.7 and 2.8, respectively, and from equivalent values for the rejuvenator X_{Rej} and Y_{Rej} for equations 2.7 and 2.8, respectively, that are reported in following sections. In the equations, *a, b and c* are the relative mass concentrations of fresh binder, RAP binder and rejuvenator, respectively $(a+b+c=1)$.

$$X_{blend\ est.\ 2} = a \cdot X_{50/70} + b \cdot X_{RAP} + c \cdot X_{Rej} \quad (2.7)$$

$$\log Y_{blend\ est.\ 2} = a \cdot \log Y_{50/70} + b \cdot \log Y_{RAP} + c \cdot \log Y_{Rej} \quad (2.8)$$

Output (estimated parameters for 15 blends)

Input (experimental parameters for 2 binders)

Input Equivalent values obtained by minimizing the distance between exp. and est. results

where:

$X = T_{R\&B}, T_{Fraass}, 2S2P1D\ parameter\ (h), T_{DSR\ high\ critical}$ and $T_{BBR\ low\ critical}$;

$Y = pen., \eta_0(T), \left|G^*(T,f)\right|, 2S2P1D\ parameters\ (\beta,\tau), a_T$;

a, b, c = relative mass concentration of fresh binder, RAP binder and rejuvenator in the final blend (values in Table 2.1).

In the equations 2.7 and 2.8, a and c could be calculated as functions of the relative mass concentration of RAP binder in the final blend, b, and the dosage of the rejuvenator by the mass of RAP binder, $r(0\%, 5\%, 10\% \text{ or } 15\%)$. Equations 2.7 and 2.8 could then be rewritten as equations 2.9 and 2.10.

$$X_{blend\ est.\ 2} = \left[1 - b \cdot (1 + r)\right] \cdot X_{50/70} + b \cdot X_{RAP} + b \cdot r \cdot X_{Rej} \quad (2.9)$$

$$log\, Y_{blend\ est.\ 2} = \left[1 - b \cdot (1 + r)\right] \cdot log\, Y_{50/70} + b \cdot log\, Y_{RAP} + b \cdot r \cdot log\, Y_{Rej} \quad (2.10)$$

Equivalent values for the rejuvenator $(X_{Rej} \text{ and } Y_{Rej})$ were obtained by minimizing the distance (D) between experimental and calculated values (equations 2.9 and 2.10). The distance D is the sum of the square of the difference between the experimental and calculated values for the 15 blends: $D = \sum_{1}^{15} (Exp. - Est.)^2$. More details are given in the following sections.

It should be highlighted that these equivalent values were used only in the context of the blending law, therefore they are not intended to reflect actual properties of the rejuvenator.

2.5 Analysis of European conventional parameters

2.5.1 Experimental results

Conventional tests were performed on all binders in order to determine penetration at 25°C (*pen.*, SR EN 1426:2015 [17]), softening point ($T_{R\&B}$, SR EN 1427:2015 [56]), ductility at 25°C (*elongation*, SR 61 [171]), Fraass breaking point (T_{Fraass}, SR EN 12593:2015 [170]), and density at 25°C (SR EN 15326+A1:2009 [172]). The Penetration Index (PI) was also calculated according to SR EN 12591:2009 [18]. The results are reported in Table 2.6.

The experimental results, analyses and the estimation of these conventional parameters, have been presented in two publications Forton et al., 2019, 2020 [128], [175]. With respect to these articles, only slight modifications have been made.

Penetration (in logarithmic scale) and softening point of all binders are plotted as functions of RAP binder content in Figure 2.13a and 2.13b.

The results obtained for the RAP binder are coherent with the expected results for an aged binder [176].

As expected, results in Table 2.6 and Figure 2.13a and 2.13b show a decrease in penetration and an increase in softening point as RAP binder content increases for the blends produced without rejuvenator. Increasing penetration values and decreasing ring and ball temperatures were observed when increasing the dosage of the rejuvenator in blends.

Fraass breaking point temperature and PI of all binders are plotted as functions of RAP binder content in Figure 2.13c and 2.13d, respectively.

An increase in both T_{Fraass} and PI values of blends without rejuvenator is observed as RAP binder content increases. On the contrary, values of both parameters decrease when the percentage of Rej in blends increases.

Similar tendencies to those observed for the T_{Fraass} and PI values were found for the values of density at 25°C (Figure 2.13e).

Regarding the results obtained for the elongation, it was not possible to observe the effect of increasing the percentage of rejuvenator on ductility results since measure span of the test machine is limited to 150 cm (Table 2.6). For the binder blends produced without rejuvenator it can be observed that the elongation is decreasing with the increase of the RAP binder content and is always lower than 150 mm.

In Figure 2.13, linear regressions were performed for values of properties of blends having the same rejuvenator content (0%, 5%, 10% and 15%).

As a general comment, it could be observed that with increasing RAP binder content properties of blends without rejuvenator tend towards those of pure RAP binder, as expected. The effect of the rejuvenator proves to counterbalance this tendency, as it could be observed from the change of slope of regressions in Figure 2.13 for different rejuvenator contents.

As it could be observed in Figure 2.13 and Table 2.6, the results obtained (for $pen.$, $T_{R\&B}$, T_{Fraass}, PI and density) for the blends produced with 5% rejuvenator by mass of the RAP binder, show the same tendencies as those obtained for the blends produced without rejuvenator. This means that the amount 5% of rejuvenator by mass of the RAP binder is not sufficient to counterbalance the effect of the RAP binder.

Moreover, the results obtained for the blends produced with 10% rejuvenator by mass of the RAP binder are similar to those obtained for fresh binder 50/70, independently of the RAP binder content. This indicates the capability of the rejuvenator (in terms of mechanical characteristics) to rejuvenate the hard-aged RAP binder and finally to provide a final product with similar properties of fresh binder. This effect can be observed in Figure 2.13 a-d, where the regression lines for the blends produced with 10% rejuvenator are close to the horizontal line. R^2 values are not meaningful since $pen.$, $T_{R\&B}$, T_{Fraass} and PI values of all blends remain approximately constant for all RAP binder contents. Thus, for the results obtained for density this observation is not valid.

On the other side, for the blends produced with 15% rejuvenator by mass of the RAP binder, an inverse effect can be observed. It is interesting to notice that blends with 15% rejuvenator appear to become softer with increasing RAP binder content. This trend can be explained by the fact that the rejuvenator content is calculated with respect to RAP binder content and also by the fact that the 10% rejuvenator amount seems to be the 'optimal dosage' in order to obtain a blend with similar mechanical characteristics as a fresh 50/70 pen. grade binder.

Table 2.6. Experimental results of the conventional tests for all tested binders presented in Table 2.1.

Materials	*pen.* (0.1 mm)	$T_{R\&B}$ (°C)	T_{Fraass} (°C)	*Elongation* (cm)	*Density* (kg/m^3)	*PI* (-)
50/70	54	48.60	-14	> 150	1016	-1.39
RAP	11	79.00	-2	52	1060	1.01
RAP + 5% Rej	27	62.00	-9	99	1054	0.03
RAP + 10% Rej	60	47.60	-15	> 150	1048	-1.41
RAP + 15% Rej	100	39.00	-18	> 150	1043	-2.92
50/70 + 25% RAP	41	54.00	-12	138	1024	-0.70
50/70 + 25% RAP + 5% Rej	46	50.40	-13	> 150	1023	-1.29
50/70 + 25% RAP + 10% Rej	53	48.60	-14	> 150	1022	-1.43
50/70 + 25% RAP + 15% Rej	60	47.60	-15	> 150	1021	-1.41
50/70 + 50% RAP	30	58.80	-10	98	1032	-0.36
50/70 + 50% RAP + 5% Rej	43	52.80	-12	> 150	1030	-0.87
50/70 + 50% RAP + 10% Rej	53	48.20	-14	> 150	1028	-1.54
50/70 + 50% RAP + 15% Rej	67	46.40	-16	> 150	1026	-1.53
50/70 + 75% RAP	23	64.00	-8	77	1041	0.08
50/70 + 75% RAP + 5% Rej	35	56.60	-11	> 150	1037	-0.48
50/70 + 75% RAP + 10% Rej	57	48.40	-14	> 150	1034	-1.32
50/70 + 75% RAP + 15% Rej	78	43.20	-16	> 150	1032	-2.07

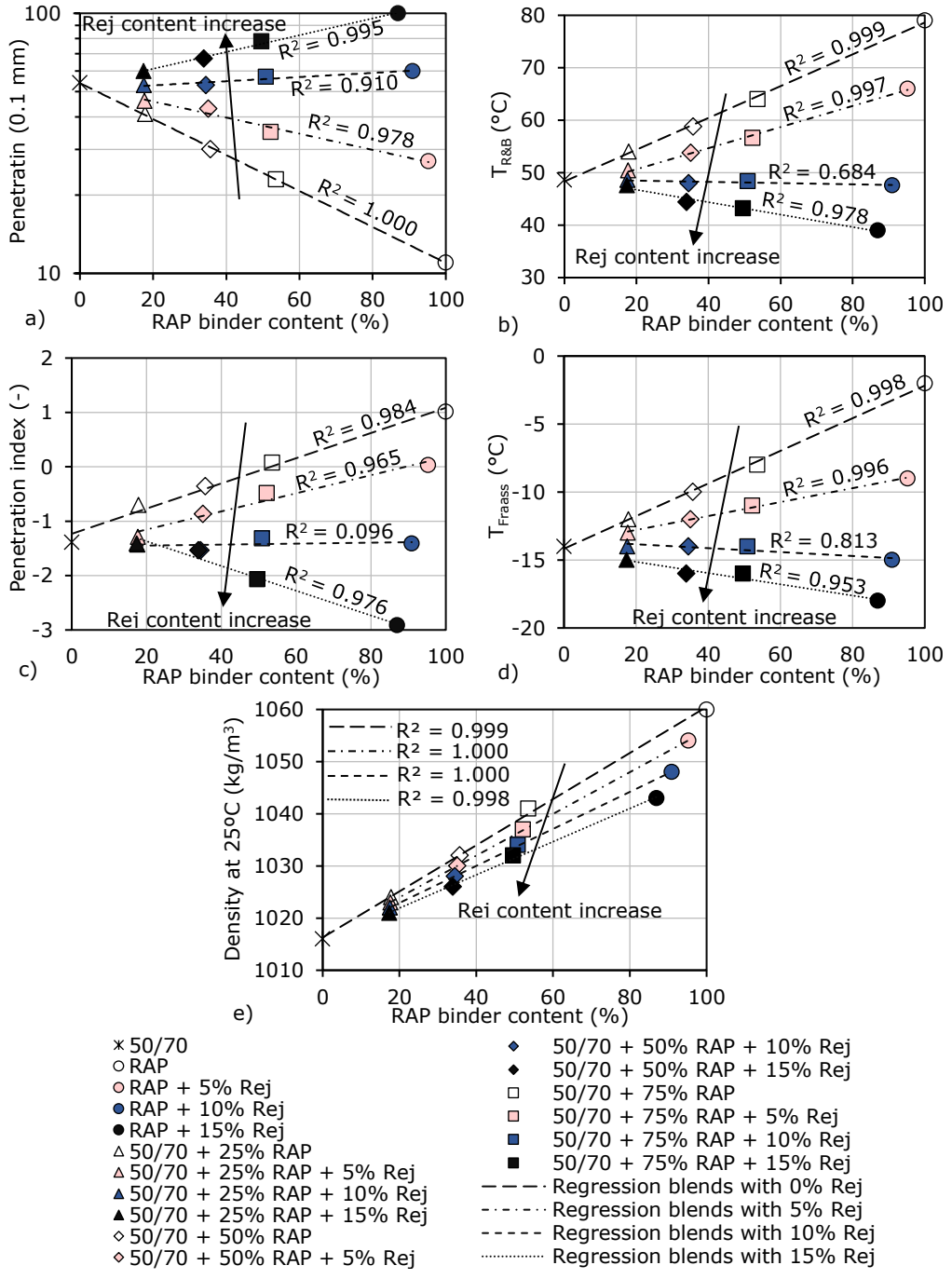

Figure 2.13. Conventional test results of all binders as a function of RAP bitumen content: (a) Penetration at 25°C; (b) Ring and ball temperature; (c) Penetration Index; (d) Fraass breaking point temperature; (e) Density at 25°C.

2.5.2 Estimation of European conventional parameters

Penetration at 25°C $(pen.)$, ring and ball temperature $(T_{R\&B})$ and Fraass breaking point temperature (T_{Fraass}) values were estimated from experimental results obtained for the base constituents, by using the two different estimation approaches presented in Section 2.4.

In order to estimate *pen.* values equation 2.6 (1st estimation) and equation 2.10 (2nd estimation) were used, respectively equation 2.5 (1st estimation) and equation 2.9 (2nd estimation) were used for the estimation of $T_{R\&B}$ and T_{Fraass}. The estimated values obtained for these three conventional parameters are reported, respectively in Table 2.7 and Table 2.8.

The estimated values determined with respect to these two proposed approaches were then rounded by following identical rules shown in Section 2.3, as follows:

- penetration values were expressed in tenths of mm rounded to the nearest integer;
- ring and ball temperature were expressed to the nearest 0.20°C;
- Fraass breaking point temperatures were rounded to the nearest integer.

Correlation plots of estimated values vs. experimental results are shown in Figure 2.14.

In each plot, coefficients of determination R^2 of both correlations 1st and 2nd estimation vs. experimental results were calculated with respect to the equality line. In the calculation of R^2, values of the following three parameters of the base constituents were not taken into account: $X_{50/70}, Y_{50/70}, X_{RAP+Rej}$ *and* $Y_{RAP+Rej}$ (5 binders) for the first approach Equations 2.5 and 2.6, $X_{50/70}, Y_{50/70}, X_{RAP}, Y_{RAP}, X_{Rej}$ *and* Y_{Rej} 2 binders and the rejuvenator for the second approach (Equations 2.9 and 2.10).

Regarding the second estimation approach, as mentioned in Section 2.4.2, equivalent values of the rejuvenator $\left(X_{Rej}\ and\ Y_{Rej}\right)$ were obtained by minimizing the distance D between experimental and estimated values of each parameter. The distance D is the sum of the square of the difference between the experimental and calculated values for the 15 blends. As already mentioned, these equivalent values of the rejuvenator were used only in the context of the estimation approach, therefore they are not intended to reflect real properties of the rejuvenator.

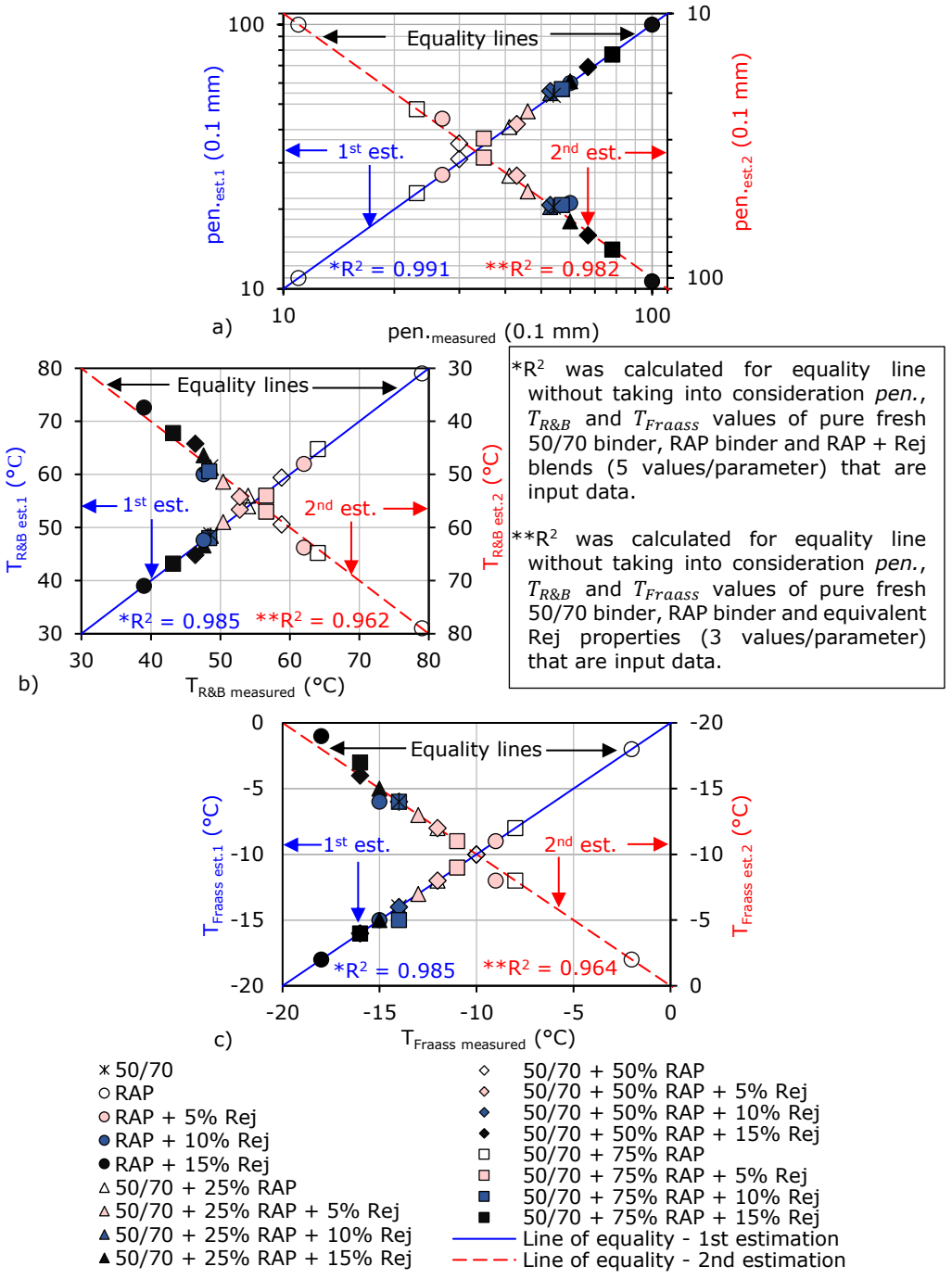

Figure 2.14. Plots of estimated vs. experimental (measured) values for all binders: (a) Penetration; (b) Ring and ball temperature; (c) Fraass breaking point temperature.

As it could be observed in Figure 2.14, greater values of the coefficient of determination were found with the first estimation approach than the second one. However, as a general observation the estimated values obtained by applying these two approaches are close to the measured values of *pen.*, $T_{R\&B}$ and T_{Fraass} for all the binder blends. The satisfactory values of R^2 found (always higher than 0.962) show that both estimation methods can be considered valid for the tested binders.

Table 2.7. Estimated values of penetration, ring and ball temperature, Fraass breaking point temperature from the 1st estimation approach for the 12 binder blends.

Binder blends	1st estimation		
	(0.1 mm)	$T_{R\&B}$ (°C)	T_{Fraass} (°C)
50/70 + 25% RAP	41	54.00	-12
50/70 + 25% RAP + 5% Rej	47	51.00	-13
50/70 + 25% RAP + 10% Rej	55	48.40	-14
50/70 + 25% RAP + 15% Rej	61	46.60	-15
50/70 + 50% RAP	31	59.40	-10
50/70 + 50% RAP + 5% Rej	42	53.40	-12
50/70 + 50% RAP + 10% Rej	56	48.20	-14
50/70 + 50% RAP + 15% Rej	69	44.80	-16
50/70 + 75% RAP	23	64.80	-8
50/70 + 75% RAP + 5% Rej	37	56.00	-11
50/70 + 75% RAP + 10% Rej	57	48.00	-15
50/70 + 75% RAP + 15% Rej	77	43.20	-16

Table 2.8. Estimated values of penetration, ring and ball temperature, Fraass breaking point temperature from the 2nd estimation approach for the 15 binder blends.

Materials	2nd estimation		
	pen. (0.1 mm)	$T_{R\&B}$ (°C)	T_{Fraass} (°C)
Rej equivalent	3×10^8	-240.20	-131
RAP + 5% Rej	25	63.80	-8
RAP + 10% Rej	52	50.00	-14
RAP + 15% Rej	103	37.40	-19
50/70 + 25% RAP	41	54.00	-12
50/70 + 25% RAP + 5% Rej	47	51.40	-13
50/70 + 25% RAP + 10% Rej	54	48.80	-14
50/70 + 25% RAP + 15% Rej	61	46.40	-15
50/70 + 50% RAP	31	59.40	-10
50/70 + 50% RAP + 5% Rej	41	54.20	-12
50/70 + 50% RAP + 10% Rej	53	49.20	-14
50/70 + 50% RAP + 15% Rej	69	44.20	-16
50/70 + 75% RAP	23	64.80	-8
50/70 + 75% RAP + 5% Rej	35	57.00	-11
50/70 + 75% RAP + 10% Rej	53	49.40	-14
50/70 + 75% RAP + 15% Rej	78	42.20	-17

2.6 Analysis of complex shear modulus

2.6.1 Experimental results

Part of the experimental results, including the determination of steady shear viscosity, analyses and the estimation of these parameters, have been presented in two publications Forton et al., 2019, 2021 [128], [177]. With respect to these articles, only slight modifications have been made.

As an example, isothermal curves of norm of complex shear modulus and phase angle for the blend 50/70 + 25% RAP + 5% Rej are shown in Figure 2.15.

In order to investigate the influence of RAP binder and rejuvenator content, isothermal master curves of norm $|G^*|$ and phase angle φ of complex shear modulus at a reference temperature of 55ºC and Black diagrams were built for all binders.

The time–temperature superposition principle was applied to obtain temperature shift factors a_T [122], [174], [178], [179]. Master curves were derived from experimental results at the reference temperature $(T_{ref} = 55°C)$. Equations 2.11 and 2.12 were considered.

$$\left|G^*(T,f)\right| = \left|G^*(T_{ref}, a_T \cdot f)\right| \tag{2.11}$$

$$\varphi(T,f) = \varphi(T_{ref}, a_T \cdot f) \tag{2.12}$$

where T and f are, respectively, the test temperature and frequency and T_{ref} is the reference temperature. Values of a_T for each binder were fitted using WLF equations.

Values of a_T shift factors and WLF constants (equation 1.26 from Section 1.5.2) for all tested binders are reported in Table 2.9.

As an example, master curves of $|G^*|$ and φ at a reference temperature of 55°C (Figure 2.16a), temperature shift factors vs. temperature and WLF curves (Figure 2.16b) and Black diagrams (Figure 2.16c) of blends of RAP binder and rejuvenator are shown in Figure 2.16. Similar graphs plotted for the other binders are reported in Figures A1.1 – A1.3 in Appendix 1.

The data presented in Black diagrams are located on a unique curve for each of the considered blends. This means that the time temperature superposition principle (TTSP) is valid for all tested binders. Then they are thermorheologically simple even when containing the rejuvenator.

As expected, master curves, Black curves and a_T shift factors of the blends produced without rejuvenator fall between corresponding master curves of fresh 50/70 binder and RAP binder. On the other side, the increase of the rejuvenator content into the blends corresponds to master curves, Black curves and shift factors progresively approaching to those of the 50/70 fresh binder.

From the data presented it results that the blends produced with fresh and RAP binders and 10% Rej by mass of the RAP binder presents close properties to those of the fresh 50/70 binder, independently of the RAP binder content, that is themaster curves and shift factors are significantly close to those of the fresh 50/70 binder. However, these blends produced with 10% Rej are stiffer and they present

much lower phase angle values compared to the fresh binder used in this study. This trend indicates that this rejuvenator is able to counterbalance the effect of the hard-aged RAP binder into the blends, in term of mechanical characteristics.

Moreover, the blends produced with fresh and RAP binders and 15% Rej by mass of the RAP binder show a behaviour which may corresponds to a 'softer binder' than the fresh binder used in this study. In Figure 2.16 it could be observed that the blend RAP + 15% Rej presents a behaviour that corresponds much more with the data obtained for the 50/70 binder. This trend can be explained by the fact that the optimal dosage of the rejuvenator is probably closer to 15% Rej by mass of the RAP binder, corresponding to 0.6% rejuvenator by mass of the RAP material for the corresponding bituminous mixture in order to obtain a blend who presents a similar behaviour as a fresh 50/70 pen. grade binder.

By increasing the rejuvenator content above this optimal percentage softer binders than the 50/70 pen. grade binder can be obtained. However, in order to determine the optimal dosage of a rejuvenator, this process must not be performed on only one direction due to the fact that this dosage may not meet all the specifications of a fresh virgin binder. Therefore, DSR tests must be combined with other tests at low temperature and also with a chemical investigation of rejuvenated binder blends in order to determine the proper optimal dosage of the rejuvenator.

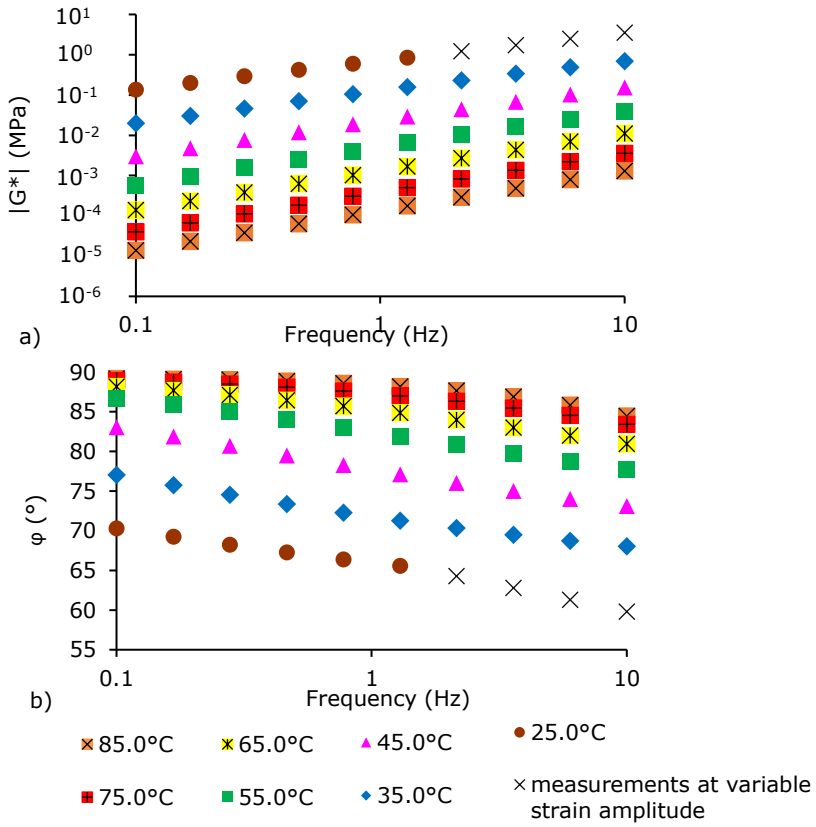

Figure 2.15. Example of complex shear modulus test results for the blend 50/70 +25% RAP + 5% Rej: (a) norm of complex shear modulus isotherms; (b) phase angle isotherms.

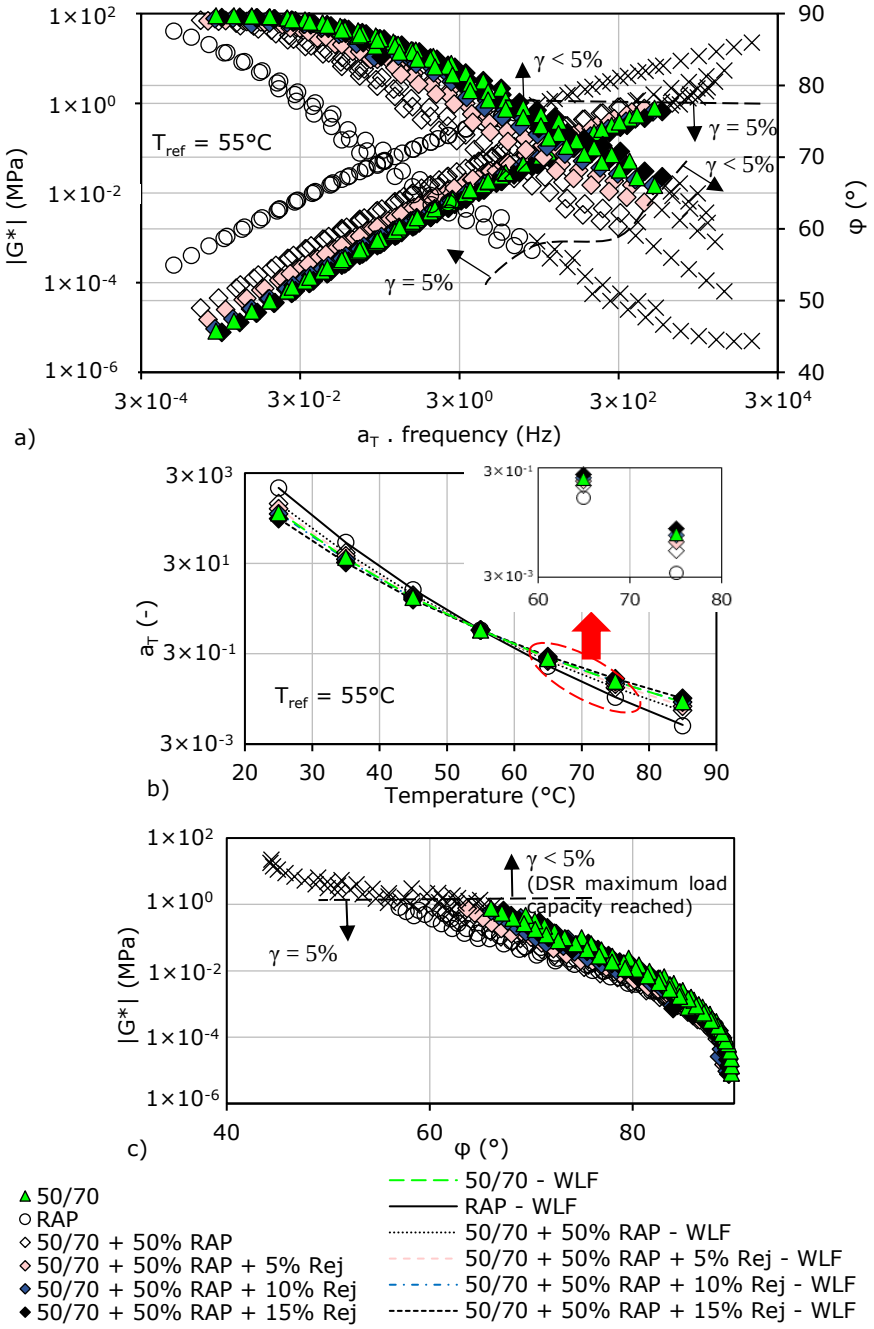

Figure 2.16. Complex shear modulus test results for the blends produced with fresh binder, 50% RAP and different dosages of rejuvenator: (a) master curves of the norm and phase angle of complex shear modulus; (b) temperature shift factors and WLF curves; (c) Black diagrams.

Table 2.9. DSR complex shear modulus test results for all binder: a_T temperature shift factors and WLF constants.

Binders	a_T (-)							C_1	C_2
	25°C	35°C	45°C	55°C	65°C	75°C	85°C		
50/70	3.96×10^{2}	41.00	5.30	1	2.36×10^{-1}	7.40×10^{-2}	2.62×10^{-2}	8.15	123.10
RAP	1.41×10^{3}	88.00	7.90	1	1.60×10^{-1}	3.30×10^{-2}	7.70×10^{-3}	12.58	149.84
RAP + 5% Rej	5.82×10^{2}	52.00	6.00	1	2.10×10^{-1}	5.30×10^{-2}	1.62×10^{-2}	10.16	140.31
RAP + 10% Rej	3.00×10^{2}	33.00	4.90	1	2.53×10^{-1}	7.70×10^{-2}	2.70×10^{-2}	8.13	133.66
RAP + 15% Rej	1.82×10^{2}	22.00	4.21	1	2.97×10^{-1}	1.02×10^{-1}	4.12×10^{-2}	7.16	124.98
50/70 + 25% RAP	5.59×10^{2}	48.00	5.70	1	2.20×10^{-1}	6.04×10^{-2}	1.97×10^{-2}	9.16	129.98
50/70 + 25% RAP + 5% Rej	4.88×10^{2}	43.50	5.50	1	2.31×10^{-1}	6.49×10^{-2}	2.20×10^{-2}	8.65	126.56
50/70 + 25% RAP + 10% Rej	4.27×10^{2}	39.80	5.30	1	2.40×10^{-1}	7.00×10^{-2}	2.44×10^{-2}	8.34	125.08
50/70 + 25% RAP + 15% Rej	3.76×10^{2}	36.90	5.08	1	2.49×10^{-1}	7.47×10^{-2}	2.70×10^{-2}	8.04	123.63
50/70 + 50% RAP	6.37×10^{2}	52.50	5.98	1	2.08×10^{-1}	5.30×10^{-2}	1.68×10^{-2}	9.95	136.46
50/70 + 50% RAP + 5% Rej	4.89×10^{2}	44.03	5.53	1	2.25×10^{-1}	6.37×10^{-2}	2.07×10^{-2}	8.97	130.03
50/70 + 50% RAP + 10% Rej	3.78×10^{2}	37.06	5.11	1	2.43×10^{-1}	7.33×10^{-2}	2.55×10^{-2}	8.25	125.41
50/70 + 50% RAP + 15% Rej	2.96×10^{2}	31.46	4.74	1	2.61×10^{-1}	8.37×10^{-2}	3.10×10^{-2}	7.79	124.54
50/70 + 75% RAP	8.75×10^{2}	63.80	6.70	1	1.92×10^{-1}	4.62×10^{-2}	1.30×10^{-2}	10.51	137.16
50/70 + 75% RAP + 5% Rej	5.85×10^{2}	48.77	5.92	1	2.16×10^{-1}	5.75×10^{-2}	1.79×10^{-2}	9.48	132.81
50/70 + 75% RAP + 10% Rej	3.99×10^{2}	37.85	5.28	1	2.42×10^{-1}	7.07×10^{-2}	2.43×10^{-2}	7.80	130.26
50/70 + 75% RAP + 15% Rej	2.78×10^{2}	29.72	4.72	1	2.69×10^{-1}	8.61×10^{-2}	3.24×10^{-2}	7.26	125.68

2.6.2 2S2P1D modelling

2.6.2.1 Experimental data fitting

Experimental data presented in Section 2.6.1 under the form of master curves of the norm and phase angle of complex shear modulus, Black and WLF curves were modelled using 2S2P1D model (Section 1.5.3, equation 1.28). Due to the fact that DSR complex shear modulus tests were performed only at intermediate and high temperature, the 2S2P1D model could not be fitted on the Cole-Cole curves.

The experimental results, analyses and the estimation of the 2S2P1D parameters was presented in one publications Forton et al., 2021 [180]. With respect to this article, only slight modifications have been made.

Taking into consideration that all binder blends were produced by mixing two base binders with and without the rejuvenator, first the experimental results obtained for fresh and RAP binders were modelled using 2S2P1D model (Figure 2.17).

All binders were tested at intermediate and high temperatures and by plotting the obtained data in a Cole-Cole representation it was observed that the experimental data fits only on the first part of the curve. By fitting the 2S2P1D model on the data obtained for the two base binders it was observed that the glassy modulus G_0 and the parameter k do not show an important variation, which characterize the 'final part' of the 2S2P1D model Cole-Cole plot. A similar comment can be made also for the shape parameter δ. Therefore, in this work the values of G_0, k *and* δ were imposed and assumed to have the same constant values for all binders. Also, for all binders $G_{00} = 0$ *MPa*.

It must be mentioned that probably this assumption could not be valid if a larger temperature range will be considered e.g. DSR tests performed at lower temperatures. Therefore, further investigation must be done on this direction.

The values of these constant parameters were established according to the 2S2P1D fitting model of fresh 50/70 and RAP binders $\left(G_{00} = 0\ MPa, G_0 = 980\ MPa, k = 0.25\ and\ \delta = 4.3\right)$.

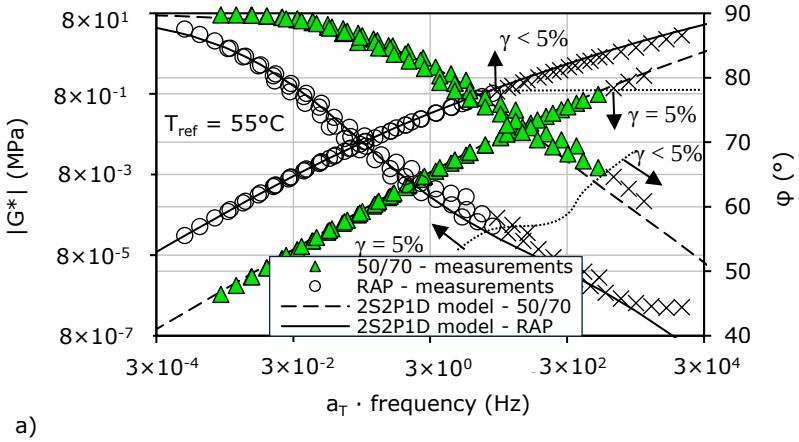

a)

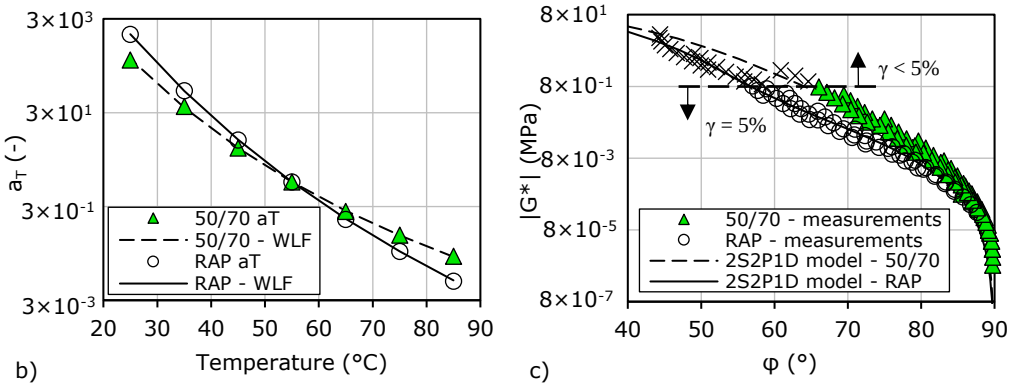

Figure 2.17. 2S2P1D model fitting of DSR complex shear modulus test results for the fresh 50/70 and RAP binders: (a) master curves of norm and phase angle of complex shear modulus $(T_{ref} = 55°C)$; (b) WLF curves; (c) Black curves.

The experimental results obtained for all binders $(T_{ref} = 55°C)$ were modelled using the same proposed approach and the results are presented in Figures A1.4 – A1.18 reported in Appendix 1.

The values of 2S2P1D parameters $(h, \beta \text{ and } \tau)$ for all tested blends are reported in Table 2.10 and in Figures 2.19a - 2.19c as a function of RAP binder content.

As it can be observed, parameters $h, \beta \text{ and } \tau$ show remarkable tendencies with the increase of RAP binder and rejuvenator contents in the final blends. Similar observation can be done also for the shift factors tendency. With this regard, the Figure 2.18d shows an example of the a_T shift factors obtained for all tested binders corresponding to the 65°C. Similar plots are presented for the a_T shift factors corresponding to the other temperatures obtained for all tested binders in Figure A1.19 reported in Appendix 1. The values of a_T shift factors for all tested binders are reported in Section 2.6.1, Table 2.9.

As already mentioned, values of $h, \log \beta, \log \tau \text{ and } \log a_T$ show linear relations with RAP binder and Rej contents. Therefore, linear regressions were performed for the blends produced with the same rejuvenator content of 0%, 5%, 10% and 15% by mass of the RAP binder content.

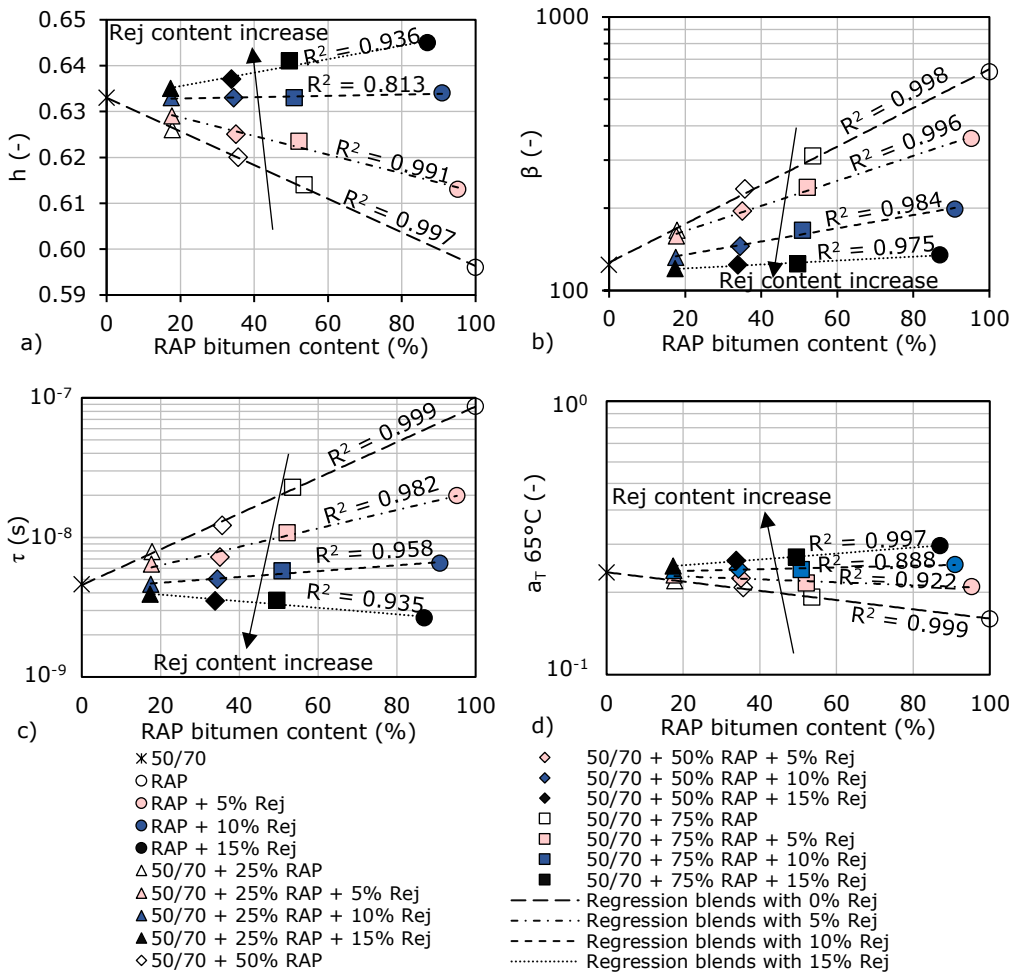

Figure 2.18. 2S2P1D parameters for all tested binders: (a) h tendency with RAP binder content; (b) β tendency with RAP binder content; (c) τ tendency with RAP binder content; (d) $a_T(65°C)$ tendency with RAP binder content.

Table 2.10. 2S2P1D parameters for all tested binders.

Binders	G_{00} (MPa)	G_0 (MPa)	k (-)	δ (-)	h (-)	β (-)	τ (s)
50/70	0	980	0.25	4.30	0.633	124	4.60×10^{-9}
RAP					0.596	630	8.70×10^{-8}
RAP + 5% Rej					0.614	360	1.99×10^{-8}
RAP + 10% Rej					0.634	198	6.53×10^{-9}
RAP + 15% Rej					0.645	135	2.65×10^{-9}
50/70 + 25% RAP					0.625	166	7.90×10^{-9}
50/70 + 25% RAP + 5% Rej					0.629	158	6.42×10^{-9}
50/70 + 25% RAP + 10% Rej					0.633	132	4.60×10^{-9}
50/70 + 25% RAP + 15% Rej					0.636	120	3.91×10^{-9}
50/70 + 50% RAP					0.620	235	1.22×10^{-8}
50/70 + 50% RAP + 5% Rej					0.627	195	7.20×10^{-9}
50/70 + 50% RAP + 10% Rej					0.632	145	5.00×10^{-9}
50/70 + 50% RAP + 15% Rej					0.637	124	3.50×10^{-9}
50/70 + 75% RAP					0.614	310	2.28×10^{-8}
50/70 + 75% RAP + 5% Rej					0.623	238	1.08×10^{-8}
50/70 + 75% RAP + 10% Rej					0.631	166	5.75×10^{-9}
50/70 + 75% RAP + 15% Rej					0.638	125	3.53×10^{-9}

As it could be observed in Figure 2.18a, parameter h shows a linear relationship with the RAP binder content. For the blends produced without rejuvenator the increase of RAP binder content corresponds to a decrease of parameter h values heading towards values of RAP binder. On the other side, the increase of rejuvenator content corresponds to an increase of h values. For the binder blends produced with 10% Rej a lower value of the R^2 of 0.813 was obtained, value that is not meaningful since the h values of all these blends remain approximately constant independently of the RAP binder content.

Similar remarks are valid for parameters β, τ and a_T temperature shift factors in a logarithmic scale (Figure 2.18b, 2.18c and 2.18d). The values of β and τ are increasing with the increase of RAP binder content and on the contrary they are decreasing with the increase of rejuvenator content. Similar tendencies were observed for the a_T shift factors (25°C, 35°C, 45°C). An inverse tendency can be observed for the a_T shift factors for the corresponding temperature at 65°C, 75°C and 85°C.

These observations suggest the possibility of the rejuvenator to balance the effect of RAP binder on the LVE behaviour of the tested binder blends.

For simplicity in the following section, the values of 2S2P1D parameters $(h, \beta \text{ and } \tau)$ and values of a_T shift factors determined for all the blends by fitting the 2S2P1D model on the experimental results, as described so far are referred to as 'experimental'.

2.6.2.2 Estimation of 2S2P1D parameters

As previously described in Section 2.6.2.1, the LVE behaviour of all binder blends depends on the content of RAP binder and rejuvenator contents, this being shown by the master curves and 2S2P1D parameters tendencies with the RAP binder content. The same procedures considering 1st and 2nd estimation approaches were used in order to estimate LVE behaviour of all binder blends over the whole temperature and frequency range from the LVE properties of the base binders: five binders for the 1st approach and the two base binders (50/70 fresh and RAP binders) and the rejuvenator and their concentrations.

In accordance with the observed tendencies i.e. parameter h shows a linear relationship with the RAP binder content, respectively parameters β, τ and a_T shift factors show similar relations but in a logarithmic scale equation 2.5 considering the linear rule for 1st approach and equation 2.9 considering the linear rule for 2nd approach were used in order to estimate the parameter h, respectively equations 2.6 as log rule for 1st approach and 2.10 as log rule for 2nd approach for the estimation of parameters β, τ and a_T shift factors.

As already mentioned in all previous sections were the estimation results were analysed for other parameters, in the second approach the equivalent values of the rejuvenator used, are not intended to reflect its actual properties and were used only in the context of the blending rule.

Equivalent values for the rejuvenator $(h_{Rej} \text{ and } X_{Rej})$ were obtained by following the same principle as already showed in the previous sections.

The experimental results as direct determination of parameters h (Figure 2.19a), β (Figure 2.19b), τ (Figure 2.19c) and of temperature shift factors, a_T corresponding to 65°C (Figure 2.19d) were plotted as a function of RAP binder content, together with the equivalent values determined for the rejuvenator. As it can be observed, linear regressions could be performed with excellent approximation, for all series of blends, by imposing as intercept point the equivalent values determined for the rejuvenator $\left(h_{Rej}\ and\ X_{Rej}\right)$. It can be noted that R^2 values are satisfactory, always greater than 0.958.

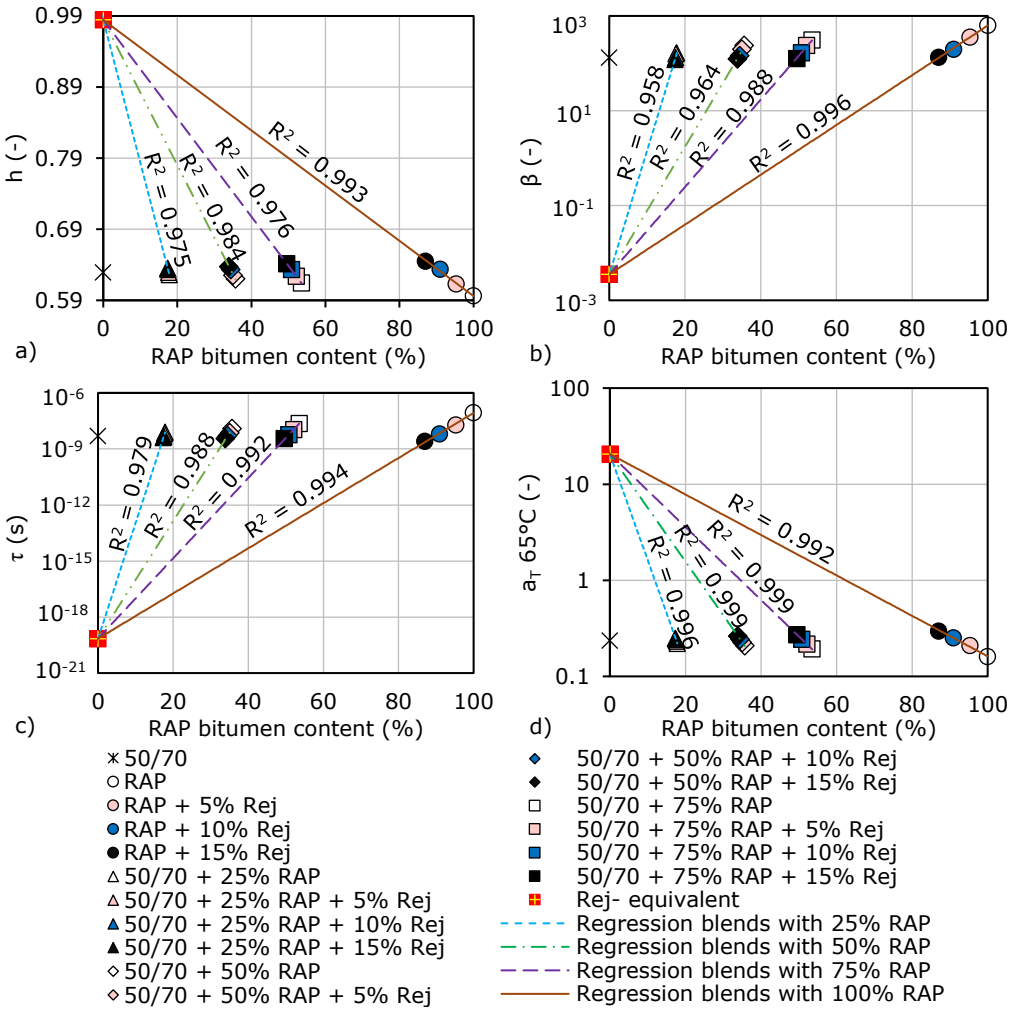

Figure 2.19. Experimental values of h, β, τ and a_T (at 65°C) and equivalent values of the rejuvenator as a function or RAP bitumen content: re-calculation of R^2 by imposing the equivalent values of the rejuvenator as an intercept point for all linear regressions.

Similar plots were built for the a_T temperature shift factors for all temperatures, as it could be observed in Figure A1.20 in Appendix 1.

Estimated values of 2S2P1D parameters $(h, \beta \text{ and } \tau)$ are shown in Table 2.11. Values for temperature shift factors are shown in Table 2.12 (1st estimation) and Table 2.13 (2nd estimation).

Figure 2.20 shows by applying 1st and 2nd estimation approaches plots of estimated vs. experimental values of 2S2P1D parameters $h, \beta \text{ and } \tau$. Similar plot was built for a_T temperature shift factors at all temperatures, as it shown in Figure 2.20d. In Appendix 1 similar plots were reported for a_T temperature shift factors for all binders for each temperature (Figure A1.21 – A1.22).

For both correlations (the coefficients of determination R^2 were calculated with respect to the equality line. R^2 values were calculated without taking into account the input values for each parameter with respect to each approach: h, β, τ and a_T values for fresh binder and RAP + Rej blends in a total of five binders for the 1st approach; h, β, τ and a_T values for the two base binders and the equivalent values for the rejuvenator for the 2nd approach.

It could be observed that for all analysed 2S2P1D parameters and temperature shift factors the obtained estimated results are significantly close to the experimental ones. Satisfactory values of R^2 higher than 0.949 were found. Slightly higher correlation with the experimental results was found for the estimated values obtained with the 2nd approach, except for the parameter τ.

As it could be observed in Figure 2.20b, the parameter β is the only 2S2P1D parameter that do not show a very strong correlation with the experimental values: for the 1st approach $R^2 = 0.949$ and for the 2nd approach $R^2 = 0.957$.

In particular, the parameters h (Figure 2.20a) and τ (characteristic time at reference temperature given in Figure 2.20c) and a_T temperature shift factors (Figure 2.20d) show good correlation. Therefore, it can be concluded that temperature sensitivity of the tested binders is dependent on the RAP binder and rejuvenator contents and it varies linearly with this in logarithmic scale for τ and a_T.

Table 2.11. Estimated values of 2S2P1D parameters for all binders.

Materials	1st estimation			2nd estimation		
	h (-)	β (-)	τ (s)	h (-)	β (-)	τ (s)
50/70	N*	N*	N*	N*	N*	N*
RAP	N*	N*	N*	N*	N*	N*
Rej equivalent	-	-	-	**0.985	**3.52×10^{-3}	**7.01×10^{-20}
RAP + 5% Rej	N*	N*	N*	0.614	354	2.31×10^{-8}
RAP + 10% Rej	N*	N*	N*	0.631	210	6.92×10^{-9}
RAP + 15% Rej	N*	N*	N*	0.647	130	2.30×10^{-9}
50/70 + 25% RAP	0.626	166	7.78×10^{-9}	0.626	166	7.78×10^{-9}
50/70 + 25% RAP + 5% Rej	0.629	151	6.04×10^{-9}	0.630	151	6.22×10^{-9}
50/70 + 25% RAP + 10% Rej	0.633	136	4.92×10^{-9}	0.633	137	4.97×10^{-9}
50/70 + 25% RAP + 15% Rej	0.636	126	4.12×10^{-9}	0.636	125	4.00×10^{-9}
50/70 + 50% RAP	0.620	222	1.31×10^{-8}	0.620	222	1.31×10^{-8}
50/70 + 50% RAP + 5% Rej	0.626	184	7.89×10^{-9}	0.626	183	8.35×10^{-9}
50/70 + 50% RAP + 10% Rej	0.633	148	5.25×10^{-9}	0.632	151	5.37×10^{-9}
50/70 + 50% RAP + 15% Rej	0.637	128	3.71×10^{-9}	0.638	126	3.52×10^{-9}
50/70 + 75% RAP	0.614	296	2.22×10^{-8}	0.613	296	2.22×10^{-8}
50/70 + 75% RAP + 5% Rej	0.622	222	1.03×10^{-8}	0.623	220	1.11×10^{-8}
50/70 + 75% RAP + 10% Rej	0.634	161	5.60×10^{-9}	0.632	167	5.79×10^{-9}
50/70 + 75% RAP + 15% Rej	0.640	130	3.36×10^{-9}	0.641	127	3.10×10^{-9}

N* - no estimation performed (direct determination results).

** - equivalent values for the rejuvenator obtained by minimizing the distance between experimental and estimated results.

Table 2.12. Estimated values of temperature shift factors a_T by applying the 1st estimation approach for all binders analysed in this approach.

Binders	1st estimation					
	a_T 25°C	a_T 35°C	a_T 45°C	a_T 65°C	a_T 75°C	a_T 85°C
50/70 + 25% RAP	4.97×10^{2}	46.99	5.69	2.20×10^{-1}	6.41×10^{-2}	2.11×10^{-2}
50/70 + 25% RAP + 5% Rej	4.25×10^{2}	42.85	5.42	2.31×10^{-1}	6.96×10^{-2}	2.40×10^{-2}
50/70 + 25% RAP + 10% Rej	3.75×10^{2}	39.32	5.22	2.39×10^{-1}	7.46×10^{-2}	2.64×10^{-2}
50/70 + 25% RAP + 15% Rej	3.39×10^{2}	36.20	5.06	2.47×10^{-1}	7.89×10^{-2}	2.87×10^{-2}
50/70 + 50% RAP	6.23×10^{2}	53.86	6.11	2.05×10^{-1}	5.55×10^{-2}	1.69×10^{-2}
50/70 + 50% RAP + 5% Rej	4.56×10^{2}	44.75	5.55	2.26×10^{-1}	6.54×10^{-2}	2.19×10^{-2}
50/70 + 50% RAP + 10% Rej	3.56×10^{2}	37.76	5.14	2.42×10^{-1}	7.51×10^{-2}	2.65×10^{-2}
50/70 + 50% RAP + 15% Rej	2.92×10^{2}	32.17	4.85	2.58×10^{-1}	8.39×10^{-2}	3.13×10^{-2}
50/70 + 75% RAP	7.82×10^{2}	61.73	6.56	1.92×10^{-1}	4.80×10^{-2}	1.36×10^{-2}
50/70 + 75% RAP + 5% Rej	4.89×10^{2}	46.70	5.67	2.21×10^{-1}	6.16×10^{-2}	2.01×10^{-2}
50/70 + 75% RAP + 10% Rej	3.39×10^{2}	36.31	5.07	2.45×10^{-1}	7.57×10^{-2}	2.66×10^{-2}
50/70 + 75% RAP + 15% Rej	2.54×10^{2}	28.75	4.65	2.69×10^{-1}	8.89×10^{-2}	3.39×10^{-2}

Table 2.13. Estimated values of temperature shift factors a_T by applying the 2nd estimation approach for all binders analysed in this approach.

Materials	2nd estimation					
	a_T 25°C	a_T 35°C	a_T 45°C	a_T 65°C	a_T 75°C	a_T 85°C
Rej equivalent	$^{*}1.67\times10^{-4}$	$^{*}2.13\times10^{-3}$	$^{*}5.36\times10^{-2}$	$^{*}20.60$	$^{*}1.83\times10^{2}$	$^{*}2.83\times10^{3}$
RAP + 5% Rej	6.60×10^{2}	53.06	6.23	2.02×10^{-1}	4.97×10^{-2}	1.42×10^{-2}
RAP + 10% Rej	3.31×10^{2}	33.49	5.02	2.49×10^{-1}	7.23×10^{-2}	2.47×10^{-2}
RAP + 15% Rej	1.76×10^{2}	22.01	4.12	3.01×10^{-1}	1.02×10^{-1}	4.09×10^{-2}
50/70 + 25% RAP	4.97×10^{2}	46.99	5.69	2.20×10^{-1}	6.41×10^{-2}	2.11×10^{-2}
50/70 + 25% RAP + 5% Rej	4.36×10^{2}	43.03	5.46	2.29×10^{-1}	6.87×10^{-2}	2.34×10^{-2}
50/70 + 25% RAP + 10% Rej	3.82×10^{2}	39.41	5.24	2.38×10^{-1}	7.37×10^{-2}	2.59×10^{-2}
50/70 + 25% RAP + 15% Rej	3.37×10^{2}	36.20	5.04	2.48×10^{-1}	7.89×10^{-2}	2.87×10^{-2}
50/70 + 50% RAP	6.23×10^{2}	53.86	6.11	2.05×10^{-1}	5.55×10^{-2}	1.69×10^{-2}
50/70 + 50% RAP + 5% Rej	4.78×10^{2}	45.10	5.63	2.23×10^{-1}	6.39×10^{-2}	2.09×10^{-2}
50/70 + 50% RAP + 10% Rej	3.70×10^{2}	37.96	5.19	2.41×10^{-1}	7.33×10^{-2}	2.56×10^{-2}
50/70 + 50% RAP + 15% Rej	2.89×10^{2}	32.18	4.80	2.60×10^{-1}	8.37×10^{-2}	3.12×10^{-2}
50/70 + 75% RAP	7.82×10^{2}	61.73	6.56	1.92×10^{-1}	4.80×10^{-2}	1.36×10^{-2}
50/70 + 75% RAP + 5% Rej	5.24×10^{2}	47.21	5.79	2.17×10^{-1}	5.95×10^{-2}	1.87×10^{-2}
50/70 + 75% RAP + 10% Rej	3.58×10^{2}	36.63	5.14	2.43×10^{-1}	7.30×10^{-2}	2.53×10^{-2}
50/70 + 75% RAP + 15% Rej	2.49×10^{2}	28.74	4.59	2.71×10^{-1}	8.87×10^{-2}	3.38×10^{-2}

* - equivalent values for the rejuvenator obtained by minimizing the distance between experimental and estimated results.

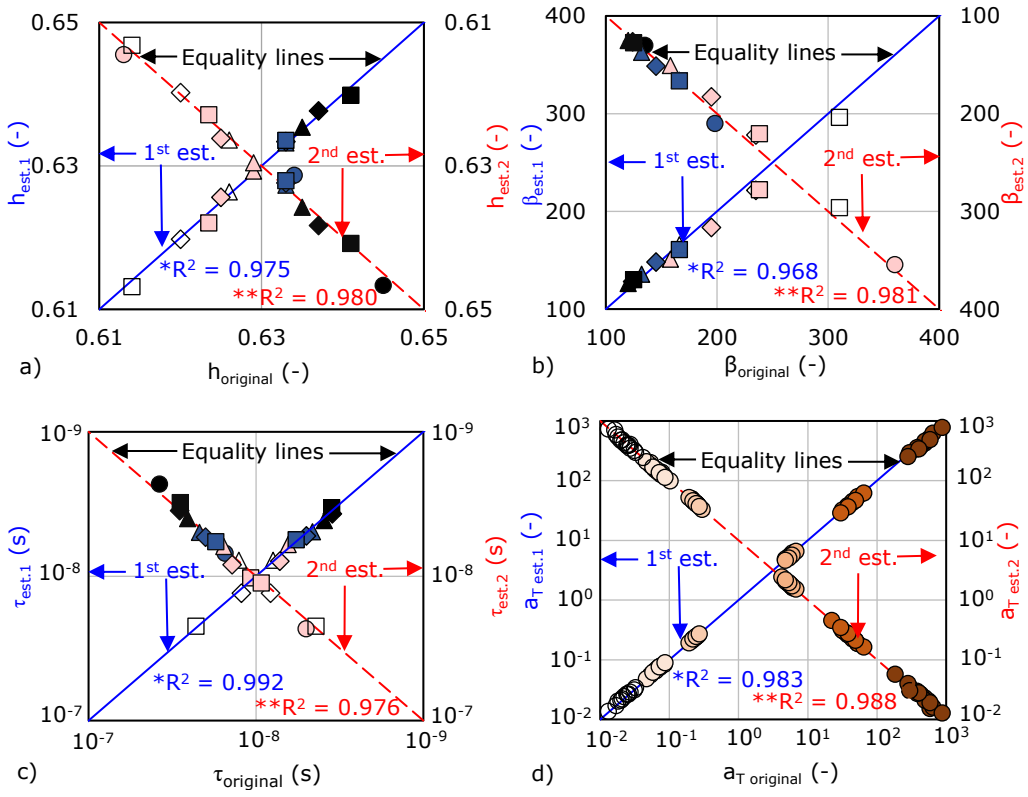

*R^2 was calculated for equality line without taking into consideration the results of pure fresh 50/70 binder, RAP binder and RAP + Rej blends (5 values/parameter) that are input data.

**R^2 was calculated for equality line without taking into consideration the results of pure fresh 50/70 binder, RAP binder and equivalent Rej properties (3 values/parameter) that are input data.

- 50/70
- RAP
- RAP + 5% Rej
- RAP + 10% Rej
- RAP + 15% Rej
- 50/70 + 25% RAP
- 50/70 + 25% RAP + 5% Rej
- 50/70 + 25% RAP + 10% Rej
- 50/70 + 25% RAP + 15% Rej
- 50/70 + 50% RAP
- 50/70 + 50% RAP + 5% Rej
- 50/70 + 50% RAP + 10% Rej
- 50/70 + 50% RAP + 15% Rej
- 50/70 + 75% RAP
- 50/70 + 75% RAP + 5% Rej
- 50/70 + 75% RAP + 10% Rej
- 50/70 + 75% RAP + 15% Rej
- Line of equality - 1st estimation
- Line of equality - 2nd estimation
- aT 25°C
- aT 35°C
- aT 45°C
- aT 65°C
- aT 75°C
- aT 85°C

Figure 2.20. Plots of estimated vs. experimental values: (a) parameter h; (b) parameter β; (c) parameter τ; (d) temperature shift factors a_T.

All estimated values reported in Table 2.11, Table 2.12 and Table 2.13 were used to estimate the prediction of LVE behaviour by re-implementing in the 2S2P1D model resulting master curves of norm and phase angle of complex shear modulus and Black curves which were compared with those built using the experimental data. As an example, Figure 2.21 shows the curves for the blend 50/70 + 75% RAP + 5%

Rej and as it could be observed master curves and Black curves are significantly close to the experimental ones. Similar plots are reported in Appendix 1 for all binders (Figures A1.23 – A1.36).

For all the blends it was observed that the estimated LVE behaviour is satisfactory close to the 2S2P1D curves based on the experimental data. The results show that these two approaches used to estimate 2S2P1D parameters and temperature shift factors, can be considered valid for the tested binders.

As an example, for the blend 50/70 + 75% RAP + 5% Rej, the errors between the measured norm of complex shear modulus $|G^*|$ and phase angle φ and the calculated $|G^*|$ and φ from the 2S2P1D parameters original direct determination and estimated values are shown in Figure 2.22. The errors were calculated for all binder blends for the results obtained at temperatures from 55°C to 85°C as temperatures for which the measurements were performed at a constant 5% shear stain amplitude over the whole frequency range of 0.1 to 10 Hz.

Acceptable errors, in accordance with the findings of Mangiafico et al. (2019) [181], were generally observed over the whole range of frequencies and temperatures for each binder blend.

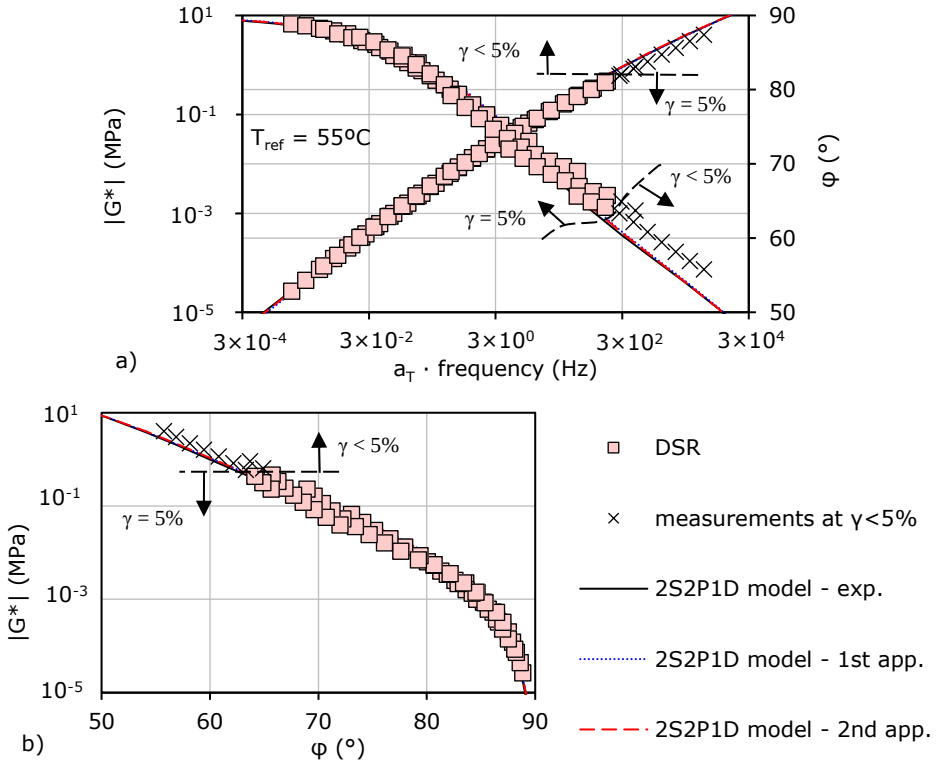

Figure 2.21. Comparison between test results, curves built using experimental and estimated 2S2P1D parameters for the 50/70 + 75% RAP + 5% Rej blend: (a) master curves of norm and phase angle of complex shear modulus $(T_{ref} = 55°C)$; (b) Black curve.

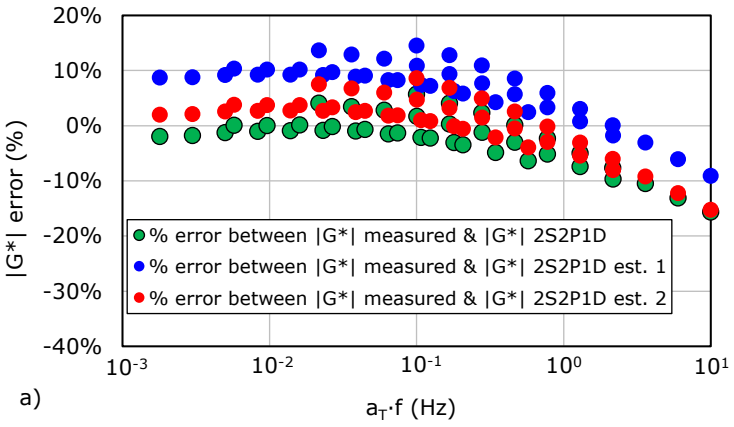

a)

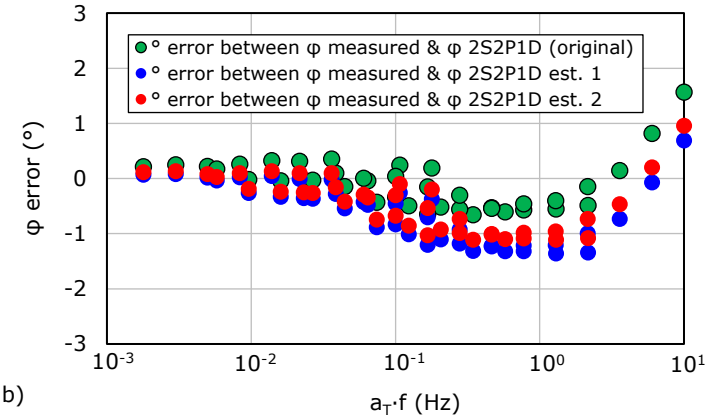

b)

$$Error\left|G^*\right|(\%) = \frac{\left|G^*\right|_{measured} - \left|G^*\right|_{2S2P1D\ original/est.1/est.2}}{\left|G^*\right|_{measured}} \times 100$$

$$Error\ \varphi\ (^\circ) = \varphi_{measured} - \varphi_{2S2P1D\ original/est.1/est.2}$$

Figure 2.22. (a) Error between $\left|G^*\right|_{measured}$ and $\left|G^*\right|_{2S2P1D}$ (from direct determination - original, from the 1st and 2nd estimation of 2S2P1D parameters) for the blend 50/70 + 75% RAP + 5% Rej; (b) Error between $\varphi_{measured}$ and φ_{2S2P1D} (from direct determination-original, from the 1st and 2nd estimation of 2S2P1D parameters) for the blend 50/70 + 75% RAP + 5% Rej.

2.7 Analysis of steady shear viscosity

2.7.1 Determination of steady shear viscosity at T_{Ref} = 85ºC

Complex viscosity η^* of a binder is defined as its complex shear modulus G^* divided by the angular frequency ω multiplied by the imaginary unit i $\left(i^2 = -1\right)$:

$$\eta^* = \frac{G^*}{i\omega} \tag{2.13}$$

Steady shear viscosity (η_0) can be obtained at a given temperature from the norm of complex viscosity $\left(\left|\eta^*\right|\right)$ at this temperature when angular frequency (ω) tends towards zero, as shown in equation 2.14.

$$\left|\eta^*\right| = \frac{\left|G^*\right|}{\omega} = \eta_0, \quad \omega \to 0, \quad \eta_0(T) = \lim_{\omega \to 0} \left|\eta^*(T,\omega)\right| \tag{2.14}$$

In a logarithmic form equation 2.15 can be written, as follows:

$$log\left|G^*\right| = log\,\omega + log\left|\eta^*\right| \tag{2.15}$$

where $\left|G^*\right|$ is the norm of complex shear modulus (in MPa), ω is the angular frequency (in rad/s) and $\left|\eta^*\right|$ is the norm of complex viscosity (in MPa·s).

Steady shear viscosity η_0 can be calculated from DSR complex modulus tests by applying the time-temperature superposition principle, as the norm of complex viscosity at very low frequencies, in the domain of Newtonian behaviour of binders.

In order to determine the steady shear viscosity, for all tested binders, $\left|G^*\right|$ was plotted as a function of ω in a log-log scale, at a reference temperature of 85°C. The high temperature/low frequency part of the curve corresponding to the isotherm obtained at 85ºC, for which a_T shift factors are equal to 1.0 was analysed in order to highlight the Newtonian behaviour of the binders in this loading domain. A linear regression was performed on this part of the curve (with an imposed 45° slope line), in order to determine η_0.

As an example, Figure 2.23 shows how η_0 values were obtained for fresh binder, RAP binder and their blends. Similar plots were built for each tested binder and reported in Figures A1.37 – A1.53 of the Appendix 1. The obtained η_0 values at 85°C for all binders are shown in Table 2.14.

As it could be observed in Figure 2.24, η_0 values at 85°C increase with the increase of RAP binder content in the blends. Linear regressions in logarithmic scale could be performed on the obtained η_0 values with good approximation. For the blends produced with 15% of rejuvenator by mass of the RAP binder, the R^2 value

of 0.231 is not meaningful since the $\eta_0(85°C)$ values of all these blends remain approximately constant for all RAP binder contents. Moreover, η_0 values decrease with the increase of rejuvenator content in the blends. However, these results were expected taking into consideration the results obtained for the complex shear modulus and for the conventional parameters of same blends.

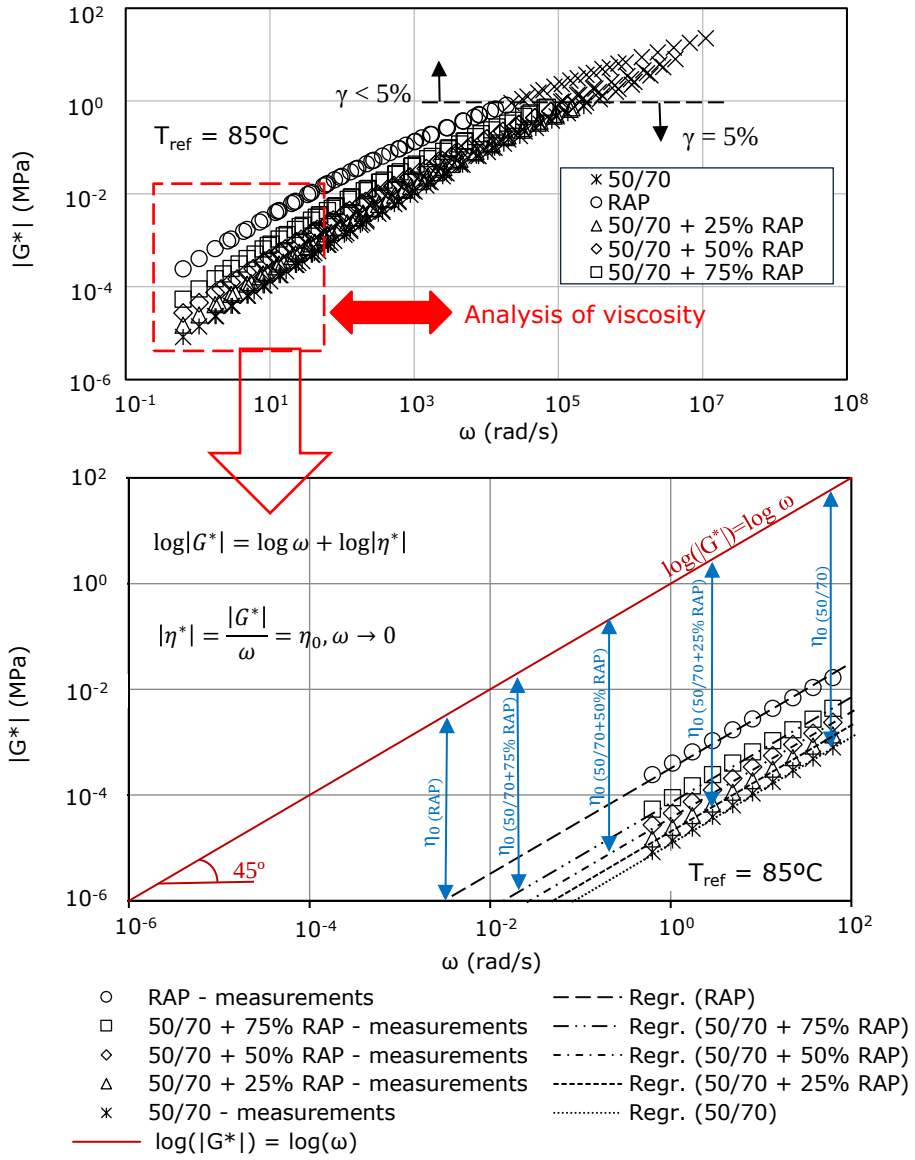

Figure 2.23. Steady shear viscosity (η_0) at 85ºC of 50/70 fresh and RAP binders and their blends.

Table 2.14. Experimental results of steady shear viscosity at $T_{ref} = 85°C$.

Binders	$\eta_0(85°C)$ (Pa·s)
50/70	1.32×10^1
RAP	3.39×10^2
RAP + 5% Rej	9.36×10^1
RAP + 10% Rej	2.90×10^1
RAP + 15% Rej	1.27×10^1
50/70 + 25% RAP	2.31×10^1
50/70 + 25% RAP + 5% Rej	2.16×10^1
50/70 + 25% RAP + 10% Rej	1.36×10^1
50/70 + 25% RAP + 15% Rej	1.14×10^1
50/70 + 50% RAP	4.17×10^1
50/70 + 50% RAP + 5% Rej	2.32×10^1
50/70 + 50% RAP + 10% Rej	1.47×10^1
50/70 + 50% RAP + 15% Rej	1.21×10^1
50/70 + 75% RAP	8.05×10^1
50/70 + 75% RAP + 5% Rej	4.01×10^1
50/70 + 75% RAP + 10% Rej	2.13×10^1
50/70 + 75% RAP + 15% Rej	1.44×10^1

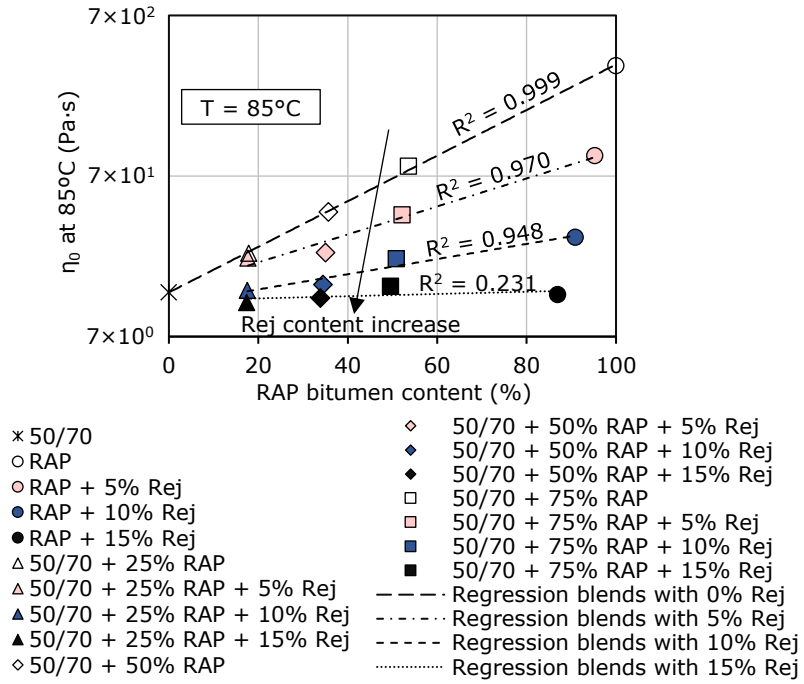

Figure 2.24. Steady shear viscosity $\eta_0(85°C)$ for all binders, as a function of RAP binder content.

2.7.2 Determination of steady shear viscosity at different temperatures

In order to calculate η_0 values for all binders at different temperatures equation 2.16 was used. In this equation, the value of the steady shear viscosity at a temperature T, $\eta_0(T)$ is calculated from the values of the steady shear viscosity at the reference temperature of 85°C, $\eta_0(T_{ref} = 85°C)$, multiplied by the temperature shift factor at temperature T, a_T. Values of temperature shift factors at a reference temperature of 85ºC were calculated from WLF (equation 1.20 from Section 1.5.2). Results are reported in Table 2.15.

$$\eta_0(T) = a_T \cdot \eta_0(T_{ref}) \tag{2.16}$$

The results obtained by applying equation 2.16 are reported in Table 2.16 and in Figure 2.25.

As expected, values of $\eta_0(T)$ decrease with the increase of temperature. Also, $\eta_0(T)$ increase with increasing RAP binder content in the blends and decrease with the increase of Rej content within blends. Linear regressions in logarithmic scale as a function of RAP binder content were performed with rather good approximation for all binders, at all considered temperatures.

As it could be observed in Figure 2.25a and 2.25b and Table 2.16, the values of $\eta_0(T)$ at low temperatures (25ºC and 35ºC) of the blends containing 10% Rej independently of the RAP binder content are close to the results obtained for the base fresh binder. This observation is not valid at higher temperatures for which $\eta_0(T)$ increases with the increasing RAP bitumen content.

For simplicity in the following sections values of $\eta_0(T)$ determined for all blends from experimental tests as described so far are referred to as 'experimental'.

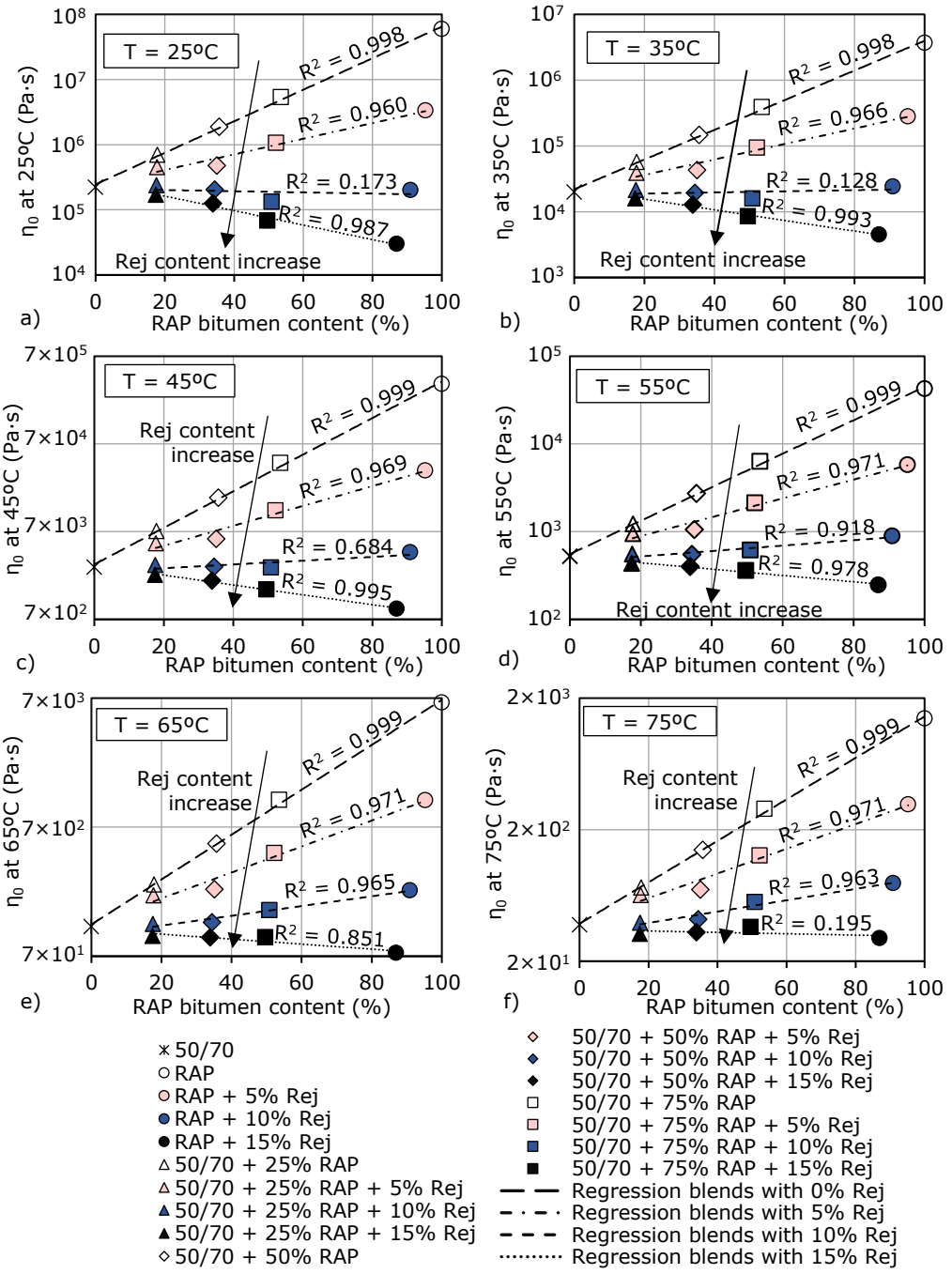

Figure 2.25. Results of steady shear viscosity at different temperatures for all binders as a function of RAP binder content: (a) T=25°C; (b) T=35°C; (c) T=45°C; (d) T=55°C; (e) T=65°C; (f) T=75°C.

Table 2.15. a_T shift factors values at a reference temperature of 85°C calculated from WLF for all tested binders.

Binders	a_T (-) at $T_{ref} = 85°C$						
	85°C	75°C	65°C	55°C	45°C	35°C	25°C
50/70	1	2.87×10^{0}	9.65×10^{0}	3.95×10^{1}	2.08×10^{2}	1.51×10^{3}	1.67×10^{4}
RAP	1	4.14×10^{0}	2.05×10^{1}	1.26×10^{2}	9.96×10^{2}	1.09×10^{4}	1.77×10^{5}
RAP + 5% Rej	1	3.33×10^{0}	1.30×10^{1}	6.17×10^{1}	3.72×10^{2}	3.02×10^{3}	3.59×10^{4}
RAP + 10% Rej	1	2.70×10^{0}	8.40×10^{0}	3.09×10^{1}	1.41×10^{2}	8.33×10^{2}	6.97×10^{3}
RAP + 15% Rej	1	2.35×10^{0}	6.24×10^{0}	1.94×10^{1}	7.30×10^{1}	3.52×10^{2}	2.35×10^{3}
50/70 + 25% RAP	1	3.14×10^{0}	1.16×10^{1}	5.28×10^{1}	3.08×10^{2}	2.47×10^{3}	3.01×10^{4}
50/70 + 25% RAP + 5% Rej	1	2.96×10^{0}	1.03×10^{1}	4.38×10^{1}	2.39×10^{2}	1.81×10^{3}	2.10×10^{4}
50/70 + 25% RAP + 10% Rej	1	2.90×10^{0}	9.83×10^{0}	4.07×10^{1}	2.16×10^{2}	1.58×10^{3}	1.76×10^{4}
50/70 + 25% RAP + 15% Rej	1	2.84×10^{0}	9.45×10^{0}	3.82×10^{1}	1.97×10^{2}	1.40×10^{3}	1.50×10^{4}
50/70 + 50% RAP	1	3.37×10^{0}	1.34×10^{1}	6.54×10^{1}	4.09×10^{2}	3.51×10^{3}	4.51×10^{4}
50/70 + 50% RAP + 5% Rej	1	3.01×10^{0}	1.06×10^{1}	4.55×10^{1}	2.48×10^{2}	1.84×10^{3}	2.04×10^{4}
50/70 + 50% RAP + 10% Rej	1	2.82×10^{0}	9.28×10^{0}	3.70×10^{1}	1.88×10^{2}	1.31×10^{3}	1.37×10^{4}
50/70 + 50% RAP + 15% Rej	1	2.72×10^{0}	8.62×10^{0}	3.29×10^{1}	1.59×10^{2}	1.05×10^{3}	1.03×10^{4}
50/70 + 75% RAP	1	3.57×10^{0}	1.51×10^{1}	7.87×10^{1}	5.28×10^{2}	4.86×10^{3}	6.69×10^{4}
50/70 + 75% RAP + 5% Rej	1	3.17×10^{0}	1.18×10^{1}	5.32×10^{1}	3.04×10^{2}	2.35×10^{3}	2.66×10^{4}
50/70 + 75% RAP + 10% Rej	1	2.64×10^{0}	8.02×10^{0}	2.88×10^{1}	1.28×10^{2}	7.50×10^{2}	6.22×10^{3}
50/70 + 75% RAP + 15% Rej	1	2.53×10^{0}	7.31×10^{0}	2.51×10^{1}	1.06×10^{2}	5.93×10^{2}	4.74×10^{3}

Table 2.16. Experimental results of steady shear viscosity, $\eta_0(T)$, at different temperatures for all tested binders.

Binders	$\eta_0(T)$, (Pa·s)					
	75°C	65°C	55°C	45°C	35°C	25°C
50/70	3.79×10^{1}	1.27×10^{2}	5.22×10^{2}	2.74×10^{3}	1.99×10^{4}	2.21×10^{5}
RAP	1.41×10^{3}	6.96×10^{3}	4.26×10^{4}	3.38×10^{5}	3.69×10^{6}	6.01×10^{7}
RAP + 5% Rej	3.12×10^{2}	1.22×10^{3}	5.78×10^{3}	3.48×10^{4}	2.83×10^{5}	3.36×10^{6}
RAP + 10% Rej	7.84×10^{1}	2.44×10^{2}	8.97×10^{2}	4.08×10^{3}	2.42×10^{4}	2.02×10^{5}
RAP + 15% Rej	2.99×10^{1}	7.96×10^{1}	2.47×10^{2}	9.30×10^{2}	4.49×10^{3}	3.02×10^{4}
50/70 + 25% RAP	7.27×10^{1}	2.69×10^{2}	1.22×10^{3}	7.11×10^{3}	5.71×10^{4}	6.95×10^{5}
50/70 + 25% RAP + 5% Rej	6.39×10^{1}	2.22×10^{2}	9.45×10^{2}	5.17×10^{3}	3.91×10^{4}	4.54×10^{5}
50/70 + 25% RAP + 10% Rej	3.93×10^{1}	1.34×10^{2}	5.52×10^{2}	2.93×10^{3}	2.14×10^{4}	2.39×10^{5}
50/70 + 25% RAP + 15% Rej	3.24×10^{1}	1.08×10^{2}	4.35×10^{2}	2.25×10^{3}	1.59×10^{4}	1.71×10^{5}
50/70 + 50% RAP	1.40×10^{2}	5.59×10^{2}	2.72×10^{3}	1.71×10^{4}	1.46×10^{5}	1.88×10^{6}
50/70 + 50% RAP + 5% Rej	7.00×10^{1}	2.47×10^{2}	1.06×10^{3}	5.76×10^{3}	4.28×10^{4}	4.74×10^{5}
50/70 + 50% RAP + 10% Rej	4.15×10^{1}	1.37×10^{2}	5.46×10^{2}	2.77×10^{3}	1.93×10^{4}	2.03×10^{5}
50/70 + 50% RAP + 15% Rej	3.31×10^{1}	1.05×10^{2}	4.00×10^{2}	1.94×10^{3}	1.27×10^{4}	1.25×10^{5}
50/70 + 75% RAP	2.88×10^{2}	1.22×10^{3}	6.34×10^{3}	4.25×10^{4}	3.91×10^{5}	5.39×10^{6}
50/70 + 75% RAP + 5% Rej	1.27×10^{2}	4.74×10^{2}	2.13×10^{3}	1.22×10^{4}	9.42×10^{4}	1.07×10^{6}
50/70 + 75% RAP + 10% Rej	5.63×10^{1}	1.71×10^{2}	6.15×10^{2}	2.74×10^{3}	1.60×10^{4}	1.67×10^{5}
50/70 + 75% RAP + 15% Rej	3.64×10^{1}	1.05×10^{2}	3.61×10^{2}	1.53×10^{3}	8.54×10^{3}	6.82×10^{4}

2.7.3 Estimation of steady shear viscosity

The two estimation approaches were applied in order to determine the estimated values of $\eta_0(T)$ at different temperatures (from 25°C to 85°C) of all binder blends. The obtained results were then compared with the experimental values.

As previously described, the 1st estimation approach considers the classical blending rule expressed in equation 2.6 in logarithmic form, which supposes that $\eta_0(T)$ values for fresh binder, RAP binder and blends of RAP + Rej at the three different dosages used in the study are used as input values. For this approach, $\eta_0(T)$ values for RAP + Rej blends must be known from experimental tests, which is a drawback as these blends should be tested for each of the three considered Rej contents of 5%, 10% and 15%.

As described in Section 2.4.2, the 2nd estimation approach consists in the three-way blending rule expressed in equation 2.10 in logarithmic form, which requires as input data only the values of $\eta_0(T)$ for the three base materials used in this study.

The estimated values of steady shear viscosity at a given temperature for any of the 15 blends $\left(\eta_0(T)_{est.2\ blend}\right)$ were calculated from the experimental results of fresh binder $\left(\eta_0(T)_{(50/70)}\right)$, RAP binder $\left(\eta_0(T)_{(RAP)}\right)$ and from equivalent values of the rejuvenator $\left(\eta_0(T)_{(Rej)}\right)$.

In order to obtain the equivalent values for the rejuvenator of $\left(\eta_0(T)_{(Rej)}\right)$ at a given temperature, it was necessary to minimize the distance between experimental and estimated values of all 15 blends. It should be mentioned that these equivalent $\eta_0(T)_{(Rej)}$ values were used only for this second estimation approach, which is valid only for rather small Rej content (up to 15%). It should be pointed that his equivalent viscosity is not equal to the viscosity of the rejuvenator used for this study.

In Figure 2.26, the experimental results of η_0 at different temperatures for RAP + Rej blends are plotted as a function of the rejuvenator content, together with the equivalent values of $\eta_0(T)_{(Rej)}$ determined for the rejuvenator. Linear regressions could be performed with excellent approximation at all considered temperatures. It was observed that all the regression lines can be obtained with the same R^2 its influence was only on the 4th decimal when considering that all lines intersect a unique point: 35% Rej content and 0.038 Pa·s. Figure 2.26 gives an overview of these results.

These results led to the idea of a 'temperature-independent constant content-viscosity couple' for the rejuvenator which is expressed in equations 2.17.

$$log\,0.038 = 0.65\,log\,\eta_0(T)_{(RAP)} + 0.35\,log\,\eta_0(T)_{(Rej)} \quad (2.17)$$

The values of $\eta_0(T)_{(Rej)}$ could be directly deduced from the following equation:

$$log\,\eta_0(T)_{(Rej)} = \frac{log\,0.038}{0.35} - \frac{0.65}{0.35}\,log\,\eta_0(T)_{(RAP)} \quad (2.18)$$

The values of $\eta_0(T)_{(Rej)}$ determined with equation 2.18 are reported in Table 2.17. Plots of the estimated results obtained from the 1st approach and the 2nd approach versus the experimental results are and shown in Figure 2.27. Estimated results of $\eta_0(T)$ for all blends are reported in Table 2.18 and Table 2.19.

Table 2.17. Equivalent values of $\eta_0(T)_{(Rej)}$ determined for the rejuvenator.

Temperature (ºC)	$\eta_0(T)_{(Rej)}$ (Pa·s)
25°C	3.13×10^{-19}
35°C	5.57×10^{-17}
45°C	4.72×10^{-15}
55°C	2.21×10^{-13}
65°C	6.40×10^{-12}
75°C	1.25×10^{-10}
85°C	1.75×10^{-09}

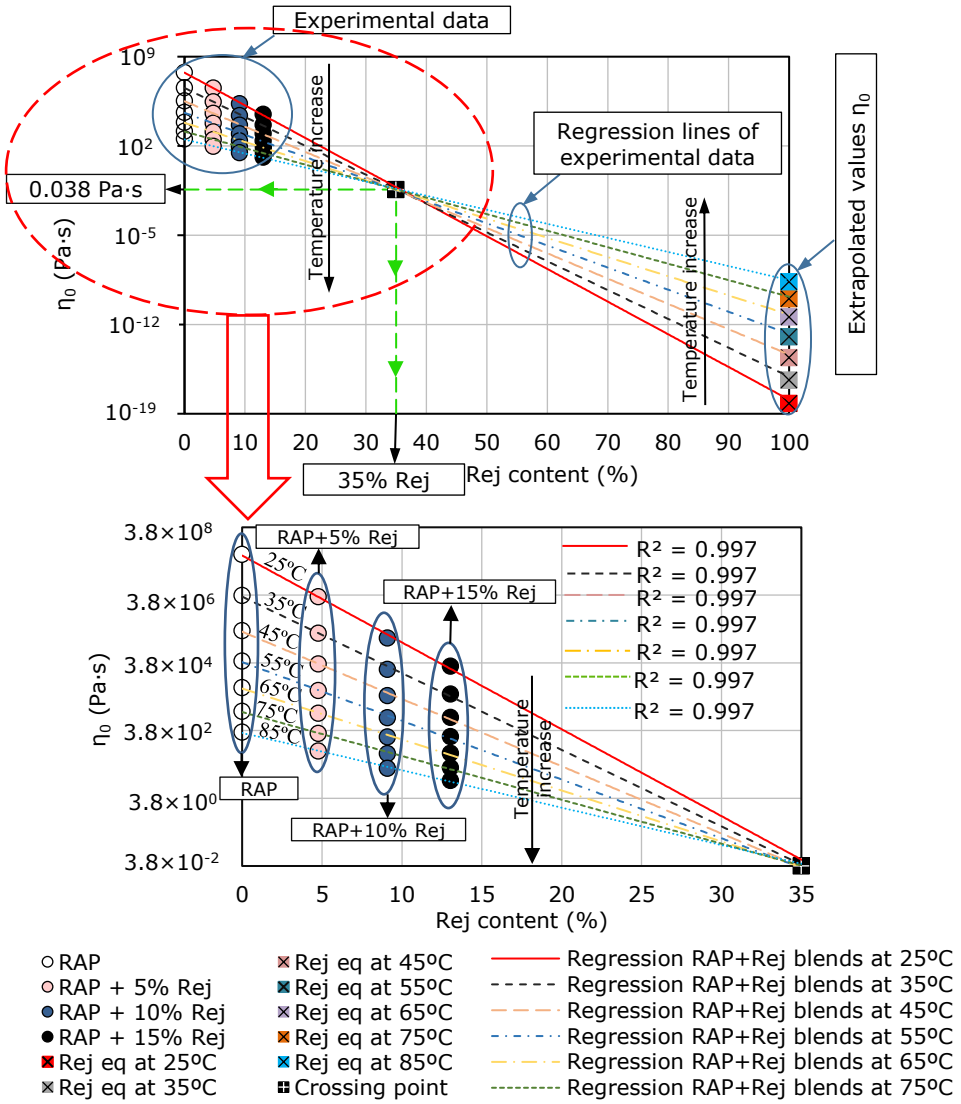

Figure 2.26. Experimental results of $\eta_0(T)$ for RAP + Rej blends, equivalent values for rejuvenator $\eta_0(T)_{(Rej)}$, plotted as a function of Rej content in the blends, at all considered temperatures.

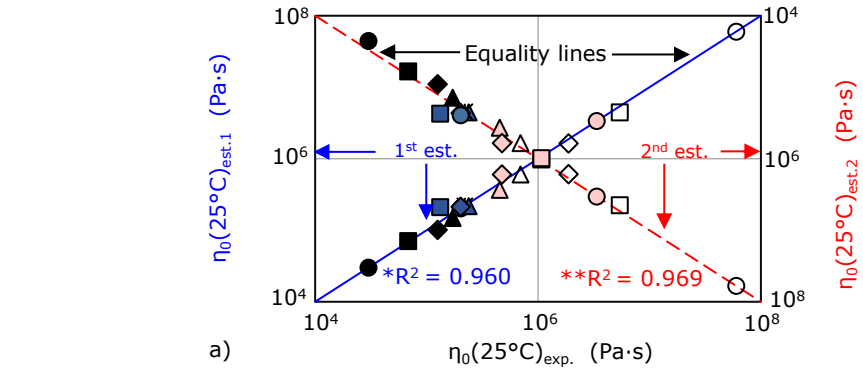

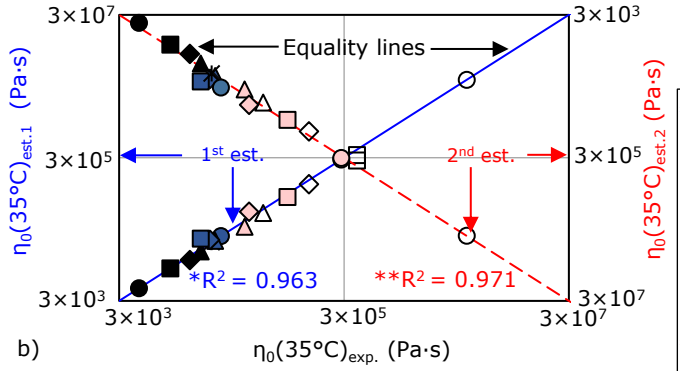

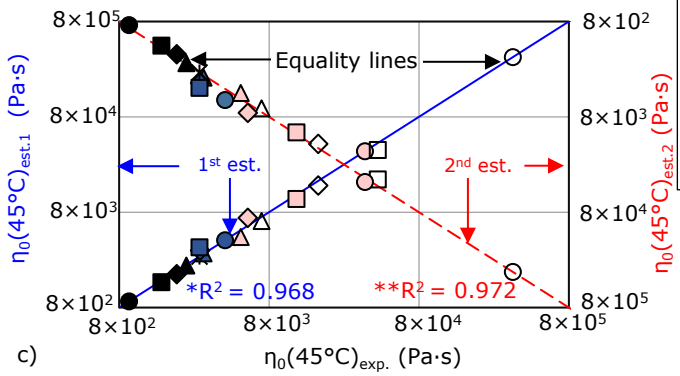

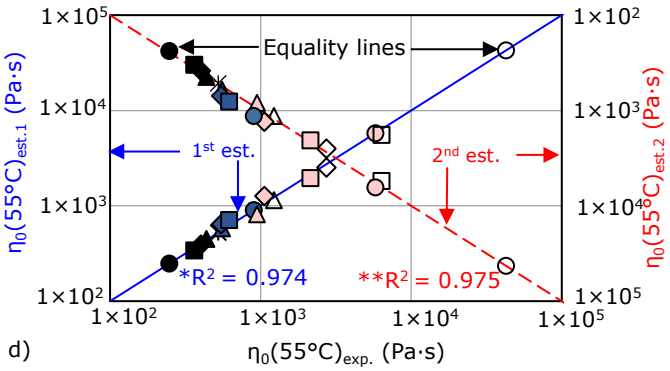

*R^2 was calculated for equality line without taking into consideration the results of pure fresh 50/70 binder, RAP binder and RAP + Rej blends (5 values/parameter) that are input data.

**R^2 was calculated for equality line without taking into consideration the results of pure fresh 50/70 binder, RAP binder and equivalent Rej properties (3 values/parameter) that are input data.

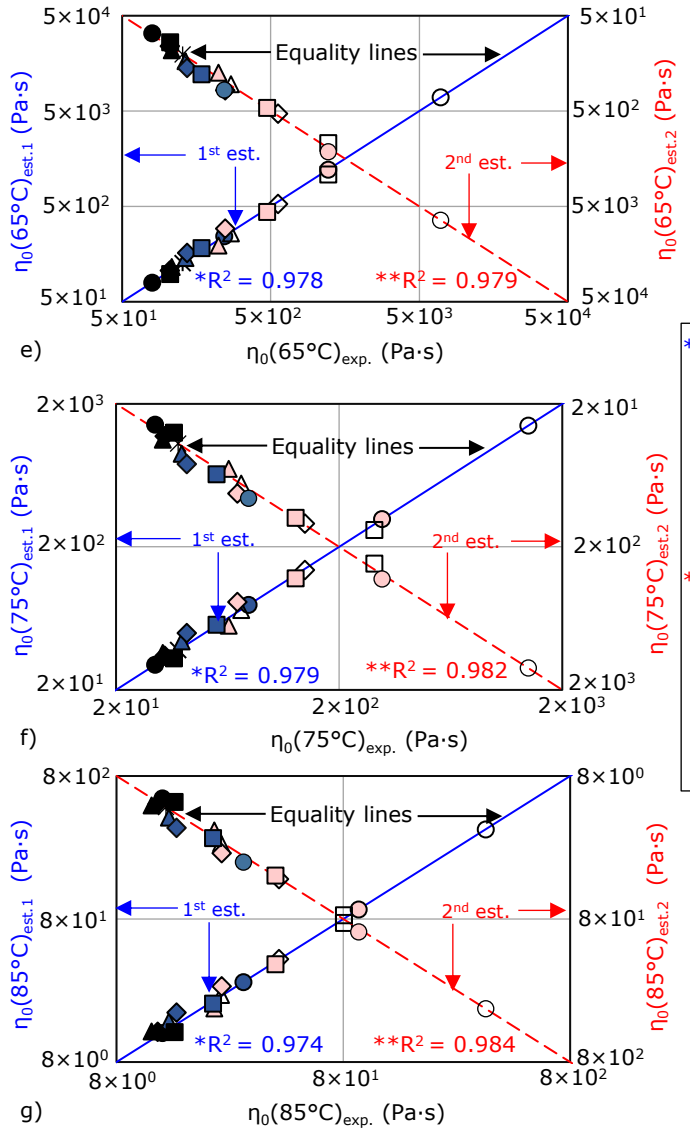

*R^2 was calculated for equality line without taking into consideration the results of pure fresh 50/70 binder, RAP binder and RAP + Rej blends (5 values/parameter) that are input data.

**R^2 was calculated for equality line without taking into consideration the results of pure fresh 50/70 binder, RAP binder and equivalent Rej properties (3 values/parameter) that are input data.

- 50/70
- RAP
- RAP + 5% Rej
- RAP + 10% Rej
- RAP + 15% Rej
- 50/70 + 25% RAP
- 50/70 + 25% RAP + 5% Rej
- 50/70 + 25% RAP + 10% Rej
- 50/70 + 25% RAP + 15% Rej
- 50/70 + 50% RAP
- 50/70 + 50% RAP + 5% Rej
- 50/70 + 50% RAP + 10% Rej
- 50/70 + 50% RAP + 15% Rej
- 50/70 + 75% RAP
- 50/70 + 75% RAP + 5% Rej
- 50/70 + 75% RAP + 10% Rej
- 50/70 + 75% RAP + 15% Rej
- Line of equality - 1st estimation
- Line of equality - 2nd estimation

Figure 2.27. Plots of estimated vs. experimental results of steady shear viscosity for all binder blends: (a) T=25°C; (b) T=35°C; (c) T=45°C; (d) T=55°C; (e) T=65°C; (f) T=75°C; (g) T=85°C.

The coefficient of determination R^2 was calculated for each plot with respect to the equality line.

In order to calculate R^2 for the 1st estimation approach, steady shear viscosity values were not taken into account for the base constituents: fresh 50/70 binder, RAP binder and the three RAP + Rej blends, for a total of five binders. Regarding the 2nd approach, R^2 was calculated without considering the steady shear viscosity values of the base constituents: fresh 50/70 binder, RAP binder and the 'temperature-independent constant content-viscosity couple' for the rejuvenator. These values are not considered because they correspond to input data, which are perfectly estimated.

As it could be observed in Figure 2.27, the estimated results $\eta_0(T)_{est.1\ blend}$ $\eta_0(T)_{est.2\ blend}$, of all binder blends are close to the corresponding experimental results. It can be noted that with the decrease of temperature from 85ºC to 25ºC R^2 values decrease but they are still satisfactory leading to R^2 values always higher than 0.960.

R^2 values obtained in the case of the 2nd estimation approach are always higher than 0.969, too and greater than the values obtained with the first approach. Considering the fair correlation with experimental points and the reduced number of input data necessary, the 2nd estimation approach can be considered more accurate than the first approach.

As a general comment, with the 2nd estimation approach a total of 105 η_0 values were estimated, at seven different temperatures for 15 blends, using as input data the experimental results of η_0 obtained at a reference temperature of 85ºC, $\eta_0(T_{ref} = 85°C)$, for fresh and RAP binders and the 'temperature-independent constant couple' for the rejuvenator.

Regarding the 1st estimation approach a total of 84 η_0 values were estimated, at seven different temperatures for 12 blends, using as input data the experimental results of η_0 obtained at a reference temperature of 85ºC, $\eta_0(T_{ref} = 85°C)$, for fresh and RAP binders and the blends of RAP and rejuvenator.

Global correlation plots between all these estimated values obtained by applying both estimation approaches and the experimental values are shown in Figure 2.28a (1st estimation approach, 12 blends) and Figure 2.28b (2nd estimation approach, 15 blends). A satisfactory global R^2 was found (0.977) for the estimations obtained with the 2nd estimation approach.

Slightly better correspondence was found between estimated η_0 values obtained with the 2nd estimation approach, which is an original input of this work, and experimental values. Thus, the R^2 values are always higher than those found with the 1st estimation approach, which is based on the classical log-log rule.

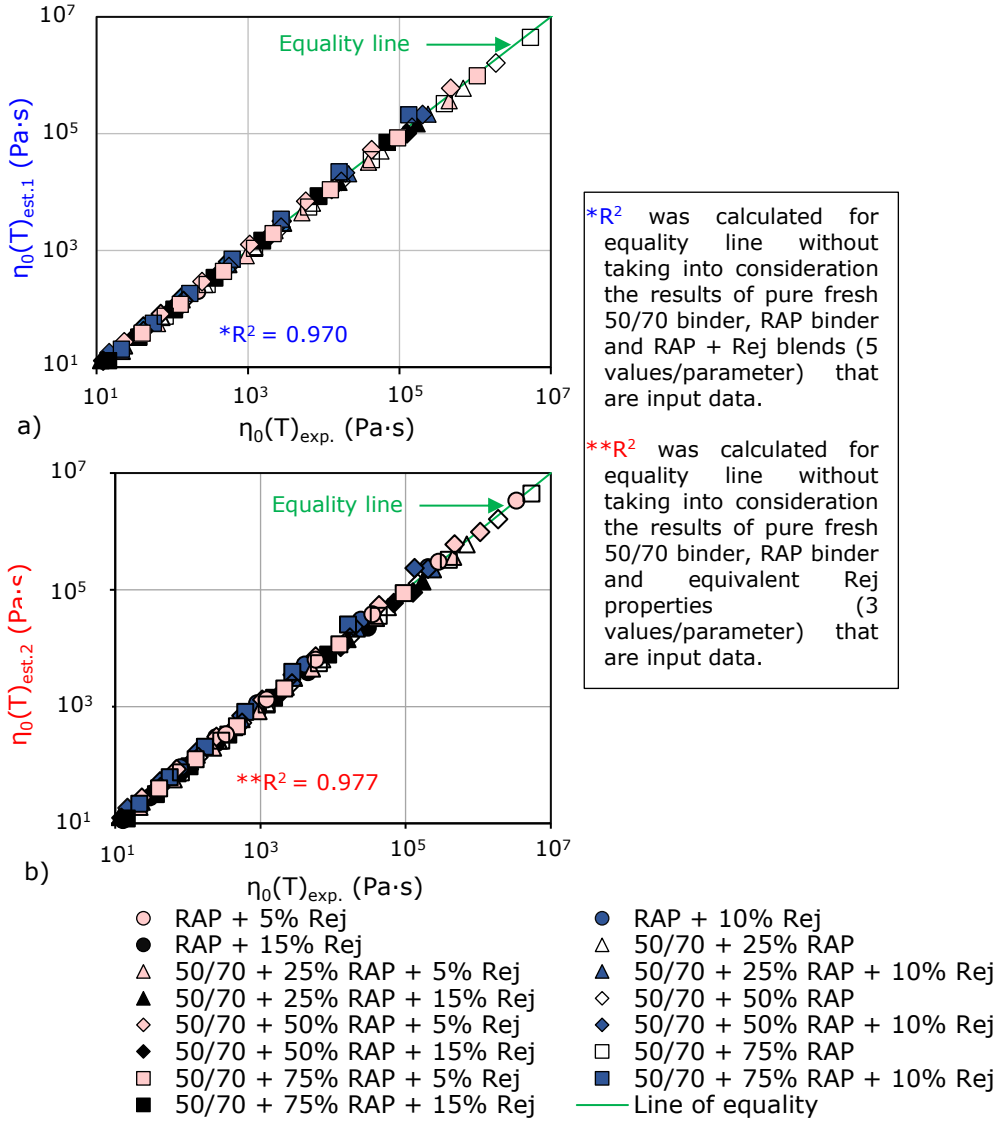

Figure 2.28. Global correlation plot of estimated vs. experimental results of $\eta_0(T)$ at temperatures from 85°C to 25°C for all binders: (a) 1st estimation approach; (b) 2nd estimation approach.

Table 2.18. Estimated values of steady shear viscosity at different temperatures from the 1st estimation approach for the 12 binder blends considered in this approach.

Blends	1st estimation						
	η_0 - Steady shear viscosity (Pa·s)						
	T = 25°C	T = 35°C	T = 45°C	T = 55°C	T = 65°C	T = 75°C	T = 85°C
50/70 + 25% RAP	6.01×10^{5}	5.06×10^{4}	6.48×10^{3}	1.15×10^{3}	2.60×10^{2}	7.23×10^{1}	2.36×10^{1}
50/70 + 25% RAP + 5% Rej	3.66×10^{5}	3.26×10^{4}	4.40×10^{3}	8.16×10^{2}	1.94×10^{2}	5.60×10^{1}	1.90×10^{1}
50/70 + 25% RAP + 10% Rej	2.17×10^{5}	2.07×10^{4}	2.96×10^{3}	5.79×10^{2}	1.44×10^{2}	4.36×10^{1}	1.54×10^{1}
50/70 + 25% RAP + 15% Rej	1.48×10^{5}	1.48×10^{4}	2.21×10^{3}	4.49×10^{2}	1.16×10^{2}	3.61×10^{1}	1.31×10^{1}
50/70 + 50% RAP	1.63×10^{6}	1.28×10^{5}	1.53×10^{4}	2.51×10^{3}	5.32×10^{2}	1.38×10^{2}	4.21×10^{1}
50/70 + 50% RAP + 5% Rej	6.02×10^{5}	5.29×10^{4}	6.99×10^{3}	1.27×10^{3}	2.93×10^{2}	8.23×10^{1}	2.72×10^{1}
50/70 + 50% RAP + 10% Rej	2.13×10^{5}	2.14×10^{4}	3.19×10^{3}	6.41×10^{2}	1.63×10^{2}	4.99×10^{1}	1.78×10^{1}
50/70 + 50% RAP + 15% Rej	1.01×10^{5}	1.11×10^{4}	1.80×10^{3}	3.90×10^{2}	1.06×10^{2}	3.46×10^{1}	1.30×10^{1}
50/70 + 75% RAP	4.45×10^{6}	3.27×10^{5}	3.62×10^{4}	5.52×10^{3}	1.09×10^{3}	2.63×10^{2}	7.52×10^{1}
50/70 + 75% RAP + 5% Rej	9.80×10^{5}	8.51×10^{4}	1.10×10^{4}	1.95×10^{3}	4.39×10^{2}	1.20×10^{2}	3.86×10^{1}
50/70 + 75% RAP + 10% Rej	2.10×10^{5}	2.22×10^{4}	3.42×10^{3}	7.06×10^{2}	1.83×10^{2}	5.69×10^{1}	2.05×10^{1}
50/70 + 75% RAP + 15% Rej	7.07×10^{4}	8.15×10^{3}	1.48×10^{3}	3.41×10^{2}	9.74×10^{1}	3.31×10^{1}	1.29×10^{1}

Table 2.19. Estimated values of steady shear viscosity at different temperatures from 2nd estimation approach for the 15 binder blends considered in this approach.

Blends	2nd estimation						
	η_0 – Steady shear viscosity (Pa·s)						
	T = 25°C	T = 35°C	T = 45°C	T = 55°C	T = 65°C	T = 75°C	T = 85°C
RAP + 5% Rej	3.37×10^{6}	3.03×10^{5}	3.84×10^{4}	6.41×10^{3}	1.34×10^{3}	3.36×10^{2}	9.85×10^{1}
RAP + 10% Rej	2.45×10^{5}	3.11×10^{4}	5.30×10^{3}	1.14×10^{3}	2.99×10^{2}	9.15×10^{1}	3.20×10^{1}
RAP + 15% Rej	2.25×10^{4}	3.90×10^{3}	8.71×10^{2}	2.37×10^{2}	7.62×10^{1}	2.79×10^{1}	1.14×10^{1}
50/70 + 25% RAP	6.01×10^{5}	5.06×10^{4}	6.48×10^{3}	1.15×10^{3}	2.60×10^{2}	7.23×10^{1}	2.36×10^{1}
50/70 + 25% RAP + 5% Rej	3.67×10^{5}	3.31×10^{4}	4.49×10^{3}	8.33×10^{2}	1.98×10^{2}	5.69×10^{1}	1.92×10^{1}
50/70 + 25% RAP + 10% Rej	2.24×10^{5}	2.16×10^{4}	3.11×10^{3}	6.06×10^{2}	1.50×10^{2}	4.48×10^{1}	1.56×10^{1}
50/70 + 25% RAP + 15% Rej	1.40×10^{5}	1.43×10^{4}	2.18×10^{3}	4.46×10^{2}	1.15×10^{2}	3.56×10^{1}	1.28×10^{1}
50/70 + 50% RAP	1.63×10^{6}	1.28×10^{5}	1.53×10^{4}	2.51×10^{3}	5.32×10^{2}	1.38×10^{2}	4.21×10^{1}
50/70 + 50% RAP + 5% Rej	6.04×10^{5}	5.43×10^{4}	7.26×10^{3}	1.32×10^{3}	3.03×10^{2}	8.48×10^{1}	2.77×10^{1}
50/70 + 50% RAP + 10% Rej	2.29×10^{5}	2.35×10^{4}	3.52×10^{3}	7.02×10^{2}	1.76×10^{2}	5.29×10^{1}	1.85×10^{1}
50/70 + 50% RAP + 15% Rej	9.07×10^{4}	1.06×10^{4}	1.76×10^{3}	3.84×10^{2}	1.04×10^{2}	3.37×10^{1}	1.25×10^{1}
50/70 + 75% RAP	4.45×10^{6}	3.27×10^{5}	3.62×10^{4}	5.52×10^{3}	1.09×10^{3}	2.63×10^{2}	7.52×10^{1}
50/70 + 75% RAP + 5% Rej	9.81×10^{5}	8.83×10^{4}	1.16×10^{4}	2.06×10^{3}	4.62×10^{2}	1.25×10^{2}	3.97×10^{1}
50/70 + 75% RAP + 10% Rej	2.35×10^{5}	2.56×10^{4}	3.97×10^{3}	8.11×10^{2}	2.06×10^{2}	6.21×10^{1}	2.17×10^{1}
50/70 + 75% RAP + 15% Rej	5.98×10^{4}	7.84×10^{3}	1.42×10^{3}	3.33×10^{2}	9.49×10^{1}	3.18×10^{1}	1.22×10^{1}

2.8 Estimation of complex shear modulus

The steps followed to estimate the complex shear modulus of all binder blends for each of the two considered estimation methods are described in Figure 2.29.

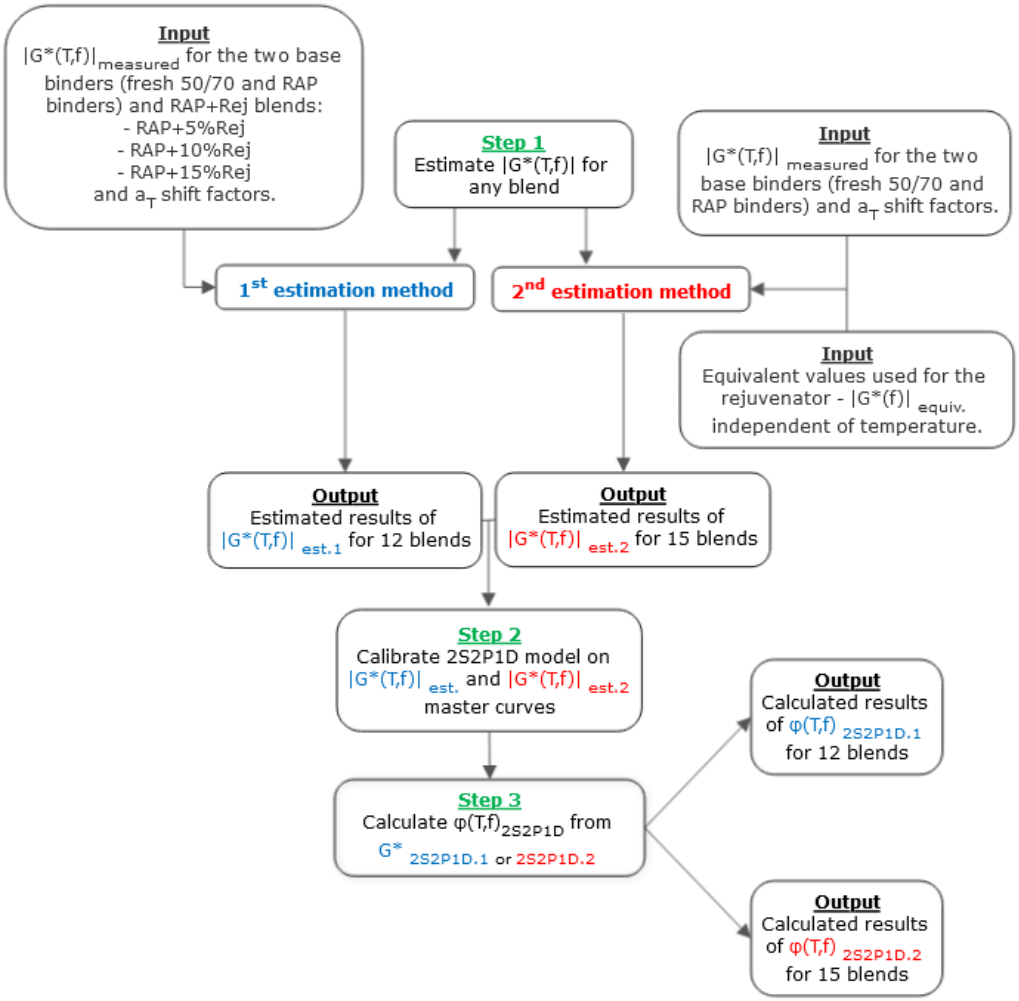

Figure 2.29. Different steps to estimate the complex shear modulus of all binder blends for each of the two considered estimation methods.

It must be mentioned that a part of this analysis was presented by the author in a conference paper Forton et al., 2020 [182].

In Section 2.7.1, steady shear viscosity (equation 2.14) was defined as a ratio between the norm of complex shear modulus $\left(\left|G^*\right|\right)$ and the angular frequency (ω). It was shown in Section 2.7.2 that values of steady shear viscosity of a blend can be successfully estimated by using a logarithmic rule from experimentally determined values of the base constituents. Both estimation approaches are based on the same hypothesis, shown in equation 2.19, which supposes that the steady shear viscosity

of a blend $\left(\eta_{0\ blend\ AB}\right)$ can be estimated as a function of the steady shear viscosity of base constituents $\left(\eta_{0\ A}, \eta_{0\ B}\right)$, known from experimental results, and their concentrations (a, b).

$$log\,\eta_{0\ blend\ AB} = a \cdot log\,\eta_{0\ A} + b \cdot log\,\eta_{0\ B} \tag{2.19}$$

Considering equation 2.14, the equation 2.19 can be written as:

$$log\frac{\left|G^*\right|_{blend\ AB}}{\omega} = a \cdot log\frac{\left|G^*\right|_{A}}{\omega} + b \cdot log\frac{\left|G^*\right|_{B}}{\omega} \quad with\ a+b=1 \tag{2.20}$$

Therefore, values of the norm of complex shear modulus of the produced binder blends can be estimated from the values of base constituents by using the two approaches (1st estimation expressed in equation 2.21, respectively, 2nd estimation expressed in equation 2.22):

$$log\left|G^*(T,f)\right|_{blend\ est.1} = a \cdot log\left|G^*(T,f)\right|_{50/70} + (1-a) \cdot log\left|G^*(T,f)\right|_{RAP+Rej} \tag{2.21}$$

$$\begin{aligned} log\left|G^*(T,f)\right|_{blend\ est.2} = {} & a \cdot log\left|G^*(T,f)\right|_{50/70} + b \cdot log\left|G^*(T,f)\right|_{RAP} + \\ & + b \cdot r \cdot log\left|G^*(T,f)\right|_{Rej} \end{aligned} \tag{2.22}$$

where:

- $\left|G^*(T,f)\right|_{50/70}$, $\left|G^*(T,f)\right|_{RAP}$ and $\left|G^*(T,f)\right|_{RAP+Rej}$ are the values of the norm of complex shear modulus at the same temperature, T and frequency, f obtained respectively for the fresh 50/70 binder, the RAP binder and the blend of RAP binder and rejuvenator;
- $\left|G^*(T,f)\right|_{Rej}$ are the equivalent values of the norm of complex shear modulus obtained for the rejuvenator;
- $\left|G^*(T,f)\right|_{blend\ est.1}$ and $\left|G^*(T,f)\right|_{blend\ est.2}$ are the estimated values of the norm of complex shear modulus (at the same temperature T and frequency f) for any of the analysed blends according to the proposed approach 1st or 2nd estimation;
- a *and* b are the relative mass concentrations of the base binders fresh binder and RAP binder and r is the percentage of the rejuvenator by the mass of RAP binder.

As shown in Section 2.7.2 a 'temperature-independent constant content-viscosity couple' for the rejuvenator was considered (35% Rej; 0.038 MPa).

Starting from this principle, in Figure 2.30 a similar analysis as in case of the steady shear viscosity was performed (for three test frequency: 0.1 Hz, 1.29 Hz and 10 Hz, the measurements of $\left|G^*\right|$ at different temperatures for RAP + Rej blends are

plotted as a function of the rejuvenator content). Similar plots are shown in Appendix 1 for the other frequencies in Figure A1.54. A similar remark can be made as in the case of $\eta_0(T)_{(Rej)}$: satisfactory R^2 values were obtained when considering that all lines intersect a unique point: 35% Rej content and $\left|G^*(f)\right|_{equiv.}$.

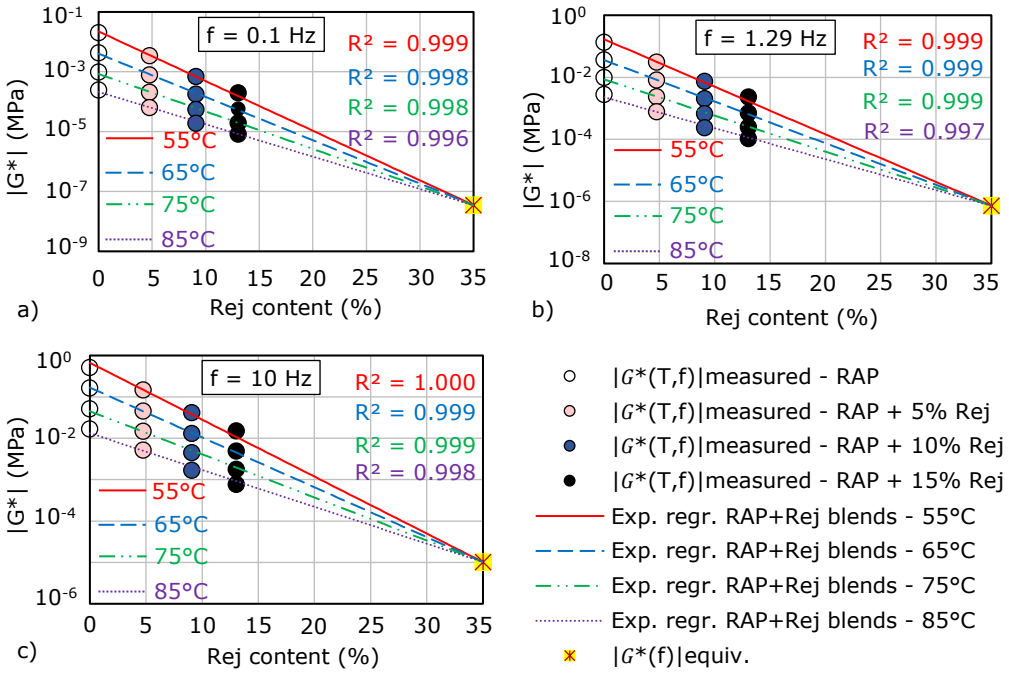

Figure 2.30. Norm of complex shear modulus measurements for the RAP + Rej blends at 0.1 Hz, 1.29 Hz and 10 Hz frequencies and $\left|G^*(f)\right|_{equiv.}$ values which are only dependent on frequency obtained by linear extrapolation for a value of 35% content Rej: (a) f=0.1 Hz; (b) f=1.29 Hz; (c) f=10.0 Hz.

These results led to the idea of a $\left|G^*(f)\right|_{equiv.}$ temperature independent constant, dependent only on frequency, for the rejuvenator which is expressed in equation 2.23.

$$log\left|G^*(T,f)\right|_{Rej} = \frac{log\left|G^*(f)\right|_{35\%\ Rej}}{0.35} - \frac{0.65}{0.35} log\left|G^*(T,f)\right|_{RAP} \qquad (2.23)$$

$\left|G^*(f)\right|_{equiv.}$ values which are dependent only on frequency obtained by linear extrapolation for a value of 35% rejuvenator content are represented as a function of the angular frequency in Figure 2.31a. Then, steady shear viscosity was determined for the rejuvenator equivalent values in Figure 2.31b, where it could be observed that

the equivalent values obtained are asymptotical to the temperature-independent constant content-viscosity couple when the angular frequency tends to 0.

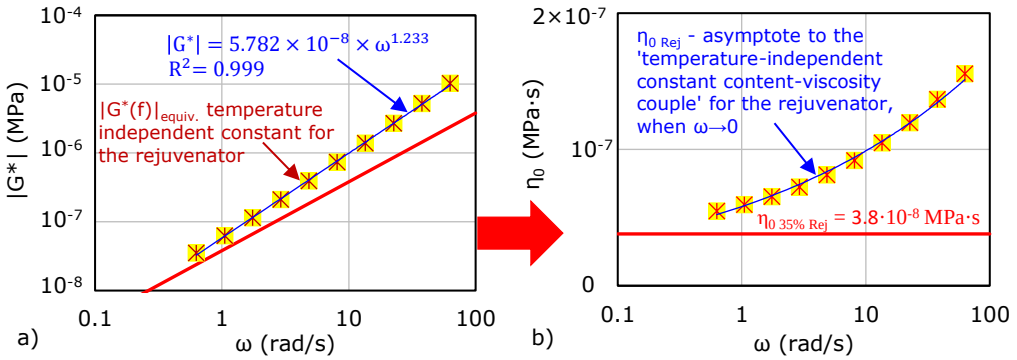

Figure 2.31. (a) $\left|G^*(f)\right|_{equiv.}$ values which are only dependent on frequency obtained by linear extrapolation for a value of 35% rejuvenator content; (b) steady shear viscosity determination for the rejuvenator equivalent values – asymptotical to the 'temperature-independent constant content-viscosity couple' when the angular frequency tends to 0.

Correlation plots of estimated vs. experimental values of $\left|G^*(T,f)\right|$ for each binder blend were built in order to highlight the validity of the proposed estimation approaches. As an example, Figure 2.32 shows the correlation plots for the blend 50/70 + 50% RAP + 10% Rej. Similar plots are reported in Appendix 1 for all binders (Figures A1.55 – A1.66).

A global correlation plot of estimated vs. the measurements of $\left|G^*(T,f)\right|$ for the blends of fresh and RAP binders and rejuvenator, with respect to each estimation method (1st estimation – 12 blends, 2nd estimation – 15 blends), is reported in Figure 2.33 by applying 1st and 2nd estimation method.

Moreover, similar correlation plots were built for each frequency test in order to highlight the imprecision of each considered estimation method. Figure 2.34 shows three examples for the frequencies 0.1Hz, 1.29 Hz and 10 Hz. Similar plots are shown for the other test frequencies in Figure A1.67 – A1.68 – Appendix 1.

The coefficient of determination R^2 for the two approaches were calculated with respect to the equality line, where: for the 1st estimation method the results for the base constituents as fresh 50/70 binder, RAP binder and the three RAP + Rej blends, for a total of five binders and for the 2nd estimation method the results for the fresh 50/70 binder, RAP binder and the 'frequency dependent constant' for the rejuvenator were not taken into account.

As it could be observed, the estimated values of $\left|G^*(T,f)\right|$ obtained by applying both estimation methods are significantly close to the measured values for all binder blends. A higher global value of R^2, determined with respect to the equality line, was found with the 1st estimation (0.987) than with the second one (0.968).

From the individual correlation plots for each binder blend (Figure 2.32 and Figures A1.55 – A1.66 – Appendix 1) it was observed that a better estimation of

$|G^*(T,f)|$ was obtained with the 2nd method for the blends produced with low rejuvenator content and RAP binder content. For the blends produced with 75% RAP binder and different amounts of rejuvenator and the blends produced only with RAP binder and rejuvenator, a better estimation was obtained with the first method.

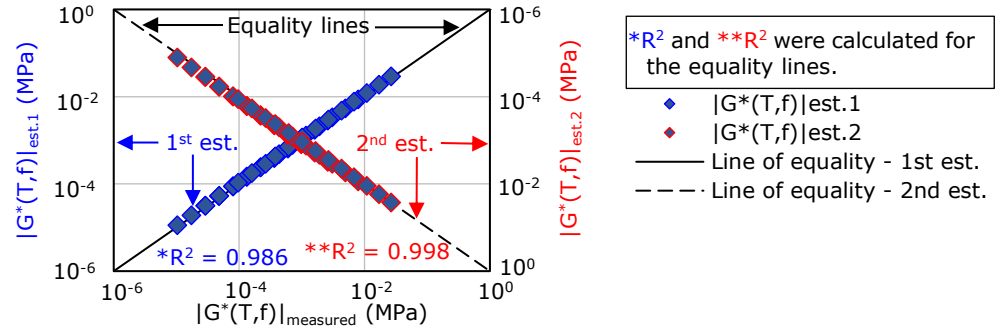

Figure 2.32. Correlation plot of estimated vs. measured $|G^*(T,f)|$ values for the binder blend 50/70 + 50% RAP + 10% Rej.

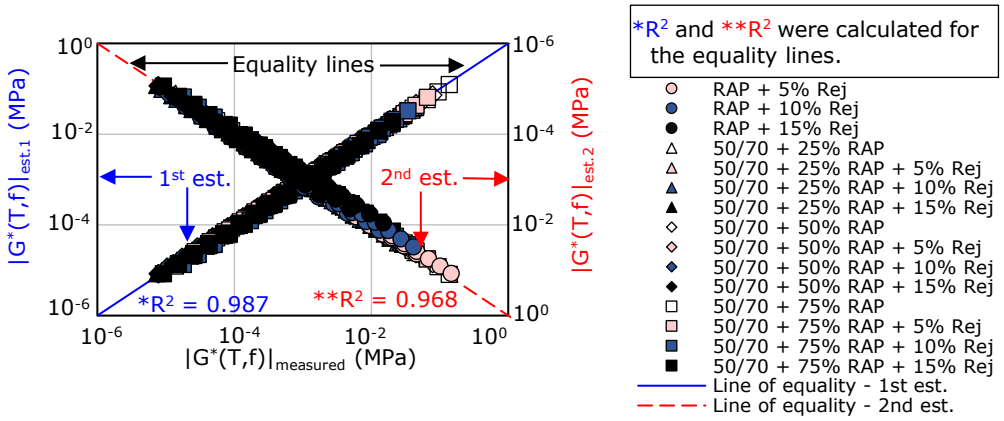

Figure 2.33. Global correlation plots of estimated vs. measured $|G^*(T,f)|$ values for all considered binder blends.

Moreover, in Figure 2.34 and Figures A1.67 – A1.68 – Appendix 1 it could be observed that for frequencies lower than 1.0 Hz a better correlation was obtained with the 2nd estimation method. On the contrary, for frequencies higher that 1.0 Hz a better correlation was obtained with the 1st estimation method. On the other side, R^2 values are increasing from 0.954 to 0.986, with the increase of frequency for the 1st estimation. A reverse tendency was observed for the second estimation, where R^2 values are decreasing from 0.981 to 0.966 with the increase of frequency.

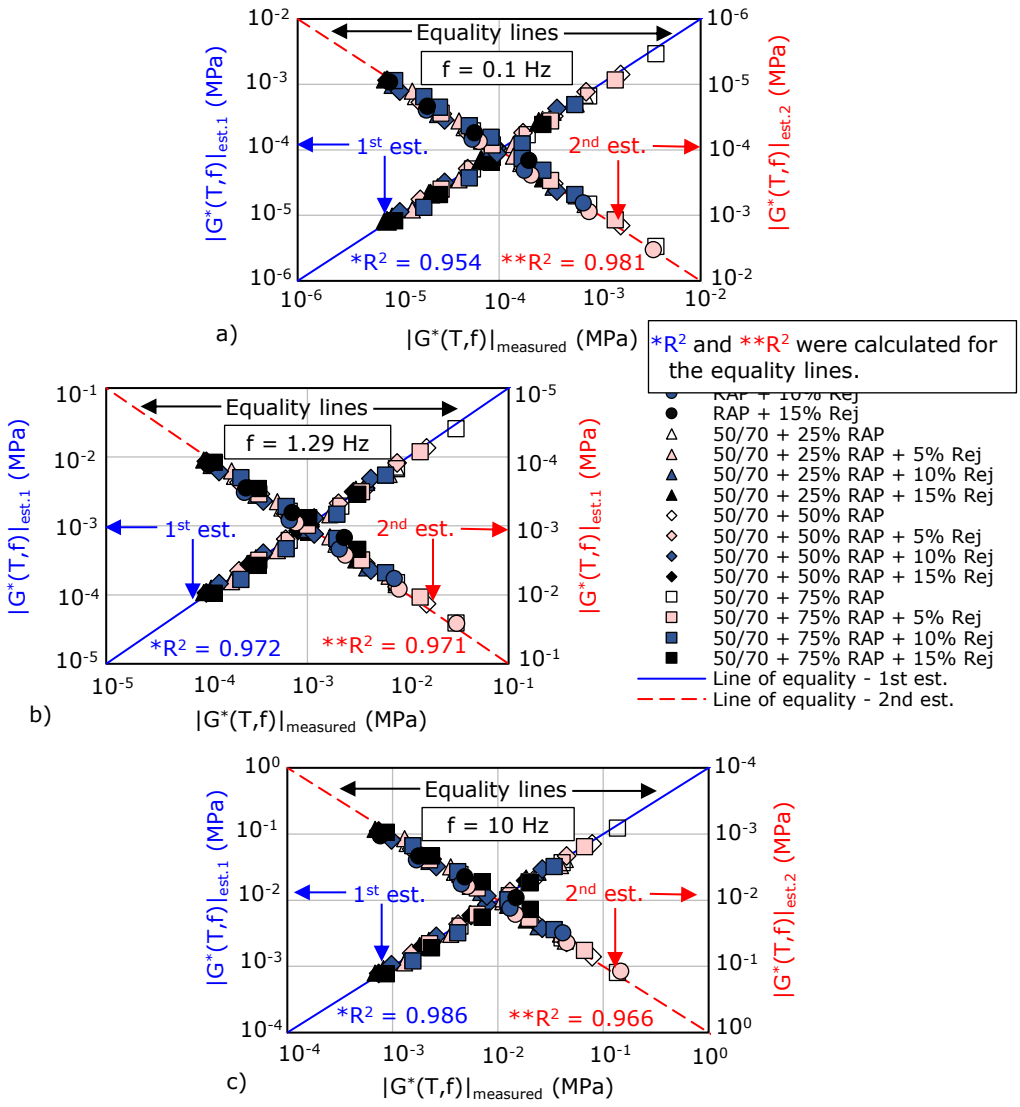

Figure 2.34. Global correlation plots of estimated vs. measured $\left|G^*(T,f)\right|$ values for all considered binder blends at different frequencies: (a) f=0.1 Hz; (b) f=1.29 Hz; (c) f=10.0 Hz.

In order to highlight the accuracy of each estimation method the errors (%) between $\left|G^*(T,f)\right|_{measured}$ and $\left|G^*(T,f)\right|_{est.1}$ or $\left|G^*(T,f)\right|_{est.2}$ were plotted in Figure 2.35 as a function of the measured values for all considered binder blends.

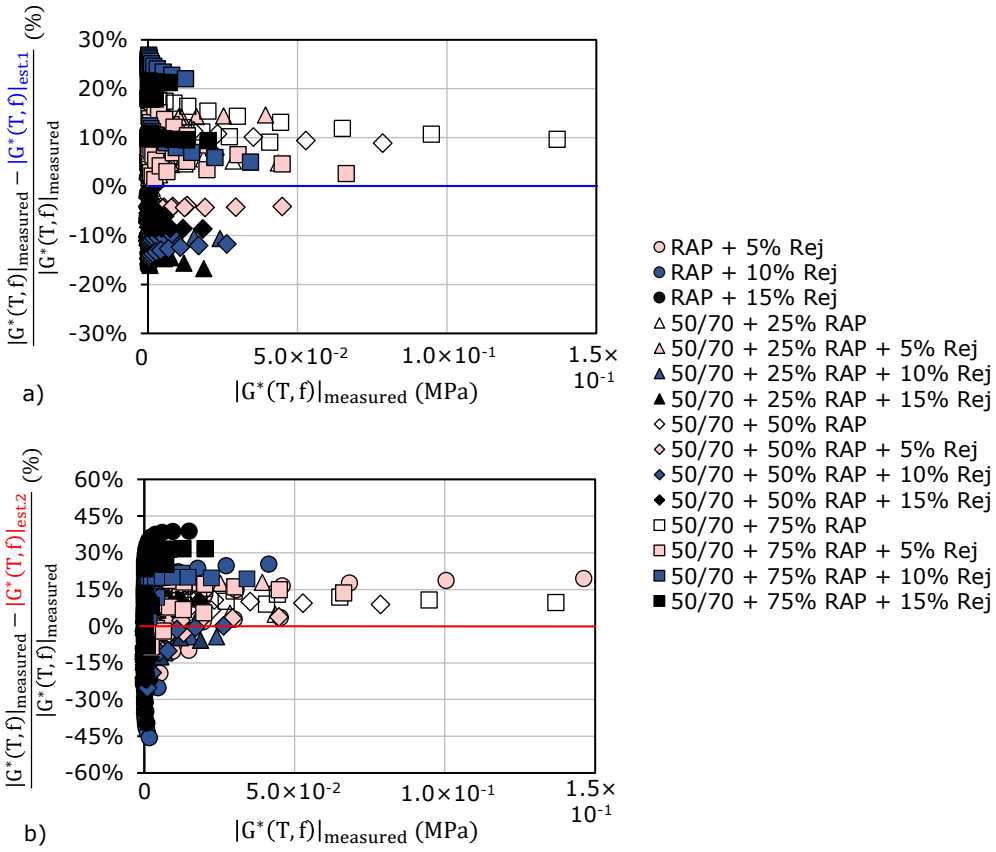

Figure 2.35. (a) Error between $|G^*(T,f)|_{measured}$ and $|G^*(T,f)|_{est.1}$ as a function of $|G^*(T,f)|_{measured}$; (b) Error between $|G^*(T,f)|_{measured}$ and $|G^*(T,f)|_{est.2}$ as a function of $|G^*(T,f)|_{measured}$.

It could be observed that the maximum errors between $|G^*(T,f)|_{measured}$ and $|G^*(T,f)|_{est.1}$ is approximatively 28%. On the other side, the errors between $|G^*(T,f)|_{measured}$ and $|G^*(T,f)|_{est.2}$ are higher than in the first estimation, approximatively -48%. In the second estimation method the higher errors were obtained for the blend produced only with RAP and rejuvenator. However, the second approach presents the advantage related to the required input data as it requires less input data than the first approach.

It must be mentioned that the estimation approaches used to obtain $\left|G^*(T,f)\right|_{est.1\ or\ 2}$ values cannot be applied for the phase angle. Therefore, it was proposed a new approach in order to obtain phase angle values of all binder blends over the whole frequency and temperature domain, starting from the hypothesis that all analysed binders are considered thermorheologically simple and they are in the LVE domain. For this purpose, the 2S2P1D model (Section 1.5.3) was used.

The overall procedure used to determine $\varphi(T,f)$ is shown in Figure 2.29. To summarize: the 2S2P1D model was calibrated on the master curves of $\left|G^*(T,f)\right|_{est.1}$ and $\left|G^*(T,f)\right|_{est.2}$ and then the vales of phase angle were calculated from $G^*_{2S2P1D.1\ or\ 2S2P1D.2}$. In order to obtain the master curves of the $\left|G^*(T,f)\right|_{est.1\ or\ 2}$, the time–temperature superposition principle was applied to obtain temperature shift factors [122], [174], [178], [179]. Values of a_T shift factors and WLF constants for all considered binder blends depending on each estimation method used, are reported in Table 2.20 and Table 2.21.

Table 2.20. a_T temperature shift factors and WLF constants for all binder blends for which 1st estimation is applied.

Binders	a_T (-)			WLF constants	
	65ºC	75ºC	85ºC	C1	C2
50/70 + 25% RAP	2.20×10^{-1}	6.41×10^{-2}	2.11×10^{-2}	8.91	129.26
50/70 + 25% RAP + 5% Rej	2.31×10^{-1}	7.00×10^{-2}	2.40×10^{-2}	8.47	126.61
50/70 + 25% RAP + 10% Rej	2.39×10^{-1}	7.50×10^{-2}	2.61×10^{-2}	8.17	125.13
50/70 + 25% RAP + 15% Rej	2.47×10^{-1}	7.85×10^{-2}	2.87×10^{-2}	7.94	123.64
50/70 + 50% RAP	2.13×10^{-1}	5.54×10^{-2}	1.71×10^{-2}	9.69	134.31
50/70 + 50% RAP + 5% Rej	2.23×10^{-1}	6.25×10^{-2}	2.16×10^{-2}	9.03	130.00
50/70 + 50% RAP + 10% Rej	2.43×10^{-1}	7.33×10^{-2}	2.55×10^{-2}	8.22	125.41
50/70 + 50% RAP + 15% Rej	2.51×10^{-1}	8.00×10^{-2}	2.95×10^{-2}	7.68	120.07
50/70 + 75% RAP	2.00×10^{-1}	4.90×10^{-2}	1.43×10^{-2}	10.29	137.17
50/70 + 75% RAP + 5% Rej	2.21×10^{-1}	6.20×10^{-2}	2.00×10^{-2}	9.40	135.68
50/70 + 75% RAP + 10% Rej	2.52×10^{-1}	7.58×10^{-2}	2.64×10^{-2}	8.72	135.68
50/70 + 75% RAP + 15% Rej	2.58×10^{-1}	8.30×10^{-2}	3.20×10^{-2}	8.42	135.71

Table 2.21. a_T temperature shift factors and WLF constants for all binder blends for which 2nd estimation is applied.

Binders	a_T (-)			WLF constants	
	65ºC	75ºC	85ºC	C1	C2
RAP + 5% Rej	2.20×10^{-1}	6.10×10^{-2}	1.85×10^{-2}	9.82	139.95
RAP + 10% Rej	3.20×10^{-1}	1.08×10^{-2}	4.20×10^{-2}	7.48	134.69
RAP + 15% Rej	3.00×10^{-1}	1.02×10^{-2}	4.10×10^{-2}	7.40	130.06
50/70 + 25% RAP	2.20×10^{-1}	6.41×10^{-2}	2.11×10^{-2}	8.91	129.26
50/70 + 25% RAP + 5% Rej	2.29×10^{-1}	6.90×10^{-2}	2.40×10^{-2}	8.56	127.39
50/70 + 25% RAP + 10% Rej	2.38×10^{-1}	7.60×10^{-2}	2.80×10^{-2}	8.11	124.96
50/70 + 25% RAP + 15% Rej	2.48×10^{-1}	8.10×10^{-2}	3.10×10^{-2}	7.72	121.38
50/70 + 50% RAP	2.13×10^{-1}	5.54×10^{-2}	1.71×10^{-2}	9.69	134.31
50/70 + 50% RAP + 5% Rej	2.26×10^{-1}	6.50×10^{-2}	2.33×10^{-2}	7.94	113.83
50/70 + 50% RAP + 10% Rej	2.52×10^{-1}	8.10×10^{-2}	2.95×10^{-2}	7.17	111.20
50/70 + 50% RAP + 15% Rej	3.00×10^{-1}	1.01×10^{-1}	3.90×10^{-2}	7.10	126.99
50/70 + 75% RAP	2.00×10^{-1}	4.90×10^{-2}	1.43×10^{-2}	10.29	137.17
50/70 + 75% RAP + 5% Rej	2.29×10^{-1}	6.60×10^{-2}	2.30×10^{-2}	9.17	132.80
50/70 + 75% RAP + 10% Rej	2.90×10^{-1}	8.78×10^{-2}	3.40×10^{-2}	8.54	130.20
50/70 + 75% RAP + 15% Rej	3.24×10^{-1}	1.20×10^{-1}	4.58×10^{-2}	7.31	138.38

As example, master curves of $\left|G^*(T,f)\right|_{est.1\ or\ 2}$ at a reference temperature of 55°C and temperature shift factors vs. temperature and WLF curves of blends produced with fresh binder and 50% RAP and different dosages of rejuvenator: 0% and 15% Rej, are shown in Figure 2.36.

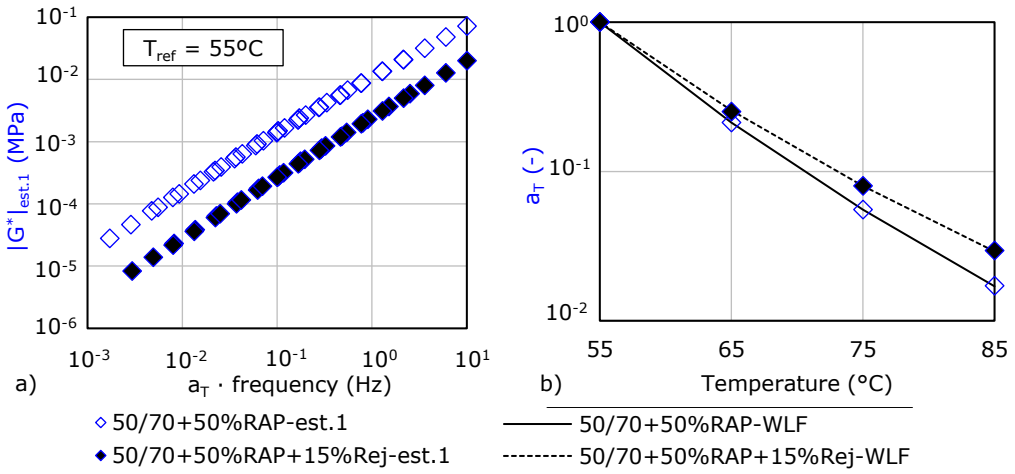

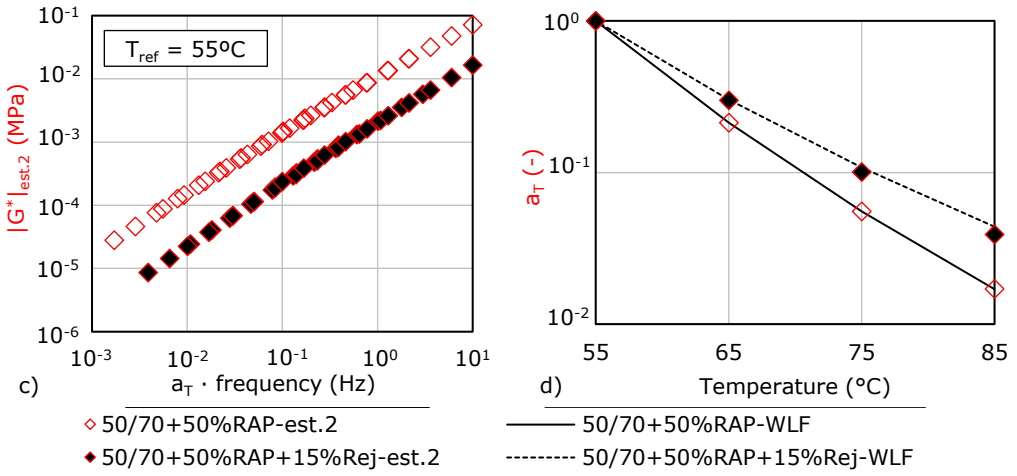

Figure 2.36. Blends produced with fresh binder and 50% RAP and different dosages (0% and 15% Rej) of rejuvenator: (a) master curves of $\left|G^*(T,f)\right|_{est.1}$; (b) temperature shift factors and WLF curves for the 1st estimation; (c) master curves of $\left|G^*(T,f)\right|_{est.2}$; (d) temperature shift factors and WLF curves for the 2nd estimation.

The 2S2P1D model was fitted on the isotherms and master curves of $\left|G^*(T,f)\right|_{est.1\ or\ 2}$ at $T_{ref} = 55°C$. The same approach as in Section 2.6.2 was used, considering constant values for G_{00}, G_0, k *and* δ. Values of 2S2P1D parameters for the considered binder blends following the estimated values of $\left|G^*(T,f)\right|_{est.1\ or\ 2}$ are reported in Table 2.22 and Table 2.23.

Therefore, equation 2.24 was used in order to calculate phase angle values corresponding to the 2S2P1D model fitted on $\left|G^*(T,f)\right|_{est.1\ or\ 2}$ values.

$$\varphi(T,f)_{2S2P1D} = atan\left(\frac{\delta(\omega\tau)^{-k}\,sin\left(\frac{k\pi}{2}\right)+(\omega\tau)^{-h}\,sin\left(\frac{h\pi}{2}\right)+(\omega\beta\tau)^{-1}}{1+\delta(\omega\tau)^{-k}\,cos\left(\frac{k\pi}{2}\right)+(\omega\tau)^{-h}\,cos\left(\frac{h\pi}{2}\right)}\right) \quad (2.24)$$

where:

- ω is the pulsation;
- τ is the characteristic time, a function of temperature and accounting for time temperature superposition principle;
- δ, k *and* h are dimensionless constants and β is a dimensionless parameter related to Newtonian viscosity η.

Table 2.22. 2S2P1D parameters for all binder blends considered in the 1st estimation.

Binders	G_{00} = 0 MPa	G_0 = 980 MPa	k = 0.25	δ = 4.30	h (-)	β (-)	τ (s)
50/70 + 25% RAP					0.626	166	7.58×10^{-9}
50/70 + 25% RAP + 5% Rej					0.629	151	6.04×10^{-9}
50/70 + 25% RAP + 10% Rej					0.633	136	4.90×10^{-9}
50/70 + 25% RAP + 15% Rej					0.636	126	4.12×10^{-9}
50/70 + 50% RAP					0.632	222	1.19×10^{-8}
50/70 + 50% RAP + 5% Rej					0.630	171	7.90×10^{-9}
50/70 + 50% RAP + 10% Rej					0.636	148	5.15×10^{-9}
50/70 + 50% RAP + 15% Rej					0.638	128	3.62×10^{-9}
50/70 + 75% RAP					0.620	296	2.03×10^{-8}
50/70 + 75% RAP + 5% Rej					0.626	202	1.05×10^{-8}
50/70 + 75% RAP + 10% Rej					0.634	161	5.30×10^{-9}
50/70 + 75% RAP + 15% Rej					0.640	130	3.30×10^{-9}

Table 2.23. 2S2P1D parameters for all binder blends considered in the 2nd estimation.

Binders	G_{00} = 0 MPa	G_0 = 980 MPa	k = 0.25	δ = 4.30	h (-)	β (-)	τ (s)
RAP + 5% Rej					0.614	354	1.89×10^{-8}
RAP + 10% Rej					0.650	195	6.01×10^{-9}
RAP + 15% Rej					0.647	130	2.48×10^{-9}
50/70 + 25% RAP					0.626	166	7.58×10^{-9}
50/70 + 25% RAP + 5% Rej					0.630	150	5.80×10^{-9}
50/70 + 25% RAP + 10% Rej					0.633	135	4.77×10^{-9}
50/70 + 25% RAP + 15% Rej					0.636	123	3.90×10^{-9}
50/70 + 50% RAP					0.632	222	1.19×10^{-8}
50/70 + 50% RAP + 5% Rej					0.626	175	7.91×10^{-9}
50/70 + 50% RAP + 10% Rej					0.632	146	4.80×10^{-9}
50/70 + 50% RAP + 15% Rej					0.638	120	3.30×10^{-9}
50/70 + 75% RAP					0.620	296	2.03×10^{-8}
50/70 + 75% RAP + 5% Rej					0.635	210	9.80×10^{-9}
50/70 + 75% RAP + 10% Rej					0.639	166	4.80×10^{-9}
50/70 + 75% RAP + 15% Rej					0.645	126	2.60×10^{-9}

Figure 2.37 shows an example of how $\varphi(T,f)$ were obtained from the optimization of 2S2P1D model on the $\left|G^*(T,f)\right|_{est.1}$ and $\left|G^*(T,f)\right|_{est.2}$ values and the plots between the experimental vs. determined values of $\varphi(T,f)$ for the 50/70 + 50% RAP + 10% Rej blend. Similar plots are reported in Appendix 1 for all binders (Figures A1.69 – A1.79).

A global plot of calculated vs. measured values of $\varphi(T,f)$ for all considered blends, according to the proposed methods of estimation i.e. 1st estimation – 12 blends, 2nd estimation – 15 blends, is reported in Figure 2.38. R^2 values were calculated for the two correlations with respect to the equality line. In order to highlight the accuracy of each calculation the errors between $\varphi(T,f)_{measured}$ and $\varphi(T,f)_{2S2P1D.1\ or\ 2S2P1D.2}$ were plotted in Figure 2.39 as a function of the measured values for all considered binder blends.

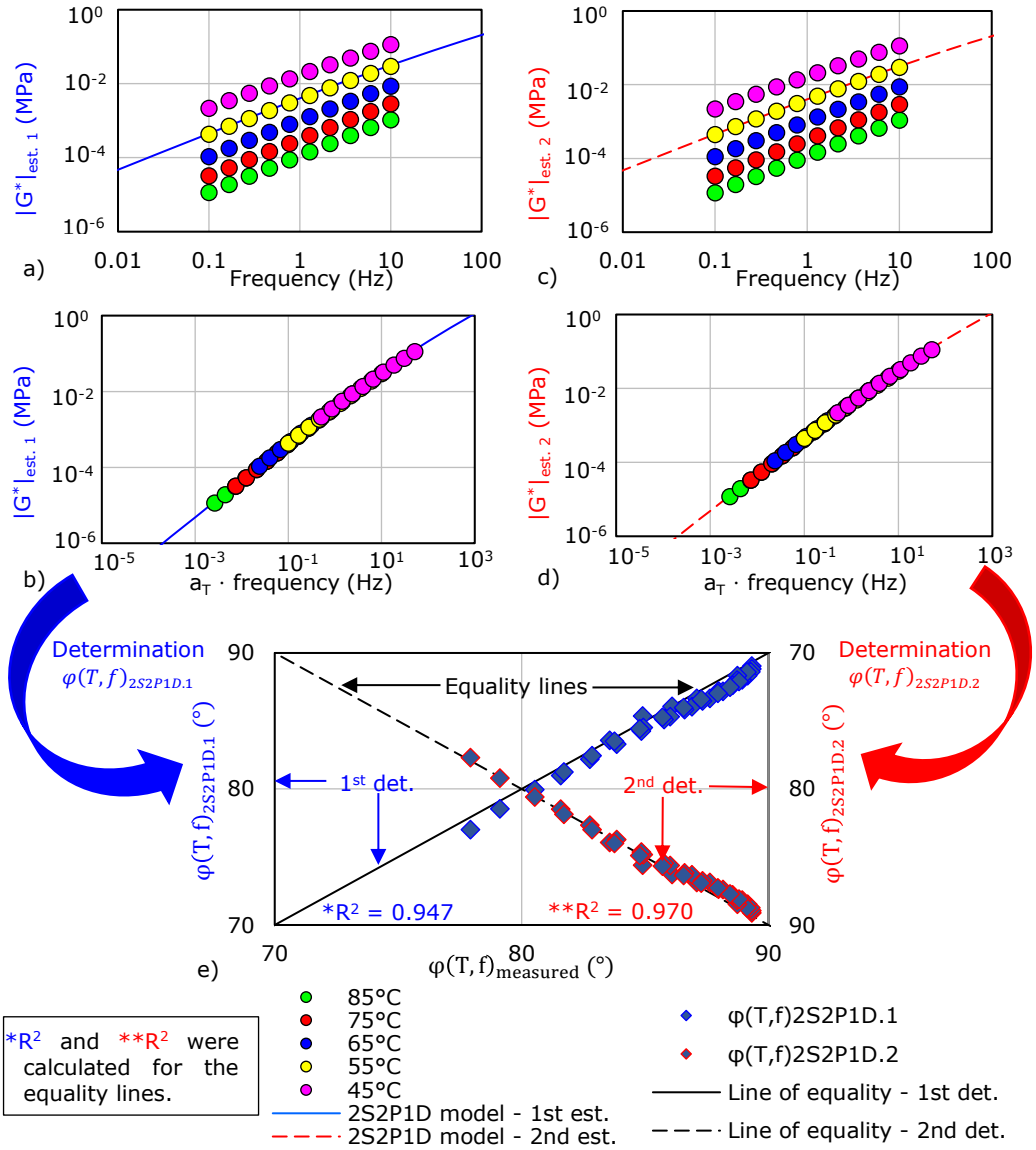

Figure 2.37. Determination of $\varphi(T,f)_{2S2P1D.1\ or\ 2S2P1D.2}$ values for the 50/70 + 50% RAP + 10% Rej blend: (a) isotherms of $\left|G^*(T,f)\right|_{est.1}$ and 2S2P1D optimization; (b) master curve of $\left|G^*(T,f)\right|_{est.1}$ and 2S2P1D optimization; (c) isotherms of $\left|G^*(T,f)\right|_{est.2}$ and 2S2P1D optimization; (d) master curve of $\left|G^*(T,f)\right|_{est.2}$ and 2S2P1D optimization; (e) plots of measured vs. calculated values of $\varphi(T,f)$.

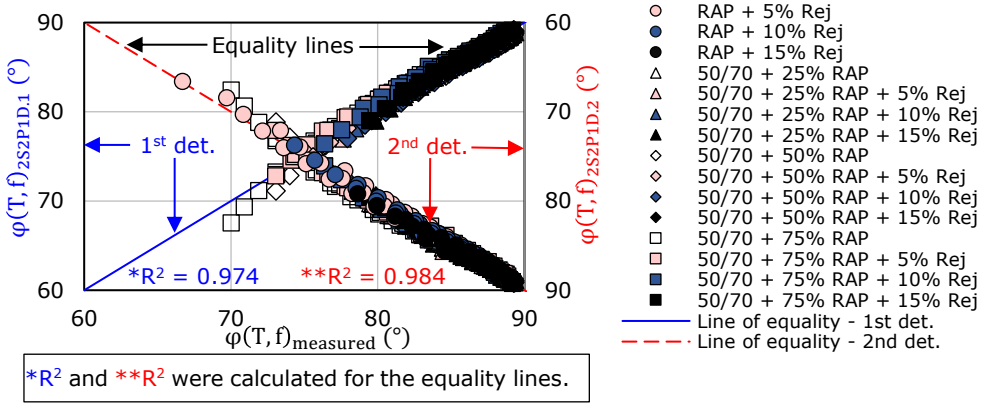

Figure 2.38. Global plot of measured vs. calculated values of $\varphi(T,f)$ for all the blends according to the proposed approaches (1st determination – 12 blends, 2nd determination – 15 blends).

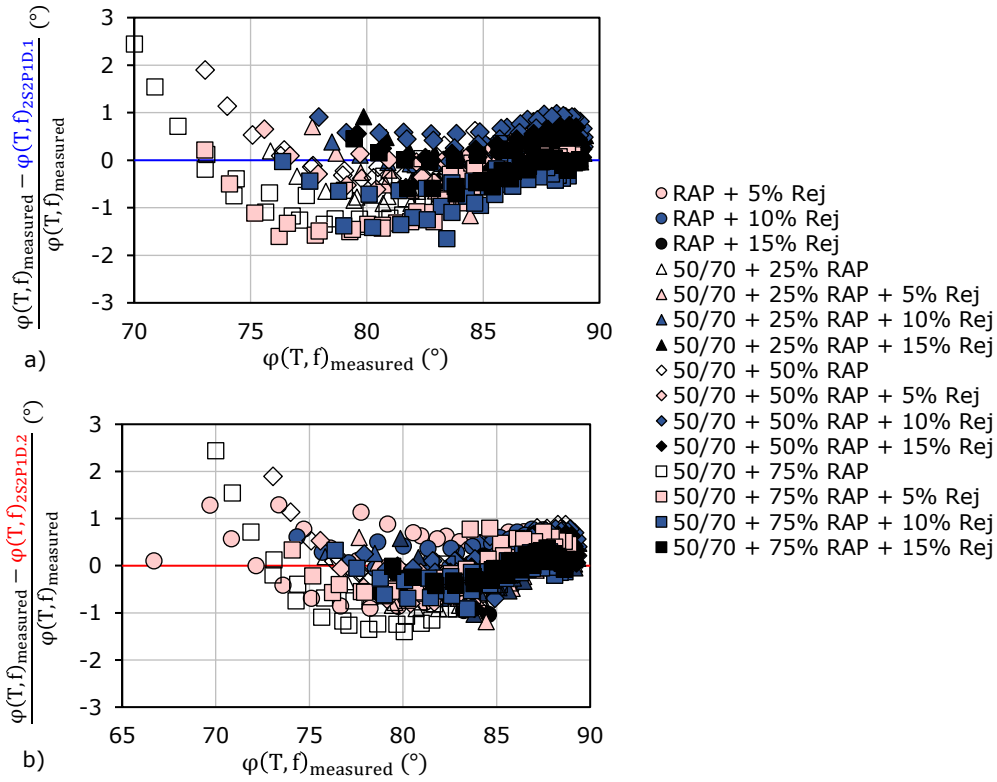

Figure 2.39. (a) Error between $\varphi(T,f)_{measured}$ and $\varphi(T,f)_{2S2P1D.1}$ as a function of $\varphi(T,f)_{measured}$; (b) Error between $\varphi(T,f)_{measured}$ and $\varphi(T,f)_{2S2P1D.2}$ as a function of $\varphi(T,f)_{measured}$.

Moreover, similar plots to the global one (Figure 2.38) were built in order to highlight the imprecision of each considered estimation method for each frequency test. Figure 2.40 shows three examples for the frequencies 0.1Hz, 1.29 Hz and 10 Hz. Similar plots are shown for the other test frequencies in Figures A1.80 – A1.81 – Appendix 1.

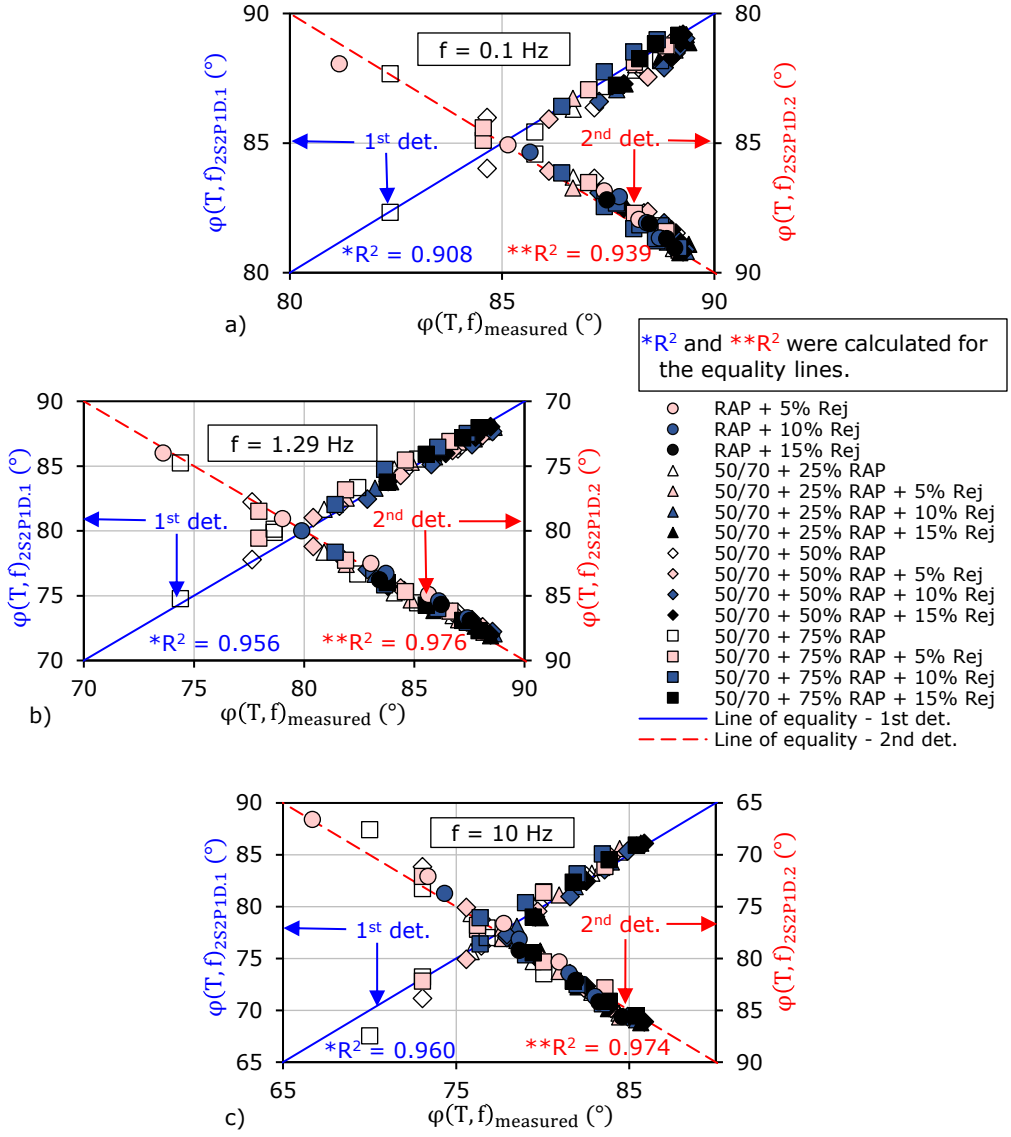

Figure 2.40. Global plots of calculated vs. measured $\varphi(T,f)$ values for all considered binder blends at different frequencies: (a) f=0.1 Hz; (b) f=1.29 Hz; (c) f=10.0 Hz.

As it can be observed, the determined values of $\varphi(T,f)$ obtained from the 2S2P1D model fitted on the estimated values of $|G^*(T,f)|$, are significantly close to the measured values for all binder blends. A higher global value of R^2 was found with the 2nd approach (0.984) than with the first one (0.974).

From the individual correlation plots for each binder blend (Figure 2.43 and Figures A1.89 – A1.99 – Appendix 1) it was observed that a better approximation was obtained for the $\varphi(T,f)_{2S2P1D.2}$ for all the binder blends with the exception for two blends: 50/70 + 25% RAP + 10% Rej and 50/70 + 50% RAP + 15% Rej. However, the difference between R^2 values obtained for these blends is not significant.

Moreover, for the blends produced without rejuvenator it could be observed that with the increase of the RAP binder content the accuracy of the estimation is decreasing (R^2 values are decreasing). The maximum errors between $\varphi(T,f)_{measured}$ and $\varphi(T,f)_{2S2P1D.1}$ or $\varphi(T,f)_{2S2P1D.2}$ is approximatively 2.5°.

From Figure 2.40 and Figures A1.80 – A1.81 – Appendix 1 it could be observed that for all frequencies a better correlation with the measurements was obtained for the $\varphi(T,f)_{2S2P1D.2}$.

Due to the satisfactory values of R^2 that were found, this approach can be considered valid for the tested blends. However, a better correlation with the experimental measurements was found for the phase angle values calculated from the 2S2P1D fitted on the $|G^*(T,f)|_{est.2}$ values.

2.9 Analysis of BBR test results

BBR tests were performed on all binder blends in order to determine the flexural creep stiffness, $S(t)$, and the *m-value,* $m(t)$ by using equations 2.3 and 2.4 presented in Section 2.3.3.

As it could be observed in Table 2.5 all binders were tested at the temperature of -15°C. As an example, in order to highlight the influence of the RAP binder and rejuvenator contents on the behaviour by means of stiffness and m-values, all tested binders at -15°C, values of $S(t)$ and $m(t)$ obtained at the loading time of 60s were plotted as a function of the RAP binder content in Figures 2.42a – 2.42b. In Figure 2.41c values of $S(60s)$ were plotted as a function of $m(60s)$.

As it can be observed, values of flexural creep stiffness $S(60s)$ increase with the increase of RAP binder content and decrease with the increase of rejuvenator content within blends. On the other side, the increase of RAP binder and rejuvenator contents leads to the opposite tendencies of $m(60s)$ values. The effect of the rejuvenator proves to counterbalance this tendency, as it could be observed from the change of slope of regressions in Figure 2.41 for different rejuvenator contents. Moreover, $S(60s)$ and $m(60s)$ values show linear relationships with the RAP binder content for the blends produced with the same amount of rejuvenator (0%, 5%, 10%

and 15% by mass of RAP binder). Linear regressions were performed and R^2 values were determined for each regression resulting values always higher than 0.961.

Figure 2.41c shows the relation between $S(60s)$ and $m(60s)$ of all binders at -15°C. An exponential regression was performed on these data and a good R^2 value of 0.977 was found.

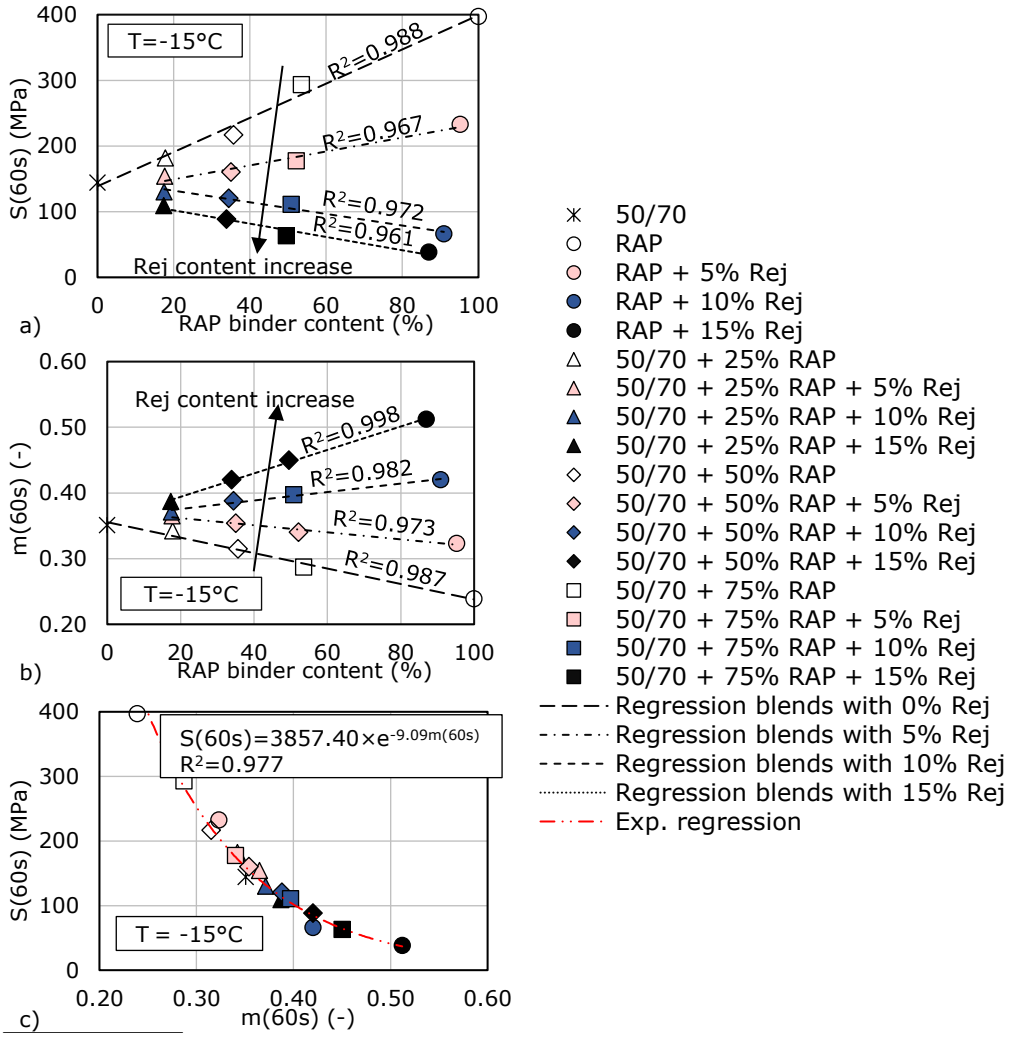

Figure 2.41. BBR test results for all the blends at -15°C: (a) $S(60s)$ values as a function of RAP binder content; (b) $m(60s)$ values as a function of RAP binder content; (c) $S(60s)$ vs. $m(60s)$.

2.10 Analysis of the high and low critical temperatures

2.10.1 Determination of DSR high critical temperature

As previously described, complex shear modulus tests were performed on all binders by using a DSR apparatus at seven temperatures and at ten frequencies. Test conditions are detailed in Table 2.3.

The determination of the DSR high critical temperatures, the experimental results and the estimation of these temperatures was presented in one publication which was accepted for publication Forton et al., 2021 [183]. With respect to this article, only slight modifications have been made.

The procedure used to calculate $T_{DSR\ high\ critical}$ is shown in Figure 2.42.

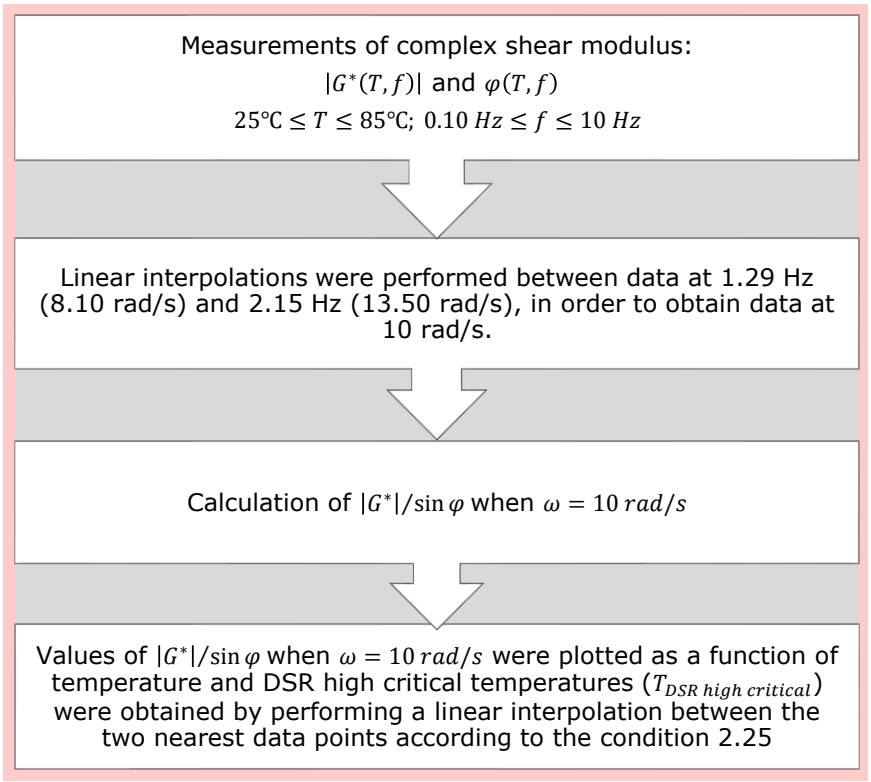

Figure 2.42. Overall description of the procedure used to determine $T_{DSR\ high\ critical}$

Performed tests and analysis are in agreement with the overall Superpave framework but some minor differences in the analysis of test results were applied to obtain the high critical temperatures of the tested binders.

High critical temperatures for all tested binders were determined considering the condition 2.25 from AASHTO T315-10 [184] for unaged binders.

$T_{DSR\ high\ critical}$ determined when $\left|G^*\right|/\sin\varphi = 1.0\ KPa$, when $\omega = 10\ rad/s$ (2.25)

Since the exact frequency corresponding to 10 rad/s (1.59 Hz) was not used in tests a linear interpolation was performed between data at 1.29 Hz (8.10 rad/s) and 2.15 Hz (13.50 rad/s), in order to obtain data at 10 rad/s. Values of $\left|G^*\right|/sin\varphi = 1.0\ kPa$ when $\omega = 10\ rad/s$ were plotted as a function of temperature, and high critical temperatures were obtained according to the condition 2.25.

Figure 2.43 shows an example of how the high critical temperature was obtained for the binder blend 50/70 + 75% RAP + 5% Rej. The same analysis was performed for all the tested binders and shown in Figure A1.82 to Figure A1.97 reported in Appendix 1.

It must be mentioned that the high critical temperature of the RAP binder was extrapolated by performing a linear regression of the values of $\left|G^*\right|/sin\varphi$ for $\omega = 10\ rad/s$ at temperatures from 25°C to 85°C since this material is an aged binder and its $T_{DSR\ high\ critical}$ value is higher than the highest test temperature (85°C). Values of $T_{DSR\ high\ critical}$ for all binder blends are reported in Table 2.24.

In order to highlight the influence of the RAP binder and the rejuvenator on the behaviour of all binder blends, $T_{DSR\ high\ critical}$ values were plotted as a function of the RAP binder content (Figure 2.44).

Table 2.24. Experimental results for all tested binders: DSR high critical temperatures.

Binders	$T_{DSR\ high\ critical}$ (ºC)
50/70	67.30
RAP	92.80
RAP + 5% Rej	84.70
RAP + 10% Rej	73.90
RAP + 15% Rej	64.40
50/70 + 25% RAP	73.10
50/70 + 25% RAP + 5% Rej	72.30
50/70 + 25% RAP + 10% Rej	67.80
50/70 + 25% RAP + 15% Rej	65.00
50/70 + 50% RAP	78.40
50/70 + 50% RAP + 5% Rej	72.90
50/70 + 50% RAP + 10% Rej	68.40
50/70 + 50% RAP + 15% Rej	65.00
50/70 + 75% RAP	83.60
50/70 + 75% RAP + 5% Rej	77.70
50/70 + 75% RAP + 10% Rej	71.70
50/70 + 75% RAP + 15% Rej	66.20

As it can be observed, values of $T_{DSR\ high\ critical}$ increase with the increase of RAP binder content and decrease with the increase of rejuvenator content within blends. Moreover, $T_{DSR\ high\ critical}$ shows a linear relationship with the RAP binder content for the blends produced with the same amount of rejuvenator: 0%, 5%, 10% and 15% by mass of the RAP binder. Linear regressions were performed and R^2 values were determined for each regression. For the blends produced with 15% of

rejuvenator by mass of the RAP binder, the R^2 value of 0.095 is not meaningful since the $T_{DSR\ high\ critical}$ values of all blends remain approximately constant for all RAP binder contents. It seems that the 15% Rej amount is the limit dosage.

It is interesting to notei that, probably, the blends produced with more than 15% Rej become softer with increasing RAP binder content. This possible trend can be explained by the fact that rejuvenator content is calculated with respect to RAP binder content and also by the fact that the 15% Rej amount seems to be the limit dosage.

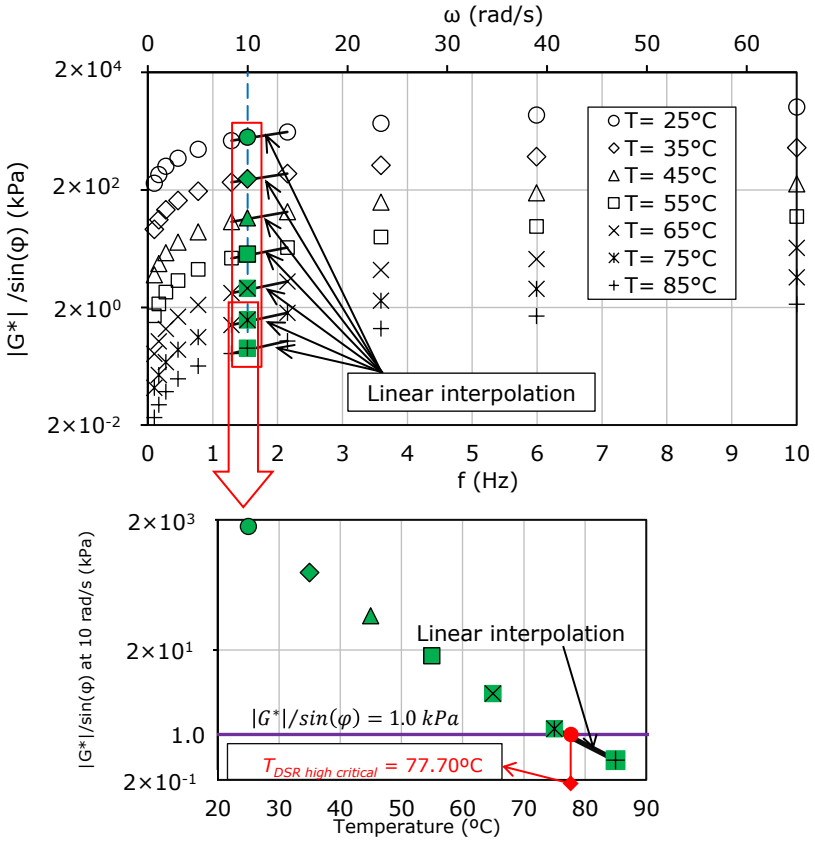

Figure 2.43. $T_{DSR\ high\ critical}$ determination from complex shear modulus test results for 50/70 + 75% RAP + 5% Rej blend.

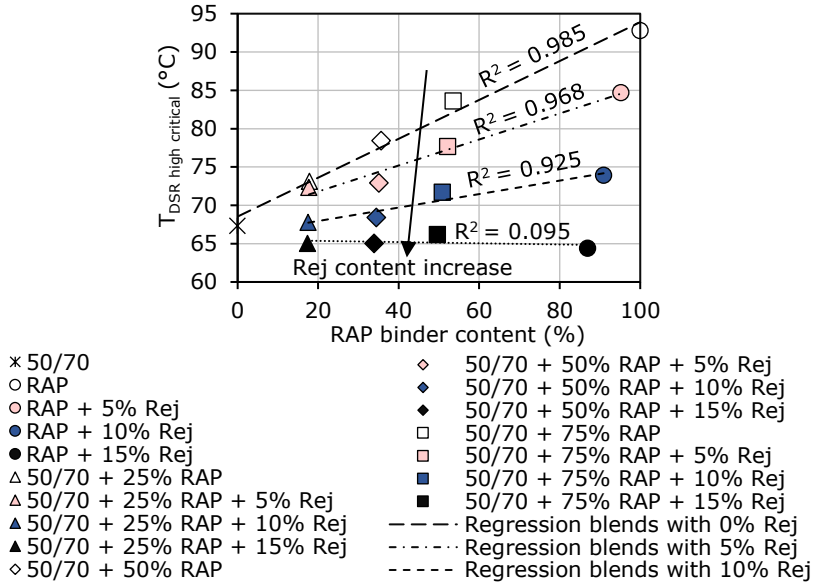

Figure 2.44. DSR high critical temperatures for all binders as a function of RAP binder content.

With respect to values of $T_{DSR\ high\ critical}$, the increase of the rejuvenator content within blends has the opposite effect of the increase of RAP binder, thus $T_{DSR\ high\ critical}$ decreases for increasing rejuvenator content. This observation suggests the possibility to balance the effect of RAP binder on $T_{DSR\ high\ critical}$ of blends with rejuvenator.

For simplicity in the following sections the values of $T_{DSR\ high\ critical}$ determined for all blends from experimental tests as described so far are referred to as 'experimental'.

2.10.2 Determination of BBR low critical temperature

The determination of the BBR low critical temperatures, the experimental results and the estimation of these temperatures was presented in one publication which was accepted for publication Forton et al., 2021 [183]. With respect to this article, only slight modifications have been made.

The most common parameters obtained from the BBR test results are the 'low critical temperatures' which in accordance with the American Standards are used for the binder classification (low PG temperature).

Performed tests and analysis are in agreement with the overall Superpave framework but some minor differences in the analysis of test results were applied to obtain the considered critical temperatures of the tested binders. Even if the critical temperatures are similar, but not equal to the two Superpave critical temperatures, the developed new approach can most probably be applied with success to Superpave values. The procedure used to calculate $T_{BBR\ low\ critical}$ is shown in Figure 2.45.

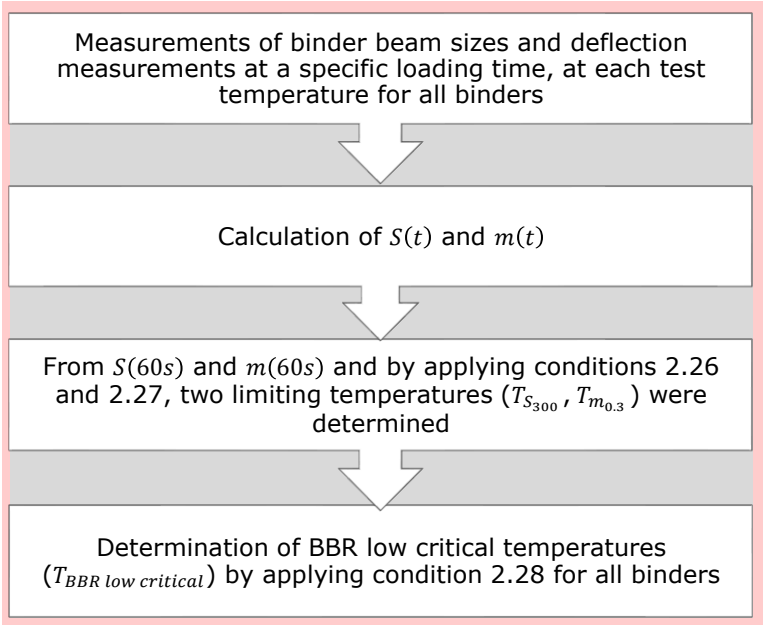

Figure 2.45. Overall description of the procedure used to determine $T_{BBR\ low\ critical}$.

The $S(t)$ and $m(t)$ were plotted as a function of the loading time (t, in s) for all test temperatures. From $S(t)$ and $m(t)$ values at the loading time of 60s, two limiting temperatures were obtained corresponding to the temperature at which $S(60s) = 300\ MPa$ and the temperature at which $m(60s) = 0.300$ respectively, as shown in equations 2.26 and 2.27.

$$S(60s) = 300\ MPa \rightarrow T_{S_{300}} \tag{2.26}$$

$$m(60s) = 0.300 \rightarrow T_{m_{0.3}} \tag{2.27}$$

Values of $S(60s)$ and $m(60s)$ were plotted as a function of temperature. The limiting temperatures were obtained by performing a linear interpolation between the two nearest data points to the conditions 2.26 and 2.27.

The BBR low critical temperature $(T_{BBR\ low\ critical})$ was defined as the highest value between the above mentioned two temperatures $T_{S_{300}}$ and $T_{m_{0.3}}$:

$$T_{BBR\ low\ critical} = max\left(T_{S_{300}}; T_{m_{0.3}}\right) \tag{2.28}$$

According to AASHTO MP1-a [185], the low PG critical temperature $(T_{PG\ low\ critical})$ is 10°C lower than the above mentioned $T_{BBR\ low\ critical}$. However, if the creep stiffness is below 300 MPa, the direct tension test is not required.

It must be mentioned that BBR tests were performed only on the original binders without aging process. The direct tensile test (DTT) was not performed. Therefore, in this work the analysis and the estimations were performed for the $T_{BBR\ low\ critical}$ values obtained only by applying the conditions 2.26, 2.27 and 2.28. Therefore, the analysed temperature is called $T_{BBR\ low\ critical}$ and is not the Superpave low critical temperature.

Figure 2.46 show an example of how $T_{BBR\ low\ critical}$ was obtained for the blend 50/70 + 50% RAP + 10% Rej. The same analysis was performed for all the tested binders (Figures A1.98 – A1.113 – Appendix 1).

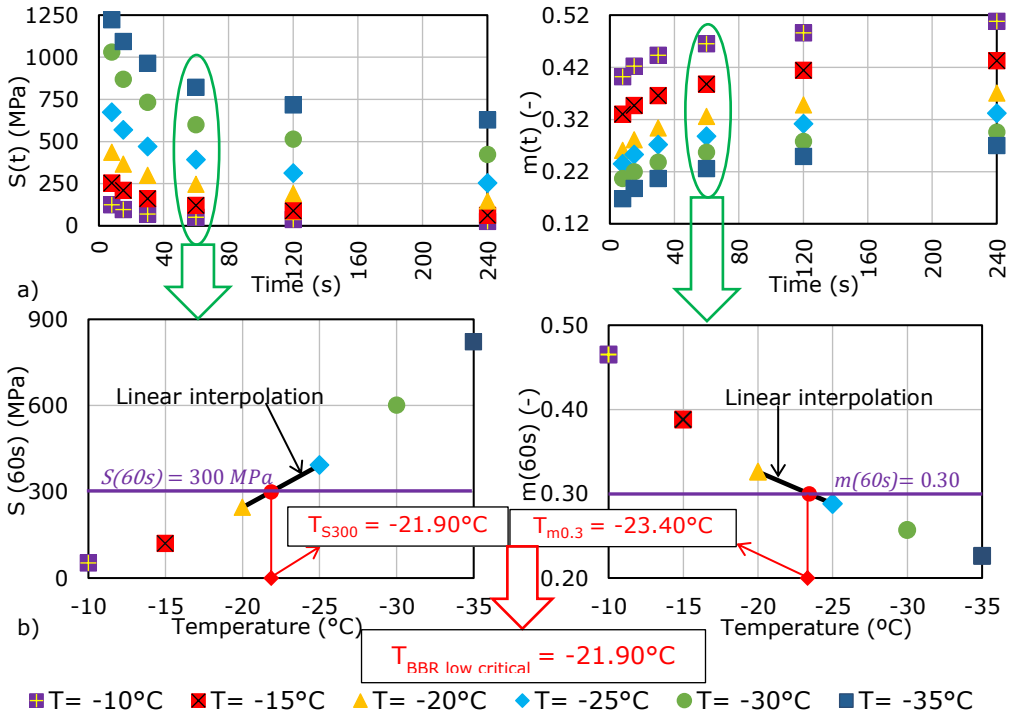

Figure 2.46. BBR test results for the blend 50/70 + 50% RAP +10% Rej: (a) flexural creep stiffness (left) and m-value (right) as a function of time; (b) determination of the limiting low temperatures: $T_{S_{300}}$ (left), $T_{m_{0.3}}$ (right) and $T_{BBR\ low\ critical}$.

In order to highlight the influence of the RAP binder and rejuvenator content on the behaviour at low temperatures of all binders, $T_{S_{300}}$, $T_{m_{0.3}}$ and $T_{BBR\ low\ critical}$ values were plotted as a function of the RAP binder content in Figure 2.47a - 2.47c. Values of $T_{S_{300}}$, $T_{m_{0.3}}$ and $T_{BBR\ low\ critical}$ of all tested binders are reported in Table 2.25.

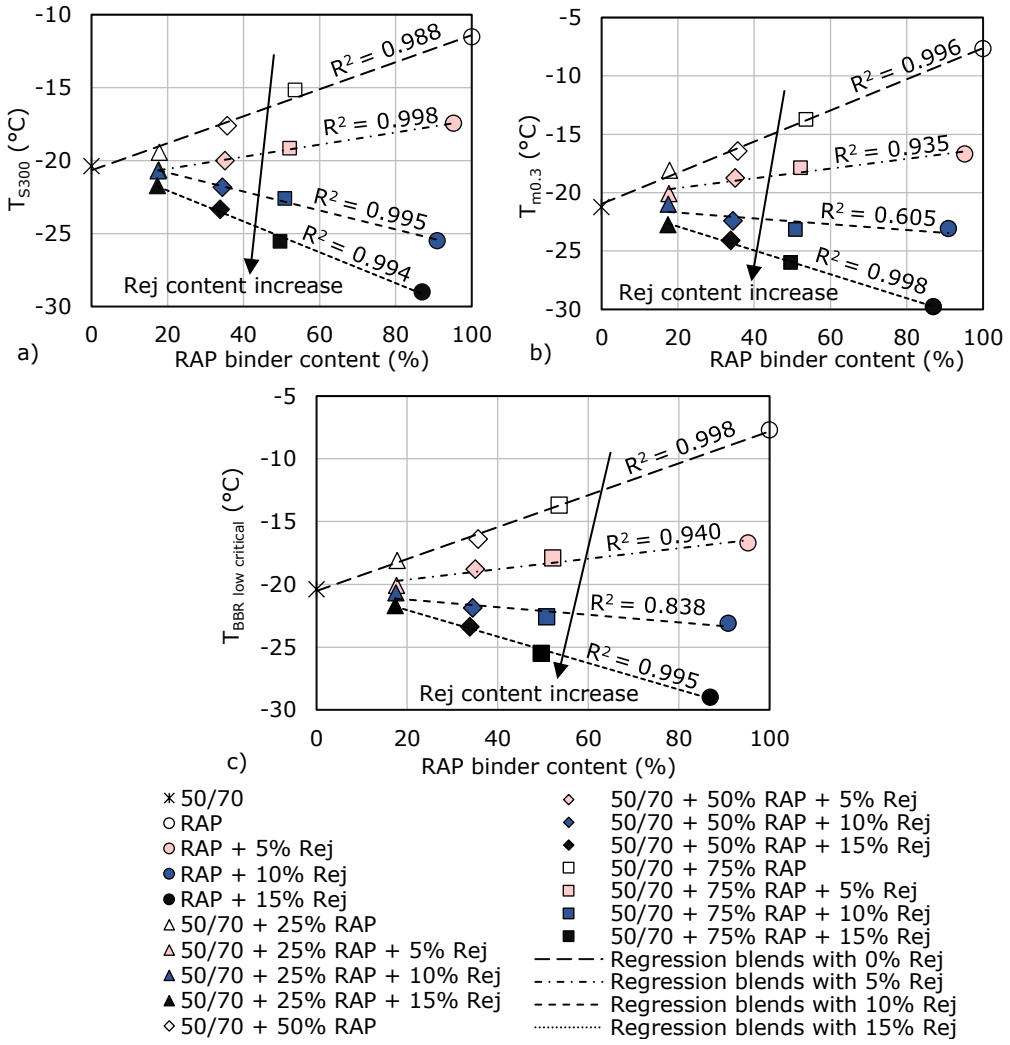

Figure 2.47. BBR temperatures as a function of RAP binder content for all binders: (a) $T_{S_{300}}$; (b) $T_{m_{0.3}}$; (c) $T_{BBR\ low\ critical}$.

As it can be observed, values of $T_{S_{300}}$, $T_{m_{0.3}}$ and $T_{BBR\ low\ critical}$ increase with the increase of RAP binder content and decrease with the increase of rejuvenator content within blends. Moreover, BBR temperatures show linear relationships with the RAP binder content for the blends produced with the same amount of rejuvenator (0%, 5%, 10% and 15% by mass of the RAP binder). Linear regressions were performed and R^2 values were determined for each regression. Similar tendencies were observed for the European conventional parameters of penetration, ring and ball temperature, Fraass temperature of the blends produced with 10% Rej: regression lines for the blends produced with 10% rejuvenator are close to the horizontal line, with a lower R^2 values. This indicates the capability of the rejuvenator to rejuvenate

the hard-aged RAP binder and to provide a final product with closer properties of fresh binder.

With respect to $T_{BBR\ low\ critical}$ values the increase of the rejuvenator content within blends have the opposite effect of the increase of RAP binder, thus $T_{BBR\ low\ critical}$ decreases for increasing rejuvenator content. The same comment made for high critical temperatures is similar to BBR low critical temperatures. The effect of the rejuvenator appears to counterbalance the effect of the RAP binder on $T_{BBR\ low\ critical}$ of blends with rejuvenator. However, it is interesting to note that a lower dosage of rejuvenator is necessary in order to obtain a similar low critical temperature as the one of the 50/70 binder than to meet the high temperature specifications.

For simplicity, in the following sections the values of $T_{BBR\ low\ critical}$ determined for all blends from experimental tests as described so far are referred to as 'experimental'.

Table 2.25. Values of $T_{S_{300}}$, $T_{m_{0.3}}$ and $T_{BBR\ low\ critical}$ of all tested binders.

Binders	$T_{S_{300}}$ (°C)	$T_{m_{0.3}}$ (°C)	$T_{BBR\ low\ critical}$ (°C)
50/70	-20.40	-21.30	-20.40
RAP	-11.50	-7.70	-7.70
RAP + 5% Rej	-17.50	-16.70	-16.70
RAP + 10% Rej	-25.50	-23.10	-23.10
RAP + 15% Rej	-29.00	-29.80	-29.00
50/70 + 25% RAP	-19.40	-18.10	-18.10
50/70 + 25% RAP + 5% Rej	-20.60	-20.10	-20.10
50/70 + 25% RAP + 10% Rej	-20.70	-21.00	-20.70
50/70 + 25% RAP + 15% Rej	-21.70	-22.80	-21.70
50/70 + 50% RAP	-17.60	-16.40	-16.40
50/70 + 50% RAP + 5% Rej	-20.00	-18.80	-18.80
50/70 + 50% RAP + 10% Rej	-21.90	-23.40	-21.90
50/70 + 50% RAP + 15% Rej	-23.40	-24.10	-23.40
50/70 + 75% RAP	-15.20	-13.70	-13.70
50/70 + 75% RAP + 5% Rej	-19.20	-17.90	-17.90
50/70 + 75% RAP + 10% Rej	-22.60	-23.20	-22.60
50/70 + 75% RAP + 15% Rej	-25.50	-26.10	-25.50

2.10.3 Estimation of the high and low critical temperatures

The two estimation approaches described in Section 2.4 were applied to determine the estimated values of $T_{DSR\ high\ critical}$ and $T_{BBR\ low\ critical}$ for all binder blends. The obtained results were then compared with the experimental values.

It must be mentioned that the first estimation approach used in this study is a 'classical' linear blending rule for high critical temperature between two binders as presented in AASHTO M 323 [186]. The second approach is a proposed estimation

method in which critical temperatures of the final blends were estimated from values determined for the two base binders and equivalent values of the rejuvenator. It must be mentioned that these equivalent values of the rejuvenator are not intended to reflect its actual properties and were used only in the context of the blending rule. The equivalent values of the rejuvenator are: $T_{Rej\ DSR\ high\ critical} = -119.90°C$, $T_{Rej\ BBR\ low\ critical} = -175.60°C$.

Correlation plot of estimated vs. experimental results of $T_{DSR\ high\ critical}$ and $T_{BBR\ low\ critical}$ are shown in Figure 2.48 and Table 2.26. All estimated results were rounded to the nearest 0.10°C.

Coefficients of determination were calculated with respect to the equality line for both correlations by 1st estimation approach and 2nd estimation approach vs. experimental results, respectively. R^2 values were calculated for the equality lines without taking into account the input values with respect to each approach: , $T_{RAP+Rej}$ i.e. five binders for the classical approach; $T_{50/70}$, T_{RAP}, T_{Rej} i.e. two binders and the equivalent values for the rejuvenator for the proposed approach.

Table 2.26. Estimated values of DSR high critical temperatures and BBR low critical temperatures for all binders.

Binders	$T_{DSR\ high\ critical}$ (°C)		$T_{BBR\ low\ critical}$ (°C)	
	1st estimation	2nd estimation	1st estimation	2nd estimation
50/70	M*	M*	M*	M*
RAP	M*	M*	M*	M*
Rej equivalent	-	-119.90**	-	-175.60**
RAP + 5% Rej	M*	82.70	M*	-15.70
RAP + 10% Rej	M*	73.50	M*	-23.00
RAP + 15% Rej	M*	65.10	M*	-29.60
50/70 + 25% RAP	71.90	71.90	-18.10	-18.10
50/70 + 25% RAP + 5% Rej	70.50	70.20	-19.70	-19.50
50/70 + 25% RAP + 10% Rej	68.60	68.50	-20.90	-20.90
50/70 + 25% RAP + 15% Rej	66.70	66.90	-22.10	-22.20
50/70 + 50% RAP	76.40	76.40	-15.90	-15.90
50/70 + 50% RAP + 5% Rej	73.70	73.00	-19.00	-18.70
50/70 + 50% RAP + 10% Rej	69.80	69.60	-21.40	-21.40
50/70 + 50% RAP + 15% Rej	66.20	66.40	-23.80	-24.00
50/70 + 75% RAP	81.00	81.00	-13.60	-13.60
50/70 + 75% RAP + 5% Rej	76.80	75.70	-18.40	-17.80
50/70 + 75% RAP + 10% Rej	71.00	70.80	-21.90	-21.80
50/70 + 75% RAP + 15% Rej	65.70	66.00	-25.30	-25.70

M* - measured (experimental results).

** - equivalent values for the rejuvenator obtained by minimizing the distance between experimental results and estimated values.

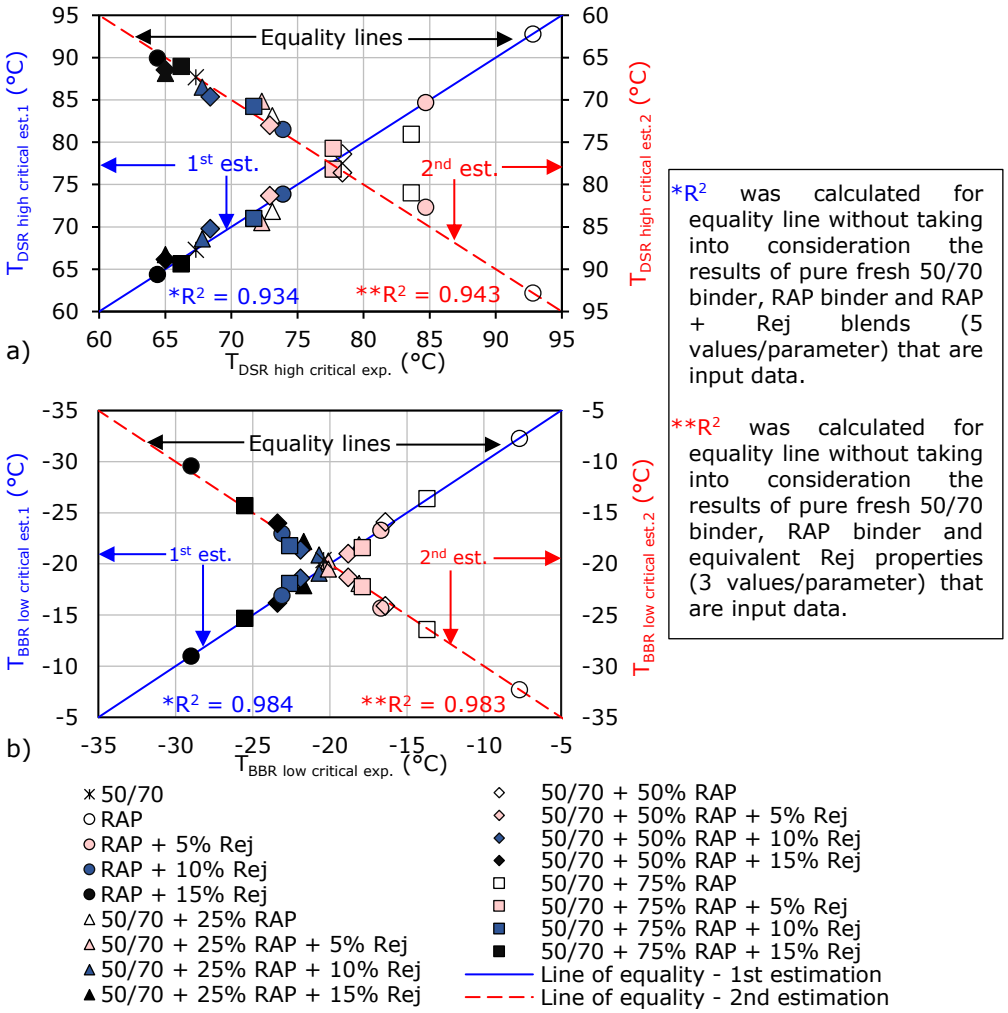

Figure 2.48. Plot of estimated vs. experimental values of for all binders: (a) DSR high critical temperatures; (b) BBR low critical temperatures.

For the high critical temperatures, satisfactory values of R^2 higher than 0.934 were found. Slightly higher correlation with the experimental results was found for the estimated values obtained with the 2nd estimation approach, which is an original input of this study.

For the low critical temperatures, a better correlation was obtained, R^2 higher than 0.983 were found. A slightly better correlation with the experimental results was found for the estimated values obtained with the 1st approach, $R^2 = 0.984$. However, in case of the second approach a close value of R^2 was obtained (0.983).

The satisfactory values of R^2 obtained with the 2nd proposed approach shows that this estimation method can be considered valid and even more advantageous because less input data is required.

For the low temperatures, the developed model should be applied on PAV aged binder. In this case, a validation process must be done in further research. A wider set of data are needed to validate the proposed approach. Also, in order to validate this proposed estimation approach a wider range of temperatures and frequencies should be considered for the DSR tests.

2.11 Relations between parameters

2.11.1 Relations between penetration and $T_{R\&B}$ and T_{Fraass}

In order to find possible relations between penetration and ring and ball temperature $(T_{R\&B})$ and Fraass breaking point temperature (T_{Fraass}), experimental values of penetration at 25°C (*pen.*, in logarithmic scale) were plotted against experimental values of $T_{R\&B}$ and T_{Fraass} for all binders (Figure 2.49).

Figure 2.49a and 2.50b show also the limits defined in standard EN 12591:2009, for traditional binders (35/50, 50/70 and 70/100).

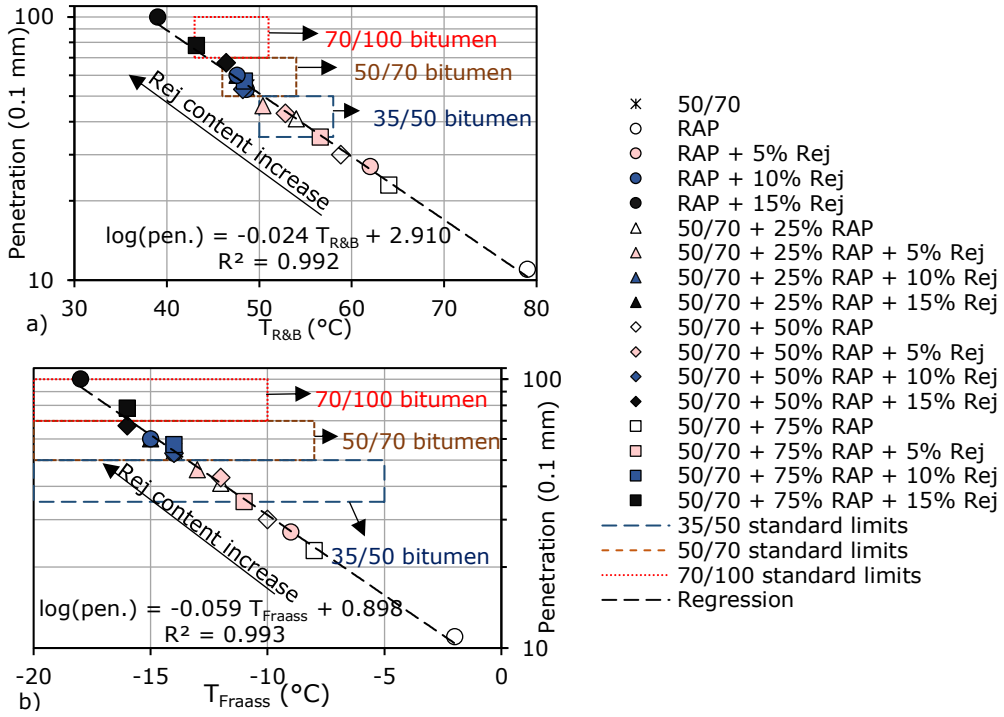

Figure 2.49. (a) Relation between ring and ball temperature and penetration for all tested blends and traditional binders limits; (b) Relation between Fraass breaking point temperature and penetration for all tested blends and traditional binders limits.

As it can be observed, the blends of RAP and fresh binders produced with 5% rejuvenator by mass of RAP binder are within the limits of a 35/50 penetration grade bitumen. Similarly, the blends produced with 10% rejuvenator by mass of RAP

bitumen are within the limits of a 50/70 penetration grade bitumen. As expected, $T_{R\&B}$ values of the tested binders increase with the decrease of penetration.

Similar observations can be made regarding penetration as a function of Fraass breaking point temperature (T_{Fraass}), as it could be observed in Figure 2.49b.

Strong correlations were found for all the linear regressions performed for the mentioned parameters.

In particular, R^2 values equal to 0.992 and 0.993 were obtained for the linear regressions between *log pen.* and $T_{R\&B}$ and *log pen.* and T_{Fraass} respectively.

2.11.2 Relation between *pen.* and steady shear viscosity at 25°C

In Figure 2.50 the possible relation between penetration and steady shear viscosity at 25ºC was investigated. The experimental values of penetration at 25ºC $(pen.)$ were plotted against experimental values of $\eta_0(25°C)$ in log-log scale.

As expected, the steady shear viscosity values at 25ºC of all tested binders increase with the decrease of penetration.

Strong correlation was found for the linear regressions performed for the mentioned parameters. In particular, R^2 value equal to 0.995 was obtained for the linear regressions between *log pen.* and $log\,\eta_0$.

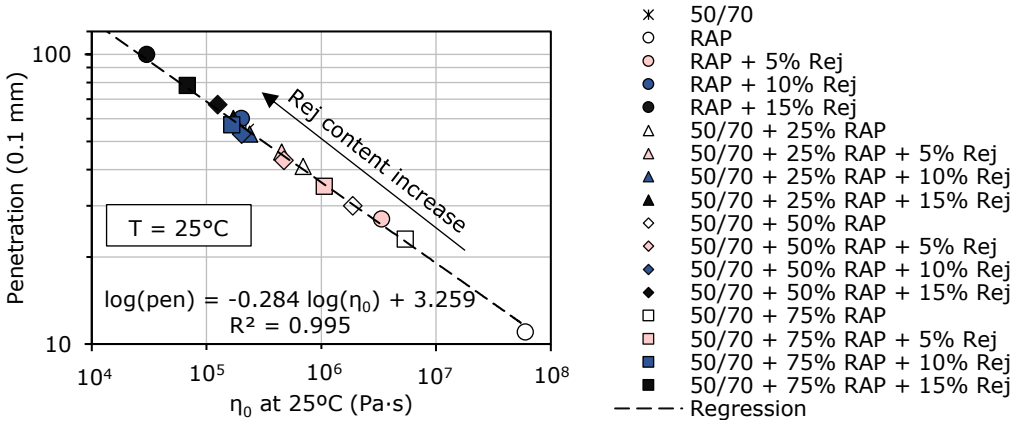

Figure 2.50. Relation between steady shear viscosity (norm of complex viscosity at 25ºC) and penetration for all the tested blends.

2.11.3 Relation between conventional parameters (*pen.*, $T_{R\&B}$) and $T_{DSR\ high\ critical}$

In Figure 2.51 the experimental values of penetration at 25ºC (*pen.*, in logarithmic scale) and $T_{R\&B}$ were plotted against experimental values of $T_{DSR\ high\ critical}$ (Figure 2.51a and Figure 2.51b) in order to highlight the possible relation between these two conventional parameters and DSR high critical temperatures.

As it can be observed, $T_{DSR\ high\ critical}$ values increase with the decrease of penetration and the increase of $T_{R\&B}$. These tendencies are caused by the increase of the RAP binder content. On the other side, it could be observed that the rejuvenator proves to have a reverse effect on the behaviour of the binder blends.

The correlations between $T_{DSR\ high\ critical}$ vs. penetration and $T_{R\&B}$, respectively, show lower values of R^2 of 0.897 and 0.906.

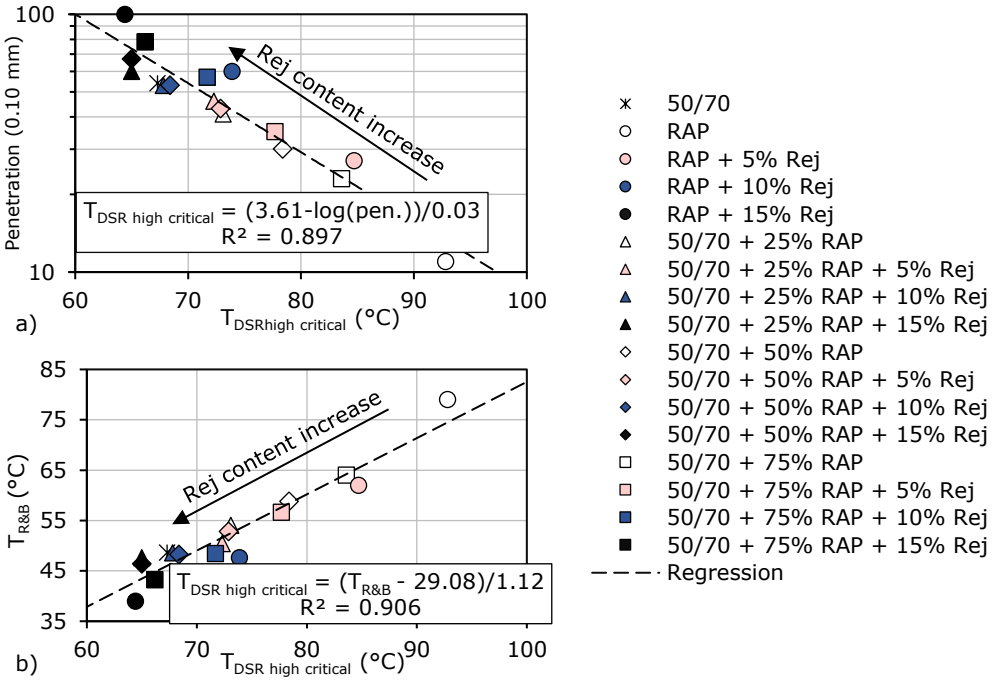

Figure 2.51. (a) Relation between penetration and DSR high critical temperature for all blends; (b) Relation between ring and ball temperature and DSR high critical temperature for all blends.

2.11.4 Relation between conventional parameters (*pen.*, T_{Fraass}) and $T_{BBR\ low\ critical}$

In order to investigate the possible relation between these two conventional parameters and BBR low critical temperatures, the experimental values of penetration at 25°C (*pen.* , in logarithmic scale) and T_{Fraass} were plotted against experimental values of $T_{BBR\ low\ critical}$ (Figure 2.52a and Figure 2.52b).

As it can be observed, $T_{BBR\ low\ critical}$ values increase with the decrease of penetration and the increase of T_{Fraass}. These tendencies are caused by the increase of the RAP binder content. On the other side, it could be observed that the rejuvenator presence proves to have a reverse effect on the behaviour of the binder blends.

Strong correlations were found for the linear regressions performed for the $T_{BBR\ low\ critical}$ vs. *pen.* and T_{Fraass}. In particular, R^2 values equal to 0.969 and 0.955 were obtained for the linear regressions between, *log pen.* and $T_{BBR\ low\ critical}$ and T_{Fraass} and $T_{BBR\ low\ critical}$, respectively.

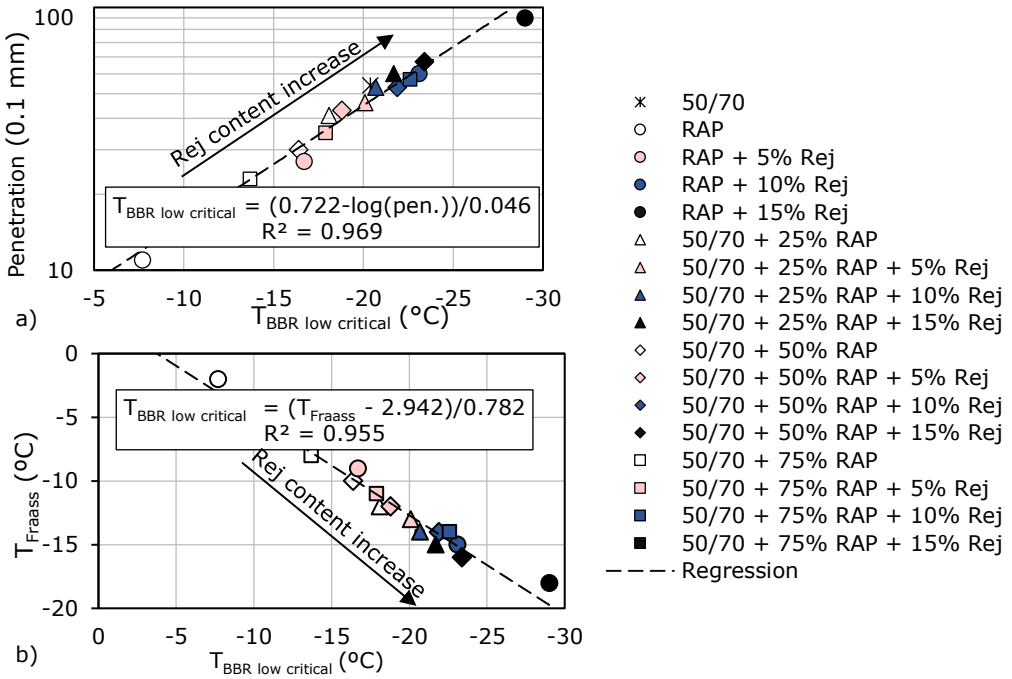

Figure 2.52. (a) Relation between penetration values and BBR low critical temperatures for all blends; (b) Relation between ring and ball temperatures and BBR low critical temperatures for all blends.

2.12 Statistical analysis

A statistical analysis was performed in order to highlight the validity of both estimation methods (1st and 2nd estimation) of conventional parameters (*pen.* at 25°C, $T_{R\&B}$, T_{Fraass}), steady shear viscosity at different temperatures $\eta_0(T)$, 2S2P1D parameters $(h, \beta\ and\ \tau)$ and a_T temperature shift factors, critical temperatures $(T_{DSR\ high\ critical}\ and\ T_{BBR\ low\ critical})$ and norm of complex shear modulus $\left(\left|G^*(T,f)\right|\right)$.

The difference (d) between experimental $\left(X_{experimental}, \log Y_{experimental}\right)$ and estimated $\left(X_{estimation\ 1\ or\ 2}, \log Y_{estimation\ 1\ or\ 2}\right)$ parameters was chosen as the response for the statistical analysis (equation 2.29).

$$d = X_{experimental} - X_{estimation\ 1\ or\ 2} \quad or \quad d = \log Y_{experimental} - \log Y_{estimation\ 1\ or\ 2} \tag{2.29}$$

Standard deviation σ was calculated for each parameter as follows:

$$\sigma = \sqrt{\frac{\sum_{i=1}^{N}\left(d_i - \bar{d}\right)}{N-1}} \tag{2.30}$$

where N corresponds to the number of binder blends (for the first estimation $N = 12$ and for the second estimation $N = 15$), and $\bar{d}$ is the average of d_i values.

A confidence interval was calculated for each parameter, as follows in equation 2.31:

$$\varepsilon = -\frac{\sigma}{\sqrt{N}} t_{(\upsilon,\alpha)} \tag{2.31}$$

where ε is the half-width of the confidence interval, t is the value of the Student-Fischer distribution as a function of υ (degrees of freedom) and α (confidence level).

As already described, with the 1st estimation method the above-mentioned parameters of 12 blends were estimated from experimental values obtained for the base binders: fresh 50/70 binder and four RAP + Rej blends, for a total of five base binders, and therefore the number of degrees of freedom for this estimation is seven.

Regarding the 2nd estimation method parameters of 15 binder blends were estimated from experimental values obtained for the two base binders (fresh 50/70 and RAP binders) and equivalent values obtained for the rejuvenator, therefore υ for this estimation is 12.

In this analysis, seven confidence levels from 90% to 99.9% were considered for the calculation in order to obtain confidence interval half-width values, ε.

Values of ε obtained for each parameter and for both estimation approaches are intended to show the maximum possible errors for a given confidence level.

In order to highlight the magnitude of the imprecision of both estimation methods, for each parameter values of ε were compared to the maximum variations (Δ) of the experimental results. Also, the inverse analysis was carried out, in which the confidence levels corresponding to a 5% ε/Δ were determined.

The output of this statistical evaluation for each parameter for both estimations are related to:

- confidence intervals half-width (ε) for different confidence levels: results reported in Table 2.27 for conventional parameters, Table 2.28 for steady shear viscosity, Table 2.29 for critical temperatures, Table 2.30 for 2S2P1D

parameters and temperature shift factors and Table 2.37 shows an example for the norm of complex shear modulus $\left|G^*\left(T, f = 1.29\ Hz\right)\right|$;

- maximum variations $\left(\Delta\right)$ of experimental values of each parameter: results reported in Table 2.31 and Table 2.39;
- confidence intervals half-width, $\left(\varepsilon\right)$ / maximum variation $\left(\Delta\right)$ for different confidence levels: results reported in Table 2.32 for conventional parameters, Table 2.33 for steady shear viscosity, Table 2.34 for 2S2P1D parameters and temperature shift factors, Table 2.35 for critical temperatures and Table 2.38 shows an example for the norm of complex shear modulus $\left|G^*\left(T, f = 1.29\ Hz\right)\right|$;
- confidence levels corresponding to 5% ε/Δ: results reported in Table 2.36 and Table 2.40.

Regarding the norm of complex shear modulus results, it must be mentioned that Tables 2.37 - 2.40 are showing the results of the statistical analysis performed on $\left|G^*\left(T, f = 1.29\ Hz\right)\right|$. The same analysis was performed for all the other frequencies, and the results are reported in Appendix 1 – Table A1.1 – A1.9.

As it could be observed in Tables 2.27 – 2.30, ε values in most cases are higher for the first estimation as the possible errors for a given confidence level are higher with the first estimation method. However, for some parameters $\left(example: \log\eta_0\left(85°C\right), T_{DSR\ high\ critical}, h, etc.\right)$ this observation is not valid ε showing values higher for the second estimation. In this case the difference between the ε values obtained for each estimation method are close (it could be observed from the values of the ratio 1st/2nd which are near to 1.0).

Table 2.27. Confidence interval half-width values ε - conventional parameters.

	Parameter	Estimation method	Confidence level α						
			90%	93%	95%	97%	99%	99.5%	99.9%
confidence interval half-width ε	$\log\left(pen.\right)$	1st	0.01	0.01	0.01	0.01	0.01	0.01	0.02
		2nd	0.01	0.01	0.02	0.02	0.02	0.02	0.03
		Ratio 1st/2nd	0.54	0.54	0.55	0.56	0.58	0.60	0.64
	$T_{R\&B}$	1st	0.46	0.51	0.57	0.65	0.84	0.97	1.30
		2nd	0.77	0.86	0.94	1.06	1.32	1.48	1.87
		Ratio 1st/2nd	0.59	0.60	0.60	0.61	0.64	0.65	0.70
	T_{Fraass}	1st	0.18	0.21	0.23	0.26	0.34	0.39	0.52
		2nd	0.32	0.35	0.39	0.44	0.54	0.61	0.77
		Ratio 1st/2nd	0.57	0.58	0.59	0.60	0.62	0.63	0.68

Table 2.28. Confidence interval half-width values ε - steady shear viscosity.

	Parameter	Estimation method	Confidence level α						
			90%	93%	95%	97%	99%	99.5%	99.9%
confidence interval half-width ε	$log\,\eta_0(25°C)$	1st	0.06	0.06	0.07	0.08	0.10	0.12	0.16
		2nd	0.06	0.07	0.07	0.08	0.11	0.12	0.15
		Ratio 1st/2nd	0.92	0.93	0.94	0.95	0.99	1.01	1.08
	$log\,\eta_0(35°C)$	1st	0.04	0.05	0.06	0.06	0.08	0.09	0.13
		2nd	0.05	0.06	0.06	0.07	0.09	0.10	0.12
		Ratio 1st/2nd	0.86	0.87	0.88	0.89	0.93	0.95	1.02
	$log\,\eta_0(45°C)$	1st	0.04	0.04	0.05	0.05	0.07	0.08	0.10
		2nd	0.04	0.05	0.05	0.06	0.08	0.08	0.11
		Ratio 1st/2nd	0.83	0.84	0.84	0.86	0.89	0.91	0.97
	$log\,\eta_0(55°C)$	1st	0.03	0.04	0.04	0.05	0.06	0.07	0.09
		2nd	0.04	0.04	0.05	0.05	0.06	0.07	0.09
		Ratio 1st/2nd	0.83	0.84	0.85	0.86	0.90	0.92	0.98
	$log\,\eta_0(65°C)$	1st	0.03	0.03	0.04	0.04	0.05	0.06	0.08
		2nd	0.03	0.04	0.04	0.05	0.05	0.06	0.08
		Ratio 1st/2nd	0.88	0.89	0.90	0.92	1.18	0.98	1.04
	$log\,\eta_0(75°C)$	1st	0.03	0.03	0.04	0.04	0.05	0.06	0.08
		2nd	0.03	0.03	0.04	0.04	0.05	0.06	0.07
		Ratio 1st/2nd	0.96	0.97	0.98	1.00	1.03	1.06	1.13
	$log\,\eta_0(85°C)$	1st	0.03	0.03	0.04	0.04	0.05	0.06	0.08
		2nd	0.03	0.03	0.04	0.04	0.05	0.06	0.07
		Ratio 1st/2nd	1.02	1.03	1.04	1.05	1.10	1.12	1.20

Table 2.29. Confidence interval half-width values ε - critical temperatures.

	Parameter	Estimation method	Confidence level α						
			90%	93%	95%	97%	99%	99.5%	99.9%
confidence interval half-width ε	$T_{DSR\ high\ critical}$	1st	0.92	1.04	1.15	1.32	1.70	1.96	2.63
		2nd	0.87	0.97	1.06	1.20	1.49	1.67	2.11
		Ratio 1st/2nd	1.06	1.07	1.08	1.10	1.14	1.17	1.25
	$T_{BBR\ low\ critical}$	1st	0.26	0.29	0.32	0.37	0.47	0.54	0.73
		2nd	0.29	0.33	0.36	0.40	0.50	0.56	0.71
		Ratio 1st/2nd	0.88	0.88	0.89	0.91	0.94	0.97	1.03

Table 2.30. Confidence interval half-width values ε - 2S2P1D parameters and temperature shift factors.

	Parameter	Estimation method	Confidence level α						
			90%	93%	95%	97%	99%	99.5%	99.9%
confidence interval half-width ε	h	1st	0.00	0.00	0.00	0.00	0.00	0.00	0.00
		2nd	0.00	0.00	0.00	0.00	0.00	0.00	0.00
		Ratio 1st/2nd	1.42	1.40	1.39	1.37	1.31	1.28	1.20
	$log(\beta)$	1st	0.01	0.01	0.02	0.02	0.02	0.03	0.03
		2nd	0.01	0.01	0.01	0.02	0.02	0.02	0.03
		Ratio 1st/2nd	0.95	0.94	0.93	0.91	0.88	0.86	0.80
	$log(\tau)$	1st	0.02	0.02	0.02	0.02	0.03	0.03	0.04
		2nd	0.02	0.02	0.03	0.03	0.04	0.04	0.05
		Ratio 1st/2nd	1.40	1.39	1.37	1.35	1.30	1.27	1.19
	$log(a_T)$ *at* 25°C	1st	0.01	0.02	0.02	0.02	0.03	0.03	0.04
		2nd	0.02	0.02	0.02	0.03	0.03	0.04	0.05
		Ratio 1st/2nd	1.42	1.41	1.39	1.37	1.32	1.29	1.21
	$log(a_T)$ *at* 35°C	1st	0.01	0.01	0.01	0.01	0.01	0.01	0.02
		2nd	0.01	0.01	0.01	0.01	0.01	0.01	0.02
		Ratio 1st/2nd	0.88	0.87	0.86	0.85	0.82	0.80	0.75
	$log(a_T)$ *at* 45°C	1st	0.01	0.01	0.01	0.01	0.01	0.01	0.02
		2nd	0.01	0.01	0.01	0.01	0.01	0.01	0.01
		Ratio 1st/2nd	0.96	0.95	0.94	0.93	0.89	0.87	0.81
	$log(a_T)$ *at* 65°C	1st	0.00	0.00	0.00	0.00	0.01	0.01	0.01
		2nd	0.00	0.00	0.00	0.00	0.01	0.01	0.01
		Ratio 1st/2nd	1.16	1.15	1.14	1.12	1.08	1.05	0.99
	$log(a_T)$ *at* 75°C	1st	0.01	0.01	0.01	0.01	0.01	0.01	0.02
		2nd	0.01	0.01	0.01	0.01	0.02	0.02	0.02
		Ratio 1st/2nd	1.73	1.71	1.69	1.66	1.60	1.56	1.47
	$log(a_T)$ *at* 85°C	1st	0.01	0.01	0.01	0.01	0.02	0.02	0.03
		2nd	0.01	0.02	0.02	0.02	0.03	0.03	0.04
		Ratio 1st/2nd	1.65	1.63	1.62	1.59	1.53	1.49	1.40

By analysing the results obtained for this statistical evaluation it could be observed that for the 1st estimation half-width values of 99.5% confidence intervals of estimated conventional parameters are always below 5% of the maximum variation of the experimental values (Table 2.27, Table 2.32 and Table 2.36). Regarding the second estimation the same observation could be made. However, the values of the estimated conventional parameters are always below 5% of the maximum variation of their experimental values for a 98.4% confidence interval.

Regarding the analysis performed over steady shear viscosity (given in Table 2.28, Table 2.33 and Table 2.36), half-width values of 97% confidence intervals of $log\,\eta_0(T)$ are always inferior to 5% of the maximum variations of their experimental values, independently of the estimation approach used. However, a more accurate estimation was performed with the 2nd method.

For the 2S2P1D parameters and temperature shift factors shown in Table 2.29, Table 2.34 and Table 2.36 for the 1st estimation, the half-width values of 95.00% confidence intervals of h, $log\,\beta$, $log\,\tau$ and $log\,a_T$ are always inferior to 5% of the maximum variations of their experimental values. A better estimation was performed with the 2nd method for which the half-width values of 98.85% confidence intervals of 2S2P1D parameters are always inferior to 5% Δ.

Similar observations can be made also for the critical temperatures by reading the Table 2.30, Table 2.35 and Table 2.36. Half-width values of 90.50% *for* $T_{DSR\ high\ critical}$, respectively 99.60% *for* $T_{BBR\ low\ critical}$ confidence intervals of the considered parameters are always inferior to 5% of Δ, independently of the estimation method used.

Table 2.31. Maximum variations Δ of experimental values of each parameter for all binder blends according to the 1st or 2nd estimation method.

	Parameter	Estimation method	Δ
Conventional parameters	$log\,(pen.)$	1st	0.53
		2nd	0.64
	$T_{R\&B}$	1st	20.80
		2nd	25.00
	T_{Fraass}	1st	8.00
		2nd	10.00
Steady shear viscosity	$log\,\eta_0\,(25°C)$	1st	1.90
		2nd	2.25
	$log\,\eta_0\,(35°C)$	1st	1.66
		2nd	1.94
	$log\,\eta_0\,(45°C)$	1st	1.44
		2nd	1.66
	$log\,\eta_0\,(55°C)$	1st	1.24
		2nd	1.41
	$log\,\eta_0\,(65°C)$	1st	1.07
		2nd	1.19
	$log\,\eta_0\,(75°C)$	1st	0.95
		2nd	1.02
	$log\,\eta_0\,(85°C)$	1st	0.85
		2nd	0.91

	Parameter	Est. method	Δ
Critical temp.	$T_{DSR\ high\ critical}$	1st	18.60
		2nd	20.30
	$T_{BBR\ low\ critical}$	1st	11.80
		2nd	15.30
2S2P1D parameters	h	1st	0.03
		2nd	0.03
	$log\,(\beta)$	1st	0.41
		2nd	0.48
	$log\,(\tau)$	1st	0.81
		2nd	0.93
Temperature shift factors	$log\,(a_T)$ *at* 25°C	1st	0.50
		2nd	0.68
	$log\,(a_T)$ *at* 35°C	1st	0.33
		2nd	0.46
	$log\,(a_T)$ *at* 45°C	1st	0.15
		2nd	0.20
	$log\,(a_T)$ *at* 65°C	1st	0.15
		2nd	0.19
	$log\,(a_T)$ *at* 75°C	1st	0.27
		2nd	0.34
	$log\,(a_T)$ *at* 85°C	1st	0.40
		2nd	0.50

Table 2.32. Confidence interval half-width values ε / maximum variation Δ ratios – conventional parameters.

	Parameter	Estimation method	Confidence level α						
			90%	93%	95%	97%	99%	99.5%	99.9%
ε / Δ	$log\,(pen.)$	1st	1.3%	1.5%	1.6%	1.9%	2.4%	2.8%	3.8%
		2nd	2.0%	2.3%	2.5%	2.8%	3.5%	3.9%	4.9%
	$T_{R\&B}$	1st	2.2%	2.5%	2.7%	3.1%	4.0%	4.7%	6.2%
		2nd	3.1%	3.4%	3.8%	4.3%	5.3%	5.9%	7.5%
	T_{Fraass}	1st	2.3%	2.6%	2.8%	3.3%	4.2%	4.8%	6.5%
		2nd	3.2%	3.5%	3.9%	4.4%	5.4%	6.1%	7.7%

Table 2.33. Confidence interval half-width values ε / maximum variation Δ ratios – steady shear viscosity.

	Parameter	Estimation method	Confidence level α						
			90%	93%	95%	97%	99%	99.5%	99.9%
ε / Δ	$log\ \eta_0\ (25°C)$	1st	3.0%	3.3%	3.7%	4.2%	5.5%	6.3%	8.5%
		2nd	2.7%	3.0%	3.3%	3.8%	4.7%	5.2%	6.6%
	$log\ \eta_0\ (35°C)$	1st	2.7%	3.0%	3.3%	3.8%	4.9%	5.7%	7.6%
		2nd	2.7%	3.0%	3.2%	3.7%	4.5%	5.1%	6.4%
	$log\ \eta_0\ (45°C)$	1st	2.5%	2.8%	3.1%	3.6%	4.7%	5.4%	7.2%
		2nd	2.6%	3.0%	3.2%	3.7%	4.5%	5.1%	6.4%
	$log\ \eta_0\ (55°C)$	1st	2.5%	2.8%	3.2%	3.6%	4.7%	5.4%	7.2%
		2nd	2.7%	3.0%	3.3%	3.7%	4.6%	5.2%	6.5%
	$log\ \eta_0\ (65°C)$	1st	2.7%	3.1%	3.4%	3.9%	5.0%	5.8%	7.8%
		2nd	2.8%	3.1%	3.4%	3.8%	4.7%	5.3%	6.7%
	$log\ \eta_0\ (75°C)$	1st	3.0%	3.4%	3.8%	4.3%	5.6%	6.4%	8.6%
		2nd	2.9%	3.3%	3.6%	4.0%	5.0%	5.6%	7.1%
	$log\ \eta_0\ (85°C)$	1st	3.5%	3.9%	4.3%	5.0%	6.4%	7.4%	9.9%
		2nd	3.2%	3.5%	3.9%	4.4%	5.4%	6.1%	7.7%

Table 2.34. Confidence interval half-width values ε / maximum variation Δ ratios – 2S2P1D parameters and temperature shift factors.

	Parameter	Estimation method	Confidence level α						
			90%	93%	95%	97%	99%	99.5%	99.9%
ε / Δ	h	1st	1.7%	1.9%	2.1%	2.4%	3.1%	3.6%	4.8%
		2nd	2.0%	2.2%	2.4%	2.7%	3.4%	3.8%	4.7%
	$log\ (\beta)$	1st	2.9%	3.3%	3.7%	4.2%	5.4%	6.3%	8.4%
		2nd	2.4%	2.7%	2.9%	3.3%	4.1%	4.6%	5.8%
	$log\ (\tau)$	1st	1.9%	2.1%	2.4%	2.7%	3.5%	4.0%	5.4%
		2nd	2.3%	2.6%	2.8%	3.2%	4.0%	4.5%	5.6%
	$log\ (a_T)$ at 25°C	1st	2.9%	3.2%	3.6%	4.1%	5.3%	6.1%	8.2%
		2nd	3.0%	3.3%	3.6%	4.1%	5.1%	5.7%	7.2%
	$log\ (a_T)$ at 35°C	1st	2.1%	2.4%	2.6%	3.0%	3.9%	4.5%	6.0%
		2nd	1.3%	1.5%	1.6%	1.9%	2.3%	2.6%	3.2%
	$log\ (a_T)$ at 45°C	1st	3.7%	4.2%	4.7%	5.4%	6.9%	7.9%	10.7%
		2nd	2.7%	3.0%	3.3%	3.7%	4.6%	5.2%	6.6%
	$log\ (a_T)$ at 65°C	1st	1.9%	2.2%	2.4%	2.8%	3.6%	4.1%	5.5%
		2nd	1.7%	1.9%	2.1%	2.4%	3.0%	3.4%	4.2%
	$log\ (a_T)$ at 75°C	1st	2.2%	2.5%	2.7%	3.1%	4.0%	4.7%	6.3%
		2nd	3.0%	3.3%	3.6%	4.1%	5.1%	5.7%	7.2%
	$log\ (a_T)$ at 85°C	1st	2.3%	2.5%	2.8%	3.2%	4.2%	4.8%	6.4%
		2nd	2.9%	3.3%	3.6%	4.1%	5.0%	5.7%	7.1%

Table 2.35. Confidence interval half-width values ε / maximum variation Δ ratios – critical temperatures.

	Parameter	Est. method	Confidence level α						
			90%	93%	95%	97%	99%	99.5%	99.9%
ε / Δ	$T_{DSR\ high\ critical}$	1st	4.9%	5.6%	6.2%	7.1%	9.1%	10.5%	14.1%
		2nd	4.3%	4.8%	5.2%	5.9%	7.3%	8.2%	10.4%
	$T_{BBR\ low\ critical}$	1st	2.2%	2.4%	2.7%	3.1%	4.0%	4.6%	6.2%
		2nd	1.9%	2.1%	2.3%	2.6%	3.3%	3.7%	4.6%

Table 2.36. Confidence levels corresponding to 5% ε/Δ ratios of each parameter for all binder blends according to the 1st or 2nd estimation method.

	Parameter	Est. met.	**confidence level corresp. to 5% ε/Δ**
Conventional param.	$log\,(pen.)$	1st	99.98%
		2nd	99.91%
	$T_{R\&B}$	1st	99.65%
		2nd	98.60%
	T_{Fraass}	1st	99.56%
		2nd	98.40%
Steady shear viscosity	$log\,\eta_0\,(25°C)$	1st	98.50%
		2nd	99.30%
	$log\,\eta_0\,(35°C)$	1st	99.10%
		2nd	99.40%
	$log\,\eta_0\,(45°C)$	1st	99.30%
		2nd	99.40%
	$log\,\eta_0\,(55°C)$	1st	99.30%
		2nd	99.40%
	$log\,\eta_0\,(65°C)$	1st	99.00%
		2nd	99.30%
	$log\,\eta_0\,(75°C)$	1st	98.30%
		2nd	99.00%
	$log\,\eta_0\,(85°C)$	1st	97.00%
		2nd	98.40%

	Parameter	Est. met.	**confidence level corresp. to 5% ε/Δ**
Critical temp.	$T_{DSR\ high\ critica}$	1st	90.50%
		2nd	94.00%
	$T_{BBR\ low\ critical}$	1st	99.68%
		2nd	99.95%
2S2P1D parameters	h	1st	99.92%
		2nd	99.93%
	$log\,(\beta)$	1st	98.50%
		2nd	99.70%
	$log\,(\tau)$	1st	99.85%
		2nd	99.77%
Temperature shift factors	$log\,(a_T)$ *at* 25°C	1st	98.70%
		2nd	98.90%
	$log\,(a_T)$ *at* 35°C	1st	99.70%
		2nd	100.00%
	$log\,(a_T)$ *at* 45°C	1st	96.00%
		2nd	99.35%
	$log\,(a_T)$ *at* 65°C	1st	99.82%
		2nd	99.97%
	$log\,(a_T)$ *at* 75°C	1st	99.65%
		2nd	98.85%
	$log\,(a_T)$ *at* 85°C	1st	99.60%
		2nd	98.90%

Similar remarks can be done for the norm of complex shear modulus $\left|G^*\left(T, f = 1.29\ Hz\right)\right|$ where the confidence levels corresponding to $5\%\ \varepsilon/\Delta$ ratios of norm of complex shear modulus is always higher than 94.8% for the 1st estimation, and 94.3% for the 2nd estimation.

The results of the statistical evaluation confirm the observations made for the correlation plots of estimated vs. experimental results of each considered parameter.

As a general comment, regarding the analysis for the 1st estimation of all parameters, the obtained confidence level corresponding to 5% ε/Δ is always 90.50%. For the 2nd estimation the obtained confidence level corresponding to 5% ε/Δ is always 94.00%.

It can be concluded that both estimation approaches can be considered valid for all analysed parameters for the materials considered in this work. However, a more accurate estimation was performed with the 2nd proposed estimation method.

Table 2.37. Confidence interval half-width values ε – norm of complex shear modulus f=1.29 Hz.

	Parameter	Estimation method	Confidence level α						
			90%	93%	95%	97%	99%	99.5%	99.9%
confidence interval half-width ε	$log\left(\left\|G^*(85°C,1.29\ Hz)\right\|\right)$	1st	0.03	0.04	0.04	0.05	0.06	0.07	0.09
		2nd	0.03	0.04	0.04	0.05	0.06	0.06	0.08
		Ratio 1st/2nd	1.00	1.01	1.02	1.04	1.08	1.11	1.18
	$log\left(\left\|G^*(75°C,1.29\ Hz)\right\|\right)$	1st	0.04	0.04	0.04	0.05	0.07	0.08	0.10
		2nd	0.03	0.04	0.04	0.04	0.06	0.06	0.08
		Ratio 1st/2nd	1.09	1.10	1.11	1.13	1.17	1.20	1.28
	$log\left(\left\|G^*(65°C,1.29\ Hz)\right\|\right)$	1st	0.04	0.04	0.05	0.05	0.07	0.08	0.11
		2nd	0.03	0.04	0.04	0.05	0.06	0.06	0.08
		Ratio 1st/2nd	1.14	1.15	1.16	1.18	1.23	1.26	1.34
	$log\left(\left\|G^*(55°C,1.29\ Hz)\right\|\right)$	1st	0.03	0.03	0.04	0.04	0.06	0.06	0.09
		2nd	0.04	0.04	0.05	0.05	0.06	0.07	0.09
		Ratio 1st/2nd	0.82	0.83	0.84	0.85	0.89	0.91	0.97

Table 2.38. Confidence interval half-width values ε / maximum variation Δ ratios – norm of complex shear modulus f=1.29 Hz.

	Parameter	Est. Meth.	Confidence level α						
			90%	93%	95%	97%	99%	99.5%	99.9%
ε / Δ	$log\left(\left\|G^*(85°C,1.29\ Hz)\right\|\right)$	1st	3.9%	4.3%	4.8%	5.5%	7.1%	8.2%	11.0%
		2nd	3.6%	4.0%	4.4%	4.9%	6.1%	6.9%	8.7%
	$log\left(\left\|G^*(75°C,1.29\ Hz)\right\|\right)$	1st	3.8%	4.3%	4.8%	5.5%	7.0%	8.1%	10.9%
		2nd	3.3%	3.7%	4.0%	4.5%	5.6%	6.3%	8.0%
	$log\left(\left\|G^*(65°C,1.29\ Hz)\right\|\right)$	1st	3.8%	4.3%	4.8%	5.5%	7.1%	8.1%	10.9%
		2nd	3.1%	3.4%	3.8%	4.3%	5.3%	5.9%	7.5%
	$log\left(\left\|G^*(55°C,1.29\ Hz)\right\|\right)$	1st	3.0%	3.4%	3.7%	4.3%	5.5%	6.3%	8.5%
		2nd	3.3%	3.7%	4.0%	4.6%	5.7%	6.3%	8.0%

Table 2.39. Maximum variations Δ of measured values of norm of complex shear modulus f=1.29 Hz for all binder blends according to the 1st or 2nd estimation method.

	Parameter	Estimation method	**Δ**
Norm of complex shear modulus	$log\left(\left\|G^*(85°C,1.29\ Hz)\right\|\right)$	1st	0.85
		2nd	0.92
	$log\left(\left\|G^*(75°C,1.29\ Hz)\right\|\right)$	1st	0.93
		2nd	0.99
	$log\left(\left\|G^*(65°C,1.29\ Hz)\right\|\right)$	1st	0.98
		2nd	1.07
	$log\left(\left\|G^*(55°C,1.29\ Hz)\right\|\right)$	1st	1.02
		2nd	1.12

Table 2.40. Confidence levels corresponding to 5% ε/Δ ratios of norm of complex shear modulus f=1.29 Hz for all binder blends according to the 1st or 2nd estimation method.

	Parameter	Est. met.	**confidence level corresp. to 5% ε/Δ**
Norm of complex shear modulus	$log\left(\left\|G^*(85°C,1.29\ Hz)\right\|\right)$	1st	95.50%
		2nd	97.10%
	$log\left(\left\|G^*(75°C,1.29\ Hz)\right\|\right)$	1st	95.70%
		2nd	98.00%
	$log\left(\left\|G^*(65°C,1.29\ Hz)\right\|\right)$	1st	95.70%
		2nd	98.60%
	$log\left(\left\|G^*(55°C,1.29\ Hz)\right\|\right)$	1st	98.40%
		2nd	98.00%

2.13 Approximation of rejuvenator properties with only one test

This approximated estimation approach was used only for the penetration, ring and ball temperature, Fraass breaking point and the two critical temperature.

If the values of the equivalent penetration/temperatures for the rejuvenator are not known from previous experiments, a good approximation can be obtained from only one test performed on the binder blend produced between the RAP binder and the maximum rejuvenator content (15% Rej by mass of the RAP binder). In this method, in addition to the tests performed on the base binders, penetration, ring and ball, Frass, DSR and BBR tests should be performed only on this binder blend RAP + 15% Rej.

It this case, by using equations 2.9 and 2.10 where the experimental penetration or temperatures for RAP binder $\left(pen_{RAP}\ or\ T_{RAP}\right)$ and for the blend RAP + 15 % Rej $\left(pen_{RAP+15\%Rej}\ or\ T_{RAP+15\%Rej}\right)$ and the concentrations $\left(b\ and\ r\right)$ for the base components (RAP binder and rejuvenator) were used in order to determine the equivalent penetration or temperatures for the rejuvenator $\left(pen_{Rej\ \ approx.}\ or\ T_{Rej\ \ approx.}\right)$, as shown in equation 2.32.

$$log\ pen_{Rej\ approx.} = \frac{\left(log\ pen_{RAP+15\%Rej} - b \cdot log\ pen_{RAP}\right)}{b \cdot r}$$

$$or \qquad (2.32)$$

$$T_{Rej\ approx.} = \frac{\left(T_{RAP+15\%Rej} - b \cdot T_{RAP}\right)}{b \cdot r}$$

where: T represents $T_{R\&B}$ or T_{Fraass} or $T_{DSR\ high\ critical}$ or $T_{BBR\ low\ critical}$.

Therefore, with this rapid and practically method the approximated equivalent values for the above mentioned parameters are the following: $pen_{Rej\ approx.} = 2.47E+08\ \ 0.10\,mm$, $T_{Rej\ approx._{R\&B}} = -228°C$, $T_{Rej\ approx._{Fraass}} = -125°C$, $T_{Rej\ approx._{DSR}} = -125°C$ and $T_{Rej\ approx._{BBR}} = -171°C$. These approximated equivalent parameters for the rejuvenator can be used to estimate the parameters for any binder blend, independent of the RAP binder and rejuvenator contents. Most probably the equivalent pen_{Rej} and all T_{Rej} values are only rejuvenator dependent. This should be confirmed in a future research.

Moreover, two additional binder blends were produced with different contents of RAP binder and rejuvenator (different from those reported in Table 2.1). Penetration, ring and ball, Fraass, DSR and BBR tests were performed under the same test conditions. $T_{R\&B}$, T_{Fraass}, $T_{DSRhighcritical}$, $T_{BBRlowcritical}$ and pen were determined from the experimental measurements following the same procedures. The blending proportions between the three base materials for the additional binder blends, are reported in Table 2.41. The obtained experimental critical temperatures for both blends are reported in Table 2.42.

Table 2.41. Experimental and estimated results obtained for the two additional binder blends using T_{Rej} or pen_{Rej} values from either the optimization approach (2nd estimation method) of previous sections "Est. Optim. App." or the approximated approach "Est. Approx. app.".

Binder blends	$T_{DSRhighcritical}$ (ºC)			$T_{BBRlowcritical}$ (ºC)		
	Exp.	Est. Optim. app.	Est. Approx. app.	Exp.	Est. Optim. app.	Est. Approx. app.
50/70 + 40% RAP + 7.5% Rej	70.7	70.1	70.4	-20.6	-20.1	-20.0
50/70 + 60% RAP + 8.5% Rej	71.8	71.3	71.1	-21.0	-20.6	-20.4

Binder blends	$T_{R\&B}$ (ºC)			T_{Fraass} (ºC)		
	Exp.	Est. Optim. app.	Est. Approx. app.	Exp.	Est. Optim. app.	Est. Approx. app.
50/70 + 40% RAP + 7.5% Rej	50.8	51	51.4	-13	-13	-13
50/70 + 60% RAP + 8.5% Rej	51.2	51	51.4	-13	-13	-13

Binder blends	*pen* (0.10 mm)		
	Exp.	Est. Optim. app.	Est. Approx. app.
50/70 + 40% RAP + 7.5% Rej	50	48	48
50/70 + 60% RAP + 8.5% Rej	52	48	48

As it can be observed, the values of the experimental critical temperatures of the two additional binder blends are close to those obtained by using the optimized estimation. The maximum difference between the experimental and estimated values of all temperatures is only ±0.60°C.

On the other hand, when the approximated estimation is used the maximum difference between the experimental and estimated values of all temperatures is only ±0.70°C.

For the penetration, the maximum difference between the experimental and estimated values, either those obtained with the optimized estimation approach or with the approximated estimation approach, is only +4.0 (0.10 mm).

In order to better highlight the accuracy of this approximated approach compared to the optimized approach, in Figure 2.53 the differences between the experimental and the estimated (proposed and approximated approach) results for all temperatures and penetration for all binder blends produced with rejuvenator (12 binder blends which are reported in Table 2.1) were plotted.

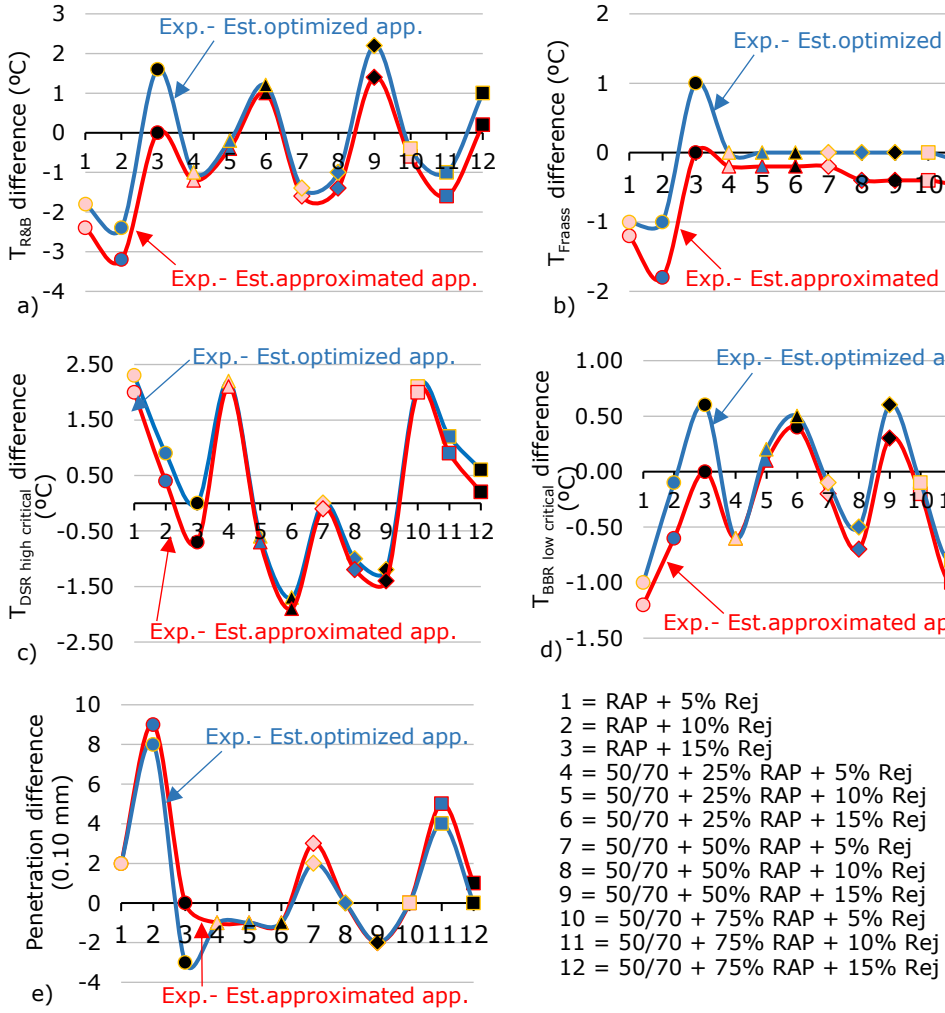

Figure 2.53. Difference between experimental and estimated results considering optimized and approximated values for the rejuvenator: (a) Ring and ball temperatures; (b) Fraass breaking point temperatures; (c) DSR high critical temperatures; (d) BBR low critical temperatures; (e) Penetration.

As it can be observed, the two series shown in Figure 2.53 (a-e) give quite similar good results. Therefore, the approximated estimation approach presents the advantage of requiring less input data (tests only for fresh binder, RAP binder and the blend of RAP binder and the maximum rejuvenator content RAP + 15% Rej) and it can be applied for any combination of RAP/rejuvenator, which is not the case for the classical approach. Indeed, classical approach needs the blend of RAP with the exact percentage of rejuvenator to be tested.

2.14 Conclusions

Conventional tests: penetration at 25°C, softening point, Fraass breaking point, elongation and density at 25°C, rheological (DSR) tests and BBR tests were performed on various blends of a pure fresh 50/70 bitumen, a RAP-extracted binder and rejuvenator, in different proportions. In total, 17 different binders including pure fresh and RAP binders were produced and tested (Table 2.1).

Several parameters were investigated in order to highlight the influence of the RAP binder and the effect of the rejuvenator on the properties of final blends.

The experimental results show a decrease in penetration and an increase in softening point $(T_{R\&B})$, Fraass breaking point temperature (T_{Fraass}) and penetration index (PI) for increasing RAP binder content and decreasing rejuvenator content in blends. Similar tendencies to those observed for the T_{Fraass} and PI values were found for the values of density at 25°C. For the binder blends produced without rejuvenator it can be observed that the elongation is decreasing with the increase of the RAP binder content and is always lower than 150 mm. It was not possible to observe the effect of increasing the percentage of rejuvenator on ductility results since measure span of the test machine is limited to 150 cm.

DSR complex modulus tests were performed from 25°C to 85°C and frequencies from 0.1 Hz to 10 Hz. The Time-Temperature Superposition Principle was validated for all tested binders.

The experimental data were analysed by using the 2S2P1D model in which four parameters $(G_0, G_{00}, k \text{ and } \delta)$ were considered constants for all tested binders and only three parameters $(h, \beta \text{ and } \tau)$ were variable. Parameters $h, \beta \text{ and } \tau$ and a_T shift factors show some remarkable tendencies with the increase of RAP binder and rejuvenator contents in the final blends. In particular, parameter h shows a linear relationship with the RAP binder content and on the other side parameters β, τ and a_T temperature shift factors follow a logarithmic trend.

Steady shear viscosity (η_0) at 85°C was obtained as the norm of complex viscosity at high temperature/low frequency in the domain of Newtonian behaviour of binders. η_0 values at temperatures from 75°C to 25°C were calculated from the experimental values of η_0 at the reference temperature of 85°C, $(\eta_0(T_{ref} = 85°C))$, multiplied by the shift factors. From the obtained results it can be concluded that, for all temperatures, η_0 values are increasing with the increase of RAP binder content and with the decrease of Rej content in the blends. The addition of the rejuvenator was observed to counterbalance the stiffening effect of the RAP binder in the blends.

Two critical temperatures were determined for the original binder blends. Tests are in agreement with the overall Superpave framework but some minor differences in the analysis of test results were applied to obtain the considered critical temperatures of the tested binders. The experimental results show that both critical temperatures increase with increasing RAP binder content in the blends and decrease with the increase of Rej content within blends. From these results, it seems that the rejuvenator can have a counterbalancing effect as this neutralizes the effect of the RAP binder. However, it is interesting to notice that a lower dosage of rejuvenator is

necessary to obtain a similar low critical temperature as the one of the 50/70 binder than to meet the high temperature specifications.

From a thermo-mechanical point of view, by analysing the conventional parameters, steady shear viscosity, 2S2P1D parameters and critical temperatures, the rejuvenating effect of the mix of vegetal oil was observed to counterbalance the effect of the aged RAP binder within binder blends.

Moreover, the results obtained for the blends produced with 10% or 15% rejuvenator by mass of the RAP binder, depending on the investigated parameter are close to those obtained for fresh binder 50/70, independently of the RAP binder content. This indicates the capability of the rejuvenator to rejuvenate the hard-aged RAP binder in terms of mechanical characteristics and finally provide a final product with similar properties of fresh binder.

Strong relations were observed between the experimental results obtained for $pen.$, $T_{R\&B}$, T_{Fraass}, steady shear viscosity at 25°C (η_0) and the critical temperatures $(T_{DSR\ high\ critical}\ and\ T_{BBR\ low\ critical})$.

Two different estimation methods were proposed and $pen.$, $T_{R\&B}$, T_{Fraass}, 2S2P1D parameters $(h, \beta\ and\ \tau)$, a_T temperature shift factors, $T_{DSR\ high\ critical}$, $T_{BBR\ low\ critical}$ and $|G^*(T,f)|$ values were estimated for all produced binder blends from experimental results obtained for the base constituents.

With both estimation methods, good correspondences were found between estimated and experimental values of all blends. Both methods can be considered valid for these tested blends.

Slightly better correspondence was found between the estimated values of all above-mentioned parameters obtained with the 2nd estimation, which is an original contribution of this work, and experimental values. Moreover, the 2nd estimation has also the great advantage to need only one data for each of the three base constituents when the dosage if fixed.

The estimation approaches used to obtain $|G^*(T,f)|_{est.1\ or\ 2}$ values cannot be applied for the phase angle, $|G^*(T,f)|$ and $\varphi(T,f)$ cannot be estimated independently. Therefore, in order to obtain phase angle values of all binder blends over the whole frequency and temperature domain, the 2S2P1D model was calibrated on master curves of $|G^*(T,f)|_{est.1\ or\ 2}$ at a reference temperature of 55°C in order to be sure that all analysed binders are thermorheologically simple.

The determined values of $\varphi(T,f)$ are significantly close to the measured values for all binder blends. A higher global value of R^2 was found for the second calculation (0.984) than using the first (0.974). Due to the satisfactory values of R^2 that were found, this approach can be considered valid for the tested blends. However, a better correlation with the experimental measurements was found for the phase angle values calculated from the 2S2P1D fitted on the $|G^*(T,f)|_{est.2}$ values.

A statistical analysis was performed in order to highlight the accuracy of both estimation methods for all parameters, considering all binder blends. Thus, a more accurate estimation resulted by applying the second estimation method.

It must be mentioned that the 2nd estimation approach could work for new combination of RAP/Rejuvenator, only if the experimental results obtained for the RAP and fresh binders and the equivalent parameters considered for the rejuvenator are available.

In addition, if the equivalent parameters for the rejuvenator are not known from previous experiments, a good approximation can be obtained from only one test performed on the binder blend produced with the RAP binder and the maximum rejuvenator content (RAP + 15% Rej in the case of this study). The results using these approximated values for the rejuvenator are very similar than the ones considering the optimized values. This conclusion is also validated on two new blends having other rejuvenator contents (7.5% and 8.5%).

The approximated proposed approach presents the great advantage of requiring less tests than the classical approach and can be used for any combination of RAP/rejuvenator, in contrast to the classical approach.

The equivalent parameters for the rejuvenator are probably only rejuvenator dependent, which is another advantage of the proposed method. This point should be confirmed with a wider range of fresh and RAP binder types.

These conclusions are based on the research that was conducted on 17 binders and therefore further investigation of the estimation of the above-mentioned parameters of binder blends is still needed and the validation of this proposed approach has to be performed on different materials such as different other binders, aged binders and different rejuvenators.

3. Performed tests on bituminous mixtures, analysis and modelling

3.1 Objectives

The main objective of the chapter is to highlight the effects of the RAP material and the rejuvenator on the thermo-mechanical properties of different bituminous mixtures produced with different amounts of RAP material and with or without a mix of vegetal origin used as a rejuvenator. One conventional Hot Mix Asphalt is considered as a reference. The possible relation between the behaviour of the bituminous mixtures and the properties of their corresponding binder blends from Chapter 2, was investigated.

All materials (aggregates, binders and RAP material) were characterized by performing a series of tests according to the specifications from the Romanian Standards [14]. The experimental plan was divided in two campaigns. In the first campaign, seven types of HMA, produced only with virgin materials, were investigated in order to determine the optimal binder content of the mix. This content is used in the second campaign where the behaviour of twelve bituminous mixtures produced with RAP material and with or without rejuvenator was investigated.

The influence of the RAP material and rejuvenator on the behaviour of all mixtures was analysed by performing the following tests and by evaluating the below mentioned parameters:

- hydrostatic measurements:
  - SSD bulk density: $\rho_{A.bit.mix.}$;
  - water absorption: $A_{V\,bit.mix.}$;
  - void content $V_{M\,bit.mix.}$ and voids in mixing aggregates and filled with bitumen: $VMA_{bit.mix.}$, $VFB_{bit.mix.}$.
- Marshall test:
  - Marshall stability: $S_{bit.mix.}$;
  - Marshall flow: $F_{bit.mix.}$;
  - Marshall tangential flow: $F_{t\,bit.mix.}$;
  - ratio between Marshall stability and flow: $S/F_{bit.mix.}$.
- indirect tension test on cylindrical samples (IT-CY) at different temperatures 10°C, 15°C, 20°C, 25°C:
  - measured and adjusted stiffness modulus: $S_M(T)$, $S_A(T)$.
- permanent deformation resistance (dynamic creep) 10000 impulses, 300 kPa, 50 kPa (confinement pressure), 50°C:
  - cumulative axial strain of specimen after 10000 impulses: ε_{10000};
  - creep rate: f_c.
- complex modulus – two-point bending test on trapezoidal samples:
  - norm of complex modulus: $\left|E^*(T,f)\right|$ and phase angle: $\varphi(T,f)$.

More details regarding the experimental results obtained for all above mentioned parameters for all bituminous mixtures, the materials characterization and the test procedures are given in the following sections.

3.2 Materials components characterization

The materials used in this work were chosen with respect to the specifications given in the Romanian Standards [14] in order to produce bituminous mixtures with the maximum aggregate size of 16 mm by adding RAP material with and without rejuvenator. The materials used in this study are:

- quarry crushed aggregates (0-4 mm; 4-8 mm and 8-16 mm);
- natural sand 0-4 mm;
- limestone filler;
- RAP material (divided into two lots: 0-8 mm; 8-22.4 mm);
- fresh 50/70 binder;
- rejuvenator (oil of vegetal origin).

Each material (Figure 3.1) was characterized starting with the fresh aggregates (the tests performed for each aggregate group and the results are show in Tables 3.1 to 3.4), RAP material (results shown in Tables 3.5 and 3.6) and finally the fresh 50/70 binder and the rejuvenator (their properties and characterization were analysed in Section 2).

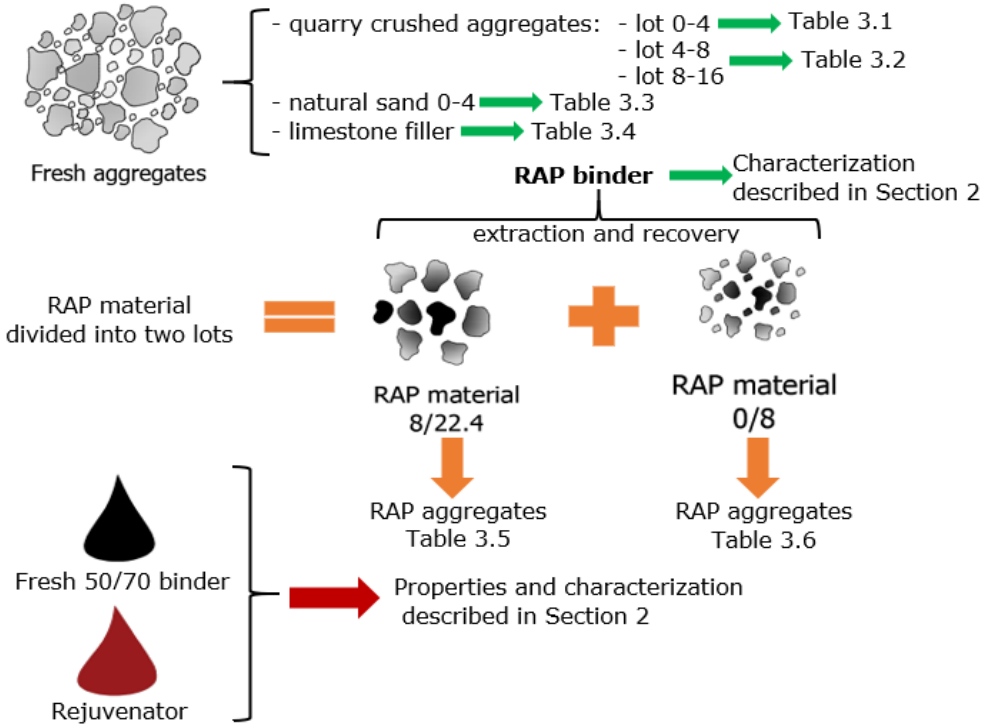

Figure 3.1. Bituminous mixtures components.

All the tests on the fresh aggregates and RAP aggregates were performed with respect to the European/Romanian Standards.

The crushed aggregates (0-4 mm, 4-8 mm and 8-16 mm) have the same origin from 'Morlaca' quarry. According to the specification of the producer the aggregate nature is dacite which is an intermediate composition between andesite and rhyolite. The natural sand 0-4 mm comes from 'Sambateni' gravel pit and the limestone filler from 'Alesd'. In order to check their quality, for each sort of aggregates some specific characteristics were determined. The results are reported in Tables 3.1 to 3.5.

Table 3.1. Crushed aggregates 0-4 mm characteristics.

Characteristics	Results	Standard procedures
Granularity sort, d/D Granularity Purity-fine particles (63µm), %	0/4 G_A 90 f 10	SR EN 933-1:2012
Assessment of fines - Methylene blue test, g/kg	MB 2	SR EN 933-9+A1:2013
Sand equivalent, %	SE 50	SR EN 933-8:2015
Dry real density, kg/m^3 Water absorption, %	2.63 WA_{24} 0.9	SR EN 1097-6:2013

Table 3.2. Crushed aggregates 4-8 mm and 8-16 mm characteristics.

Characteristics	Sort 4-8	Sort 8-16	Standard procedures
Granularity sort, d/D Granularity Purity-fine particles (63µm), %	4/8 G_C 90/10 f 1.5	8/16 G_C 90/10 f 0.5	SR EN 933-1:2012
Shape index, %	SI 25	SI 20	SR EN 933-4:2008
Flakiness index, %	FI 20	FI 20	SR EN 933-3:2012
Dry real density, kg/m^3 Water absorption, %	2.65 WA_{24} 0.8	2.65 WA_{24} 0.6	SR EN 1097-6:2013
Resistance to fragmentation - Los Angeles coefficient	LA 15	LA 15	SR EN 1097-2:2010
Resistance to wear - micro-Deval coefficient	M_{DE} 10	M_{DE} 10	SR EN 1097-1:2011
Affinity between aggregate and bitumen (fresh 50/70 binder), %	Af 89	Af 89.5	SR EN 12697-11:2012
Adhesivity between binder (fresh 50/70 binder) and aggregate - spectrophotometric method, %	85	85.8	SR 10969:2007

Table 3.3. Natural sand 0-4 mm characteristics.

Characteristics	Results	Standard procedures
Granularity sort, d/D Granularity Purity-fine particles (63µm), %	0/4 G_F 85 f 3	SR EN 933-1:2012
Sand equivalent, %	SE 88	SR EN 933-8:2015
Dry real density, kg/m^3 Water absorption, %	2.55 WA_{24} 1.3	SR EN 1097-6:2013

Table 3.4. Limestone filler characteristics.

Characteristics	Results	Standard procedure
Granularity, % passing through:		
- sieve 2 mm	100.0	
- sieve 0.125 mm	93.0	SR EN
- sieve 0.063 mm	77.2	13043:2003/AC:2004
Moisture content, %	0.9	
Real specific gravity, kg/m^3	2.64	

All the results obtained for each material are consistent with the Standard specifications, therefore these materials can be used in the production of bituminous mixtures.

The RAP material was obtained from a national road from Timis county, Romania. It was classified and described by performing the tests required by SR EN 13108-8 [51], regarding the characteristics of the material before and after the binder extraction as characteristics of the RAP aggregates and of the RAP binder. The RAP material was divided into two lots: 0-8 mm and 8-22.4 mm.

It must be specified that the RAP material used for each mix has identical proportion of 25% RAP 0-8 mm + 75% RAP 8-22.4 mm. Complete binder extraction was performed in the Road Laboratory from University Politehnica Timisoara, by using the 'asphaltanalysor' according to SR EN 12697-3 [53]. The binder content of this RAP material mix, measured trough extraction and recovery is 4% (determined as the average value over 30 measurements). After each extraction the gradation curve of the RAP aggregates and the resistance to wear - micro-Deval coefficient were determined. The average values are reported in Table 3.5.

Table 3.5. RAP aggregates characteristics.

Characteristics	Results	Standard procedure
Granularity, % passing through:		
- sieve 22.4 mm	100.0	
- sieve 16 mm	100.0	
- sieve 8 mm	64.60	SR EN 933-1:2012
- sieve 4 mm	43.70	
- sieve 2 mm	27.50	
- sieve 0.125 mm	13.00	
- sieve 0.063 mm	7.50	
Resistance to wear - micro-Deval coefficient	M_{DE} 10	SR EN 1097-1:2011

A 50/70 pen. grade binder was used as fresh binder. A mixture of vegetal oils was used as a rejuvenator. The characterisation of these two materials together with the RAP extracted binder is described in Chapter 2. It is important to notice that the same binders and blends as the ones tested in Chapter 2 are introduced in the tested mixtures.

3.3 Experimental plan

The experimental plan regarding the bituminous mixtures was divided in two campaigns:

- first campaign, seven types of HMA, produced only with virgin materials, were investigated to determine the optimal binder content of the mix considered as the conventional mix. This content is used in the second campaign.
- second campaign, twelve bituminous mixtures produced with different amounts of RAP material with or without rejuvenator, all having the same grading curve as the conventional HMA and the same binder content without rejuvenator were tested in order to highlight the influence/effect of the rejuvenator and RAP material on the thermomechanical properties of the final bituminous mixtures.

The experimental plan is presented in Figure 3.2. More details regarding all tested bituminous mixtures such as composition, samples production, etc. are given in Section 3.4. The experimental procedures used in order to perform all tests are described in Section 3.5.

3.3.1 First campaign

For the HMA produced only with virgin materials a series of tests according to the Romanian Standards were performed to determine the optimal binder content. Hydrostatic measurements, Marshall tests and indirect tension tests at 20°C were performed to determine the volumetric characteristics, mechanical and thermomechanical properties of all HMAs. Figure 3.2 shows the determined parameters.

All seven HMAs tested in order to determine the optimal binder content were named as follows (see Table 3.6):

- ”HMA.” for Hot Mix Asphalt;
- fresh binder content: ”5.2”, ”5.4”, ”5.6”, ”5.7”, ”5.8”, ”6.0”, ”6.2”.

Table 3.6. Bituminous mixtures HMAs name and characteristics.

Bituminous mixtures HMA names	Characteristics
HMA.5.2	
HMA.5.4	No RAP material.
HMA.5.6	No rejuvenator.
HMA.5.7	Same grading curve.
HMA.5.8	Different binder content
HMA.6.0	from 5.2% up to 6.2%.
HMA.6.2	

More details regarding the mix design and analysis of the obtained results for these HMAs are given in Section 3.6.

3.3.2 Second campaign

Twelve different bituminous mixtures were produced with different amounts of RAP material with/without rejuvenator. Proportions of the base components were

calculated to produce bituminous mixtures with a total binder content of 5.6% rejuvenator not included, containing 25%, 50% and 75% RAP material and different dosages of rejuvenator: 0%, 0.2%, 0.4% and 0.6% by mass of the RAP material. One conventional HMA bituminous mixture produced with virgin materials was used as reference.

All 13 bituminous mixtures have the following common characteristics:

- continuous 16 mm grading curve;
- 5.60% total binder content by weight of the final mix not including here the rejuvenator;
- the RAP material used for each mix has the same proportion: 25% RAP 0-8 mm + 75% RAP 8-22.4 mm. The binder content of this RAP material mix, measured trough extraction and recovery is 4%.

Table 3.7 shows the 13 types of bituminous mixtures produced with RAP material and with or without rejuvenator and their corresponding binder blends which were tested in Chapter 2. It is important to notice that the same binders and blends as the ones tested in Chapter 2 are introduced in the tested mixtures. However, it is important to mention that the binder blends investigated in Chapter 2 were perfectly blended in the laboratory. Even if the percentages between fresh, RAP binder and rejuvenator are the same, some differences between these perfect blends (Chapter 2) and the blends from the mixtures can occur.

All 13 bituminous mixtures were named as follows:

- ”D.” for dosage;
- RAP material amount in percentage: ”0.”, ”25.”, ”50.”, ”75.”;
- ”R.” for rejuvenator;
- rejuvenator amount by the mass of RAP material: ”0”, ”0.2”, ”0.4”, ”0.6”.

Table 3.7. Bituminous mixtures and corresponding binder blends tested in Chapter 2.

Bituminous mixtures	Corresponding binder blends
D.0.R.0	50/70
D.25.R.0	50/70+25%RAP
D.25.R.0.2	50/70+25%RAP+5%Rej
D.25.R.0.4	50/70+25%RAP+10%Rej
D.25.R.0.6	50/70+25%RAP+15%Rej
D.50.R.0	50/70+50%RAP
D.50.R.0.2	50/70+50%RAP+5%Rej
D.50.R.0.4	50/70+50%RAP+10%Rej
D.50.R.0.6	50/70+50%RAP+15%Rej
D.75.R.0	50/70+75%RAP
D.75.R.0.2	50/70+75%RAP+5%Rej
D.75.R.0.4	50/70+75%RAP+10%Rej
D.75.R.0.6	50/70+75%RAP+15%Rej

As an example, the mixture produced with 75% RAP material and 0.4% of rejuvenator by mass of the RAP material is called: D.75.R.0.4.

Hydrostatic measurements, Marshall tests, indirect tension tests on cylindrical specimens at different temperatures, cyclic compression tests with confinement and complex modulus tests: two-point bending test on trapezoidal specimens, were performed on all mixtures from Table 3.7. The parameters that will be investigated in the following sections are presented in Figure 3.2.

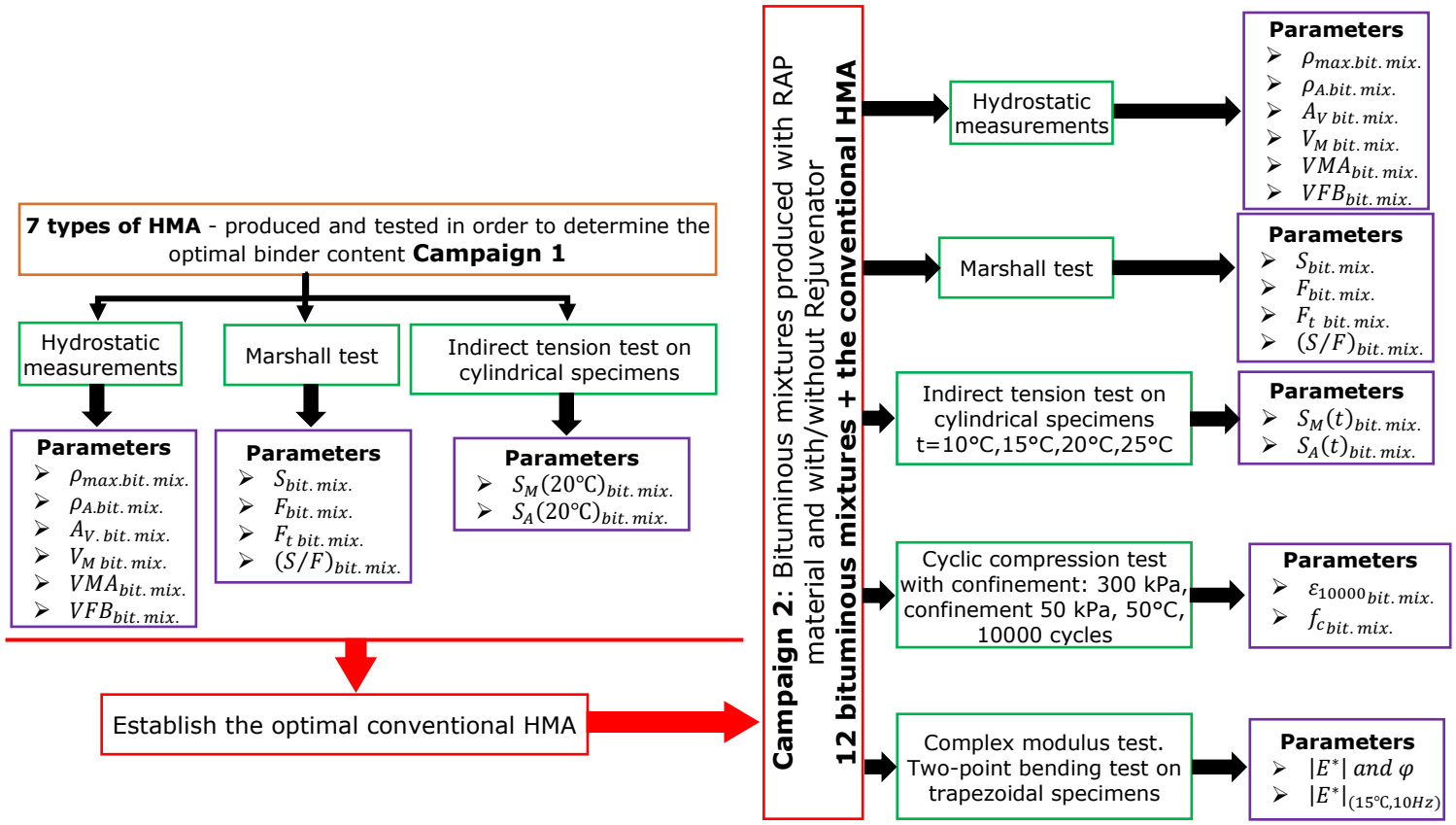

Figure 3.2. Scheme of the two experimental campaigns for bituminous mixtures.

3.4 Tested materials

3.4.1 Tested bituminous mixtures

As mentioned in the previous section, seven HMAs were produced and tested in order to determine the optimal binder content. For this purpose, the same grading curve was used with different binder content. The proportions by weight of the final mix for the considered HMA's are reported in Table 3.6.

Figure 3.3 shows the grading curve used for the considered HMAs presented in Table 3.8, together with the minimum and maximum limitations specified in the Romanian Standards for a bituminous mixture with a 16 mm maximum aggregate size.

Table 3.8. Proportions by weight of the final mix for the considered HMAs (Campaign 1).

Mix design	Proportions by weight of the final mix, %					
	C.R. 8-16	C.R. 4-8	C.R. 0-4	N.S. 0-4	Filler	Bitumen
HMA.5.2	23.70	20.86	40.76	2.84	6.64	5.20
HMA.5.4	23.65	20.81	40.68	2.84	6.62	5.40
HMA.5.6	23.60	20.77	40.59	2.83	6.61	5.60
HMA.5.7	23.58	20.75	40.55	2.83	6.60	5.70
HMA.5.8	23.55	20.72	40.51	2.83	6.59	5.80
HMA.6.0	23.50	20.68	40.42	2.82	6.58	6.00
HMA.6.2	23.45	20.64	40.33	2.81	6.57	6.20

*C.R. - crushed aggregates
*N.S. - natural sand

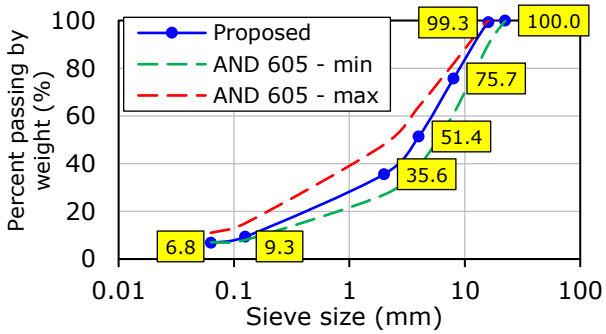

Figure 3.3. Grading curve used for the bituminous mixtures presented in Table 3.8 (Campaign 1).

The conventional HMA bituminous mixture HMA.5.6 was found to be optimal mix, details are given in Section 3.6. This bituminous mixture was then used as the reference one and named D.0.R.0. On this basis, twelve different bituminous mixtures were produced with a total binder content of 5.6%, not considering the rejuvenator and containing 25%, 50% and 75% RAP material and different dosages of rejuvenator: 0%, 0.2%, 0.4% and 0.6% by mass of the RAP material.

A similar grading curve, as the one presented in Figure 3.3, was used for the considered bituminous mixtures, considered in Table 3.9 and Table 3.10 (Campaign 2), together with the minimum and maximum limitations specified in the Romanian

Standards [14]. As example, Figure 3.4 shows the grading curves used for the mixtures D.25.R.0, D.50.R.0 and D.75.R.0 form Campaign 2. It can be observed that some small differences between the grading curves used for the three mixtures produced with RAP material and the one used for the conventional mix, were obtained.

It must be mentioned that for the bituminous mixtures produced with 75% RAP material and different percentages of rejuvenator (Table 3.10) in order to reproduce the same continuous 16 mm grading curve as for the other bituminous mixtures, the crushed aggregates 0-4 mm was sieved and separate fractions (0.125, 2 and respectively 4 mm) were used.

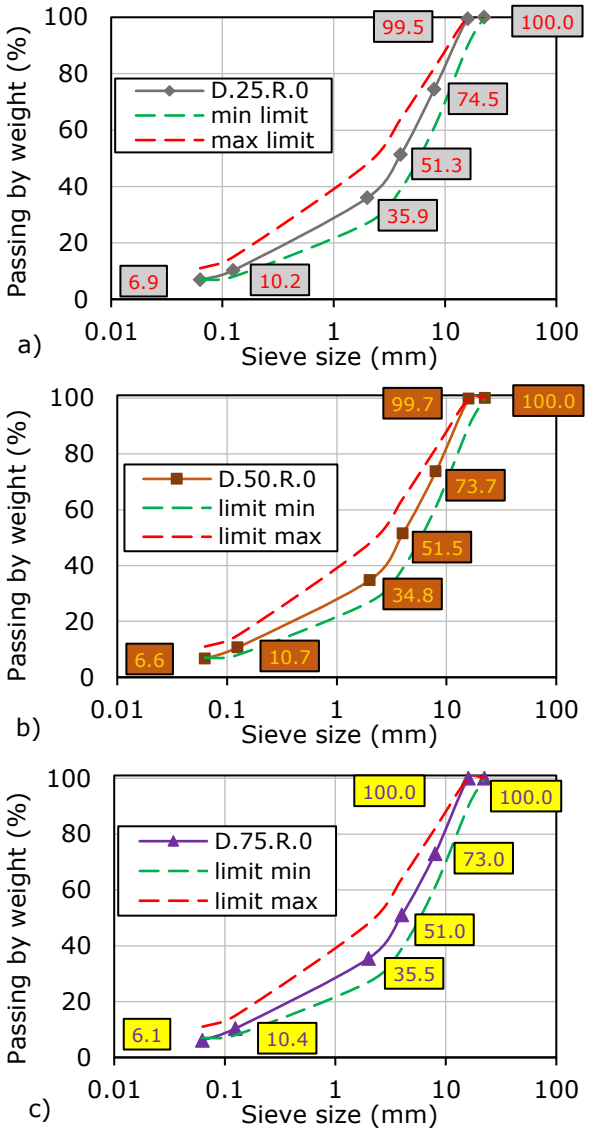

Figure 3.4. Grading curves used for the bituminous mixtures: (a) D.25.R.0; (b) D.50.R.0; (c) D.75.R.0.

Table 3.9. Proportions in percent (%) of base materials within the bituminous mixtures produced only with virgin materials, 25% RAP material and 50% RAP with/without rejuvenator (Campaign 2).

Bituminous mixtures	Proportions in percent (%)									
	Crushed aggregates			Natural sand 0-4	Filler	RAP material			Fresh binder	Rej.
	8-16	4-8	0-4			Agg. from RAP 8-22.4	Agg. from RAP 0-8	RAP binder		
D.0.R.0	23.60	20.77	40.59	2.83	6.61	-	-	-	5.60	-
D.25.R.0	16.10	12.94	35.87	0.87	4.62	18.00	6.00	1.00	4.60	-
D.25.R.0.2	16.09	12.93	35.85	0.87	4.62	17.99	6.00	1.00	4.60	0.05
D.25.R.0.4	16.08	12.93	35.83	0.87	4.62	17.98	5.99	1.00	4.60	0.10
D.25.R.0.6	16.07	12.92	35.82	0.87	4.61	17.97	5.99	1.00	4.60	0.15
D.50.R.0	8.02	7.98	28.13	-	2.27	36.00	12.00	2.00	3.60	-
D.50.R.0.2	8.02	7.97	28.10	-	2.26	35.95	12.00	2.00	3.60	0.10
D.50.R.0.4	8.01	7.96	28.08	-	2.26	35.92	11.97	2.00	3.60	0.20
D.50.R.0.6	8.00	7.96	28.05	-	2.26	35.88	11.95	2.00	3.60	0.30

Table 3.10. Proportions in percent (%) of base materials within the bituminous mixtures produced with 75% RAP material with/without rejuvenator (Campaign 2).

Bituminous mixtures	Proportions in percent (%)											
	Crushed aggregates					Natural sand 0-4	Filler	RAP material			Fresh binder	Rej.
	8-16	4-8	0-4					Agg. from RAP 8-22.4	Agg. from RAP 0-8	RAP binder		
			fr. 0.125	fr. 2	fr. 4							
D.75.R.0	-	-	13.21	3.78	4.94	-	0.47	54.00	18.00	3.00	2.60	-
D.75.R.0.2	-	-	13.20	3.77	4.93	-	0.47	53.92	17.97	3.00	2.60	0.15
D.75.R.0.4	-	-	13.18	3.76	4.91	-	0.47	53.84	17.94	3.00	2.60	0.30
D.75.R.0.6	-	-	13.16	3.75	4.90	-	0.47	53.76	17.91	3.00	2.60	0.45

3.4.2 Production of bituminous mixture specimens

The mixing temperature used in order to produce all bituminous mixtures was chosen with respect to the European and Romanian Standard SR EN 12697-35 [187] and AND 605 [14] for bituminous mixtures realized with RAP material and fresh crushed aggregates with a 16 mm maximum aggregate size. Therefore, the mixing temperature was 160±10°C.

All materials were preheated/conditioned as follows:

- the fresh aggregates of crushed aggregates, natural sand and filler were preheated at 160±10°C for 12 hours;
- the fresh binder was preheated at 160±10°C for 4 hours;
- the RAP material was preheated at a 165±10°C for 2 hours;
- the rejuvenator was not preheated.

The mixing process was performed by using a heated mechanical mixer (Figure 3.5). First the fresh aggregates were inserted into the mixer, then RAP material, fresh binder and rejuvenator. The mixing time was equal to 5 min. A total of 30 kg of bituminous mixture was produced per each mix process.

Figure 3.5. Matest mixer - University Politehnica Timisoara.

Three types of compaction were performed, as follows:

- Marshall impact compaction – cylindrical specimens compacted at 50 blows/part – SR EN 12697-30 [188]. The Marshall impact compactor which was used is shown in Figure 3.6a;
- gyratory compaction – cylindrical specimens compacted at 80 gyrations – SR EN 12697-31 [189]. The gyratory press which was used is shown in Figure 3.6b;
- slabs produced according to SR EN 12697-33 [190] by using a steel roller compactor show in Figure 3.6c.

A total of 69 Marshall cylindrical specimens, 82 cylindrical gyratory specimens and 13 slabs were produced. All bituminous mixtures and all specimens were produced in the Road Laboratory from University Politehnica Timisoara. Table 3.11 presents the number of specimens produced for each type of compaction per each type of bituminous mixture.

All slabs, regardless of the bituminous mixture type, were compacted by using the same level of compaction by 39 passes. The levels of compaction per each group of passes are shown in Table 3.12.

Trapezoidal specimens for complex modulus two-point bending test were cut from slabs. Four specimens were cut per each slab. The coring plan for one slab is presented in Figure 3.7.

A selection between the trapezoidal specimens was performed according to void content, the dimensions of specimens. Therefore, a lot of two specimens which meet the accuracy of ±1 mm for each dimension and which has the average void content as similar as possible, were selected for the complex modulus two-point bending test.

(a) (b) (c)

Figure 3.6. (a) Matest Marshall impact compactor; (b) Matest gyratory compactor; (c) Roller compactor - Road Laboratory, University Politehnica Timisoara.

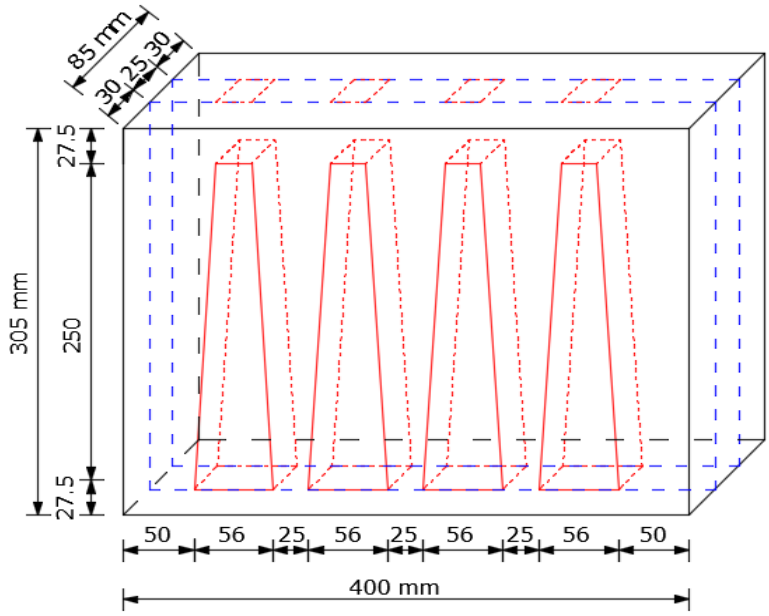

Figure 3.7. Coring plan of slabs followed at the Road Laboratory - University Politehnica Timisoara.

Table 3.11. Specimens produced and tested/each bituminous mixture/each compaction type in Campaign 1 and Campaign 2.

	Bituminous mixtures	Marshall cylindrical specimens	Cylindrical specimens gyratory compaction	Slabs
Campaign 1	HMA.5.2	3	3	-
	HMA.5.4	3	3	-
	HMA.5.6	3	3	-
	HMA.5.7	3	3	-
	HMA.5.8	3	3	-
	HMA.6.0	3	3	-
	HMA.6.2	3	3	-
Campaign 2	D.0.R.0	3	4	1
	D.25.R.0	3	4	1
	D.25.R.0.2	3	4	1
	D.25.R.0.4	3	4	1
	D.25.R.0.6	3	4	1
	D.50.R.0	3	4	1
	D.50.R.0.2	3	4	1
	D.50.R.0.4	3	4	1
	D.50.R.0.6	3	4	1
	D.75.R.0	3	4	1
	D.75.R.0.2	3	4	1
	D.75.R.0.4	3	4	1
	D.75.R.0.6	3	4	1

Table 3.12. Slabs compaction specifications (slabs prepared by roller compactor) – Campaign 2.

Passes	Compaction load, kN
2	0.5
4	1.0
8	2.0
8	3.0
8	7.0
9	11.0

3.5 Experimental procedures

3.5.1 Bulk density and water absorption. Determination of void content. Hydrostatic method

For all bituminous mixture specimens, regardless of the compaction type, the bulk density, water absorption and void content were determined by using the

hydrostatic method according to the Romanian/European Standards SR EN 12697-6 [191] bulk density, AND 605-Annex B [14] water absorption and SR EN 12697-8 [192] voids content. On the other side, for each type of bituminous mixture the maximum density was determined by using the hydrostatic method, according to SR EN 12697-5 [193].

In order to perform all the above determinations, the following apparatus were used: callipers 0.1 mm, in order to determine the dimensions of specimens according to SR EN 12697-29 [194], balance with an accuracy of 0.01 g, water-bath, thermometer, vacuum system, ventilated oven and other auxiliary tools.

The procedure used to determine the bulk density of all specimens was the so-called SSD procedure (saturated surface dry), which is described in Figure 3.7.

As presented in Figure 3.8 - step 2, the density of the water (ρ_w in kg/m^3) was calculated at the test temperature t in °C. According to SR EN 12697-8 [192], equation 3.1 was considered.

$$\rho_w = 1.00025205 + \left(\frac{7.59 \times t - 5.32 \times t^2}{10^6} \right) \tag{3.1}$$

where:

t – temperature of the water, in °C;

ρ_w – water density, in kg/m^3.

After determining by weighing the mass of the dry specimen, in g, M, the mass of the saturated specimen in water, in g, m_1, and the mass of the saturated surface-dried specimen in air, in g, m_2, the SSD bulk density $\left(\rho_{specimen}\right)$ of the specimen was calculated by using equation 3.2.

$$\rho_{specimen} = \frac{M}{m_2 - m_1} \times \rho_w \tag{3.2}$$

where:

$\rho_{specimen}$ – SSD bulk density of the specimen, in kg/m^3;

M – mass of the dry specimen, in g;

m_1 – mass of the specimen after 1 h maintained in water, measured in air, in g;

m_2 – mass of the specimen after 1 h maintained in water, measured in water, in g;

ρ_w – water density (determined by using equation 3.1).

Specimens production

Cylindrical specimens:
- Marshall specimens: 50 blows/part (SR EN 12697-30);
- gyratory press specimens: 80 gyrations (SR EN 12697-31).

Trapezoidal specimens: cored from slabs. The same level of compaction was used SR EN 12697-33.

↓

After compaction

Rest period 4 days at ambient temperature. For trapezoidal specimens more details given in Section 3.4.2.

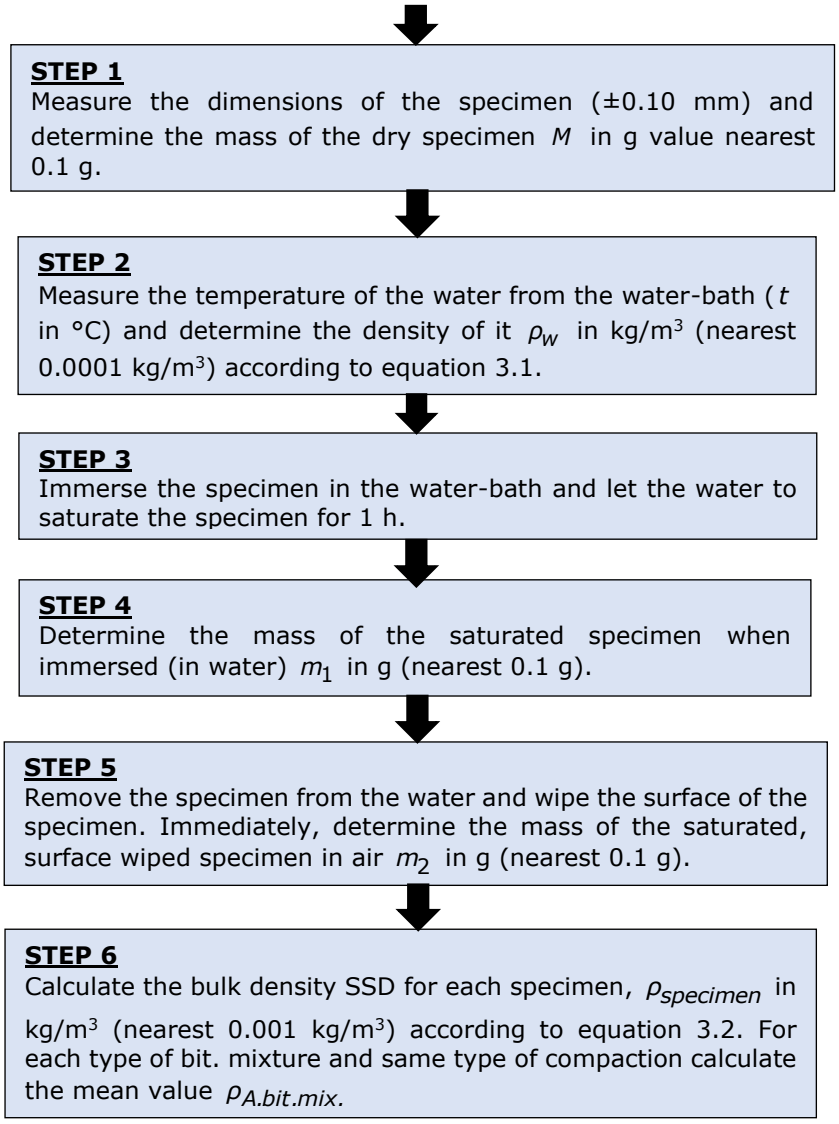

Figure 3.8. Procedure used in order determine the bulk SSD density.

The procedure followed in order to determine the water absorption for each specimen consist in continuing the procedure used for bulk density and described in Figure 3.7 with the steps presented in Figure 3.9.

A mean value of the SSD bulk density $(\rho_{A.bit.mix.})$ was calculated as the average value of all $\rho_{specimen}$ values obtained for all the specimens produced for each type of bituminous mixture and by using the same type of compaction.

In order to calculate the initial (V_1) and the final (V_2) volume of the specimen, kept in water equations 3.3 and 3.4 were used. The density of the water from the exicator (ρ_{w1} in kg/m³) was calculated by using equation 3.1.

$$V_1 = \frac{m_2 - m_1}{\rho_w} \tag{3.3}$$

$$V_2 = \frac{m_3 - m_4}{\rho_{w1}} \tag{3.4}$$

where:

V_1 – initial volume of the specimen after 1 h keeping in water, in cm^3;

m_1 – mass of the specimen after 1 h keeping in water, measured in air, in g;

m_2 – mass of the specimen after 1 h keeping in water, measured in water, in g;

ρ_w – water density determined by using equation 3.1;

V_2 – final volume of the specimen after 3 h keeping in water + vacuum and 2 h in water at atmospheric pressure, in cm^3;

m_3 – mass of the specimen after 3 h keeping in water + vacuum and 2 h in water at atmospheric pressure, in air, in g;

m_4 – mass of the specimen after 3 h keeping in water + vacuum and 2 h in water at atmospheric pressure, in water, in g;

ρ_{w1} – water density determined by using equation 3.1.

In order to determine the water absorption $\left(A_{V\,specimen}\ in\ \%vol.\right)$ reported to the volume of the specimen equations 3.5 and 3.6 were considered, depending on the difference between the two volumes $\left(V_1\ and\ V_2\right)$.

$$If\ V_1 > V_2 \rightarrow A_{V\,specimen} = \frac{(m_3 - M)/\rho_{w1}}{(m_2 - m_1)/\rho_w} \times 100 \tag{3.5}$$

$$If\ V_2 > V_1 \rightarrow A_{V\,specimen} = \frac{\left\{(m_3 - M) - \left[(m_3 - m_4) - (m_2 - m_1)\right]\right\}/\rho_{w1}}{(m_2 - m_1)/\rho_w} \times 100 \tag{3.6}$$

A mean value of the water absorption $\left(A_{V\,mean}\right)$ was calculated as the average value of all $A_{V\,specimen}$ values obtained for all the specimens produced for each type of bituminous mixture and by using the same type of compaction.

STEP 1
Follow the procedure presented in Figure 3.7 and calculate the volume of the specimen, V_1 in cm^3.

STEP 2
The specimens are introduced in a vacuum exicator which is fill with water. Measure the temperature of the water (t_1 in °C) and determine the density of it ρ_{w1} in kg/m^3.

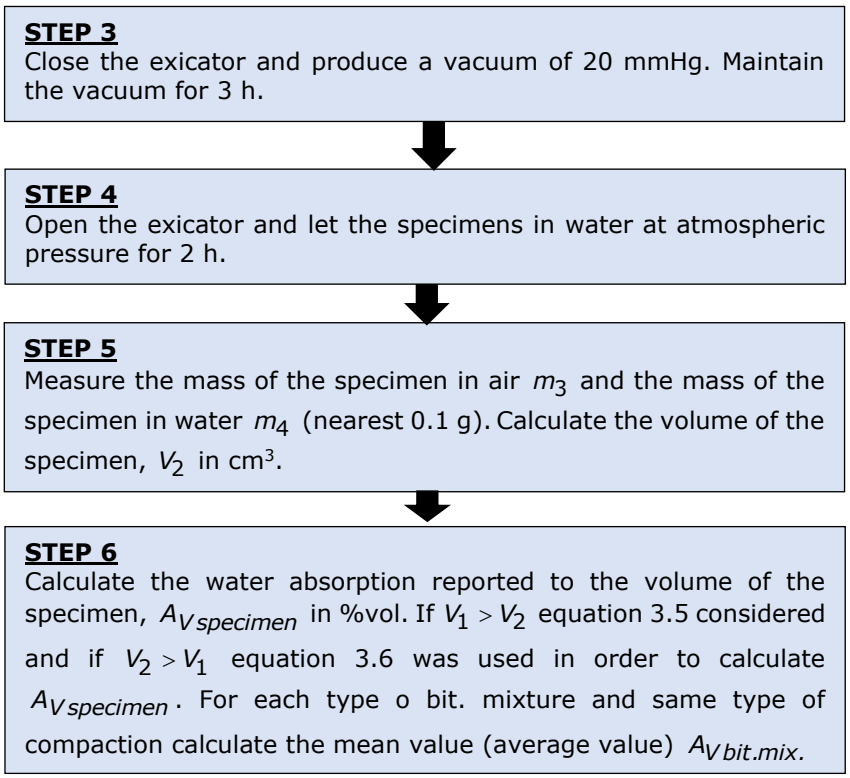

Figure 3.9. Procedure used in order determine the water absorption.

The procedure used to determine the maximum density of each type of bituminous mixture is described in Figure 3.10.

In order to determine the maximum density $\left(\rho_{max.bit.mix.}\right)$ of each bituminous mixture, equations 3.7 was considered.

$$\rho_{max.bit.mix.} = \frac{m_{III} - m_I}{(m_{III} - m_I) - (m_{IV} - m_{II})} \times \rho_w \qquad (3.7)$$

where:

$\rho_{max.bit.mix.}$ – maximum density of the bituminous mixture determined by hydrostatic method, in kg/m^3;

m_I – mass in air of the glass container, in g;

m_{II} – mass under water of the glass container, in g;

m_{III} – mass in air of the glass container + bit. mix. specimen, in g;

m_{IV} – mass under water of the glass container + bit. mix. specimen, in g;

ρ_w – water density at the test temperature 25°C (determined by using equation 3.1).

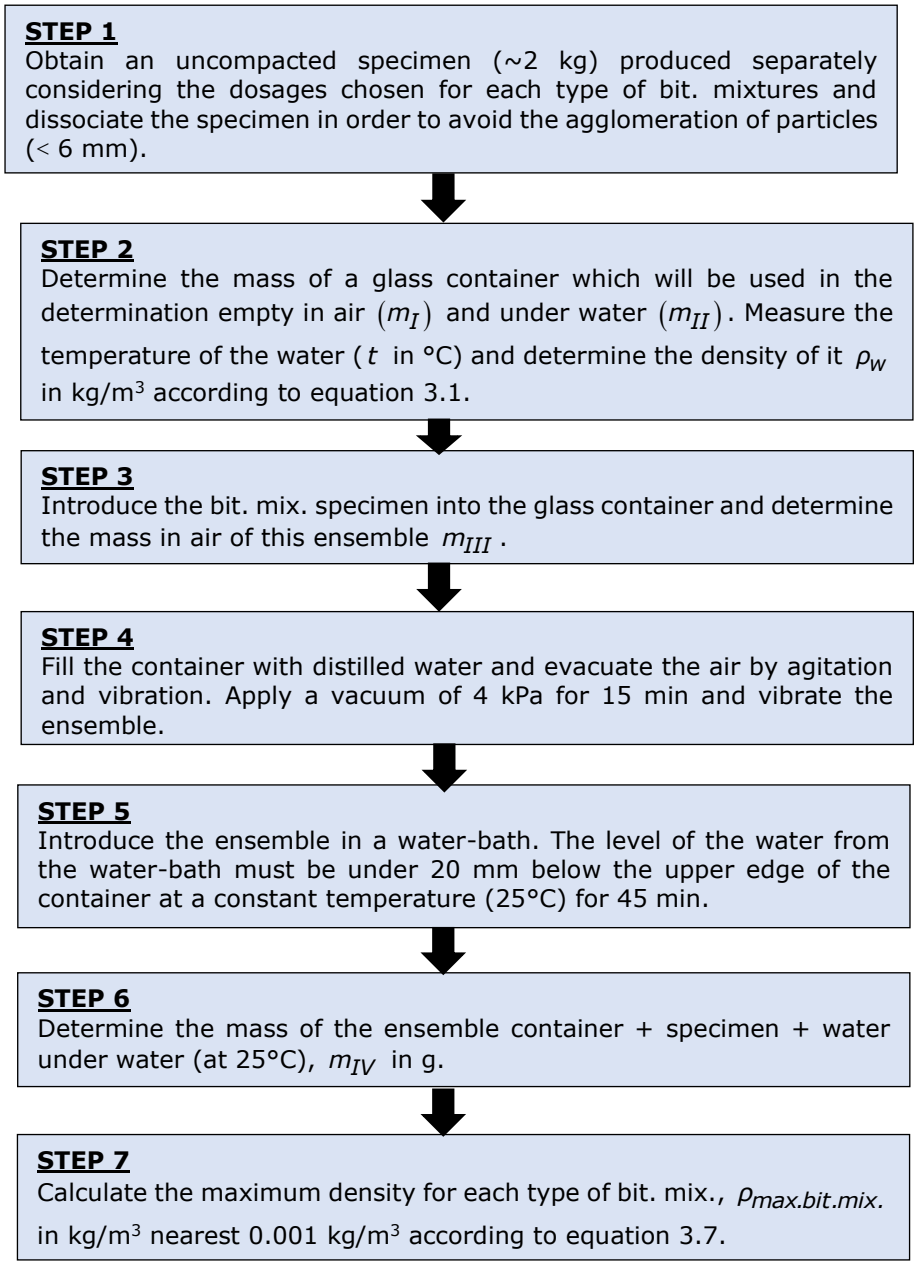

Figure 3.10. Procedure used in order determine the maximum density.

For each specimen the percent of the air voids $\left(V_{M\,specimen}\right)$ was calculated with 0.1% (v/v) accuracy by using equation 3.8. A mean value of the air voids $\left(V_{M\,mean}\right)$ was calculated as the average value of all V_M values obtained for all the

specimens produced for each type of bituminous mixture and by using the same type of compaction.

$$V_{M\,specimen} = \frac{\rho_{max.bit.mix.} - \rho_{specimen}}{\rho_{max.bit.mix.}} \times 100 \quad (3.8)$$

where:

$V_{M\,specimen}$ – air voids content in the specimen, in % (v/v);

$\rho_{max.bit.mix.}$ – maximum density of the bituminous mixture determined by hydrostatic method, in kg/m^3, determined with equation 3.7;

$\rho_{specimen}$ – SSD bulk density of specimen, in kg/m^3, determined with equation 3.2.

Based on the previous determinations, the percent of the void in mixed aggregates $\left(VMA_{specimen}\right)$ and the percent of the voids filled with bitumen $\left(VFB_{specimen}\right)$ can be calculated with 0.1% (v/v) accuracy by using equations 3.9 and 3.10.

The mean values of the percent of the void in mixed aggregates $\left(VMA_{mean}\right)$ and of the percent of the voids filled with bitumen $\left(VFB_{mean}\right)$ were calculated as the average values of all $VMA_{specimen}$ and $VFB_{specimen}$ values obtained for all the specimens produced for each type of bituminous mixture and by using the same type of compaction.

$$VMA_{specimen} = V_{M\,specimen} + b \times \frac{\rho_{specimen}}{\rho_b} \times 100 \quad (3.9)$$

$$VFB_{specimen} = \frac{b \times \rho_{specimen} / \rho_b}{VMA_{specimen}} \times 100 \quad (3.10)$$

where:

$VMA_{specimen}$ – percent of voids in mixed aggregates in the specimen, in 0.1% (v/v);

$VFB_{specimen}$ – percent of voids filled with bitumen in the specimen, in 0.1% (v/v);

$V_{M\,specimen}$ – air voids content in the specimen, in 0.1% (v/v);

b – percent of the binder from the specimen (100% bit. mixture), in 0.1% (v/v);

$\rho_{specimen}$ – SSD bulk density of specimen, in kg/m^3, determined with equation 3.2.

ρ_b – binder density at 25°C determined by using equation 2.2 – Section 2.3.1.6.

3.5.2 Marshall test

Marshall tests were performed according to SR EN 12697-34 [195] by using a load-deformation recorder (console) with a load cell and LVDT transducers.

The Marshall characteristics of a cylindrical specimen are related to its stability (S) and flow (F) which is a measure of deformation of the specimen during the test. Usually, Marshall stability represents the peak resistance load obtained during a

constant rate (50 mm/min) of deformation loading sequence (ASTM D6927-15 [196]). However, when the failure of the specimen is nor clearly observed, the peak stability can be considered as the point on the curve which is shifted six flow points (1.5 mm) to the right part of the curve, as shown in Figure 3.11.

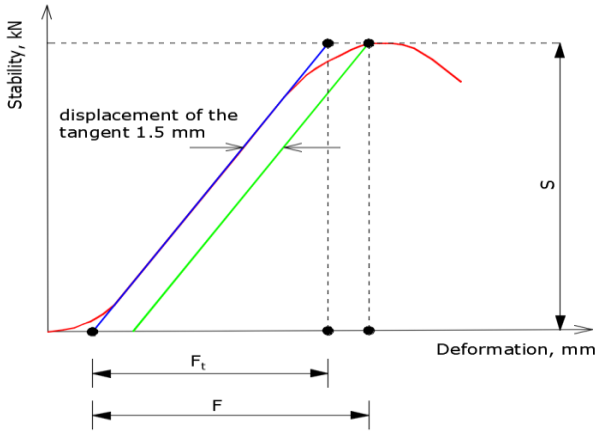

Figure 3.11. Marshall stability and flow determination.

The main characteristics of the Marshall press together with its illustration, are shown in Figure 3.12. The procedure followed in order to determine the Marshall characteristics for each type of bituminous mixtures is described in Figure 3.13.

The mean values of the Marshall stability (S_{mean}), Marshall flow (F_{mean}), Marshall tangential flow $(F_{t\,mean})$ and the ratio between them (S_{mean}/F_{mean}) were calculated as the average value of all S, F, F_t and S/F values obtained for all the specimens produced for each type of bituminous mixture and by using the same type of compaction.

Technical data
- Electric cell 50Kn
- Displacement transducer 50 mm
- 8 channels digital display unit
- Displays at the same time the stability in kN and the flow in mm
- Auxiliar equipment: Digital Water bath, with cooling device, temperature range: +3 to +95°C, accuracy ± 1°C

(a) (b)

Figure 3.12. (a) Main characteristics of the Marshall press; (b) Matest Marshall press - Road Laboratory, University Politehnica Timisoara.

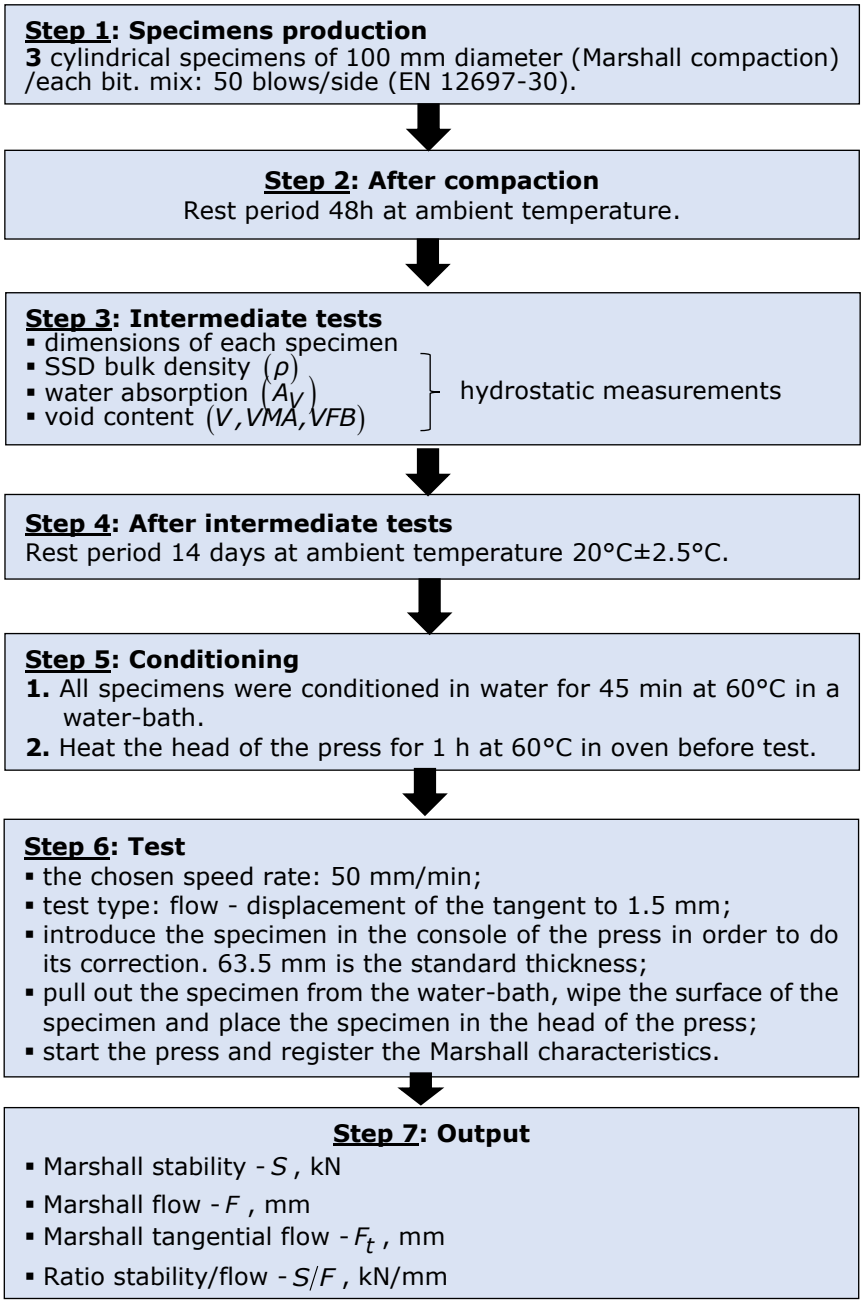

Figure 3.13. Procedure used in order performed the Marshall test.

3.5.3 Indirect tension test on cylindrical specimen (IT-CY)

Indirect tension tests were performed according to SR EN 12697-26 [197], with some differences regarding the test temperature, etc.

The equipment used in order to perform this test is shown in Figure 3.14, including the instrumentation: thermal chamber, auxiliary instruments, etc. More details are given in the description of the procedure and Figure 3.15.

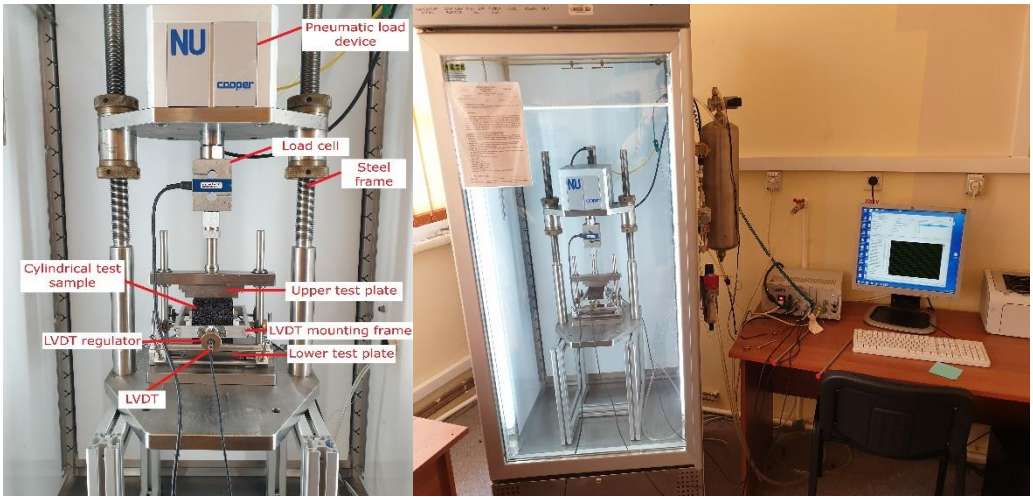

(a) (b)

Figure 3.14. (a) Test equipment; (b) Cooper Research Technology CRT-UTM-NU testing machine - Road Laboratory, University Politehnica Timisoara.

The procedure followed in order to determine the stiffness modulus (S_M, in MPa) for each type of bituminous mixtures is the following: two cylindrical specimens 100 mm diameter produced with the gyratory press at 80 gyrations/each type of bit. mix. is described in Figure 3.15.

Based on the measurements (vertical load, horizontal deformation, load-area factor, etc.) from the 5 impulses of the test/each side of the specimen, a measured stiffness modulus $\left(S_{Mi}\right)$ for each impulse can be calculated by using equation 3.11. The impulse repetition time is 3 s. Therefore, two mean values of the measured stiffness modulus/each side of the specimen, i.e. initial position and rotated at 90° around its axis, are obtained $\left(S_{MA}, S_{MB}\right)$ by using equation 3.12. If the difference between S_{MA} and S_{MB} is out of +10% or -20% from their mean value, the test must be rejected, and the test should be done on another specimen. Otherwise, the mean values between S_{MA} and S_{MB} will be reported as the measured stiffness modulus of the specimen $\left(S_M\right)$, according to equation 3.13.

$$S_{Mi} = \frac{F \times (\upsilon + 0.27)}{d \times h} \tag{3.11}$$

where:

S_{Mi} – measured stiffness modulus value corresponding to impulse i, in MPa;

F – maximum value of the applied vertical load, in N;

υ – Poisson coefficient;

d – amplitude of the horizontal deformation determined for the impulse i, in mm;

h – the thickness of the cylindrical specimen, in mm.

According to SR EN 12697-26 [197], if the Poisson coefficient was not determined, a value of 0.35 can be considered for all test temperatures.

$$S_{MA/B} = \frac{S_{M1A/B} + S_{M2A/B} + S_{M3A/B} + S_{M4A/B} + S_{M5A/B}}{5} \quad (3.12)$$

where:

$S_{MA/B}$ – the mean values of the measured stiffness modulus/each side A and B of the specimen (initial position and rotated at 90° around its axis), in MPa;

$S_{M1...5A/B}$ – the measured stiffness modulus value corresponding to impulse 1…5/each side A and B of the specimen, in MPa.

$$S_M = \frac{S_{MA} + S_{MB}}{2} \quad (3.13)$$

where:

S_M – the measured stiffness modulus of the specimen, in MPa;

$S_{MA/B}$ – the mean values of the measured stiffness modulus/each side A and B of the specimen (initial position and specimen rotated at 90° around its axis), in MPa.

Therefore, the measured stiffness modulus must be adapted to the load-area factor with 0.60, by using equation 3.14.

$$S_{adjusted} = S_M \times \left[1 - 0.322 \times \left(log\, S_M - 1.82\right) \times \left(0.60 - k\right)\right] \quad (3.14)$$

where:

$S_{adjusted}$ – the adjusted stiffness modulus of the tested specimen, adapted to the load-area factor with 0.60, in MPa;

S_M – the measured stiffness modulus of the tested specimen corresponding to the k load-area factor, in MPa;

k – the measured load-area factor.

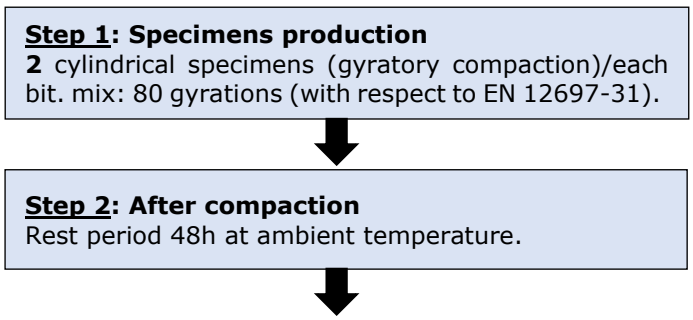

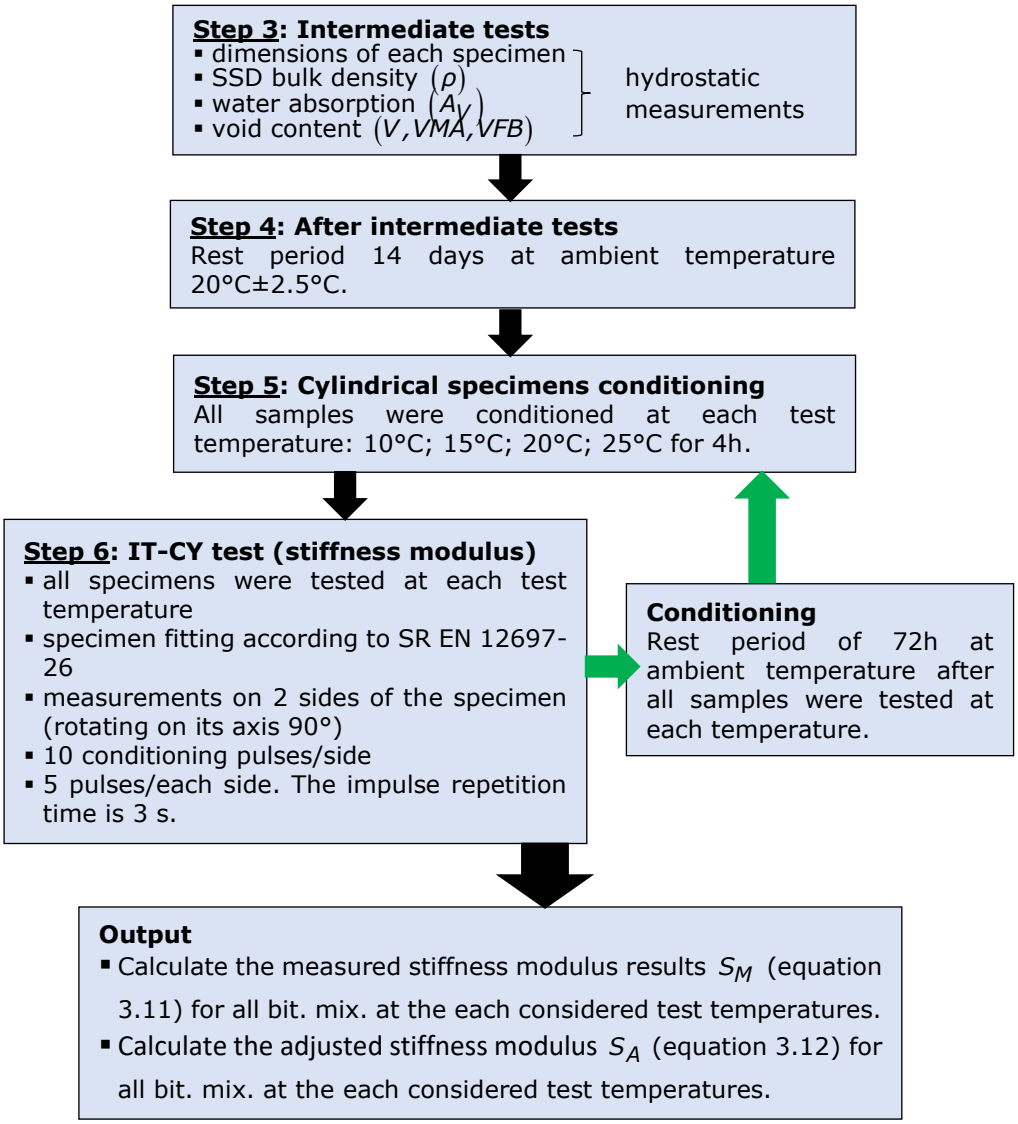

Figure 3.15. Procedure used in order performed IT-CY test (stiffness modulus).

3.5.4 Cyclic compression test with confinement

The cyclic compression with confinement tests were performed according to SR EN 12697-25 [198] – Method B in order to determine the resistance to permanent deformation at a constant temperature of a cylindrical specimen prepared in the laboratory subjected to a triaxial cyclic compression load i.e. gyratory press at 80 gyrations.

The equipment used in order to perform the triaxial cyclic compression test is shown in Figure 3.16, including the testing system thermal chamber, auxiliary instruments, etc.

During the test, the specimen conditioned at the test temperature 50°C for 4 h is placed between two plan parallel loading platens and subjected to a cyclic axial block-pulse pressure $\sigma_{axial}(t)$ with the height σ_a superposed with a static confining pressure $\sigma_{confining}$, equation 3.15. More details regarding the test conditions are given in Figure 3.17.

$$\sigma_{axial}(t) = \sigma_a(t) + \sigma_{confining} \tag{3.15}$$

where:

$\sigma_{axial}(t)$ – the cyclic axial pressure as a function of time which is equal to σ_a during the pulse duration (T_P) and is equal to $\sigma_{confining}$ during the rest period (T_R), in kPa;

σ_a – the height of the block pulse, in kPa;

$\sigma_{confining}$ – the confining pressure, in kPa.

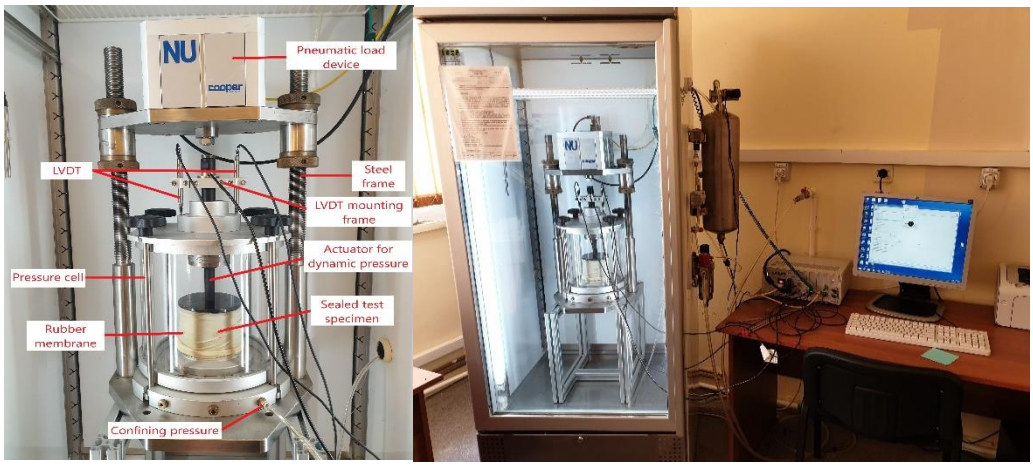

(a) (b)

Figure 3.16. (a) Test equipment; (b) Cooper Research Technology CRT-UTM-NU testing machine - Road Laboratory, University Politehnica Timisoara.

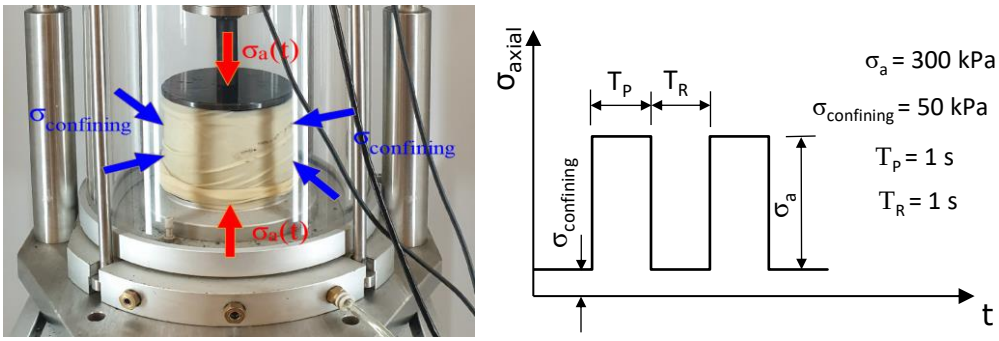

Figure 3.17. Test conditions – block-pressure cyclic loading.

The procedure followed in order to determine the resistance to permanent deformation is by applying 10000 impulses for each type of bituminous mixtures on two cylindrical specimens of 100 mm in diameter produced with the gyratory press at 80 gyrations/each type of bit. mix. and shown in Figure 3.18.

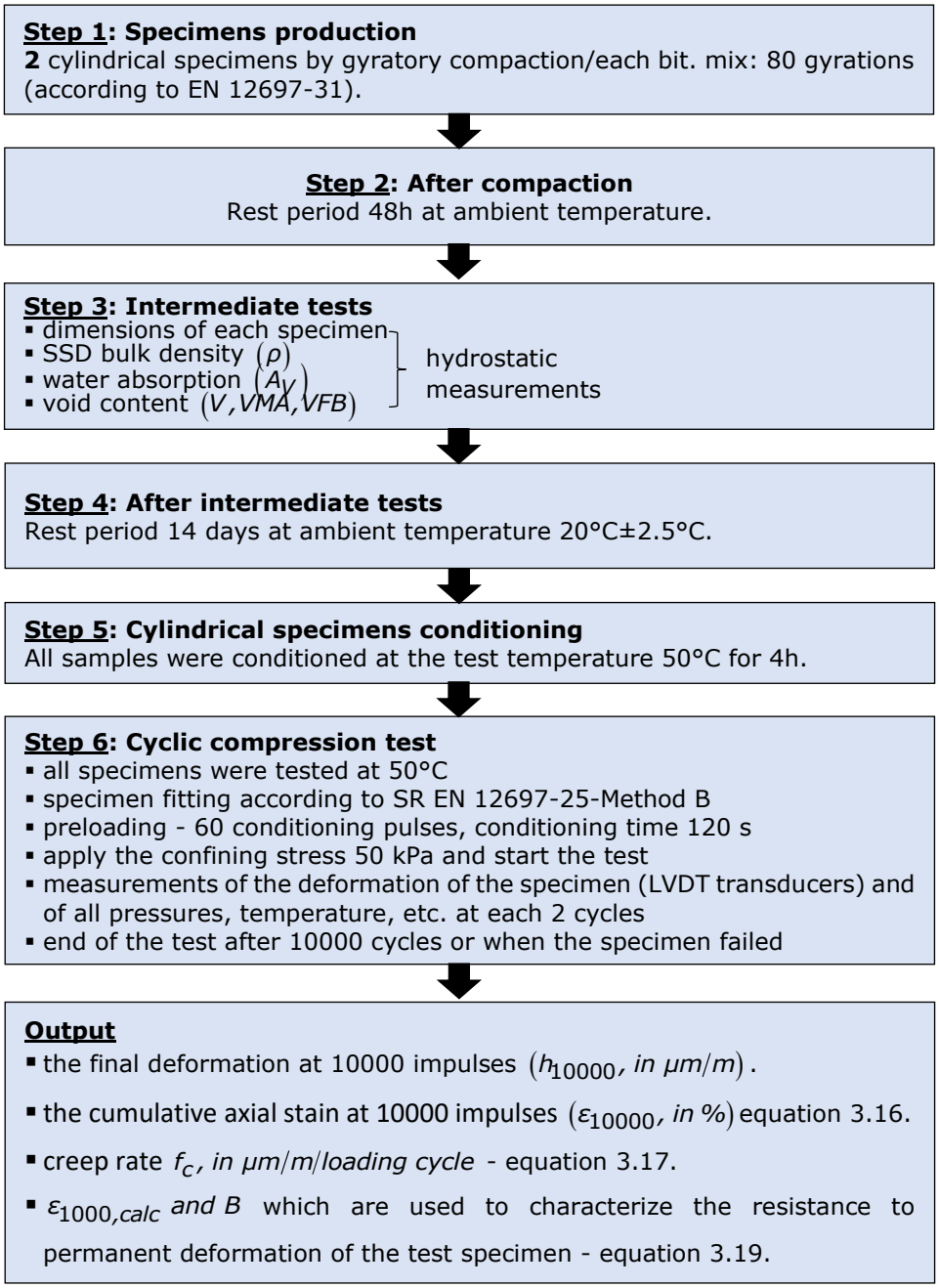

Figure 3.18. Procedure - cyclic compression test with confinement.

Figure 3.19 shows an example of a creep curve in order to define the three stages of the behaviour. It should be mentioned that the third stage was absent during the tests performed in this work.

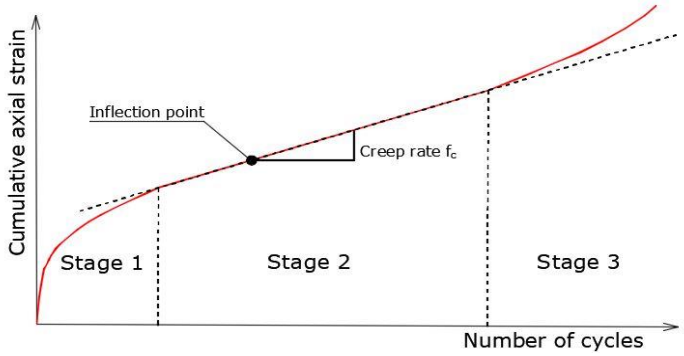

where:

Stage 1 – the initial part of the curve where the increase of the cycles corresponds to a decrease of the slope of the creep curve;

Stage 2 – creep curve with quasi-constant slope (creep rate f_C);

Stage 3 – increase of cycles corresponds to an increase of the slope of the creep curve.

Figure 3.19. Creep curve - stages.

In order to determine the outputs mentioned in Figure 3.17, the following equations were considered.

$$\varepsilon_{10000} = \frac{h_0 - h_{10000}}{h} \times 100 \tag{3.16}$$

where:

ε_{10000} – cumulative axial strain of the test specimen after 10000 impulses, in %;

h_0 – the mean deformation - position of the upper plate measured by the two LVDTs of the specimen, after the preload by 60 conditioning impulses, in mm;

h_{10000} – the mean deformation - position of the upper plate measured by the two LVDTs of the specimen, after 10000 loading cycles, in mm;

h – the initial thickness of the specimen, in mm.

To determine the creep rate f_C the slope B_1 from the least square linear fit of the quasi-linear part of the creep curve was determined (equations 3.17 and 3.18).

$$f_C = B_1 \times 10^4 \tag{3.17}$$

$$\varepsilon_n = A_1 + B_1 \cdot n \tag{3.18}$$

where:

ε_n – the cumulative axial strain of the test specimen after n impulses, in %;

f_C – creep rate, in $\mu m/m/loading\ cycle$;

n – number of the impulses (loading cycles);

A_1, B_1 – regression constants.

To determine the two parameters $\varepsilon_{1000,calc}$ *and* B that are used to characterize the resistance to permanent deformation of a bituminous mixture specimen, the least square power fit of the quasi-linear part of the creep curve were calculated.

$$\varepsilon_{1000,calc} = A \cdot 1000^{B} + C \tag{3.19}$$

where:

$\varepsilon_{1000,calc}$ – cumulative axial strain of the test specimen after 1000 impulses, in %;

A – regression constant;

B – slope from the least square linear fit on the $log\left(\varepsilon_{1000,calc} - C\right)$ *vs.* $log\left(n\right)$ values;

C – factor to correct deformation at the beginning of the loading.

3.5.5 Complex modulus test – Two-point bending test on trapezoidal specimens

Complex modulus tests in two-point bending configuration were performed on trapezoidal specimens according to SR EN 12697-26 [197] – Annex A specifications.

In the two-point bending test a trapezoidal specimen obtained as shown in Section 3.4.2, is fixed on the base extremity and on the other one a cyclic sinusoidal displacement (centred at zero) is imposed. All tests were performed in strain control. Figure 3.20 shows the test device used at the Road Laboratory-University Politehnica Timisoara.

For each trapezoidal specimen the void contents were determined by performing hydrostatic measurements. All specimens whose dimensions do not meet the accuracy of ±1 mm over the dimensions specified in the Standard for a bituminous mixture with a 16 mm maximum aggregate size, shown in Figure 3.21a, were rejected. The dimensions of all specimens were measured with the system shown in Figure 3.21b. Two specimens for each type of bituminous mixture were glued by using the system shown in Figure 3.21c.

The complex modulus test was performed at seven different temperatures from -5°C to 25°C at a frequency range from 0.5 Hz to 20 Hz, in order to determine the viscoelastic properties of all tested materials. Tests were performed in strain control with the imposed strain loading amplitude of 50 μm/m. Figure 3.22 shows the procedure which was followed in this study.

A conditioning time of 2 h at each change of temperature, where no loading is applied on the specimens, was considered in order to assure a homogenous temperature in the interior of specimens.

At each frequency level applied on the specimen a cyclic sinusoidal displacement is imposed for a predefined time (120 s), the data obtained over the last 10 seconds is acquired and the mean of these values are recoded and reported at the end of the test. After each frequency a rest period of 5 minutes was considered.

Moreover, after performing the test at each temperature over the hole considered frequency range, the first frequency test 0.5 Hz was again considered in order to verify if the specimen was damaged or not during the test. If the differences between the first and the last measurements at 0.5 Hz at the same temperature is higher than 3%, the specimen is considered damaged, and the test cannot continue at other temperatures.

Technical data
Thermal chamber: -20…+30°C
Frequency range: 0.10…30 Hz
Two LVDT's: ±1 mm range
Two force transducers: max. 2.5 kN

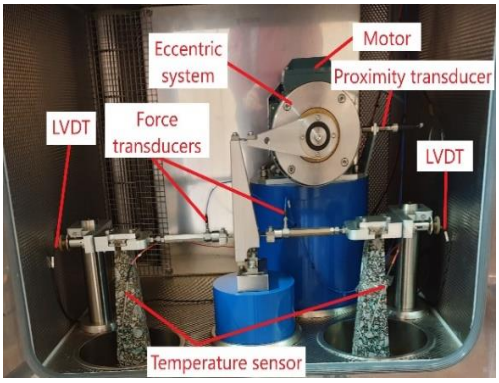

(a) (b)

Figure 3.20. (a) Main characteristics of the equipment; (b) Cooper Research Technology CRT-2PT testing machine - Road Laboratory, University Politehnica Timisoara.

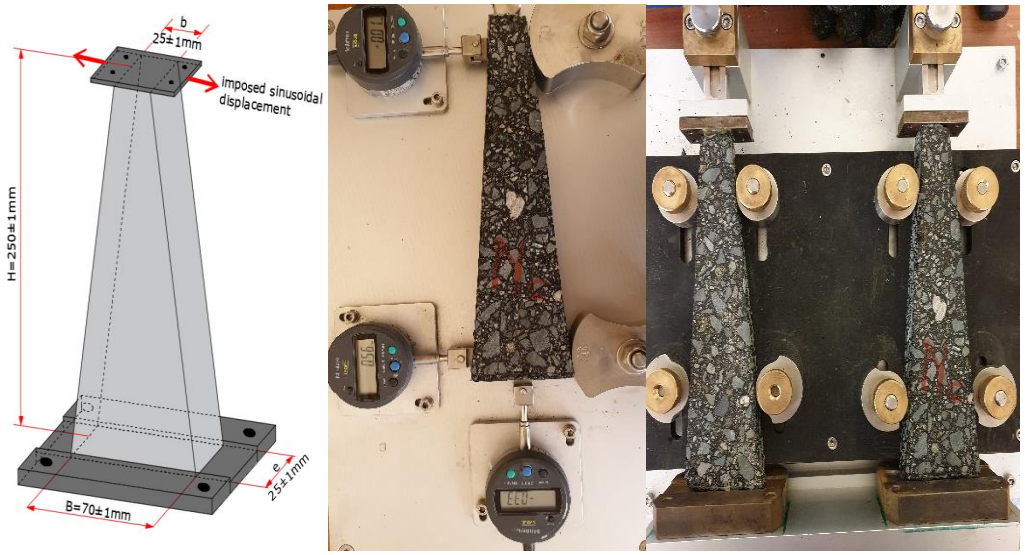

(a) (b) (c)

Figure 3.21. (a) Trapezoidal specimen size; (b) Specimen measuring system; (c) Equipment – gluing the upper and lower plates on in the specimen.

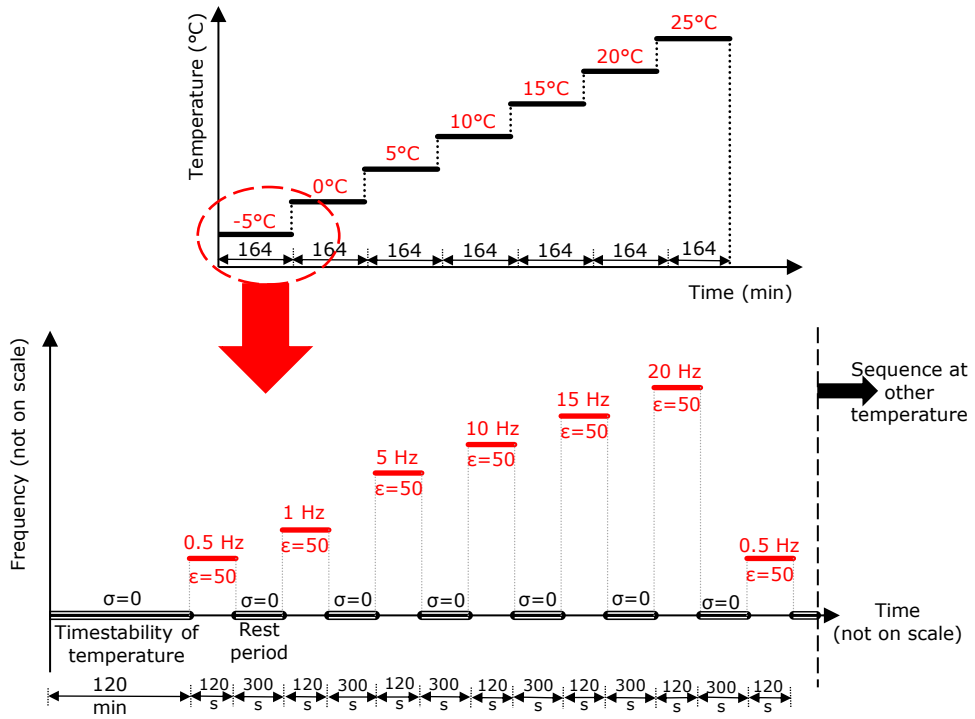

Figure 3.22. Procedure for complex modulus test.

At each temperature and each frequency, the maximum applied force F, the displacement z and the phase angle φ were directly measured and the real part, respectively, the imaginary part of the complex modulus are obtained using the following equations specified in the norm:

$$\left|E^*\right| = \sqrt{E_1^2 + E_2^2} \tag{3.20}$$

$$E_1 = \gamma\left(\frac{F}{z}\cos\varphi + \frac{\mu\omega^2}{10^6}\right) \tag{3.21}$$

$$E_2 = \gamma\frac{F}{z}\sin\varphi \tag{3.22}$$

$$\omega = 2\pi f \tag{3.23}$$

$$\gamma = \frac{12H^3}{e(B-b)^3}\left[\left(2-\frac{b}{2B}\right)\frac{b}{B} - \frac{3}{2} - \ln\frac{b}{B}\right] \tag{3.24}$$

$$\mu = 0.135M + m \tag{3.25}$$

where:

$|E^*|$ – the norm of complex modulus, in MPa;

E_1 – the real part of complex modulus, in MPa;

E_2 – the imaginary part of complex modulus, in MPa;

φ – the phase angle of complex modulus, in °;

F – maximum applied force, in N;

z – the displacement, in mm;

γ – a form factor depending on the form of the specimen and its dimensions;

μ – a mass factor, considering inertial effects of movable parts;

ω – angular frequency, rad/s;

f – frequency, in Hz;

H – the height of the trapezoidal specimen (Figure 3.20 a), in mm;

e – the thickness of the trapezoidal specimen (Figure 3.20 a), in mm;

B – the length of greater base of the trapezoidal specimen (Figure 3.20 a), in mm;

b – the length of smaller base of the trapezoidal specimen (Figure 3.20 a), in mm;

M – the mass of the trapezoidal specimen, in g;

m – the mass of the movable parts, in g.

3.6 HMA mix design: Campaign 1

3.6.1 Determination of the optimal binder content - HMA's without RAP material – Marshall mix design

In order to determine the optimal binder content seven HMA's were produced having the same grading curve and different binder content starting from 5.2% up to 6.2%. The optimal binder content was established based on the experimental results obtained for the above-mentioned bituminous mixtures compared to the limitations regarding the water absorption, void content, Marshall stability, flow and stiffness specified in the Romanian Standard AND 605 [14] for a bituminous mixture produced with virgin materials with 16 mm maximum aggregate size.

After establishing the optimal binder content, three grading curves for the mix design were considered. More details were given in Section 3.4.2. The same tests as for the above-mentioned seven bituminous mixtures were performed. A detailed procedure is showed in Figure 3.23.

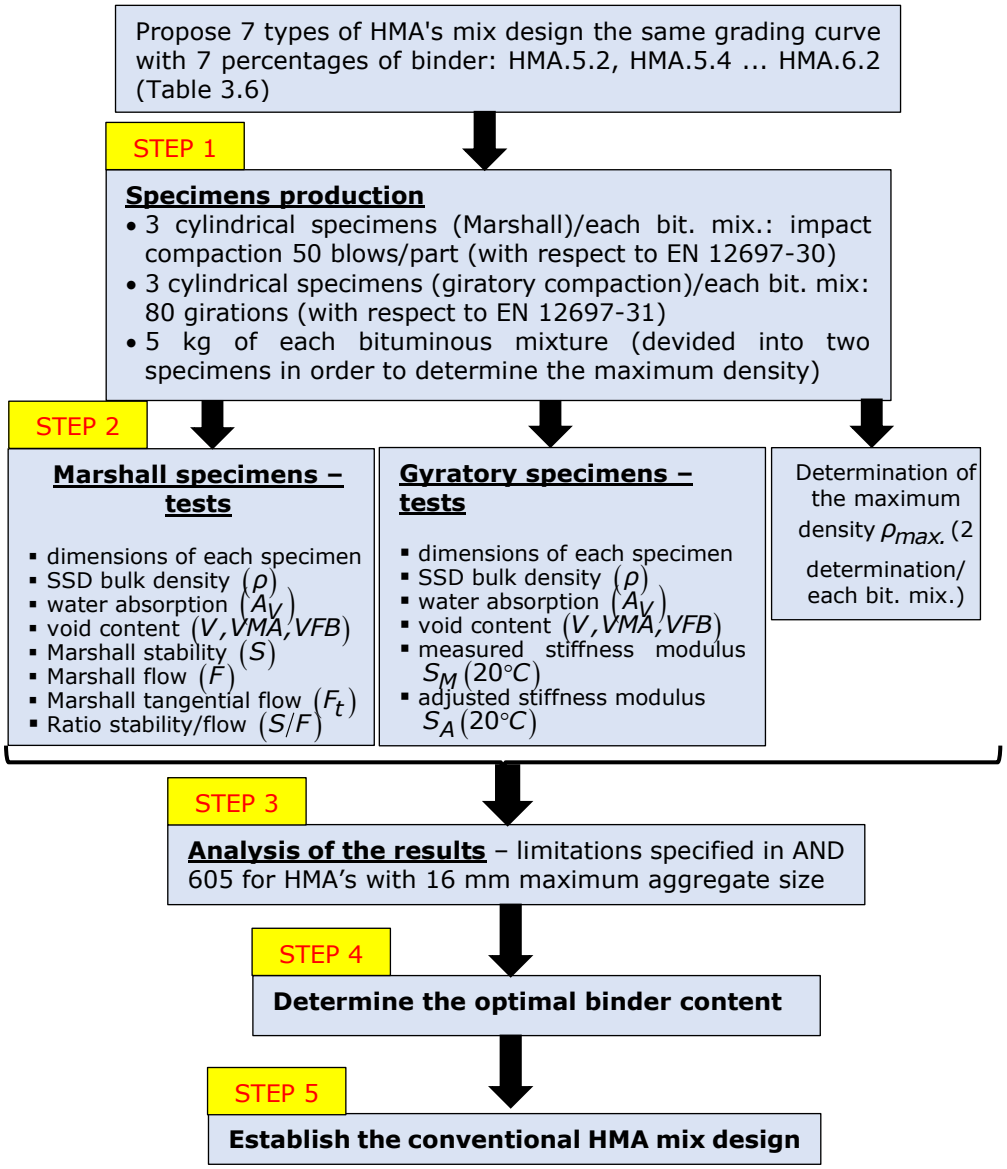

Figure 3.23. Procedure used in order to establish the optimal mix design for an HMA.

3.6.2 Results and analysis: Campaign 1

The experimental results as average value/each parameter obtained for the SSD bulk density $(\rho_{A.bit.mix.})$, water absorption $(A_{V\,bit.mix.})$, Marshall stability $(S_{bit.mix.})$, Marshall flow $(F_{bit.mix.})$, ratio between them $(S/F_{bit.mix.})$ on the Marshall

specimens, air void content $\left(V_{M\,bit.mix.}\right)$, void in mixed aggregates $\left(VMA_{bit.mix.}\right)$, voids filled with bitumen $\left(VFB_{bit.mix.}\right)$, stiffness $\left(S_M\left(20°C\right)_{bit.mix.}\right)$ on the gyratory cylindrical specimens and the maximum density $\left(\rho_{max.bit.mix.}\right)$ of all considered HMAs were plotted as a function of their binder content as shown in Figure 3.24, Figure 3.25 and Figure 3.26.

The limitations specified in the Romanian Standard AND 605 [14] for an HMA produced with virgin materials with a 16 mm maximum aggregate size regarding the water absorption, Marshall characteristics, void content and stiffness, were represented in the same figures. The following limitations, presented as red zones in the following figures were considered:

- water absorption: $5.0 \le A_{V\,bit.mix.} \le 1.5\ (\%vol.)$;
- Marshall stability: $6.5 \le S_{bit.mix.} \le 13.0\ (kN)$;
- Marshall flow: $1.5 \le F_{bit.mix.} \le 4.0\ (mm)$;
- ratio between Marshall stability and flow: $S/F_{bit.mix.}$ *min.* $1.6\ (kN/mm)$;
- air void content of specimens compacted at 80 gyrations: $V_{M\,bit.mix.}$ *max.* $6.0\ (\%)$;
- stiffness at 20°C: $S_M\left(20°C\right)_{bit.mix.}$ *min.* $4000\ (MPa)$.

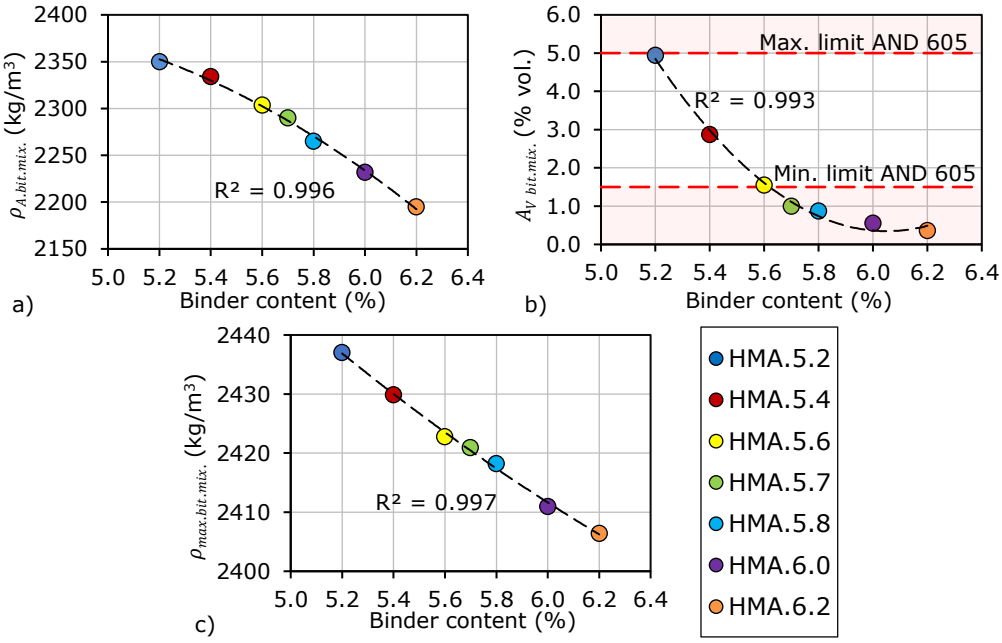

Figure 3.24. Hydrostatic measurement results as a function of the binder content of the seven bituminous mixtures and the limits specified in AND 605 [14]: (a) SSD bulk density; (b) water absorption; (c) maximum density.

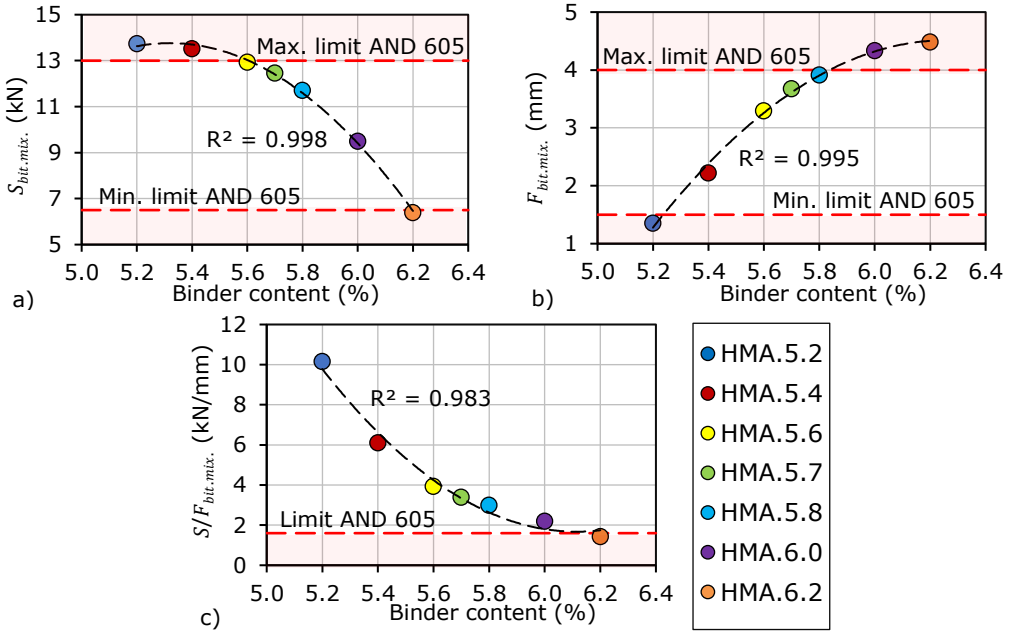

Figure 3.25. Marshall test results as a function of the binder content of the seven bituminous mixtures and the limits specified in AND 605 [14]: (a) Marshall stability; (b) Marshall flow; (c) Stability/flow.

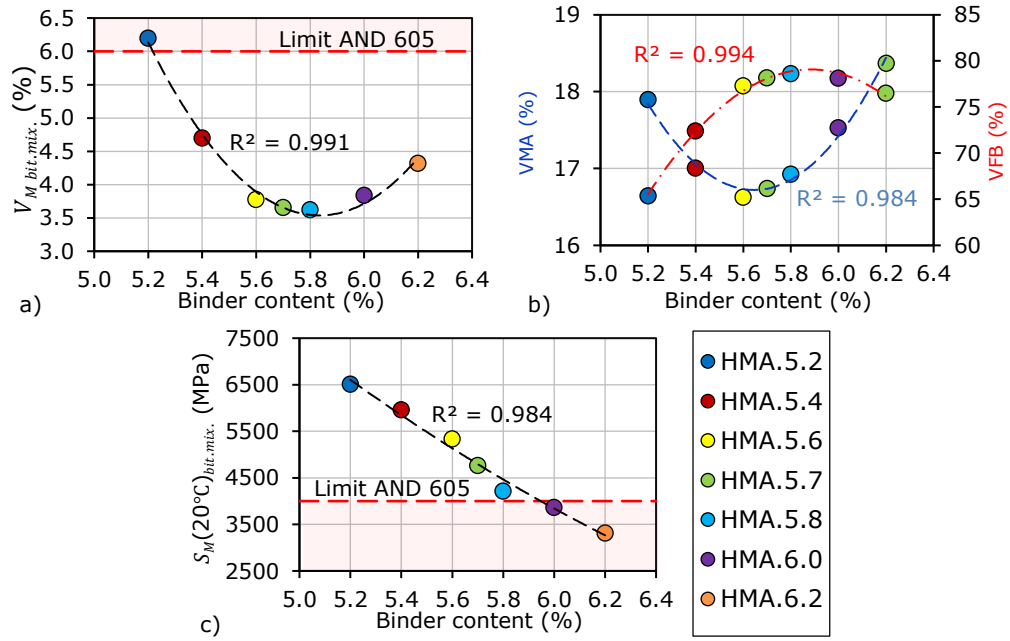

Figure 3.26. Test results obtained on the gyratory specimens as a function of the binder content for the seven bituminous mixtures and the limits specified in AND 605 [14]: (a) void content; (b) VMA and VFB; (c) Stiffness at 20°C.

In each plot, polynomial regressions were performed and R^2 are shown.

By analysing the results shown in Figure 3.24, it could be observed that only three HMAs (HMA.5.2, HMA.5.4 and HMA.5.6) respect the specifications from the Romanian Standard concerning the water absorption. Regarding the results obtained for the Marshall characteristics (Figure 3.25), void contents and stiffness at 20°C (Figure 3.26), the extremes HMA's (lowest/highest binder content) do not meet the requirements specified in AND 605 [14] for an HMA with a 16 mm maximum aggregate size.

Therefore, by analysing all these experimental measurements it could be observed that only the bituminous mixture produced with 5.6% binder content (HMA.5.6) respects the specifications from the Romanian Standard.

It must be mentioned that in the Romanian Standard AND 605 [14] a minimum binder content of 5.7% from the total mass of the mixture for a 'BA16' (Hot Mix Asphalt – concrete asphalt with a 16 mm maximum aggregate size) is indicated. However, based on the results obtained for the HMA.5.6 analysed in this study, this binder content (5.6%) was considered to be the optimal one.

Therefore, all the following twelve bituminous mixtures produced with RAP material with or without rejuvenator will be produced with a 5.6% total binder content, rejuvenator not included and similar grading curve.

3.7 Results and analysis: Campaign 2

3.7.1 Marshall stability and Marshall flow

Marshall tests were performed on all 13 bituminous mixtures: 12 bituminous mixtures produced with RAP material with and without rejuvenator and one conventional bituminous mixture. Three cylindrical specimens were produced using the Marshall compaction with 50 blows/part according to SR EN 12697-30 [188]. Marshall tests were performed according to SR EN 12697-34 [195]. The Marshall characteristics of each cylindrical specimen and their average values related to stability $\left(S_{bit.mix.}\ in\ kN\right)$, flow $\left(F_{bit.mix.}\ in\ mm\right)$, tangential flow $\left(F_{T\,bit.mix.}\ in\ mm\right)$ and the ratio between stability and flow $\left(S/F_{bit.mix.}\ in\ kN/mm\right)$ were determined and obtained results are presented in the following figures. Usually, Marshall stability represents the peak resistance load obtained during a constant rate of deformation loading sequence of 50 mm/min (ASTM D6927-15 [196]). The procedure used in order to obtain the above-mentioned characteristics is presented in Section 3.5.2.

Before performing the Marshall tests, some intermediate measurements were performed for each bituminous mixture specimen. Therefore, for each specimen the SSD bulk density, the water absorption, void contents, VMA, VFB and the maximum density were determined by hydrostatic measurements. The average values obtained for each type of bituminous mixture are reported in Table 3.13.

By increasing the amount of the RAP material in the mass of the bituminous mixtures it could be observed that all the values of the above-mentioned parameters, except $VFB_{bit.mix.}$, are increasing. These results were expected due to the fact that the RAP material is an aged material. Moreover, it is interesting to note that by adding and increasing the amounts of the rejuvenator in the mass of the bituminous mixtures, a reverse effect was obtained excepting $\rho_{Abit.mix.}$.

Table 3.13. Intermediate test results (average values of three specimens) determined for the Marshall specimens for all considered bituminous mixtures.

Bit. mix.	$\rho_{Abit.mix.}$ (kg/m^3)	$\rho_{max.bit.mix.}$ (kg/m^3)	$A_{Vbit.mix.}$ (%vol.)	$V_{Mbit.mix.}$ (%)	$VMA_{bit.mix.}$ (%)	$VFB_{bit.mix.}$ (%)
D.0.R.0	2305	2423	1.50	4.90	17.60	72.20
D.25.R.0	2339	2444	1.70	4.30	17.10	74.80
D.25.R.0.2	2349	2442	1.50	3.80	16.80	77.40
D.25.R.0.4	2354	2442	1.30	3.60	16.70	78.30
D.25.R.0.6	2361	2438	1.00	3.10	16.40	80.90
D.50.R.0	2345	2465	1.90	4.90	17.60	72.40
D.50.R.0.2	2352	2461	1.70	4.40	17.40	74.70
D.50.R.0.4	2359	2457	1.50	4.00	17.30	76.80
D.50.R.0.6	2370	2453	1.20	3.40	17.00	80.10
D.75.R.0	2382	2565	2.20	7.10	19.90	64.30
D.75.R.0.2	2395	2546	1.80	5.90	19.20	69.00
D.75.R.0.4	2407	2543	1.40	5.30	19.00	71.90
D.75.R.0.6	2418	2537	1.10	4.70	18.80	75.00

As already mentioned, three specimens were tested for each type of bituminous mixture. The average values of Marshall characteristics are reported in Figure 3.27 (3.27a – Marshall stability; 3.27b – Marshall flow; 3.27c – ratio between stability and flow; 3.27d – tangential flow).

As expected, the increase of the RAP material within the new bituminous mixtures leads to an increase of the Marshall characteristics, except S/F ratio. It could be observed that for the bituminous mixtures produced with more than 25% RAP the stability is higher than the maximum limit from the AND 605 Standard [14] for a bituminous mixture produced with virgin materias with 16 mm maximum aggregate size. In this case, a rejuvenator should be used in order to decrease the stiffness of the mix.

Regarding the bituminous mixtures produced with the lowest percentages of RAP material, a small increase of the stability and flow was observed. Therefore, it can be considered that, probably, the use of less than 25% of the RAP material in the production of a new bituminous mixture leads to a final mix that is still within the limits imposed by the Romanian Standard [14].

By increasing the amounts of the rejuvenator within the mass of the bituminous mixtures a decrease of the stability and of the S/F ratio and an increase of the Marshall flow and tangential flow could be observed.

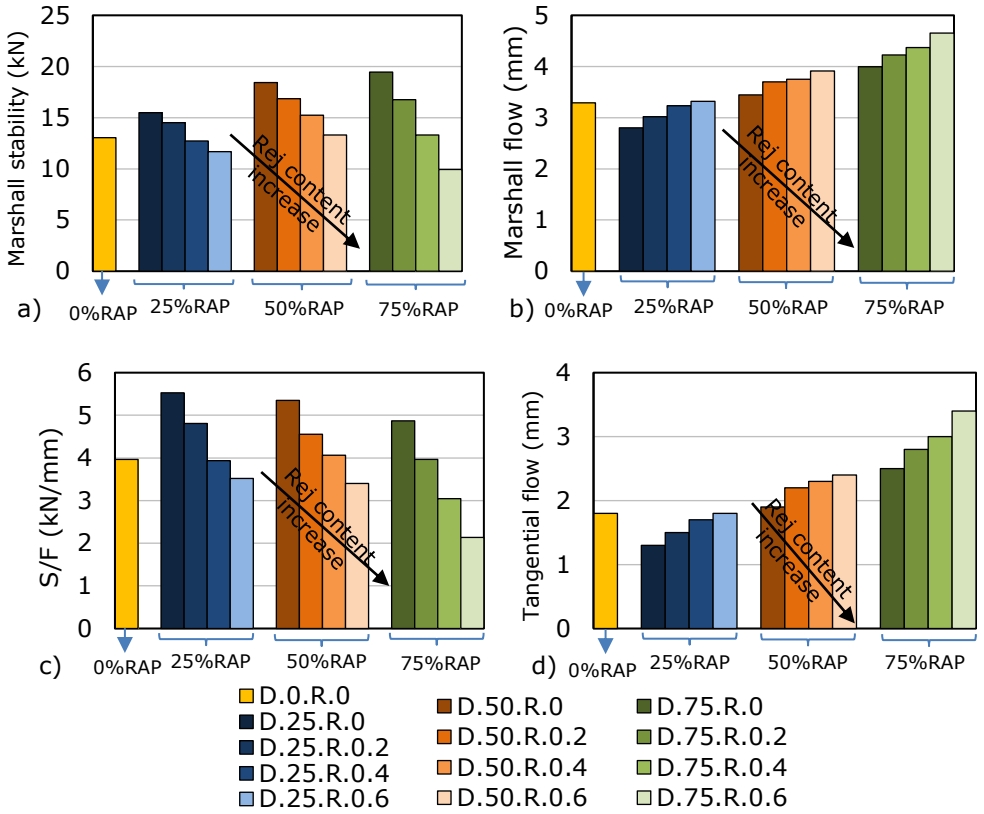

Figure 3.27. Marshall test results for all considered bituminous mixtures: (a) Marshall stability; (b) Marshall flow; (c) Ratio stability/flow; (d) Tangential flow.

To highlight the variation of the experimental results obtained for the Marshall characteristics with the increase of RAP material and rejuvenator percentages used for each bituminous mixture, Figure 3.28 shows all the results plotted as a function of the RAP material content.

Some linear relationship with the RAP material content for the bituminous mixtures produced with the same amount of rejuvenator of 0%, 0.2%, 0.4% and 0.6% by mass of the RAP material, can be observed for the Marshall characteristics, excepting the stability. Linear regressions were performed and R^2 values were determined for each regression.

Regarding the Marshall flow and the tangential flow, it could be observed that satisfactory R^2 values always higher than 0.966 were obtained. Moreover, Table 3.14 shows the experimental results obtained for the Marshall characteristics for all 13 bituminous mixtures. Also, $S_{bit.mix.}$, $F_{bit.mix.}$, $F_{t\,bit.mix.}$ and $S/F_{bit.mix.}$ values were normalized with respect to the values measured for the conventional HMA (D.0.R.0). Normalized values are reported in Table 3.14.

As a general comment it can be concluded that the effect of increasing the RAP material content leads to a stiffer behaviour of the bituminous mixtures as the stability increases. The influence of increasing the rejuvenator content was observed as a reverse effect which is counterbalancing the effect of the RAP material.

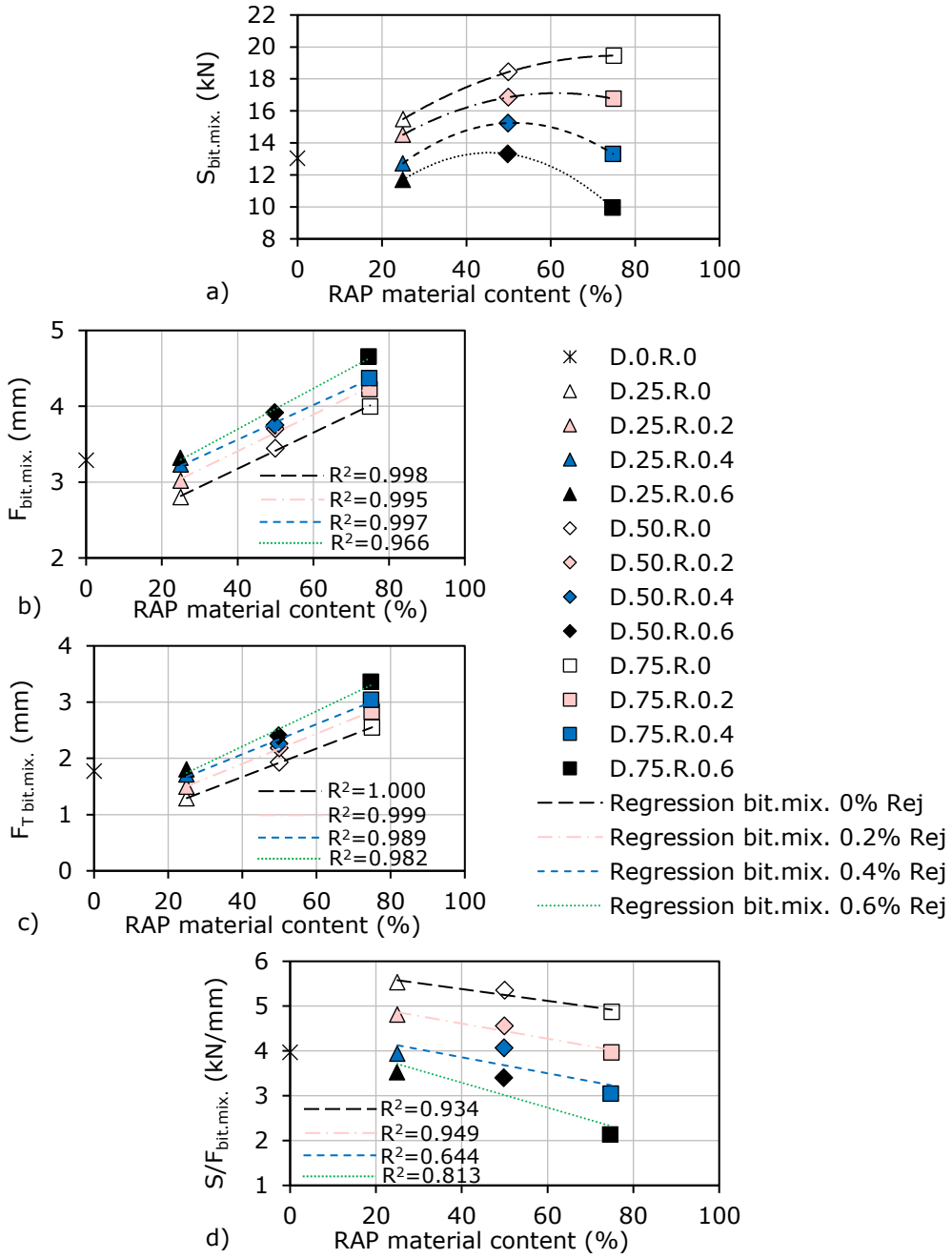

Figure 3.28. Marshall test results as a function of RAP material content for all bituminous mixtures: (a) Marshall stability; (b) Marshall flow; (c) Tangential flow; (d) Ratio stability/flow.

Table 3.14. Experimental results and normalized (to D.0.R.0) Marshall characteristics for all considered bituminous mixtures.

Bit. mix.	S (kN)	$S/S_{0\%}$ (-)	F (mm)	$F/F_{0\%}$ (-)	S/F (kN/mm)	$(S/F)/(S/F)_{0\%}$ (-)	F_t (mm)	$F_t/F_{t0\%}$ (-)
D.0.R.0	13.0	1.00	3.3	1.00	4.0	1.00	1.8	1.00
D.25.R.0	15.5	1.19	2.8	0.85	5.5	1.39	1.3	0.73
D.25.R.0.2	14.5	1.11	3.0	0.92	4.8	1.21	1.5	0.84
D.25.R.0.4	12.7	0.98	3.2	0.98	3.9	0.99	1.7	0.97
D.25.R.0.6	11.7	0.90	3.3	1.01	3.5	0.89	1.8	1.02
D.50.R.0	18.4	1.41	3.4	1.05	5.3	1.35	1.9	1.09
D.50.R.0.2	16.9	1.29	3.7	1.12	4.6	1.15	2.2	1.23
D.50.R.0.4	15.2	1.17	3.8	1.14	4.1	1.02	2.3	1.27
D.50.R.0.6	13.3	1.02	3.9	1.19	3.4	0.86	2.4	1.35
D.75.R.0	19.5	1.49	4.0	1.21	4.9	1.23	2.5	1.44
D.75.R.0.2	16.8	1.28	4.2	1.28	4.0	1.00	2.8	1.60
D.75.R.0.4	13.3	1.02	4.4	1.33	3.0	0.77	3.0	1.72
D.75.R.0.6	9.9	0.76	4.7	1.41	2.1	0.54	3.4	1.90

It would be interesting to investigate the relation between the Marshall characteristics of the mixtures and the properties of the corresponding binder blends. Therefore, results of the Marshall stability and flow were plotted as a function on the penetration results obtained for the binder blends in Figure 3.29 a and b. A global linear regression was performed. The coefficient of determination was determined.

A good relation between the Marshall stability of mixtures and the penetration results of the corresponding blends was obtained. However, it could be observed in Figure 3.29a that by performing some linear regression for the mixtures produced with the same RAP material content (25%, 50% and 75%) and different rejuvenator content, some strong relations were found, R^2 always higher than 0.987. Similar analysis was performed for the Marshall flow (Figure 3.29b) and for the void content of Marshall specimens (Figure 3.29c).

It could be observed that for all these three parameters of mixtures and the penetration of binder blends stronger relations, R^2 always higher than 0.908, where found for the mixtures produced with constant RAP content (25%, 50% and 75%), than in the case when all materials were considered (total R^2).

These tendencies could be explained by the fact that most probably when the RAP material was added in the new bituminous mixtures some differences between the grading curves of these mixtures and the one used for the conventional mix were obtained. Also, as the rejuvenator content was established by the mass of the RAP material, as all specimens were produced by using the same compaction energy and as the density of the aggregates from the RAP material is most probably higher than the density of the virgin aggregates, the mixture specimens become more dense with the increase of the RAP material and rejuvenator contents (see Table 3.13). For these reasons, for the mixtures/binder blends produced with the same amount of RAP content good linear relations could be performed.

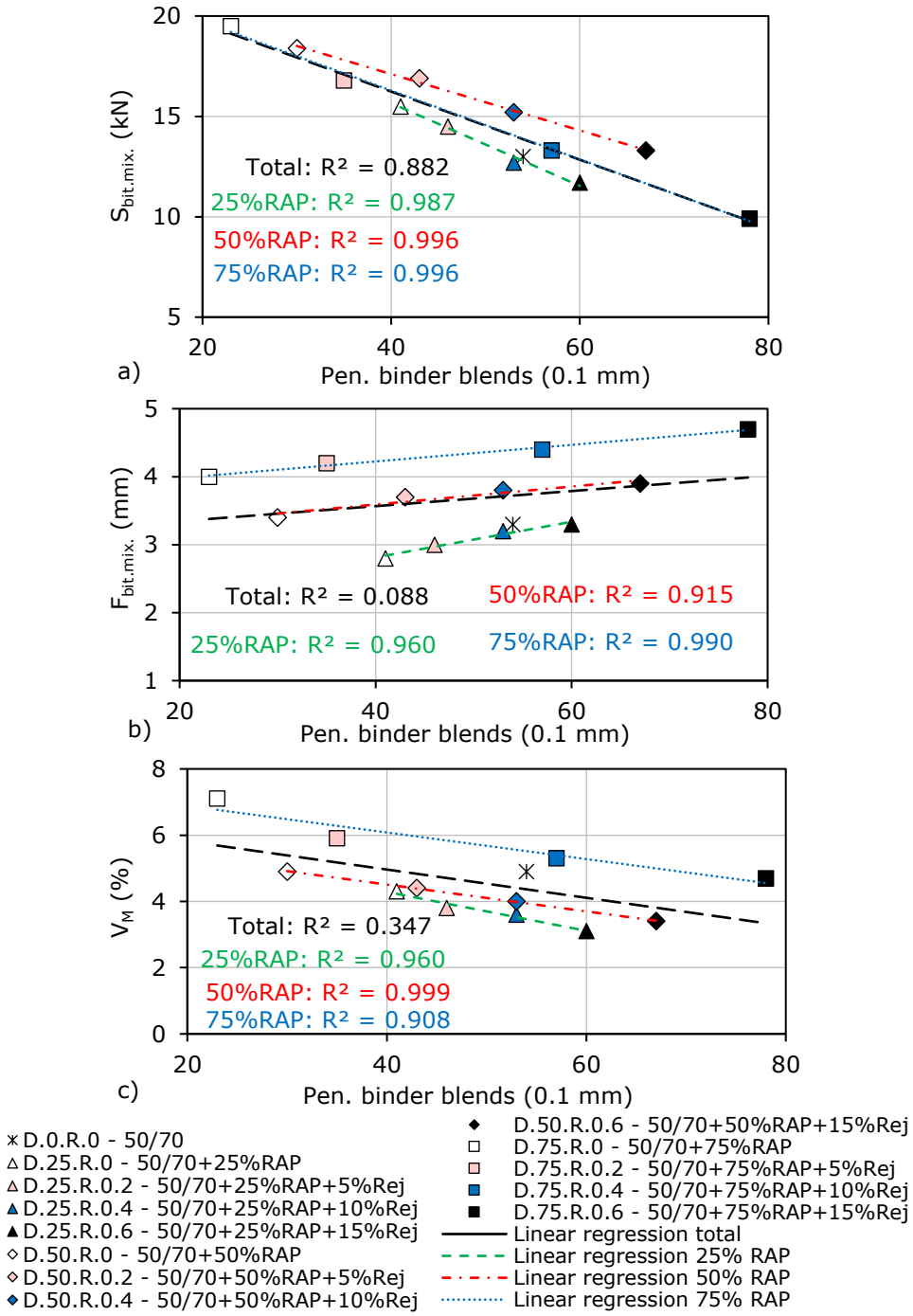

Figure 3.29. (a) Marshall stability vs. binder blends penetration; (b) Marshall flow vs. binder blends penetration; (c) Void content vs. binder blends penetration.

3.7.2 Stiffness modulus from indirect tension tests

Indirect tension tests were performed for all 13 bituminous mixtures according to SR EN 12697-26 [197] with some differences, in order to obtain their stiffness modulus. Two cylindrical specimens were produced using the gyratory compaction according to SR EN 12697-31 [189] by using the same compaction energy through 80 gyrations.

Before performing the IT-CY tests, the same intermediate measurements, as in the case of the Marshall tests, were performed for each bituminous mixture cylindrical specimen. The average values obtained for these hydrostatic measurements each type of bituminous mixture are reported in Table 3.15.

The comment stated in the case of the Marshall specimens is valid in the case of the analysed cylindrical specimens compacted with the gyratory press. The increase of the RAP material content within the mass of the bituminous mixtures corresponds to an increase of all values of the above-mentioned parameters, except $VFB_{bit.mix.}$.

Moreover, when the rejuvenator was used, the increase of its amount corresponds to a reverse influence, i.e., a decrease of the intermediate test results, except $\rho_{A.bit.mix.}$ and $VFB_{bit.mix.}$.

IT-CY tests were performed on each specimen at four temperatures: 10°C, 15°C, 20°C and 25°C. More details regarding the procedure that was followed during these tests, are given in Section 3.5.3.

Based on the measurements obtained by applying 5 impulses on each side of the specimen, a measured stiffness modulus $\left(S_{Mi}\right)$ for each impulse was calculated and two mean values of the measured stiffness modulus/each side of the specimen (specimen rotated at 90° around its axis) were obtained $\left(S_{MA}, S_{MB}\right)$. For all specimens the differences between S_{MA} and S_{MB} were in +10% or -20% from their mean value. Therefore, a mean value S_M was reported as the measured stiffness modulus of the specimen.

As the Poisson coefficient was not determined, a unique value of 0.35 was considered, according to SR EN 12697-26 [197], for all test temperatures for all specimens.

Moreover, the measured stiffness modulus corresponding to each applied impulse, were adapted to the load-area factor with 0.60, and the adjusted stiffness moduli S_{Ai} were obtained. Also, a mean value of the adjusted stiffness modulus was calculated for each specimen.

As an example, a test results report is shown in Figure 3.30 for one specimen for the bituminous mixture D.25.R.0.4 where the row measurements are presented together with the S_M and S_A values.

Figure 3.31 shows an example for the bituminous mixtures produced with 50% RAP material and different percentages of rejuvenator where the experimental results obtained for the measured stiffness modulus were plotted as a function of the test temperature in order to highlight the influence of the temperature on the S_M values. Similar plots were built in Figure 3.32 for the same materials for the adjusted stiffness modulus results. Similar plots are shown in Appendix 2 form Figure A2.1 to Figure A2.6.

Table 3.15. Intermediate test results (average values of two specimens) determined for cylindrical specimens produced at 80 gyrations for all considered bituminous mixtures.

Bit. mix.	$\rho_{A\,bit.mix.}$ (kg/m^3)	$A_{V\,bit.mix.}$ (%vol.)	$V_{M\,bit.mix.}$ (%)	$VMA_{bit.mix.}$ (%)	$VFB_{bit.mix.}$ (%)
D.0.R.0	2297	1.10	5.20	17.90	70.90
D.25.R.0	2344	2.10	4.10	16.90	75.90
D.25.R.0.2	2354	1.50	3.60	16.60	78.30
D.25.R.0.4	2363	1.30	3.20	16.40	80.40
D.25.R.0.6	2369	1.30	2.80	16.10	82.50
D.50.R.0	2350	2.60	4.70	17.40	73.20
D.50.R.0.2	2362	1.80	4.00	17.10	76.40
D.50.R.0.4	2366	1.20	3.70	17.00	78.20
D.50.R.0.6	2372	1.10	3.30	16.90	80.40
D.75.R.0	2394	3.70	6.70	19.50	65.90
D.75.R.0.2	2401	2.60	5.70	19.00	70.00
D.75.R.0.4	2415	1.80	5.00	18.80	73.20
D.75.R.0.6	2434	1.20	4.10	18.30	77.80

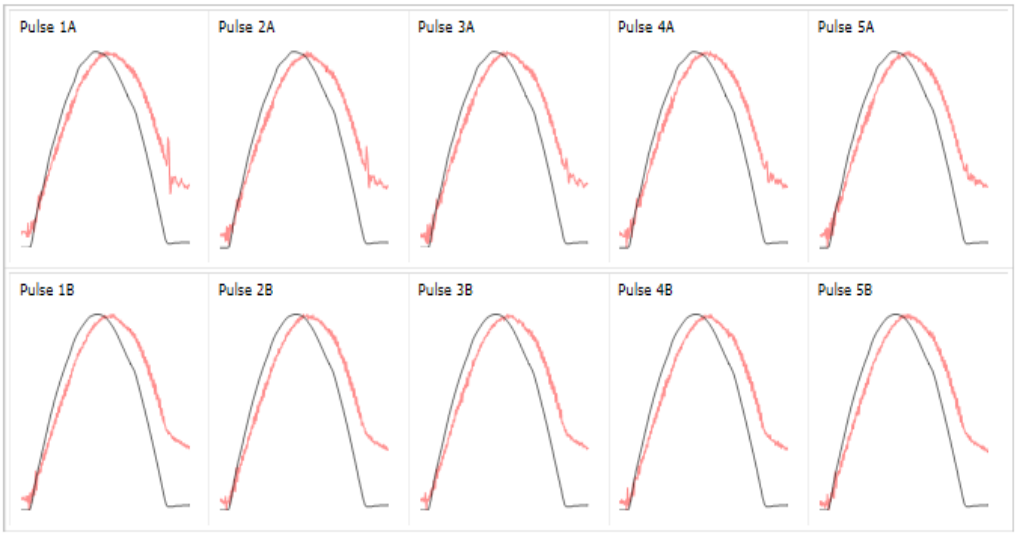

Test Results

	1A	2A	3A	4A	5A	Mean A	1B	2B	3B	4B	5B	Mean B	**Mean A&B**
Load Peak to Peak (kN)	4.032	4.030	4.028	4.030	4.027	4.029	4.361	4.359	4.360	4.360	4.360	4.360	**4.195**
Horizontal Stress (kPa)	383.3	383.1	383.0	383.1	382.9	383.1	414.6	414.4	414.5	414.6	414.6	414.5	**398.8**
Load-Area Factor	0.65	0.65	0.65	0.65	0.65	0.65	0.65	0.65	0.65	0.65	0.65	0.65	**0.65**
Horizontal Deformation (um)	4.415	4.364	4.279	4.252	4.241	4.310	4.718	4.650	4.698	4.704	4.626	4.679	**4.495**
Load Rise Time (ms)	127	127	127	127	127	127	124	124	124	124	124	124	**125**
Measured Stiffness (MPa)	8456	8551	8716	8776	8792	8658	8559	8680	8593	8582	8727	8628	**8643**
Adjusted Stiffness Modulus (MPa)	8743	8842	9014	9076	9093	8953	8850	8976	8885	8874	9025	8922	**8938**

Figure 3.30. Example IT-CY test results bituminous mixture D.25.R.0.4.

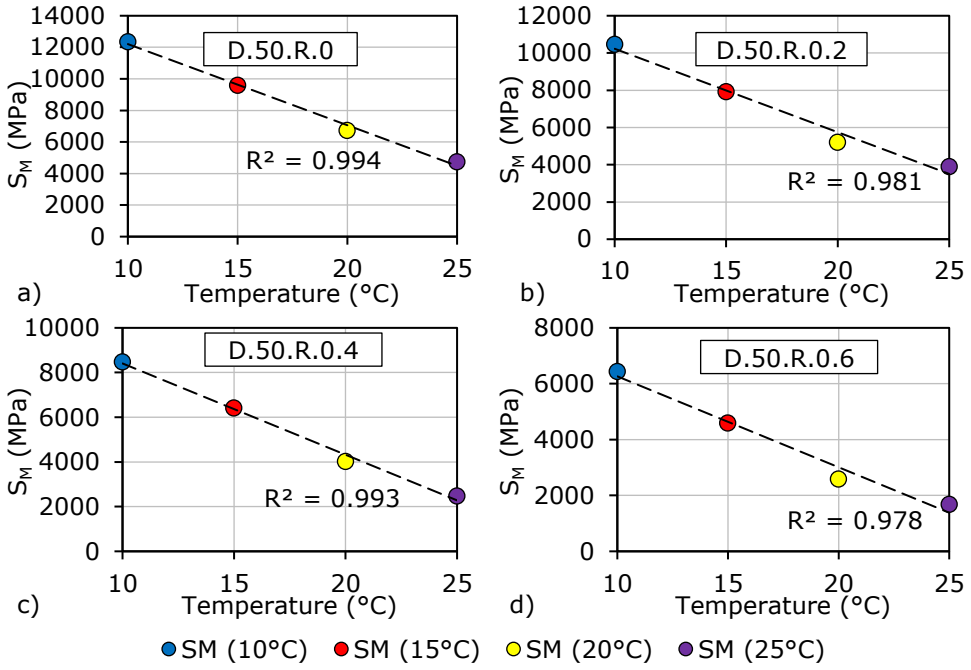

Figure 3.31. Measured stiffness modulus as a function of the test temperature for the bituminous mixtures: (a) D.50.R.0; (b) D.50.R.0.2; (c) D.50.R.0.4; (d) D.50.R.0.6.

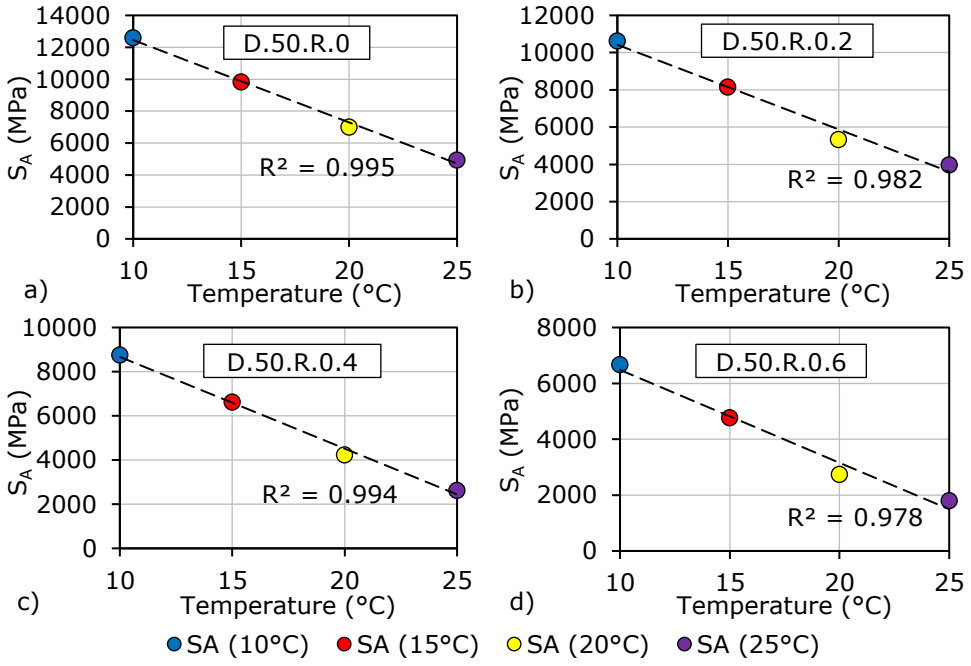

Figure 3.32. Adjusted stiffness modulus as a function of the test temperature for the bituminous mixtures: (a) D.50.R.0; (b) D.50.R.0.2; (c) D.50.R.0.4; (d) D.50.R.0.6.

As it could be observed for all the tested materials, both S_M and S_A show a linear relationship with the increase of temperature. Therefore, some linear regressions were performed and the R^2 was calculated for each regression for each tested bituminous mixture.

Satisfactory R^2 values were obtained, always higher than 0.962 in the case of the measured stiffness, and always higher than 0.963 in the case of the adjusted stiffness. It is interesting to note that the lowest R^2 value was obtained for the bituminous mixture D.75.R.0.6. However, these observed tendencies are very important because they show that the increase of temperature leads to a linear decrease of the bituminous mixture stiffness.

Figure 3.33 shows the average values obtained for S_M and S_A at each test temperature for all considered bituminous mixtures.

As expected, the increase of the RAP material content within the mass of the bituminous mixtures corresponds to an increase of the S_M and S_A values. Also, the increase of the temperature leads to a decrease of stiffness.

On the other side, when the rejuvenator was used a decrease of the stiffness was observed with the increase of its percentage within the mass of the mixtures.

Moreover, the obtained $S_A(t)$ results in logarithmic scale for all bituminous mixtures were plotted as a function of the RAP material content in Figure 3.34 in order to highlight if there are any relationships between them.

Exponential regressions were performed for each series of bituminous mixtures produced with the same amount of rejuvenator (0%, 0.2%, 0.4% and 0.6% by mass of the RAP material) by mass of the RAP material. R^2 values were determined for each regression.

It is interesting to note that for the lowest temperature (10°C) the results obtained for the adjusted stiffness for the bituminous mixtures produced with different amounts of RAP material (25%, 50% and 75%) without rejuvenator, present a small increase with the increase of the RAP material. On the other side, the increase of the temperature corresponds to an increase of this tendency.

For the bituminous mixtures produced with 0% and 0.2% of rejuvenator by mass of the RAP material, at the lowest temperature the R^2 is not meaningful due to the fact that the differences between $S_A(10°C)$ values is small as the regression line presents a small slope. For the other two series of 0.4% and 0.6% rejuvenator, a change of slope was observed, $S_A(10°C)$ values are decreasing with the increase of the RAP material content. Similar tendencies were observed for all the other temperatures.

In order to better observe the effects of the RAP material and the rejuvenator the $S_M(t)$ and $S_A(t)$ values were normalized with respect to the results obtained for the conventional bituminous mixture D.0.R.0. All $S_M(t)$ and $S_A(t)$ values together with the normalized values for all tested bituminous mixtures are reported in Table 3.16 for the measured stiffness and Table 3.17 for the adjusted stiffness.

It could be observed that the stiffness of the bituminous mixtures produced with rejuvenator show a variation with the increase of RAP material, with respect to the conventional mixture. This tendency can be explained since the rejuvenator content is fixed as a percentage of 0%, 0.2%, 0.4% and 0.6% of the RAP material

content. Therefore, the bituminous mixtures produced with a higher RAP material amount have also a higher rejuvenator content.

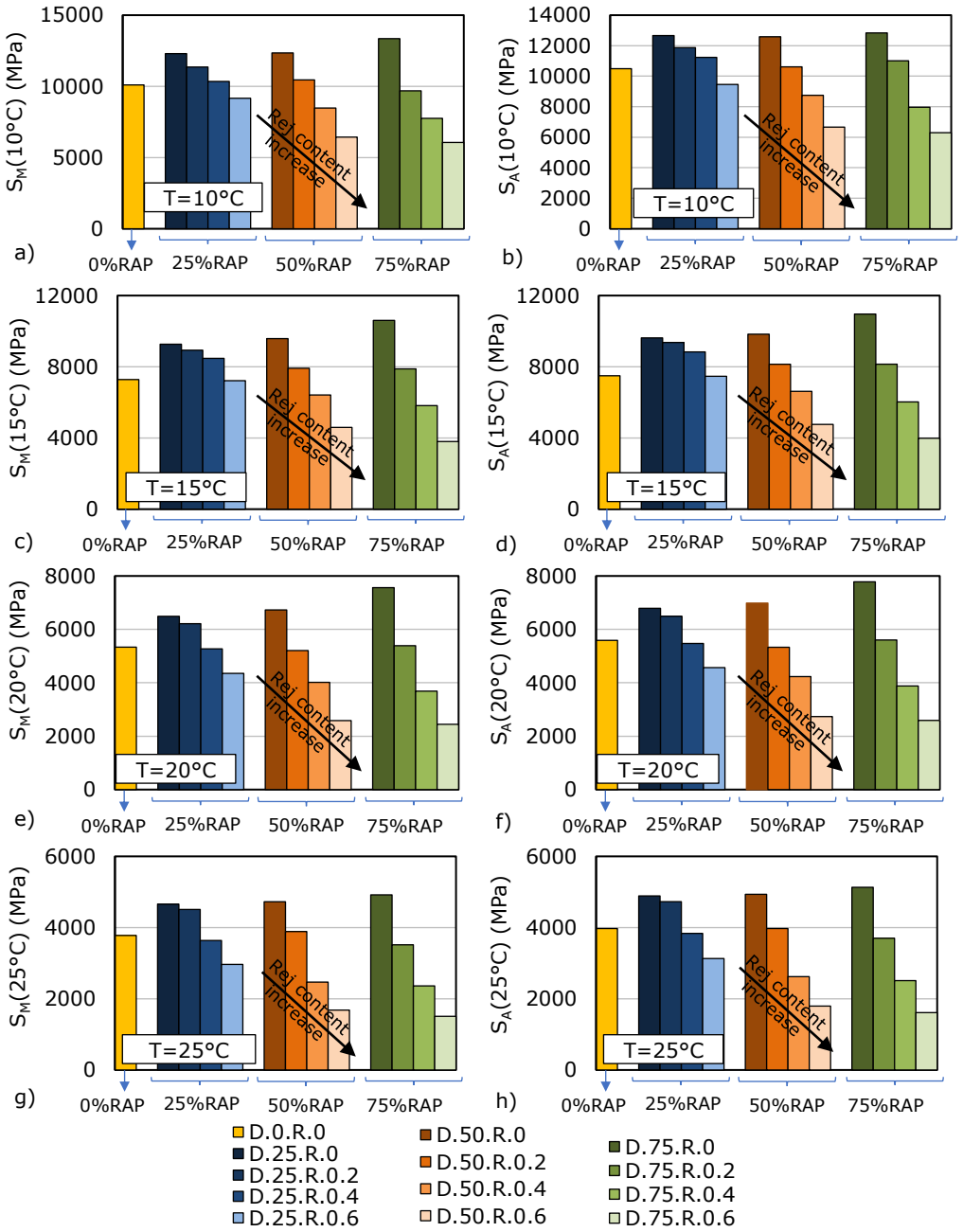

Figure 3.33. Stiffness modulus for all considered bituminous mixtures at each test temperature: (a) $S_M(10°C)$; (b) $S_A(10°C)$; (c) $S_M(15°C)$; (d) $S_A(15°C)$; (e) $S_M(20°C)$; (f) $S_A(20°C)$; (g) $S_M(25°C)$; (h) $S_A(25°C)$.

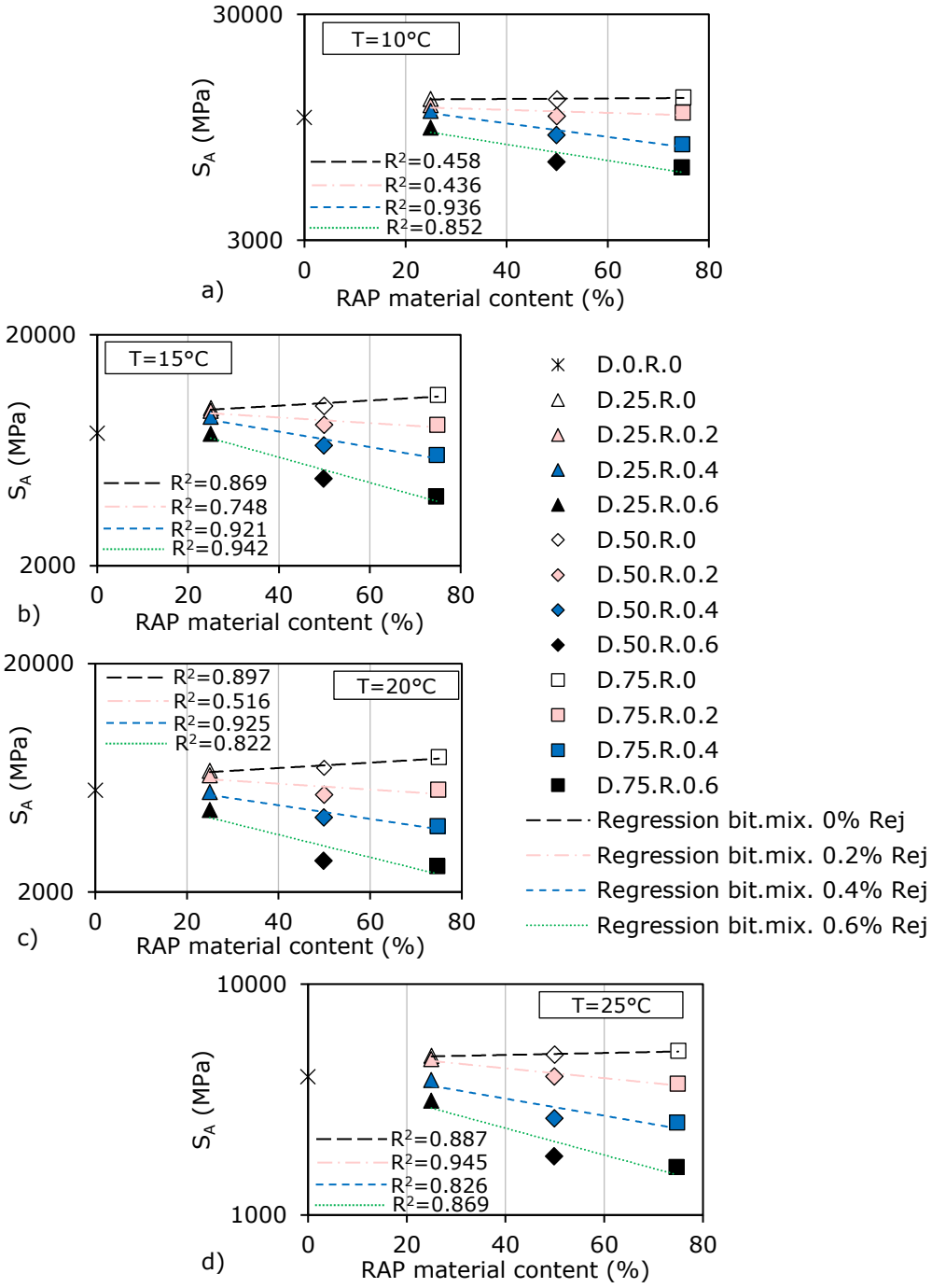

Figure 3.34. Adjusted stiffness modulus as a function of the RAP material content for all considered bituminous mixtures at each test temperature: (a) T=10°C; (b) T=15°C; (c) T=20°C; (d) T=25°C.

Table 3.16. Experimental results and normalized (to D.0.R.0) of the measured stiffness modulus for all considered bituminous mixtures.

Bit. mix.	$S_M(T)\,(MPa)$				$S_M/S_{M\,0\%}(T)\,(-)$			
	T=10°C	T=15°C	T=20°C	T=25°C	T=10°C	T=15°C	T=20°C	T=25°C
D.0.R.0	10100	7282	5335	3779	1.00	1.00	1.00	1.00
D.25.R.0	12298	9267	6490	4658	1.22	1.27	1.22	1.23
D.25.R.0.2	11358	8931	6214	4510	1.12	1.23	1.16	1.19
D.25.R.0.4	10345	8473	5271	3638	1.02	1.16	0.99	0.96
D.25.R.0.6	9165	7218	4352	2966	0.91	0.99	0.82	0.78
D.50.R.0	12348	9583	6729	4726	1.22	1.32	1.26	1.25
D.50.R.0.2	10453	7916	5207	3889	1.03	1.09	0.98	1.03
D.50.R.0.4	8477	6415	4016	2469	0.84	0.88	0.75	0.65
D.50.R.0.6	6436	4593	2584	1683	0.64	0.63	0.48	0.45
D.75.R.0	13352	10606	7564	4920	1.32	1.46	1.42	1.30
D.75.R.0.2	9687	7882	5389	3516	0.96	1.08	1.01	0.93
D.75.R.0.4	7754	5818	3687	2362	0.77	0.80	0.69	0.63
D.75.R.0.6	6061	3800	2445	1507	0.60	0.52	0.46	0.40

Table 3.17. Experimental results and normalized (to D.0.R.0) of the adjusted stiffness modulus for all considered bituminous mixtures.

Bit. mix.	$S_A(T)\,(MPa)$				$S_A/S_{A\,0\%}(T)\,(-)$			
	T=10°C	T=15°C	T=20°C	T=25°C	T=10°C	T=15°C	T=20°C	T=25°C
D.0.R.0	10492	7495	5589	3974	1.00	1.00	1.00	1.00
D.25.R.0	12662	9623	6790	4890	1.21	1.28	1.21	1.23
D.25.R.0.2	11872	9365	6492	4728	1.13	1.25	1.16	1.19
D.25.R.0.4	11233	8835	5473	3837	1.07	1.18	0.98	0.97
D.25.R.0.6	9458	7466	4568	3131	0.90	1.00	0.82	0.79
D.50.R.0	12586	9830	6985	4935	1.20	1.31	1.25	1.24
D.50.R.0.2	10612	8141	5330	3975	1.01	1.09	0.95	1.00
D.50.R.0.4	8747	6620	4232	2622	0.83	0.88	0.76	0.66
D.50.R.0.6	6662	4762	2734	1795	0.63	0.64	0.49	0.45
D.75.R.0	12836	10961	7782	5132	1.22	1.46	1.39	1.29
D.75.R.0.2	11008	8145	5603	3702	1.05	1.09	1.00	0.93
D.75.R.0.4	7965	6025	3881	2511	0.76	0.80	0.69	0.63
D.75.R.0.6	6296	3985	2590	1612	0.60	0.53	0.46	0.41

From the presented results a general conclusion could be raised, that the effect of increasing the RAP material content conduce to an increase of stiffness. The influence of the temperature was observed: the increase of temperature leads to a linear decrease of the stiffness modulus. On the other side, the increase of the rejuvenator content within the mass of mixtures corresponds to a reverse effect as the stiffness decreases with the increase of the rejuvenator content.

As in case of the Marshall characteristics it would be interesting to investigate the relation between the stiffness modulus of the mixtures and the penetration of the corresponding binder blends. Figure 3.35 shows the adjusted stiffness modulus results

obtained at different temperature as a function on the penetration results obtained for the binder blends. Similar analysis as in case of the Marshall characteristics was performed: linear regressions for the mixtures produced with constant RAP material content and a global linear regression were performed.

It could be observed that for the mixtures produced with the same RAP material content (25%, 50% and 75%) and different rejuvenator content, some strong relations were found, R^2 always higher than 0.917. However, the global relation between stiffness and penetration is not so strong, R^2 is lower than 0.825.

As mentioned in the previous section, these tendencies could be explained by the fact that most probably when the RAP material was added in the new bituminous mixtures some differences between the grading curves of these mixtures and the one used for the conventional mix were obtained. Also, as the rejuvenator content was established by the mass of the RAP material, the total binder content is increasing with the increase of RAP material. As all specimens were produced by using the same compaction energy and as the density of the aggregates from the RAP material is most probably higher than the density of the virgin aggregates, the mixture specimens become more dense with the increase of the RAP material and rejuvenator contents (see Table 3.15). For these reasons, for the mixtures/binder blends produced with the same amount of RAP content good linear relations could be performed.

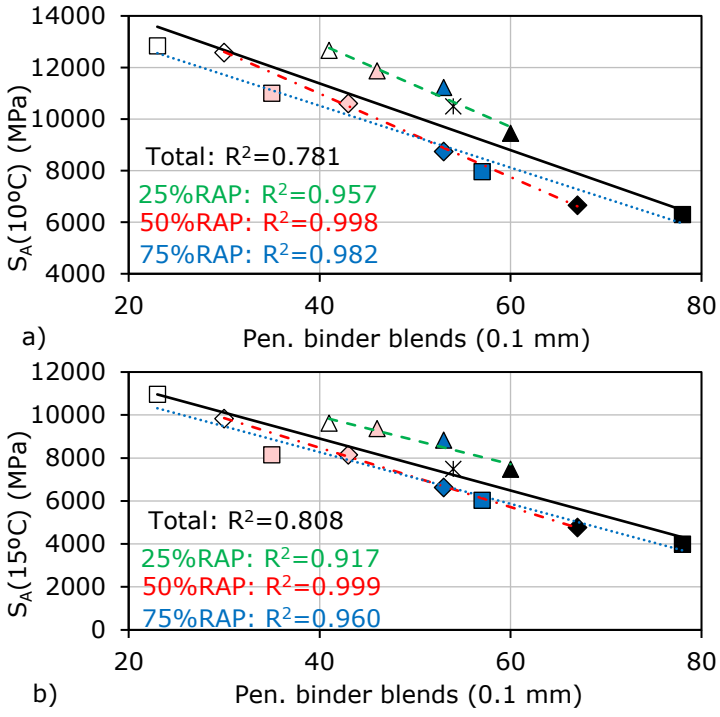

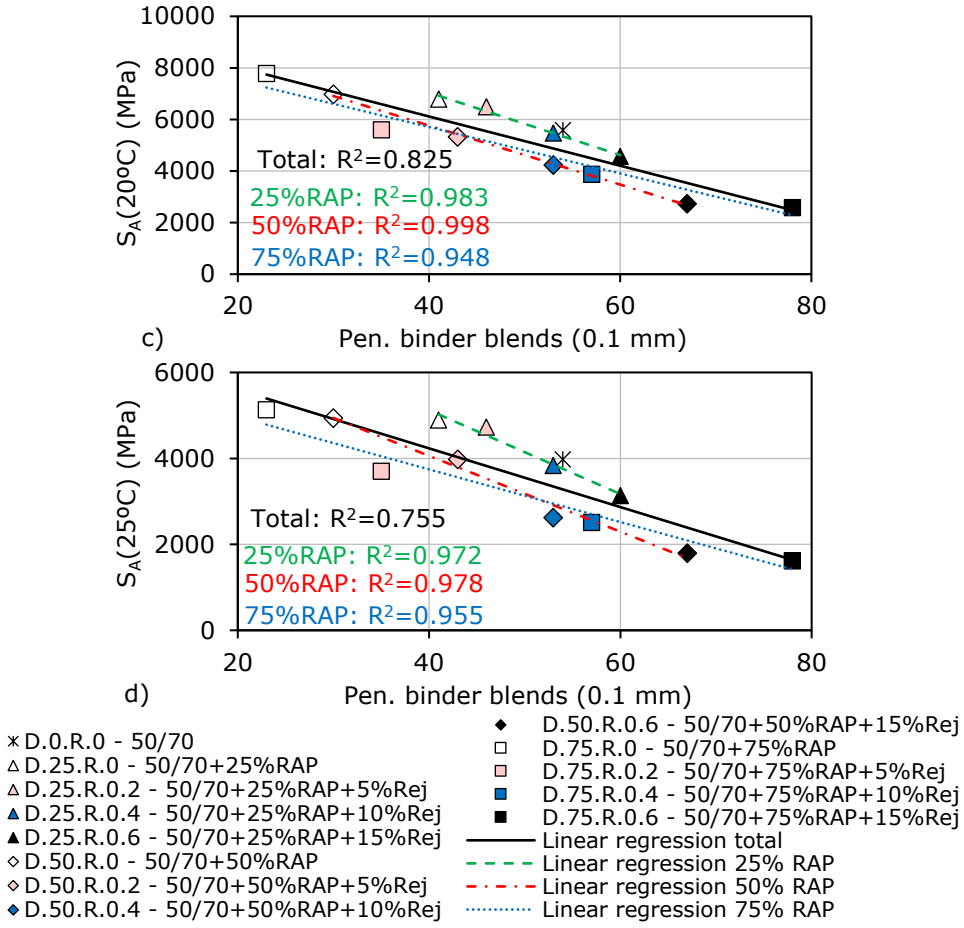

Figure 3.35. (a) Adjusted stiffness at 10ºC vs. binder blends penetration; (b) Adjusted stiffness at 15ºC vs. binder blends penetration; (c) Adjusted stiffness at 20ºC vs. binder blends penetration; (d) Adjusted stiffness at 25ºC vs. binder blends penetration.

3.7.3 Permanent deformation resistance (dynamic creep)

The cyclic compression with confinement tests were performed according to SR EN 12697-25 [198]– Method B in order to determine the resistance to permanent deformation at a constant temperature of 50°C, on a cylindrical specimen subjected to a cyclic axial block-pulse pressure of 300 kPa, superposed with a static confining pressure of 50 kPa.

The procedure followed in order to determine the resistance to permanent deformation after applying 10000 impulses in described in Section 3.5.3. For each considered bituminous mixture, two cylindrical specimens with a 100 mm diameter were produced with the gyratory press at 80 gyrations.

Identical intermediate measurements, as in the case of the IT-CY tests, were performed for each bituminous mixture cylindrical specimen. The values obtained for all specimens for each bituminous mixture are reported in Table 3.18.

The same remarks as in the case of the specimens considered for the IT-CY test, are valid in the case of the analysed cylindrical specimens. By increasing the RAP material content within the mass of the bituminous mixtures, it results an increase of all values of the above-mentioned parameters, except $VFB_{bit.mix.}$. The increase of the rejuvenator content corresponds to a reverse effect, a decrease of the intermediate test results, except $\rho_{A.bit.mix.}$ and $VFB_{bit.mix.}$.

Cyclic compression with confinement tests were performed on all specimens and based on the obtained measurements the creep curve was built for each tested specimen. The quasi-linear stage of the creep curve was obtained by performing a linear fit on this stage. It must be mentioned that for all tests only the first stage i.e. initial part of the curve where the increase of the cycles corresponds to a decrease of the slope of the creep curve and the second stage i.e. the part of the creep curve with quasi-constant slope of the creep cures were observed. The third stage corresponding to an increase of the slope is missing for all tests.

Figure 3.36 shows as an example the creep curve obtained for the specimen 8a for the mixture D.50.R.0.4, together with the linear fit performed on the second stage of the creep curve.

The outputs determined by performing the cyclic compression with confinement tests that were analysed in this study are:

- the mean deformation of the specimen, after 10000 loading cycles, h_{10000} in mm found as position of the upper plate measured by the two LVDTs;
- the cumulative axial strain of the test specimen after 10000 impulses, ε_{10000} in μm/m;
- creep rate, f_C in μm/m/loading cycle;
- the slope from the least square linear fit on the $log\left(\varepsilon_{1000,calc} - C\right)$ *vs.* $log\left(n\right)$ values, B;
- the cumulative axial strain of the test specimen after 1000 impulses, $\varepsilon_{1000,calc}$ in %.

All outputs were calculated by using the equations 3.16 – 3.19 which are described in Section 3.5.4.

As already mentioned, two cylindrical specimens were tested for each type of bituminous mixture. The average results determined for the above-mentioned output parameters are reported in Table 3.19 for all considered mixtures.

Moreover, Figure 3.37 shows the results obtained for the cumulative axial strain after 10000 impulses and the creep rate for all bituminous mixtures.

Table 3.18. Intermediate test results for each specimen determined for cylindrical specimens produced at 80 gyrations for all considered bituminous mixtures.

Bit. mix.	Specimen	$\rho_{Abit.mix.}$ (kg/m^3)	$A_{V\,bit.mix.}$ (%vol.)	$V_{Mbit.mix.}$ (%)	$VMA_{bit.mix.}$ (%)	$VFB_{bit.mix.}$ (%)
D.0.R.0	1a	2295	1.20	5.30	17.90	70.50
	1b	2299	1.00	5.10	17.80	71.30
D.25.R.0	2a	2343	2.20	4.10	16.90	75.70
	2b	2345	2.00	4.00	16.90	76.10
D.25.R.0.2	3a	2357	1.50	3.50	16.50	79.00
	3b	2351	1.60	3.70	16.70	77.70
D.25.R.0.4	4a	2361	1.20	3.30	16.50	79.90
	4b	2365	1.50	3.10	16.30	80.80
D.25.R.0.6	5a	2373	1.20	2.70	16.00	83.40
	5b	2365	1.30	3.00	16.30	81.70
D.50.R.0	6a	2340	2.50	5.10	17.80	71.40
	6b	2359	2.70	4.30	17.10	74.90
D.50.R.0.2	7a	2362	1.80	4.00	17.10	76.40
	7b	2361	1.70	4.10	17.10	76.30
D.50.R.0.4	8a	2372	1.30	3.40	16.80	79.50
	8b	2359	1.20	4.00	17.30	76.80
D.50.R.0.6	9a	2365	1.10	3.60	17.10	79.10
	9b	2378	1.10	3.00	16.70	81.80
D.75.R.0	10a	2395	3.60	6.60	19.50	66.00
	10b	2393	3.90	6.70	19.60	65.80
D.75.R.0.2	11a	2406	2.60	5.50	18.80	70.80
	11b	2396	2.60	5.90	19.20	69.20
D.75.R.0.4	12a	2411	1.80	5.20	18.90	72.60
	12b	2419	1.80	4.90	18.60	73.80
D.75.R.0.6	13a	2434	1.10	4.10	18.30	77.70
	13b	2435	1.20	4.00	18.20	77.90

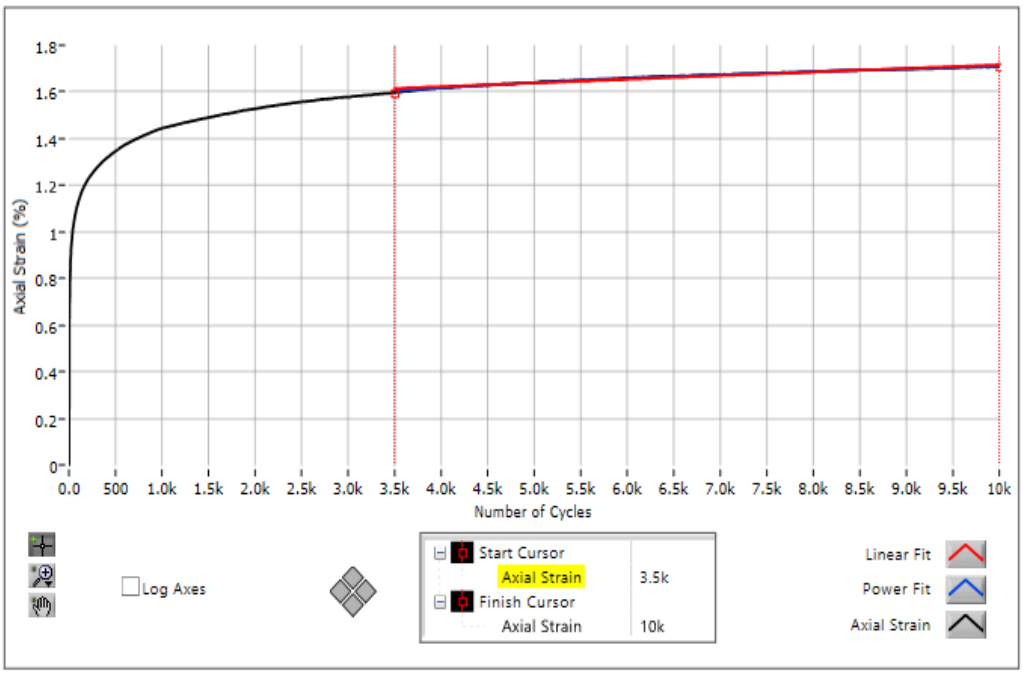

Figure 3.36. Example creep curve test results for specimen 8a, bituminous mixture D.50.R.0.4.

Table 3.19. Cyclic compression with confinement test results (average values of two specimens) determined for cylindrical specimens produced at 80 gyrations for all considered bituminous mixtures.

Bit. mix.	h_0 *(mm)*	h_{10000} *(mm)*	ε_{10000} *(μm/m)*	f_c *(μm/m/loading cycle)*	*Power fit B (-)*	$\varepsilon_{1000,calc.}$ *(-)*
D.0.R.0	0.007	0.669	9593	0.153	0.146	0.558
D.25.R.0	0.017	0.777	12051	0.096	0.065	0.844
D.25.R.0.2	0.022	1.126	16392	0.102	0.066	0.868
D.25.R.0.4	0.024	1.423	20681	0.145	0.039	2.084
D.25.R.0.6	0.029	1.924	27866	0.171	0.042	2.319
D.50.R.0	0.033	1.030	15107	0.123	0.065	1.111
D.50.R.0.2	0.039	1.344	20380	0.156	0.061	1.487
D.50.R.0.4	0.053	1.712	25134	0.266	0.116	1.265
D.50.R.0.6	0.061	2.022	30650	0.399	0.234	2.454
D.75.R.0	0.052	1.244	18626	0.160	0.071	1.264
D.75.R.0.2	0.062	1.647	25141	0.264	0.123	1.210
D.75.R.0.4	0.024	2.029	32329	0.579	0.134	2.180
D.75.R.0.6	0.062	2.348	38088	0.863	0.185	2.252

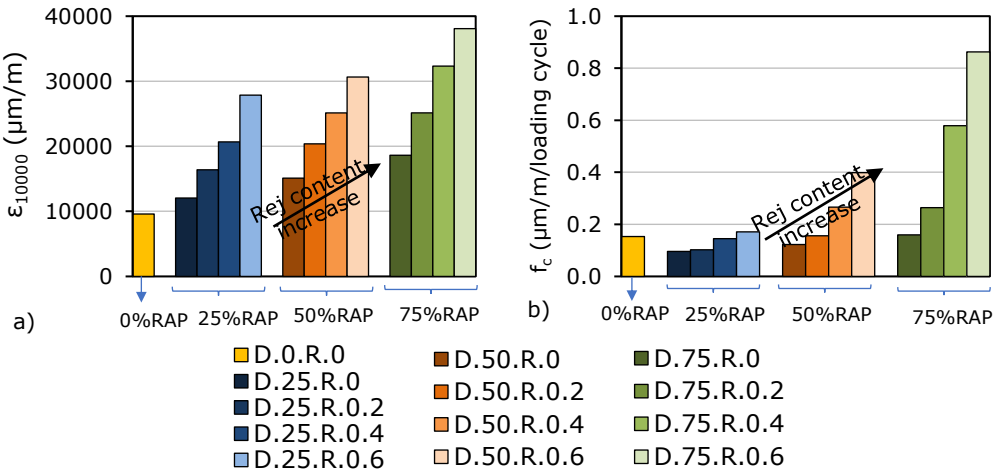

Figure 3.37. Permanent deformation test results for all considered bituminous mixtures at each test temperature: (a) cumulative axial strain of the test specimen after 10000 impulses; (b) creep rate.

It could be noted that the increase of the RAP material content within the mass of mixtures leads to an increase of the h_{10000}, ε_{10000} and f_c values. Similarly, the increase of the rejuvenator content conduced to a same tendency.

It must be mentioned that no specimens failed before the 10000 loading cycles.

The obtained results for the ε_{10000} and f_c for all bituminous mixtures were plotted as a function of the RAP material content in Figure 3.38 in order to highlight if there are any obvious variation with the increase of both RAP material and rejuvenator contents.

As it could be observed in Figure 3.38, ε_{10000} and f_c values increase with the increase of RAP content and some linear trends were observed. Therefore, linear regressions were performed on the obtained outputs results for all mixtures produced with the same amount of rejuvenator of 0%, 0.2%, 0.4% and 0.6% by mass of the RAP material and the R^2 values were determined for each regression with good approximation. R^2 values always higher than 0.935.

It worth noting that the values of ε_{10000} obtained for each series of mixtures produced with the same amount of rejuvenator by mass of the RAP material, presents approximatively the same tendency, the slope of each linear regression being approximatively the same. It seems that ε_{10000} values are proportional with the rejuvenator content. However, this remark is not valid in case of the creep rate.

Moreover, it is interesting to note that for the mixtures produced without rejuvenator, a small increase of the creep rate was observed with the increase of the RAP material content as the linear regression is close to horizontal line. The rate of the increase of the f_c values is higher for the other series of bituminous mixtures produced with 0.2%, 0.4% and 0.6% rejuvenator. This can be observed by increasing the slope of the linear regressions.

As an example, for the mixtures produced with the highest rejuvenator content 0.6% by mass of the RAP material, an important increase of the creep rate

was observed. These tendencies can be explained by the fact that the rejuvenator content is calculated as a percentage of the RAP material. Therefore, the increase of the RAP material content corresponds to an increase of the rejuvenator content.

As a general comment on these test results, it could be concluded that the effect of increasing the RAP material content leads to an increase of the cumulative strain after 10000 loading cycles and of the creep rate. On the other side, the increase of the rejuvenator content within the mass of mixtures corresponds to a reverse effect.

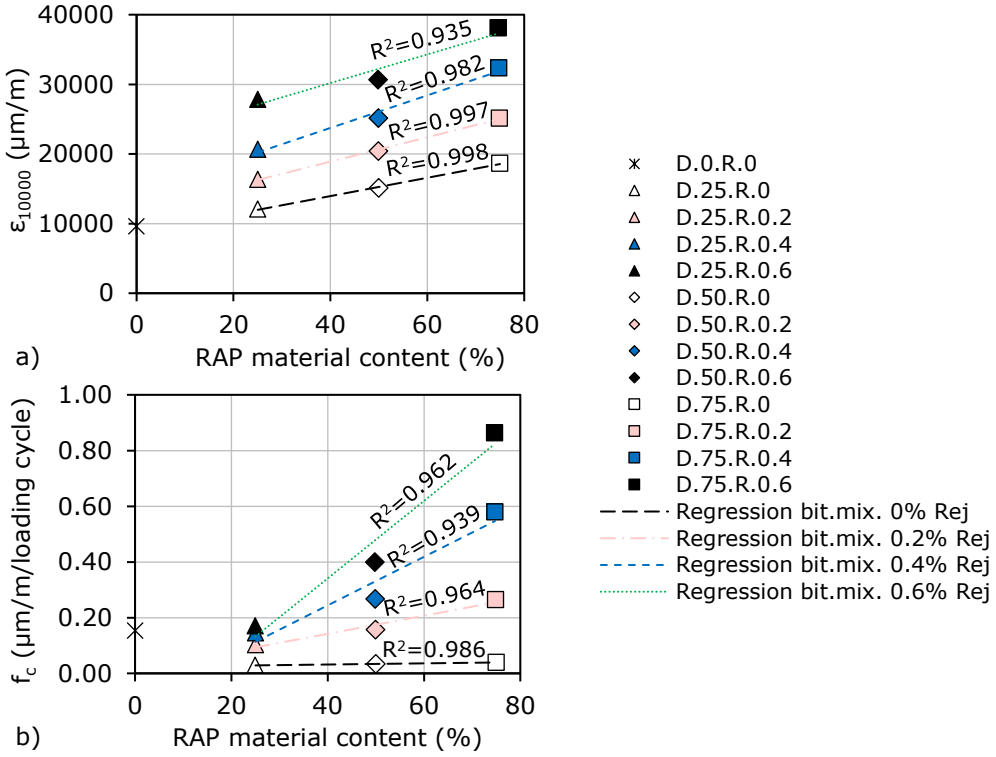

Figure 3.38. Permanent deformation test results as a function of the RAP material content for all considered bituminous mixtures: (a) ε_{10000}; (b) f_c.

As in case of the stiffness modulus and Marshall characteristics the relation between the cumulative axial strain after 10000 impulses of the mixtures and the penetration of the corresponding binder blends was investigated as shown in Figure 3.39. Similar analysis as in case of the Marshall characteristics was performed: linear regressions for the mixtures produced with constant RAP material content and a global linear regression were performed.

Some strong relations were found, R^2 always higher than 0.982, for the mixtures produced with the same RAP material content (25%, 50% and 75%). However, the global relation between stiffness and penetration is not so strong, R^2 is lower than 0.428. As mentioned in previous sections, these tendencies could be explained by the fact that most probably the use of the RAP material leads to a change of the grading curves of the final mixtures. Also, the use of the same energy compaction of all mixtures, the rejuvenator content which was established as a

function of the mass of the RAP material and the difference between the density of the RAP aggregates and the virgin aggregates lead to these results.

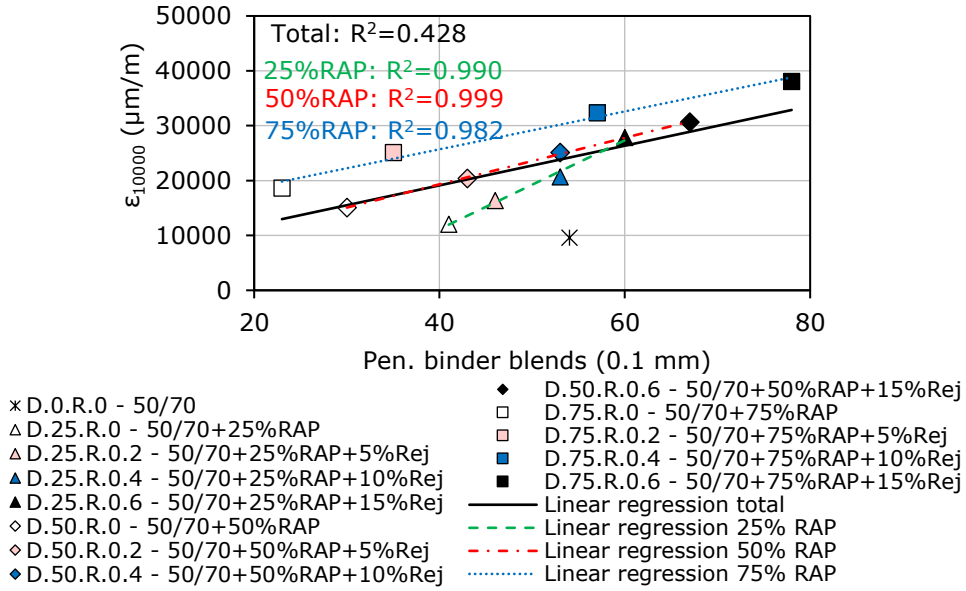

Figure 3.39. Cumulative axial strain after 10000 impulses of mixtures vs. binder blends penetration.

3.7.4 Complex modulus test - two-point bending test

3.7.4.1 Experimental results

Complex modulus tests in two-point bending configuration were performed on trapezoidal specimens according to SR EN 12697-26 – Annex A [197].

As described in Section 3.4.2, four trapezoidal specimens were cut from each slab produced for each considered mixtures. It is important to mention that same energy of compaction was used in order to produce the slabs. The coring plan for one slab is presented in Figure 3.7 in Section 3.4.2.

A selection between the trapezoidal specimens according to their void contents and their dimensions was performed. The dimensions and the void contents for each specimen are reported in Table 3.20 where the specimens marked by '*' are chosen to be tested. Therefore, a lot of two specimens which meet the accuracy of ±1 mm for each dimension as specified in the Standard for a mixture with a 16 mm maximum aggregate size and which has the average void content as similar as possible, were selected for the evaluation of complex modulus two-point bending test.

Table 3.20. Dimensions and void contents of all cut trapezoidal specimens.

Bit. mix.	Specimen	Trapezoidal specimens dimensions (mm)				Void content
		H	B	b	e	(%)
D.0.R.0	1.1	250.33	70.12	24.88	23.93	4.10
	1.2*	250.97	69.46	24.50	24.60	4.50
	1.3	250.11	70.77	25.75	23.88	4.30
	1.4*	250.71	69.68	24.49	25.90	4.90
D.25.R.0	2.2	248.94	70.25	25.12	25.14	4.90
	2.3	250.22	68.98	24.93	24.99	5.20
	2.4*	249.72	69.70	24.89	25.12	5.00
	2.5*	250.45	69.84	24.79	24.10	5.10
D.25.R.0.2	3.1	250.56	70.05	23.91	25.02	4.90
	3.2*	250.97	69.89	25.06	24.90	4.90
	3.3*	250.56	69.98	24.75	25.50	4.70
	3.4	248.87	69.84	25.01	24.96	4.10
D.25.R.0.4	4.1*	249.42	70.39	25.29	25.60	4.30
	4.2*	249.23	70.35	25.17	25.10	4.30
	4.3	248.92	70.25	25.23	25.45	3.80
	4.4	248.89	70.33	25.15	25.11	4.20
D.25.R.0.6	5.1*	250.63	69.56	24.52	25.25	3.80
	5.2*	250.05	69.64	24.43	25.20	3.60
	5.3	250.12	69.78	23.88	25.10	3.50
	5.4	250.55	69.82	24.56	23.84	3.80
D.50.R.0	6.1*	249.59	69.60	24.94	25.50	5.70
	6.2	250.85	69.68	25.04	25.08	5.10
	6.3*	251.00	69.45	24.91	25.00	5.50
	6.4	248.89	69.96	25.93	25.18	5.60
D.50.R.0.2	7.1*	250.52	69.38	24.47	25.80	4.90
	7.2	248.88	70.28	25.06	25.36	4.80
	7.3	249.52	70.37	25.26	23.85	4.90
	7.4*	251.00	69.97	24.88	25.00	4.90
D.50.R.0.4	8.1	248.79	70.18	25.14	25.18	3.60
	8.2*	251.00	69.71	25.09	24.70	3.90
	8.3*	250.57	70.03	25.24	25.30	3.70
	8.4	250.63	70.44	25.13	25.19	3.10
D.50.R.0.6	9.1*	249.00	70.03	24.30	25.65	2.90
	9.2	248.80	70.08	24.83	23.97	2.80
	9.3*	249.42	70.12	25.54	26.00	2.90
	9.4	248.98	70.37	25.68	23.96	2.90
D.75.R.0	10.1*	249.00	70.44	25.82	25.00	6.20
	10.2*	249.09	70.14	25.49	25.30	6.40
	10.3	249.01	70.33	23.93	24.08	6.10
	10.4	249.08	70.25	23.91	23.97	6.00
D.75.R.0.2	11.1	248.91	69.86	24.99	24.86	4.70
	11.2	249.03	68.94	23.97	24.15	4.70
	11.3*	250.02	70.45	25.93	24.20	5.30
	11.4*	249.17	70.29	26.00	26.00	5.10
D.75.R.0.4	12.1	249.69	68.95	23.87	25.04	3.20
	12.2*	249.78	70.45	26.00	25.00	3.50
	12.3*	251.00	69.71	25.70	24.30	3.00
	12.4	249.61	68.92	25.45	25.12	3.30
D.75.R.0.6	13.1	248.93	70.17	25.28	25.10	2.30
	13.2	248.90	70.22	24.97	23.96	2.00
	13.3*	249.99	70.45	25.74	24.10	2.30
	13.4*	249.61	70.33	25.02	25.00	2.10

Complex modulus tests were performed in strain control with the imposed strain loading amplitude of 50 µm/m at seven temperatures starting from -5°C up to 25°C at a frequency range from 0.5 Hz to 20 Hz.

At each frequency and each temperature, a cyclic sinusoidal displacement is imposed on the specimen for a predefined time of 120 s. The data obtained over the last 10 seconds is acquired and the mean of these values are recoded and reported at the end of each test. More details regarding the procedure that was followed during these tests, are given in Section 3.5.5.

As an example, Figure 3.40 shows the isothermal curves of the norm and the phase angle of the complex modulus for the bituminous mixture produced with 25% RAP material and 0.4% rejuvenator by mass of the RAP material.

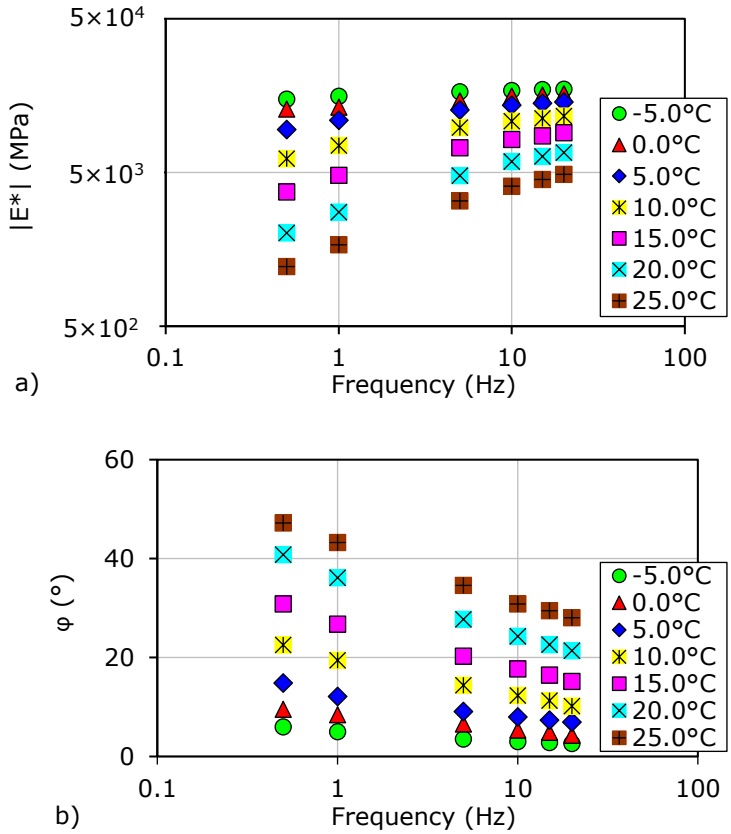

Figure 3.40. Example of complex modulus two-point bending test results for the bituminous mixture D.25.R.0.4: (a) norm of complex modulus isotherms; (b) phase angle isotherms.

Also, Cole-Cole and Black diagrams were built in order to verify if the time temperature superposition principle (TTSP) is valid. Figure 3.41 shows an example for the mixture D.25.R.0.4.

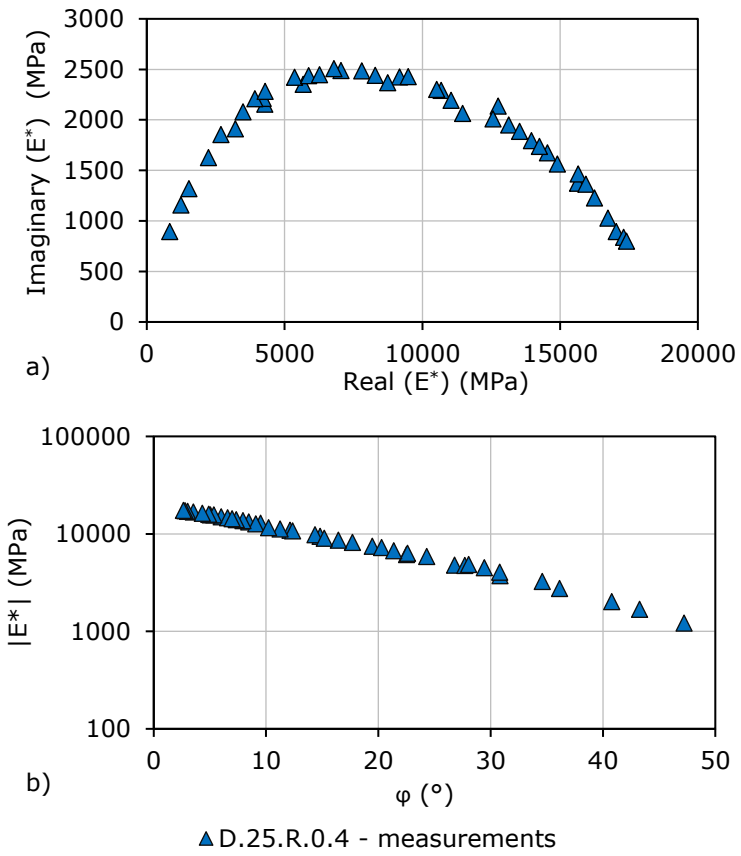

Figure 3.41. Example of complex modulus two-point bending test results for the bituminous mixture D.25.R.0.4: (a) Cole-Cole diagram; (b) Black diagram.

As it could be observed, the data presented in Cole-Cole and Black diagrams are located on a unique curve, independently of the test temperature and frequency, for each of the considered mixtures.

This observed trend means that the time temperature superposition principle (TTSP) is valid for all tested bituminous mixtures and moreover they can be considered as thermorheologically simple materials [11] even when containing the rejuvenator.

Cole-Cole and Black curves of the mixtures produced without rejuvenator present an expected trend with the increase of the RAP material content within mixtures. On the other side, the increase of the rejuvenator content into mixtures corresponds to a reverse effect by counterbalancing the effect of the aged RAP material.

For the same bituminous mixture (D.25.R.0.4) isothermal master curves of the norm of complex modulus $|E^*|$ and phase angle φ were built at a reference temperature (T_{ref}) of 15°C in Figure 3.42. Also, Figure 3.42c shows the values of the temperature shift factors a_T as a function of test temperature. It must be mentioned

that same WLF constants as those obtained for each corresponding binder blends at the same reference temperature (15°C) of each mixture were used. The use of the same WLF constants is a step in order to apply the SHStS transformation (presented in Section 1.5.4).

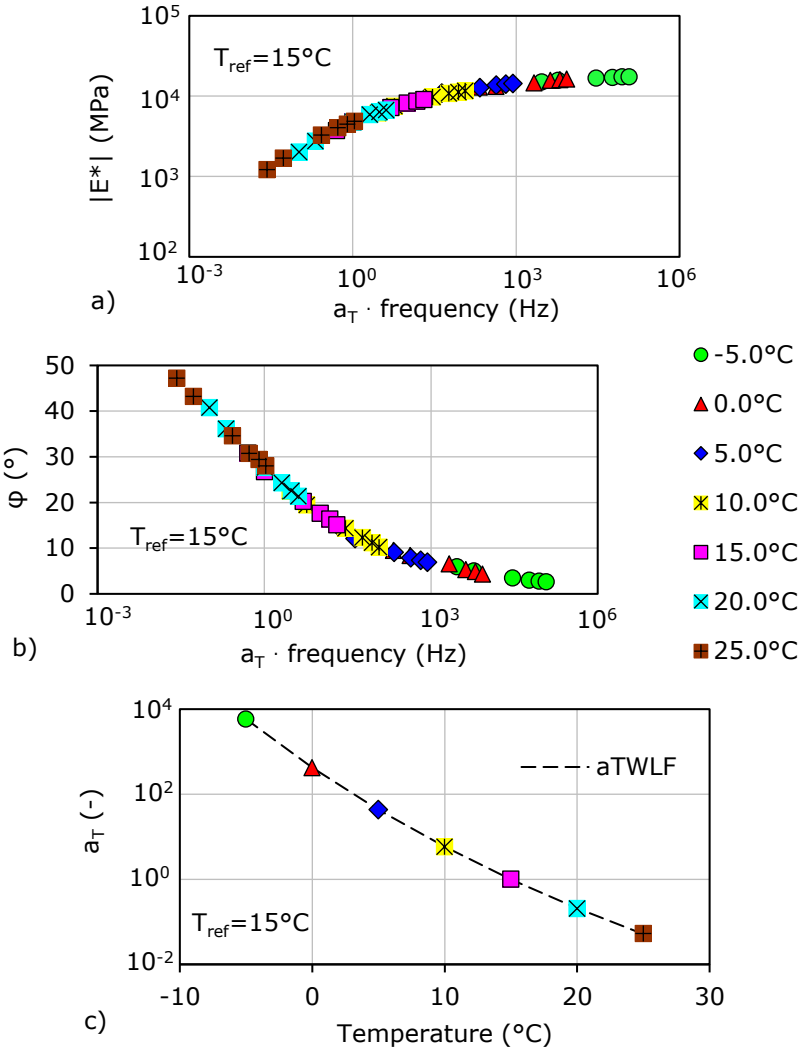

Figure 3.42. Complex modulus two-point bending test results for the bituminous mixture D.25.R.0.4: (a) master curve of the norm of complex modulus; (b) master curve of the phase angle of complex modulus; (c) a_T shift factors versus temperature.

Similar plots to those presented in Figure 3.42 were made for all the other mixtures. All plots together with the 2S2P1D modelling are reported in Appendix 2. Table 3.21 lists the values of a_T temperature shift factors together with WLF constants for all tested mixtures.

Table 3.21. Complex modulus two-point bending test results for all mixtures: (a) a_T temperature; (b) WLF constants.

a)

Bit. mix.	a_T shift factors (-)						
	-5°C	0°C	5°C	10°C	15°C	20°C	25°C
D.0.R.0	6693.00	450.00	43.00	4.98	1	0.234	0.066
D.25.R.0	6028.00	441.00	44.00	5.92	1	0.200	0.047
D.25.R.0.2	6335.00	448.00	33.20	5.08	1	0.210	0.050
D.25.R.0.4	5833.00	420.00	43.00	5.77	1	0.204	0.053
D.25.R.0.6	4222.00	394.00	40.60	5.11	1	0.222	0.055
D.50.R.0	4011.00	381.20	40.50	5.65	1	0.202	0.055
D.50.R.0.2	4060.80	280.20	35.20	5.77	1	0.235	0.059
D.50.R.0.4	2564.00	220.80	30.10	5.01	1	0.214	0.053
D.50.R.0.6	2483.80	197.90	24.50	4.56	1	0.260	0.065
D.75.R.0	4852.00	385.00	42.23	6.20	1	0.220	0.052
D.75.R.0.2	3839.60	283.00	28.50	4.90	1	0.250	0.060
D.75.R.0.4	757.60	143.60	31.20	4.54	1	0.250	0.055
D.75.R.0.6	981.40	104.30	20.50	5.01	1	0.235	0.063

b)

Bit. mix.	C_1	C_2
D.0.R.0	12.07	83.10
D.25.R.0	13.23	89.98
D.25.R.0.2	12.65	86.56
D.25.R.0.4	12.26	85.08
D.25.R.0.6	11.88	83.63
D.50.R.0	14.08	96.46
D.50.R.0.2	12.96	90.03
D.50.R.0.4	12.12	85.41
D.50.R.0.6	11.47	84.54
D.75.R.0	14.84	97.16
D.75.R.0.2	13.57	92.81
D.75.R.0.4	11.56	88.44
D.75.R.0.6	12.29	92.79

In order to highlight the influence of increasing the RAP material and the rejuvenator contents on the thermomechanical behaviour of mixtures, master curves of the norm and phase angle of the complex modulus for the mixtures produced with 50% RAP material and different amounts of rejuvenator and the conventional mixture were plotted in Figure 3.43.

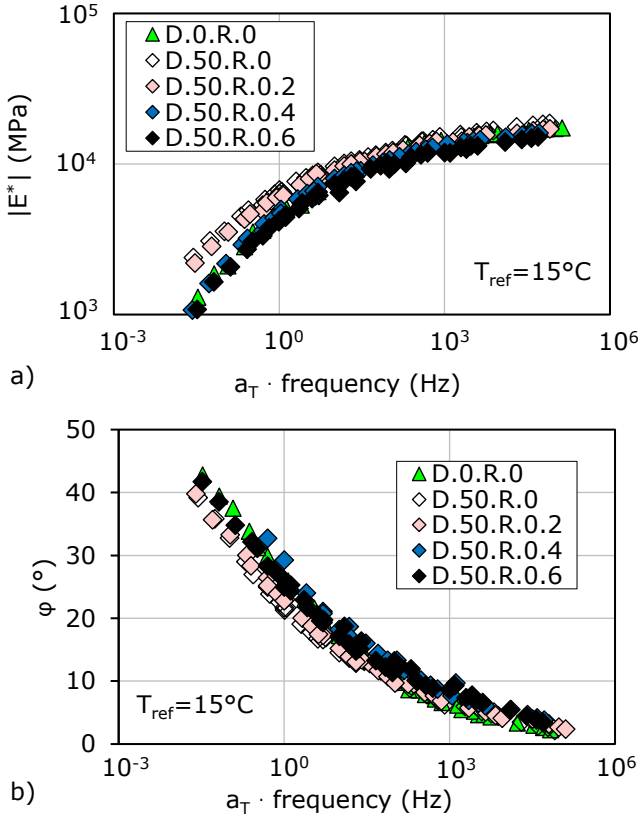

Figure 3.43. Complex shear modulus test results for the mixtures produced with 50% RAP and different dosages of rejuvenator and the conventional mixtures: (a) master curves of the norm of complex modulus; (b) master curves of the phase angle of complex modulus.

As expected, master curves of mixtures produced without rejuvenator are falling away from the corresponding master curves of the conventional one. $|E^*|$ values are increasing with the increase of RAP material content while the φ values are decreasing with the increase of RAP material content. On the other side, the increase of the rejuvenator content into mixtures corresponds to master curves and shift factors progresively approaching to those of the conventional mixture.

From these results, the mixture produced with 50% RAP mateial and 0.6% Rej by mass of the RAP material presents an aproximatively close behaviour to the one of the conventional mixture. Thus, the master curves are close to those of the conventional HMA.

This tendency confirms the conclusions from Chapter 2 where it was shown that the corresponding binder blend of D.50.R.0.6 presents similar conventional and rheological properties to those of the used fresh 50/70. Practically the rejuvenating effect of the rejuvenator is counterbalancing the effect of the aged RAP binder within this binder blend.

3.7.4.2 2S2P1D modelling

Experimental data were fitted with 2S2P1D model (equation 1.28 Section 1.5.3) which is presented in Section 1.5.3. As an example, Black, Cole-Cole and complex modulus and phase angle master curves at a reference temperature of 15°C for mixture D.50.R.0.2 are reported in Figure 3.44. 2S2P1D model parameters, for all tested mixtures are listed in Table 3.22, excepting the parameters corresponding to Poisson ratio which were not investigated. 2S2P1D model fittings of master curves of complex modulus and phase angle, WLF curves, Black curves and Cole-Cole curves obtained for all other mixtures are reported in Appendix 2 from Figure A2.7 to Figure A2.18.

It must be mentioned that the same values of h and β parameters as those used in case of the binder blends (Table 2.10 from Section 2.6.2.1), were used for each corresponding bituminous mixture.

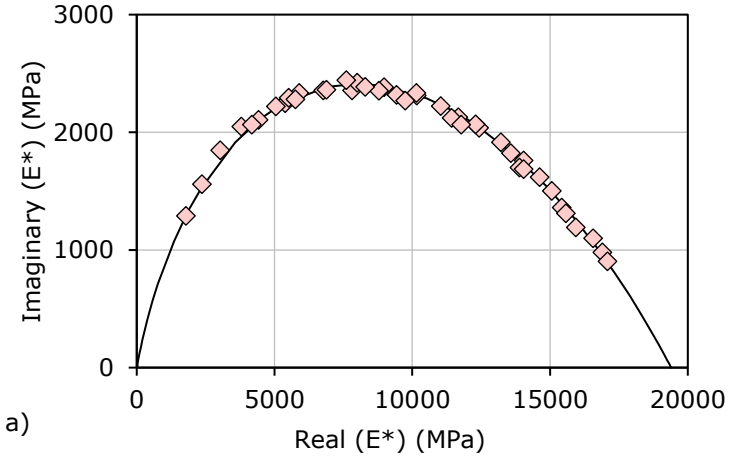

a)

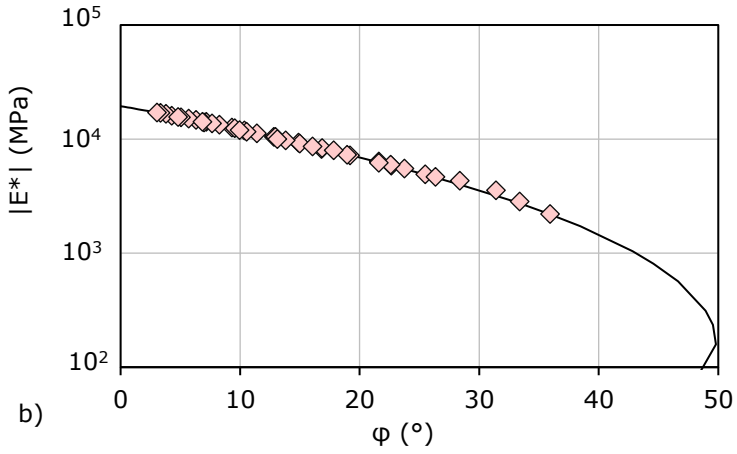

b)

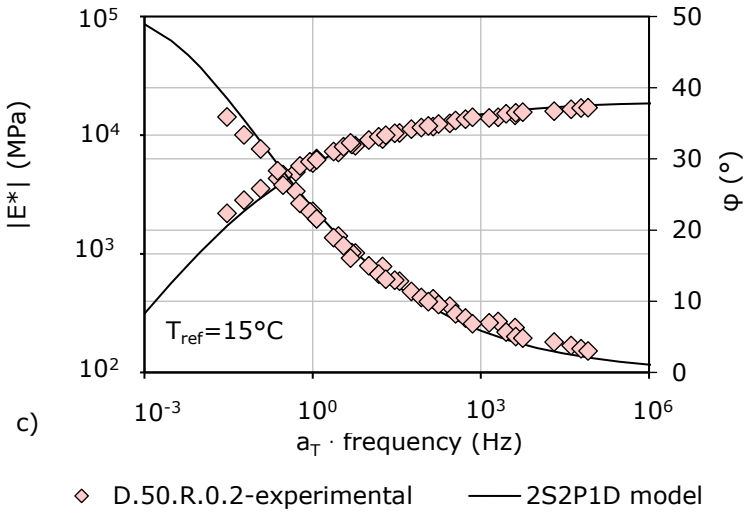

Figure 3.44. 2S2P1D model fitting of complex modulus test results for mixture D.50.R.0.2: (a) Cole-Cole curve; (b) Black curve; (c) master curves of the norm of complex modulus and phase angle.

Table 3.22. 2S2P1D parameters obtained for the considered bituminous mixtures.

Bit. mix.	2S2P1D parameters						
	E_{00} (MPa)	E_0 (MPa)	k (-)	h (-)	δ (-)	τ (s)	β (-)
D.0.R.0	10	19000	0.277	0.633	2.35	0.184	124
D.25.R.0	15	19300	0.262	0.626	2.02	0.233	166
D.25.R.0.2	15	18720	0.262	0.629	2.37	0.312	158
D.25.R.0.4	10	19400	0.267	0.643	2.11	0.131	132
D.25.R.0.6	10	17500	0.268	0.635	2.38	0.182	120
D.50.R.0	15	20600	0.253	0.620	2.16	0.258	235
D.50.R.0.2	15	19400	0.265	0.625	2.28	0.298	195
D.50.R.0.4	10	18900	0.268	0.633	1.86	0.097	145
D.50.R.0.6	10	17600	0.274	0.638	2.63	0.198	124
D.75.R.0	25	21900	0.254	0.614	2.36	0.468	310
D.75.R.0.2	15	20000	0.288	0.624	2.32	0.180	238
D.75.R.0.4	10	19280	0.292	0.633	1.51	0.040	166
D.75.R.0.6	10	14500	0.239	0.641	2.69	0.532	125

Values of the 2S2P1D parameters were then plotted as a function of RAP material content, as shown in Figure 3.45 a-g. Illustratively, an example of the shift factors at 5°C as a function of RAP material content within the mixture is shown in Figure 3.45h.

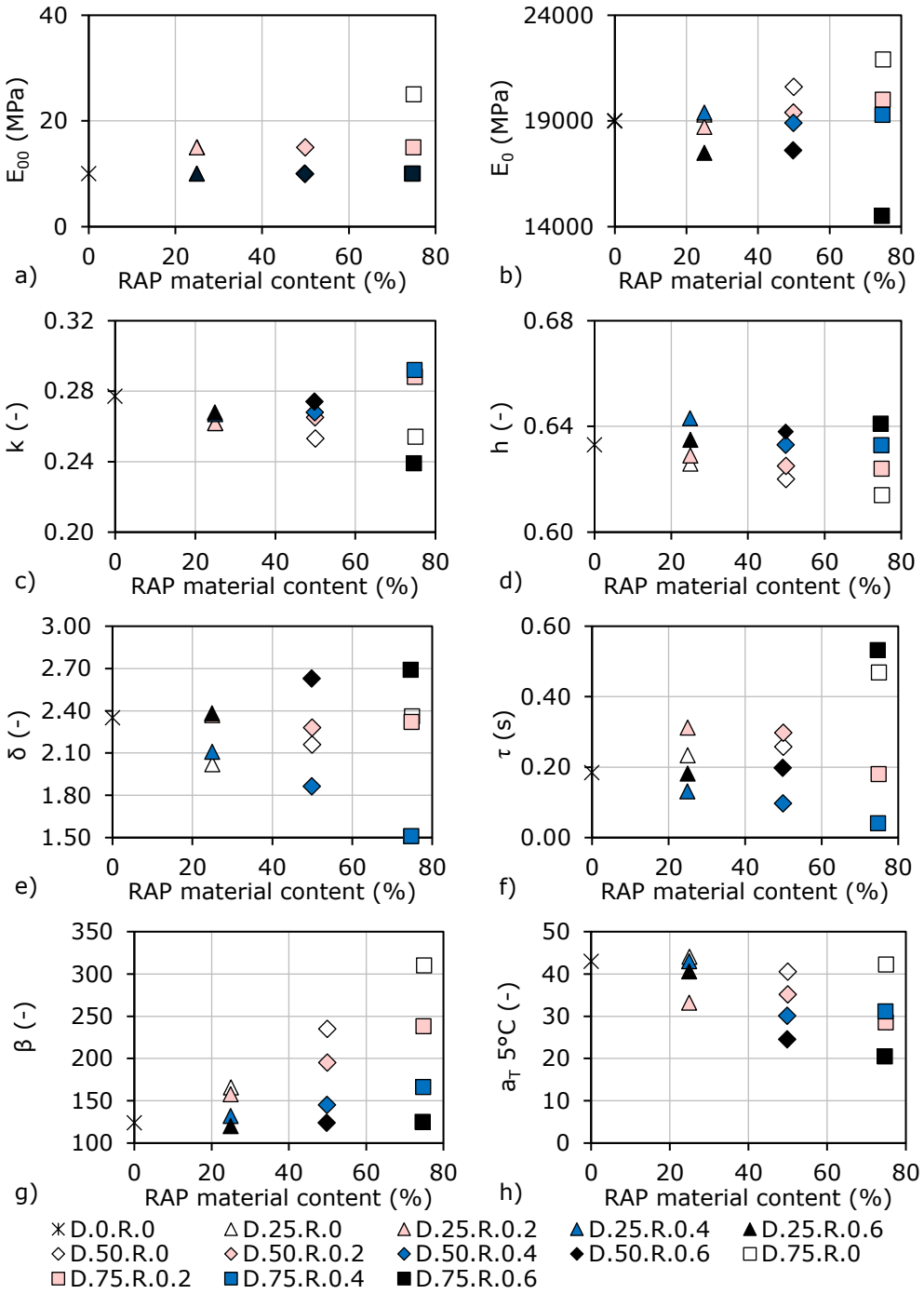

Figure 3.45. 2S2P1D parameters values as a function of the RAP material content for all mixtures: (a) E_{00} ; (b) E_0 ; (c) k ; (d) h ; (e) δ ; (f) τ ; (g) β ; (h) $a_T 5°C$.

It could be observed that 2S2P1D parameters and the a_T shift factors of mixtures do not appear to follow a clear tendency with the increase of the RAP material and rejuvenator contents. This observation is in contrast with the linear tendencies of these parameters with the RAP binder content which were observed for the corresponding binder blends.

Further, the parameter τ was investigated due to the fact that this is the only 2S2P1D parameter that is related to the thermal sensitivity of both binders and mixtures and therefore it can be used to highlight the influence of binder characteristics on the bituminous mixtures behaviour.

The possible relation between the glassy modulus (E_0) of all mixtures and the penetration of the corresponding binder blends was investigated as shown in Figure 3.46. A linear regression was performed. The coefficient of determination was calculated.

It could be observed that E_0 values show an important dependence with the RAP material and the rejuvenator contents and penetration of the corresponding binder blends, R^2 = 0.842. The increase of the RAP material content leads to an increase of E_0 with the increase of penetration of the corresponding binder blends. A reverse was observed when the rejuvenator content increase.

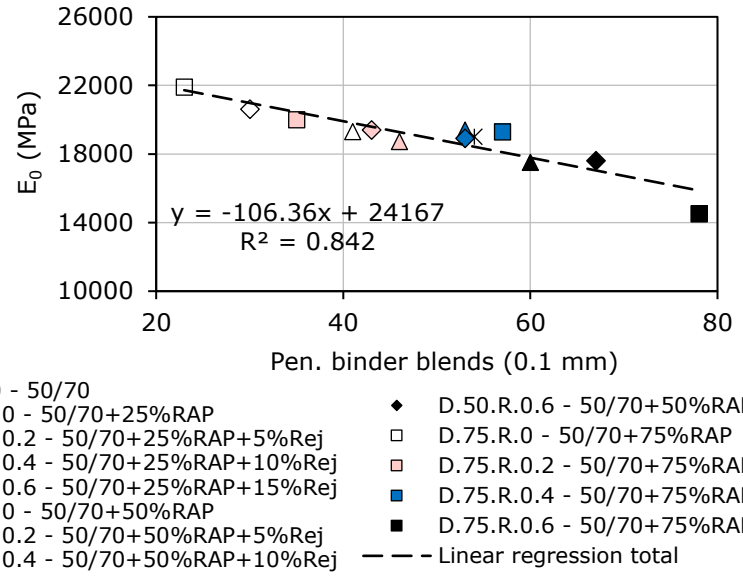

Figure 3.46. Glassy modulus E_0 of mixtures as a function of binder blends penetration.

3.7.4.3 Link between binders and mixtures: SHStS transformation

By using the SHStS transformation (Section 1.54, equation 1.40) the LVE behaviour of a bituminous mixture can be predicted from the LVE behaviour of the corresponding binder. Also, the inverse procedure is valid, regardless of the aggregate skeleton. The SHStS transformation is presented in Section 1.5.4.

Complex modulus values obtained from the 2PT bending tests for all 13 bituminous mixtures were normalized to corresponding parameters E_0 and E_{00} which are reported in Table 3.22.

The same procedure was applied for the complex modulus values obtained from the DSR tests reported in Chapter 2 for the corresponding binder blends.

As an example, the normalized Cole-Cole curves and the plots of the normalized norm of complex modulus as a function of the normalized phase angle were plotted in Figure 3.47 for the mixture D.50.R.0.2 and its corresponding binder blend 50/70+50%RAP+5%Rej.

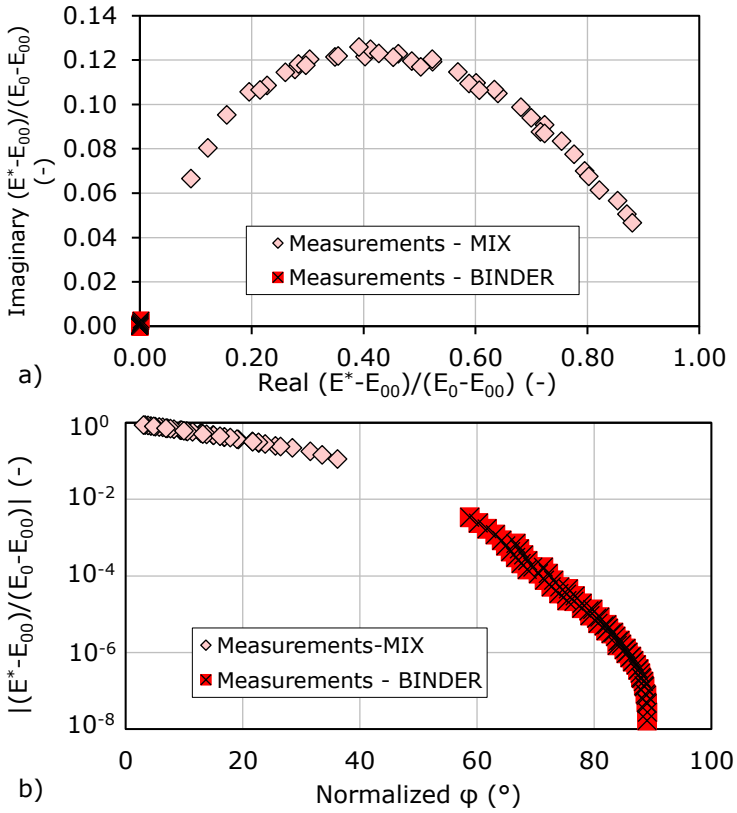

Figure 3.47. (a) Normalized Cole-Cole curves for mixture D.50.R.0.2 and the corresponding binder blend 50/70+50%RAP+5%Rej; (b) Normalized Black curves for mixture D.50.R.0.2 and the corresponding binder blend 50/70+50%RAP+5%Rej in logarithmic scale.

As it could be observed, due to the fact that the DSR measurements on binders were limited, the tests were performed only at intermediate and high temperatures, a reasonable superposition is not obvious.

Therefore, by using the normalized values of the complex modulus and the two parameters E_0 and E_{00} and the parameter α, the SHStS transformation was applied in order to simulate the LVE behaviour of mixtures from the DSR data obtained for the corresponding binders. Based on the above comment, the 2S2P1D model that

was fitted on the experimental data obtained for the mixtures was used in order to highlight if the SHStS transformation is valid or not.

As shown in Section 2.6.2.1 some constant values for k and δ were used for all binder blends do to the fact that DSR test were performed only at high temperatures. Therefore, in order to apply the SHStS transformation the values of parameters k and δ obtained for the mixtures were reintroduced in case of the corresponding binder blends.

Thus, for each mixture and for each corresponding binder blend the same WLF constants and same values of k, δ, h and β parameters were considered.

In order to determine the values for the parameter α, the WLF constants which are shown in Chapter 2 were used in order to calculate the values of the τ parameter of all biner blends at the same reference temperature (15°C) which was used in case of mixtures. Equations 1.39 and 1.40 were used. 2S2P1D parameters for both mixtures and binder blends are reported in Table 2.23.

The values of E_0, E_{00} and α which were used to apply the SHStS transformation are reported in Table 3.24. Also, the variation of the parameter α with the increase of the RAP and rejuvenator contents was investigated, as shown in Figure 3.48.

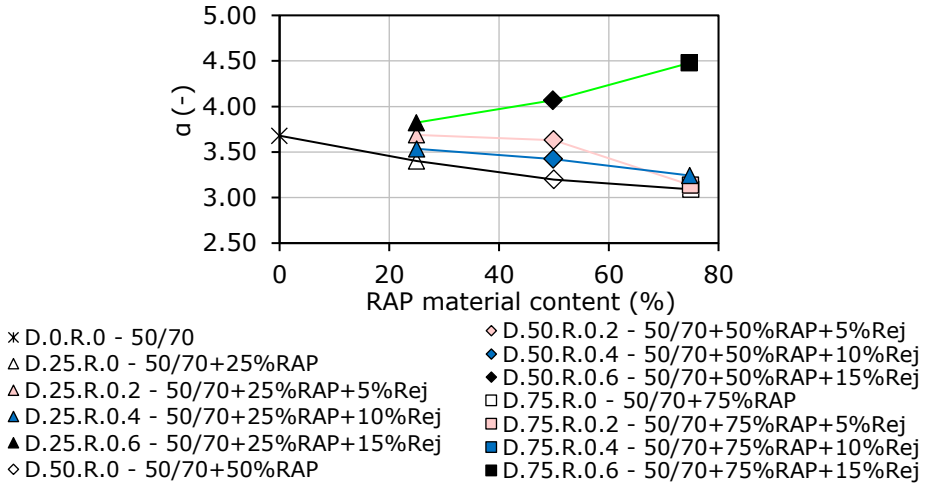

Figure 3.48. Parameter α variation with the RAP content for all binder blends and bituminous mixtures.

No clearly tendencies of the parameter α with the increase of the RAP content or with the increase of the rejuvenator content is observed. This suggests that the parameter α which is defined as the ratio between τ values obtained for the biner blends and the corresponding mixtures is not directly related to the RAP content or the rejuvenator content in the mixtures. This aspect can be influenced by the fact that all the mixtures considered in this research presents the same granular curve. According to Di Benedetto et al. (2004) [130], Olard and Di Benedetto (2003) [129], Mangiafico (2014) [71] this variation of the parameter α can be explained by the fact that it depends on the design of mixtures and the aging process that can occur on the binder during the mixing process.

Table 3.23. 2S2P1D parameters values used for mixtures and binder blends (T_{ref}=15ºC).

Binder blend	Mixture	k (-)	h (-)	δ (-)	β (-)	τ_{binder} (s)	τ_{mix} (s)
50/70	D.0.R.0	0.277	0.633	2.35	124	3.85×10^{-5}	0.184
50/70+25%RAP	D.25.R.0	0.262	0.626	2.02	166	9.29×10^{-5}	0.233
50/70+25%RAP+5%Rej	D.25.R.0.2	0.262	0.629	2.37	158	6.40×10^{-5}	0.312
50/70+25%RAP+10%Rej	D.25.R.0.4	0.267	0.643	2.11	132	3.82×10^{-5}	0.131
50/70+25%RAP+15%Rej	D.25.R.0.6	0.268	0.635	2.38	120	2.73×10^{-5}	0.182
50/70+50%RAP	D.50.R.0	0.253	0.620	2.16	235	1.63×10^{-4}	0.258
50/70+50%RAP+5%Rej	D.50.R.0.2	0.265	0.625	2.28	195	6.97×10^{-5}	0.298
50/70+50%RAP+10%Rej	D.50.R.0.4	0.268	0.633	1.86	145	3.66×10^{-5}	0.097
50/70+50%RAP+15%Rej	D.50.R.0.6	0.274	0.638	2.63	124	1.69×10^{-5}	0.198
50/70+75%RAP	D.75.R.0	0.254	0.614	2.36	310	3.80×10^{-4}	0.468
50/70+75%RAP+5%Rej	D.75.R.0.2	0.288	0.624	2.32	238	1.31×10^{-4}	0.180
50/70+75%RAP+10%Rej	D.75.R.0.4	0.292	0.633	1.51	166	2.29×10^{-5}	0.040
50/70+75%RAP+15%Rej	D.75.R.0.6	0.239	0.641	2.69	125	1.77×10^{-5}	0.532

Table 3.24. Parameters that were used for the SHStS transformation for mixtures and their corresponding binder blends.

Binder blend	Mixture	$E_{00,binder} = 0$ MPa	$E_{0,binder} = 2940$ MPa	$E_{00,mix}$ (MPa)	$E_{0,mix}$ (MPa)	α
50/70	D.0.R.0			10	19000	3.68
50/70+25%RAP	D.25.R.0			15	19300	3.40
50/70+25%RAP+5%Rej	D.25.R.0.2			15	18720	3.69
50/70+25%RAP+10%Rej	D.25.R.0.4			10	19400	3.54
50/70+25%RAP+15%Rej	D.25.R.0.6			10	17500	3.82
50/70+50%RAP	D.50.R.0			15	20600	3.20
50/70+50%RAP+5%Rej	D.50.R.0.2			15	19400	3.63
50/70+50%RAP+10%Rej	D.50.R.0.4			10	18900	3.42
50/70+50%RAP+15%Rej	D.50.R.0.6			10	17600	4.07
50/70+75%RAP	D.75.R.0			25	21900	3.09
50/70+75%RAP+5%Rej	D.75.R.0.2			15	20000	3.14
50/70+75%RAP+10%Rej	D.75.R.0.4			10	19280	3.24
50/70+75%RAP+15%Rej	D.75.R.0.6			10	14500	4.48

As an example, for the mixture D.50.R.0.2 and the corresponding binder blend 50/70+50%RAP+5%Rej, the plots obtained by applying the SHStS transformation together with the experimental data obtained from the 2PT complex modulus tests on the mixtures and the 2S2P1D model fitted on the experimental data, are reported in Figure 3.49 and Figure 3.50. The temperature shift factors and the WLF curves for both, binder and mixture, are reported in Figure 3.51.

Similar plots were built for all the other materials. All plots are reported in Appendix 2 from Figure A2.19 to Figure A2.78.

It was observed that the SHStS transformation works satisfactory in order to predict the LVE behaviour of mixtures from the experimental results obtained for the corresponding binder blend. Although the experimental result on binders are limited, it could be observed that the obtained prediction of the mixture is well fitted on the 2S2P1D model which was fitted only on the experimental measurements on mixtures. Therefore, in order to better investigate the SHStS transformation of binder behaviour to mixtures a larger set of data on the binders must be considered in a future work, such as DSR tests performed at low temperatures.

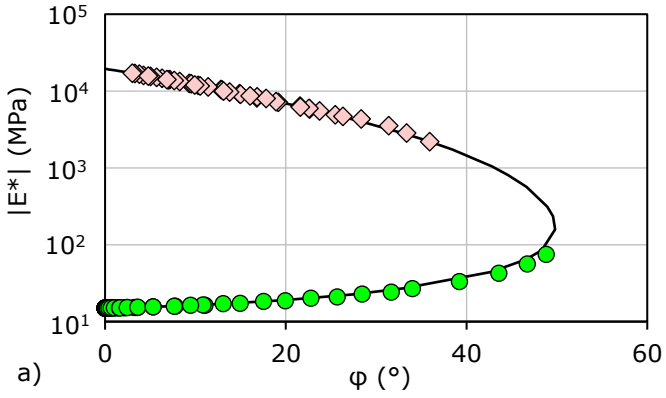

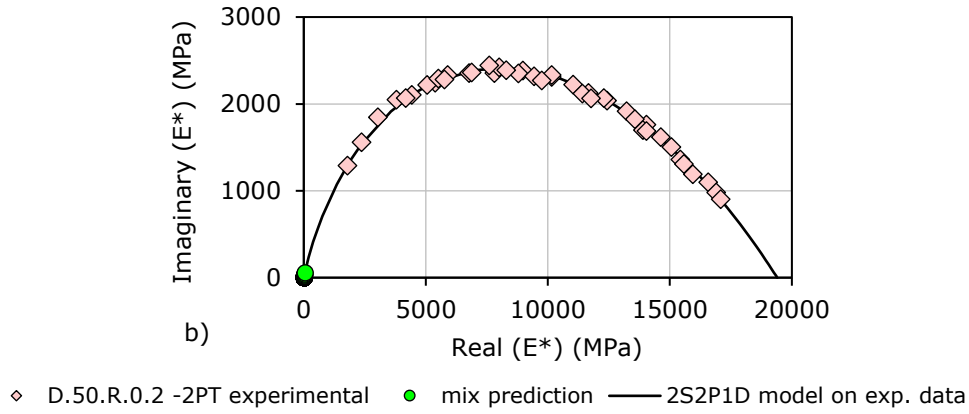

Figure 3.49. Simulation of LVE behaviour from DSR tests on binder blend 50/70 + 50% RAP + 5% Rej for mixture D.50.R.0.2 by using SHStS transformation: (a) Black curves; (b) Cole-Cole curves.

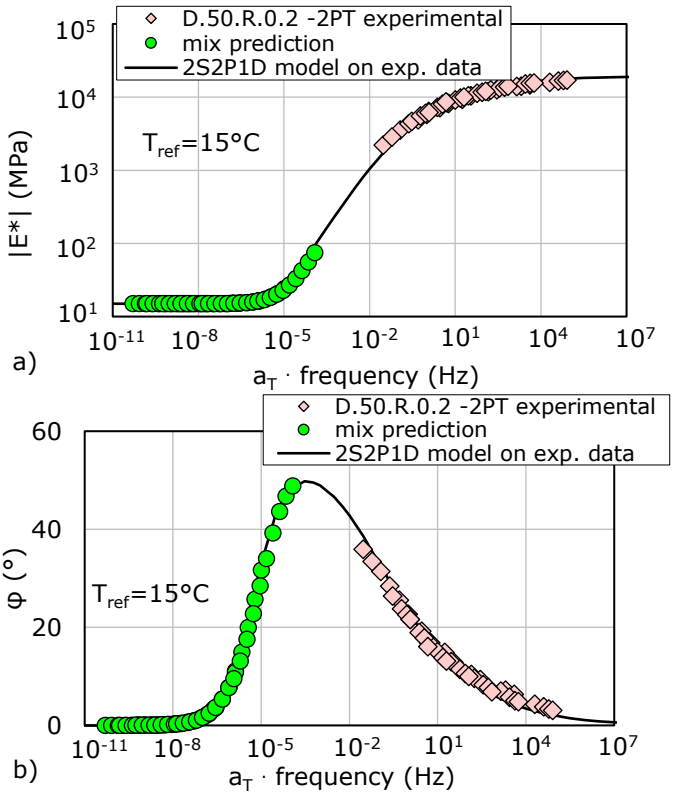

Figure 3.50. Simulation of LVE behaviour from DSR tests on binder blend 50/70 + 50% RAP + 5% Rej for mixture D.50.R.0.2 by using SHStS transformation: (a) $|E^*|$ master curves at $T_{ref} = 15°C$; (b) φ master curves at $T_{ref} = 15°C$.

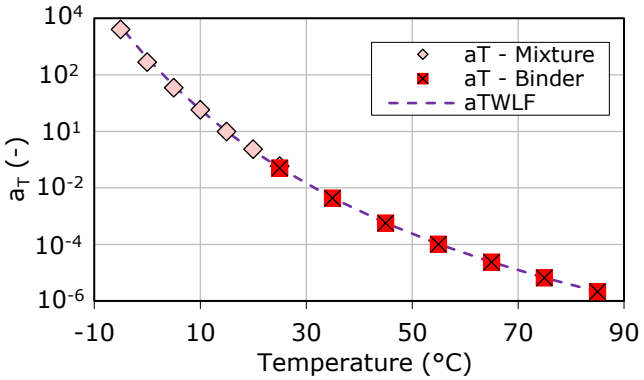

Figure 3.51. Temperature shift factors and WLF curves for the binder 50/70 + 50% RAP + 5% Rej and mixture D.50.R.0.2.

3.7.4.4 Complex modulus of bituminous mixtures at 15°C and 10Hz

3.7.4.4.1 Effect of RAP material and rejuvenator contents

In order to better highlight the effects of the RAP material and of the rejuvenator an investigation on the obtained values for the norm of the complex modulus at 15°C and 10Hz was performed.

As mentioned in the previous section, the void content was determined for each tested specimen by performing hydrostatic measurements.

In order to better observe the effects of the RAP material and the rejuvenator the values of $|E^*|$ at 15°C and 10Hz were normalized with respect to the results obtained for the conventional mixture D.0.R.0.

All $|E^*|$ at 15°C and 10Hz values and the void content of each trapezoidal specimen from Table 3.20 and their mean values, together with the normalized values for all tested bituminous mixtures are reported in Table 3.25.

All values of the void content are rounded to the nearest 0.10% and the values of $|E^*|$ are rounded to the closest ten.

Also, the mean values obtained for each type of bituminous mixture regarding the $|E^*|$ at 15°C and 10Hz values and the normalized $|E^*|$ values are plotted in histogram form in Figure 3.52.

Table 3.25. Two-point bending complex modulus test results and the normalized values of $|E^*|(15°C, 10Hz)$ for all considered bituminous mixtures.

Bit. mix.	Void content (%)	Average void content (%)	$\|E^*\|$ $(15°C, 10Hz)$ (MPa)	Average (MPa)	$\|E^*\| / \|E^*_{0\%RAP\&Rej}\|$ $(15°C, 10Hz)$
D.0.R.0	4.50 4.90	4.70	8230 8120	8180	1.00
D.25.R.0	5.00 5.10	5.10	8630 8840	8740	1.07
D.25.R.0.2	4.90 4.70	4.80	8640 8400	8520	1.04
D.25.R.0.4	4.30 4.30	4.30	8180 8060	8120	0.99
D.25.R.0.6	3.60 3.80	3.70	7520 7580	7550	0.92
D.50.R.0	5.70 5.50	5.60	9680 9370	9530	1.17
D.50.R.0.2	4.90 4.90	4.90	9100 8460	8780	1.07
D.50.R.0.4	3.90 3.70	3.80	8020 8040	8030	0.98
D.50.R.0.6	2.90 2.90	2.90	7390 7350	7370	0.90
D.75.R.0	6.20 6.40	6.30	10820 9700	10260	1.25
D.75.R.0.2	5.30 5.10	5.20	8610 9770	9190	1.12
D.75.R.0.4	3.50 3.00	3.30	7480 7870	7680	0.94
D.75.R.0.6	2.30 2.10	2.20	6550 6690	6620	0.81

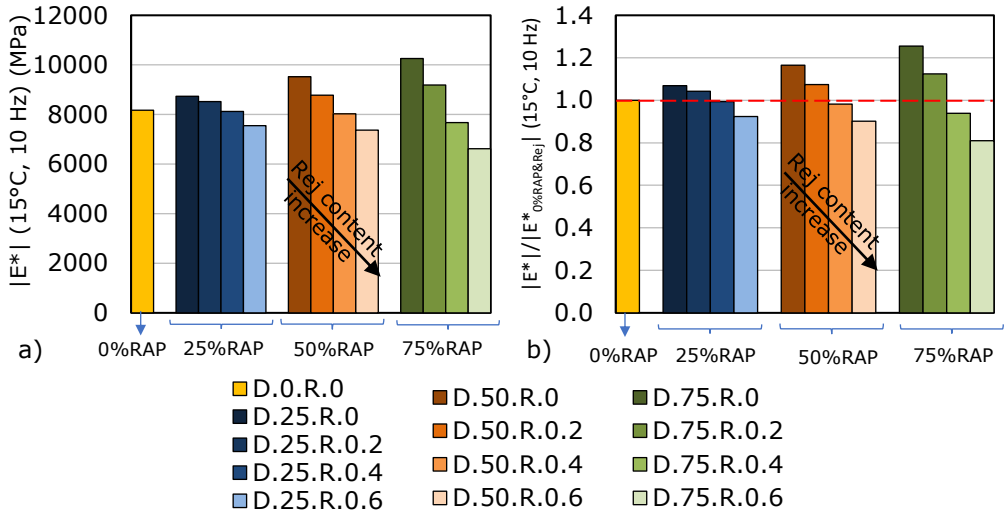

Figure 3.52. Two-point bending complex modulus test results (average values of two specimens) for all considered bituminous mixtures: (a) $|E^*|$ values at 15°C and 10Hz; (b) normalized $|E^*|$ values at 15°C and 10Hz with respect to the conventional HMA D.0.R.0.

As expected, $|E^*|$ at 15°C and 10 Hz values are increasing with the increase of the RAP material content. Similar tendency was observed for the void contents results.

The influence of the rejuvenator was observed by the fact that complex modulus values are decreasing with the increase of the rejuvenator content for the same amount of RAP material within the mass of the mixture.

From the normalized $|E^*|$ values it could be observed that the mixtures produced with 0.4% rejuvenator by mass of the RAP material, independently of the RAP material content present, similar $|E^*|$ values to the one obtained for the conventional mixture. A small decrease of the normalized $|E^*|$ values for the above-mentioned mixtures was observed. This trend can be explained by the fact that the rejuvenator content was calculated as a percentage of the RAP material content. Therefore, the increase of the RAP material content corresponds also to an increase of the rejuvenator content.

In order to better highlight these tendencies and the effects of the RAP material and the rejuvenator on values of $|E^*|$ at 15°C and 10Hz, in Figure 3.53 $|E^*|$ values at 15°C and 10Hz are presented as a function of the RAP material content.

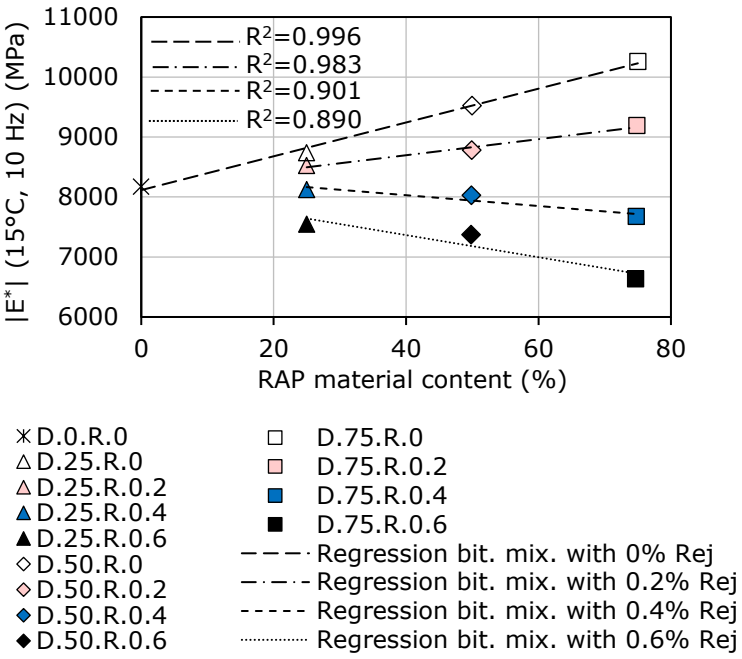

Figure 3.53. Norm of complex modulus at 15°C and 10Hz obtained for all bituminous mixtures as a function of the RAP material content.

As a general comment, it could be observed that $|E^*|$ values at 15°C and 10Hz for the mixtures produced with the same amount of rejuvenator by mass of the bituminous mixtures show a linear relation with the RAP material content. Therefore, linear regressions were performed on the obtained results for all mixtures produced with the same amount of rejuvenator of 0%, 0.2%, 0.4% and 0.6%, by mass of the RAP material. R^2 values were determined for each regression. The $|E^*|$ values plotted versus RAP material content show a decrease of the R^2 values with the increase of the rejuvenator content.

Besides, it could be observed that for the mixtures produced with 0.2% rejuvenator by mass of the RAP material present a similar tendency as the ones obtained for the mixtures produced without rejuvenator.

$|E^*|(15°C, 10Hz)$ values obtained for the mixtures produced with 0.4% rejuvenator by mass of the RAP material are closer to those obtained for the conventional HMA. However, a small decrease of $|E^*|(15°C, 10Hz)$ value could be observed with the increase of the RAP material content.

These observed tendencies indicate the capability of this mix of vegetal oil to rejuvenate the hard-aged RAP binder from the RAP material and finally to provide a bituminous mixture with similar properties of those obtained for the conventional HMA.

On the other side, for the mixtures produced with 0.6% rejuvenator by mass of the RAP material, an inverse effect can be observed by the change of the slope. This trend can be explained by the fact that the rejuvenator content is calculated with respect to RAP material content.

It could be observed that the values of the void content obtained for the mixtures produced with the same amount of RAP material of 25%, 50% and 75% and different rejuvenator content, show a decrease with the increase of the rejuvenator content. For this reason, $|E^*|(15°C, 10Hz)$ were corrected using the formula 3.26 according to Delorme et al. [199]. As an arbitrary void content, a reference void content of 5.8% was chosen for the correction. Equations 3.27 and 3.28 were used in order to determine the void content difference and the corrected $|E^*|(15°C, 10Hz)$ values.

$$\Delta|E^*|(15°C, 10Hz) = (310 \cdot b - 2000) \cdot \Delta V \quad (3.26)$$

where:

$\Delta|E^*|(15°C, 10Hz)$ – the norm of complex modulus at 15°C and 10 Hz difference;

b – the binder content by weight of aggregates and RAP material;

ΔV – the void content difference with respect to the reference void content.

$$\Delta V = V_{measured} - 5.80 \quad (3.27)$$

where:

$V_{measured}$ – the mean measured value void content for each type of mixture;

5.80 – the chosen reference void content.

$$|E^*|(15°C, 10Hz)_{corrected} = |E^*|(15°C, 10Hz)_{measured} - \Delta|E^*|(15°C, 10Hz) \quad (3.28)$$

where:

$|E^*|(15°C, 10Hz)_{measured}$ – the measured values of norm of complex modulus at 15°C and 10 Hz;

$|E^*|(15°C, 10Hz)_{corrected}$ – the corrected values of norm of complex modulus at 15°C and 10 Hz.

It must be mentioned that the formula 3.26 was developed for a specific mixture analysed by Delorme et al. [199]. The validity of this formula for other mixture it was nor proved. Therefore, the corrected values determined in this work were used only as an indication.

All the experimental values of $|E^*|(15°C, 10Hz)$ and void content together with the binder content by weight of the aggregates and the corrected values of $|E^*|$ for all considered mixtures are reported in Table 3.26.

Table 3.26. Two-point bending complex modulus test results and the normalized values of $|E^*|(15°C, 10Hz)$ for all considered bituminous mixtures.

Bit. mix.	Experimental measured values			Corrected values
	Void content (%)	$\|E^*\|(15°C, 10Hz)$ (MPa)	Binder content by weight of aggregates (%)	$\|E^*\|(15°C, 10Hz)$ (MPa)
D.0.R.0	4.70	8180	5.93	7160
D.25.R.0	5.10	8740	5.93	8060
D.25.R.0.2	4.80	8520	5.99	7660
D.25.R.0.4	4.30	8120	6.04	6960
D.25.R.0.6	3.70	7550	6.09	6100
D.50.R.0	5.60	9530	5.93	9320
D.50.R.0.2	4.90	8780	6.04	8080
D.50.R.0.4	3.80	8030	6.14	6870
D.50.R.0.6	2.90	7370	6.25	6230
D.75.R.0	6.30	10260	5.93	10730
D.75.R.0.2	5.20	9190	6.09	8780
D.75.R.0.4	3.30	7680	6.25	6680
D.75.R.0.6	2.20	6620	6.41	6310

All corrected $|E^*|(15°C, 10Hz)$ values obtained for each series of mixtures produced with the same RAP material content of 25%, 50% and 75% and different rejuvenator content of 0.2%, 0.4% and 0.6% are plotted in histogram form in Figures 3.54, 3.55 and 3.56.

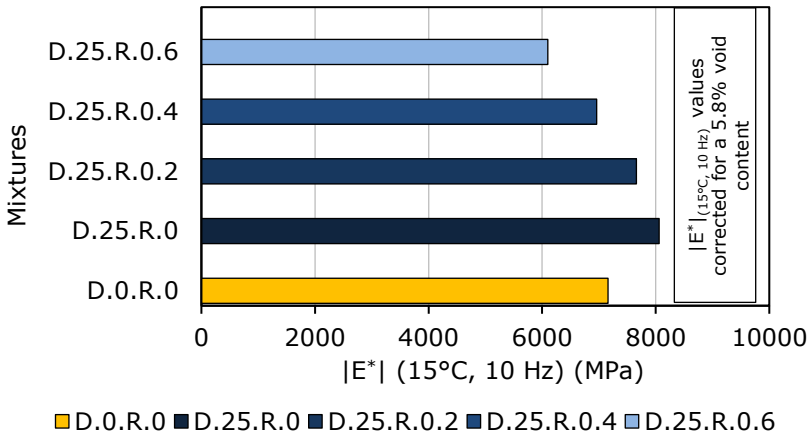

Figure 3.54. Two-point bending complex modulus test results for mixtures produced with 25% RAP and different dosages of rejuvenator and the conventional mixtures: corrected values of |E*| at 15°C and 10 Hz for a 5.8% void content.

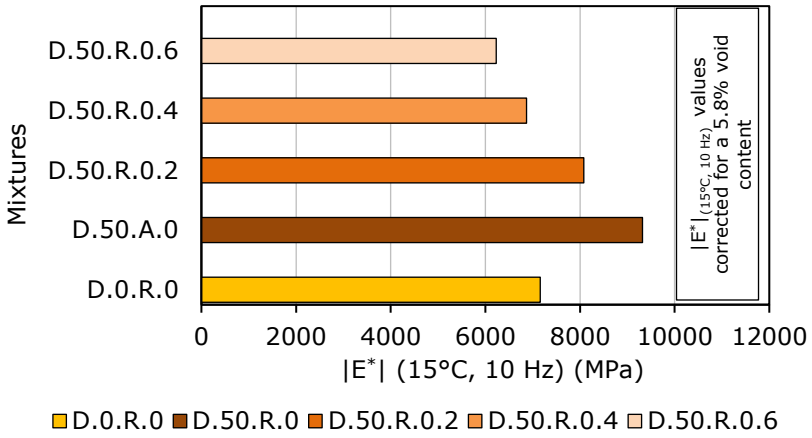

Figure 3.55. Two-point bending complex modulus test results for mixtures produced with 50% RAP and different dosages of rejuvenator and the conventional mixtures: corrected values of |E*| at 15°C and 10 Hz for a 5.8% void content.

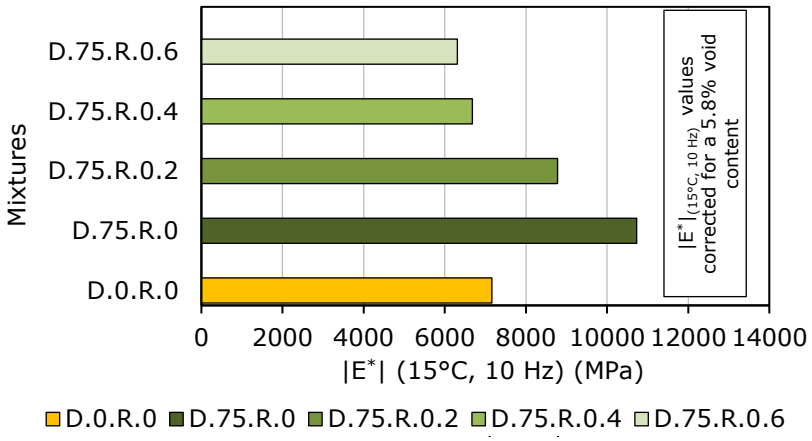

Figure 3.56. Two-point bending complex modulus test results for mixtures produced with 75% RAP and different dosages of rejuvenator and the conventional mixtures: corrected values of |E*| at 15°C and 10 Hz for a 5.8% void content.

As it could be observed in Figure 3.54, Figure 3.55 and Figure 3.56 for a specific void content of 5.8% (identical value considered for all mixtures) similar tendencies were obtained with the increase of rejuvenator content. A similar comment can be done here regarding the mixtures produced with 0.4% rejuvenator.

As a final conclusion, it could be observed that all tendencies presented in this section partially confirms the conclusions of Chapter 2.

3.7.4.4.2 |E*| at 15°C and 10Hz of the mixtures obtained from corresponding binder blends behaviour and the three SHStS constants

In this section, the norm of complex modulus at 15ºC and 10 Hz of the bituminous mixtures presented in Table 3.7, were calculated from their corresponding binder blends behaviour and with the three SHStS constants (E_0, E_{00} and α values presented in Table 3.24).

For the calibrated 2S2P1D model on the experimental results of the binder a reference temperature of 15°C was considered. The real part $\left(E_{1\ binder}\right)$ and the imaginary part $\left(E_{2\ binder}\right)$ of norm of complex modulus of the binder blends were calculated by using equations 3.29 and 3.30 for a frequency of $10^{\alpha+1}$ (values of α are reported in Table 3.24). The values of 2S2P1D parameters used in equations 3.29 and 3.30 are those presented in Table 3.23 and E_0, E_{00} from Table 3.24 for the binder blends. As E_{00} is nil for all binders the following equation were written without this parameter.

$$E_{1\ binder} = \frac{E_0\left[1+\delta(\omega\tau)^{-k}\cos\left(\frac{k\pi}{2}\right)+(\omega\tau)^{-h}\cos\left(\frac{h\pi}{2}\right)\right]}{\left[1+\delta(\omega\tau)^{-k}\cos\left(\frac{k\pi}{2}\right)+(\omega\tau)^{-h}\cos\left(\frac{h\pi}{2}\right)\right]^2+\left[\delta(\omega\tau)^{-k}\sin\left(\frac{k\pi}{2}\right)+(\omega\tau)^{-h}\sin\left(\frac{k\pi}{2}\right)+(\omega\beta\tau)^{-1}\right]^2} \quad (3.29)$$

$$E_{2\ binder} = \frac{E_0\left[\delta(\omega\tau)^{-k}\sin\left(\frac{k\pi}{2}\right)+(\omega\tau)^{-h}\sin\left(\frac{h\pi}{2}\right)+(\omega\beta\tau)^{-1}\right]}{\left[1+\delta(\omega\tau)^{-k}\cos\left(\frac{k\pi}{2}\right)+(\omega\tau)^{-h}\cos\left(\frac{h\pi}{2}\right)\right]^2+\left[\delta(\omega\tau)^{-k}\sin\left(\frac{k\pi}{2}\right)+(\omega\tau)^{-h}\sin\left(\frac{k\pi}{2}\right)+(\omega\beta\tau)^{-1}\right]^2} \quad (3.30)$$

Therefore, equations 3.31 and 3.32 were used in order to determine the simulated real and imaginary parts of the norm of complex modulus for the mixtures. The values of $\left|E^*\right|(15°C,10Hz)_{mix\ simulated}$ were calculated by using equation 3.33. Results are reported in Table 3.27 together with the experimental results.

$$E_1(15°C,10Hz)_{mix\ simulated} = E_{00,mix} + \left(E_{0,mix} - E_{00,mix}\right)\frac{E_{1\ binder}}{E_{0,binder}} \quad (3.31)$$

$$E_2(15°C,10Hz)_{mix\ simulated} = \left(E_{0,mix} - E_{00,mix}\right)\frac{E_{2\ binder}}{E_{0,binder}} \quad (3.32)$$

$$\left|E^*\right|(15°C,10Hz)_{mix\ simulated} = \sqrt{\left(E_{1\ mix\ simulated}\right)^2+\left(E_{2\ mix\ simulated}\right)^2} \quad (3.33)$$

Table 3.27. Experimental and simulated values of $|E^*|(15°C, 10Hz)$ for all bituminous mixtures (Campaign 2).

Mixture	$\|E^*\|(15°C, 10Hz)$ (MPa)	
	Experimental values	Simulated values
D.0.R.0	8180	8263
D.25.R.0	8740	9152
D.25.R.0.2	8520	8691
D.25.R.0.4	8120	8279
D.25.R.0.6	7550	7456
D.50.R.0	9530	9552
D.50.R.0.2	8780	9146
D.50.R.0.4	8030	8087
D.50.R.0.6	7370	7292
D.75.R.0	10260	10682
D.75.R.0.2	9190	9219
D.75.R.0.4	7680	7608
D.75.R.0.6	6620	6598

Figure 3.57 shows a correlation plot between the simulated and experimental values of the norm of complex modulus at 15ºC and 10 Hz of the 13 types of bituminous mixtures. A linear regression was performed and the coefficient of determination R^2 was determined. As it could be observed a good correlation was obtained, the simulated results are significantly close to the experimental ones. This satisfactory correlation is proven by the R^2 value of 0.981.

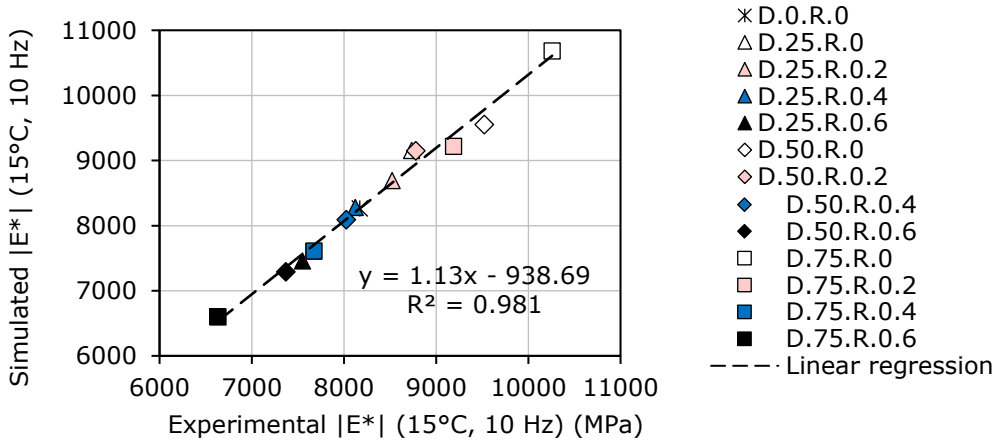

Figure 3.57. Norm of complex modulus at 15°C, 10 Hz of all bituminous mixtures (Campaign 2): experimental vs. simulated results.

In order to better highlight this correlation, the relative errors between the experimental $\left(\left|E^*\right|(15°C,10Hz)_{mix\ exp.}\right)$ and the simulated $\left(\left|E^*\right|(15°C,10Hz)_{mix\ simulated}\right)$ results of norm of complex modulus at 15ºC and 10Hz were calculated for all 13 mixtures by using equation 3.34.

$$Error = \frac{\left|E^*\right|(15°C,10Hz)_{mix\ exp.} - \left|E^*\right|(15°C,10Hz)_{mix\ simulated}}{\left|E^*\right|(15°C,10Hz)_{mix\ exp.}} x\ 100 \qquad (3.34)$$

The calculated relative errors were plotted in Figure 3.58. As it could be observed, for all mixtures from Campaign 2 the errors between the experimental and the simulated results of the norm of complex modulus at 15ºC and 10Hz are always lower than 5%.

Therefore, the method used to simulate the values of the norm of complex modulus at 15ºC and 10Hz of the bituminous mixtures from their corresponding binder blends behaviour and with the three SHStS constants can be considered valid for the 13 mixtures considered in this study.

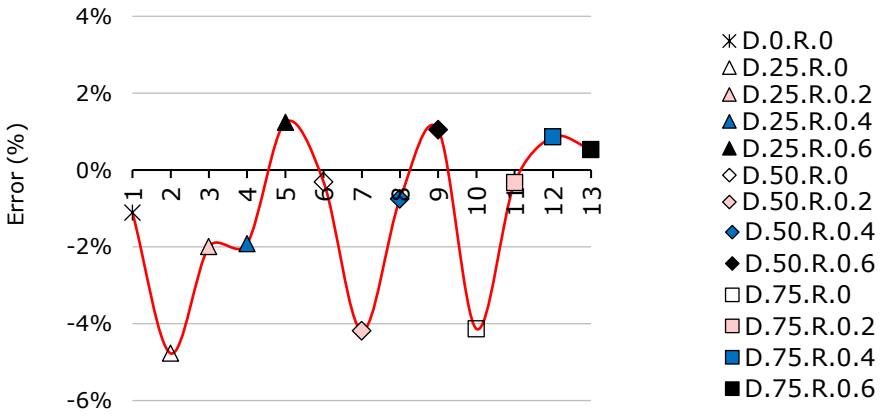

Figure 3.58. Error between experimental and simulated results of the norm of complex modulus at 15°C, 10Hz of all bituminous mixtures (Campaign 2).

3.7.4.4.3 Relation between experimental |E*| values at 15°C and 10Hz of mixtures and *pen.* values of the corresponding binder blends

It this section the possible relation between the experimental norm of complex modulus values determined at 15°C and 10 Hz for mixtures and the penetration results obtained for the corresponding binder blends is investigated.

Therefore, $\left|E^*\right|(15°C,10Hz)_{mix\ exp.}$ values for the mixtures which are reported in Table 3.27 are plotted as a function of the penetration values of the corresponding binder blends, reported in Section 2.5.1 in Table 2.6, in Figure 3.59. A

linear regression is performed. The coefficient of determination is determined for the performed regression.

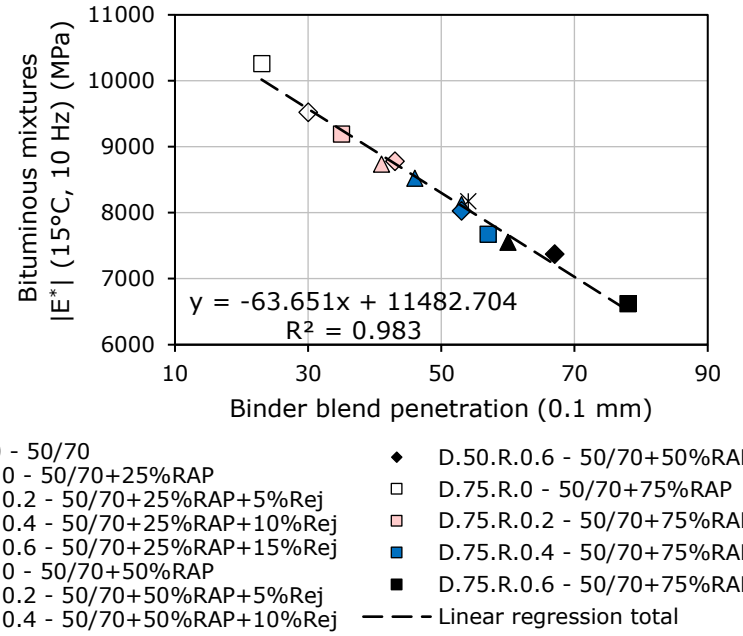

Figure 3.59. Norm of complex modulus at 15°C and 10 Hz values of all bituminous mixtures (Campaign 2) versus penetration values of the corresponding binder blends.

A good relationship between these two parameters was found $\left(R^2 = 0.983\right)$.

The norm of complex modulus of the bituminous mixtures shows an important dependence of RAP material and rejuvenator contents and also the penetration of the corresponding binder blends.

As described in Section 2.5.2, the penetration values of binder blends were estimated by using a blending rule starting from experimental results obtained for the base constituents. A good correlation between the experimental and the estimated result by 2nd estimation method (equation 2.8) of penetration was observed.

It worth mentioning that for the investigation of the relation between the $\left|E^*\right|(15°C, 10Hz)$ values for the mixtures and the estimated values of penetration for the binder blends the Figure 3.60 is plotted.

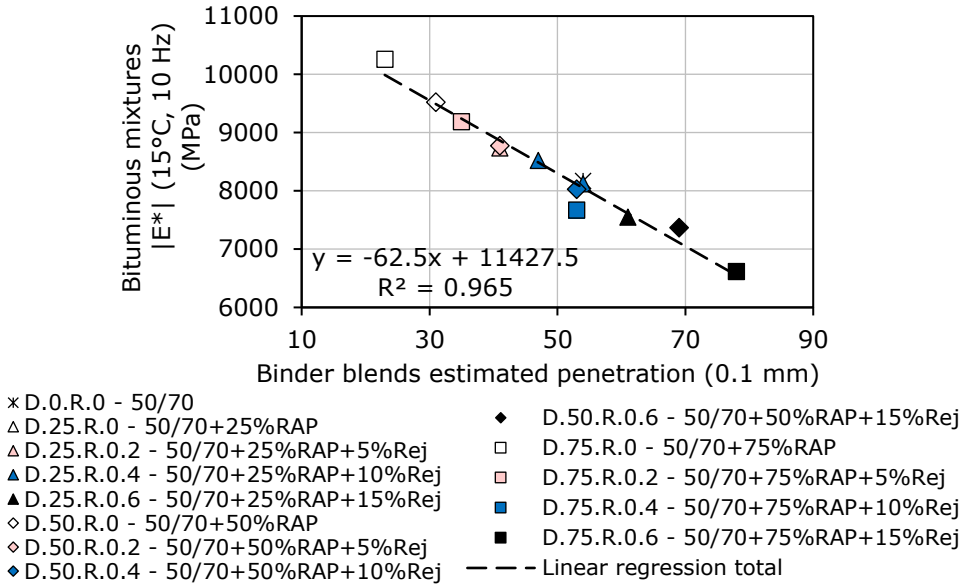

Figure 3.60. Norm of complex modulus at 15°C and 10 Hz values of all bituminous mixtures versus estimated penetration values of the corresponding binder blends.

A small decrease of the coefficient of determination is observed, however, a good relation is found (R^2 value of 0.965). Therefore, it can be concluded that for the tested materials the norm of the complex modulus values at 15°C and 10 Hz of mixtures presents a good relationship with penetration of the corresponding binder blends.

3.8 Conclusions

In this chapter, the experimental plan regarding the bituminous mixtures was divided in two campaigns. In the first campaign, seven types of HMA, produced only with virgin materials, were investigated in order to determine the optimal binder content of the mix considered as the conventional mix. This content is used in the second campaign. A series of tests were performed on these seven types of mixtures were performed according to the Romanian Standards. Based on the obtained results the percentage of 5.6% binder content was considered to be the optimal one.

In the second campaign, twelve bituminous mixtures produced with different amounts of RAP material (25%, 50% and 75% RAP material) with or without rejuvenator (0%, 0.2%, 0.4% and 0.6% by mass of the RAP material). The conventional HMA was considered as reference.

All 13 bituminous mixtures considered in Campaign 2 have the following common characteristics:

- continuous 16 mm grading curve;
- 5.60% total binder content by weight of the final mix not including here the rejuvenator;

- the RAP material used for each mix has the same proportion: 25% RAP 0-8 mm + 75% RAP 8-22.4 mm. The binder content of this RAP material mix, measured trough extraction and recovery is 4%.

It is important to notice that the binder blends of the different mixture types are the sane than the ones tested in Chapter 2. Then the general effect of binder on mixture properties could be a focus of the study. However, it is important to mention that the binder blends investigated in Chapter 2 were perfectly blended in the laboratory. Even if the percentages between fresh, RAP binder and rejuvenator are the same, some differences between these perfect blends (Chapter 2) and the blends from the mixtures can occur.

A series of tests were performed on the mixtures considered in the second Campaign were performed to highlight the influence/effect of the rejuvenator and RAP material on the thermomechanical properties of the final bituminous mixtures.

Regarding the Marshall characteristics it was observed that the effect of increasing the RAP material content conduced to a stiffer behaviour of the bituminous mixtures, thus stability increases as expected. The influence of increasing the rejuvenator content conduced to a reverse effect which can counterbalance the effect of the RAP material. Some linear relationship with the RAP material content for the bituminous mixtures produced with the same amount of rejuvenator was observed, with exception of the results recorder for the stability.

The IT-CY tests were performed at four temperatures starting from 10°C up to 25°C and the experimental results obtained for the stiffness modulus were investigated in order to highlight the influence of the RAP material and rejuvenator. The conclusion of the test results indicates that the effect of increasing the RAP material content conduced to an increase of stiffness. Also, the influence of the temperature was observed where the increase of temperature leads to a linear decrease of the stiffness modulus. On the other side, the increase of the rejuvenator content within the mass of mixtures corresponds to a reverse effect as stiffness is decreasing with the increase of the rejuvenator content.

It is interesting to note that regarding the cyclic compression with confinement test, the values of the final deformation h_{10000} and values of ε_{10000} obtained for each series of mixtures produced with the same amount of rejuvenator by mass of the RAP material, presents approximatively the same tendency, the slope of each linear regression is approximatively the same. It seems that h_{10000} and ε_{10000} values are direct proportionally with the rejuvenator content. This remark is not valid in case of the creep rate.

For the mixtures produced without rejuvenator, a small increase of the creep rate was observed with the increase of the RAP material content for a nearly horizontal linear regression. The rate of the increase of the f_c values is higher for the other series of bituminous mixtures produced with 0.2%, 0.4% and 0.6% rejuvenator. This can be observed by the incrementation of the slope of the linear regressions. These tendencies can be explained by the fact that the rejuvenator content is calculated as a percentage of the RAP material. Therefore, the increase of the RAP material content corresponds to an increase of the rejuvenator content.

For all above parameters (Marshall characteristics, stiffness modulus and ε_{10000}) the relation between them and the penetration of the corresponding binder blends was investigated. Some strong relations were found for the mixtures/binder blends produced with the same RAP material/binder content (25%, 50% and 75%). However, the global relation between these parameters and penetration is not so

strong. These tendencies could be explained by the fact that most probably the use of the RAP material leads to a change of the grading curves of the final mixtures. Also, the use of the same energy compaction of all mixtures, the rejuvenator content which was established as a function of the mass of the RAP material and the difference between the density of the RAP aggregates and the density of the virgin aggregates lead to these results.

Complex modulus tests were performed in strain control with the imposed strain loading amplitude of 50 μm/m at seven temperatures starting from -5°C up to 25°C at a frequency range from 0.5 Hz to 20 Hz.

The data presented in Cole-Cole and Black diagrams are located on a unique curve, independently of the test temperature and frequency, for each of the considered mixtures. This means that the time temperature superposition principle (TTSP) is valid for all tested bituminous mixtures and moreover they can be considered as thermorheologically simple materials even when containing the rejuvenator.

As expected, the master curves and a_T shift factors of the blends produced without rejuvenator are falling away from the corresponding master curves of the conventional one. $|E^*|$ values are increasing with the increase of RAP material content and φ values are decreasing with the increase of RAP material content. On the other side, the increase of the rejuvenator content into the blends corresponds to master curves and shift factors progresively approaching to those of the conventional mixture.

Experimental data were fitted with 2S2P1D model. It was observed that 2S2P1D parameters and the a_T shift factors of mixtures do not appear to follow a clear tendency with the increase of the RAP material and rejuvenator contents. This observation is in contrast with the linear tendencies of these parameters with the RAP binder content which were observed for the corresponding binder blends. The glassy modulus E_0 of mixtures presents a satisfactory relation with the penetration of the corresponding binder blends.

SHStS transformation was applied. A satisfactory prediction was obtained even by using the limited DSR measurements on binders. 2S2P1D model was used in order to better highlight the eficacity of the prediction. Although the experimental result on binders are limited, it was observed that the obtained prediction of the mixture is well fitted on the 2S2P1D model which was fitted only on the experimental measurements on mixtures. Therefore, in order to better investigate the SHStS transformation of binder behaviour to mixtures a larger set of data on the binders must be considered in a future work.

Regarding the $|E^*|$ at 15°C and 10 Hz values, the influence of the rejuvenator was observed by the fact that complex modulus values are decreasing with the increase of the rejuvenator content for the same amount of RAP material within the mass of the mixture. From the normalized $|E^*|$ values it could be observed that the mixtures produced with 0.4% rejuvenator by mass of the RAP material, some close $|E^*|$ values to the one obtained for the conventional mixture, were obtained. A small decrease of the normalized $|E^*|$ values for the above-mentioned mixtures was

observed. This trend can be explained by the fact that the rejuvenator content was calculated as a percentage of the RAP material content. Therefore, the increase of the RAP material content corresponds also to an increase of the rejuvenator content.

The values of $|E^*|$ at 15°C and 10Hz for the mixtures produced with the same amount of rejuvenator by mass of the bituminous mixtures show a linear relation with the RAP material content. A satisfactory relation between $|E^*|$ values at 15°C and 10 Hz obtained for the mixtures and the penetration values of the corresponding binder blends was found $\left(R^2 = 0.983\right)$.

On the other hand, the norm of complex modulus at 15ºC and 10 Hz of the bituminous mixtures from Campaign 2 were simulated from their corresponding binder blends behaviour and with the three SHStS constants (E_0, E_{00} and α values). A good correlation between the experimental and simulated results of the norm of complex modulus at 15°C and 10Hz was obtained, proven by the satisfactory R^2 value of 0.981 and by the relative errors which are always lower than 5%.

As a final conclusion, it worth mentioning that all tendencies presented in this chapter partially confirms the conclusions drawn within Chapter 2.

4. Environmental impact of the fabrication processes for different types of bituminous mixtures

4.1 Objectives

This chapter of the thesis is focused on the investigation of the potential environmental impact related to the production of several types of bituminous mixtures containing different dosages of Reclaimed Asphalt Pavement (RAP) and Rejuvenator (Rej). All materials considered in the presented study are specific and generally used for pavements in Romania.

It must be specified that all bituminous mixtures which were tested and for which different parameters were investigated in Chapter 3, were considered in this part of the research. Therefore, the potential environmental impact of the production process of thirteen different types of bituminous mixtures was investigated. One conventional bituminous mixture produced with virgin materials used as reference was also considered in the study.

The Environmental Impact Assessment (EIA) was estimated for the production process defined by the following three stages: raw material supply, transportation and manufacturing, of one tonne (1 T) of the considered bituminous mixtures while all the other processes were assumed to be similar. EIA was performed by using GaBi software [200].

It is important to mention that EIA was performed based on the calculation of the environmental indicators according to the following European Standards EN 15804+A1:2013 and the new version EN 15804+A2:2019 which includes explicitly biogenic carbon uptake and re-emission.

4.2 Introduction

In recent years several researches were devoted to highlight the environmental impacts of a road pavement by performing Life Cycle Assessments (LCA) and / or evaluating the carbon footprint through Green-House Gas (GHG) emissions [201]–[203]. The Environmental Impact Assessment (EIA) represents the process from which information are given about the effects of the implementation of a product or process etc. has on the environment, leading to a final environmental load, based on evaluated emissions, classification and aggregation of the results. The decisions taken are based on the interpretation of obtained results, by evaluating their impacts, to continue / stop or to adjust the initial project, process, etc. Aurangzeb et al. (2014) [204], Bressi et al. (2019) [205], Lu et al. (2019) [206] and Vallette (2017) [207] showed that the use of RAP materials and rejuvenators in the production of new bituminous mixtures leads to a decrease of impacts on the environment and also to a cost efficiency.

Over the last decades, several methods of evaluation of environmental impact were employed in order to better highlight the potential environmental impact of different products/materials/ processes. In most of these methods the term

environment was defined on the basis of three impact categories: the human health, the ecosystem quality and the resources. Each of these represents the sum of quantified emissions of several sub-sequent impact categories. The output values of this analysis are given in *Eco-points* which represents quantified values that express the total environmental impact of the defined production process of asphalt mixtures. The eco-point unit (Pt) is representative for 1/1000 of the yearly environmental load of one average European inhabitant [208].

Currently, several software companies developed software applications in order to better investigate the potential environmental impact based on a wider data base over a larger range of materials, processes, resources, etc. As mentioned in the previous section, the present study was performed by using GaBi software following the European specifications mentioned in the European Standards EN 15804+A1:2013 and the new version EN 15804+A2:2019 which includes explicitly biogenic carbon uptake and re-emission.

4.3 Materials. Inventory

The purpose of the environmental impact study is to investigate the potential environmental impact related to the production of one tonne (1 T) of several types of bituminous mixtures containing different dosages of RAP and rejuvenator. The input inventory of this EIA study is grouped in three categories: materials, energy and transport.

All materials considered in this analysis, gathered as input inventory for the EIA are presented in Figure 4.1. As already showed in Chapter 3 where the characterization of each material and bituminous mixture was presented, all materials were chosen with respect to the specifications from the Romanian Standards to produce bituminous mixtures with the maximum aggregate size of 16 mm.

The crushed aggregates (0-4 mm, 4-8 mm and 8-16 mm) have identical provenance and according to the specification of the producer the rock nature is dacite - intermediate in composition between andesite and rhyolite.

In this analysis the RAP material was considered as being obtained from milling the bituminous surface layer of an old, deteriorated road pavement from Timis county, Romania. The characteristics of the material before and after the binder extraction, i.e. characteristics of the RAP aggregates and of the RAP binder are shown in Chapter 3. The RAP material was considered as being divided into two lots: 0-8 mm and 8-22.4 mm and stored close to an asphalt mix plant. Also, in order to evaluate the transportation distances, it was considered that the asphalt mix plant is located near the city of Timisoara.

As fresh binder a 50/70 penetration grade binder was used, and a mixture of vegetal oils was used as rejuvenator, their characteristics being shown in Chapter 2.

A total of 13 types of bituminous mixtures, including one 'conventional' bituminous mixture produced with virgin materials used as reference, were considered.

As shown in Figure 4.1 and as described in Chapter 3, the proportions of the base components were determined in order to produce bituminous mixtures containing 0%, 25%, 50% and 75% RAP material and different dosages of rejuvenator. Materials proportions for all considered bituminous mixtures are reported in Chapter 3 in Tables 3.9 – 3.10.

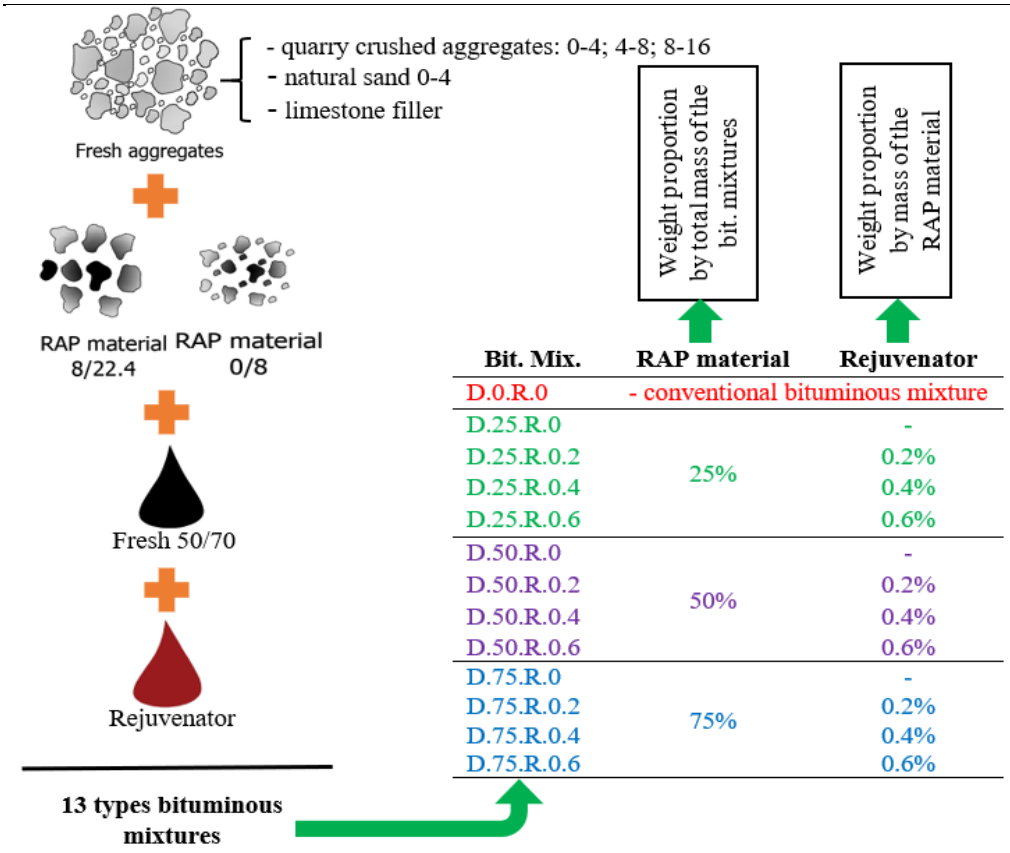

Figure 4.1. Materials used to produce the analysed bituminous mixtures.

The notations regarding the names of the bituminous mixtures, were considered identical to the ones used in Chapter 3. To summarize, all bituminous mixtures have the following common characteristics:

- similar continuous 16 mm grading curve;
- 5.60% total binder content by weight of the final mix not including here the rejuvenator;
- the RAP material used for each mix has the same proportion: 25% RAP 0-8 mm + 75% RAP 8-22.4 mm.

Therefore, Table 4.1 sums the amounts of input materials for the production of 1 tonne of mixture. The values are given in kg.

Table 4.1. Amounts of base materials, in kg, within all considered bituminous mixtures.

Bituminous mixtures	Crushed aggregates			Natural sand 0-4	Filler	RAP material	Fresh binder 50/70	Rej.
	8-16	4-8	0-4					
D.0.R.0	236.0	207.7	405.9	28.3	66.1	-	56.0	-
D.25.R.0	161.0	129.4	358.7	8.7	46.2	250.0	46.0	-
D.25.R.0.2	160.9	129.4	358.5	8.7	46.2	249.9	45.9	0.5
D.25.R.0.4	160.8	129.3	358.4	8.7	46.1	249.8	45.9	1.0
D.25.R.0.6	160.7	129.2	358.3	8.7	46.1	249.6	45.9	1.5
D.50.R.0	80.2	79.8	281.3	-	22.7	500.0	36.0	-
D.50.R.0.2	80.2	79.7	281.0	-	22.6	499.5	36.0	1.0
D.50.R.0.4	80.1	79.6	280.8	-	22.6	499.0	35.9	2.0
D.50.R.0.6	80.0	79.5	280.5	-	22.6	498.5	35.9	3.0
D.75.R.0	-	-	219.3	-	4.7	750.0	26.0	-
D.75.R.0.2	-	-	219.0	-	4.7	748.9	25.9	1.5
D.75.R.0.4	-	-	218.6	-	4.7	747.8	25.9	3.0
D.75.R.0.6	-	-	218.3	-	4.7	746.6	25.9	4.5

For the transportation of all materials integrated in the analysis, Table 4.2 shows the road distances from each quarry, refinery, etc. to the asphalt mix plant considered as located in Timisoara. This process includes the emissions generated during the transportation, including here the fuel use. The unit used for this process is tkm as it represents the transport of one tonne of material over one kilometre in a heavy lorry.

It is important to mention that for the transportation of each material some ratios between the driving share of the transport were considered as a function of the road types that are shared: motorway, rural and urban roads. Table 4.3 shows the driving share of motorway, rural and urban roads considered for each transport process.

Table 4.2. Transport distances to the asphalt mix plant.

Material		Transport distance to asphalt mix plant, (km)
Crushed aggregates	8-16	120
	4-8	
	0-4	
Natural sand 0.4		70
Limestone filler		210
Fresh 50/70 binder		100
Rejuvenator		100
RAP material		50

Table 4.3. Transport driving share motorway/rural/urban to the asphalt mix plant.

Material		Driving share, %		
		Motorways	Rural	Urban
Crushed aggregates	8-16 mm	70	23	7
	4-8 mm			
	0-4 mm			
RAP material				
Natural sand 0.4 mm		29	26	45
Limestone filler				
Fresh 50/70 binder				
Rejuvenator				

Additionally, in the production of bituminous mixtures, the following processes were considered, based on the technical data that were consulted and obtained from combined information offered by two mix plants near to Timisoara:

- heating process of the fresh aggregates: energy use – natural gas + electricity;
- heating process of the RAP material: energy use – diesel + electricity;
- heating process of the fresh binder: energy use – natural gas + electricity;
- mixing process: energy use – natural gas + electricity.

It must be specified that the rejuvenator is added to the fresh binder tank when all materials are already heated and ready for the mixing process.

The amounts of energy used to produce 1 T of bituminous mixture were estimated according to the technical data that were offered by the two producers near to Timisoara and based on the studied literature. Table 4.4 sums the amounts heating processes (energy in MJ) used to produce one tonne of each type of bituminous mixture.

Table 4.4. Energy, in MJ, used to produce one tonne of each type of bituminous mixture.

Bituminous mixtures	Energy, MJ Natural gas + diesel + electricity
D.0.R.0	280
D.25.R.0 D.25.R.0.2 D.25.R.0.4 D.25.R.0.6	227
D.50.R.0 D.50.R.0.2 D.50.R.0.4 D.50.R.0.6	175
D.75.R.0 D.75.R.0.2 D.75.R.0.4 D.75.R.0.6	123

4.4 EIA procedure and system boundaries

The Environmental Impact Assessment (EIA) was estimated for the production process of the analysed bituminous mixtures by using GaBi software [200].

The steps followed in the EIA assessment are:

- definition of the purpose of the calculation and define the system boundaries of the analysed process;
- collection or association of the input values as resources and emissions for each material, production process, transport process, energy, etc.;
- quantification of the impact of inventory - materials and processes;
- evaluation the total impact;
- interpretation the obtained results.

The system boundaries considered in this analysis are shown in Figure 4.2. It must be mentioned that for the RAP material only its transportation was considered in the analysis. The milling and the sorting processes of the RAP material were excluded from the analysis as these processes are similar for all mixtures at End-of-life (EOL). From the same reasons, all the processes included in the construction stage (laying, compaction, etc.) were excluded from the analyses. This is because the similar processes will bring similar inputs and outputs in the EI analyses.

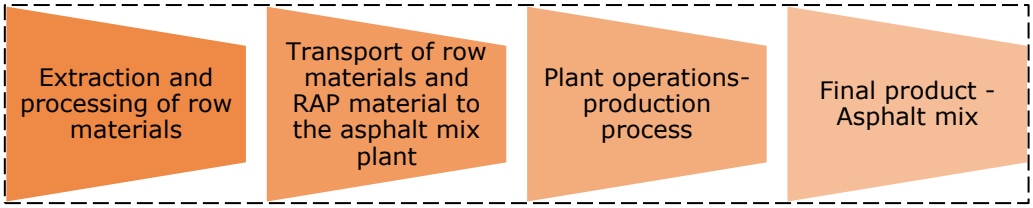

Figure 4.2. System boundaries.

In the extraction and production of the raw materials for crushed aggregates, natural sand, filler, binder and RAP material all processes from the extraction of the rock up to the last processing stage, including transportation within the quarry, were considered. For each process the corresponding emissions were evaluated.

The RAP material was obtained from the milling process of an old existing pavement. Thus, in the EIA the RAP material was considered as stored near to the asphalt mix plant and it was divided into two lots: 0-8 mm and 8-22.4 mm. The analysis was performed by considering the RAP as an inert material with zero original environmental impact. In this manner, no processes, emissions, or energy use were associated to the production of this material. This scenario for the RAP material was proposed by taking into consideration that the milling, transportation or other processes are part of the LCA of original mix and thus out of the actual system boundaries. Thus, for the EIA only the transportation process was considered for the RAP material. Also, as it can be observed in Table 4.4 (Section 4.3) a part of the total energy used in the production process of bituminous mixtures is associated to the heating process of the RAP material considering diesel and electricity as source of heating.

Figure 4.3 shows the LC flow scheme. The life cycle of the final product was considered from the early stages, including production and acquisition of the raw materials, and the production process of bituminous mixtures while the End-of-Life (EOL) phase considered the recycling and the final disposal of material. The EOL scenario considers that after the construction and the service life of the road, the

disassembly is made by milling the surface layer and the resulting material will be transported, sorted and reused in the production of other new bituminous mixtures as another RAP material. Thus, in a new LCA, the RAP material is ready-to-use, as it is considered in the current analysis.

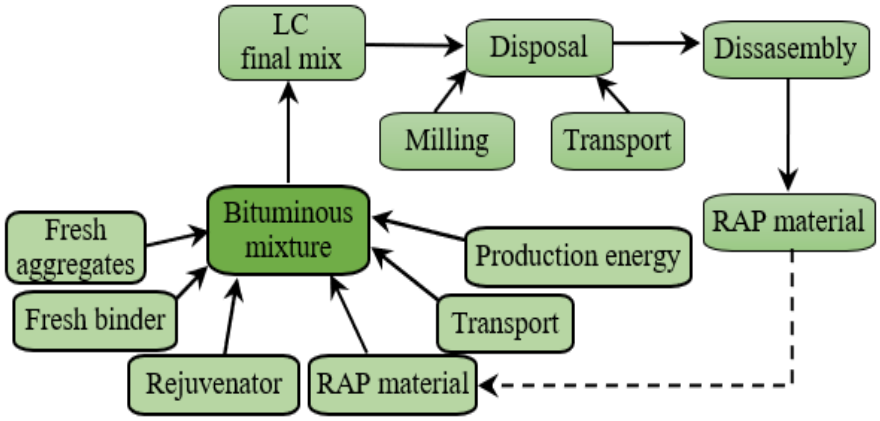

Figure 4.3. Life cycle of the final product.

Concluding, the EIA performed in this study covers the raw material supply, transportation, manufacturing, and other associated processes. Therefore, only the production stage which is composed of A1: raw material extraction and processing, A2: transport to manufacturer and A3: manufacturing, was considered. The EIA was performed according to the European specifications mentioned in the European Standards EN 15804+A1:2013 and the new version EN 15804+A2:2019 which includes explicitly biogenic carbon uptake and re-emission.

All parameters/indicators that were presented in Section 1.7.3, were calculated by using the GaBi software for the production phase of all considered bituminous mixtures. Figure 4.4 shows the flow chart of the analysed processes considered in GaBi software.

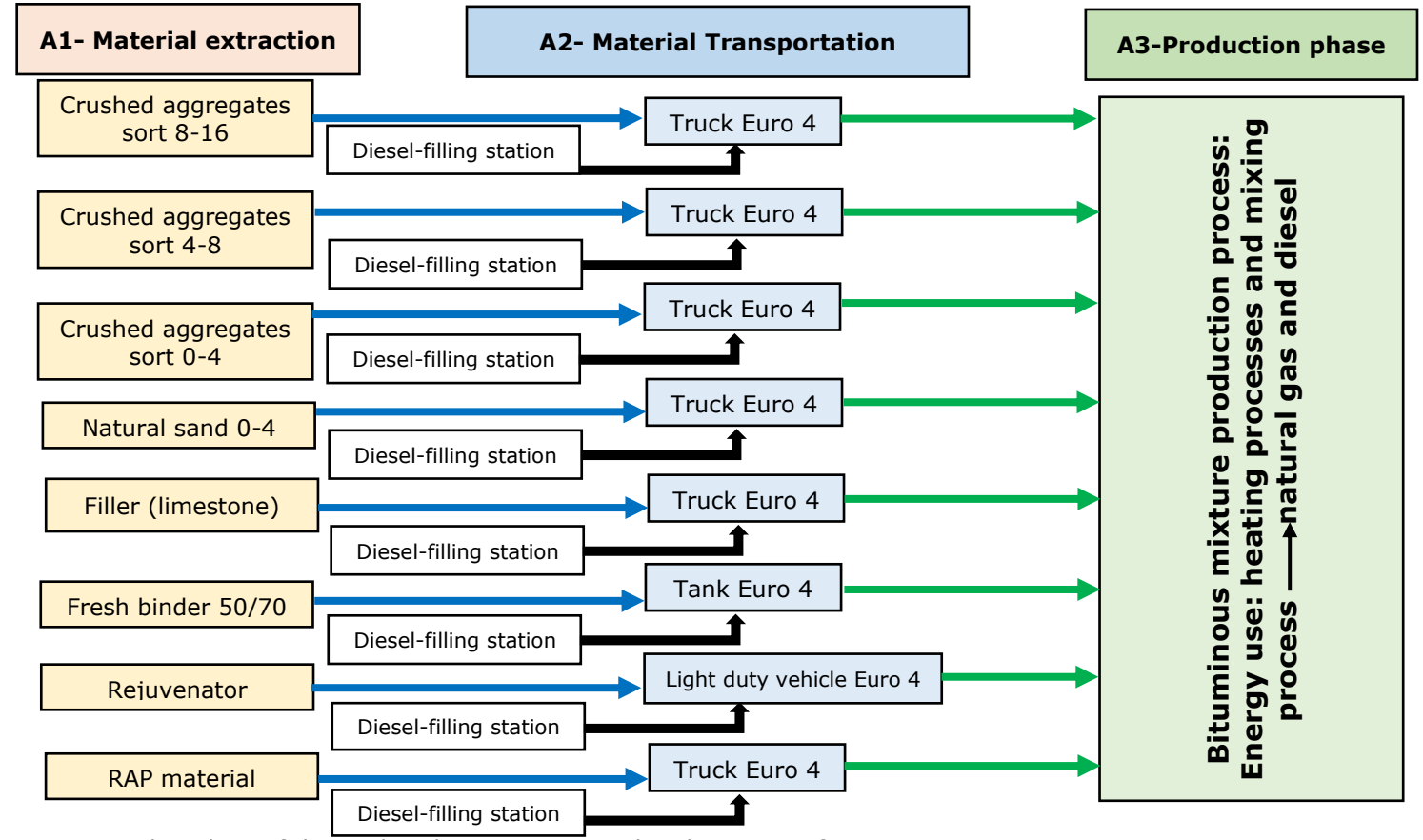

Figure 4.4. Flow chart of the analysed processes considered in GaBi software.

4.5 Environmental Impact Assessment (EIA) results

4.5.1 Comparative analysis

An evaluation of the total environmental impact and an interpretation of the obtained results are presented in this section.

A part of these results were presented by the author in a conference paper Forton et al., 2020 [209].

The EIA results are given in terms of environmental indicators/parameters for two impact categories. These indicators were obtained for each module/stage A1, A2 and A3 and a global value for each indicator obtained for the product stage A1-A3.

The environmental impacts, indicators and parameters evaluated according to EN 15804+A1 were determined for all 13 bituminous mixtures, for each module and the total impact/production phase.

The results obtained for the total production stage A1-A3 are reported in Table 4.5 for all bituminous mixtures. Also, in order to highlight the tendencies of the environmental impacts with the increase of the RAP material and rejuvenator contents, the results are shown in Figure 4.5 and Figure 4.6 for each parameter separately. Moreover, the values obtained for each impact category, those specified in EN 15804+A1, for each type of bituminous mixture for each module (A1, A2 and A3) are presented in Section 4.5.2. All results are reported in Appendix 3 in Tables A3.1 – A3.12.

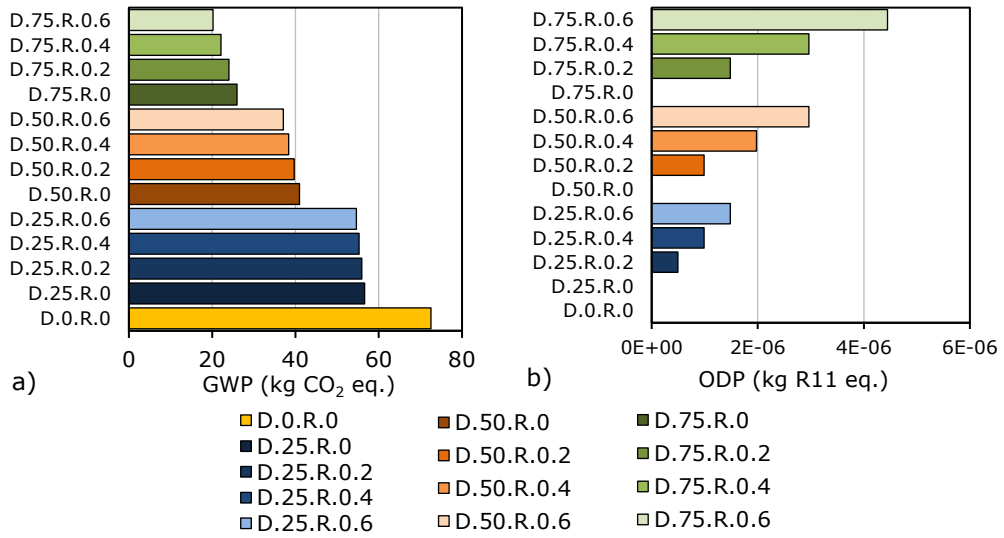

Figure 4.5. Environmental impact indicators (total impact for stages from A1 to A3) per declared unit for all considered bituminous mixtures, according to EN 15804+A1: (a) Global Warming Potential (GWP); (b) Ozone Depletion Potential of the stratospheric ozone layer (ODP).

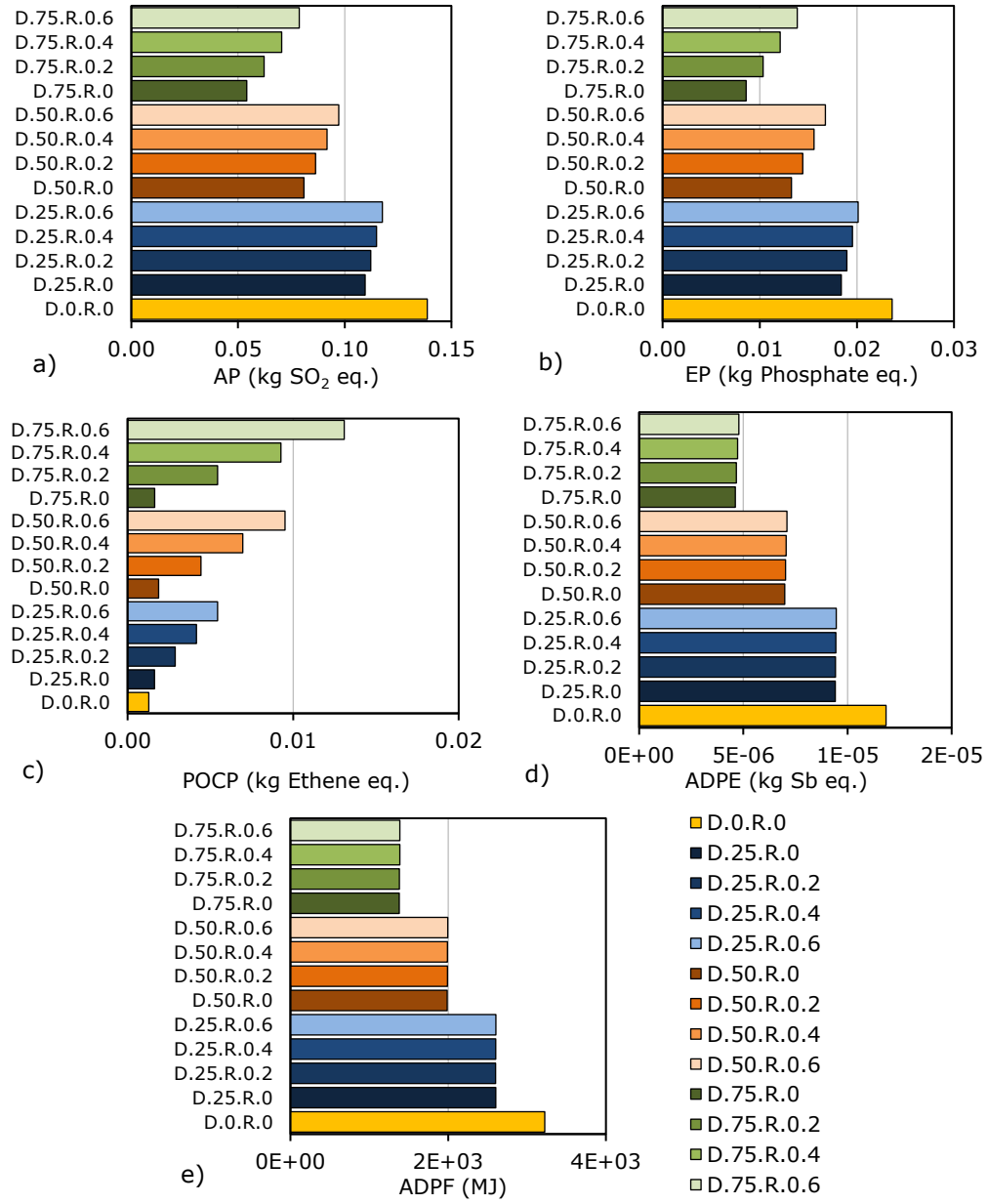

Figure 4.6. Environmental impact indicators (total impact for stages from A1 to A3) per declared unit for all considered bituminous mixtures, according to EN 15804+A1: (a) Acidification Potential of soil and water (AP); (b) Eutrophication Potential (EP); (c) Photochemical Ozone Creation Potential (POCP); (d) Abiotic depletion potential for non-fossil resources (ADPE); (e) Abiotic depletion potential for fossil resources (ADPF).

Table 4.5. Potential environmental impact indicators (total stages from A1 to A3) per declared unit of for all considered bituminous mixtures, according to EN 15804+A1.

Potential environmental impact			D.0.R.0	D.25.R.0	D.25.R.0.2	D.25.R.0.4	D.25.R.0.6	D.50.R.0	D.50.R.0.2	D.50.R.0.4	D.50.R.0.6	D.75.R.0	D.75.R.0.2	D.75.R.0.4	D.75.R.0.6
Environmental impact indicators	Parameter	Unit	A1-A3	A1-A3	A1-A3	A1-A3	A1-A3	A1-A3	A1-A3	A1-A3	A1-A3	A1-A3	A1-A3	A1-A3	A1-A3
	Global warming potential (GWP)	kg CO_2 eq.	72.54	56.61	55.93	55.28	54.63	40.97	39.68	38.37	37.09	25.97	24.02	22.11	20.20
	Ozone Depletion Potential (ODP)	kg R11 eq.	1.66E-13	1.25E-13	4.94E-07	9.88E-07	1.48E-06	8.29E-14	9.88E-07	1.98E-06	2.96E-06	3.99E-14	1.48E-06	2.96E-06	4.45E-06
	Acidification potential (AP)	kg SO_2 eq.	0.139	0.110	0.112	0.115	0.118	0.081	0.086	0.092	0.097	0.054	0.062	0.070	0.079
	Eutrophication potential (EP)	kg Phosphate eq.	0.024	0.018	0.019	0.020	0.020	0.013	0.014	0.016	0.017	0.009	0.010	0.012	0.014

Potential environmental impact			D.0.R.0	D.25.R.0	D.25.R.0.2	D.25.R.0.4	D.25.R.0.6	D.50.R.0	D.50.R.0.2	D.50.R.0.4	D.50.R.0.6	D.75.R.0	D.75.R.0.2	D.75.R.0.4	D.75.R.0.6
	Photochemical Ozone Creation Potential (POCP)	kg Ethene eq.	1.28E-03	1.63E-03	2.88E-03	4.16E-03	5.44E-03	1.87E-03	4.43E-03	6.96E-03	9.51E-03	1.64E-03	5.44E-03	9.26E-03	1.31E-02
	Abiotic depletion potential for non-fossil resources (ADPE)	kg Sb eq.	1.18E-05	9.41E-06	9.42E-06	9.44E-06	9.46E-06	6.99E-06	7.03E-06	7.06E-06	7.09E-06	4.62E-06	4.67E-06	4.73E-06	4.79E-06
	Abiotic depletion potential for fossil resources (ADPF)	MJ	3224.55	2603.59	2601.19	2602.95	2604.84	1987.42	1991.17	1990.74	1994.57	1379.79	1381.44	1387.34	1393.28

As expected, Figures 4.5 – 4.6 and Table 4.5 prove that the increase of the RAP material content leads to a net decrease of environmental impact. As an example, for the bituminous mixtures produced with RAP material without rejuvenator the obtained results for the global warming potential (GWP) show a decrease of near 22% for D.25.R.0, 43% for D.50.R.0 and near to 54% for D.75.R.0 compared to the GPW obtained for the conventional HMA D.0.R.0.

When the rejuvenator is used, a decrease of the GPW values of 1% up to near 6% could be observed, depending on the percentage of the rejuvenator. On the other hand, it could be observed that the increase of the rejuvenator corresponds to an increase of the ODP parameter. Thus, for the mixtures produced without rejuvenator, the values of ODP parameter are very low as 10^{-13}…10^{-14} kg R11 eq./one tonne of mixture. The tendency shown in Figure 4.5 b can be explained by the fact that the rejuvenator content was used by mass of the RAP material.

Regarding the acidification (AP) and eutrophication potential (EP) a significant decrease of impact can be observed in Figures 4.6a and 4.6b with the increase of the RAP material content, from 21% for D.25.R.0 up to 43% for D.75.R.0 compared to the results obtained for the conventional/traditional mixture. On the other hand, the increase of the rejuvenator content leads to an increase of these two parameters. However, for all mixtures produced with RAP and rejuvenator, the total impact of AP and EP is always lower than in case of a conventional/traditional mixture.

For the other environmental indicators such as ADPE (Figure 4.6d) and ADPF (Figure 4.6e) a proportional decrease of their values was observed with the increase of RAP material content and a small increase of these values was obtained with the increase of rejuvenator content.

For the Photochemical Ozone Creation Potential (POCP) indicator an increase was observed with the increase of both RAP material and rejuvenator amounts. However, the values of POCP parameter are low, the maximum value is near to 0.013 kg Ethene equivalent/ 1 tonne of mixture.

According to the new version of the European Standard EN 15804+A2:2019 which includes explicitly biogenic carbon uptake and re-emission different environmental impacts/indicators/parameters must be reported. Therefore, the results obtained for A1-A3 (total) for all environmental indicators (EN 15804+A2) are reported in Table 4.6 for all bituminous mixtures. Moreover, in order to highlight the tendencies of the environmental impacts with the increase of the RAP material and rejuvenator contents into the mass of the bituminous mixtures, the results are shown in Figures 4.7 - 4.9 for each parameter separately.

For detailed interpretation, the values obtained for each impact parameter (those specified in EN 15804+A2) for each type of bituminous mixture and for each module A1, A2 and A3 were analysed in Section 4.5.2. All results are reported in Appendix 3 in Tables A3.13 – A3.25.

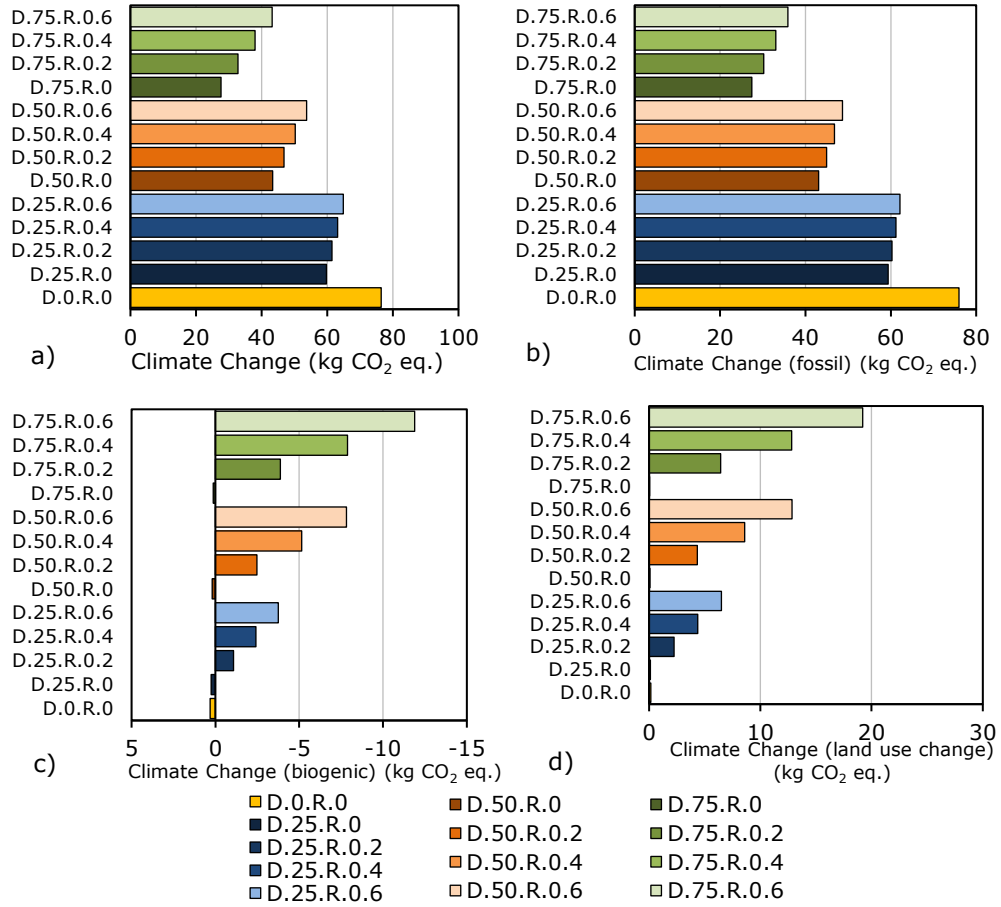

Figure 4.7. Environmental impact indicators (total impact A1-A3) per declared unit for all considered bituminous mixtures: (a) Climate change; (b) Climate change (fossil); (c) Climate change (biogenic); (d) Climate change (land use change).

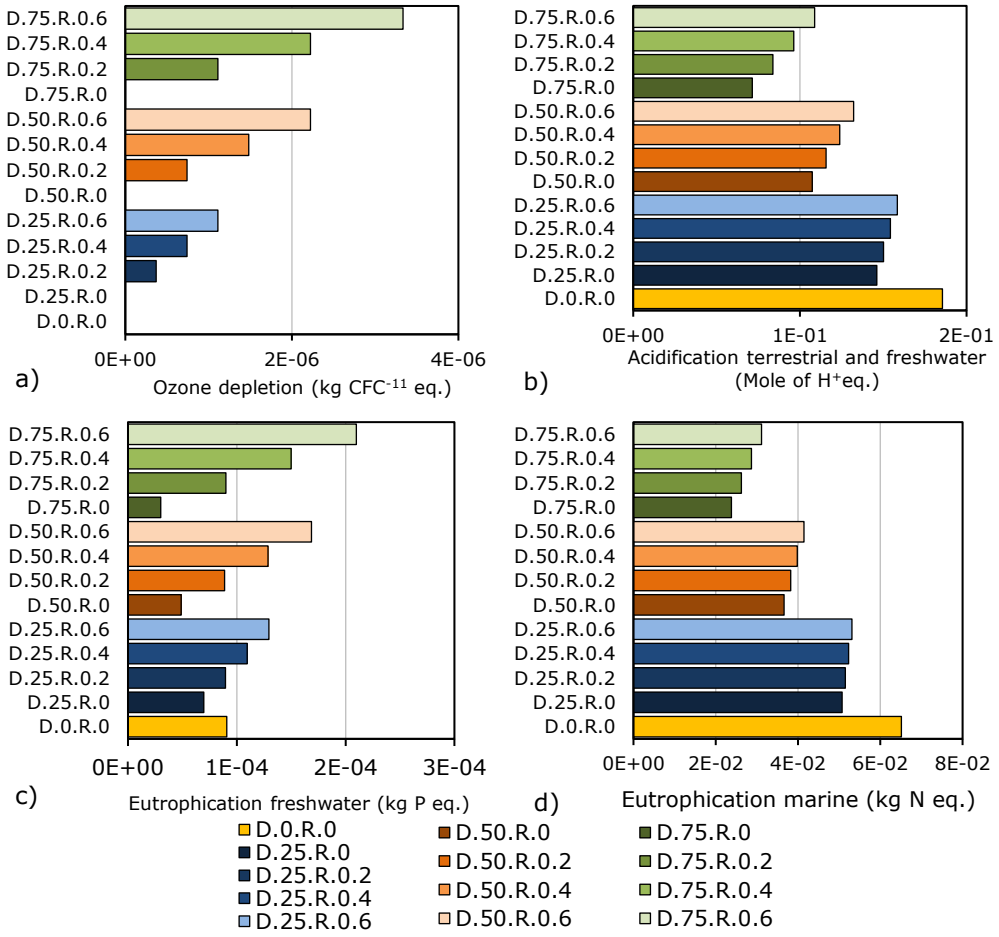

Figure 4.8. Environmental impact indicators (total impact A1-A3) per declared unit for all considered bituminous mixtures, according to EN 15804+A2: (a) Ozone depletion; (b) Acidification terrestrial and freshwater; (c) Eutrophication freshwater; (d) Eutrophication marine.

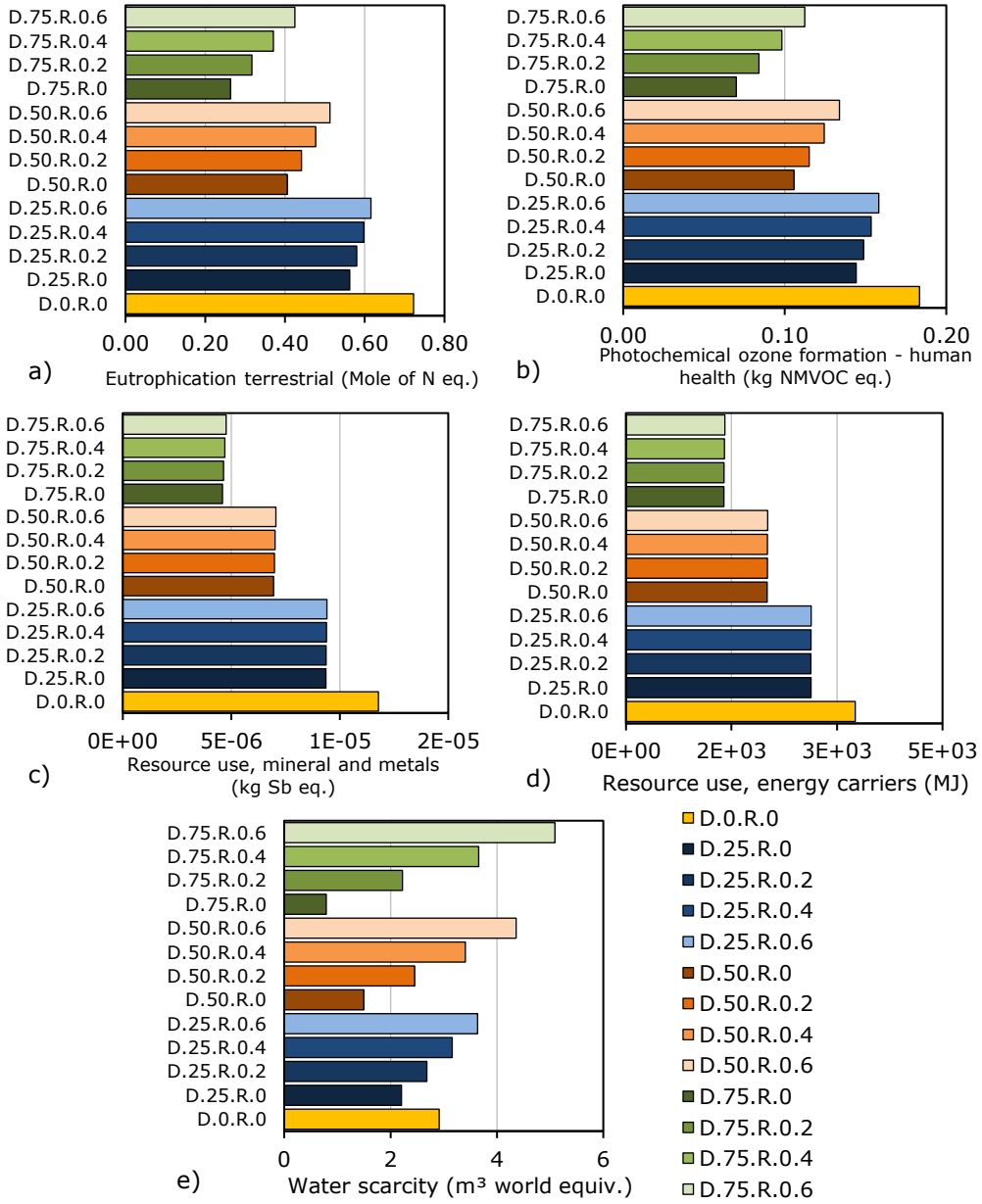

Figure 4.9. Environmental impact indicators (total impact A1-A3) per declared unit for all considered bituminous mixtures, according to EN 15804+A2: (a) Eutrophication terrestrial; (b) Photochemical ozone formation - human health; (c) Resource use, mineral and metals; (d) Resource use, energy carriers; (e) water scarcity.

Table 4.6. Potential environmental impact indicators (total stages from A1 to A3) per declared unit of for all considered bituminous mixtures, according to EN 15804+A2.

Potential environmental impact			D.0.R.0	D.25.R.0	D.25.R.0.2	D.25.R.0.4	D.25.R.0.6	D.50.R.0	D.50.R.0.2	D.50.R.0.4	D.50.R.0.6	D.75.R.0	D.75.R.0.2	D.75.R.0.4	D.75.R.0.6
Environmental impact indicators	Parameter	Unit	A1-A3	A1-A3	A1-A3	A1-A3	A1-A3	A1-A3	A1-A3	A1-A3	A1-A3	A1-A3	A1-A3	A1-A3	A1-A3
	Climate Change	kg CO_2 eq.	76.44	59.74	61.43	63.16	63.16	43.35	46.81	50.24	53.70	27.61	32.78	37.99	43.20
	Climate Change (fossil)	kg CO_2 eq.	75.97	59.38	60.27	61.20	61.20	43.08	44.95	46.80	48.67	27.43	30.22	33.05	35.88
	Climate Change (biogenic)	kg CO_2 eq.	0.31	0.25	-1.08	-2.42	-2.42	0.19	-2.48	-5.15	-7.82	0.13	-3.88	-7.88	-11.89
	Climate Change (land use change)	kg CO_2 eq.	0.15	0.12	2.24	4.37	4.37	0.08	4.33	8.59	12.85	0.05	6.43	12.82	19.20
	Ozone depletion	kg CFC-11 eq.	1.25E-13	9.40E-14	3.71E-07	7.41E-07	7.41E-07	6.22E-14	7.41E-07	1.48E-06	2.22E-06	2.99E-14	1.11E-06	2.22E-06	3.33E-06

Potential environmental impact			D.0.R.0	D.25.R.0	D.25.R.0.2	D.25.R.0.4	D.25.R.0.6	D.50.R.0	D.50.R.0.2	D.50.R.0.4	D.50.R.0.6	D.75.R.0	D.75.R.0.2	D.75.R.0.4	D.75.R.0.6
	Acidification terrestrial and freshwater	Mole of H+ eq.	0.19	0.15	0.15	0.15	0.15	0.11	0.12	0.12	0.13	0.07	0.08	0.10	0.11
Environmental impact indicators	Eutrophication freshwater	kg P eq.	9.08E-05	6.97E-05	8.96E-05	1.10E-04	1.10E-04	4.89E-05	8.88E-05	1.29E-04	1.69E-04	3.01E-05	9.00E-05	1.50E-04	2.10E-04
	Eutrophication marine	kg N eq.	6.51E-02	5.07E-02	5.15E-02	5.23E-02	5.23E-02	3.66E-02	3.82E-02	3.98E-02	4.14E-02	2.38E-02	2.62E-02	2.87E-02	3.11E-02
	Eutrophication terrestrial	Mole of N eq.	0.72	0.56	0.58	0.60	0.60	0.41	0.44	0.48	0.51	0.26	0.32	0.37	0.42
	Photochemical ozone formation - human health	kg NMVOC eq.	0.18	0.14	0.15	0.15	0.15	0.11	0.12	0.12	0.13	0.07	0.08	0.10	0.11
	Resource use, mineral and metals	kg Sb eq.	1.18E-05	9.36E-06	9.37E-06	9.39E-06	9.39E-06	6.95E-06	6.99E-06	7.02E-06	7.05E-06	4.59E-06	4.64E-06	4.70E-06	4.76E-06

Potential environmental impact			D.0.R.0	D.25.R.0	D.25.R.0.2	D.25.R.0.4	D.25.R.0.6	D.50.R.0	D.50.R.0.2	D.50.R.0.4	D.50.R.0.6	D.75.R.0	D.75.R.0.2	D.75.R.0.4	D.75.R.0.6
	Resource use, energy carriers	MJ	3259.48	2630.97	2628.59	2630.40	2630.40	2007.12	2010.96	2010.62	2014.54	1391.71	1393.50	1399.56	1405.66
	Water scarcity	m³ world equiv.	2.91	2.21	2.68	3.16	3.16	1.50	2.45	3.41	4.36	0.79	2.22	3.66	5.09

It can generally be observed in Figures 4.7 – 4.9 and Table 4.6 that the increase of the RAP material amount into the mass of mixtures, leads to a net decrease of environmental impact. It was highlighted that for the bituminous mixtures produced with RAP material and without rejuvenator, the obtained results for the environmental indicator climate change (total) show a decrease proportional with the increase of RAP material amount, compared to the conventional HMA D.0.R.0. However, Figure 4.7a also indicates that the increase of the rejuvenator content corresponds to a limited increase of the impact for the climate change.

The values obtained for the climate change indicator could be divided in three main categories: fossil, biogenic and land use change (Figure 4.7b, c and d). Thus, the obtained values show that the major impact of increasing the RAP material content is on the fossil indicator due to the use of resources, both for raw materials and energy. For the other two categories the impact is smaller than in case of the above-mentioned indicator, and an increase of these indicators was observed with the increase of the rejuvenator content. The negative values of the climate change (biogenic) that were obtained for the mixtures produced with more than 0.2% rejuvenator, by mass of the RAP material, can be interpreted as an environmental credit.

Regarding the parameter ozone depletion which is related to the reduction of the amount of ozone in the stratosphere, thus an increase of this parameter was observed with the increase of the rejuvenator due to the origin of the product which is made by a mixture of vegetal oil.

Another important parameter that characterizes the ecosystem quality impact category is the acidification terrestrial and freshwater indicator. The increase of the RAP material leads to a net decrease of the acidification indicator, compared to a conventional HMA. The increase of the rejuvenator content has a minor impact on the values obtained for this parameter as it can be observed in Figure 4.8b.

In this analysis the eutrophication parameter could be divided and reported in three indicators: eutrophication freshwater (Figure 4.8c), eutrophication marine (Figure 4.8d) and eutrophication terrestrial (Figure 4.9a). As expected, the production process of bituminous mixtures has a higher impact on the terrestrial indicator. For all three parameters the same tendencies were observed: the values for these eutrophication parameters decrease with the increase of the RAP material content and respectively increase with the increase of the rejuvenator content. A similar tendency was observed for the photochemical ozone formation - human health (Figure 4.9b).

For the eutrophication freshwater indicator, the impact is higher for the mixtures produced with more than 0.2% rejuvenator by mass of the RAP material, than the impact obtained for the conventional mixture. However, this impact is rather small, the maximum impact of 2.10×10^{-4} kg P equivalent was obtained for the mixture D.75.R.0.6. Similar tendency was observed for the water scarcity (Figure 4.9e).

Regarding the indicators related to the use of resources: resource use-mineral and metals (Figure 4.9c), resource use-energy carriers (Figure 4.9d) an important decrease was obtained with the increase of RAP material content. For these two indicators the increase of rejuvenator content corresponds to a small impact increase.

As a general comment, taking into consideration the results shown in Chapter 3 and the results of the EIA it can be concluded that when less than 25% of the considered RAP is used in the production of a new bituminous mixture, the characteristics of the final mix can be within the limits specified in the Romanian Standards for a bituminous mixture with a 16 mm maximum aggregate size. Therefore, a decrease of the environmental impact is near to 20% for this solution

compared to the conventional one. Moreover, the results prove that the addition of RAP material leads to a net decrease of the environmental impact.

When high amounts of RAP are used in the production of a new bituminous mixture, depending on the properties of this material, rejuvenators should be used. The solution with 75% RAP (D.75.R.0) was considered only to highlight the environmental impact potential of this 100% recyclable material. In this case, a substantial decrease of the environmental impact as more than half of the conventional solution could be obtained.

On the other side, the increase of the rejuvenator content corresponds to a small increase of the impact. A considerable impact was observed for the land use, due to the fact that the rejuvenator considered in this study is a mix of vegetal oils.

Regarding the production process of bituminous mixtures containing RAP material and different amounts of rejuvenator, an increase of the environmental impact was observed with the increase of the rejuvenator content compared to those produced only with RAP material. However, this does not represent a major increase in impact, approximately 1.5% increase per 0.2% rejuvenator content by the total mass of the final bituminous mixture.

From the results obtained in the laboratory (as described in Chapter 3) it was observed that the characteristics of the D.50.R.0.4 bituminous mixture are closer to the conventional bituminous mixture. The environmental impact for this solution (D.50.R.0.4) leads to a decrease of approximatively 35% (depending on the analysed environmental indicator) than the conventional one. It can be concluded that when rejuvenators are used in this process, they can affect the energy balance and reduce the gain in environmental impact.

In order to better highlight the environmental potential of the production of these recycled bituminous mixtures, Figure 4.10 shows a comparison between four environmental indicators: climate change, acidification terrestrial and freshwater, eutrophication terrestrial and resource use, energy carriers, which were obtained for the production of two mixtures produced with RAP material and rejuvenator (D.25.R.0.4 and D.50.R.0.4) and the conventional mixture (D.0.R.0).

Therefore, it could be be observed that for the environmental impact a net decrease of 16.8%...19.3%, depending on the evaluated environmental indicator, compared to the conventional solution, can be obtained when 25% RAP material and 0.4% of rejuvenator by mass of the RAP material are used to produce a recycled mixture.

A more important EI reduction of 33.2%...38.3%, depending on the evaluated environmental indicator, compared to the conventional solution, could be obtained when 50% RAP material and 0.4% of rejuvenator by mass of the RAP material are used to produce a recycled mixture.

All these tendencies are due to the fact that the RAP material is a recycled, reused material which do not bring additional environmental load in A1 stage. Also, it can be observed that the rejuvenator which is a mixture of vegetal oils that do not have a significant influence on the potential environmental impact in the production process of bituminous mixtures containing RAP material and rejuvenator.

These findings prove that when RAP materials and rejuvenators are used in the production of a new bituminous mixture a substantial decrease of the potential environmental impact is obtained. It must be specified that the type and the dosage of the rejuvenator plays an important role in the EIA analysis.

Therefore, for each analysis is important to know the proper dosage of RAP material and rejuvenator that must be used in order to obtain a bituminous mixture

that has similar characteristics as a conventional one, and finally to evaluate the EI gains.

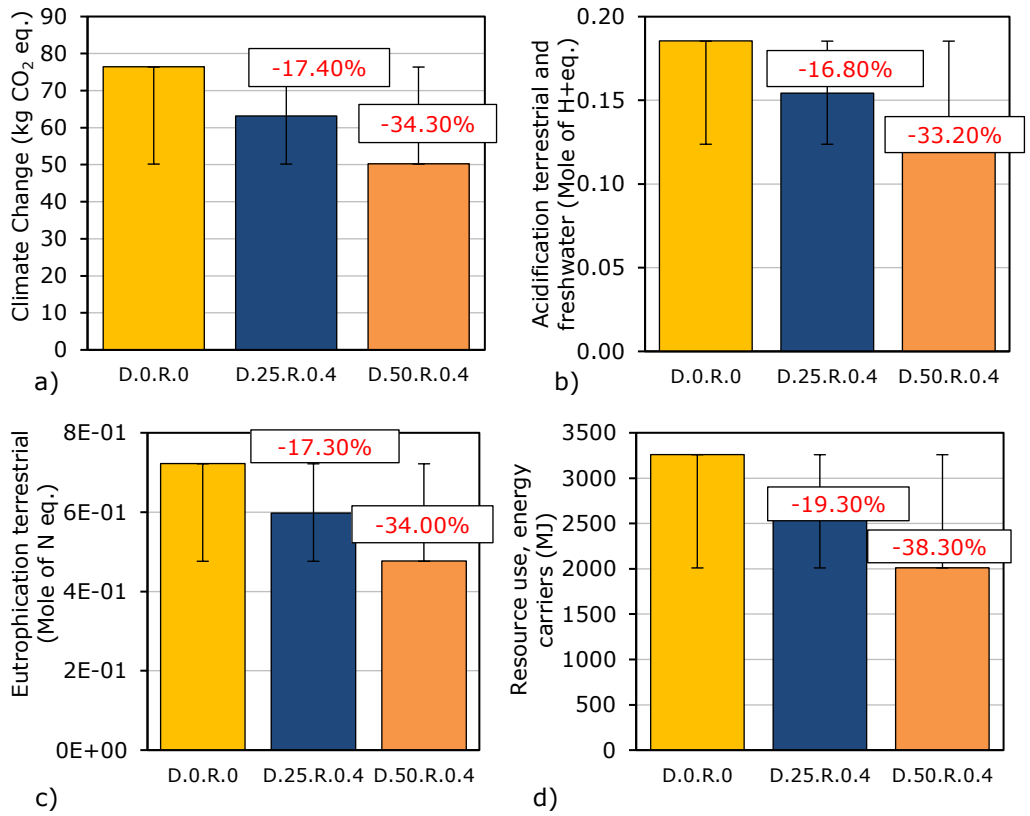

Figure 4.10. Comparison between the environmental impact indicators (total impact A1-A3) per declared unit for the conventional HMA D.0.R.0 and D.25.R.0.4 and D.50.R.0.4.: (a) Climate change; (b) Acidification terrestrial and freshwater; (c) Eutrophication freshwater; (d) Resource use, energy carriers.

4.5.2 Internal analysis

In order to observe the impact rates within one mixture an internal analysis was performed for the production stage. As an example, the values obtained for the environmental indicators for the mixture D.25.R.0.4 are presented per each module A1, A2 and A3 in Table 4.7. Similarly, the results obtained for all environmental indicators for all the other mixtures for all indicators from EN 15804+A1 are reported in Tables A3.1-A3.12 in Appendix 3.

Figure 4.11 shows the results obtained for each stage A1, A2 and A3 for the GWP, AP and EP environmental indicators for the mixture produced with 50% RAP material and 0.4% rejuvenator by mass of the RAP material. Results show that the highest impact is given by the extraction and processing of materials. It could be observed that for the Global Warming Potential the impact of the production phase is half of the A1 - material extraction and processing impact.

It could be observed that for all bituminous mixtures the stage A1 – materials extraction shows the highest impact for most of the environmental indicators, exception EP in case of the mixtures produced without rejuvenator and with small amount of rejuvenator 0.2%. As expected, the production process (A3) and the transportation process (A2) have a lower impact that the one obtained for the stage A1 – extraction and processing.

Table 4.7. Environmental impact indicators obtained for stages A1, A2 and A3, per declared unit for the bituminous mixture D.25.R.0.4, according to EN 15804+A1.

Potential environmental impact			**D.25.R.0.4**		
Environmental impact indicators	**Parameter**	**Unit**	**A1**	**A2**	**A3**
	Global warming potential (GWP)	kg CO2 eq.	30.65	10.93	13.70
	Ozone Depletion Potential (ODP)	kg R11 eq.	9.88E-07	2.96E-15	5.36E-16
	Acidification potential (AP)	kg SO2 eq.	0.069	0.038	0.008
	Eutrophication potential (EP)	kg Phosphate eq.	0.008	0.009	0.002
	Photochemical Ozone Creation Potential (POCP)	kg Ethene eq.	1.59E-02	-1.28E-02	1.08E-03
	Abiotic depletion potential for non-fossil resources (ADPE)	kg Sb eq.	6.69E-06	9.97E-07	1.76E-06
	Abiotic depletion potential for fossil resources (ADPF)	MJ	2225.08	148.08	229.80

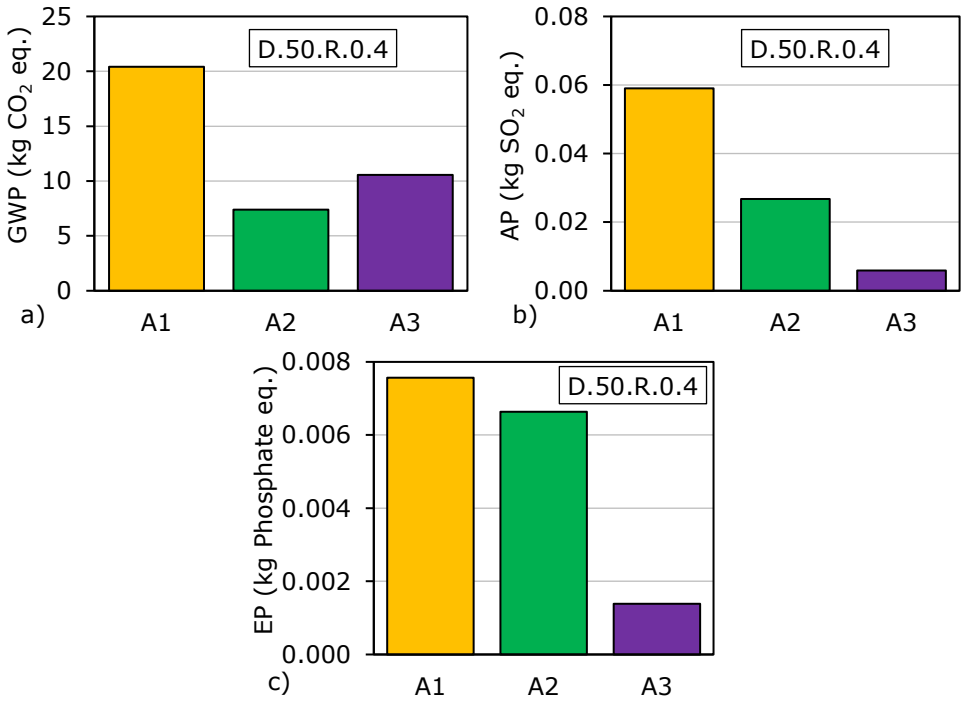

Figure 4.11. Comparison between the environmental impact indicators per each stage A1, A2, A3 per declared unit for the mixture D.50.R.0.4.: (a) GWP; (b) AP; (c) EP.

As an example, the values obtained for the environmental indicators from EN 15804+A2 for the mixture D.25.R.0.4 are presented per each module A1, A2 and A3 in Table 4.8. Similarly, the results obtained for all environmental indicators for all the other mixtures for all indicators from EN 15804+A2 are reported in Tables A3.13-A3.24 in Appendix 3.

Figure 4.12 shows the results obtained for each stage A1, A2 and A3 for the climate change environmental indicator, total impact and the impacts divided for fossil, biogenic and land use, for the mixture produced with 50% RAP material and 0.4% rejuvenator by mass of the RAP material. Results show that the highest impact is given by the extraction and processing of materials. It could be observed that for the climate change total the impact of the production phase is near to 30% of the A1 - material extraction and processing impact. The negative values of the climate change – biogenic (Figure 4.12c) can be interpreted as an environmental credit. As expected, the extraction and processing (A1) has a major impact on the land use (Figure 4.12d) indicator compared to the transportation and the production process

A similar comment can be made as in case of the indicators evaluated according to the EN 15804+A1, i.e. the first stage – materials extraction A1 shows the highest values for most of the environmental indicators, with the exception the environmental indicators related to the eutrophication marine and terrestrial for the mixtures produced without rejuvenator where the major impact was given by the transportation process.

Table 4.8. Environmental impact indicators (EN 15804+A2) obtained for stages A1, A2 and A3, per declared unit for the bituminous mixture D.25.R.0.4.

Potential environmental impact			**D.25.R.0.4**		
	Parameter	**Unit**	**A1**	**A2**	**A3**
Environmental impact indicators	Climate Change	kg CO_2 eq.	38.05	11.20	13.91
	Climate Change (fossil)	kg CO_2 eq.	36.18	11.12	13.90
	Climate Change (biogenic)	kg CO_2 eq.	-2.4E+00	-1.34E-02	5.64E-03
	Climate Change (land use change)	kg CO_2 eq.	4.28E+00	9.18E-02	7.22E-04
	Ozone depletion	kg CFC-11 eq.	7.41E-07	2.22E-15	4.02E-16
	Acidification terrestrial and freshwater	Mole of H+ eq.	8.76E-02	5.56E-02	1.10E-02
	Eutrophication freshwater	kg P eq.	7.57E-05	3.34E-05	4.79E-07
	Eutrophication marine	kg N eq.	2.03E-02	2.67E-02	5.27E-03
	Eutrophication terrestrial	Mole of N eq.	2.43E-01	2.97E-01	5.81E-02
	Photochemical ozone formation - human health	kg NMVOC eq.	8.54E-02	5.32E-02	1.48E-02
	Resource use, mineral and metals	kg Sb eq.	6.64E-06	9.95E-07	1.76E-06
	Resource use, energy carriers	MJ	2250.93	149.58	229.88
	Water scarcity	m^3 world equiv.	3.05E+00	1.04E-01	5.56E-03

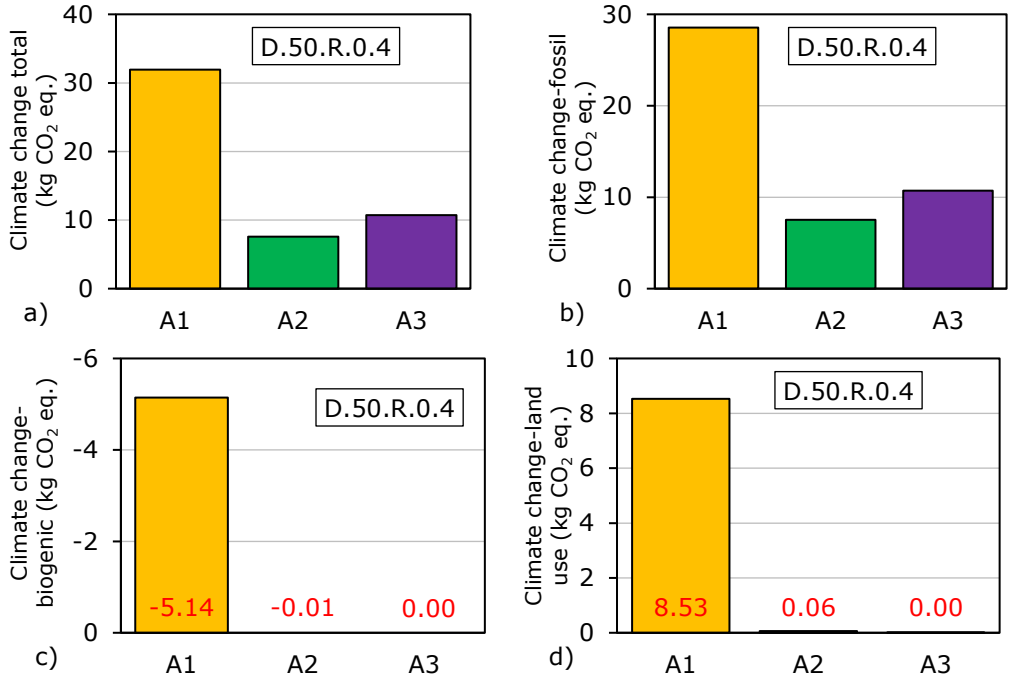

Figure 4.12. Comparison between the climate change indicator per each stage A1, A2, A3 per declared unit for the mixture D.50.R.0.4.: (a) total; (b) fossil; (c) biogenic; (d) land use change.

4.6 EIA conclusions

The objective of this analysis was to investigate the potential environmental impact related to the production of one tonne of several types of bituminous mixtures containing different amounts of Reclaimed Asphalt Pavement (RAP) and Rejuvenator (Rej). All materials considered in this study are specific and generally used for pavements in Romania.

Three bituminous mixtures containing 25%, 50% and 75% of RAP material were considered and for each mixture produced with a specific RAP material content a rejuvenator consisting in a mixture of vegetal oils was used in three dosages of 0.2%, 0.4% and 0.6% by mass of RAP material. One conventional bituminous mixture produced with virgin materials, was used as reference. A total of 13 types of bituminous mixtures were considered in this analysis.

The environmental impact was investigated for the production process defined by the following three stages: raw material supply, transportation and manufacturing (production) of one tonne of ready-to-use mixture while all the other processes were excluded by boundary conditions. The EIA was performed by using GaBi software.

It is important to mentioned that the EIA was performed based on the calculation of the environmental indicators according to the European Standards EN 15804+A1:2013 and the new version EN 15804+A2:2019 which includes explicitly biogenic carbon uptake and re-emission.

The input values were collected and associated for each material and process by using the 2016 - 2018databases associated to the GaBi software. The materials and energy were quantified for the production of one tonne of bituminous mixture and finally an evaluation of the total impact and an interpretation of the obtained results were performed.

Two sets of parameters were analysed in order to evaluate the potential environmental impact: one set of parameters specified in EN 15804+A1:2013 and another one specified in EN 15804+A2:2019. Other impact categories can be evaluated such as: the potential impact of the resource use, the potential impact on the waste categories per declared unit and the potential impact of the production process on the human health.

The following conclusions can be drawn:

- the production process of the conventional bituminous mixture leads to the highest environmental impact;
- the increase of RAP material within bituminous mixtures corresponds to a net decrease of the environmental impact due to the reuse of materials;
- it was observed that for all bituminous mixtures the extraction and manufacturing of the raw material (A1) show the highest impact values for most of the analysed indicators. These tendencies were expected.
- the addition of RAP material leads to a net decrease of the energy use and environmental impact;
- when rejuvenators are used in this process, they can affect the energy balance and reduce the difference in environmental impact;
- when less than 25% of the considered RAP is used in the production of a new bituminous mixture, the characteristics of the final mix can be within the limits specified in the Romanian Standards for a bituminous mixture with a 16 mm maximum aggregate size. Therefore, a decrease of the environmental impact is near to 20% for this solution compared to the conventional one;
- when high amounts of RAP are used in the production of a new bituminous mixture, depending on the properties of this material, rejuvenators should be used. The solution with 75% RAP (D.75.R.0) was considered only to highlight the environmental impact potential of this 100% recyclable material. In this case, a substantial decrease of the environmental impact as more than half of the conventional solution could be obtained. By using an optimal rejuvenator content this solution could be improved;
- for the production process of bituminous mixtures containing RAP material and different amounts of rejuvenator, an increase of the environmental impact was observed with the increase of the rejuvenator content compared to those produced only with RAP material. However, this does not represent a major increase in impact, approximately 1.5% increase per 0.2% rejuvenator content by the total mass of the final bituminous mixture. A considerable impact was observed for the land use, due to the fact that the rejuvenator considered in this study is a mix of vegetal oils;
- based on the experimental work and on the results presented in Chapters 2 and 3, the mix design D.50.R.0.4/the corresponding binder blend (50/70 + 50% RAP + 10% Rej) presents a closer behaviour to the one of the conventional bituminous mixture/the corresponding fresh binder (50/70). The environmental impact for this solution (D.50.R.0.4) leads to a decrease of approximatively 33-40% than the conventional HMA depending on the analysed indicator/parameter.

5. Conclusions and perspectives

The work presented in this report was devoted to the possible reuse of RAP in new bituminous mixtures. Therefore, the two declared objectives of the thesis are, i) the characterization of the thermomechanical performances of binder blends and bituminous mixtures produced with Reclaimed Asphalt Pavement (RAP) and rejuvenator (Rej) and, ii) the evaluation of the potential environmental impact related to the production of a mixture containing different amounts of RAP material and rejuvenator.

In order to achieve these objectives, comprehensive experimental investigations were performed on binders and mixtures. All tests on binders and mixtures were performed in the Road Laboratory of the University Politehnica Timisoara, including the environmental impact assessment. On the other hand, the analyses, estimations, and predictions of most parameters/characteristics of binders and mixtures were performed at ENTPE, Lyon. The study on binders focused on the properties of different binder blends produced by mixing one type of fresh binder (a straight run 50/70 pen. grade), a RAP-extracted binder and a rejuvenator of vegetal origin. The experimental plan includes a total of 17 binders consisting of the 50/70 fresh bitumen with and without the RAP-extracted binder with and without rejuvenator. Blending proportions between RAP binder, fresh bitumen and rejuvenator were calculated in order to reproduce ratios between these components within corresponding tested bituminous mixtures (with a 5.6% total binder content, the rejuvenator was not considered as part of it) containing 25%, 50%, and 75% RAP material and 0.00%, 0.20%, 0.40% and 0.60% of rejuvenator by mass of RAP material. These proportions for mixtures gave 0%, 5%, 10% and 15% of rejuvenator by mass of the RAP binder in the blends. All results are reported in Chapter 2. The following conclusions can be drawn:

- Conventional tests: penetration at 25°C, softening point, Fraass breaking point, elongation, and density at 25°C were performed on all 17 binders including pure fresh and RAP binders. The experimental results show a decrease in penetration and an increase in softening point, Fraass breaking point temperature and penetration index for the increase of RAP binder content and decreasing rejuvenator content in blends. Similar tendencies to those observed for the Fraass breaking point temperature and the penetration index values were found for the values of density at 25°C. For the binder blends produced without rejuvenator the elongation is decreasing with the increase of the RAP binder content and is always lower than 150 mm.
- DSR complex modulus tests were performed from 25°C to 85°C and frequencies from 0.1 Hz to 10 Hz. The Time-Temperature Superposition Principle was validated for all tested binders. Data obtained with the DSR tests for all binders were successfully modelled by using the 2S2P1D model. The experimental data were analysed by using the 2S2P1D model in which four parameters $(G_0, G_{00}, k \text{ and } \delta)$ were considered constants for all tested binders and only three parameters $(h, \beta \text{ and } \tau)$ were variable. Parameters $h, \beta \text{ and } \tau$ and a_T shift factors show some remarkable tendencies with the increase of RAP binder and rejuvenator

contents in the final blends. In particular, parameter h shows a linear relationship with the RAP binder content and on the other side parameters β, τ and a_T temperature shift factors follow a logarithmic trend.

- Steady shear viscosity at 85°C was obtained as the norm of complex viscosity at high temperature/low frequency in the domain of Newtonian behaviour of binders. η_0 values at temperatures from 75°C to 25°C were calculated from the experimental values obtained at the reference temperature of 85°C. For all temperatures, η_0 values are increasing with the increase of RAP binder content and with the decrease of Rej content in the blends. The addition of the rejuvenator was observed to counterbalance the stiffening effect of the RAP binder in the blends.
- High and low critical temperatures were determined from the data obtained with the DSR and BBR tests. The tests are in agreement with the overall Superpave framework but some minor differences in the analysis of test results were applied to obtain the considered critical temperatures of the tested binders. The experimental results show that both critical temperatures increase with the increase of RAP binder content in the blends, and they decrease with the increase of Rej content within blends. It seems that the rejuvenator can have a counterbalancing effect as it neutralizes the effect of the RAP binder. However, it is interesting to notice that a lower dosage of rejuvenator is necessary to obtain a similar low critical temperature as the one of the 50/70 binder than to meet the high temperature specifications.
- For most of the analysed parameters, the results obtained for the blends produced with 10% or 15% rejuvenator by mass of the RAP binder, are closer to those obtained for fresh binder 50/70, independently of the RAP binder content. The 10% or 15% rejuvenator dosage depends on the investigated parameter. Practically, this indicates the capability of the rejuvenator, in terms of mechanical characteristics, to rejuvenate the hard-aged RAP binder and finally to provide a final product with similar properties of fresh binder.
- Strong relations were observed between the experimental results obtained for $pen.$, $T_{R\&B}$, T_{Fraass}, steady shear viscosity at 25°C (η_0) and the critical temperatures $\left(T_{DSR\ high\ critical}\ and\ T_{BBR\ low\ critical}\right)$.
- Two different estimation methods were proposed and $pen.$, $T_{R\&B}$, T_{Fraass} 2S2P1D parameters $(h, \beta\ and\ \tau)$, a_T temperature shift factors, $T_{DSR\ high\ critical}$, $T_{BBR\ low\ critical}$ and $\left|G^*(T,f)\right|$ values were estimated for all produced binder blends from experimental results obtained for the base constituents and the equivalent values obtained for the rejuvenator. Equivalent values for the rejuvenator were obtained by minimizing the distance between experimental and calculated values. It should be highlighted that these equivalent values were used only in the context of the blending law, therefore they are not intended to reflect actual properties of the rejuvenator. Slightly better correspondence was found

between the estimated values of all above-mentioned parameters obtained with the 2nd estimation, which is an original input of this work, and experimental values. Moreover, the 2nd estimation has the great advantage to only require parameters for each of the three base constituents when the dosage if fixed.

- In order to obtain phase angle from the estimated values of $|G^*(T,f)|$ for all binder blends over the whole frequency and temperature domain, the 2S2P1D model was calibrated on master curves of $|G^*(T,f)|_{est.1\ or\ 2}$ at a reference temperature of 55°C in order to be sure that all analysed binders are thermorheologically simple. The determined values of $\varphi(T,f)$ are close to the measured values for all binder blends. A better correlation with the experimental measurements was found for the phase angle values calculated from the 2S2P1D fitted on the $|G^*(T,f)|_{est.2}$ values.
- The statistical analysis performed in order to highlight the accuracy of both estimation methods for all parameters, considering all binder blends, shows that a more accurate estimation resulted by applying the second estimation method.
- If the equivalent parameters for the rejuvenator are not known from previous experiments, a good approximation can be obtained from only one test performed on the binder blend produced with the RAP binder and the maximum rejuvenator content: RAP + 15% Rej in the case of this study. In these conditions, the results used for the approximated values for the rejuvenator are very similar in comparison to the ones considering the optimized values. This conclusion is also validated on two new binder blends having other rejuvenator contents of 7.5% and respectively 8.5%. This proposed approach presents the great advantage of requiring less testing than the classical approach and can be used for any combination of RAP/rejuvenator, in contrast to the classical approach.
- The equivalent parameters for the rejuvenator are probably only rejuvenator dependent, which is another advantage of the proposed method. This point should be confirmed with a wider range of fresh and RAP binder types.

The effects of the RAP material and the rejuvenator on the thermo-mechanical properties of 13 bituminous mixtures produced with different amounts of RAP material and with or without a mix of vegetal origin used as a rejuvenator were investigated. One conventional Hot Mix Asphalt was used as a reference. All results are reported in Chapter 3. The following conclusions could be drawn:

- Considering the Marshall characteristics, it was observed that the effect of increasing the RAP material content leads to a stiffer behaviour of the bituminous mixtures, thus stability increases as expected. The influence of increasing the rejuvenator content resulted in a reverse effect. A linear

relationship with the RAP material content for the bituminous mixtures produced with the same amount of rejuvenator was observed with the exception of stability.

- For the IT-CY tests the stiffness modulus was obtained at four temperatures starting from 10°C up to 25°C, every 5°C. The effect of increasing the RAP material content led to an increase of stiffness and the influence of the temperature was observed for the cases where the increase of temperature leads to a linear decrease of the stiffness modulus. On the other side, the increase of the rejuvenator content within the mass of mixtures corresponds to a counterbalancing of the effect, namely stiffness is decreasing with the increase of the rejuvenator content.
- In the case of the cyclic compression with confinement test at 50°C it resulted that h_{10000} and ε_{10000} values are directly proportional with the rejuvenator content. For the mixtures produced without rejuvenator a small increase of the creep rate was observed with the increase of the RAP material content. The rate of the increase of the f_c values is higher for the other series of bituminous mixtures produced with 0.2%, 0.4% and 0.6% rejuvenator. This clearly resulted from the increasing of the slope of the linear regressions as the rejuvenator content is calculated as a percentage of the RAP material.
- For the above parameters (Marshall characteristics, stiffness modulus and ε_{10000}), their variations with the penetration of the corresponding binder blends resulted in strong relationships for the mixtures/binder blends produced with the same RAP material/binder content (25%, 50% and 75%). However, the overall relation between these parameters and the penetration is not so strong. These tendencies could be explained by the fact that most probably the use of the RAP material leads to a change in the grading curves of the final mixtures. Besides, the use of the same compaction energy for all mixtures, the rejuvenator content which was established as a function of the mass of the RAP material and the difference between the density of the RAP aggregates and the density of the virgin aggregates are all leading to scattered results.
- The data obtained from the complex modulus tests were presented in Cole-Cole and Black diagrams and they are located on a unique curve, independently of the test temperature and frequency, for each of the considered mixtures. Master curves and shift factors of the mixtures produced without rejuvenator are falling away from the corresponding master curves of the conventional one.
- Experimental data were fitted with 2S2P1D model. It was observed that 2S2P1D parameters and the a_T shift factors of mixtures do not appear to follow a clear tendency with the increase of the RAP material and rejuvenator contents. This observation is in contrast with the linear tendencies of these parameters with the RAP binder content which were observed for the corresponding binder blends. The glassy modulus E_0 of mixtures presents a satisfactory relation with the penetration of the corresponding binder blends.
- A satisfactory prediction of the mixtures behaviour was obtained by applying the SHStS transformation by using the limited DSR measurements on binders. 2S2P1D model was used in order to better

highlight the efficiency of the prediction. Although the experimental results on binders are limited, it was observed that the obtained prediction of the mixture is well fitted on the 2S2P1D model which was calibrated only on the experimental measurements on mixtures.

- The influence of the rejuvenator on $|E^*|$ at 15°C and 10 Hz values was observed by the fact that complex modulus values are decreasing with the increase of the rejuvenator content for the same amount of RAP material within the mass of the mixture. Considering the normalized $|E^*|$ values it could be observed that the mixtures produced with 0.4% rejuvenator present close $|E^*|$ values to the one obtained for the conventional mixture. The values of $|E^*|$ at 15°C and 10Hz for the mixtures produced with the same amount of rejuvenator by mass of the bituminous mixtures show a linear relation with the RAP material content. A satisfactory relation between $|E^*|$ values at 15°C and 10 Hz was obtained for the mixtures and the penetration values of the corresponding binder blends.
- The norm of complex modulus at 15ºC and 10 Hz of the bituminous mixtures from Campaign 2 were simulated from their corresponding binder blends behaviour and with the three SHStS constants (E_0, E_{00} and α values). A good correlation between the experimental and simulated results of the norm of complex modulus at 15°C and 10Hz was obtained, proven by the satisfactory R^2 value of 0.981 and by the relative errors which are always lower than 5%.

Based on the possible use of RAP material and rejuvenator in new mixtures the third part of this study was focused on the evaluation of the potential environmental impact related to the production of one tonne of 12 types of bituminous mixtures containing different amounts of Reclaimed Asphalt Pavement (RAP) and Rejuvenator (Rej) and one HMA, used as a reference mixture. The analyses were made by considering an Environmental Impact software. All results are reported in Chapter 4. The following conclusions resulted from the analyses:

- The production process of the conventional HMA mixture leads to the highest environmental impact.
- The addition of RAP material leads to a clear decrease of the energy use and environmental impact. On the other side, when rejuvenators are used in this process, they can affect the energy balance and reduce the difference in environmental impact. However, the increase of the rejuvenator content corresponds to a small increase of the impact. A considerable impact was observed for the land use, due to the fact that the rejuvenator considered in this study is a mix of vegetal oils.
- When less than 25% of the considered RAP is used in the production of a new bituminous mixture, the characteristics of the final mix could be considered within the limits specified in the Romanian Standards for a bituminous mixture with a 16 mm maximum aggregate size. Therefore, the decrease of the environmental load is close to 20% for this solution compared to the conventional one.

- When high amounts of RAP are used in the production of a new bituminous mixture, rejuvenators should be used, too. Although the solution with 75% RAP (D.75.R.0) was considered to highlight the environmental impact potential of this 100% recyclable RAP material. A substantial decrease of the environmental impact as more than half of the conventional solution could be obtained.
- For the production process of bituminous mixtures containing RAP material and different amounts of rejuvenator, an increase of the environmental impact was observed with the increase of the rejuvenator content compared to those produced with RAP material only. However, this only represents approximately 1.5% of the environmental load increase per 0.2% rejuvenator content by the total mass of the final bituminous mixture.
- Based on the experimental work and on the results presented in Chapters 2 and 3, the mix design D.50.R.0.4/the corresponding binder blend (50/70 + 50% RAP + 10% Rej) presents a closer behaviour to the one of the conventional bituminous mixture/the corresponding fresh binder (50/70). The environmental impact for this solution (D.50.R.0.4) leads to a decrease of approximately 33-40% (depending on the analysed indicator/parameter) than the conventional HMA.

Several points of the study are worth further investigation. Therefore, as perspectives the following points could continue the work developed in the presented thesis:

- The proposed method (2nd approach) to estimate the conventional properties, LVE properties, steady shear viscosity, norm of complex shear modulus and critical temperatures of binder blends produced with RAP binder and rejuvenator, is promising but still needs validation on a larger number of different binders and rejuvenators.
- A future investigation should be carried out by performing DSR tests on a larger temperature and frequency ranges and also by performing an investigation at low temperature of the aged (RTFOT or PAV aging) binder blends. Also, a study of the linearity could be performed.
- Another important aspect that should be investigated is related to the relation between the composition in terms of chemical properties and microstructure and the 2S2P1D parameters of binder blends that are produced with RAP binder and rejuvenators. This could bring information on the chemical and thermomechanical effects of the rejuvenator on the long-term behaviour of binder blends.
- Different blending conditions should be taken into consideration in a future work in order to compare the estimated results with the experimental data.
- Regarding the study of the thermomechanical behaviour of mixtures produced with RAP material and rejuvenator, further research could be carried out on fatigue, rutting and thermal cracking in order to investigate the effect of the rejuvenator on these characteristics. Also, complex modulus tests could be investigated over a larger temperature and frequency ranges by performing tension-compression tests.
- Further analysis should be carried out on the relations of mechanical properties between binders and mixtures. In particular, correspondence between fatigue performances and rutting performances of mixtures and the corresponding binder properties could be investigated.

- An important point that worth investigation is the comparison between the behaviour and properties of corresponding binder blends, mastics, and mixtures. This research could lead to some interesting data regarding the self-healing of cracks and the recovery of the linear visco-elastic properties.
- Continuing the analyses on environmental impact for the solutions presented in this study, a Life Cycle Assessment could be made considering all the other processes excluded by the system boundaries in this study. Thus, the Life Cycle Costing (LCC) analysis could complete the LCA for mixtures produced with RAP material and rejuvenator by considering the local costs and materials.
- All conclusions that were drawn in this study are based on laboratory measurements and related analyses. Therefore, a validation with in-situ through observations regarding the performances of mixtures should be performed.

Bibliography

[1] Institutul Național de Statistică din România [National Institute of Statistics from Romania]. https://insse.ro/cms/ro/content/lungimea-căilor-de-transport-la-sfârşitul-anului-2019 (accessed Nov. 07, 2020).

[2] C.N.A.D.N.R. website, "H.G. 43/1997." http://www.cnadnr.ro/sites/default/files/pagini-statice/1 OG nr. 43_1997 privind regimul drumurilor.pdf (accessed Nov. 07, 2020).

[3] Wikipedia website. https://ro.wikipedia.org/wiki/Rețeaua_rutieră_din_România (accessed Nov. 07, 2020).

[4] Institutul Național de Statistică din România [National Institute of Statistics from Romania]. https://insse.ro/cms/ro.

[5] Wikipedia website. https://en.wikipedia.org/wiki/Roads_in_Romania.

[6] Master Planul General de Transport al Romaniei din 2016 [General Transport Master Plan of Romania 2016]. http://arf.gov.ro/web/wp-content/uploads/2020/04/Anexă-la-HG-666-2016.pdf (accessed Nov. 07, 2020).

[7] Ministerului Lucrărilor Publice, Dezvoltării și Administrației al României [Ministery of Public Works, Development and Administration of Romania website]: National program of local development from Romania. https://www.mlpda.ro/pages/programulnationaldezvoltarelocala (accessed Nov. 07, 2020).

[8] World Economic Forum, "The Global Competitiveness Report 2019." www.weforum.org/gcr (accessed Dec. 07, 2020).

[9] Programul Operațional de Transport (POT) 2021-2027 din România [Operational Transport Program (POT) 2021-2027 of Romania]. http://mfe.gov.ro/wp-content/uploads/2020/07/7809a76648585e195992ef0239798351.pdf (accessed Nov. 07, 2020).

[10] Wikipedia website. https://ro.wikipedia.org/wiki/Coridoare_pan-europene (accessed Dec. 07, 2020).

[11] J.-F. Corté and H. Di Benedetto, *Matériaux routiers bitumineux 1: Description et propriétés des constituants [Bituminous paving materials 1: Description and constituent properties]*. Paris: Hermes-Lavoisier, 2005.

[12] H. Di Benedetto and J.-F. Corté, *Matériaux routiers bitumineux 2: Constitution et propriétés thermomécaniques des mélanges [Bituminous paving materials 2: Constitution and thermomechanical properties of mixtures]*. Paris: Hermes-Lavoisier, 2005.

[13] G. Lucaci, I. Costescu, and F. Belc, *Construcţia drumurilor [Roads construction]*. Bucharest: Editura Tehnica, 2000.

[14] AND 605 - Mixturi asfaltice executate la cald. Conditii tehnice privind proiectarea, prepararea si punerea în operă [Hot Mix Asphalt. Technical conditions regarding design, production and implementation], 2016.

[15] SR EN 13043:2003 - Agregate pentru amestecuri bituminoase şi pentru finisarea suprafeţelor, utilizate la construcţia şoselelor, a aeroporturilor şi a altor zone cu trafic [Aggregates for bituminous mixtures and surface treatments for roads, airfields and other trafficked areas], p. 48, 2003.

[16] PIARC Website. https://www.piarc.org/en/activities/Road-Dictionary-

Terminology-Road-Transport/.
[17] SR EN 1426 - Bitum şi lianţi bituminoşi. Determinarea penetraţiei cu ac [Bitumen and bituminous binders - Determination of needle penetration], p. 15, 2015.
[18] SR EN 12591 - Bitum şi lianţi bituminoşi. Specificaţii pentru bitumuri rutiere [Bitumen and bituminous binders. Specifications for paving grade bitumens], p. 32, 2009.
[19] D. A. Anderson *et al.*, "Binder characterization and evaluation. Volume 3: Physical characterization (Strategic Highway Research Program A-369 Report)," Washington, DC: National Research Council, DC: National Research Council, 1994.
[20] M. Duriez, *Traité de matériaux de construction [Treatise on construction materials]*. Paris: Dunod, 1950.
[21] R. Franke and K. Ksaibati, A methodology for cost-benefit analysis of recycled asphalt pavement (RAP) in various highway applications, *Int. J. Pavement Eng.*, vol. 16, no. 7, pp. 660–666, Aug. 2015, doi: 10.1080/10298436.2014.943217.
[22] F. Hong and J. A. Prozzi, "Evaluation of recycled asphalt pavement using economic, environmental, and energy metrics based on long-term pavement performance sections," *Road Mater. Pavement Des.*, vol. 19, no. 8, pp. 1–16, Nov. 2018, doi: 10.1080/14680629.2017.1348306.
[23] Directive 2008/98/EC on waste.
[24] European Asphalt Pavement Association (EAPA), "Recommendations for Road Authorities to achieve circular economy through the re-use and recycling of asphalt. Technical Briefing," 2020.
[25] G. Mazzoni, E. Bocci, and F. Canestrari, "Influence of rejuvenators on bitumen ageing in hot recycled asphalt mixtures," *J. Traffic Transp. Eng. (English Ed.*, vol. 5, no. 3, pp. 157–168, 2018, doi: https://doi.org/10.1016/j.jtte.2018.01.001.
[26] F. Yin, F. Kaseer, E. Arámbula-Mercado, and A. Epps Martin, "Characterising the long-term rejuvenating effectiveness of recycling agents on asphalt blends and mixtures with high RAP and RAS contents," *Road Mater. Pavement Des.*, vol. 18, no. sup4, pp. 273–292, Nov. 2017, doi: 10.1080/14680629.2017.1389074.
[27] N. Tapsoba, C. Sauzéat, H. Di Benedetto, H. Baaj, and M. Ech, "Behaviour of asphalt mixtures containing reclaimed asphalt pavement and asphalt shingle," *Road Mater. Pavement Des.*, vol. 15, no. 2, pp. 330–347, Apr. 2014, doi: 10.1080/14680629.2013.871091.
[28] K. H. Moon, A. C. Falchetto, M. Marasteanu, and M. Turos, "Using recycled asphalt materials as an alternative material source in asphalt pavements," *KSCE J. Civ. Eng.*, vol. 18, no. 1, pp. 149–159, 2014, doi: 10.1007/s12205-014-0211-1.
[29] Y. A.-S. Sun Yiren A4 - Wang, Weiying A4 - Chen, Jingyun, Y. Sun, W. Wang, J. Chen, and Y. A.-S. Sun Yiren A4 - Wang, Weiying A4 - Chen, Jingyun, "Investigating impacts of warm-mix asphalt technologies and high reclaimed asphalt pavement binder content on rutting and fatigue performance of asphalt binder through MSCR and LAS tests," *J. Clean. Prod.*, vol. 219, pp. 879–893, 2019, doi: https://doi.org/10.1016/j.jclepro.2019.02.131.
[30] W. Song, B. Huang, and X. Shu, "Influence of warm-mix asphalt technology and rejuvenator on performance of asphalt mixtures containing 50%

reclaimed asphalt pavement," *J. Clean. Prod.*, vol. 192, pp. 191–198, Aug. 2018, doi: https://doi.org/10.1016/j.jclepro.2018.04.269.
[31] Technical report NAPA-Survey, 9th Annual Asphalt Pavement Industry, 2019.
[32] European Environment Agency. https://www.eea.europa.eu/data-and-maps/daviz/mineral-waste-from-construction-and#tab-googlechartid_chart_13 (accessed Oct. 05, 2020).
[33] A. Behnood, "Application of rejuvenators to improve the rheological and mechanical properties of asphalt binders and mixtures: A review," *J. Clean. Prod.*, vol. 231, pp. 171–182, Dec. 2019, doi: 10.1016/j.jclepro.2019.05.209.
[34] L. P. Ingrassia, X. Lu, G. Ferrotti, and F. Canestrari, "Renewable materials in bituminous binders and mixtures: Speculative pretext or reliable opportunity?," *Resour. Conserv. Recycl.*, vol. 144, pp. 209–222, 2019, doi: https://doi.org/10.1016/j.resconrec.2019.01.034.
[35] F. Kaseer *et al.*, "Strategies for Producing Asphalt Mixtures with High RAP Content," *J. Mater. Civ. Eng.*, vol. 31, no. 11, p. 5019002, Nov. 2019, doi: 10.1061/(ASCE)MT.1943-5533.0002910.
[36] V. Antunes, A. Freire, and J. Neves, "A review on the effect of RAP recycling on bituminous mixtures properties and the viability of multi-recycling," *Constr. Build. Mater.*, vol. 211, pp. 453–469, Mar. 2019, doi: 10.1016/j.conbuildmat.2019.03.258.
[37] A. Grilli, M. I. Gnisci, and M. Bocci, "Effect of ageing process on bitumen and rejuvenated bitumen," *Constr. Build. Mater.*, vol. 136, pp. 474–481, Apr. 2017, doi: 10.1016/J.CONBUILDMAT.2017.01.027.
[38] N. Saboo and P. Kumar, "Use of flow properties for rheological modeling of bitumen," *Int. J. Pavement Res. Technol.*, vol. 9, no. 1, pp. 63–72, Jan. 2016, doi: https://doi.org/10.1016/j.ijprt.2016.01.005.
[39] W. S. Mogawer, E. H. Fini, A. J. Austerman, A. Booshehrian, and B. Zada, "Performance characteristics of high reclaimed asphalt pavement containing bio-modifier," *Road Mater. Pavement Des.*, vol. 17, no. 3, pp. 753–767, Jul. 2016, doi: 10.1080/14680629.2015.1096820.
[40] G. Liu, E. Nielsen, J. Komacka, G. Leegwater, and M. van de Ven, "Influence of soft bitumens on the chemical and rheological properties of reclaimed polymer-modified binders from the 'old' surface-layer asphalt," *Constr. Build. Mater.*, vol. 79, pp. 129–135, Mar. 2015, doi: https://doi.org/10.1016/j.conbuildmat.2015.01.002.
[41] M. Zaumanis, R. B. Mallick, and R. Frank, "Determining optimum rejuvenator dose for asphalt recycling based on Superpave performance grade specifications," *Constr. Build. Mater.*, vol. 69, pp. 159–166, Oct. 2014, doi: https://doi.org/10.1016/j.conbuildmat.2014.07.035.
[42] X. Yu, M. Zaumanis, S. Santos, L. D. Poulikakos, S. dos Santos, and L. D. Poulikakos, "Rheological, microscopic, and chemical characterization of the rejuvenating effect on asphalt binders," *Fuel*, vol. 135, pp. 162–171, Jul. 2014, doi: 10.1016/j.fuel.2014.06.038.
[43] J.-S. Chen, C. Huang, P. Chu, and K. Lin, "Engineering characterization of recycled asphalt concrete and aged bitumen mixed recycling agent," *J. Mater. Sci.*, vol. 42, pp. 9867–9876, Dec. 2007, doi: 10.1007/s10853-007-1713-8.
[44] E. Y. Hajj, M. I. Souliman, M. Z. Alavi, and L. G. L. Salazar, "Influence of Hydrogreen Bioasphalt on Viscoelastic Properties of Reclaimed Asphalt Mixtures," *Transp. Res. Rec.*, vol. 2371, no. 1, pp. 13–22, Jan. 2013, doi:

10.3141/2371-02.
[45] S. Junan, A. Serji, and A. M. Jennifer, "Effects of Rejuvenating Agents on Superpave Mixtures Containing Reclaimed Asphalt Pavement," *J. Mater. Civ. Eng.*, vol. 19, no. 5, pp. 376–384, May 2007, doi: 10.1061/(ASCE)0899-1561(2007)19:5(376).
[46] H. K. Bailey and S. E. Zoorob, "The use of vegetable oil in asphalt mixtures, in laboratory and field," 2012.
[47] S. Mangiafico, C. Sauzéat, H. Di Benedetto, S. Pouget, F. Olard, and L. Planque, "Complex modulus and fatigue performances of bituminous mixtures with reclaimed asphalt pavement and a recycling agent of vegetable origin," *Road Mater. Pavement Des.*, vol. 18, no. 2, pp. 315–330, Mar. 2017, doi: 10.1080/14680629.2016.1213509.
[48] W. S. Mogawer, A. Booshehrian, S. Vahidi, and A. J. Austerman, "Evaluating the effect of rejuvenators on the degree of blending and performance of high RAP, RAS, and RAP/RAS mixtures," *Road Mater. Pavement Des.*, vol. 14, no. sup2, pp. 193–213, Aug. 2013, doi: 10.1080/14680629.2013.812836.
[49] L. Noferini, A. Simone, C. Sangiorgi, and F. Mazzotta, "Investigation on performances of asphalt mixtures made with Reclaimed Asphalt Pavement: Effects of interaction between virgin and RAP bitumen," *Int. J. Pavement Res. Technol.*, vol. 10, no. 4, pp. 322–332, Jul. 2017, doi: https://doi.org/10.1016/j.ijprt.2017.03.011.
[50] D. Oldham, A. Hung, M. M. Parast, and E. H. Fini, "Investigating bitumen rejuvenation mechanisms using a coupled rheometry-morphology characterization approach," *Constr. Build. Mater.*, vol. 159, pp. 37–45, Jan. 2018, doi: https://doi.org/10.1016/j.conbuildmat.2017.10.113.
[51] SR EN 13108-8 - Mixturi asfaltice. Specificaţii de material. Partea 8: Asfalt recuperat [Bituminous mixtures. Material specifications. Reclaimed asphalt], p. 14, 2016.
[52] SR EN 12697-42 - Mixturi asfaltice. Metode de încercare pentru mixturi asfaltice preparate la cald. Partea 42: Cantitatea de materiale străine în asfaltul recuperat [Bituminous mixtures. Test methods for hot mix asphalt. Amount of foreign matter in reclai, p. 22, 2013.
[53] SR EN 12697-3:2013+A1:2019 Mixturi asfaltice. Metode de încercare. Partea 3: Recuperarea bitumului: Evaporator rotativ [Bituminous mixtures. Test methods. Bitumen recovery: Rotary evaporato], p. 14, 2019.
[54] SR EN 12697-4 - Mixturi asfaltice. Metode de încercare pentru mixturi asfaltice preparate la cald. Partea 4: Recuperarea bitumului: Coloană de fracţionare [Bituminous mixtures. Test methods. Bitumen recovery: Fractionating column], p. 18, 2015.
[55] SR EN 12697-1 - Mixturi asfaltice. Metode de încercare pentru mixturi asfaltice preparate la cald. Partea 1: Conţinut de liant solubil [Bituminous mixtures. Test methods. Soluble binder content], p. 50, 2012.
[56] SR EN 1427 - Bitum şi lianţi bituminoşi. Determinarea punctului de înmuiere. Metoda cu inel şi bilă [Bitumen and bituminous binders. Determination of the softening point. Ring and Ball method], p. 19, 2015.
[57] SR EN 12596 - Bitum şi lianţi bituminoşi. Determinarea viscozităţii dinamice cu viscozimetrul capilar sub vid [Bitumen and bituminous binders. Determination of dynamic viscosity by vacuum capillary], p. 22, 2015.
[58] SR EN 12697-2+A1 - Mixturi asfaltice. Metode de încercare. Partea 2: Determinarea granulozității [Bituminous mixtures. Test methods. Determination of particle size distribution], p. 9, 2019.

[59] A.R.R.A., "Hot In-Place Recycling, Presented by the Hot In-Place Recycling Technical Committee," 1996.
[60] P. Costel and E. Plescan, "ASPHALT PAVEMENT RECYCLING," *Bull. Transilv. Univ. Brasov*, vol. 8(57), p. 256, Nov. 2015.
[61] AND 554 - Normativ privind întreținerea drumurilor publice [Norm regarding the maintenance of public roads], 2002.
[62] A. Copeland, "Report No. FHWA-HRT-11-021: Reclaimed asphalt pavement in asphalt mixtures: state of the practice," 2011.
[63] A. Eddhahak-Ouni *et al.*, "Experimental investigation of the homogeneity of the blended binder of a high rate recycled asphalt," *Road Mater. Pavement Des.*, vol. 13, no. 3, pp. 566–575, Sep. 2012, doi: 10.1080/14680629.2012.700269.
[64] E. Y. Hajj, P. E. Sebaaly, and R. Shrestha, "Laboratory Evaluation of Mixes Containing Recycled Asphalt Pavement (RAP)," *Road Mater. Pavement Des.*, vol. 10, no. 3, pp. 495–517, Jan. 2009, doi: 10.1080/14680629.2009.9690211.
[65] R. C. Jerry, "Recycled asphalt pavement (RAP) preparation system," 2005.
[66] B. Visintine, N. P. Khosla, and A. Tayebali, "Effects of higher percentage of recycled asphalt pavement on pavement performance," *Road Mater. Pavement Des.*, vol. 14, no. 2, pp. 432–437, Jun. 2013, doi: 10.1080/14680629.2013.779310.
[67] G. Valdés, F. Pérez-Jiménez, R. Miró, A. Martínez, and R. Botella, "Experimental study of recycled asphalt mixtures with high percentages of reclaimed asphalt pavement (RAP)," *Constr. Build. Mater.*, vol. 25, no. 3, pp. 1289–1297, 2011, doi: https://doi.org/10.1016/j.conbuildmat.2010.09.016.
[68] J. Sias Daniel, N. Gibson, S. Tarbox, A. Copeland, and A. Andriescu, "Effect of long-term ageing on RAP mixtures: laboratory evaluation of plant-produced mixtures," *Road Mater. Pavement Des.*, vol. 14, no. sup2, pp. 173–192, Aug. 2013, doi: 10.1080/14680629.2013.812840.
[69] D. Swiertz, E. Mahmoud, and H. U. Bahia, "Estimating the Effect of Recycled Asphalt Pavements and Asphalt Shingles on Fresh Binder, Low-Temperature Properties without Extraction and Recovery," *Transp. Res. Rec.*, vol. 2208, no. 1, pp. 48–55, Jan. 2011, doi: 10.3141/2208-07.
[70] R. S. McDaniel, A. Shah, G. A. Huber, and A. Copeland, "Effects of reclaimed asphalt pavement content and virgin binder grade on properties of plant produced mixtures," *Road Mater. Pavement Des.*, vol. 13, no. sup1, pp. 161–182, Jun. 2012, doi: 10.1080/14680629.2012.657066.
[71] S. Mangiafico, "Linear viscoelastic properties and fatigue of bituminous mixtures produced with Reclaimed Asphalt Pavement and corresponding binder blends.," University of Lyon, 2014.
[72] A. R. & R. A. (U.S.) and U. S. F. H. Administration, "Basic Asphalt Recycling Manual," 2001.
[73] VAASPHALT Website. https://vaasphalt.org/pavement-recycling/ (accessed Nov. 07, 2020).
[74] ARRA Website. https://www.arra.org/ (accessed Sep. 03, 2020).
[75] NE-026-2004 - Normativul privind reciclarea la cald a îmbrăcăminților rutiere bituminoase [Romanian Norm hot recycling of bituminous road pavements], 2004.
[76] DD 509-2003 - Normativ privind reciclarea mixturilor asfaltice la cald, în stații fixe [Romanaian Norm regarding the recycling of hot asphalt mixtures, in fixed stations], 2003.

[77] AND 532-1997 - Normativ privind reciclarea la rece a îmbracăminţilor rutiere [Romanian Norm - cold recycling of road surface layers], 1997.
[78] X. Li, M. O. Marasteanu, R. C. Williams, and T. R. Clyne, "Effect of Reclaimed Asphalt Pavement (Proportion and Type) and Binder Grade on Asphalt Mixtures," *Transp. Res. Rec.*, vol. 2051, no. 1, pp. 90–97, Jan. 2008, doi: 10.3141/2051-11.
[79] R. MCDANIEL and R. M. ANDERSON, "NCHRP Report 452 - Recommended Use of Reclaimed Asphalt Pavement in the Superpave Mix Design Method: Technician's Manual," WASHINGTON, D.C, D.C, 2001.
[80] B. Huang, Z. Zhang, W. Kingery, and G. Zuo, "Fatigue crack characteristics of HMA mixtures containing RAP," in *Fifth International RILEM Conference on Reflective Cracking in Pavements*, 2004, pp. 631–638.
[81] V. Loise *et al.*, "A Review on Bitumen Rejuvenation: Mechanisms, Materials, Methods and Perspectives," *Appl. Sci.*, vol. 9, no. 20, p. 4316, Oct. 2019, doi: 10.3390/app9204316.
[82] R. L. Terrel and J. A. Epps, "USING ADDITIVES AND MODIFIERS IN HOT MIX ASPHALT," 1989.
[83] R. and T. A. of Canada, "Study of Asphalt Cement Additives and Extenders," Ontario, 1983.
[84] R. Willis and N. H. Tran, "LEED GA REJUVENATORS: Bring Life Back to Aging Asphalt Binder," *Asphalt Pavement Magazine*, pp. 36–41, 2015.
[85] NCAT, "NCAT Researchers Explore Multiple Uses of Rejuvenators," 2014.
[86] M. Elkashef, J. Podolsky, R. C. Williams, and E. W. Cochran, "Introducing a soybean oil-derived material as a potential rejuvenator of asphalt through rheology, mix characterisation and Fourier Transform Infrared analysis," *Road Mater. Pavement Des.*, vol. 19, no. 8, pp. 1750–1770, Nov. 2018, doi: 10.1080/14680629.2017.1345781.
[87] A. Grilli, L. Iori, and L. Porot, "Effect of bio-based additives on bitumen properties," *Road Mater. Pavement Des.*, vol. 20, no. 8, pp. 1864–1879, Nov. 2019, doi: 10.1080/14680629.2018.1474790.
[88] Z. Zhou, X. Gu, Q. Dong, F. Ni, and Y. Jiang, "Low- and intermediate-temperature behaviour of polymer-modified asphalt binders, mastics, fine aggregate matrices, and mixtures with Reclaimed Asphalt Pavement material," *Road Mater. Pavement Des.*, vol. 21, no. 7, pp. 1872–1901, Oct. 2020, doi: 10.1080/14680629.2019.1574233.
[89] P. Karki and F. Zhou, "Effect of Rejuvenators on Rheological, Chemical, and Aging Properties of Asphalt Binders Containing Recycled Binders," *Transp. Res. Rec.*, vol. 2574, no. 1, pp. 74–82, Jan. 2016, doi: 10.3141/2574-08.
[90] G. Nsengiyumva, H. F. Haghshenas, Y.-R. Kim, and S. R. Kommidi, "Mechanical-Chemical Characterization of the Effects of Type, Dosage, and Treatment Methods of Rejuvenators in Aged Bituminous Materials," *Transp. Res. Rec.*, vol. 2674, no. 3, pp. 126–138, Feb. 2020, doi: 10.1177/0361198120909110.
[91] I. Menapace *et al.*, "Effect of recycling agents in recycled asphalt binders observed with microstructural and rheological tests," *Constr. Build. Mater.*, vol. 158, pp. 61–74, 2018, doi: https://doi.org/10.1016/j.conbuildmat.2017.10.017.
[92] M. Radenberg, S. Boetcher, and N. Sedaghat, "Effect and efficiency of rejuvenators on aged asphalt binder – German Experiences," 2016.
[93] C. Somé, *Rheological behavior of vegetable oil-modified asphaltite binders and mixes*. 2016.

[94] A. J. del Barco Carrión, D. Lo Presti, S. Pouget, G. Airey, and E. Chailleux, "Linear viscoelastic properties of high reclaimed asphalt content mixes with biobinders," *Road Mater. Pavement Des.*, vol. 18, no. sup2, pp. 241–251, May 2017, doi: 10.1080/14680629.2017.1304253.
[95] Z. Lei, H. Bahia, T. Yi-qiu, and C. Ling, "Effects of refined waste and bio-based oil modifiers on rheological properties of asphalt binders," *Constr. Build. Mater.*, vol. 148, pp. 504–511, 2017, doi: https://doi.org/10.1016/j.conbuildmat.2017.05.101.
[96] J. B. Król, K. J. Kowalski, Ł. Niczke, and P. Radziszewski, "Effect of bitumen fluxing using a bio-origin additive," *Constr. Build. Mater.*, vol. 114, pp. 194–203, 2016, doi: https://doi.org/10.1016/j.conbuildmat.2016.03.086.
[97] H. Zhu, G. Xu, M. Gong, and J. Yang, "Recycling long-term-aged asphalts using bio-binder/plasticizer-based rejuvenator," *Constr. Build. Mater.*, vol. 147, pp. 117–129, Aug. 2017, doi: 10.1016/j.conbuildmat.2017.04.066.
[98] J. Jie *et al.*, "Effectiveness of Vegetable Oils as Rejuvenators for Aged Asphalt Binders," *J. Mater. Civ. Eng.*, vol. 29, no. 3, p. D4016003, Mar. 2017, doi: 10.1061/(ASCE)MT.1943-5533.0001769.
[99] L. W. Corbett, "Reaction Variables in the Air Blowing of Asphalt," *Ind. Eng. Chem. Process Des. Dev.*, vol. 14, no. 2, pp. 181–187, Apr. 1975, doi: 10.1021/i260054a015.
[100] J. C. Petersen, "Chapter 14 Chemical Composition of Asphalt as Related to Asphalt Durability," in *Asphaltenes and Asphalts, 2*, vol. 40, T. F. Yen and G. V. B. T.-D. in P. S. Chilingarian, Eds. Elsevier, 2000, pp. 363–399.
[101] H. D. Lee, A. Mokhtari, and C. Williams, "TR 693- Development of Quality Standards for Inclusion of High Recycled Asphalt Pavement Content in Asphalt Mixtures – Phase III," 2018.
[102] J. Shen and Y. Ohne, "Determining Rejuvenator Content for Recycling Reclaimed Asphalt Pavement by SHRP Binder Specifications," *Int. J. Pavement Eng.*, vol. 3, no. 4, pp. 261–268, Dec. 2002, doi: 10.1080/1029843021000083685.
[103] A. Bonicelli, P. Calvi, G. Martinez-Arguelles, L. Fuentes, and F. Giustozzi, "Experimental study on the use of rejuvenators and plastomeric polymers for improving durability of high RAP content asphalt mixtures," *Constr. Build. Mater.*, vol. 155, 2017, doi: 10.1016/j.conbuildmat.2017.08.013.
[104] P. Kriz *et al.*, "Blending and diffusion of reclaimed asphalt pavement and virgin asphalt binders," *Road Mater. Pavement Des.*, vol. 15, no. sup1, pp. 78–112, Jun. 2014, doi: 10.1080/14680629.2014.927411.
[105] J. W. H. Oliver, "Diffusion of Oils in Asphalts," *Prod. R&D*, vol. 13, no. 1, pp. 65–70, Mar. 1974, doi: 10.1021/i360049a013.
[106] S. H. Carpenter and J. R. Wolosick, "Modifier influence in the characterization of hotmix recycled material," in *Transportation Research Record*, 1980, no. 777, pp. 15–22, [Online]. Available: http://onlinepubs.trb.org/onlinepubs/trr/1980/777/777-003.pdf.
[107] M. Zaumanis, L. D. Poulikakos, and M. N. Partl, "Performance-based design of asphalt mixtures and review of key parameters," *Mater. Des.*, vol. 141, pp. 185–201, 2018, doi: https://doi.org/10.1016/j.matdes.2017.12.035.
[108] D. Kuang, Z. Feng, J. Yu, X. Chen, and B. Zhou, "A new approach for evaluating rejuvenator diffusing into aged bitumen," *J. Wuhan Univ. Technol. Sci. Ed.*, vol. 26, no. 1, pp. 43–46, 2011, doi: 10.1007/s11595-011-0164-x.
[109] C. R. Dugan, C. R. Sumter, S. Rani, S. A. Ali, E. A. O'Rear, and M. Zaman, "Rheology of Virgin Asphalt Binder Combined with High Percentages of RAP

Binder Rejuvenated with Waste Vegetable Oil," *ACS Omega*, vol. 5, no. 26, pp. 15791–15798, Jul. 2020, doi: 10.1021/acsomega.0c00377.
[110] S. Rajib, M. R. S., K. Bishal, B. Anthony, and G. D. S., "Effect of Bio-Oils on Binder and Mix Properties with High RAP Binder Content," *J. Mater. Civ. Eng.*, vol. 32, no. 3, p. 4020007, Mar. 2020, doi: 10.1061/(ASCE)MT.1943-5533.0003057.
[111] T. Bennert, C. Ericson, and D. Pezeshki, "Rejuvenating Agents with RAP in Hot Mix Asphalt (HMA)," 2015. [Online]. Available: https://www.nj.gov/transportation/business/research/reports/FHWA-NJ-2015-008.pdf.
[112] H. F. Haghshenas, H. Nabizadeh, Y.-R. Kim, and K. Santosh, "Research on High-RAP Asphalt Mixtures with Rejuvenators and WMA Additives," 2016. [Online]. Available: https://rosap.ntl.bts.gov/view/dot/31604.
[113] M. Zaumanis, R. B. Mallick, L. Poulikakos, and R. Frank, "Influence of six rejuvenators on the performance properties of Reclaimed Asphalt Pavement (RAP) binder and 100% recycled asphalt mixtures," *Constr. Build. Mater.*, vol. 71, pp. 538–550, 2014, doi: https://doi.org/10.1016/j.conbuildmat.2014.08.073.
[114] F. Zhou, S. Im, D. Morton, R. Lee, S. Hu, and T. Scullion, "Rejuvenator Characterization, Blend Characteristics, and Proposed Mix Design Method," *J. Assoc. Asph. Paving Technol.*, vol. 84, pp. 675–704, 2015.
[115] A. Blanchette, S. T. Lee, and T. Wood, "Asphalt Mix Rejuvenators Synthesis," 2020. [Online]. Available: http://www.dot.state.mn.us/research/reports/2020/NRRA202002.pdf.
[116] N. H. Tran, A. Taylor, and R. Willis, "NCAT Report 12-05 - Effect of rejuvenator on performance properties of HMA mixtures with high RAP and RAS contents," 2012. [Online]. Available: http://www.ncat.us/files/reports/2012/rep12-05.pdf.
[117] S. Im, F. Zhou, R. Lee, and T. Scullion, "Impacts of rejuvenators on performance and engineering properties of asphalt mixtures containing recycled materials," *Constr. Build. Mater.*, vol. 53, pp. 596–603, 2014, doi: https://doi.org/10.1016/j.conbuildmat.2013.12.025.
[118] P. T. Marc, "Conceperea și realizarea unor structuri rutiere cu performanțe ridicate [Design and construction of high-performance road structures]," University Politehnica Timisoara, 2011.
[119] Y. H. Huang, *Pavement analysis and design*, 2nd ed. 2004.
[120] H. Di Benedetto, "Modélisation: écart entre état des connaissances et applications. Paper presented at Journée technique LAVOC, Lausanne," 1998.
[121] F. Olard, H. Di Benedetto, A. Dony, and J.-C. Vaniscote, "Properties of bituminous mixtures at low temperatures and relations with binder characteristics," *Mater. Struct.*, vol. 38, no. 1, pp. 121–126, 2005, doi: 10.1007/BF02480584.
[122] H. Di Benedetto, D. Brice, and S. Cédric, "Three-Dimensional Linear Behavior of Bituminous Materials: Experiments and Modeling," *Int. J. Geomech.*, vol. 7, no. 2, pp. 149–157, Mar. 2007, doi: 10.1061/(ASCE)1532-3641(2007)7:2(149).
[123] S. N. Sahasrabudhe, V. Rodriguez-Martinez, M. O'Meara, and B. E. Farkas, "Density, viscosity, and surface tension of five vegetable oils at elevated temperatures: Measurement and modeling," *Int. J. Food Prop.*, vol. 20, no. sup2, pp. 1965–1981, Dec. 2017, doi: 10.1080/10942912.2017.1360905.
[124] M. R. Nivitha and J. Murali Krishnan, "Rheological characterisation of

unmodified and modified bitumen in the 90–200°C temperature regime," *Road Mater. Pavement Des.*, vol. 21, no. 5, pp. 1341–1358, Jul. 2020, doi: 10.1080/14680629.2018.1552890.
[125] T. Nierat, S. Musameh, and I. Ashqer, "Temperature-dependence of olive oil viscosity," *Mater. Sci.*, vol. 11, pp. 233–238, Jun. 2014.
[126] J. Salencon, *Viscoélasticité pour le calcul des structures*. 2009.
[127] J. D. Ferry, *Viscoelastic Properties of Polymers*, 3rd editio. New York: NY: John Wiley & Sons, 1980.
[128] A. Forton, H. Di Benedetto, S. Mangiafico, C. Sauzéat, and P. Marc, "Rheological properties of fresh and RAP bitumen blends with or without regenerating agent," in *Bituminous Mixtures and Pavements VII- Proceedings of the 7th International Conference on Bituminous Mixtures and Pavements, ICONFBMP 2019*, 2019, pp. 13–19, doi: 10.1201/9781351063265-2.
[129] F. Olard and H. Di Benedetto, "General '2S2P1D' Model and Relation Between the Linear Viscoelastic Behaviours of Bituminous Binders and Mixes," *Road Mater. Pavement Des.*, vol. 4, no. 2, pp. 185–224, Jan. 2003, doi: 10.1080/14680629.2003.9689946.
[130] H. Di Benedetto, F. Olard, C. Sauzéat, and B. Delaporte, "Linear viscoelastic behaviour of bituminous materials: From binders to mixes," *Road Mater. Pavement Des.*, vol. 5, no. sup1, pp. 163–202, Jan. 2004, doi: 10.1080/14680629.2004.9689992.
[131] F. M. Boza and C. Gallegos, "Encyclopedia of Life Support Systems (EOLSS) HIGH PRESSURE RHEOLOGY.," 2011.
[132] J. C. MAXWELL, "On the Dynamical Theory of Gases," in *The Kinetic Theory of Gases*, vol. Volume 1, PUBLISHED BY IMPERIAL COLLEGE PRESS AND DISTRIBUTED BY WORLD SCIENTIFIC PUBLISHING CO., 2003, pp. 197–261.
[133] O. E. Meyer, "Theorie der elastischen Nachwirkung," *Ann. Phys.*, vol. 227, no. 1, pp. 108–119, Jan. 1874, doi: https://doi.org/10.1002/andp.18742270106.
[134] O. E. Meyer, "Ueber die elastische Nachwirkung," *Ann. Phys.*, vol. 240, no. 6, pp. 249–267, Jan. 1878, doi: https://doi.org/10.1002/andp.18782400607.
[135] W. Thomson, "IV. On the elasticity and viscosity of metals," *Proc. R. Soc. London*, vol. 14, pp. 289–297, Jan. 1865, doi: 10.1098/rspl.1865.0052.
[136] W. Thomson, "XXI. Elements of a mathematical theory of elasticity," *Philos. Trans. R. Soc. London*, vol. 146, pp. 481–498, Jan. 1856, doi: 10.1098/rstl.1856.0022.
[137] W. Voigt, "Ueber innere Reibung fester Körper, insbesondere der Metalle," *Ann. Phys.*, vol. 283, no. 12, pp. 671–693, Jan. 1892, doi: https://doi.org/10.1002/andp.18922831210.
[138] C. Huet, "Étude par une méthode d'impédance du comportement viscoélastique des matériaux hydrocarbonés [Study of viscoelastic behavior of hydrocarbon-treated materials by means of an impedance method]," Université de Paris, Paris, 1963.
[139] G. Sayegh, "Variations des modules de quelques bitumes purs et enrobés bitumineux [Modulus variations of some pure bitumens and bituminous mixtures]," Université de Paris, Paris, 1965.
[140] F. Olard, "Comportement thermomécanique des enrobés bitumineux à basses temperatures: Relations entre les propriétés du liant et de l'enrobé [Thermomechanical behavior of bituminous mixtures at low temperatures: Relations between binder and mixture properties]," ENTPE-INSA Lyon, Lyon, 2003.

[141] D. W. Christensen and D. A. Anderson, "INTERPRETATION OF DYNAMIC MECHANICAL TEST DATA FOR PAVING GRADE ASPHALT CEMENTS (WITH DISCUSSION)," *J. Assoc. Asph. Paving Technol.*, vol. 61, 1992.
[142] M. O. Marasteanu, "Inter-conversions of the linear viscoelastic functions used for the rheological characterization of asphalt binders," Pennsylvania State University, State College, PA, 1999.
[143] S. Havriliak and S. Negami, "A complex plane analysis of α-dispersions in some polymer systems," *J. Polym. Sci. Part C Polym. Symp.*, vol. 14, no. 1, pp. 99–117, Jan. 1966, doi: https://doi.org/10.1002/polc.5070140111.
[144] A. Gudmarsson, N. Ryden, H. Di Benedetto, C. Sauzéat, N. Tapsoba, and B. Birgisson, "Comparing Linear Viscoelastic Properties of Asphalt Concrete Measured by Laboratory Seismic and Tension–Compression Tests," *J. Nondestruct. Eval.*, vol. 33, no. 4, pp. 571–582, 2014, doi: 10.1007/s10921-014-0253-9.
[145] D. Perraton *et al.*, "3Dim experimental investigation of linear viscoelastic properties of bituminous mixtures," *Mater. Struct.*, vol. 49, no. 11, pp. 4813–4829, 2016, doi: 10.1617/s11527-016-0827-3.
[146] SR EN 13108-1 - Mixturi asfaltice. Specificaţii pentru materiale. Partea 1: Betoane asfaltice [Bituminous mixtures - Material specifications - Part 1: Asphalt Concrete], p. 49, 2016.
[147] I. L. Al-Qadi, S.-H. Yang, S. H. Dessouky, and J.-F. Masson, "Development of crack sealant bending beam rheometer (CSBBR) testing to characterize hot-poured bituminous crack sealant at low temperature," *J. Assoc. Asph. Paving Technol.*, vol. 76, pp. 85–121, 2007.
[148] P. UGE, G. GEST, A. GRAVOIS, and F. BONNAURE, "Nouvelle méthode de calcul du module complexe des mélanges bitumineux [New calculation method of complex modulus of bituminous mixtures]," 1977.
[149] D. W. Jr, T. Pellinen, and R. F. Bonaquist, "Hirsch model for estimating the modulus of asphalt concrete," *Asph. Paving Technol. Assoc. Asph. Paving Technol. Tech. Sess.*, vol. 72, pp. 97–121, Jan. 2003.
[150] M. W. Witczak and O. A. Fonseca, "Revised Predictive Model for Dynamic (Complex) Modulus of Asphalt Mixtures," *Transp. Res. Rec.*, vol. 1540, no. 1, pp. 15–23, Jan. 1996, doi: 10.1177/0361198196154000103.
[151] S. Pouget, "Influence des propriétés élastiques ou viscoélastiques des revêtements sur le comportement des ponts à dalle orthotrope [Influence of elastic or viscoelastic properties of coatings on the behavior of orthotropic deck bridges]," ENTPE, Lyon, 2011.
[152] S. Pouget, C. Sauzéat, H. Di Benedetto, and F. Olard, "From the Behavior of Constituent Materials to the Calculation and Design of Orthotropic Bridge Structures," *Road Mater. Pavement Des.*, vol. 11, no. sup1, pp. 111–144, Jan. 2010, doi: 10.1080/14680629.2010.9690329.
[153] S. Pouget, C. Sauzéat, H. Di Benedetto, and F. Olard, "Modeling of viscous bituminous wearing course materials on orthotropic steel deck," *Mater. Struct.*, vol. 45, no. 7, pp. 1115–1125, 2012, doi: 10.1617/s11527-011-9820-z.
[154] J. Bonnot, "Essais mécaniques pratiques de formulation et de contrôle des enrobés bitumineux rapport général," pp. 79–90, 1984.
[155] H. Di Benedetto, "Nouvelle approche du comportement des enrobés bitumineux : résultats expérimentaux et formulation rhéologique. Mechanical Tests for Bituminous Mixes, Characterization, Design and Quality Control," 1990.

[156] WCED, "Report of the World Commission on Environment and Development: Our Common Future," Berlin, 1987. [Online]. Available: https://sustainabledevelopment.un.org/content/documents/5987our-common-future.pdf.
[157] ESCAP, "ESCAP report - Chapter 1 The challenge: sustainable road transport." [Online]. Available: https://www.unescap.org/sites/default/files/roadprice_ch1.pdf.
[158] N. Ademovic, *SUSTAINABLE DEVELOPMENT AND CONCRETE BRIDGES*. 2018.
[159] National sustainable development strategy Romania 2013-2020-2030. Government of Romania. Ministry of environment and sustainable development. United Nations development program national centre for sustainable development, Bucharest, 2008.
[160] Sustainable Transport Policies 2000. EUROPEAN CONFERENCE OF MINISTERS OF TRANSPORT," 2000. [Online]. Available: https://www.itf-oecd.org/sites/default/files/docs/00sustain_0.pdf.
[161] European Asphalt Pavement Association (EAPA), "Asphalt in figures 2017," 2017. [Online]. Available: https://eapa.org/wp-content/uploads/2019/08/Asphalt-in-figures_2017.pdf.
[162] Industrial minerals. Your world is made of them. https://www.ima-europe.eu/eu-policy/environment/life-cycle-assessment.
[163] X. Zheng, S. M. Easa, T. Ji, and Z. Jiang, "Modeling life-cycle social assessment in sustainable pavement management at project level," *Int. J. Life Cycle Assess.*, vol. 25, no. 6, pp. 1106–1118, 2020, doi: 10.1007/s11367-020-01743-7.
[164] EN 15804:2012+A1:2013 and EN 15804+A2:2019 - Sustainability of construction works - Environmental product declarations - Core rules for the product category of construction products.
[165] Research Fund for Coal and Steel of the European Community, "Large Valorisation on Sustainability of Steel Structures BACKGROUND DOCUMENT," 2017.
[166] Wikipedia website. https://en.wikipedia.org/wiki/Global_warming_potential.
[167] R. Heijungs *et al.*, "Environmental Life Cycle Assessment of Products—Guide and Backgrounds," Jan. 1992.
[168] M. Huijbregts, "Uncertainty and variability in environmental life-cycle assessment," University of Amsterdam. The Netherlands.
[169] J. B. Guinée *et al.*, *Handbook on life cycle assessment. Operational guide to the ISO standards. I: LCA in perspective. IIa: Guide. IIb: Operational annex. III: Scientific background*. Kluwer Academic Publishers, 2002.
[170] SR EN 12593 - Bitum şi lianţi bituminoşi. Determinarea punctului de rupere Fraass [Bitumen and bituminous binders. Determination of the Fraass breaking point], p. 18, 2015.
[171] SR 61 - Bitum. Determinarea ductilităţii [Romanian Norm. Bitumen. Ductility determination], 1997.
[172] SR EN 15326+A1 - Bitum şi lianţi bituminoşi. Măsurarea densităţii şi a densităţii relative. Metoda picnometrului cu dop capilar [Bitumen and bituminous binders. Measurement of density and specific gravity. Capillary-stoppered pyknometer method], p. 14, 2009.
[173] SR EN 14771 - Bitum şi lianţi bituminoşi. Determinarea modulului de rigiditate la încovoiere. Reometru cu bară de încovoiere (BBR) [Bitumen and bituminous binders. Determination of the flexural creep stiffness. Bending Beam Rheometer (BBR)], p. 16, 2012.

[174] S. Mangiafico, H. Di Benedetto, C. Sauzéat, F. Olard, S. Pouget, and L. Planque, "New method to obtain viscoelastic properties of bitumen blends from pure and reclaimed asphalt pavement binder constituents," *Road Mater. Pavement Des.*, vol. 15, no. 2, pp. 312–329, Apr. 2014, doi: 10.1080/14680629.2013.870639.
[175] A. Forton, S. Mangiafico, C. Sauzéat, H. Di Benedetto, and P. Marc, "Properties of blends of fresh and RAP binders with rejuvenator: Experimental and estimated results," *Constr. Build. Mater.*, vol. 236, 2020, doi: https://doi.org/10.1016/j.conbuildmat.2019.117555.
[176] B. Hofko *et al.*, "Effect of short-term ageing temperature on bitumen properties," *Road Mater. Pavement Des.*, vol. 18, no. sup2, pp. 108–117, May 2017, doi: 10.1080/14680629.2017.1304268.
[177] A. Forton, S. Mangiafico, C. Sauzéat, H. Di Benedetto, and P. Marc, "Steady shear viscosity of blends of fresh and RAP binders with rejuvenator: Experimental and estimated results," *Constr. Build. Mater.*, vol. 269, p. 121236, 2021, doi: https://doi.org/10.1016/j.conbuildmat.2020.121236.
[178] H. M. Nguyen, S. Pouget, H. Di Benedetto, and C. Sauzéat, "Time-temperature superposition principle for bituminous mixtures," *Eur. J. Environ. Civ. Eng.*, vol. 13, no. 9, pp. 1095–1107, Oct. 2009, doi: 10.1080/19648189.2009.9693176.
[179] Q. T. Nguyen, H. Di Benedetto, C. Sauzéat, and N. Tapsoba, "Time Temperature Superposition Principle Validation for Bituminous Mixes in the Linear and Nonlinear Domains," *J. Mater. Civ. Eng.*, vol. 25, pp. 1181–1188, Sep. 2013, doi: 10.1061/(ASCE)MT.1943-5533.0000658.
[180] A. Forton, S. Mangiafico, C. Sauzéat, H. Di Benedetto, and P. Marc, "Behaviour of binder blends: experimental results and modelling from LVE properties of pure binder, RAP binder and rejuvenator," *Road Mater. Pavement Des.*, pp. 1–17, Mar. 2021, doi: 10.1080/14680629.2021.1905699 - article in press.
[181] S. Mangiafico, C. Sauzéat, and H. Di Benedetto, "Comparison of different blending combinations of virgin and RAP-extracted binder: Rheological simulations and statistical analysis," *Constr. Build. Mater.*, vol. 197, pp. 454–463, 2019, doi: https://doi.org/10.1016/j.conbuildmat.2018.11.217.
[182] A. Forton, S. Mangiafico, C. Sauzéat, H. Di Benedetto, and P. Marc, "Estimation of complex shear modulus of binder blends produced with RAP binder and rejuvenator," 2020, Conference ISBM Lyon - poster presentation.
[183] A. Forton, S. Mangiafico, C. Sauzeat, H. Di Benedetto, and P. Marc, "Critical temperatures blending chart for binder blends produced with RAP binder and rejuvenator," *J. Test. Eval.*, 2021 - paper accepted for publication.
[184] AASHTO T315-10 - Determining the Rheological Properties of Asfhalt Binder Using a Dynamic Shear Rheometer (DSR), 2010.
[185] AASHTO MP 1 - Standard Specification for Performance Graded Asphalt Binder, 1998.
[186] AASHTO M 323 - Standard Specification for Superpave Volumetric Mix Design, 2017.
[187] SR EN 12697-35 - Mixturi asfaltice. Metode de încercare. Partea 35: Malaxare în laborator [Bituminous mixtures. Test methods. Laboratory mixing], p. 25, 2016.
[188] SR EN 12697-30 - Mixturi asfaltice. Metode de încercare. Partea 30: Confecționarea epruvetelor cu compactorul cu impact [Bituminous mixtures. Test methods. Specimen preparation by impact compactor], p. 23, 2019.

[189] SR EN 12697-31 - Mixturi asfaltice. Metode de încercare. Partea 31: Confecționarea epruvetelor cu presa cu compactare giratorie [Bituminous mixtures. Test methods. Specimen preparation by gyratory compactor], p. 24, 2019.
[190] SR EN 12697-33 - Mixturi asfaltice. Metode de încercare. Partea 33: Confecționarea epruvetelor cu compactorul cu placă [Bituminous mixtures. Test method. Specimen prepared by roller compactor], p. 23, 2019.
[191] SR EN 12697-6 - Mixturi asfaltice. Metode de încercare. Partea 6: Determinarea densității aparente a epruvetelor bituminoase [Bituminous mixtures. Test methods. Determination of bulk density of bituminous specimens], p. 17, 2012.
[192] SR EN 12697-8 - Mixturi asfaltice. Metode de încercare. Partea 8: Determinarea caracteristicilor volumetrice ale epruvetelor bituminoase [Bituminous mixtures. Test methods. Determination of void characteristics of bituminous specimens], p. 10, 2019.
[193] SR EN 12697-5 - Mixturi asfaltice. Metode de încercare. Partea 5: Determinarea densității maxime [Bituminous mixtures. Test methods. Determination of the maximum density], p. 22, 2019.
[194] SR EN 12697-29 - Mixturi asfaltice. Metode de încercare. Partea 29: Determinarea dimensiunilor epruvetelor bituminoase [Bituminous mixtures. Test methods for hot mix asphalt. Determination of the dimensions of a bituminous specimen], p. 6, 2003.
[195] SR EN 12697-34 - Mixturi asfaltice. Metode de încercare. Partea 34: Încercare Marshall [Bituminous mixtures. Test methods. Marshall test], p. 12, 2012.
[196] ASTM D6927 - 15 - Standard Test Method for Marshall Stability and Flow of Asphalt Mixtures, 2015.
[197] SR EN 12697-26 - Mixturi asfaltice. Metode de încercare. Partea 26: Rigiditate [Bituminous mixtures. Test methods. Stiffness], p. 49, 2018.
[198] SR EN 12697-25 - Mixturi asfaltice. Metode de încercare. Partea 25: Încercare la compresiune ciclică [Bituminous mixtures. Test methods. Cyclic compression test], p. 36, 2016.
[199] J.-L. Delorme *et al.*, *Manuel LPC d'aide à la formulation des enrobés à chaud [LPC guidelines for hot bituminous mixture design]*. Paris, 2015.
[200] PE INTERNATIONAL AG, "GaBi software Manual," 2012. [Online]. Available: http://www.gabi-software.com/fileadmin/GaBi_Manual/GaBi_6_manual.pdf.
[201] G. J *et al.*, "Future use of life-cycle assessment in civil engineering," *Proc. Inst. Civ. Eng. Constr. Mater.*, vol. 166, no. 4, pp. 204–2012, 2013, doi: http://dx.doi.org/10.1680/coma.12.00037.
[202] H. Li, A. Saboori, and X. Cao, "Information synthesis and preliminary case study for life cycle assessment of reflective coatings for cool pavements," *Int. J. Transp. Sci. Technol.*, vol. 5, no. 1, pp. 38–46, 2016, doi: https://doi.org/10.1016/j.ijtst.2016.06.005.
[203] M. Kayhanian, H. Li, J. T. Harvey, and X. Liang, "Application of permeable pavements in highways for stormwater runoff management and pollution prevention: California research experiences," *Int. J. Transp. Sci. Technol.*, vol. 8, no. 4, pp. 358–372, 2019, doi: https://doi.org/10.1016/j.ijtst.2019.01.001.
[204] Q. Aurangzeb, I. L. Al-Qadi, H. Ozer, and R. Yang, "Hybrid life cycle assessment for asphalt mixtures with high RAP content," *Resour. Conserv. Recycl.*, vol. 83, pp. 77–86, 2014, doi:

https://doi.org/10.1016/j.resconrec.2013.12.004.
[205] S. Bressi, J. Santos, M. Orešković, and M. Losa, "A comparative environmental impact analysis of asphalt mixtures containing crumb rubber and reclaimed asphalt pavement using life cycle assessment," *Int. J. Pavement Eng.*, pp. 1–15, Jun. 2019, doi: 10.1080/10298436.2019.1623404.
[206] G. Lu, Y. Wang, H. Li, D. Wang, and M. Oeser, "The environmental impact evaluation on the application of permeable pavement based on life cycle analysis," *Int. J. Transp. Sci. Technol.*, vol. 8, no. 4, pp. 351–357, 2019, doi: https://doi.org/10.1016/j.ijtst.2019.05.006.
[207] J. Vallette, *Optimizing Recycling Reclaimed Asphalt Pavement (RAP) in Building & Construction*. 2017.
[208] A damage oriented method for Life Cycle Impact Assessment. Eco-indicator 99, 2000.
[209] A. Forton, A. Ciutina, and P. Marc, "Environmental impact of bituminous mixtures produced with reclaimed asphalt pavement and rejuvenator," 2020, EENVIRO Conference, Bucharest, Romania - poster presentation.

Appendices

TABLE OF CONTENTS APPENDICES

Appendix 1

– Binders -

A.1.1. Complex shear modulus test results

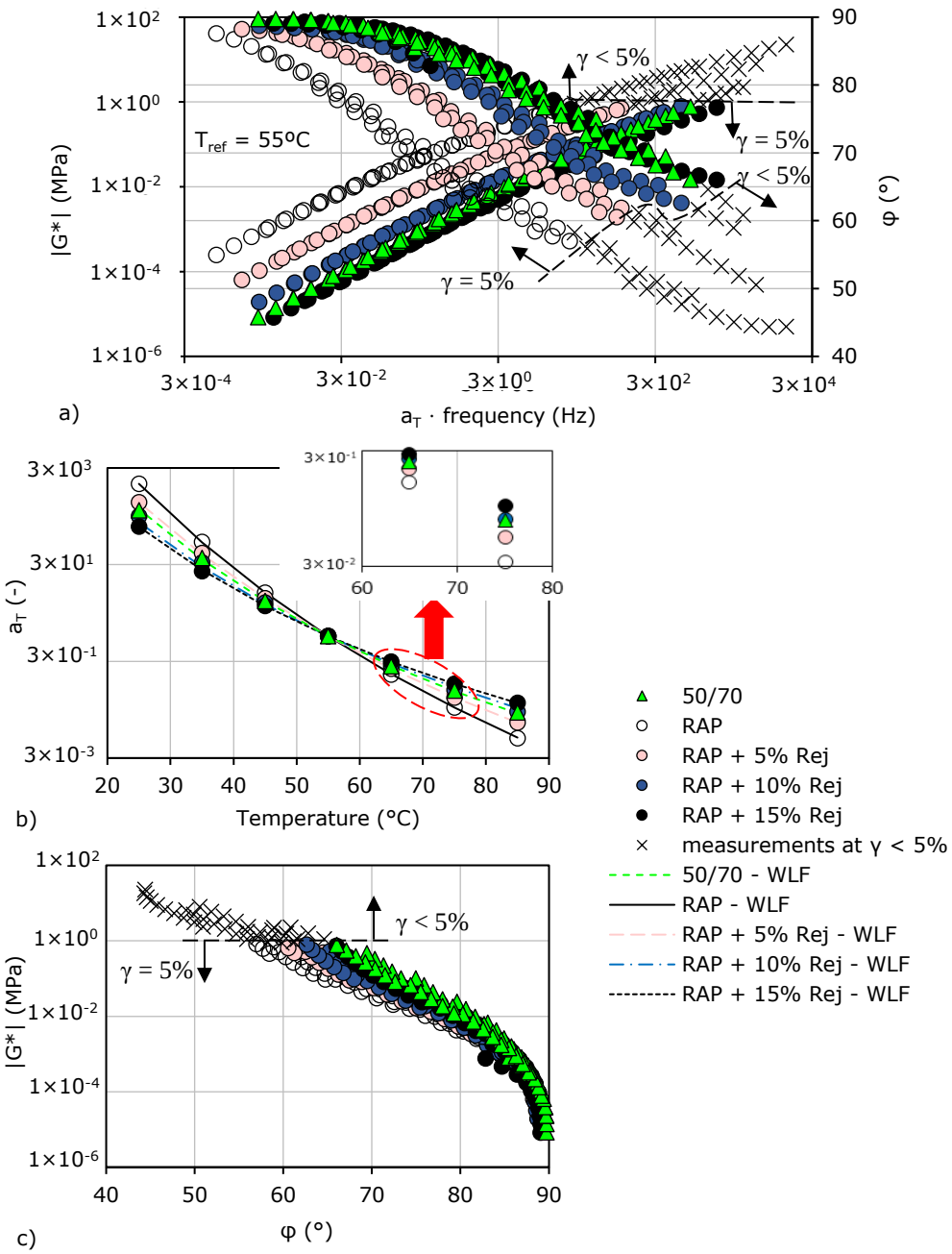

Figure A1.1. Complex shear modulus test results for the blends of RAP binder and rejuvenator: (a) master curves of the norm of complex shear modulus and phase angle; (b) temperature shift factors and WLF curves; (c) Black diagrams.

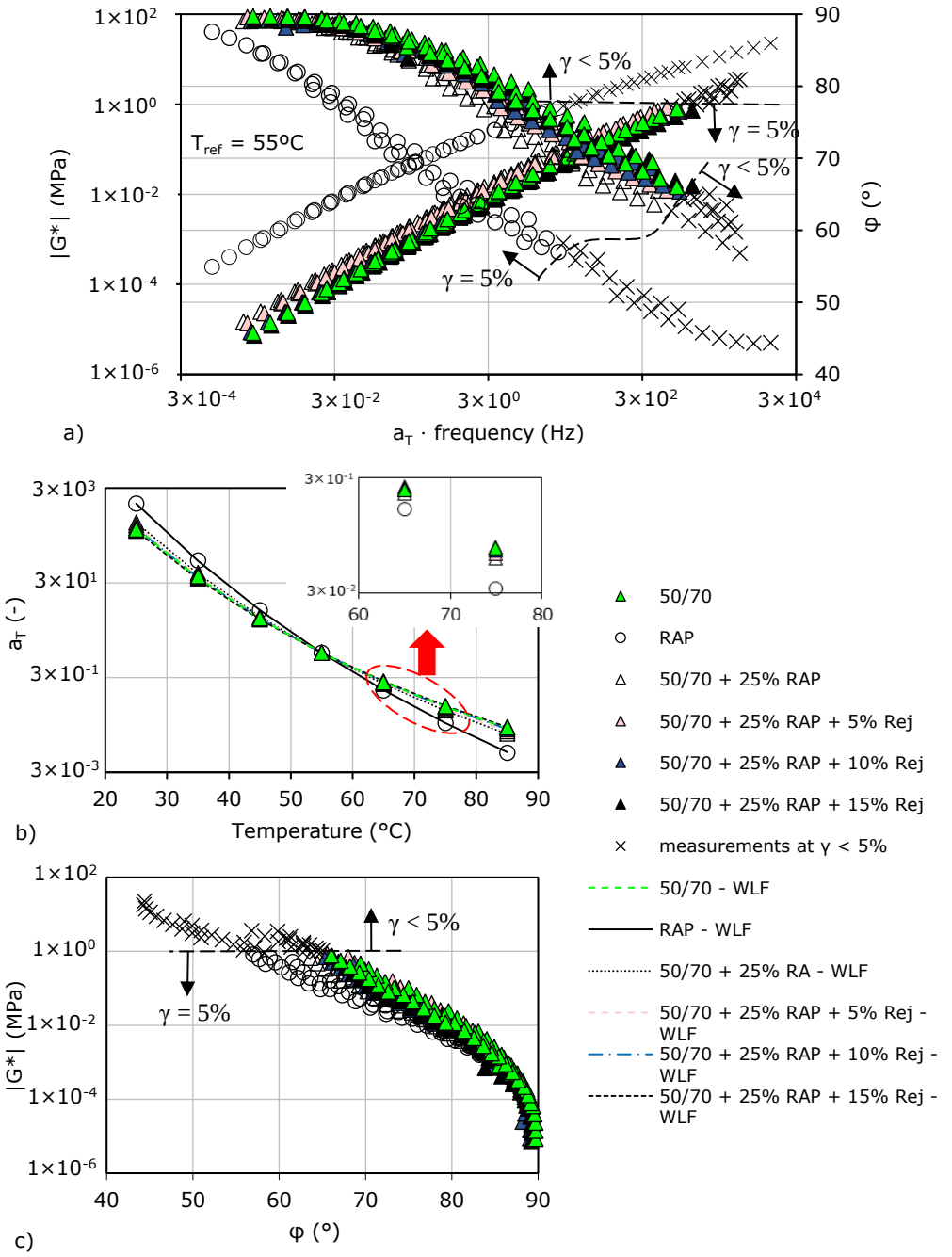

Figure A1.2. Complex shear modulus test results for the blends produced with fresh binder, 25% RAP and different dosages of rejuvenator: (a) master curves of the norm of complex shear modulus and phase angle; (b) temperature shift factors and WLF curves; (c) Black diagrams.

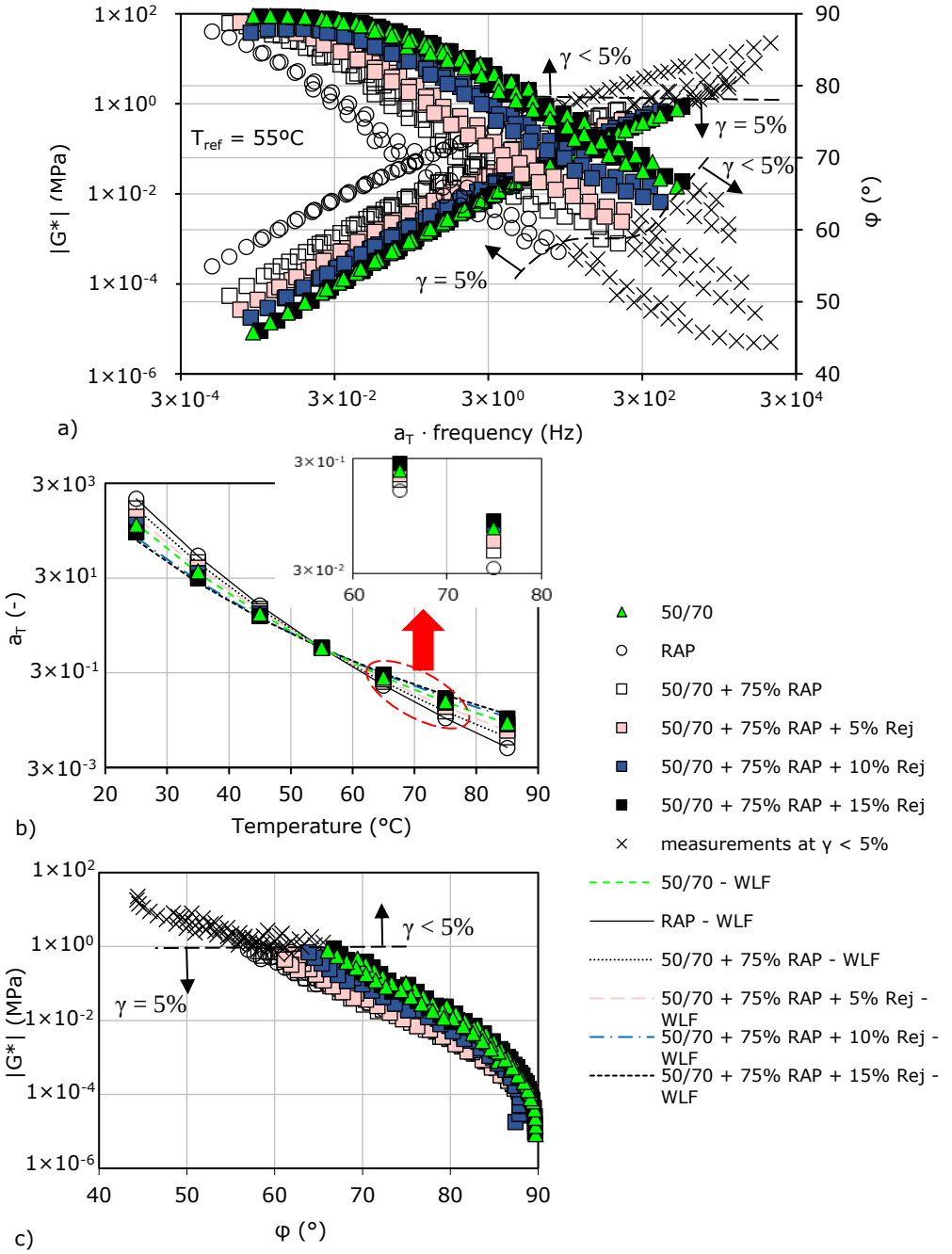

Figure A1.3. Complex shear modulus test results for the blends produced with fresh binder, 75% RAP and different dosages of rejuvenator: (a) master curves of the norm of complex shear modulus and phase angle; (b) temperature shift factors and WLF curves; (c) Black diagrams.

A.1.2. 2S2P1D model fitting of complex shear modulus results

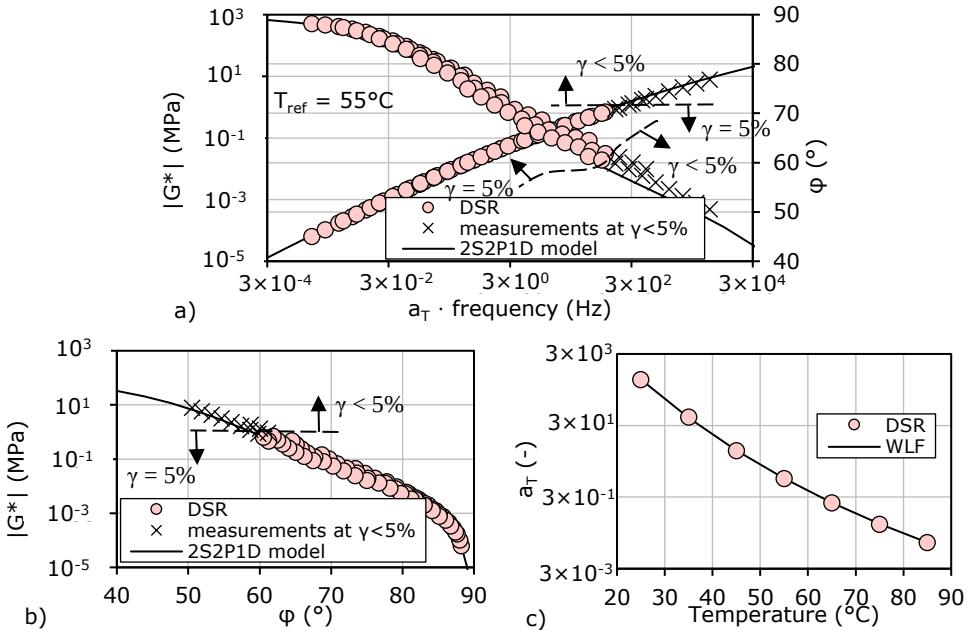

Figure A1.4. 2S2P1D model fitting of complex shear modulus test results for the binder RAP + 5% Rej: (a) master curves; (b) Black curve; (c) WLF curve.

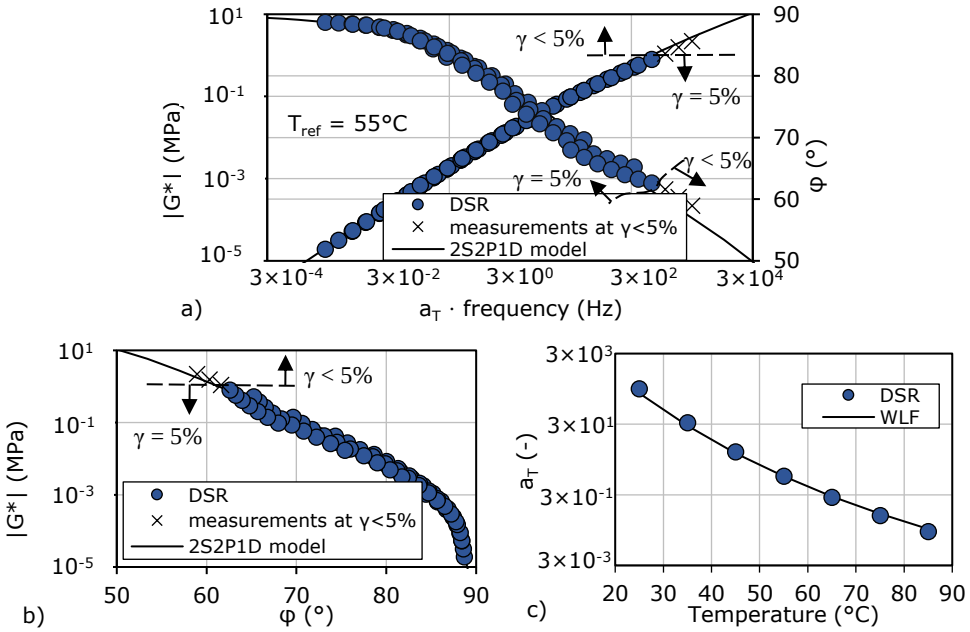

Figure A1.5. 2S2P1D model fitting of complex shear modulus test results for the binder RAP + 10% Rej: (a) master curves; (b) Black curve; (c) WLF curve.

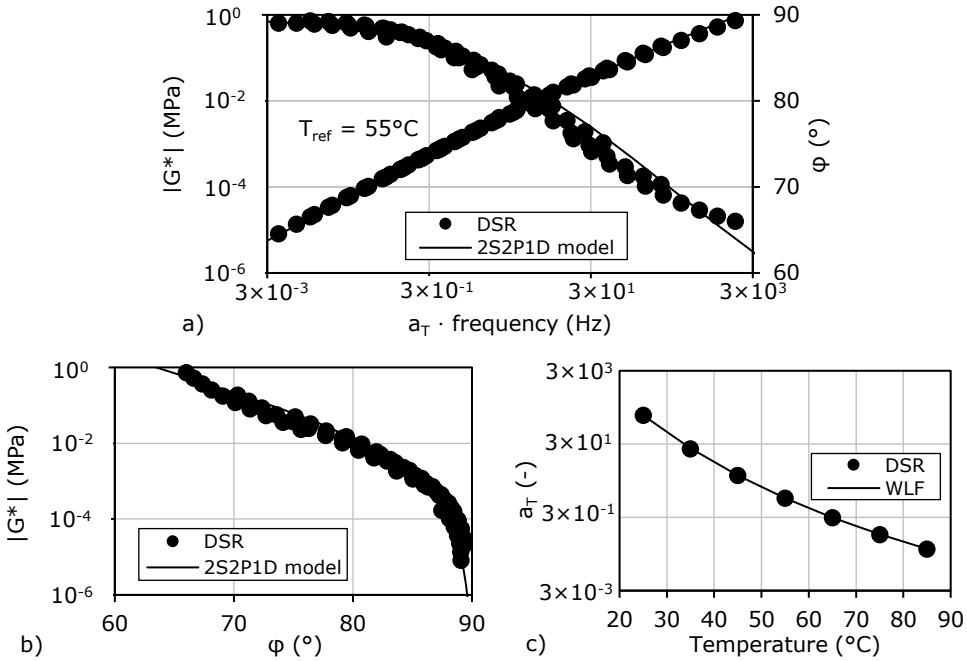

Figure A1.6. 2S2P1D model fitting of complex shear modulus test results for the binder RAP + 15% Rej: (a) master curves; (b) Black curve; (c) WLF curve.

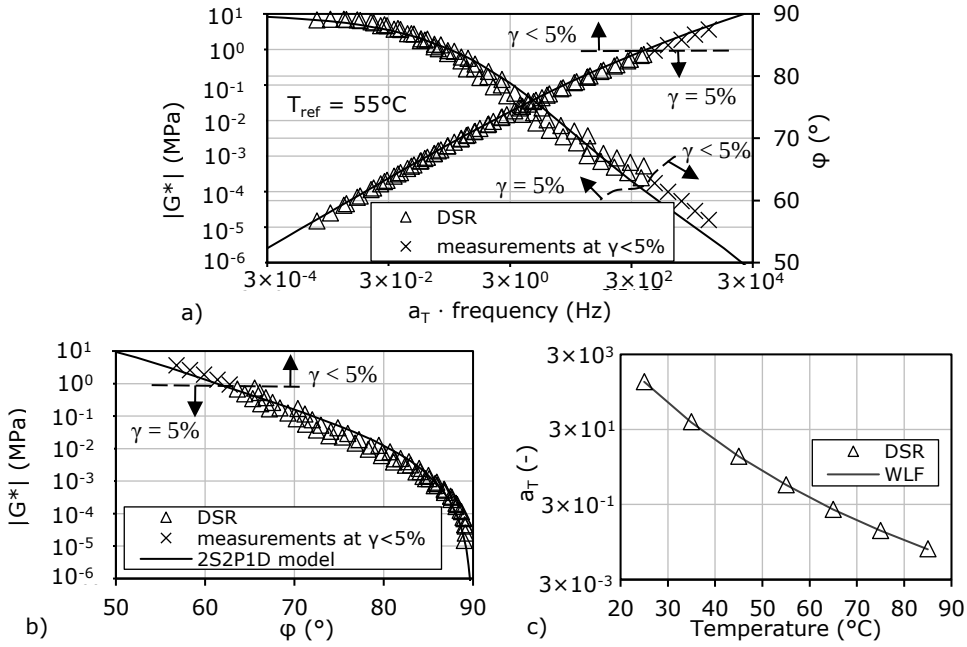

Figure A1.7. 2S2P1D model fitting of complex shear modulus test results for the binder 50/70 + 25% RAP: (a) master curves; (b) Black curve; (c) WLF curve.

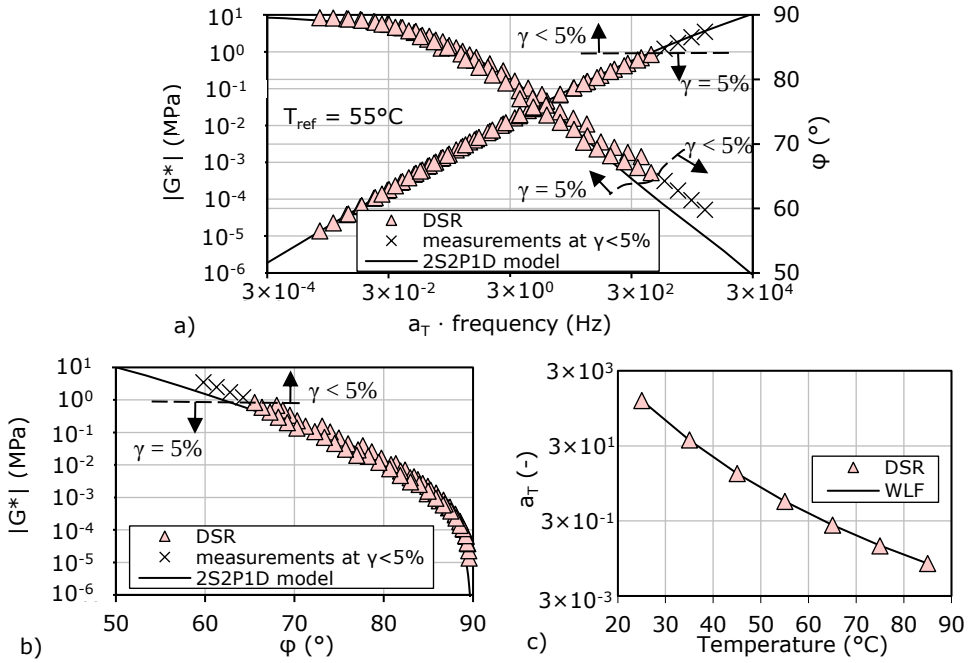

Figure A1.8. 2S2P1D model fitting of complex shear modulus test results for the binder 50/70+25% RAP+5% Rej: (a) master curves; (b) Black curve; (c) WLF curve.

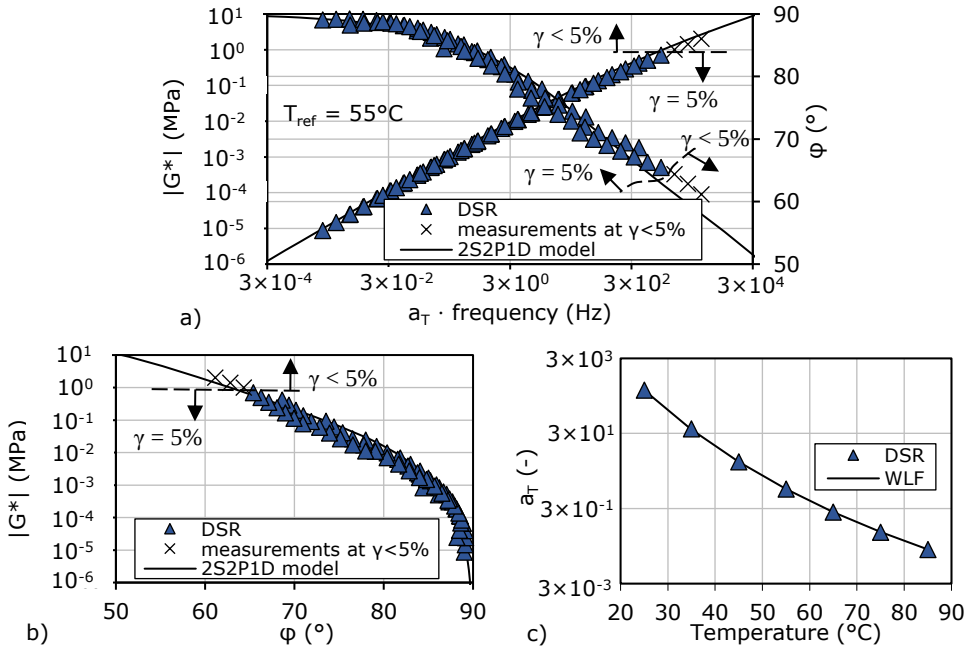

Figure A1.9. 2S2P1D model fitting of complex shear modulus test results for the binder 50/70+25% RAP+10% Rej: (a) master curves; (b) Black curve; (c) WLF curve.

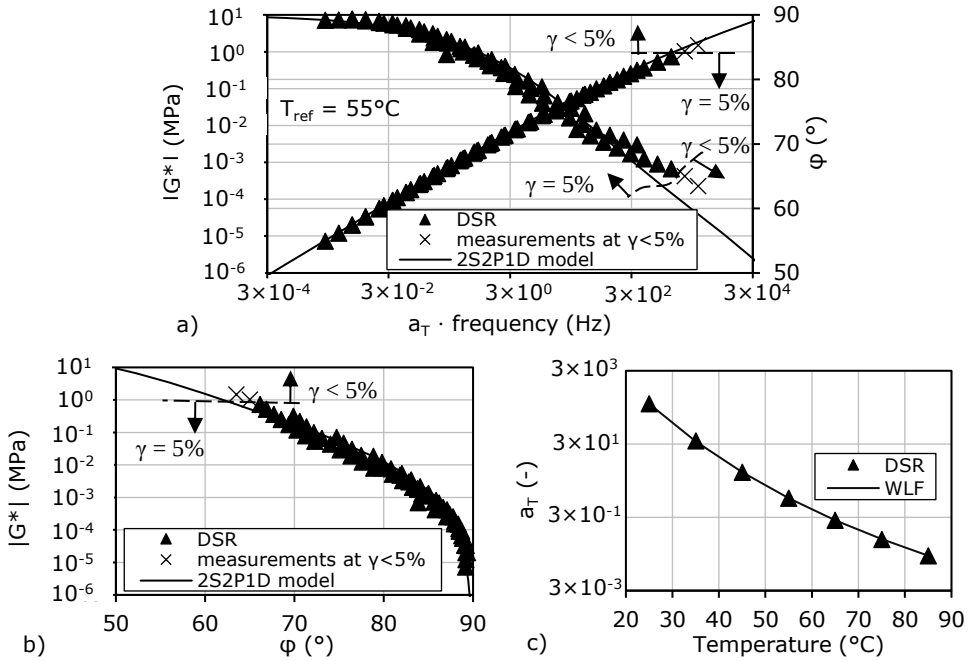

Figure A1.10. 2S2P1D model fitting of complex shear modulus test results for the binder 50/70+25% RAP+15% Rej: (a) master curves; (b) Black curve; (c) WLF curve.

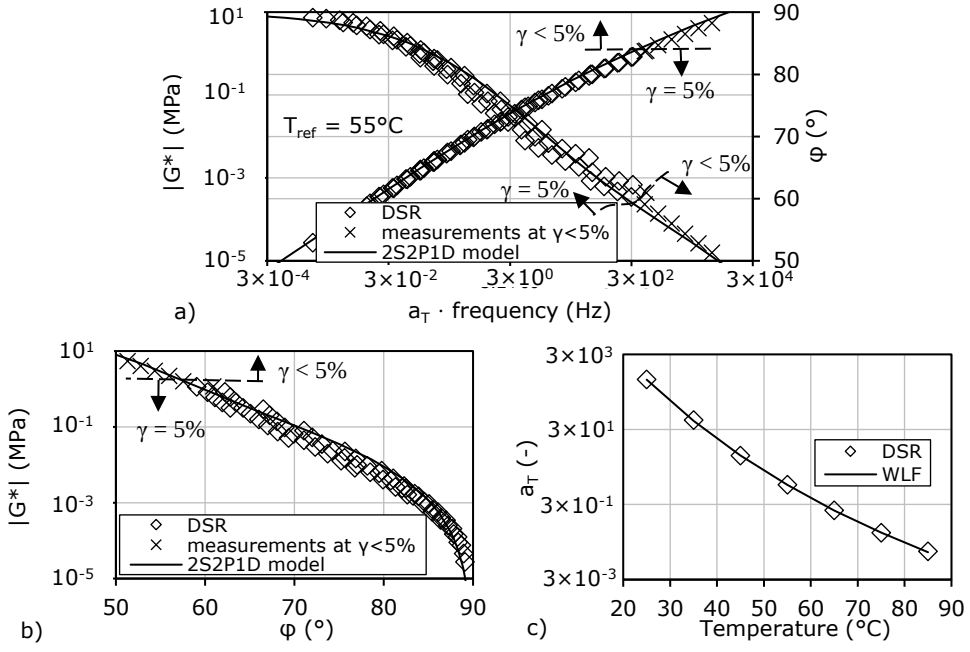

Figure A1.11. 2S2P1D model fitting of complex shear modulus test results for the binder 50/70+50% RAP: (a) master curves; (b) Black curve; (c) WLF curve.

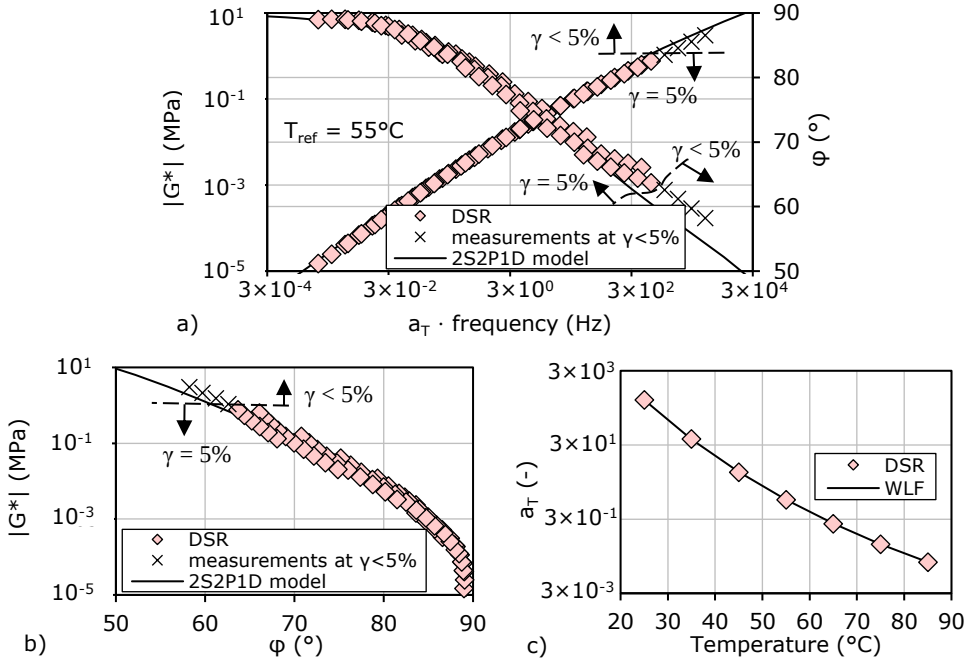

Figure A1.12. 2S2P1D model fitting of complex shear modulus test results for the binder 50/70+50% RAP+5% Rej: (a) master curves (b) Black curve; (c) WLF curve.

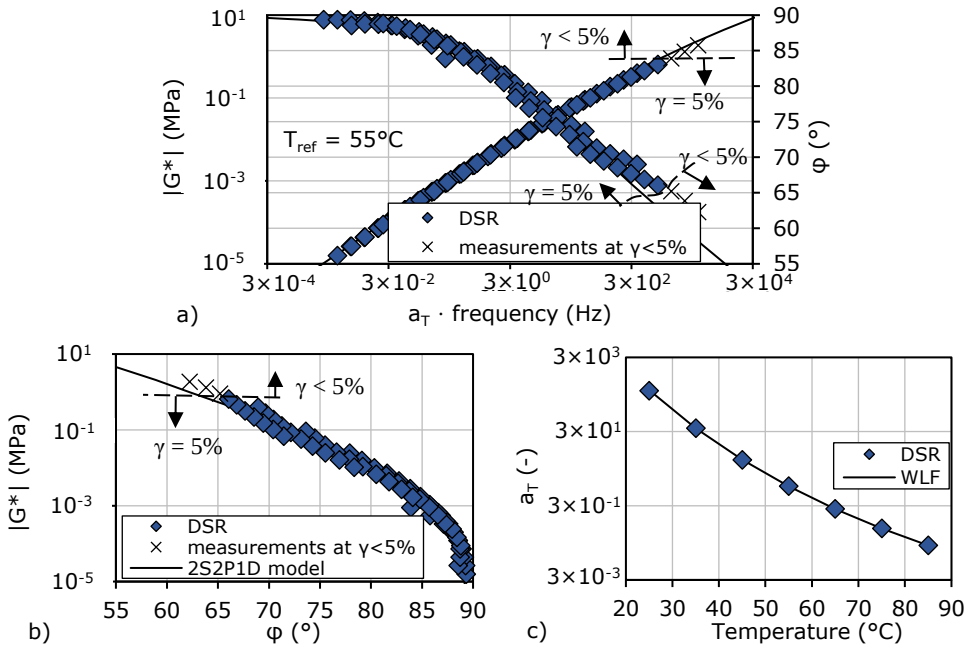

Figure A1.13. 2S2P1D model fitting of complex shear modulus test results for the binder 50/70+50% RAP+10% Rej: (a) master curves; (b) Black curve; (c) WLF curve.

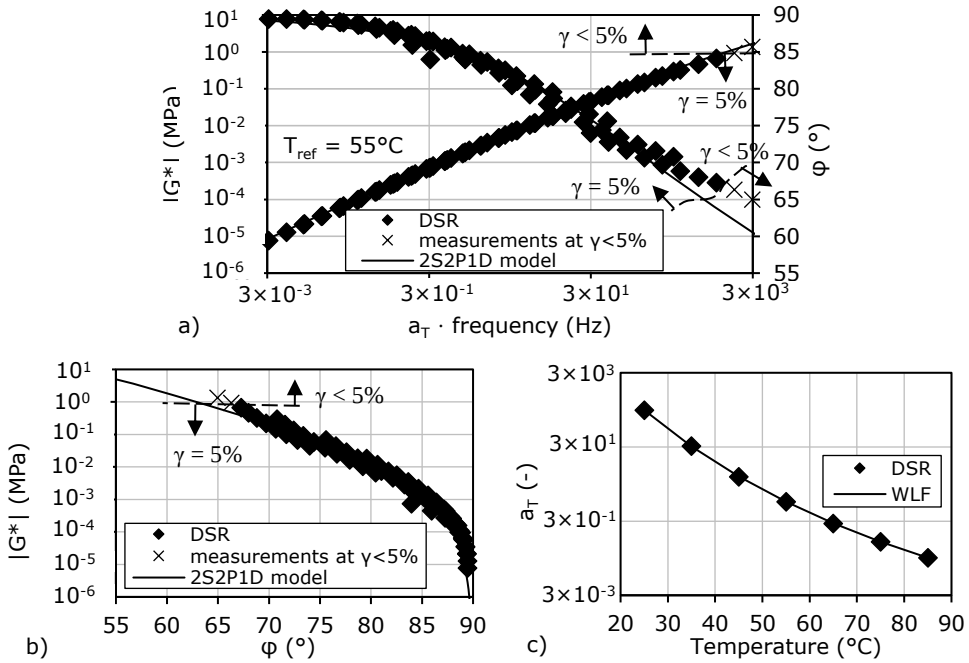

Figure A1.14. 2S2P1D model fitting of complex shear modulus test results for the binder 50/70+50% RAP+15% Rej: (a) master curves; (b) Black curve; (c) WLF curve.

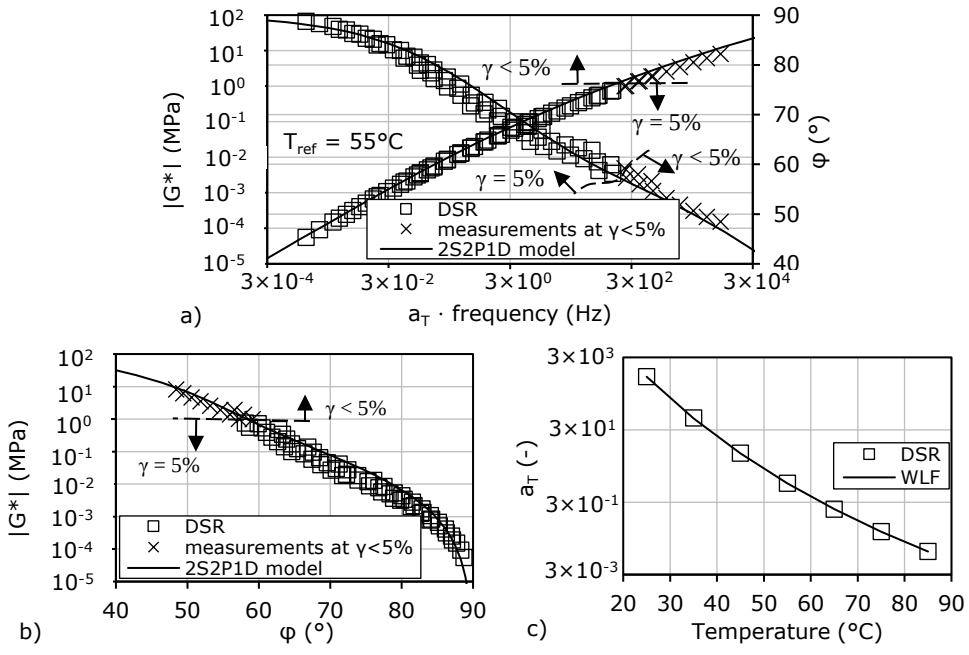

Figure A1.15. 2S2P1D model fitting of complex shear modulus test results for the binder 50/70+75% RAP: (a) master curves; (b) Black curve; (c) WLF curve.

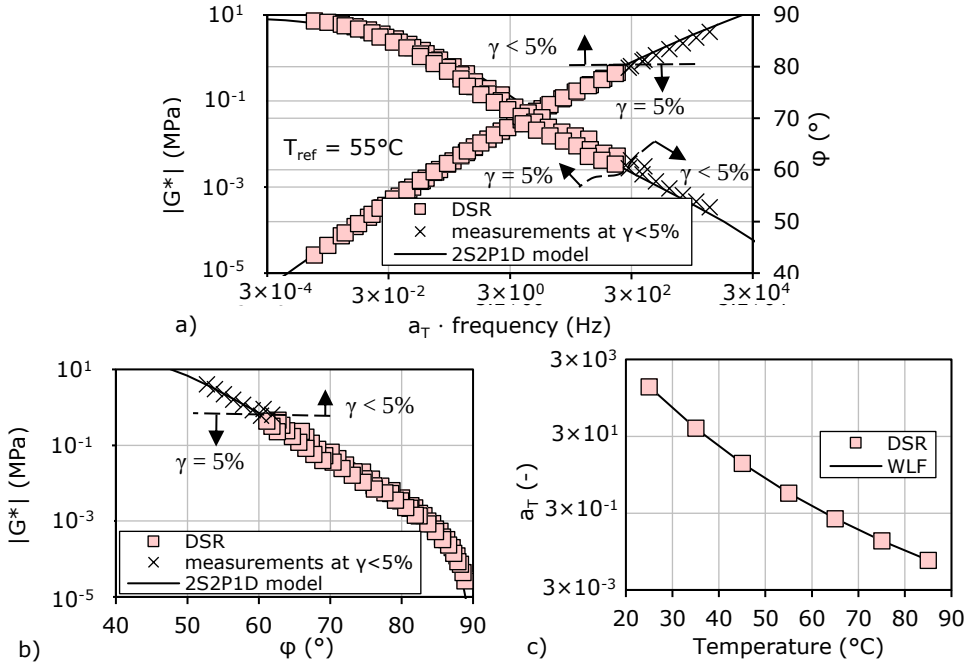

Figure A1.16. 2S2P1D model fitting of complex shear modulus test results for the binder 50/70+75% RAP+5% Rej: (a) master curves; (b) Black curve; (c) WLF curve.

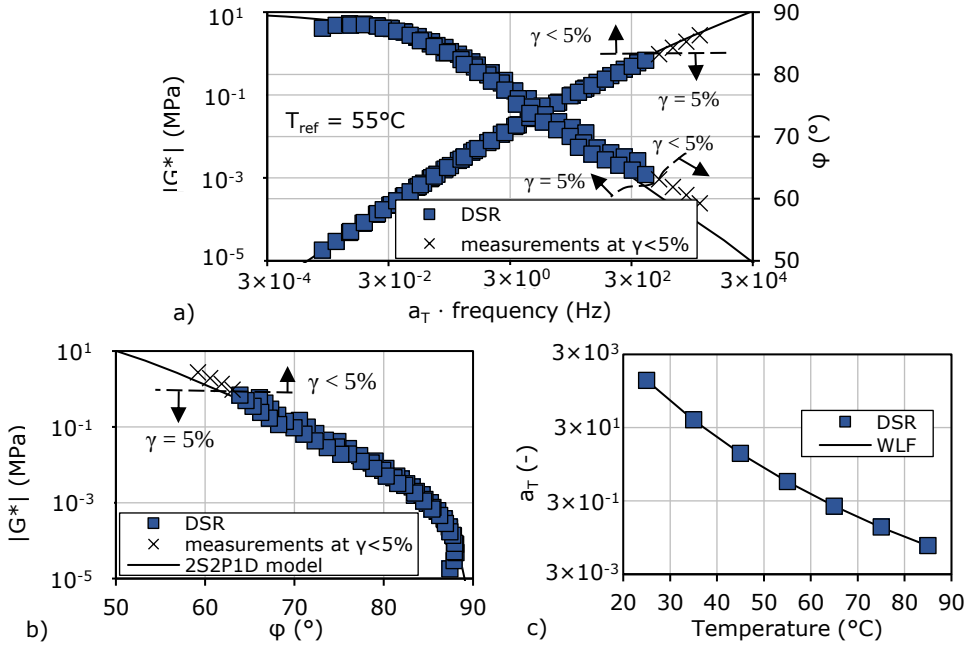

Figure A1.17. 2S2P1D model fitting of complex shear modulus test results for the binder 50/70+75% RAP+10% Rej: (a) master curves; (b) Black curve; (c) WLF curve.

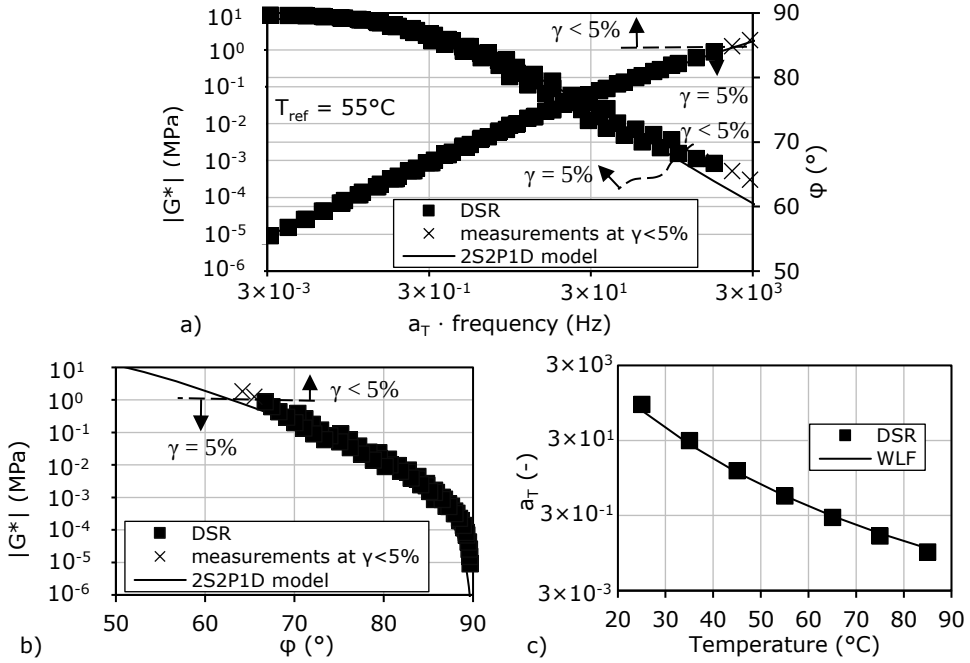

Figure A1.18. 2S2P1D model fitting of complex shear modulus test results for the binder 50/70+75% RAP+15% Rej: (a) master curves; (b) Black curve; (c) WLF curve.

A.1.3. Temperature shift factors experimental and estimated results

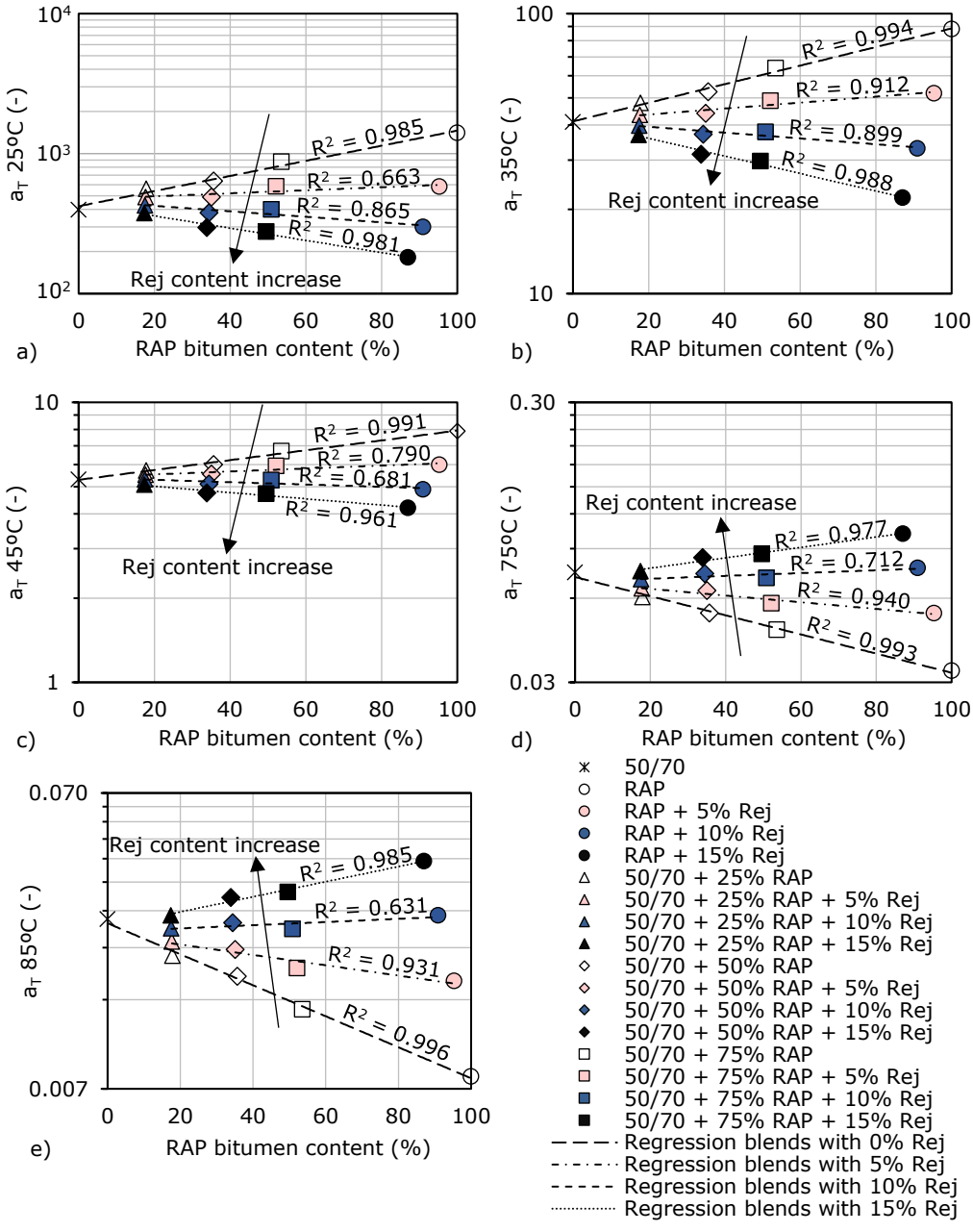

Figure A1.19. Temperature shift factors a_T values for all tested binders as a function of RAP binder content: (a) 25ºC; (b) 35ºC; (c) 45ºC; (d) 75ºC; (e) 85ºC.

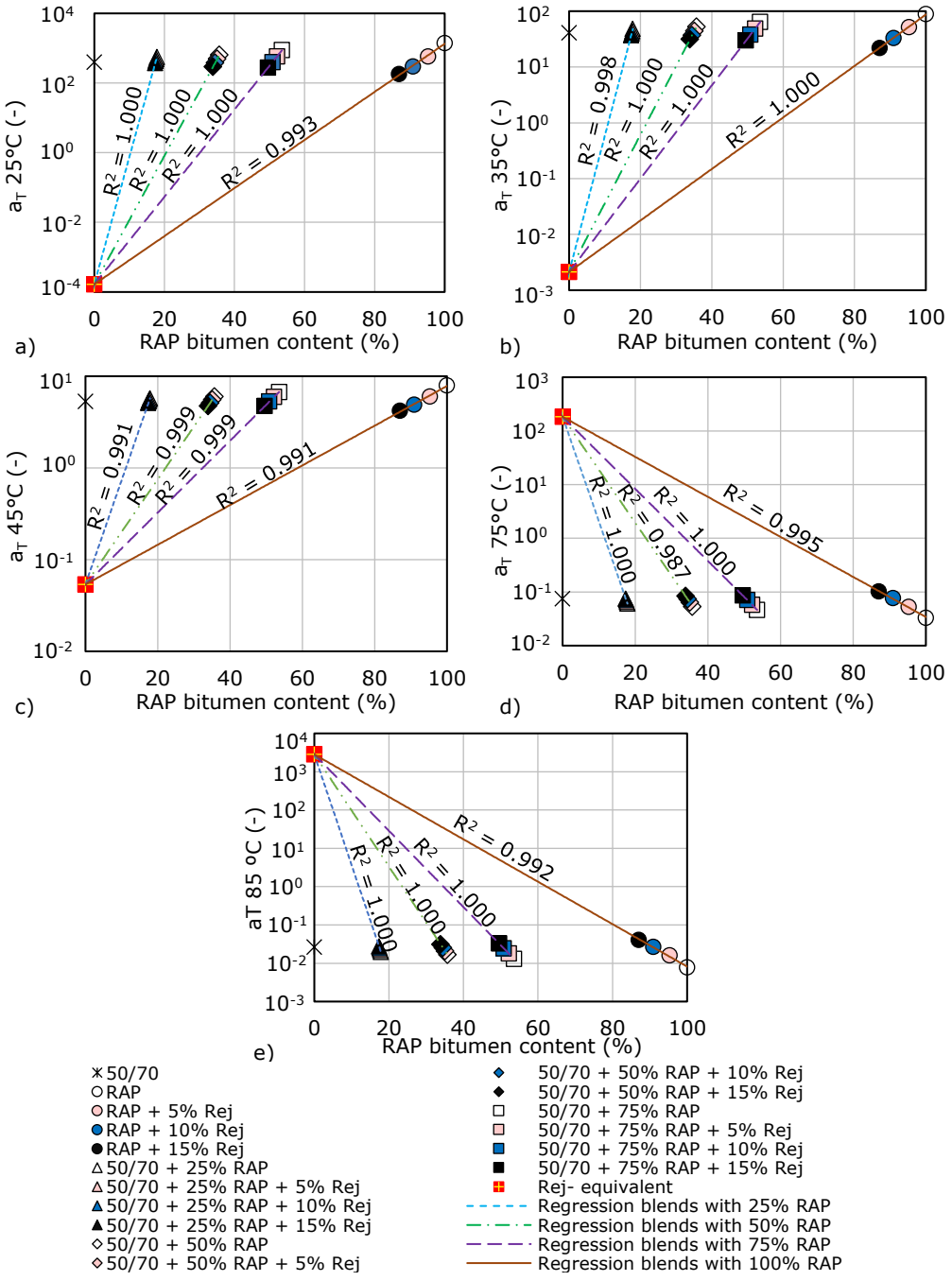

Figure A1.20. Experimental a_T values and equivalent values of rejuvenator, as a function or RAP binder content: re-calculation of R^2 by imposing the equivalent values of the rejuvenator as an intercept point for all linear regressions: (a) 25ºC; (b) 35ºC; (c) 45ºC; (d) 75ºC; (e) 85ºC.

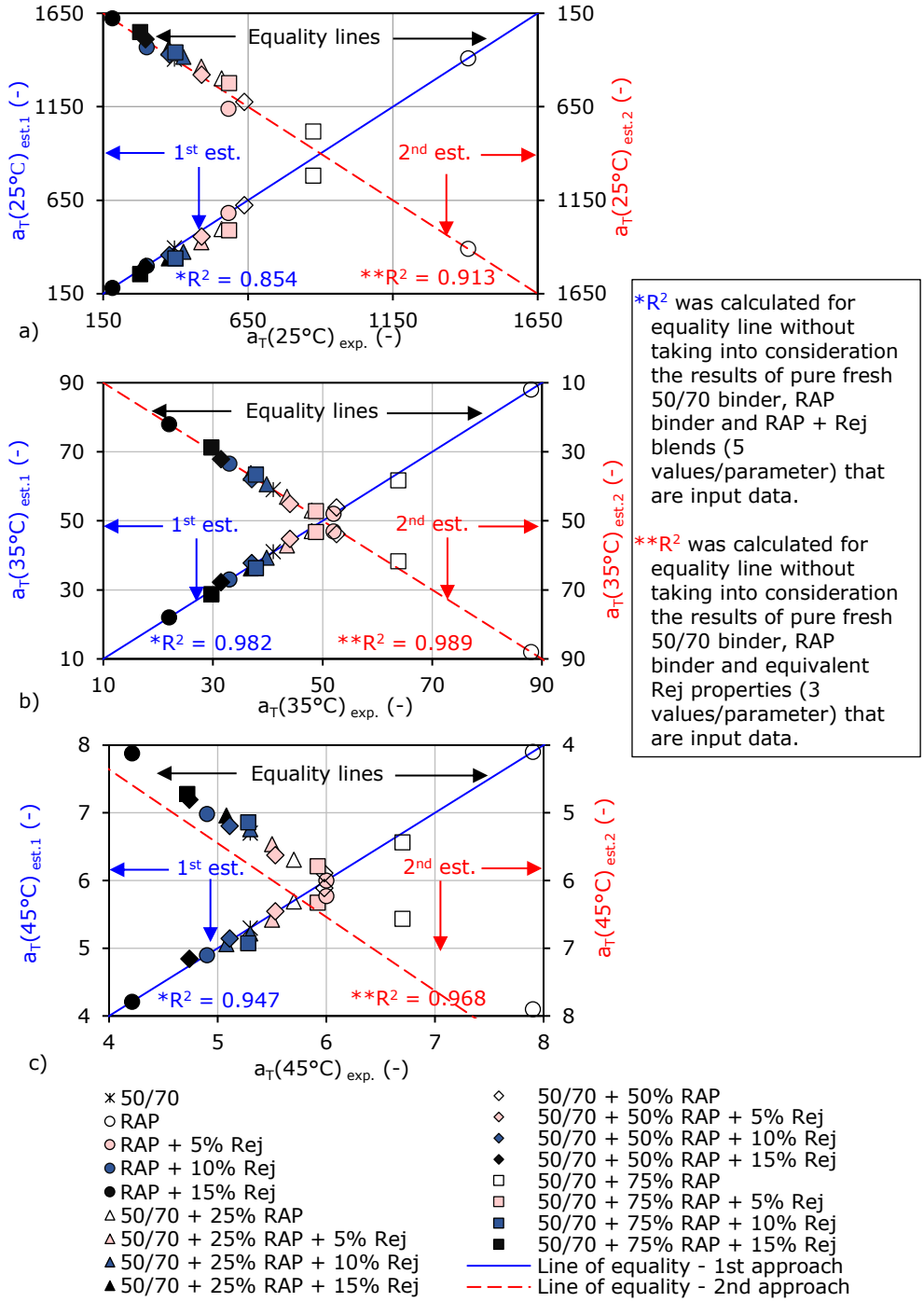

Figure A1.21. Plot of estimated vs. experimental values of temperature shift factors a_T for all binders: (a) 25ºC; (b) 35ºC; (c) 45ºC.

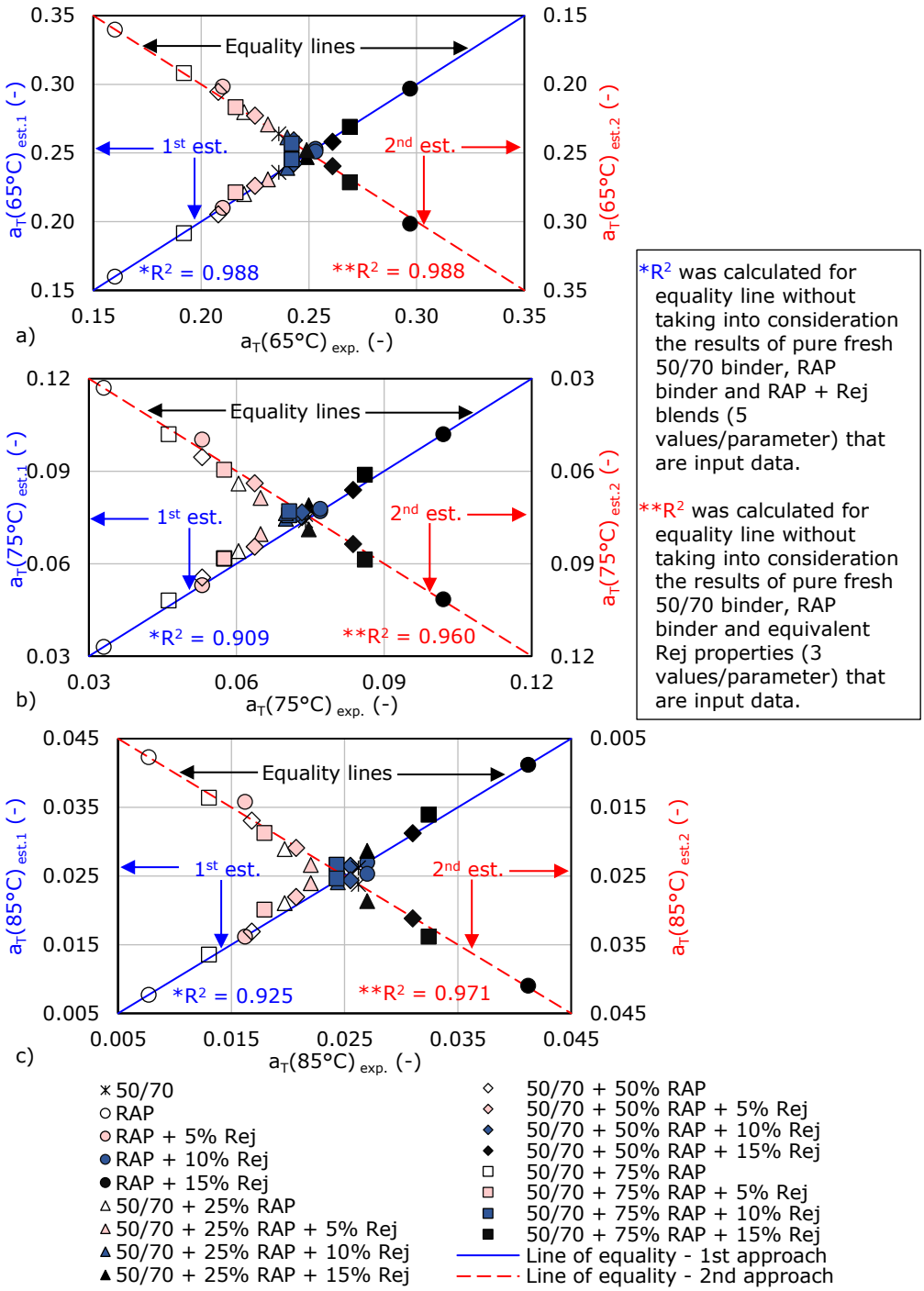

Figure A1.22. Plot of estimated vs. experimental values of temperature shift factors a_T for all binders: (a) 65ºC; (b) 75ºC; (c) 85ºC.

A.1.4. Comparison between experimental and estimated 2S2P1D model

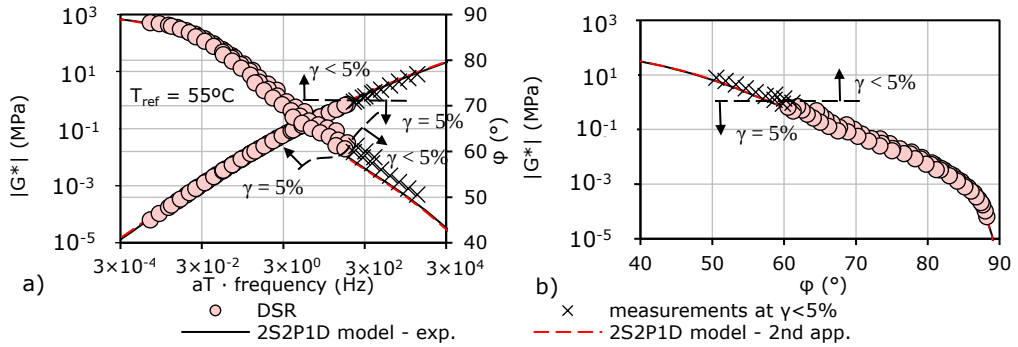

Figure A1.23. Comparison between test results, curves built using experimental and estimated 2S2P1D parameters for the RAP + 5% Rej blend: (a) master curves; (b) Black curve.

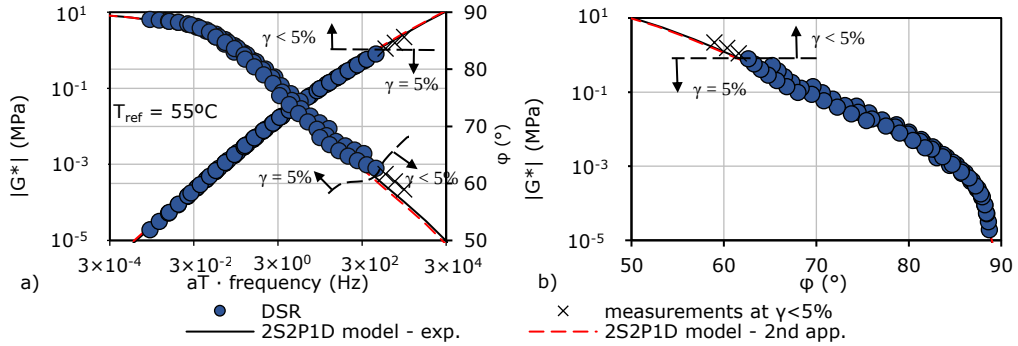

Figure A1.24. Comparison between test results, curves built using experimental and estimated 2S2P1D parameters for the RAP + 10% Rej blend: (a) master curves; (b) Black curve.

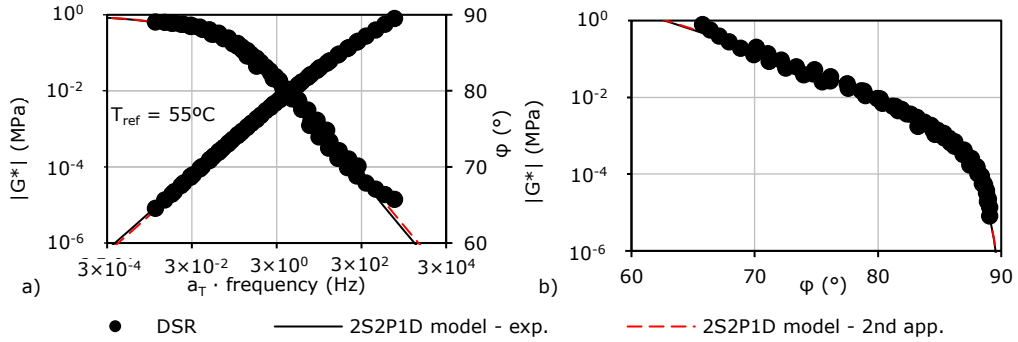

Figure A1.25. Comparison between test results, curves built using experimental and estimated 2S2P1D parameters for the RAP + 15% Rej blend: (a) master curves; (b) Black curve.

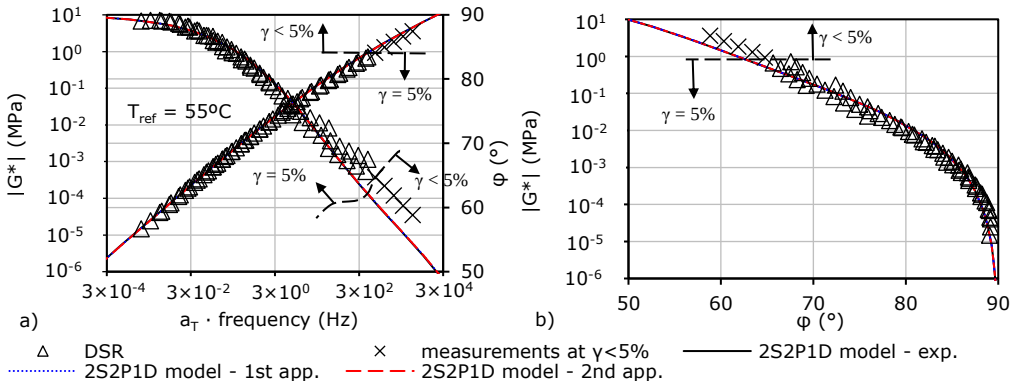

Figure A1.26. Comparison between test results, curves built using experimental and estimated 2S2P1D parameters for the 50/70 + 25% RAP blend: (a) master curves; (b) Black curve.

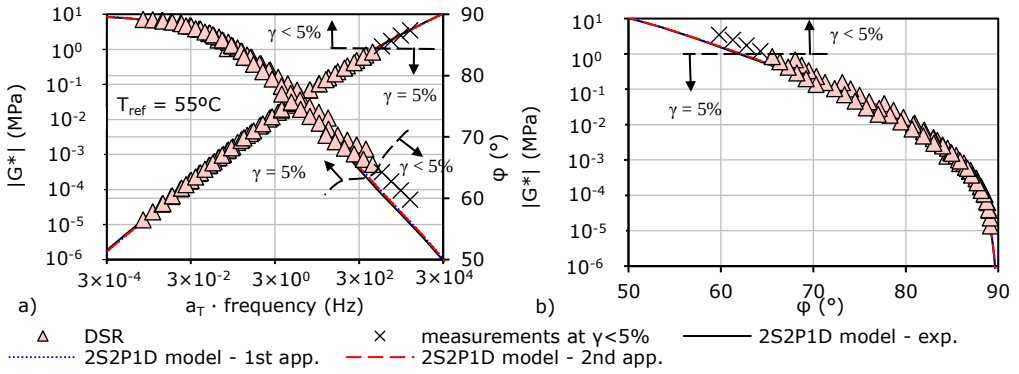

Figure A1.27. Comparison between test results, curves built using experimental and estimated 2S2P1D parameters for the 50/70 + 25% RAP + 5% Rej blend: (a) master curves; (b) Black curve.

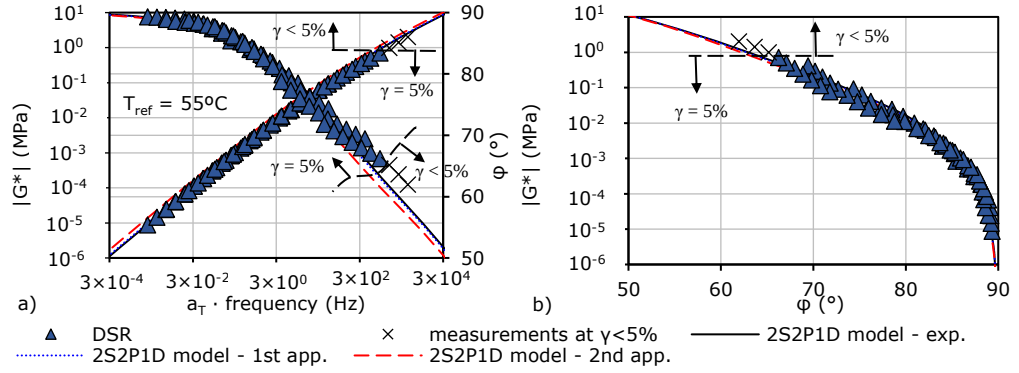

Figure A1.28. Comparison between test results, curves built using experimental and estimated 2S2P1D parameters for the 50/70 + 25% RAP + 10% Rej blend: (a) master curves; (b) Black curve.

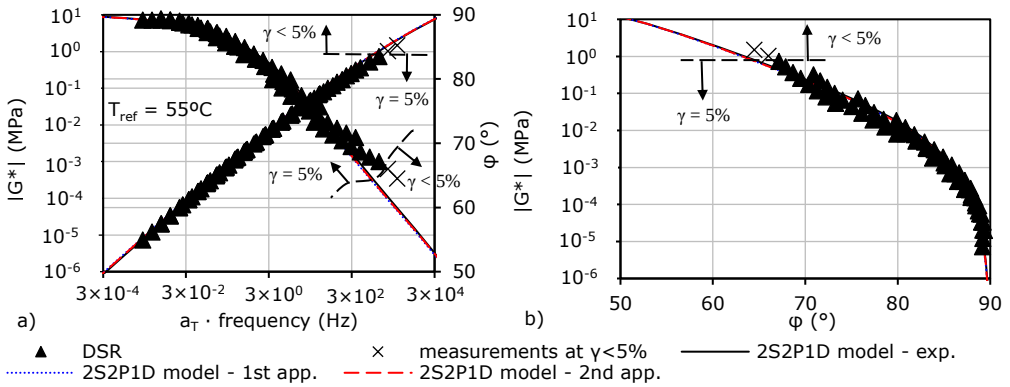

Figure A1.29. Comparison between test results, curves built using experimental and estimated 2S2P1D parameters for the 50/70 + 25% RAP + 15% Rej blend: (a) master curves; (b) Black curve.

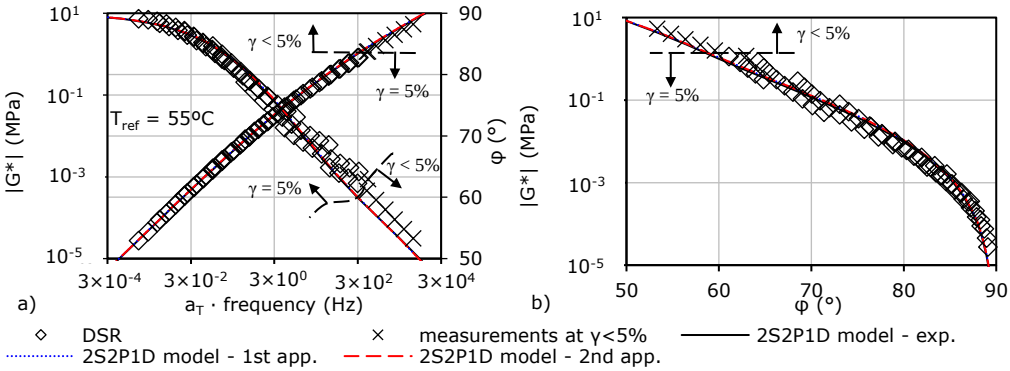

Figure A1.30. Comparison between test results, curves built using experimental and estimated 2S2P1D parameters for the 50/70 + 50% RAP blend: (a) master curves; (b) Black curve.

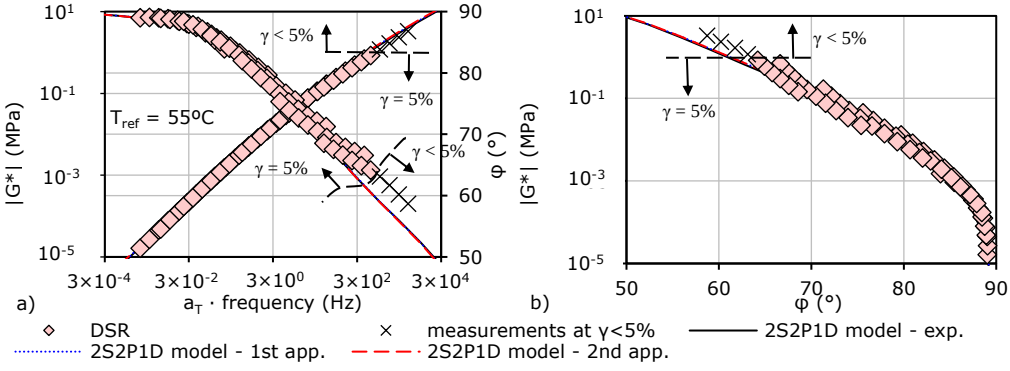

Figure A1.31. Comparison between test results, curves built using experimental and estimated 2S2P1D parameters for the 50/70 + 50% RAP + 5% Rej blend: (a) master curves; (b) Black curve.

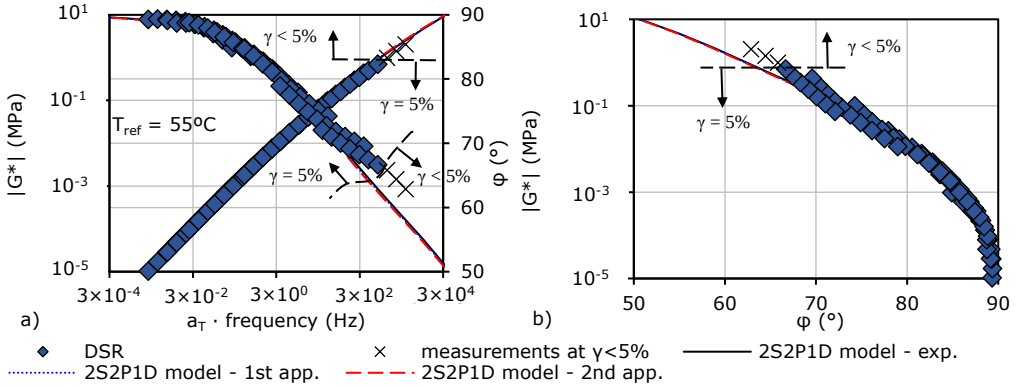

Figure A1.32. Comparison between test results, curves built using experimental and estimated 2S2P1D parameters for the 50/70 + 50% RAP + 10% Rej blend: (a) master curves; (b) Black curve.

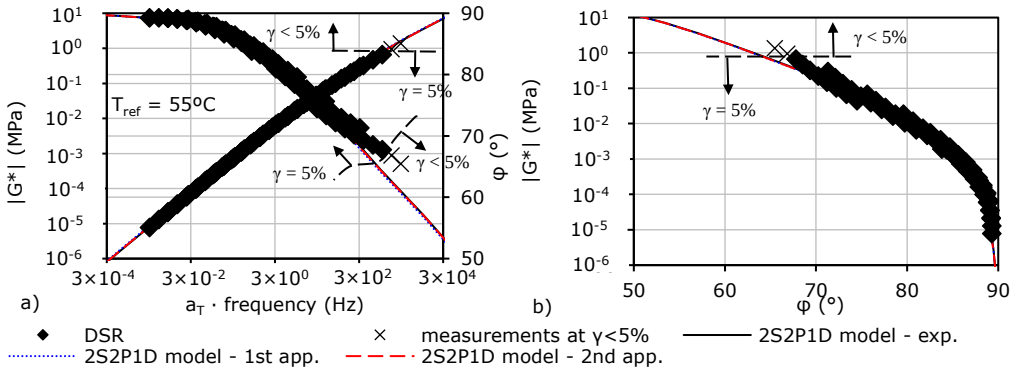

Figure A1.33. Comparison between test results, curves built using experimental and estimated 2S2P1D parameters for the 50/70 + 50% RAP + 15% Rej blend: (a) master curves; (b) Black curve.

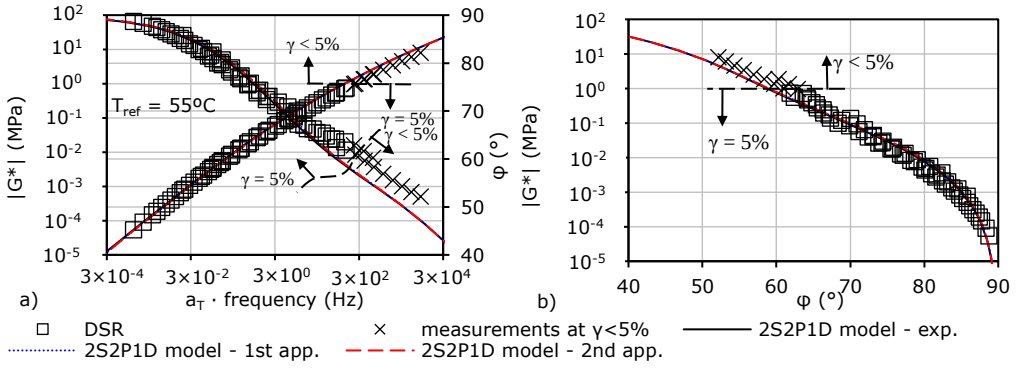

Figure A1.34. Comparison between test results, curves built using experimental and estimated 2S2P1D parameters for the blend 50/70 + 75% RAP: (a) master curves; (b) Black curve.

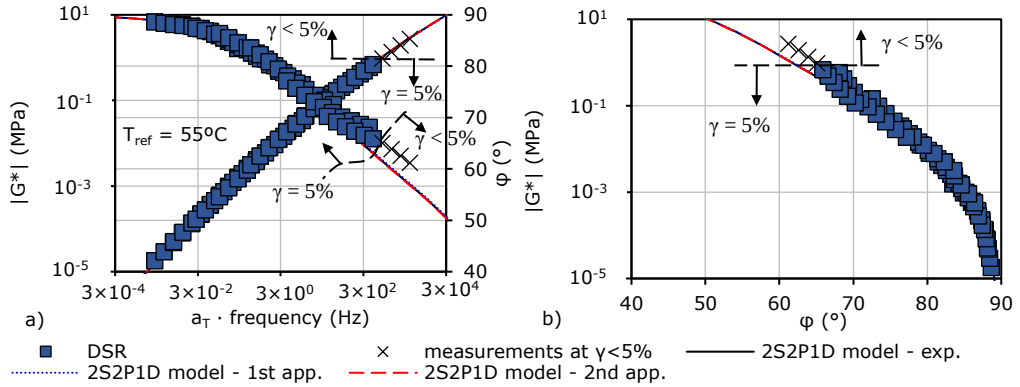

Figure A1.35. Comparison between test results, curves built using experimental and estimated 2S2P1D parameters for the blend 50/70 + 75% RAP + 10% Rej: (a) master curves; (b) Black curve.

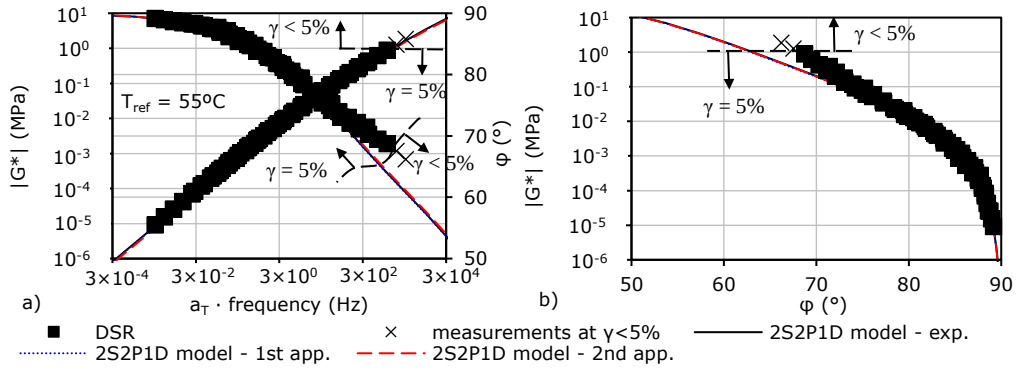

Figure A1.36. Comparison between test results, curves built using experimental and estimated 2S2P1D parameters for the blend 50/70 + 75% RAP + 15% Rej: (a) master curves; (b) Black curve.

A.1.5. Determination of steady shear viscosity at 85ºC

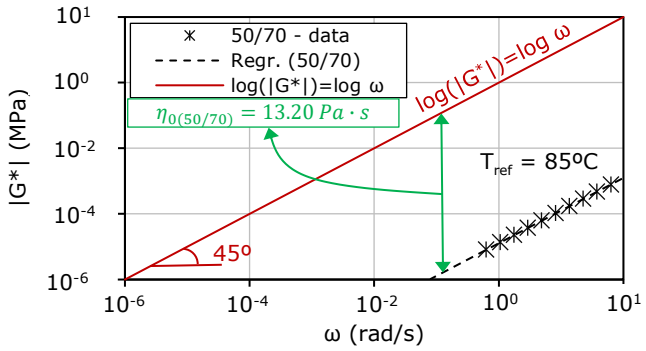

Figure A1.37. Determination of steady shear viscosity (η_0) at 85ºC for the fresh binder.

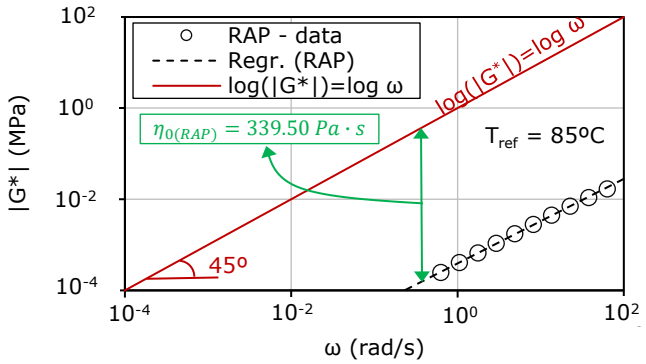

Figure A1.38. Determination of steady shear viscosity (η_0) at 85ºC for the RAP binder.

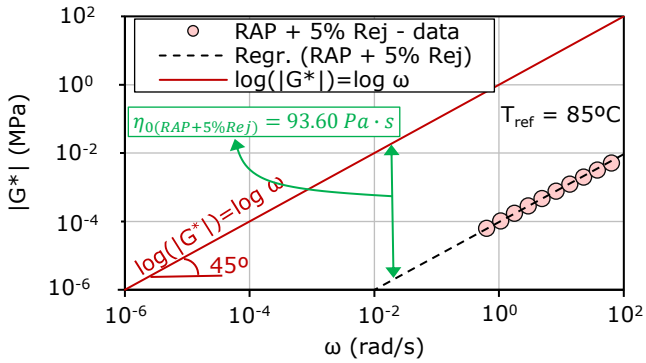

Figure A1.39. Determination of steady shear viscosity (η_0) at 85ºC for the blend RAP + 5% Rej.

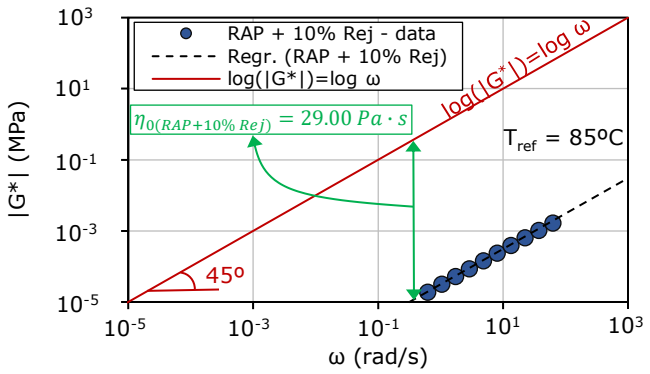

Figure A1.40. Determination of steady shear viscosity (η_0) at 85ºC for the blend RAP + 10% Rej.

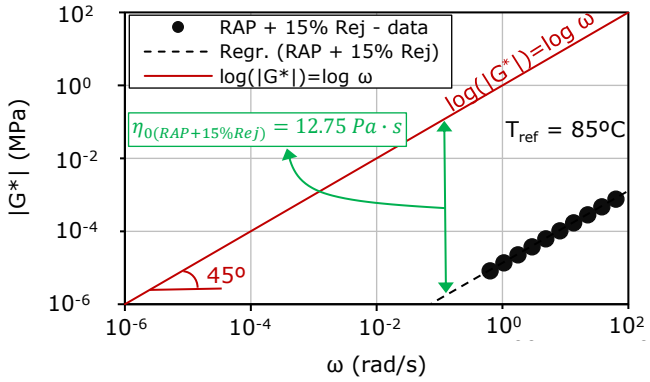

Figure A1.41. Determination of steady shear viscosity (η_0) at 85ºC for the blend RAP + 15% Rej.

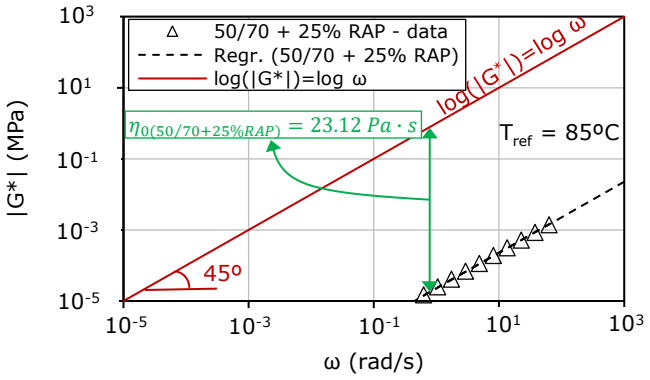

Figure A1.42. Determination of steady shear viscosity (η_0) at 85ºC for the blend 50/70 + 25% RAP.

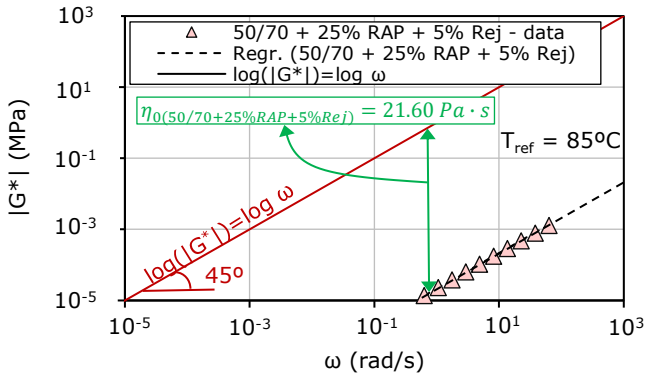

Figure A1.43. Determination of steady shear viscosity (η_0) at 85ºC for the blend 50/70 + 25% RAP + 5% Rej.

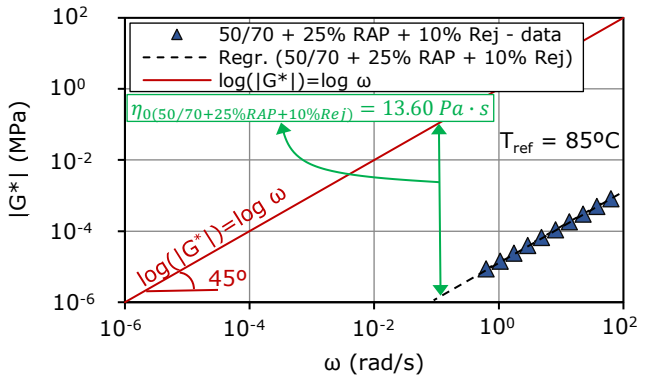

Figure A1.44. Determination of steady shear viscosity (η_0) at 85ºC for the blend 50/70 + 25% RAP + 10% Rej.

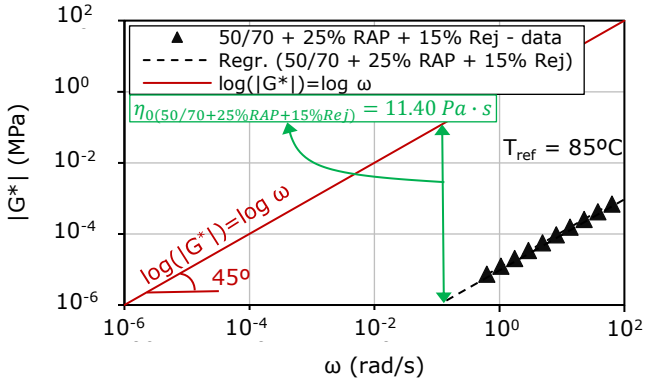

Figure A1.45. Determination of steady shear viscosity (η_0) at 85ºC for the blend 50/70 + 25% RAP + 15% Rej.

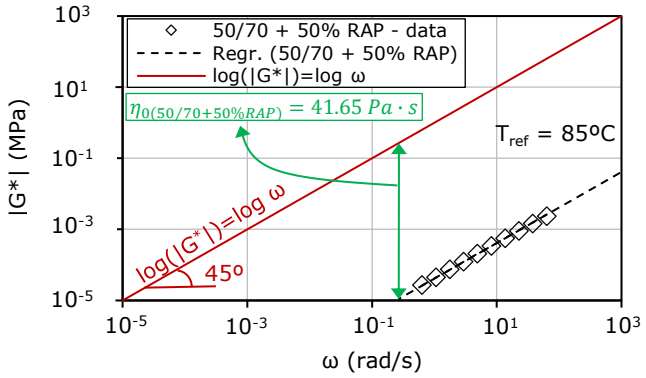

Figure A1.46. Determination of steady shear viscosity (η_0) at 85ºC for the blend 50/70 + 50% RAP.

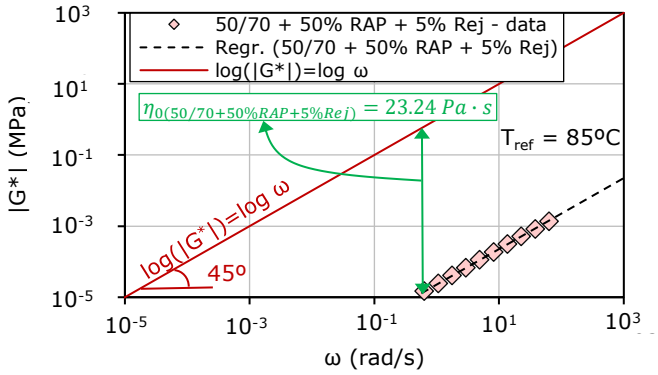

Figure A1.47. Determination of steady shear viscosity (η_0) at 85ºC for the blend 50/70 + 50% RAP + 5% Rej.

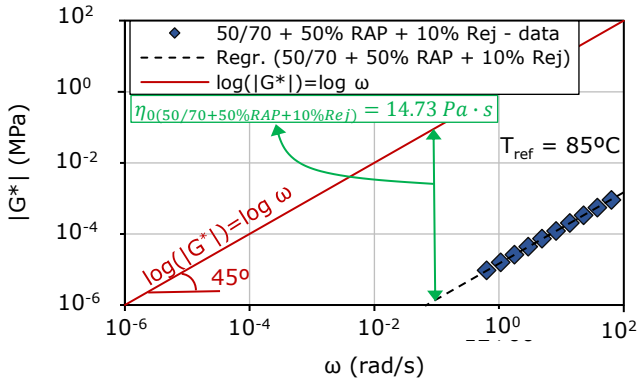

Figure A1.48. Determination of steady shear viscosity (η_0) at 85ºC for the blend 50/70 + 50% RAP + 10% Rej.

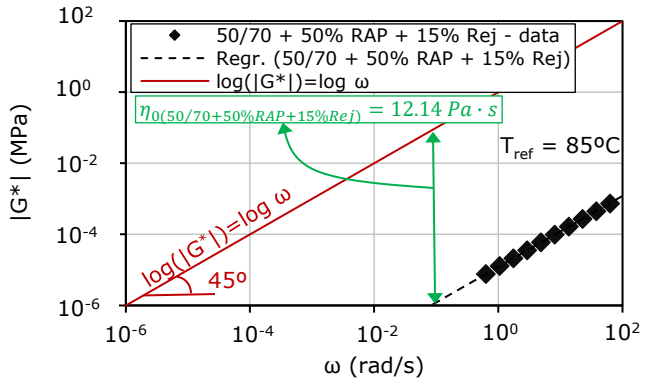

Figure A1.49. Determination of steady shear viscosity (η_0) at 85ºC for the blend 50/70 + 50% RAP + 15% Rej.

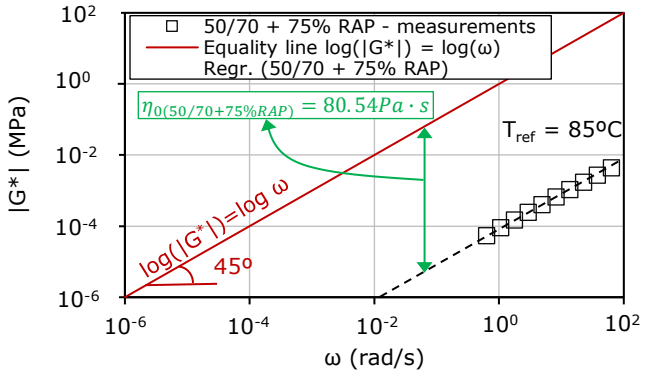

Figure A1.50. Determination of steady shear viscosity (η_0) at 85ºC for the blend 50/70 + 75% RAP.

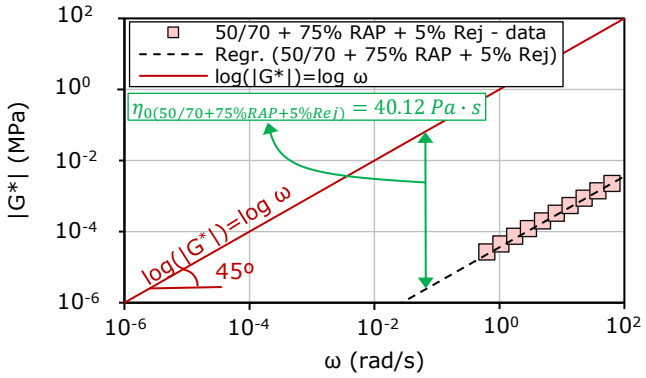

Figure A1.51. Determination of steady shear viscosity (η_0) at 85ºC for the blend 50/70 + 75% RAP + 5% Rej.

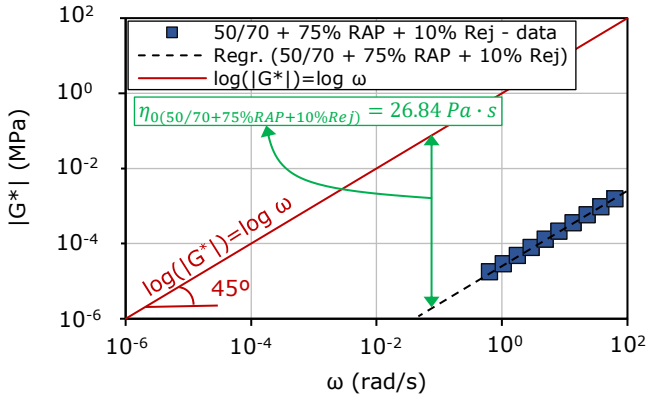

Figure A1.52. Determination of steady shear viscosity (η_0) at 85ºC for the blend 50/70 + 75% RAP + 10% Rej.

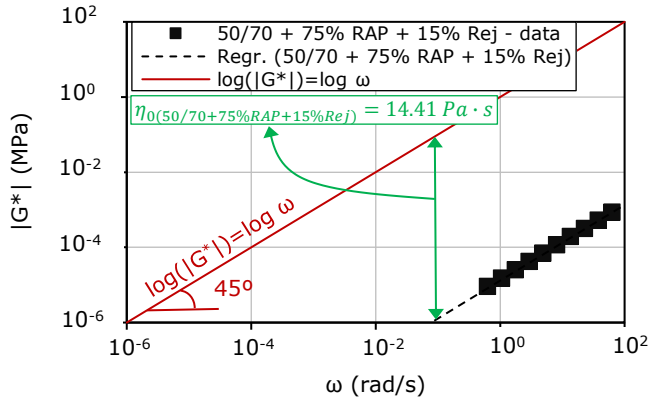

Figure A1.53. Determination of steady shear viscosity (η_0) at 85ºC for the blend 50/70 + 75% RAP + 15% Rej.

A.1.6. Norm of complex shear modulus measurements and estimations

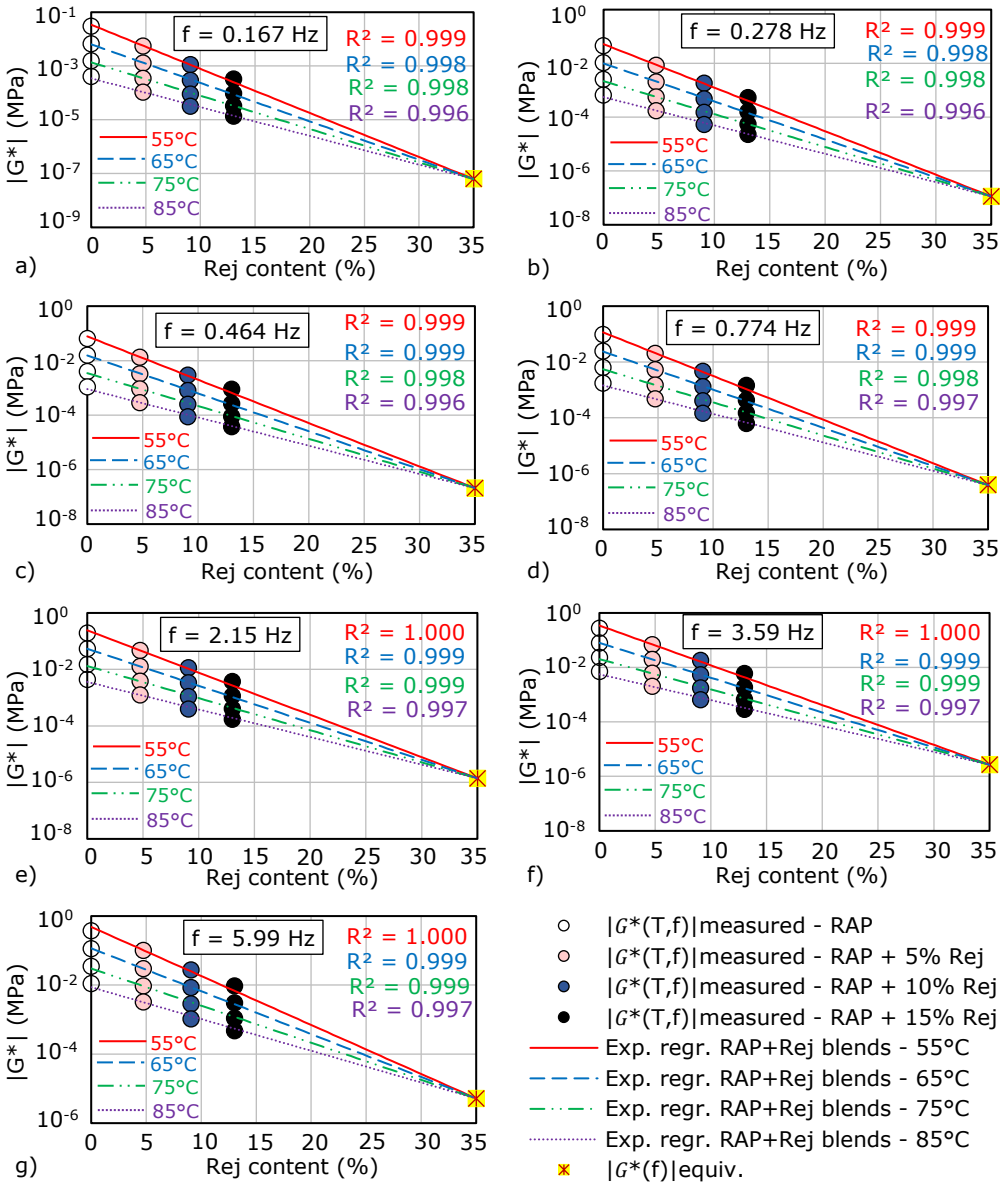

Figure A1.54. Norm of complex shear modulus measurements for the RAP + Rej blends at different frequencies and $|G^*(f)|_{equiv.}$ values which are only dependent on frequency obtained by linear extrapolation for a values of 35% content Rej: (a) f=0.167 Hz; (b) f=0.278 Hz; (c) f=0.464 Hz; (d) f=0.774 Hz; (e) f=2.15 Hz; (f) f=3.59 Hz; (g) f=5.99 Hz.

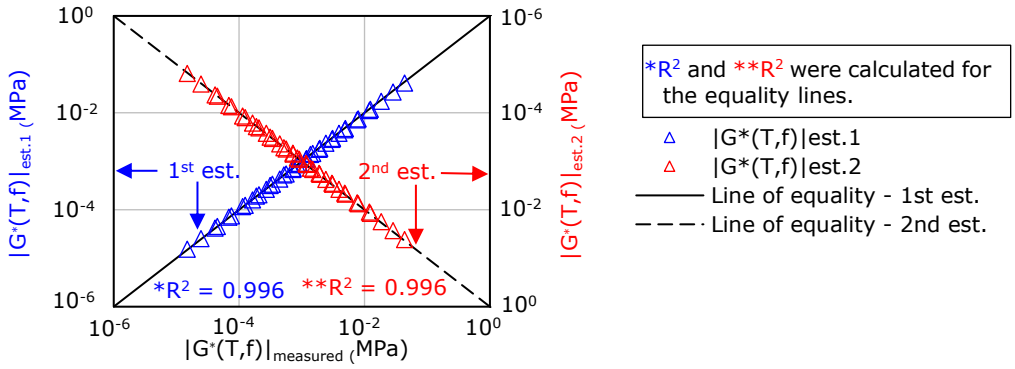

Figure A1.55. Correlation plot of estimated vs. measured $\left|G^*(T,f)\right|$ values for the binder blend 50/70 + 25% RAP.

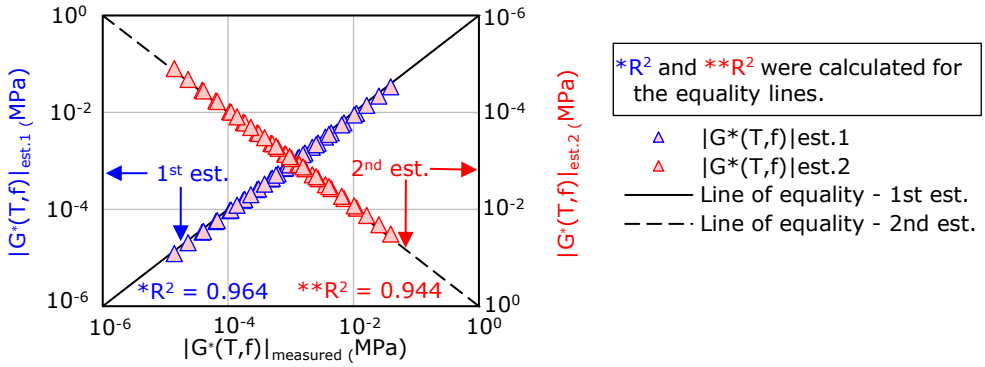

Figure A1.56. Correlation plot of estimated vs. measured $\left|G^*(T,f)\right|$ values for the binder blend 50/70 + 25% RAP + 5% Rej.

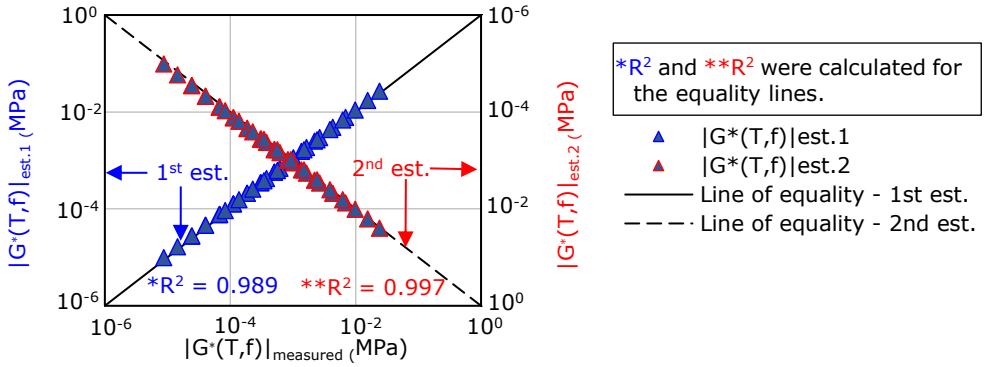

Figure A1.57. Correlation plot of estimated vs. measured $\left|G^*(T,f)\right|$ values for the binder blend 50/70 + 25% RAP + 10% Rej.

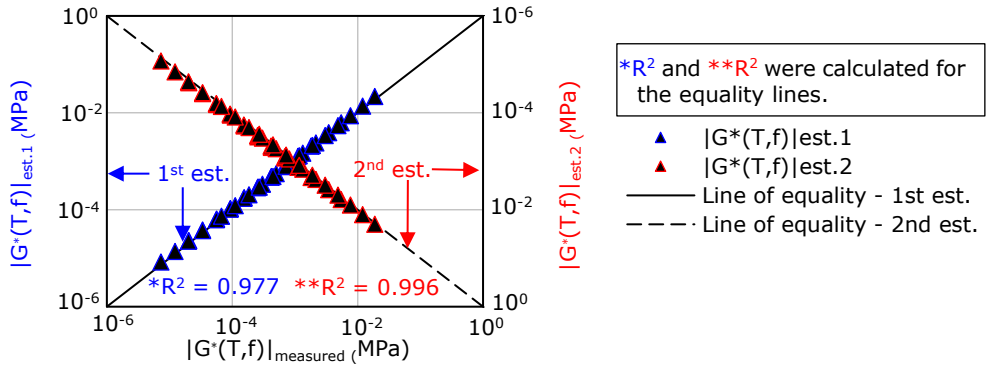

Figure A1.58. Correlation plot of estimated vs. measured $|G^*(T,f)|$ values for the binder blend 50/70 + 25% RAP + 15% Rej.

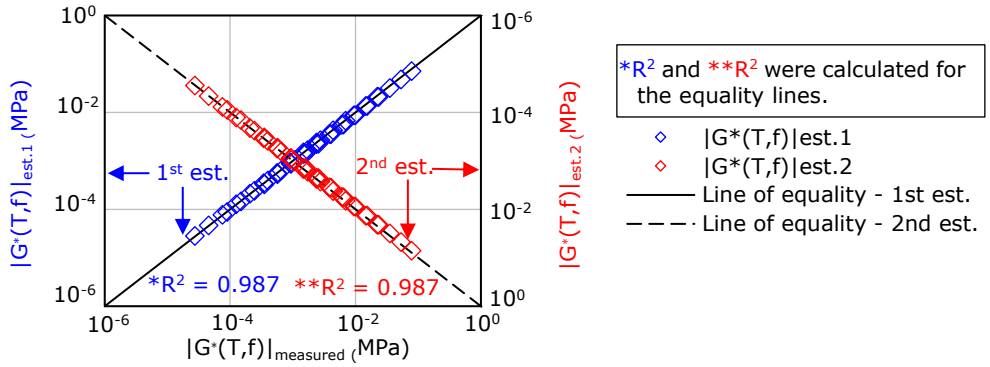

Figure A1.59. Correlation plot of estimated vs. measured $|G^*(T,f)|$ values for the binder blend 50/70 + 50% RAP.

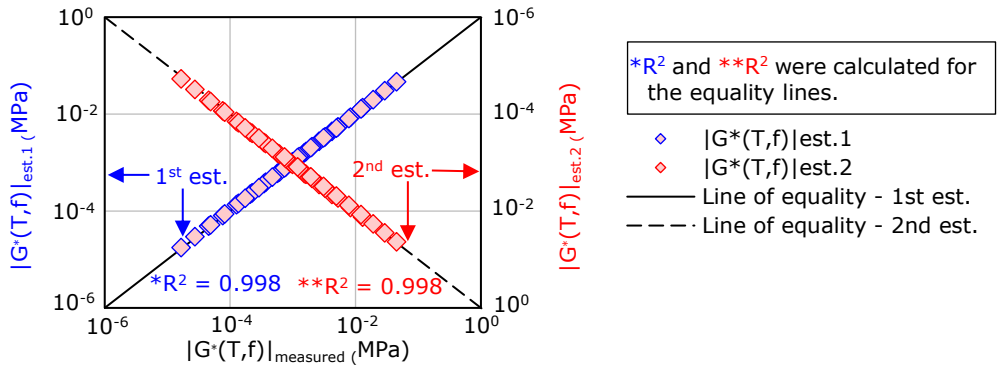

Figure A1.60. Correlation plot of estimated vs. measured $|G^*(T,f)|$ values for the binder blend 50/70 + 50% RAP + 5% Rej.

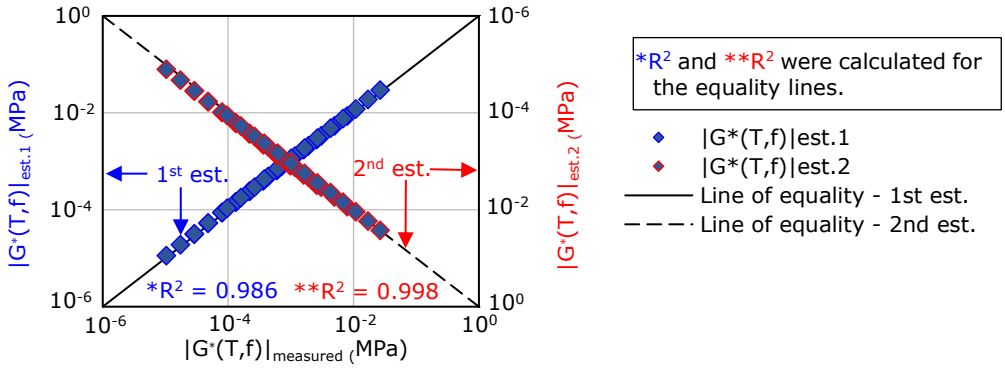

Figure A1.61. Correlation plot of estimated vs. measured $\left|G^*(T,f)\right|$ values for the binder blend 50/70 + 50% RAP + 10% Rej.

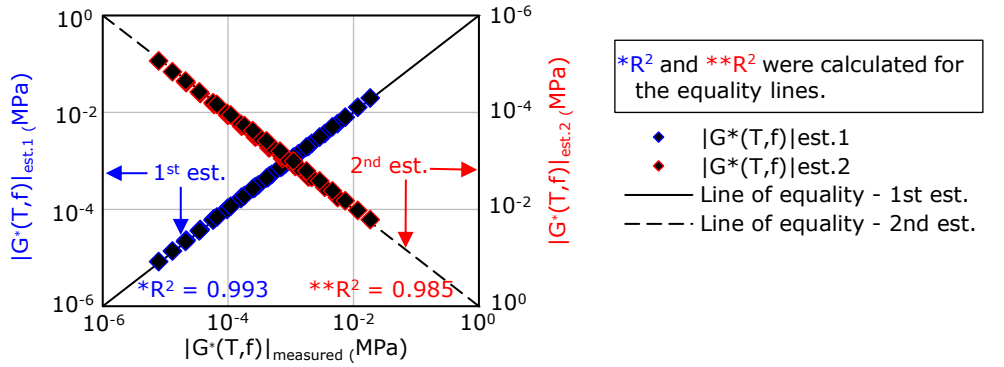

Figure A1.62. Correlation plot of estimated vs. measured $\left|G^*(T,f)\right|$ values for the binder blend 50/70 + 50% RAP + 15% Rej.

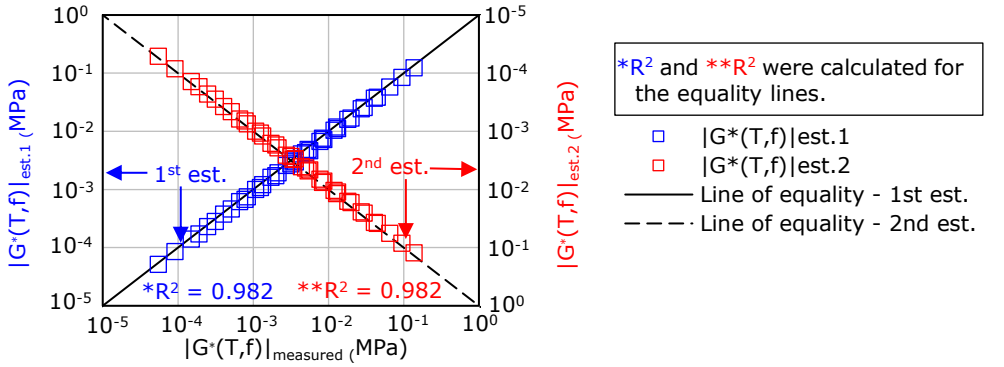

Figure A1.63. Correlation plot of estimated vs. measured $\left|G^*(T,f)\right|$ values for the binder blend 50/70 + 75% RAP.

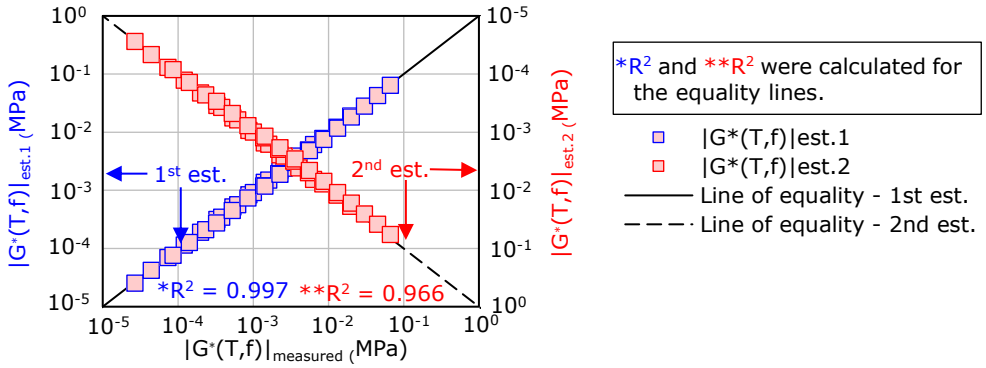

Figure A1.64. Correlation plot of estimated vs. measured $|G^*(T,f)|$ values for the binder blend 50/70 + 75% RAP + 5% Rej.

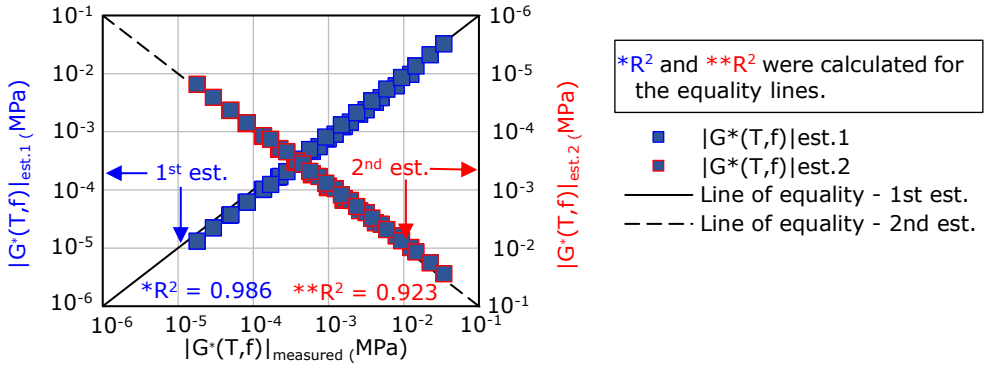

Figure A1.65. Correlation plot of estimated vs. measured $|G^*(T,f)|$ values for the binder blend 50/70 + 75% RAP + 10% Rej.

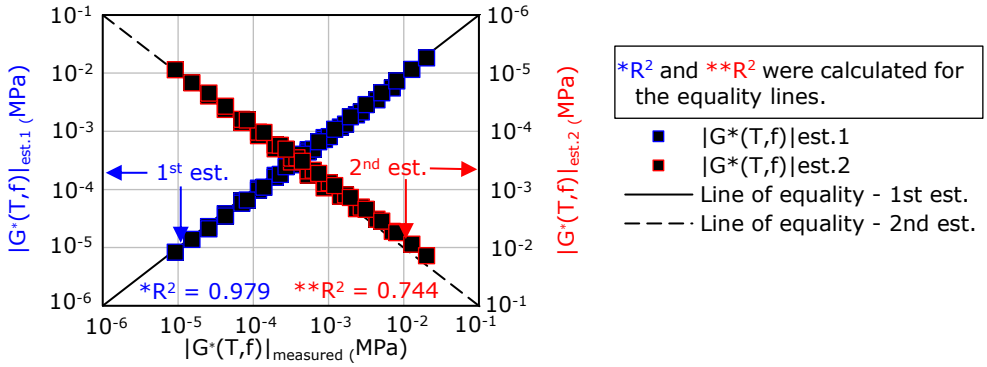

Figure A1.66. Correlation plot of estimated vs. measured $|G^*(T,f)|$ values for the binder blend 50/70 + 75% RAP + 15% Rej.

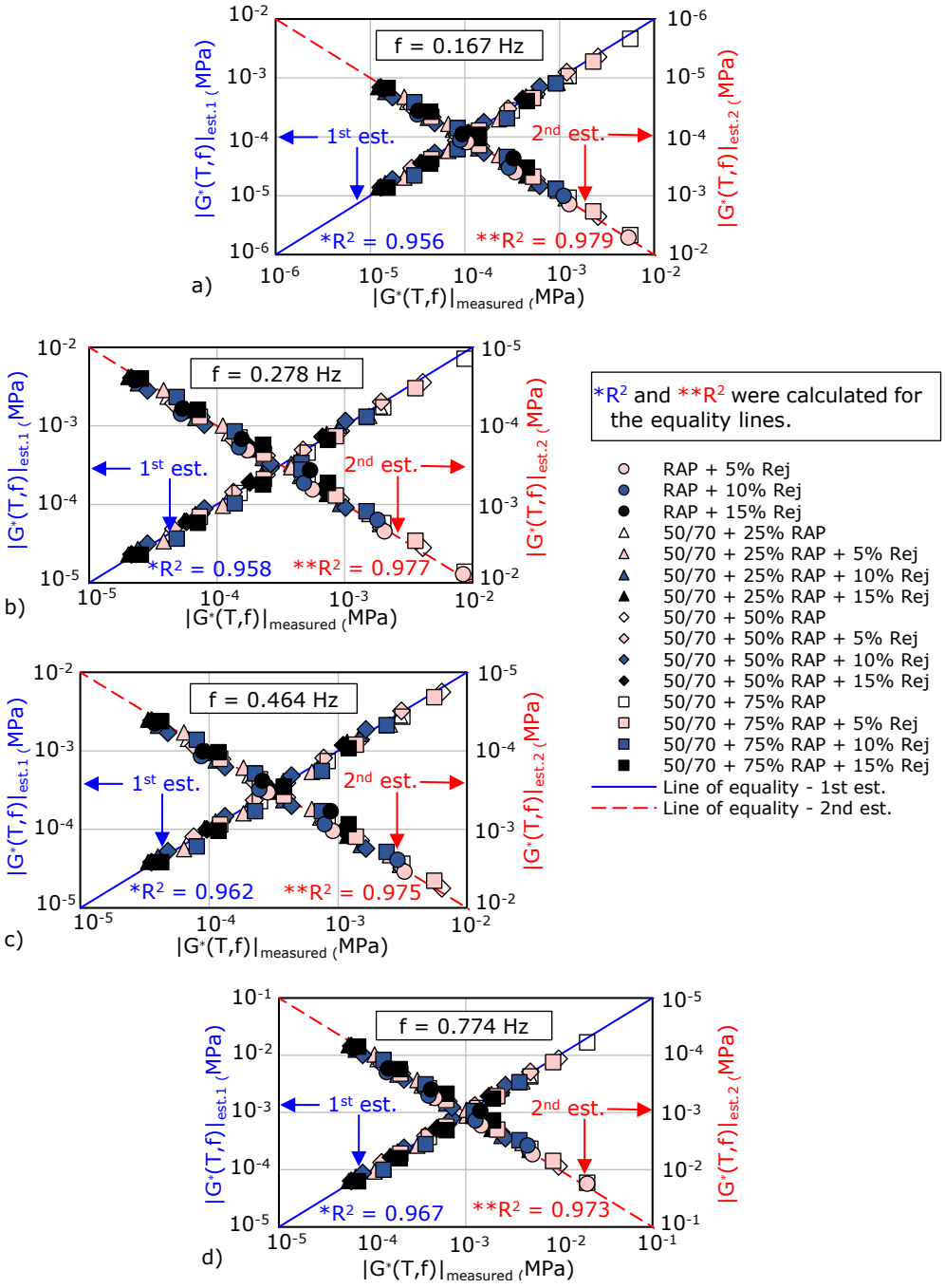

Figure A1.67. Global correlation plots of estimated vs. measured $\left|G^*(T,f)\right|$ values for all considered binder blends at different frequencies: (a) f=0.167 Hz; (b) f=0.278 Hz; (c) f=0.464 Hz; (d) f=0.774 Hz.

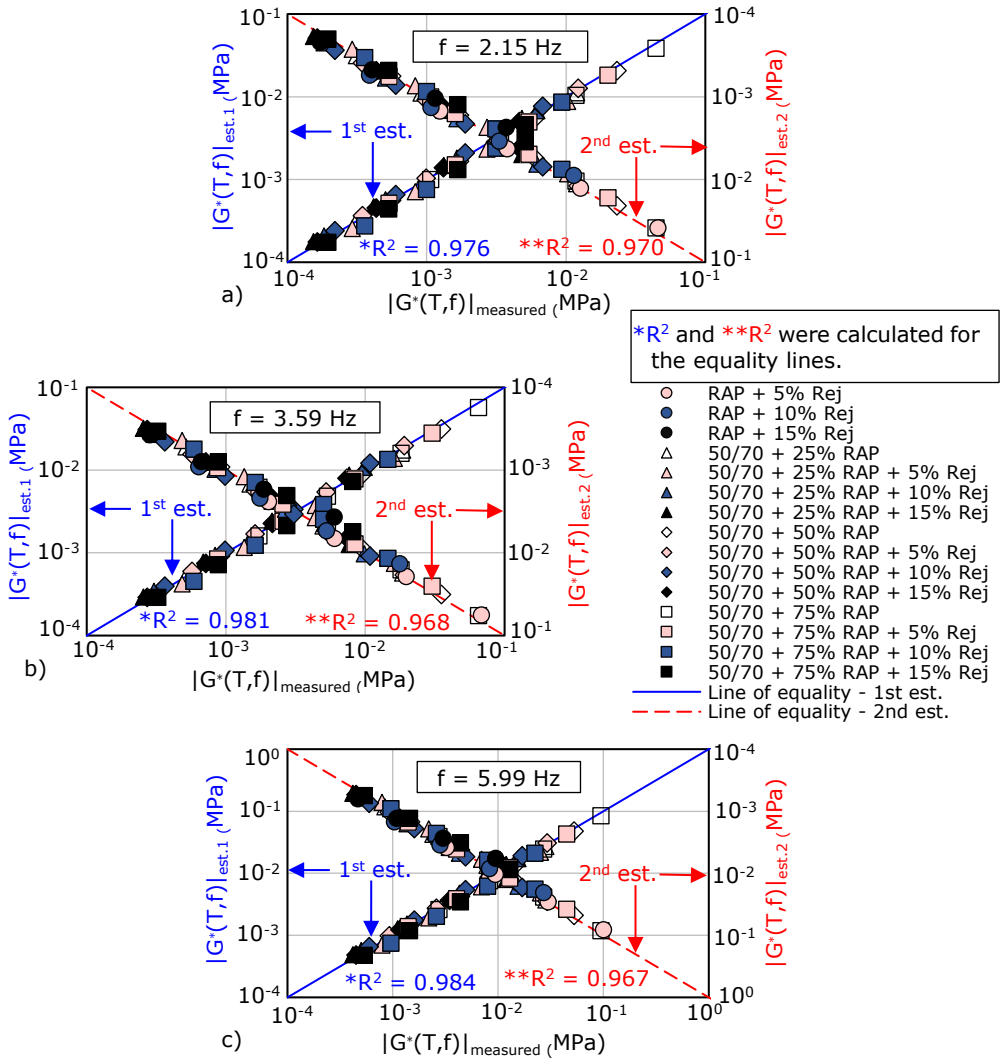

Figure A1.68. Global correlation plots of estimated vs. measured $\left|G^*(T,f)\right|$ values for all considered binder blends at different frequencies: (a) f=2.15 Hz; (b) f=3.59 Hz; (c) f=5.99 Hz.

A.1.7. Phase angle measurements vs. calculated values

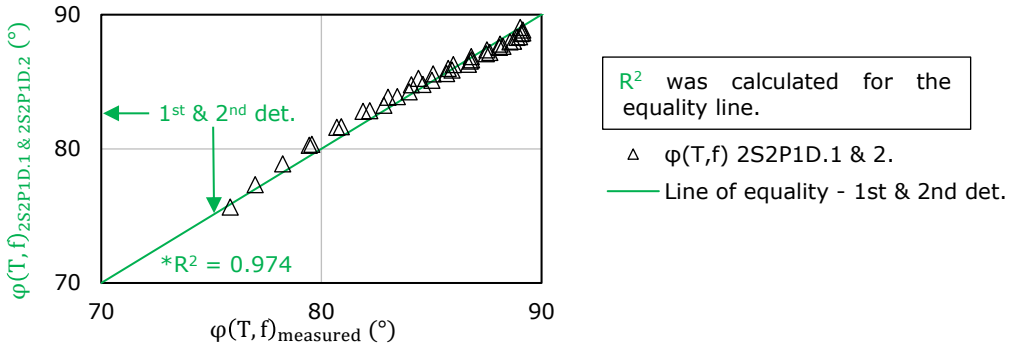

Figure A1.69. Plot of calculated vs. measured $\varphi(T,f)$ values for the binder blend 50/70 + 25% RAP.

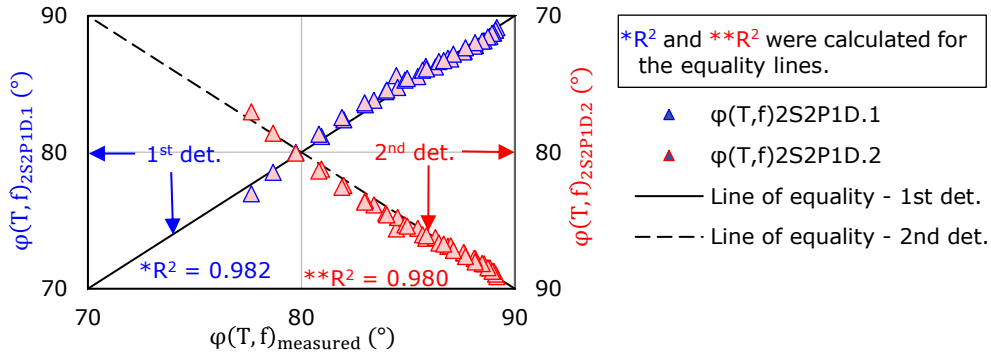

Figure A1.70. Plot of calculated vs. measured $\varphi(T,f)$ values for the binder blend 50/70 + 25% RAP + 5% Rej.

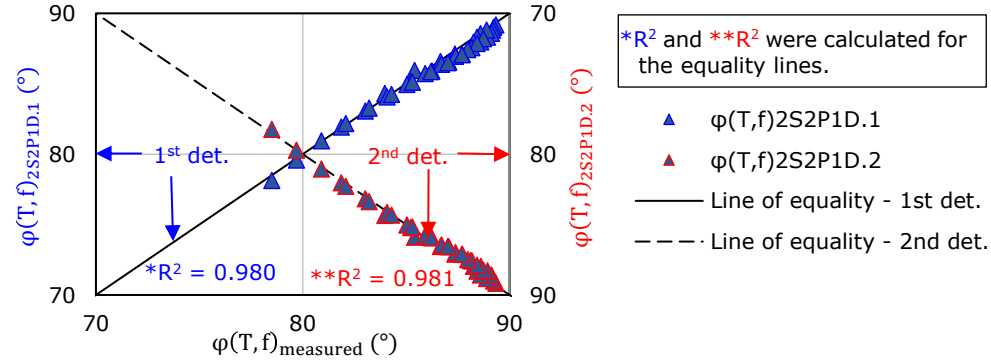

Figure A1.71. Plot of calculated vs. measured $\varphi(T,f)$ values for the binder blend 50/70 + 25% RAP + 10% Rej.

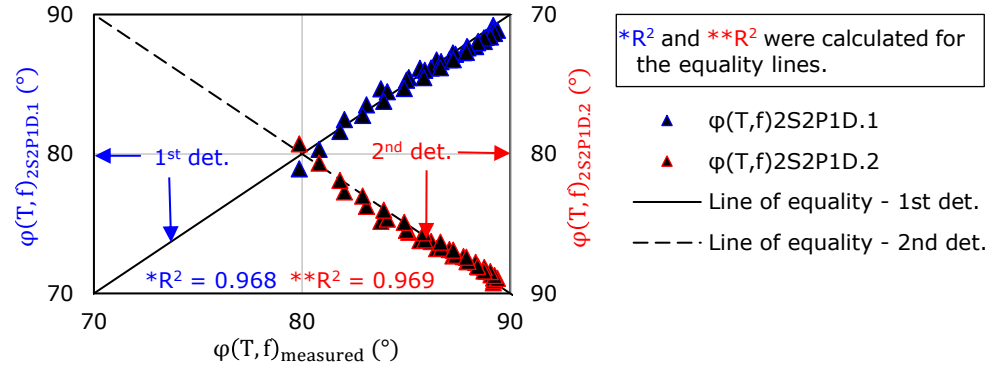

Figure A1.72. Plot of calculated vs. measured $\varphi(T,f)$ values for the binder blend 50/70 + 25% RAP + 15% Rej.

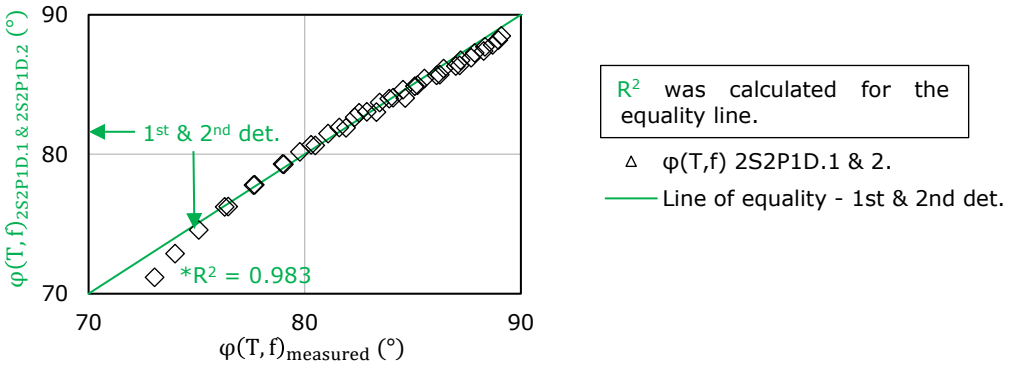

Figure A1.73. Plot of calculated vs. measured $\varphi(T,f)$ values for the binder blend 50/70 + 50% RAP.

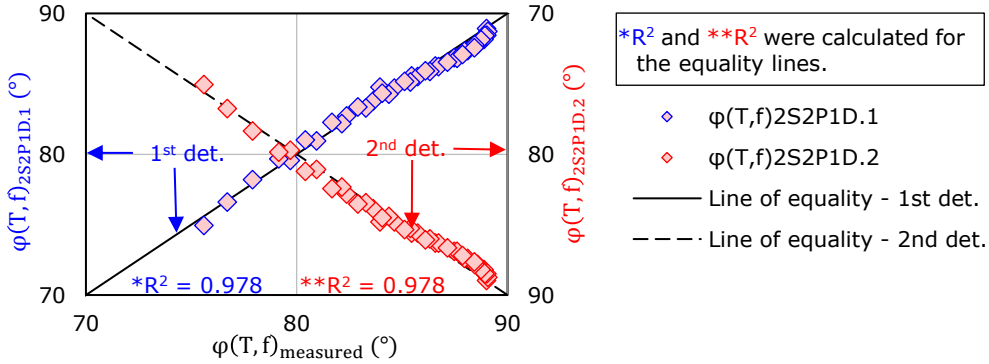

Figure A1.74. Plot of calculated vs. measured $\varphi(T,f)$ values for the binder blend 50/70 + 50% RAP + 5% Rej.

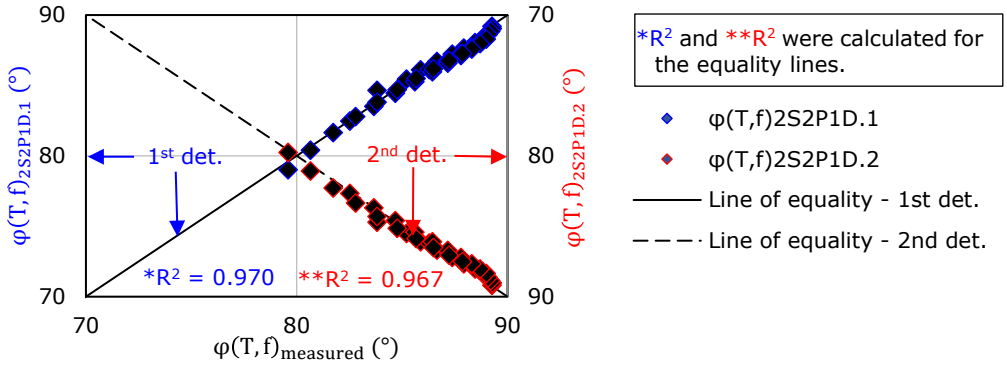

Figure A1.75. Plot of calculated vs. measured $\varphi(T,f)$ values for the binder blend 50/70 + 50% RAP + 15% Rej.

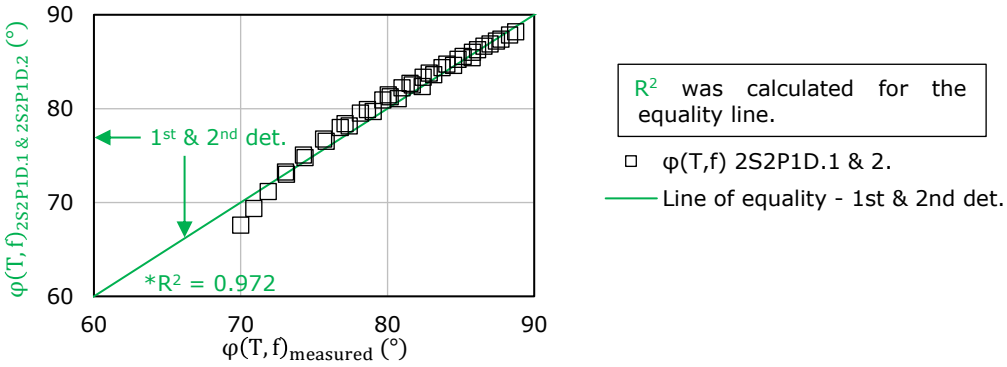

Figure A1.76. Plot of calculated vs. measured $\varphi(T,f)$ values for the binder blend 50/70 + 75% RAP.

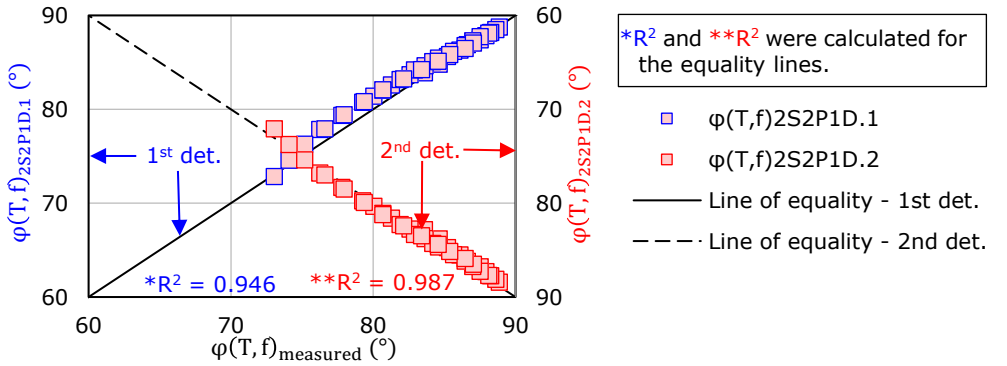

Figure A1.77. Plot of calculated vs. measured $\varphi(T,f)$ values for the binder blend 50/70 + 75% RAP + 5% Rej.

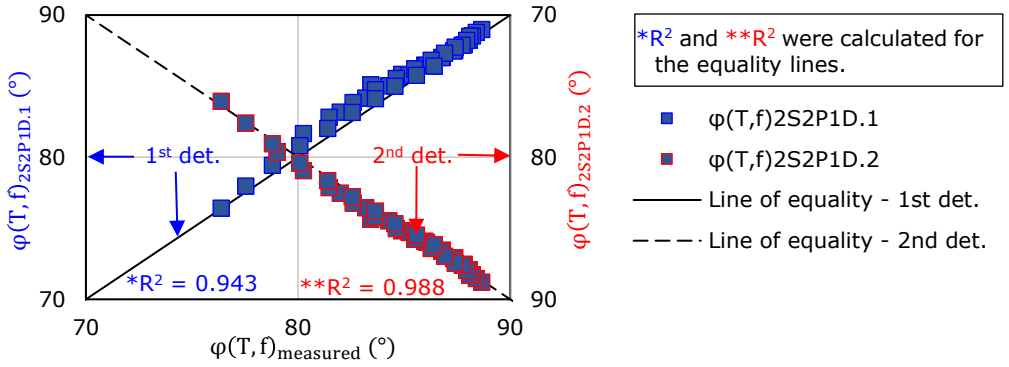

Figure A1.78. Plot of calculated vs. measured $\varphi(T,f)$ values for the binder blend 50/70 + 75% RAP + 10% Rej.

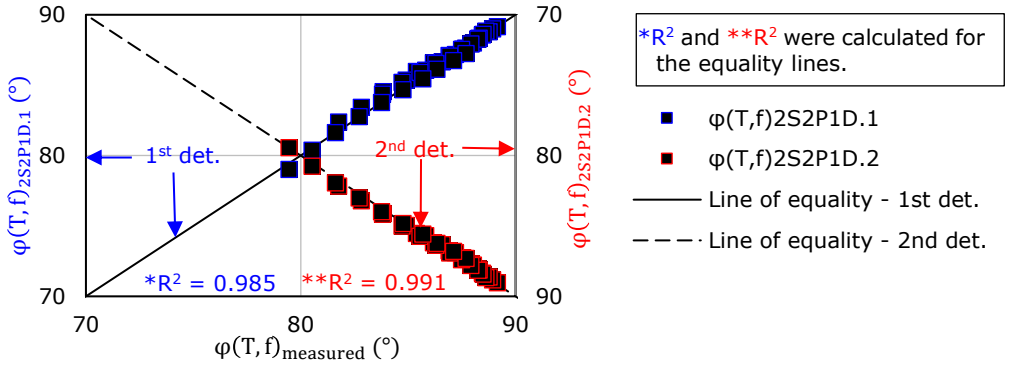

Figure A1.79. Plot of calculated vs. measured $\varphi(T,f)$ values for the binder blend 50/70 + 75% RAP + 15% Rej.

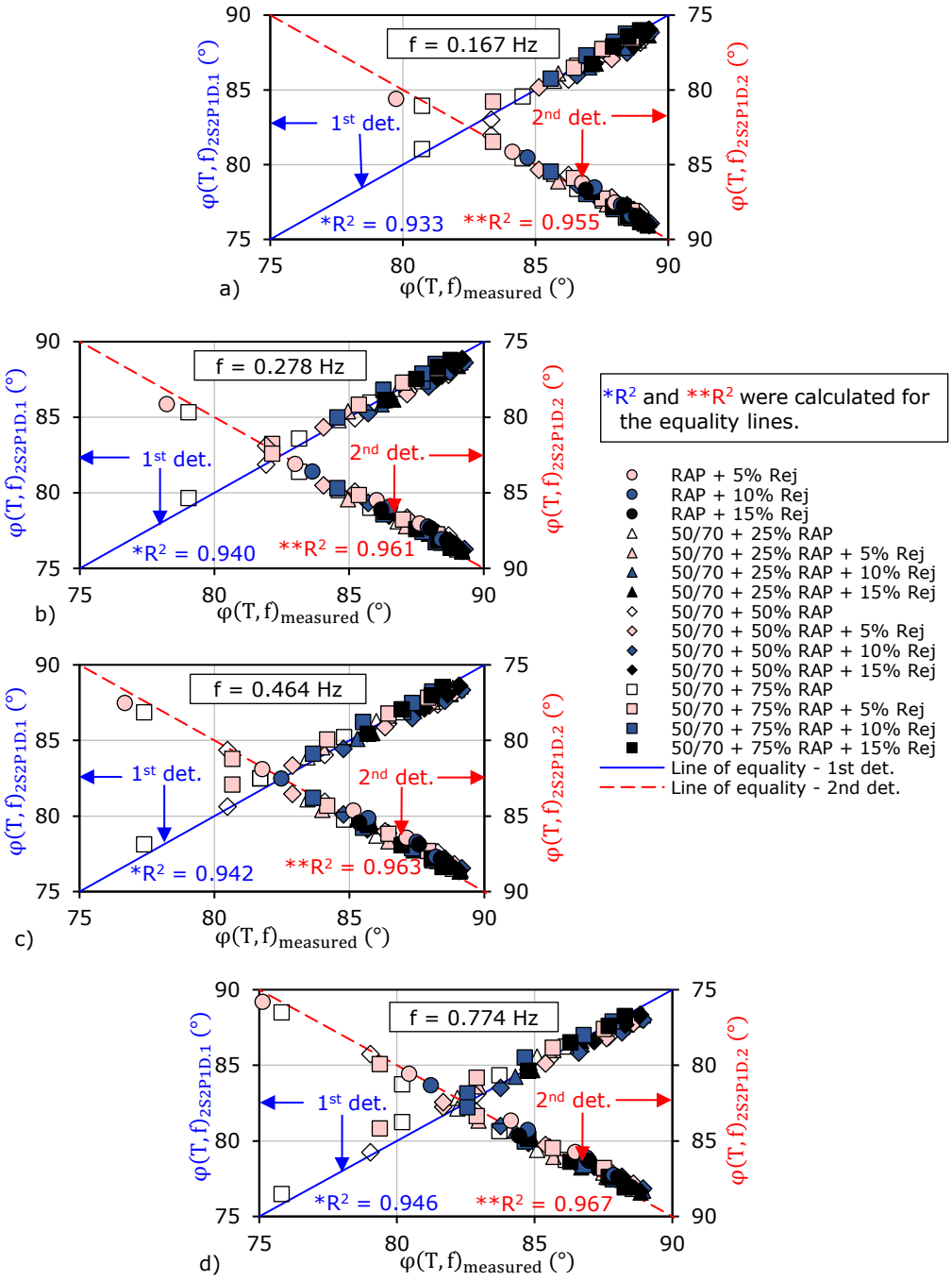

Figure A1.80. Global plots of measured vs. determined $\varphi(T,f)$ values for all considered binder blends at different frequencies: (a) f=0.167 Hz; (b) f=0.278 Hz; (c) f=0.464 Hz; (d) f=0.774 Hz.

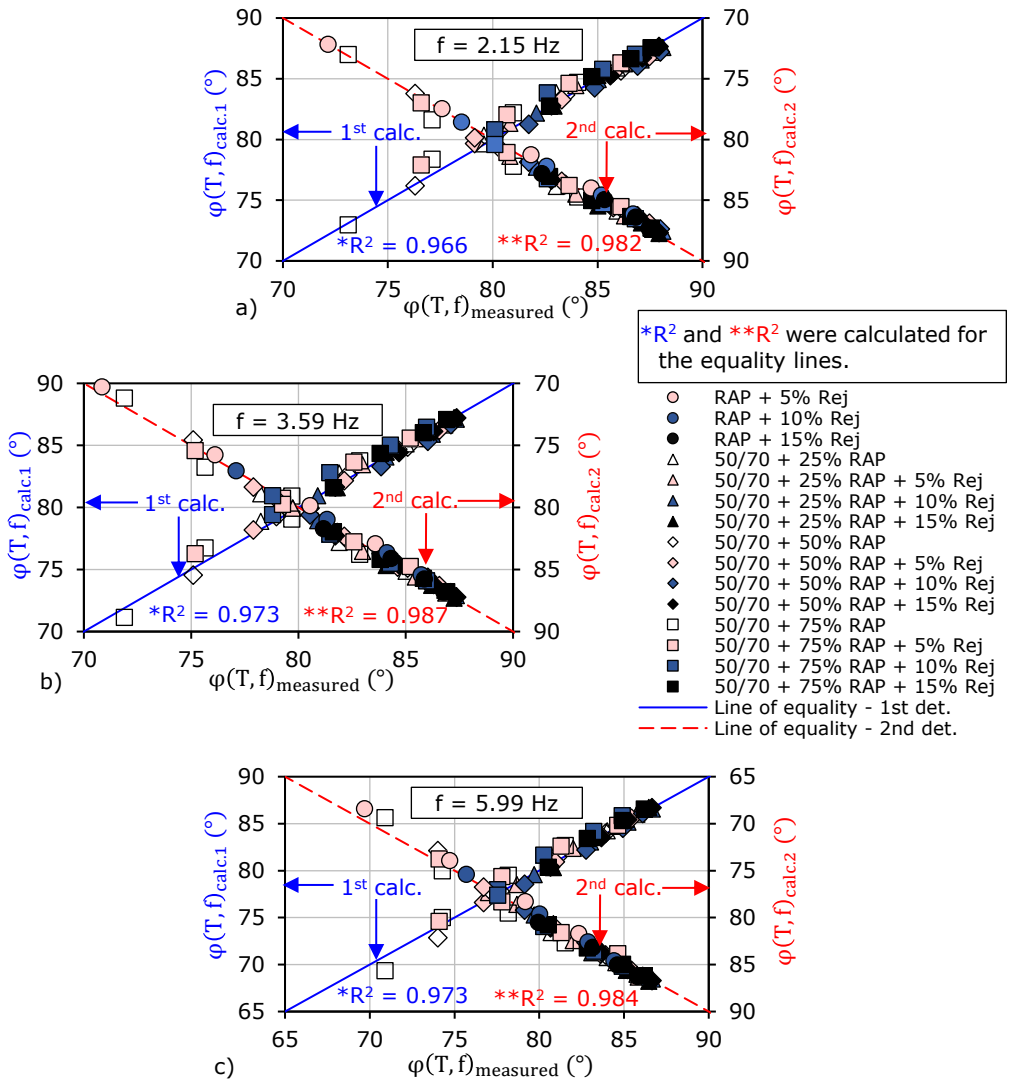

Figure A1.81. Global plots of measured vs. determined $\varphi(T,f)$ values for all considered binder blends at different frequencies: (a) f=2.15 Hz; (b) f=3.59 Hz; (c) f=5.99 Hz.

A.1.8. DSR high critical temperature determination

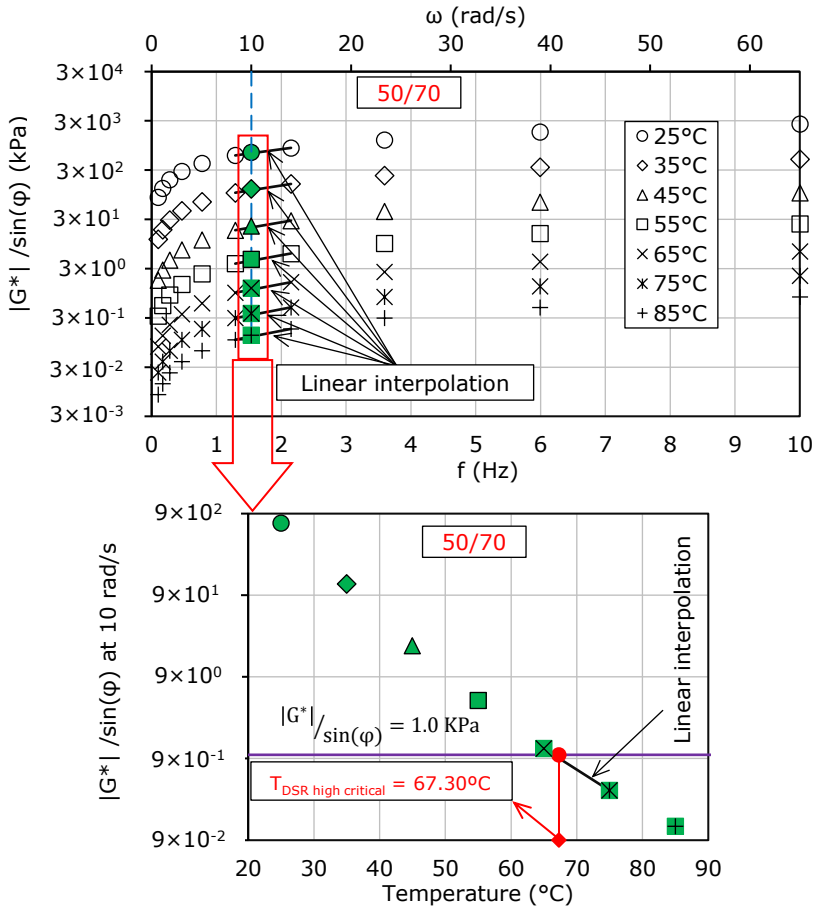

Figure A1.82. $T_{DSR\ high\ critical}$ determination from complex shear modulus test results for fresh 50/70 binder.

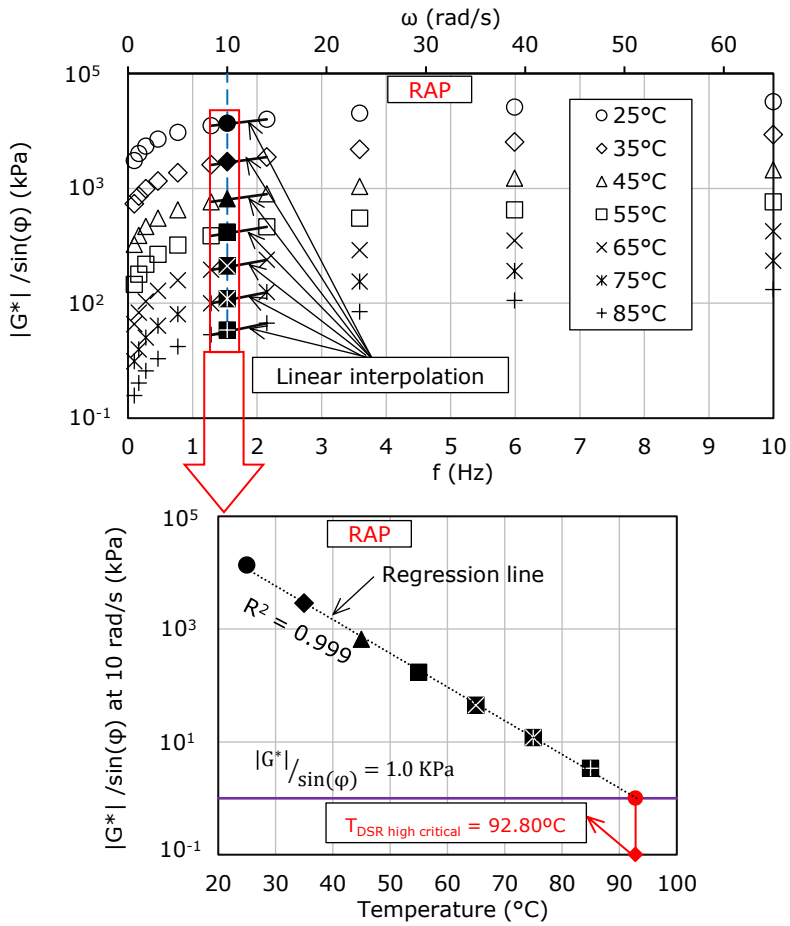

Figure A1.83. $T_{DSR\ high\ critical}$ determination from complex shear modulus test results for RAP binder.

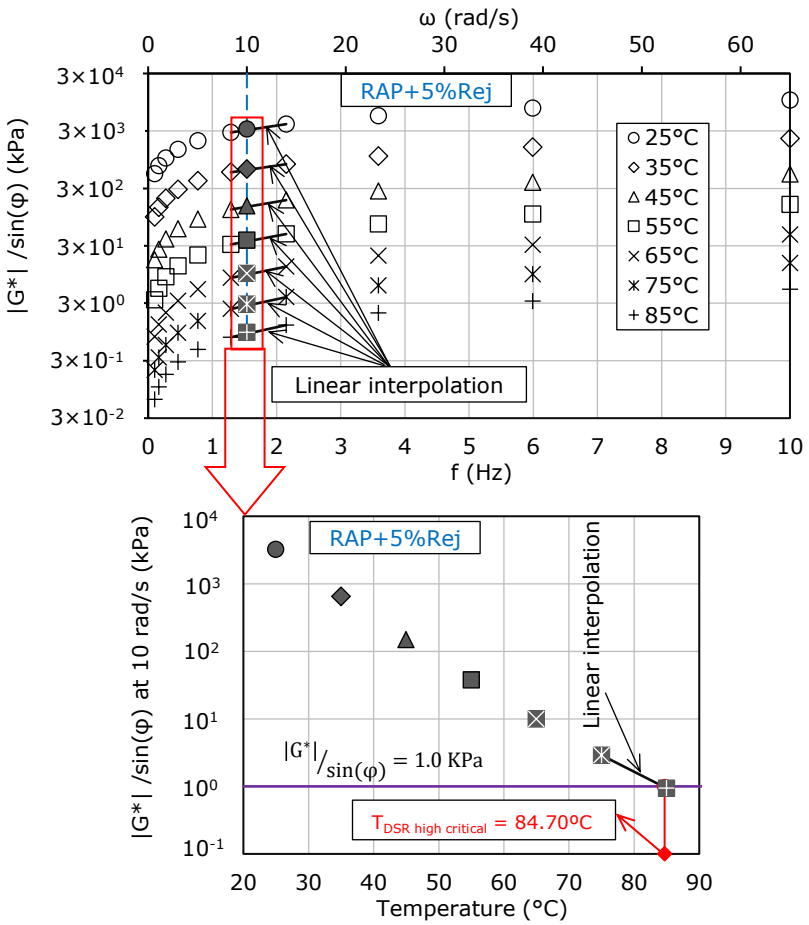

Figure A1.84. $T_{DSR\ high\ critical}$ determination from complex shear modulus test results for the blend RAP + 5% Rej.

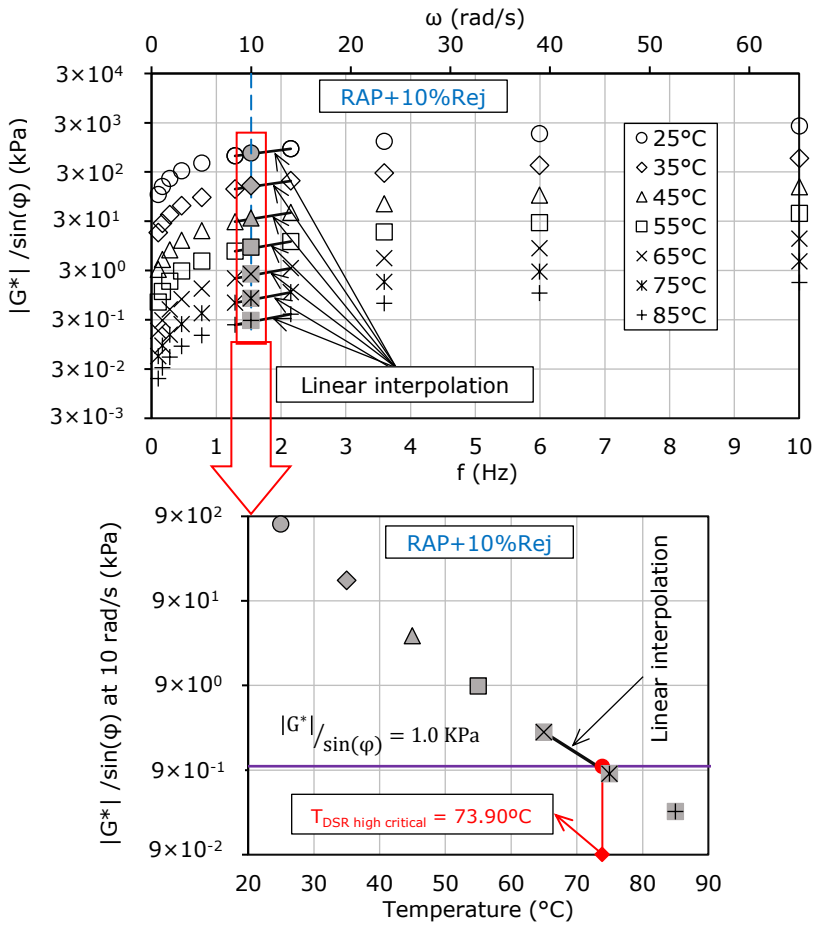

Figure A1.85. $T_{DSR\ high\ critical}$ determination from complex shear modulus test results for the blend RAP + 10% Rej.

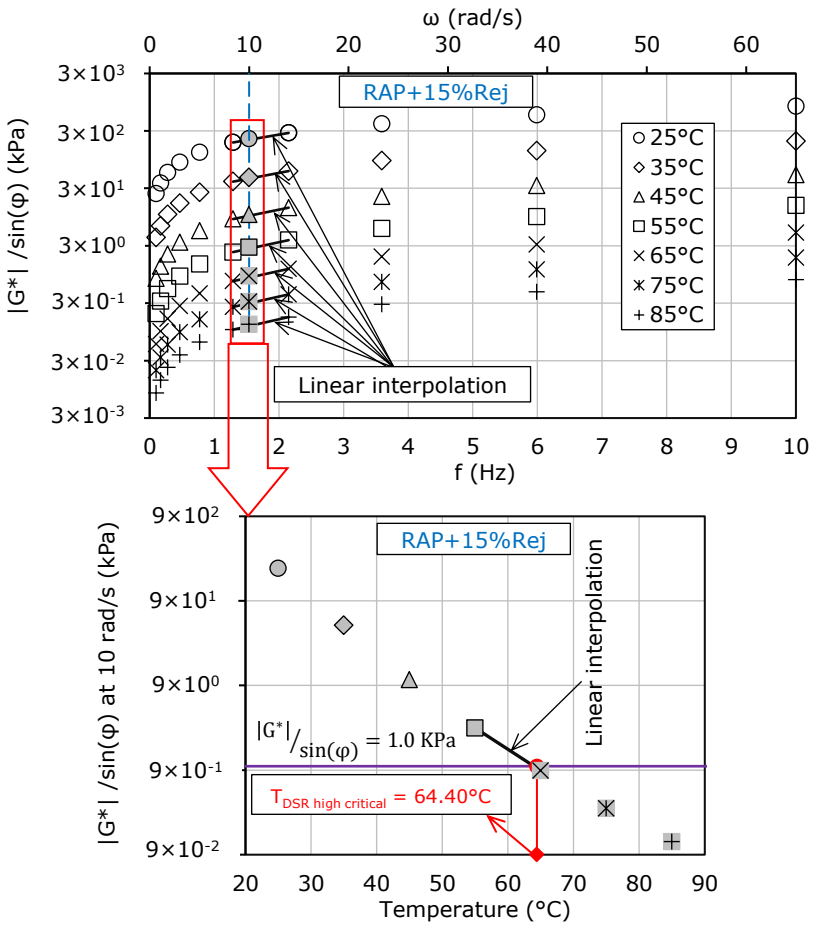

Figure A1.86. $T_{DSR\ high\ critical}$ determination from complex shear modulus test results for the blend RAP + 15% Rej.

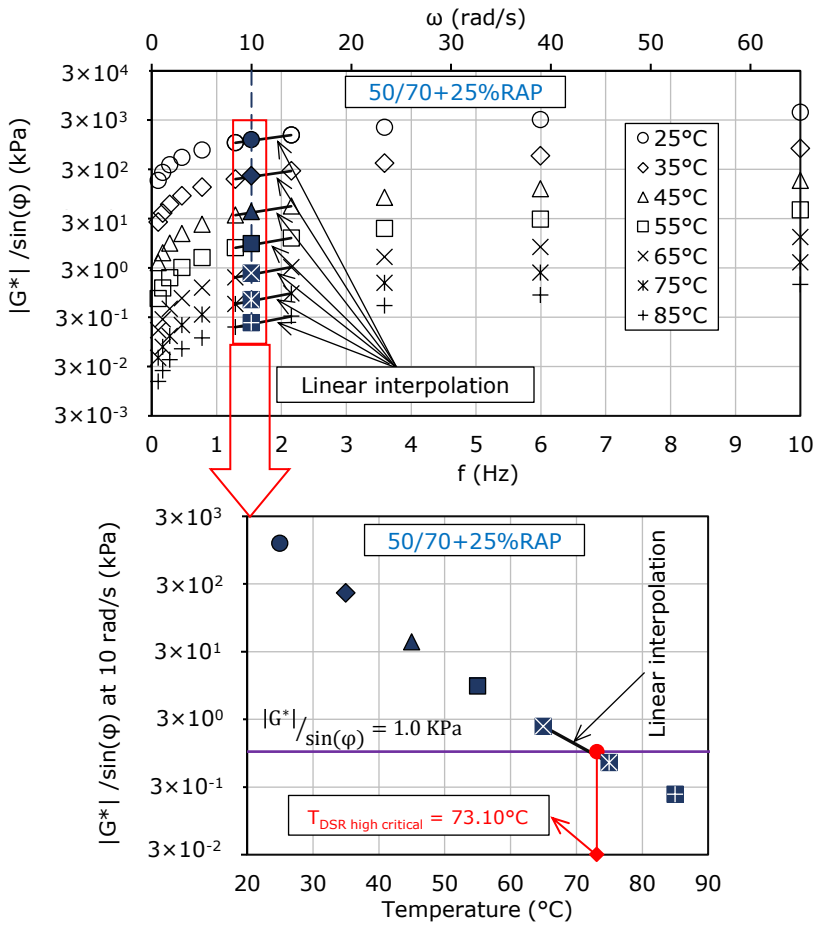

Figure A1.87. $T_{DSR\ high\ critical}$ determination from complex shear modulus test results for the blend 50/70 + 25% RAP.

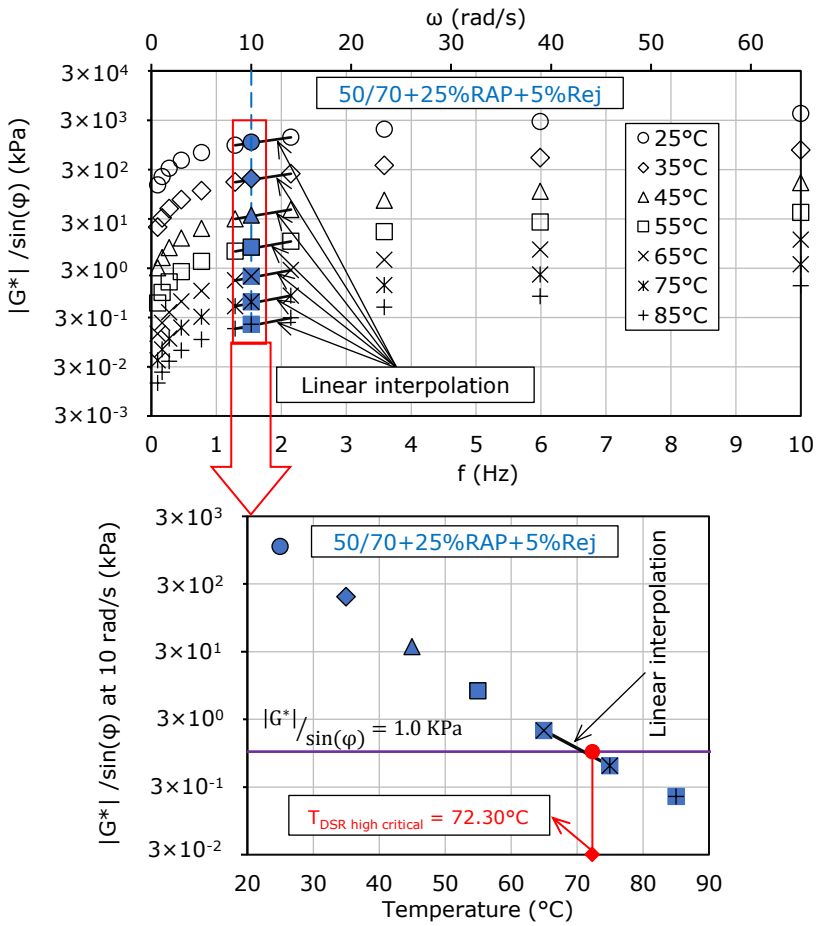

Figure A1.88. $T_{DSR\ high\ critical}$ determination from complex shear modulus test results for the blend 50/70 + 25% RAP + 5% Rej.

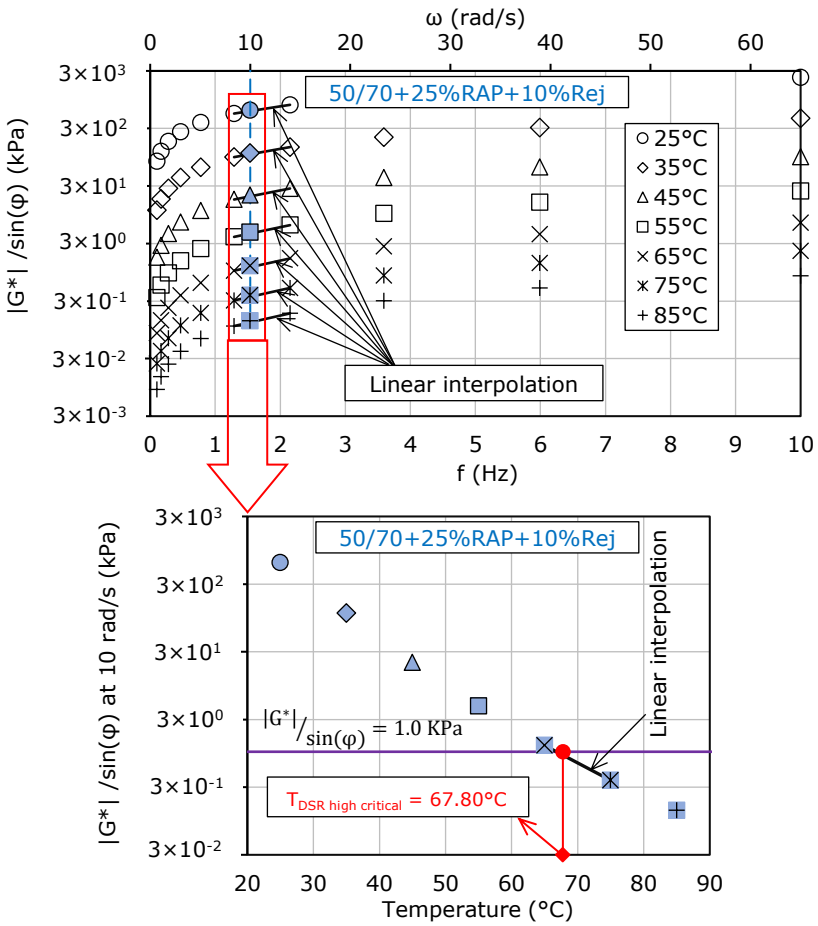

Figure A1.89. $T_{DSR\ high\ critical}$ determination from complex shear modulus test results for the blend 50/70 + 25% RAP + 10% Rej.

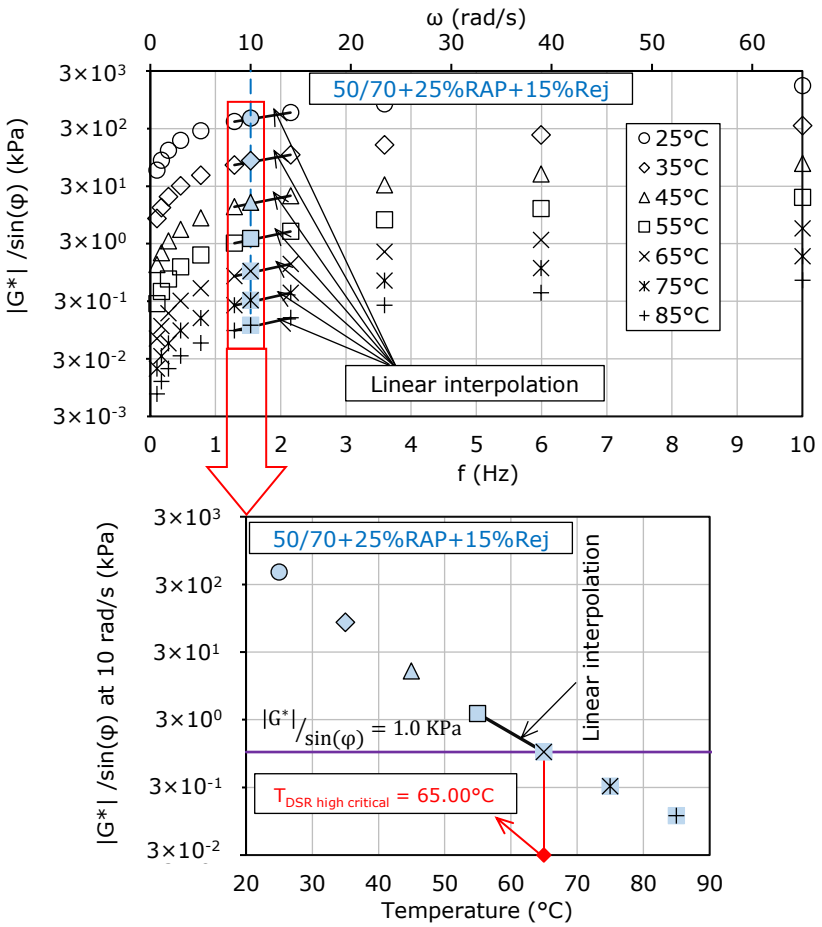

Figure A1.90. $T_{DSR\ high\ critical}$ determination from complex shear modulus test results for the blend 50/70 + 25% RAP + 15% Rej.

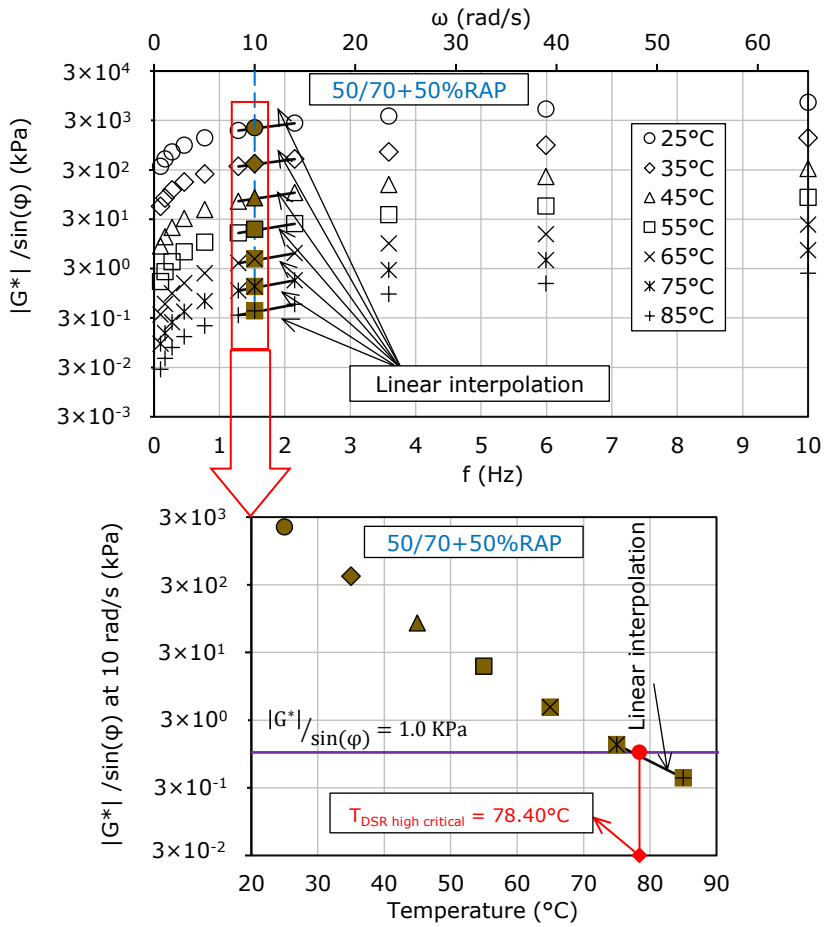

Figure A1.91. $T_{DSR\ high\ critical}$ determination from complex shear modulus test results for the blend 50/70 + 50% RAP.

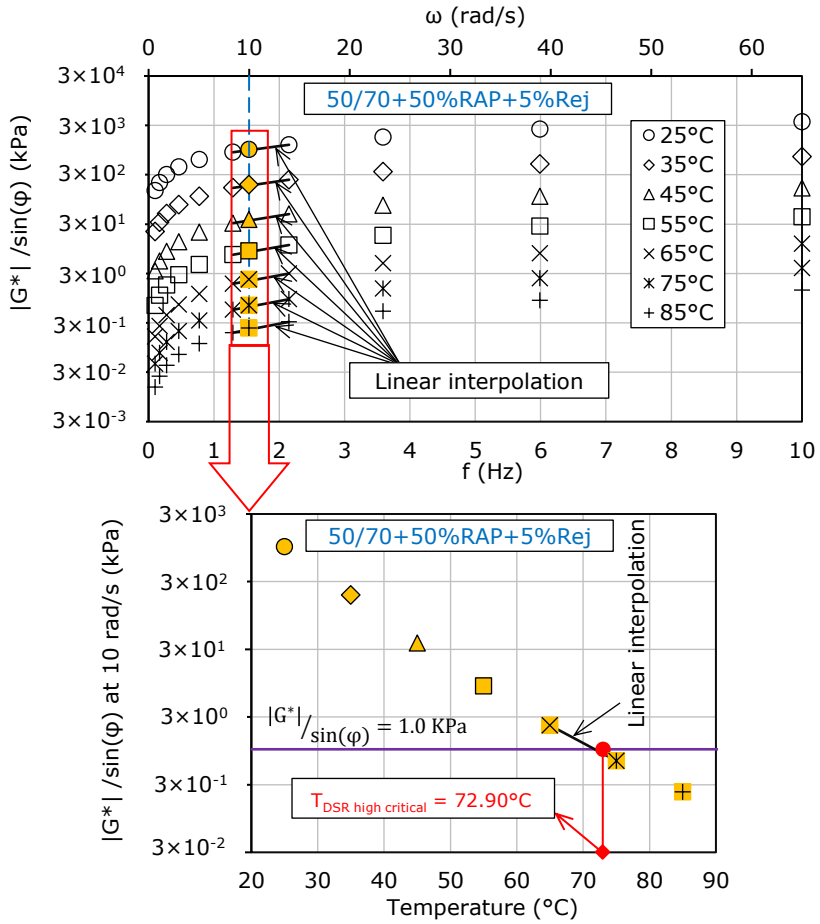

Figure A1.92. $T_{DSR\ high\ critical}$ determination from complex shear modulus test results for the blend 50/70 + 50% RAP + 5% Rej.

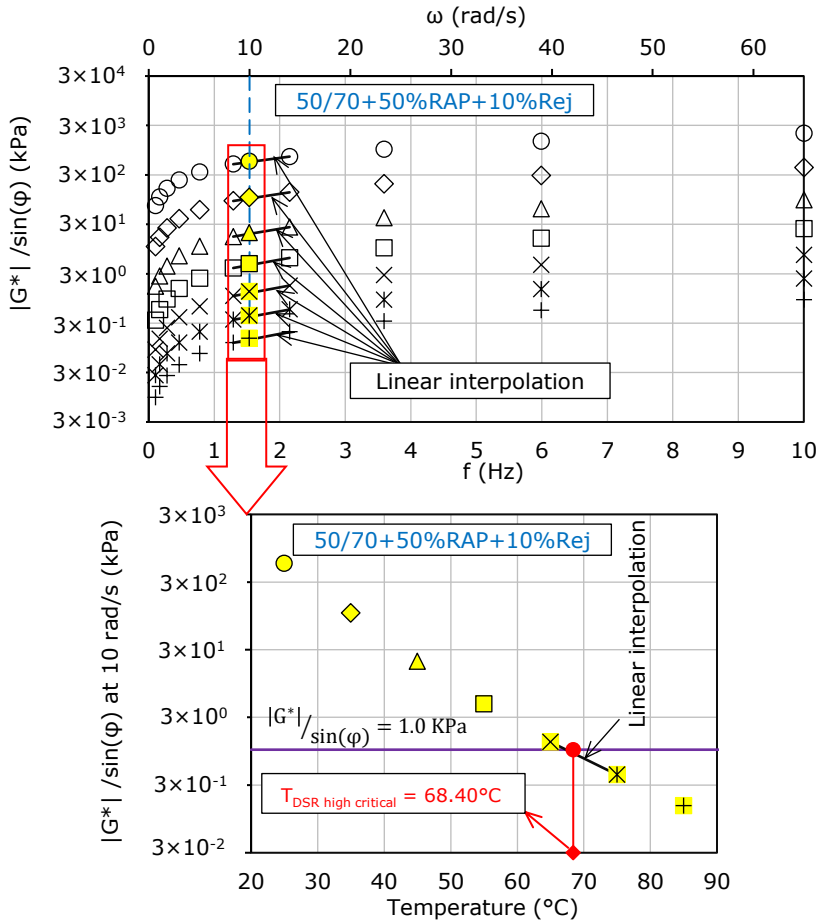

Figure A1.93. $T_{DSR\ high\ critical}$ determination from complex shear modulus test results for the blend 50/70 + 50% RAP + 10% Rej.

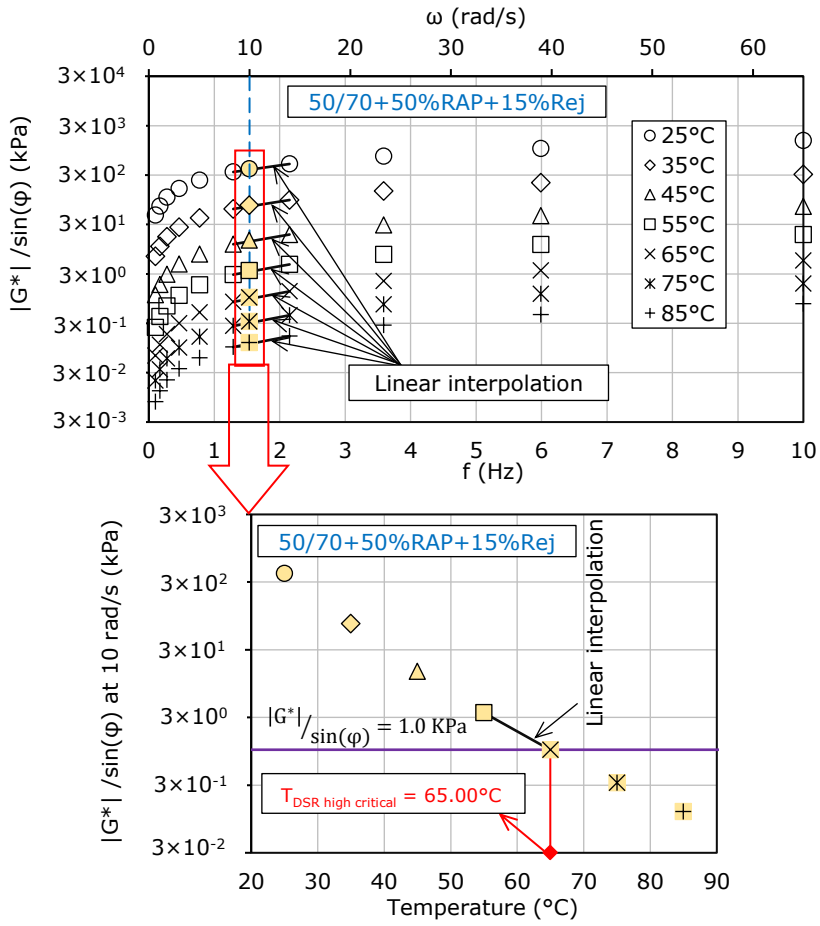

Figure A1.94. $T_{DSR\ high\ critical}$ determination from complex shear modulus test results for the blend 50/70 + 50% RAP + 15% Rej.

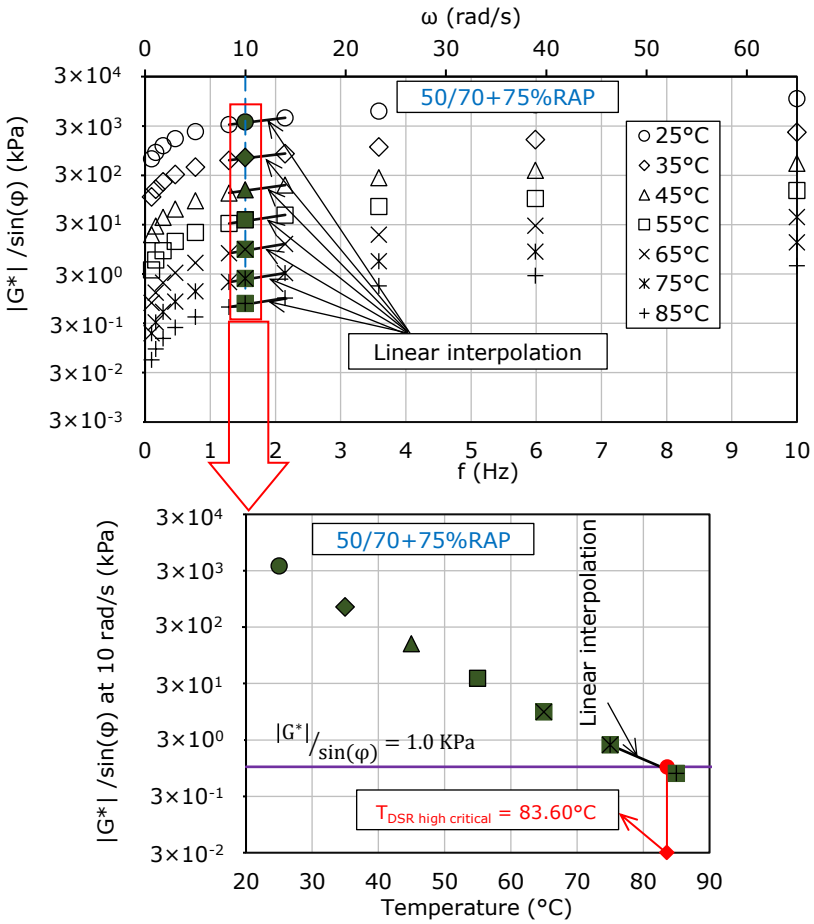

Figure A1.95. $T_{DSR\ high\ critical}$ determination from complex shear modulus test results for the blend 50/70 + 75% RAP.

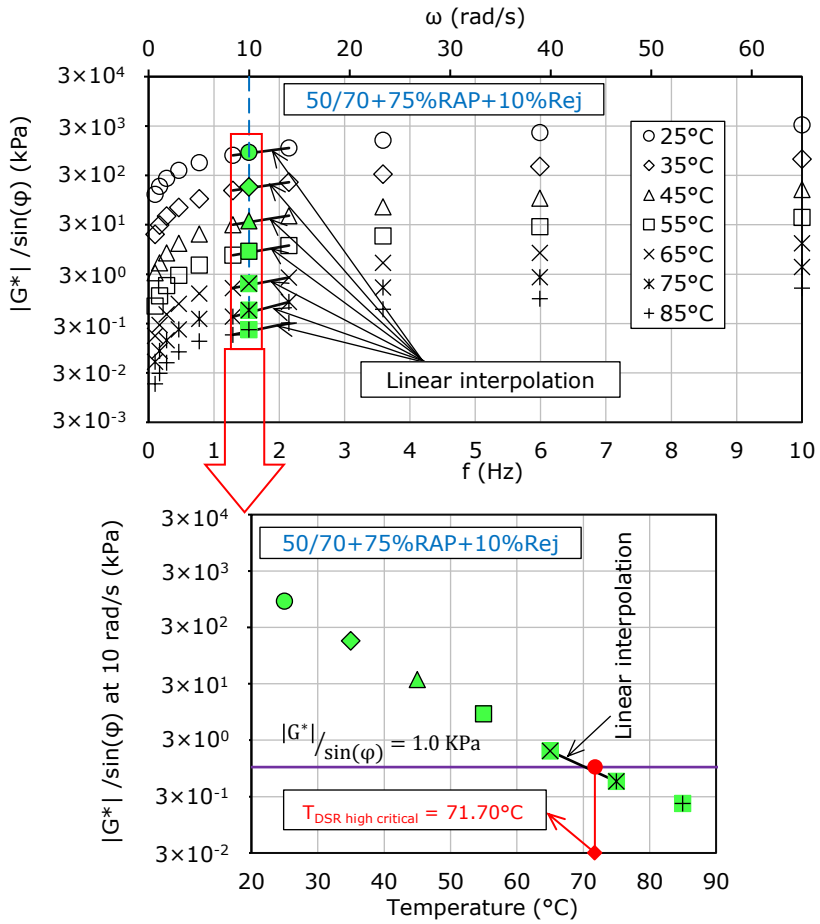

Figure A1.96. $T_{DSR\ high\ critical}$ determination from complex shear modulus test results for the blend 50/70 + 75% RAP + 10% Rej.

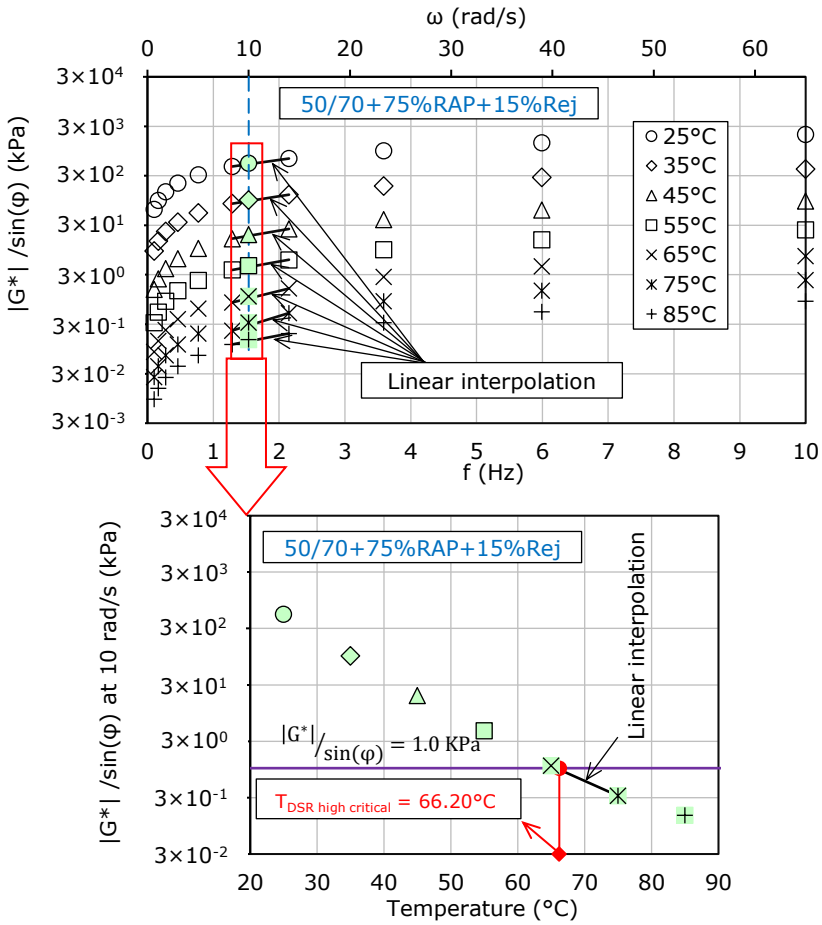

Figure A1.97. $T_{DSR\ high\ critical}$ determination from complex shear modulus test results for the blend 50/70 + 75% RAP + 15% Rej.

A.1.9. BBR low critical temperatures determination

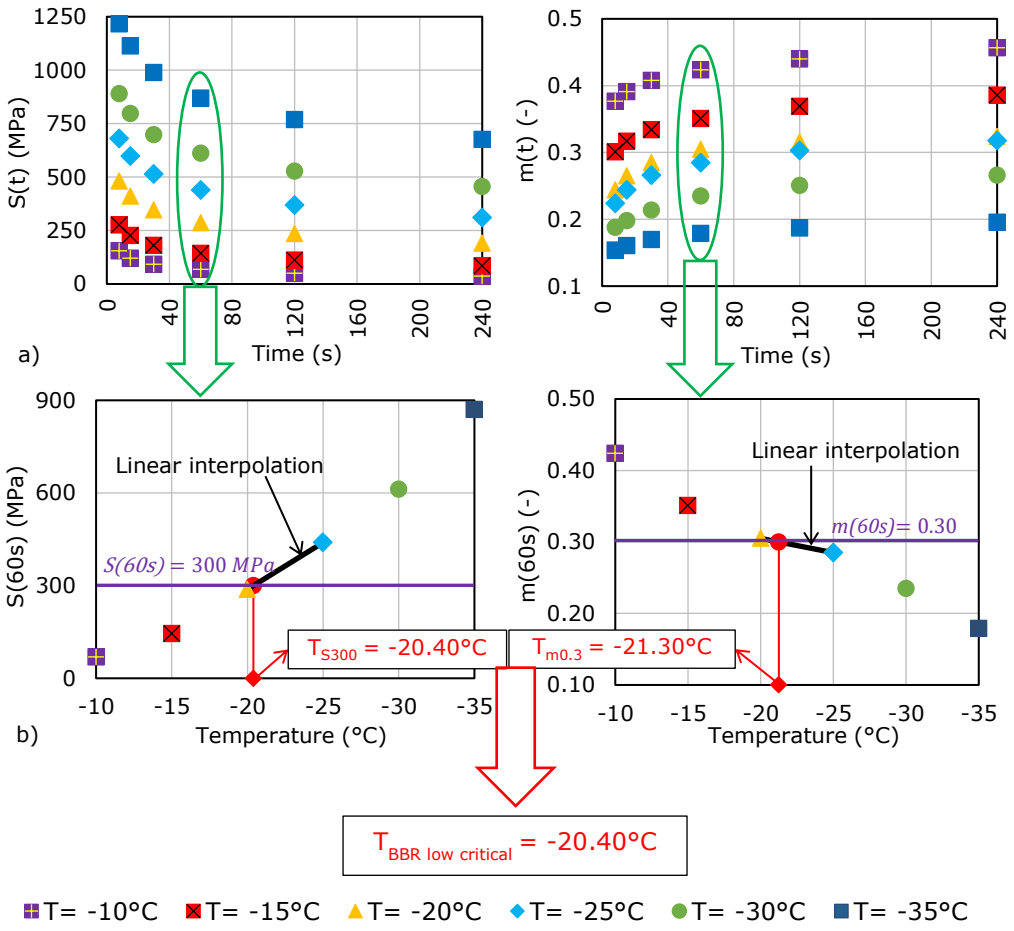

Figure A1.98. BBR test results for the fresh binder 50/70: (a) flexural creep stiffness (left) and m-value (right) as a function of time; (b) determination of the limiting low temperatures: T_{S300} (left) and $T_{m0.3}$ (right) and $T_{BBR\ low\ critical}$.

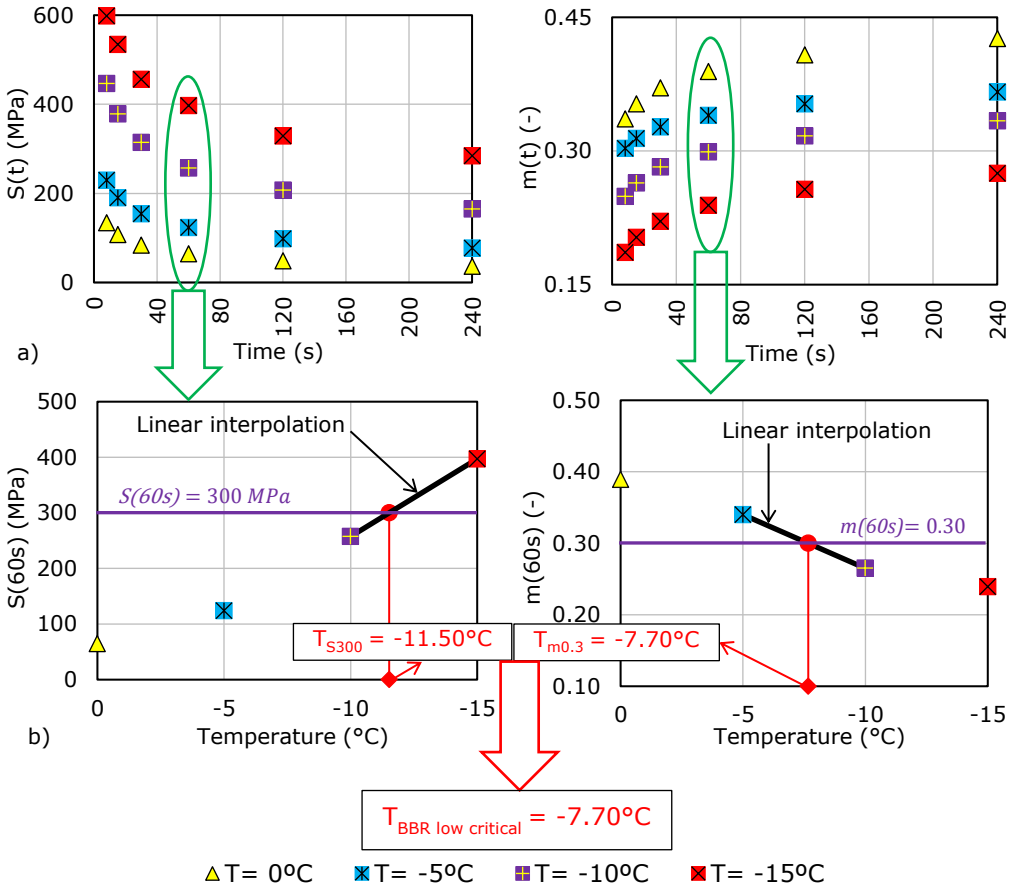

Figure A1.99. BBR test results for the RAP binder: (a) flexural creep stiffness (left) and m-value (right) as a function of time; (b) determination of the limiting low temperatures: T_{S300} (left) and $T_{m0.3}$ (right) and $T_{BBR\ low\ critical}$.

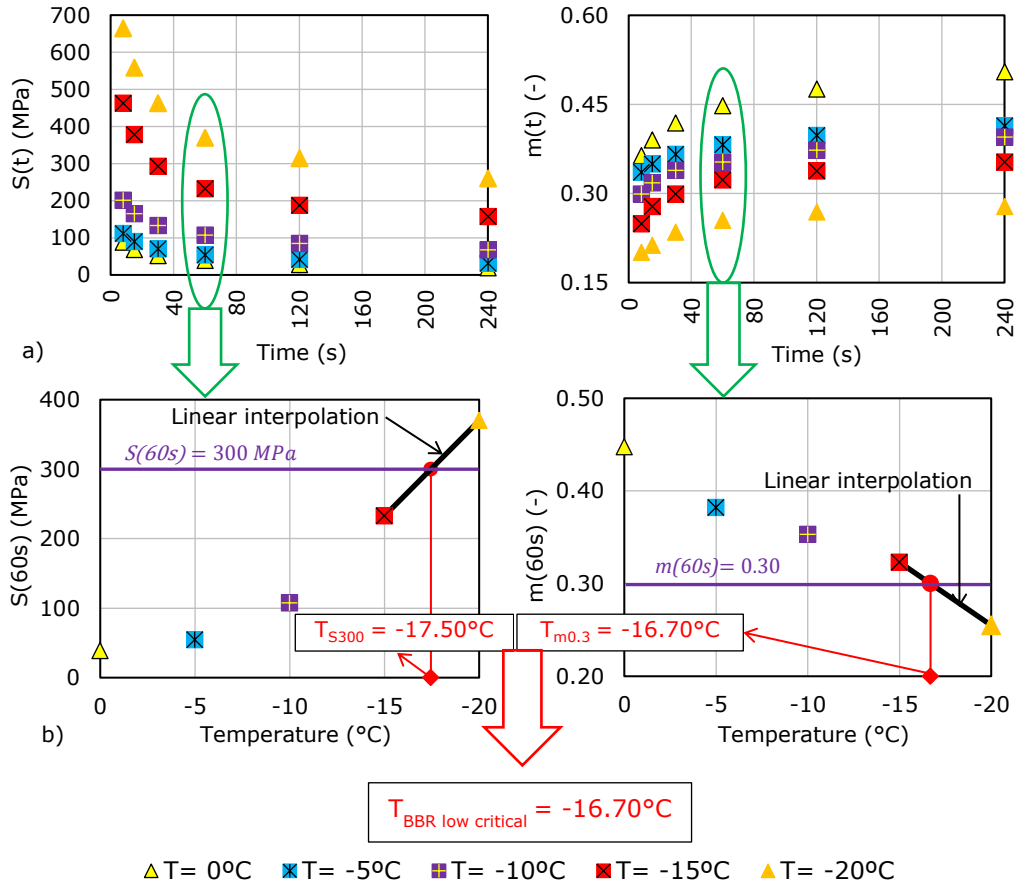

Figure A1.100. BBR test results for the blend RAP + 5% Rej: (a) flexural creep stiffness (left) and m-value (right) as a function of time; (b) determination of the limiting low temperatures: T_{S300} (left) and $T_{m0.3}$ (right) and $T_{BBR\ low\ critical}$.

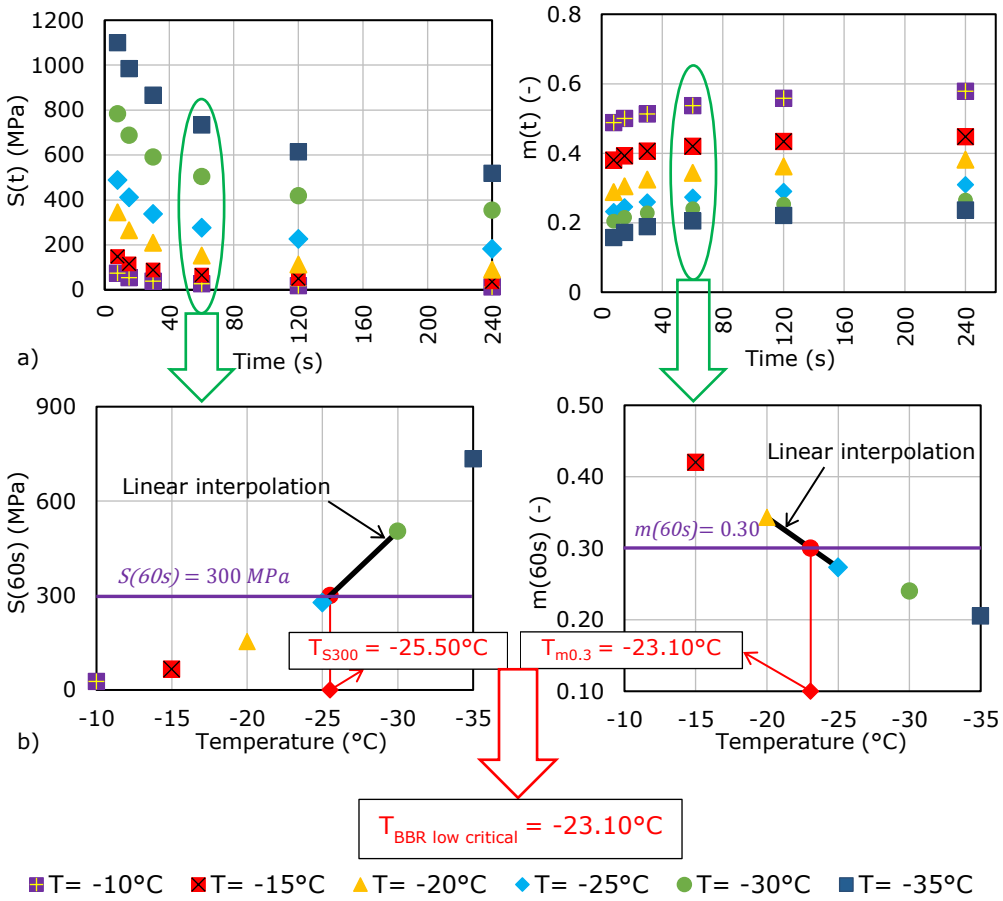

Figure A1.101. BBR test results for the blend RAP + 10% Rej: (a) flexural creep stiffness (left) and m-value (right) as a function of time; (b) determination of the limiting low temperatures: T_{S300} (left) and $T_{m0.3}$ (right) and $T_{BBR\ low\ critical}$.

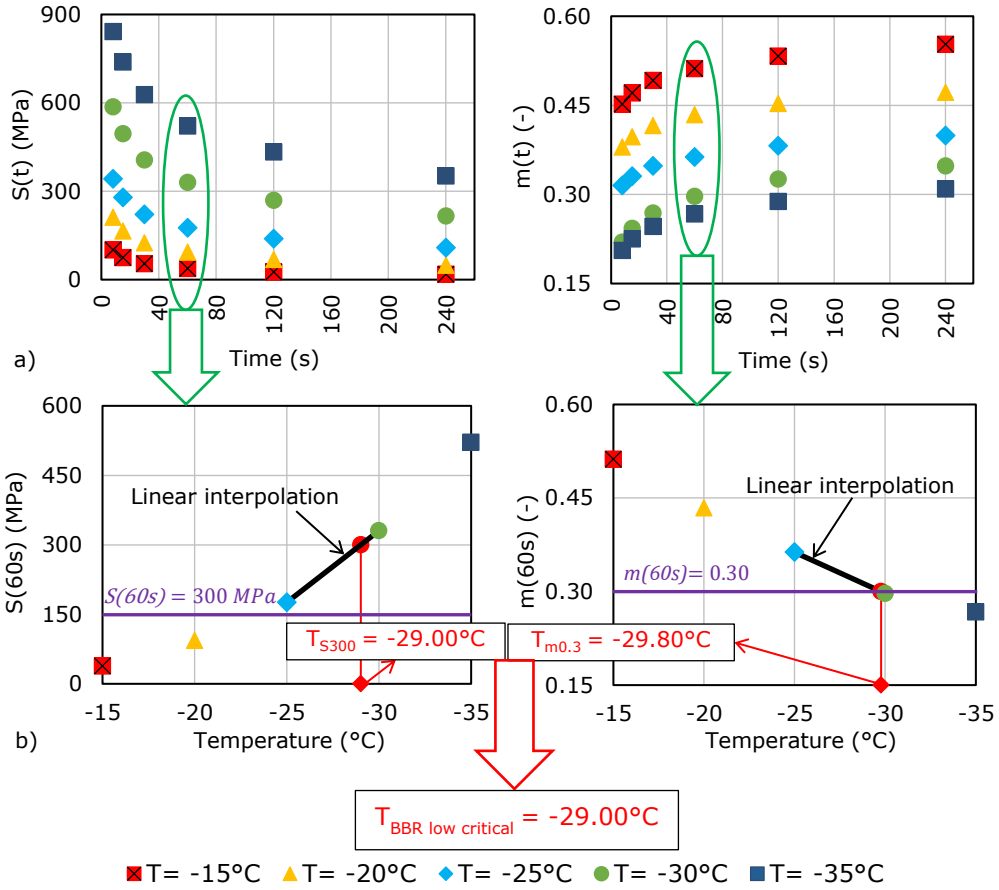

Figure A1.102. BBR test results for the RAP + 15% Rej blend: (a) flexural creep stiffness (left) and m-value (right) as a function of time; (b) determination of the limiting low temperatures: T_{S300} (left) and $T_{m0.3}$ (right) and $T_{BBR\ low\ critical}$.

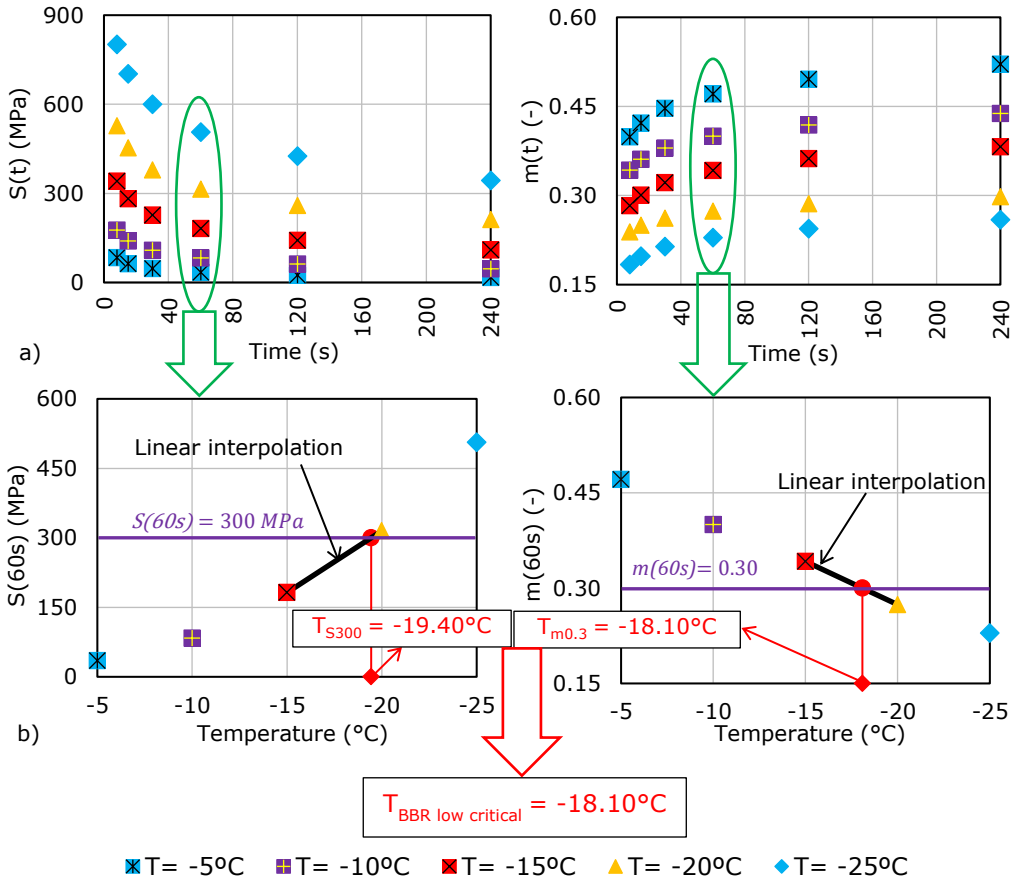

Figure A1.103. BBR test results for the blend 50/70 + 25% RAP: (a) flexural creep stiffness (left) and m-value (right) as a function of time; (b) determination of the limiting low temperatures: T_{S300} (left) and $T_{m0.3}$ (right) and $T_{BBR\ low\ critical}$.

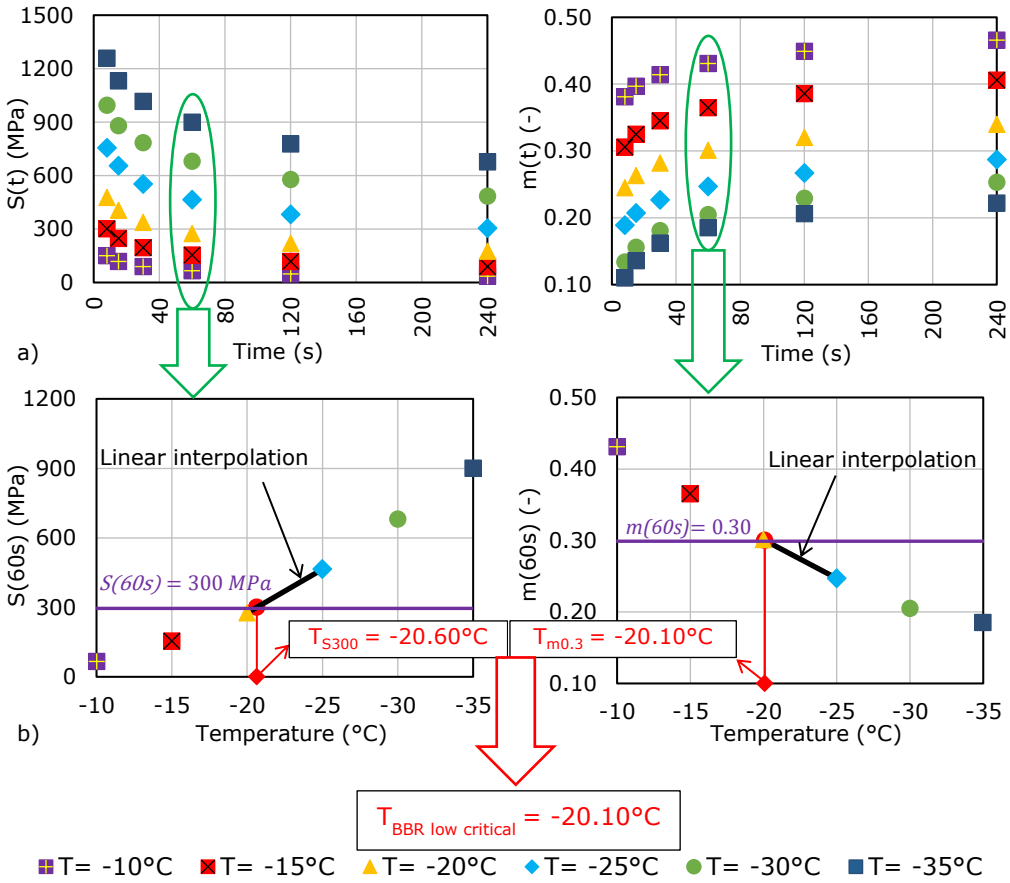

Figure A1.104. BBR test results for the blend 50/70 + 25% RAP + 5% Rej: (a) flexural creep stiffness (left) and m-value (right) as a function of time; (b) determination of the limiting low temperatures: T_{S300} (left) and $T_{m0.3}$ (right) and $T_{BBR\ low\ critical}$.

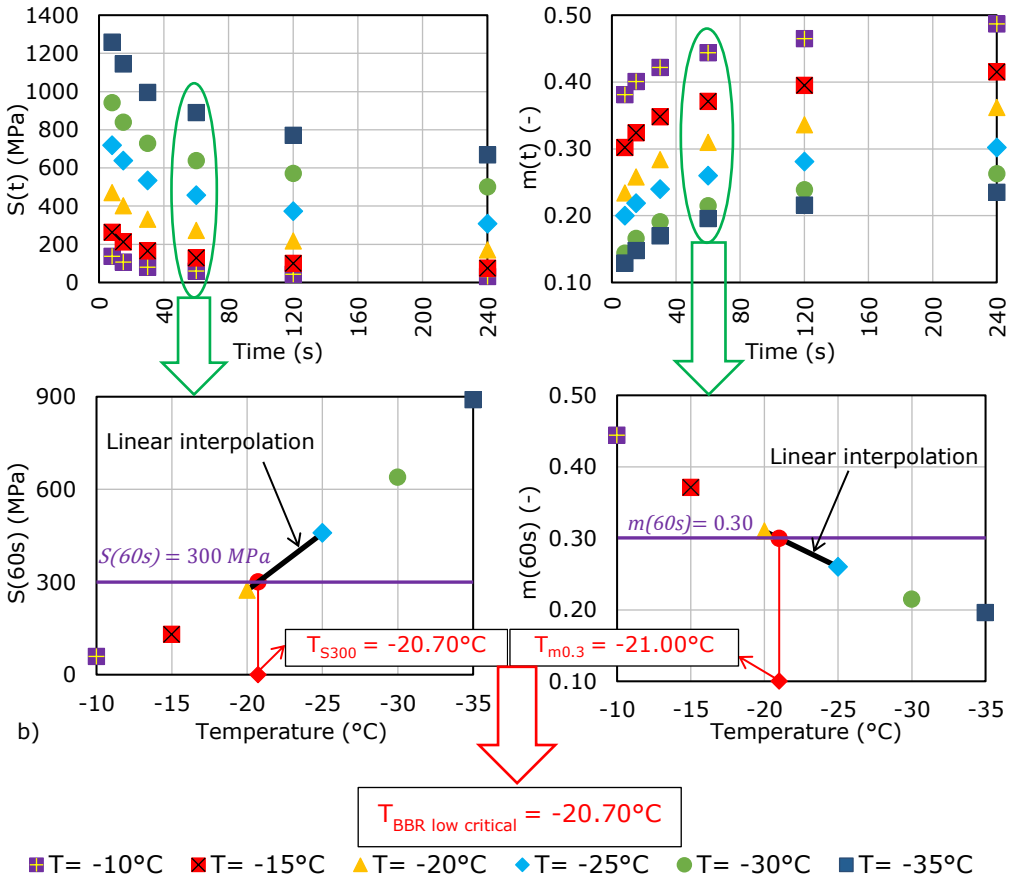

Figure A1.105. BBR test results for the blend 50/70 + 25% RAP + 10% Rej:
(a) flexural creep stiffness (left) and m-value (right) as a function of time;
(b) determination of the limiting low temperatures: T_{S300} (left) and $T_{m0.3}$ (right) and $T_{BBR\ low\ critical}$.

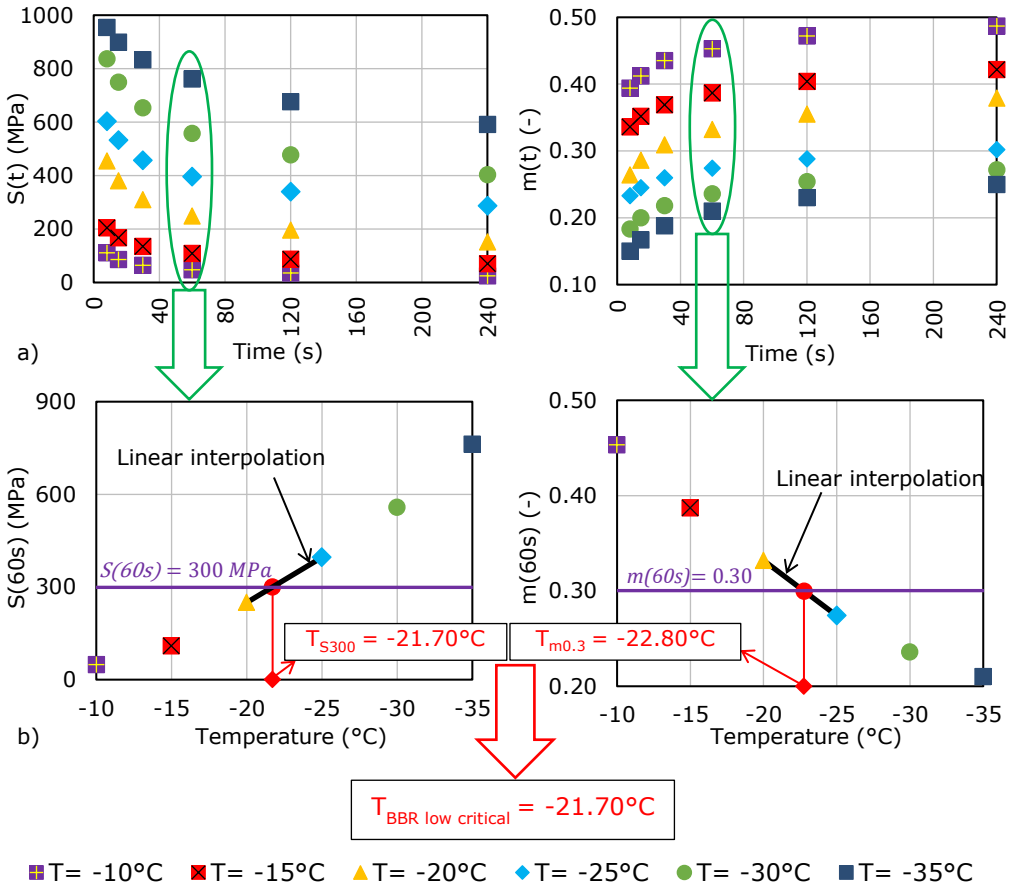

Figure A1.106. BBR test results for the blend 50/70 + 25% RAP + 15% Rej:
(a) flexural creep stiffness (left) and m-value (right) as a function of time;
(b) determination of the limiting low temperatures: T_{S300} (left) and $T_{m0.3}$ (right) and $T_{BBR\ low\ critical}$.

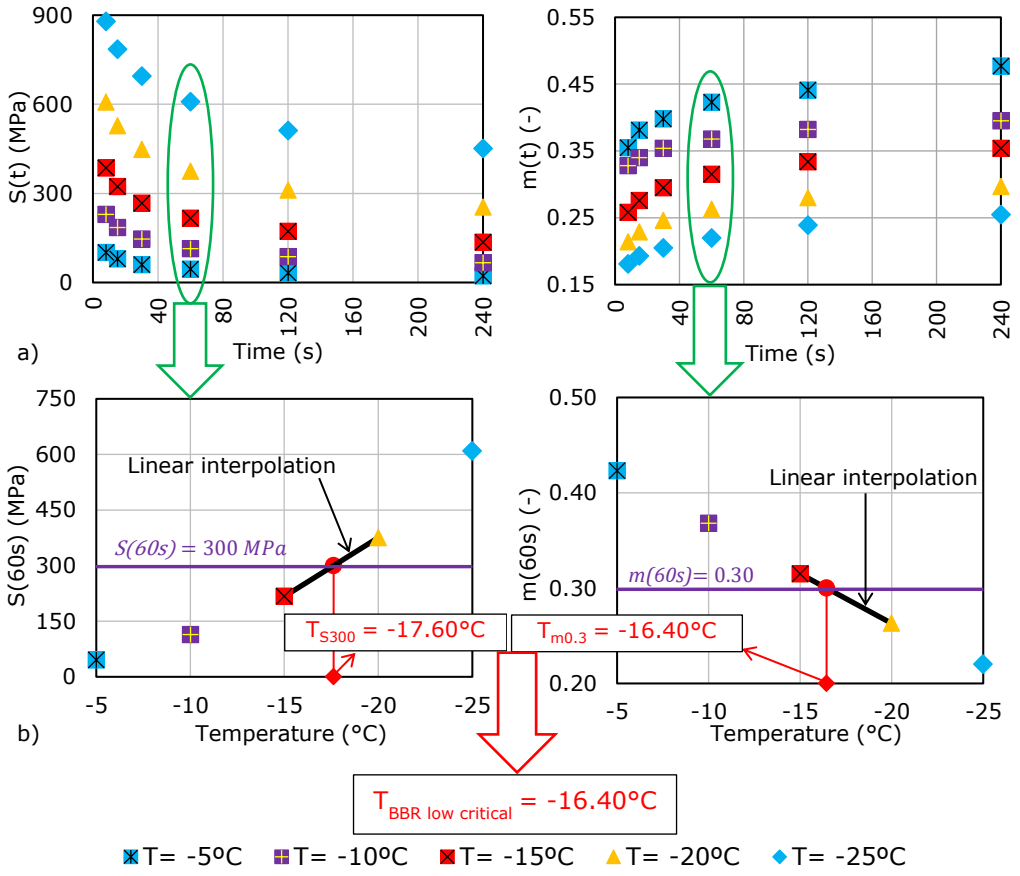

Figure A1.107. BBR test results for the blend 50/70 + 50% RAP: (a) flexural creep stiffness (left) and m-value (right) as a function of time; (b) determination of the limiting low temperatures: T_{S300} (left) and $T_{m0.3}$ (right) and $T_{BBR\ low\ critical}$.

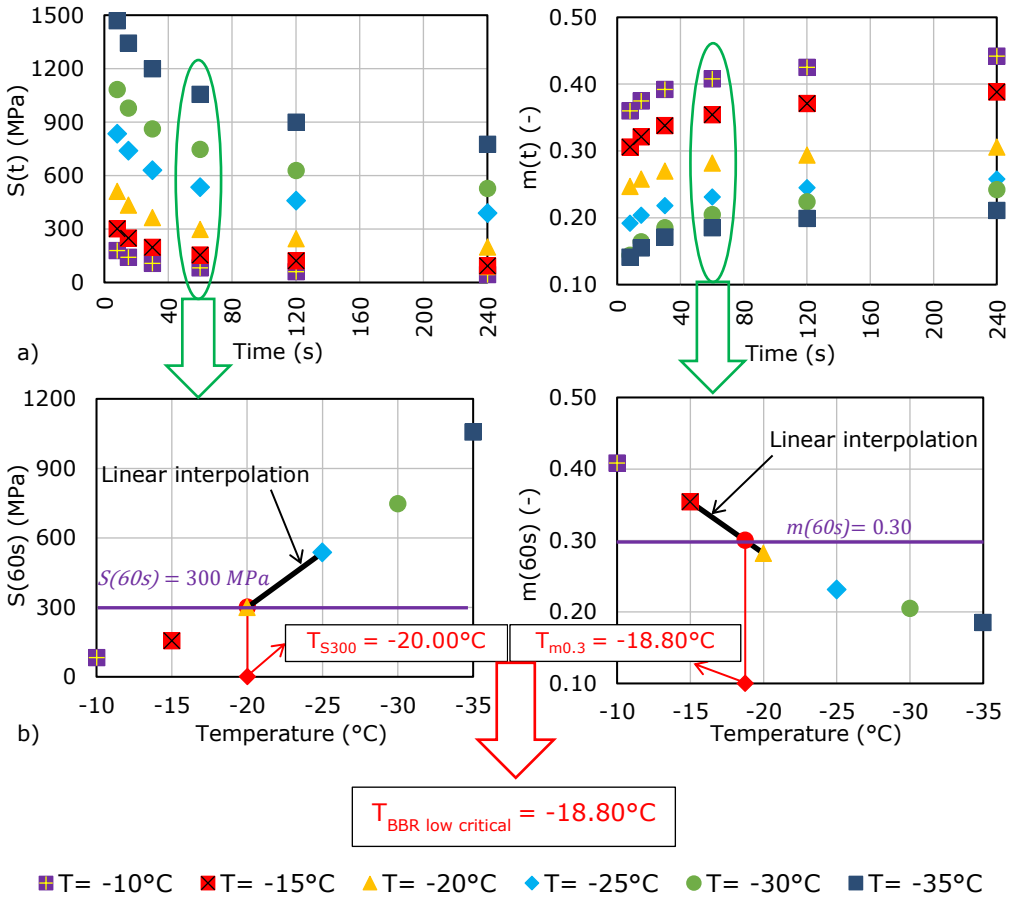

Figure A1.108. BBR test results for the blend 50/70 + 50% RAP + 5% Rej: (a) flexural creep stiffness (left) and m-value (right) as a function of time; (b) determination of the limiting low temperatures: T_{S300} (left) and $T_{m0.3}$ (right) and $T_{BBR\ low\ critical}$.

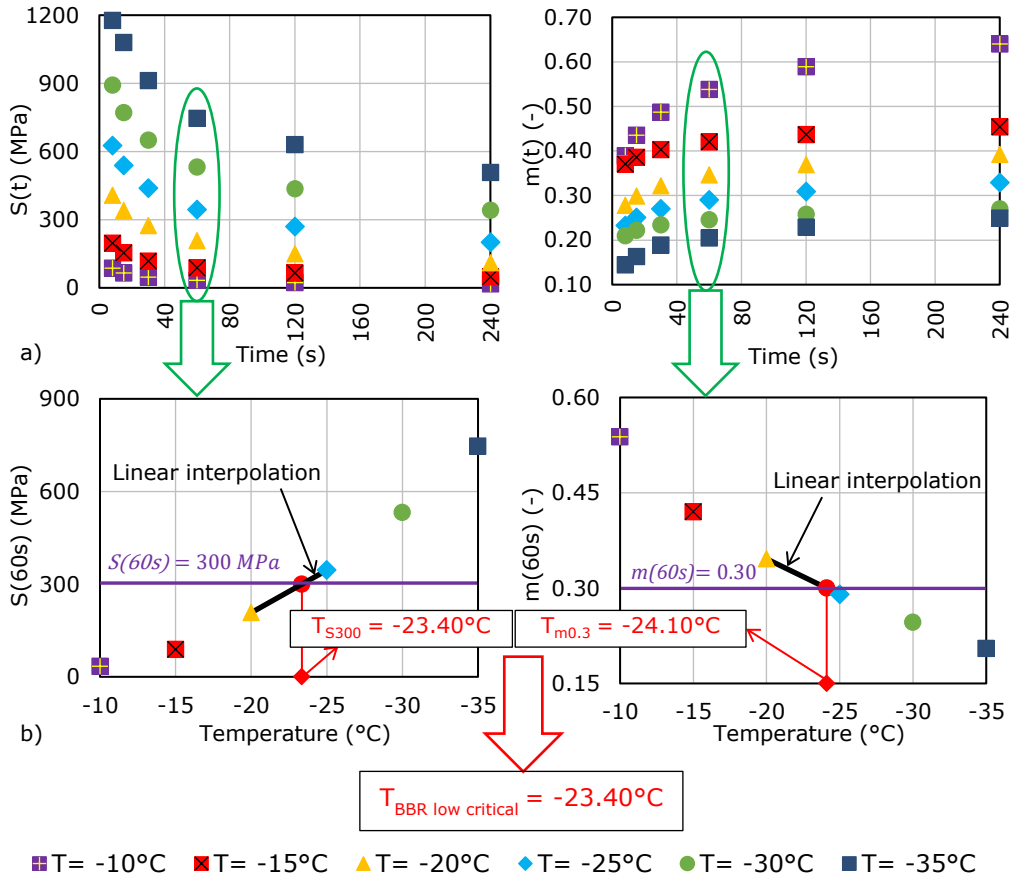

Figure A1.109. BBR test results for the blend 50/70 + 50% RAP + 15% Rej:
(a) flexural creep stiffness (left) and m-value (right) as a function of time;
(b) determination of the limiting low temperatures: T_{S300} (left) and $T_{m0.3}$ (right) and $T_{BBR\ low\ critical}$.

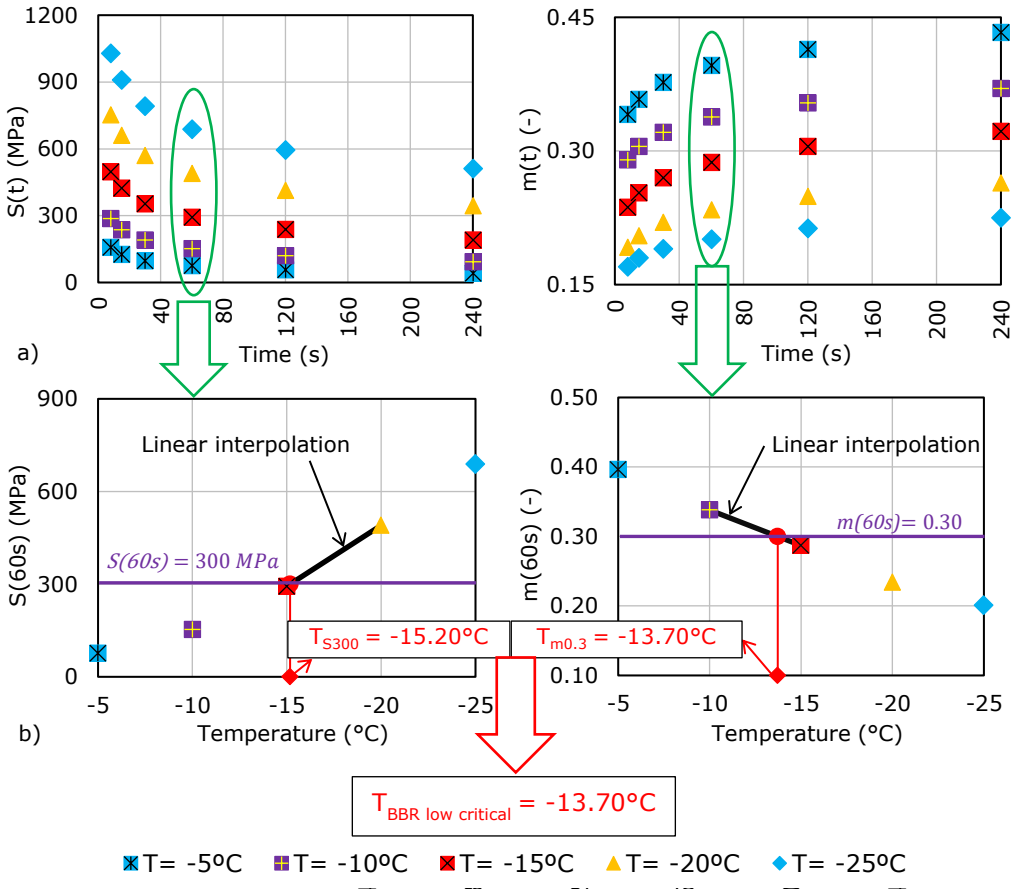

Figure A1.110. BBR test results for the blend 50/70 + 75% RAP: (a) flexural creep stiffness (left) and m-value (right) as a function of time; (b) determination of the limiting low temperatures: T_{S300} (left) and $T_{m0.3}$ (right) and $T_{BBR\ low\ critical}$.

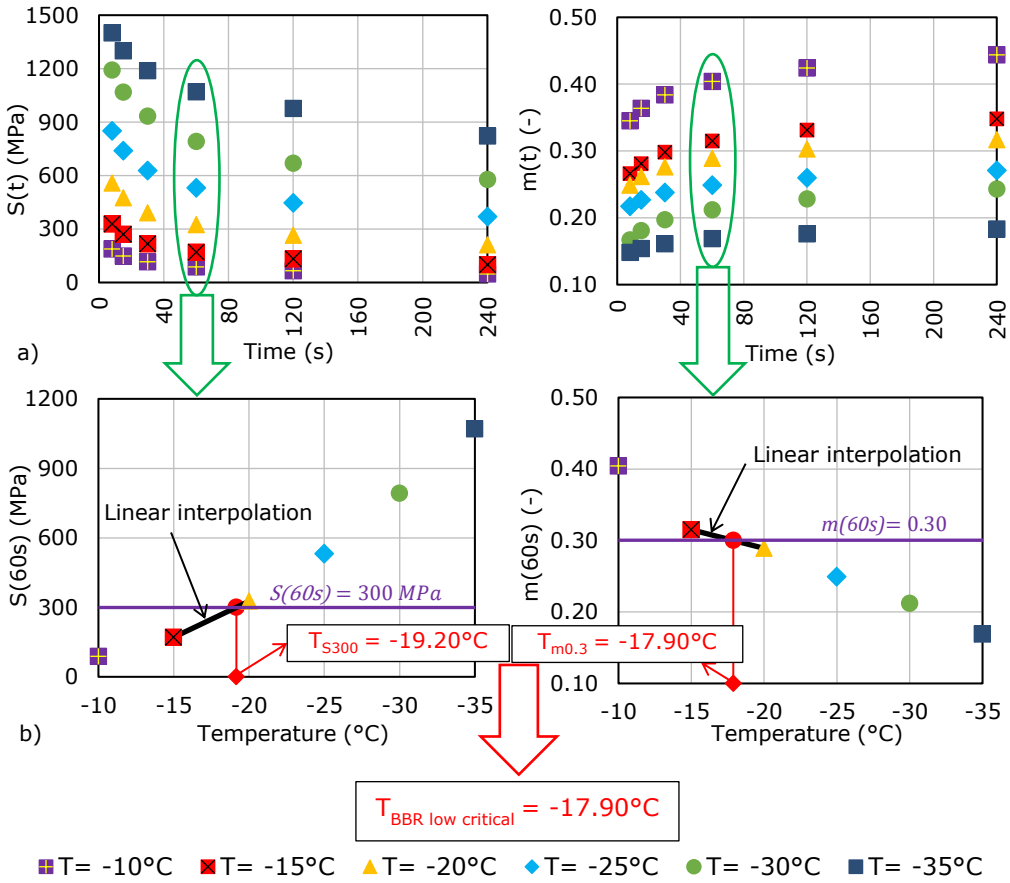

Figure A1.111. BBR test results for the blend 50/70 + 75% RAP + 5% Rej: (a) flexural creep stiffness (left) and m-value (right) as a function of time; (b) determination of the limiting low temperatures: T_{S300} (left) and $T_{m0.3}$ (right) and $T_{BBR\ low\ critical}$.

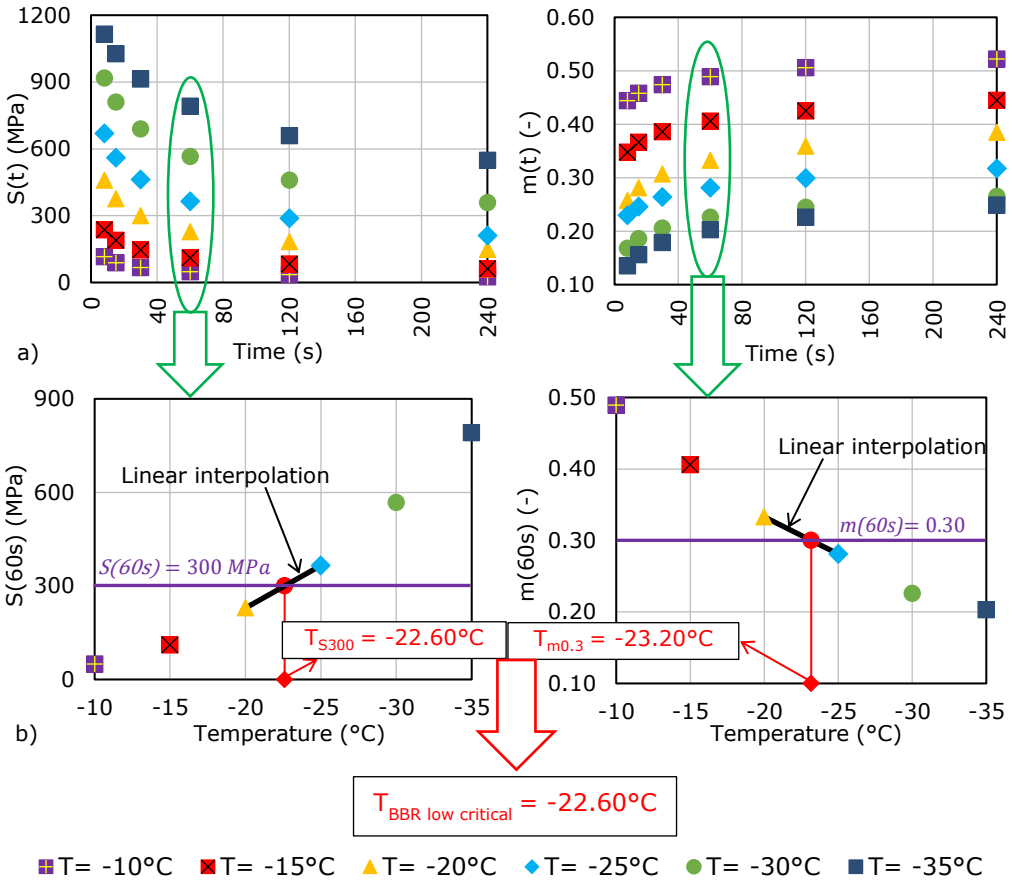

Figure A1.112. BBR test results for the blend 50/70 + 75% RAP + 10% Rej:
(a) flexural creep stiffness (left) and m-value (right) as a function of time;
(b) determination of the limiting low temperatures: T_{S300} (left) and $T_{m0.3}$ (right) and $T_{BBR\ low\ critical}$.

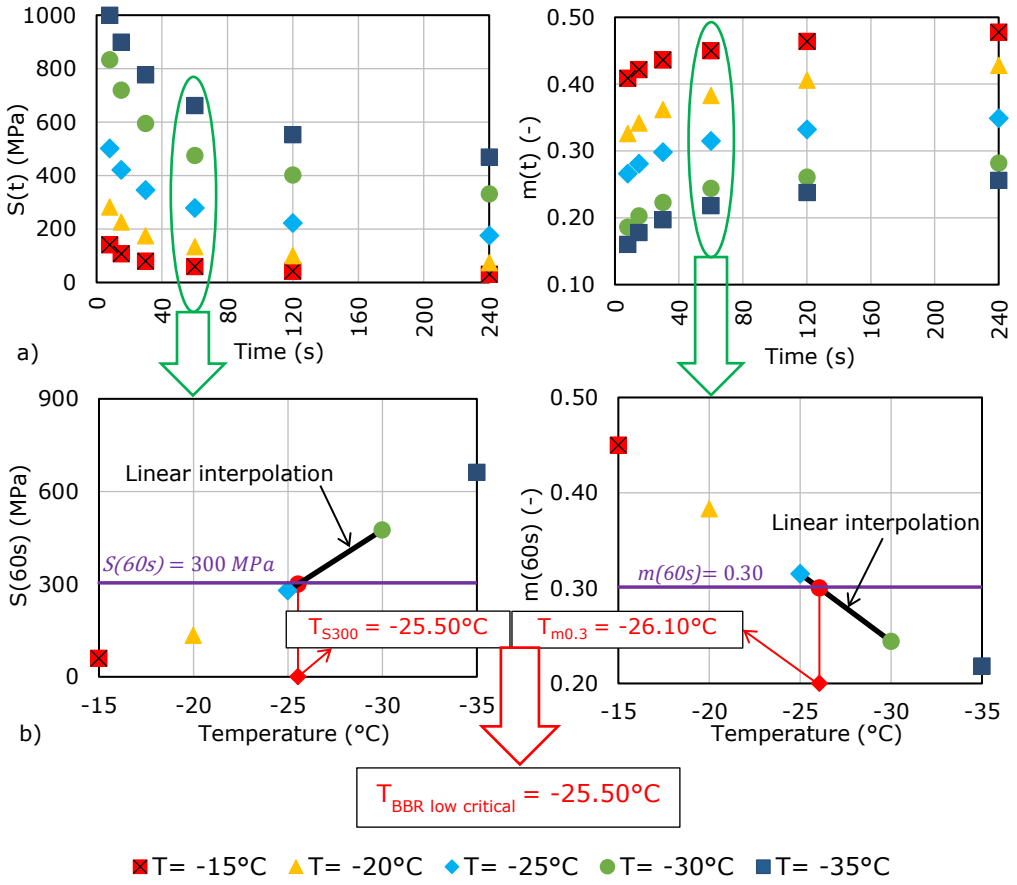

Figure A1.113. BBR test results for the blend 50/70 + 75% RAP + 15% Rej:
(a) flexural creep stiffness (left) and m-value (right) as a function of time;
(b) determination of the limiting low temperatures: T_{S300} (left) and $T_{m0.3}$ (right) and $T_{BBR\ low\ critical}$.

A.1.10. Statistical analysis results

Table A1.1. Confidence interval half-width values ε – norm of complex shear modulus for frequencies: 0.10 Hz, 0.167 Hz and 0.278 Hz.

		Temp.	Estimation method	Confidence level α						
				90 %	93%	95%	97%	99%	99.5 %	99.9 %
confidence interval half-width ε	***log(|G*(T, f=0.1 Hz)|)***	85°C	1st	0.03	0.04	0.04	0.05	0.06	0.07	0.10
			2nd	0.03	0.03	0.04	0.04	0.05	0.06	0.07
			Ratio 1st/2nd	1.14	1.15	1.16	1.18	1.23	1.26	1.34
		75°C	1st	0.04	0.04	0.05	0.05	0.07	0.08	0.11
			2nd	0.03	0.04	0.04	0.05	0.06	0.06	0.08
			Ratio 1st/2nd	1.11	1.12	1.13	1.15	1.19	1.22	1.30
		65°C	1st	0.04	0.04	0.05	0.06	0.07	0.08	0.11
			2nd	0.04	0.04	0.04	0.05	0.06	0.07	0.09
			Ratio 1st/2nd	1.11	1.13	1.14	1.16	1.20	1.23	1.31
		55°C	1st	0.03	0.04	0.04	0.05	0.06	0.07	0.10
			2nd	0.03	0.04	0.04	0.05	0.06	0.06	0.08
			Ratio 1st/2nd	1.01	1.02	1.03	1.05	1.09	1.12	1.19
	log(|G*(T, f=0.167 Hz)|)	85°C	1st	0.03	0.04	0.04	0.05	0.06	0.07	0.10
			2nd	0.03	0.03	0.04	0.04	0.05	0.06	0.07
			Ratio 1st/2nd	1.02	1.03	1.04	1.06	1.10	1.13	1.20
		75°C	1st	0.04	0.04	0.05	0.05	0.07	0.08	0.10
			2nd	0.03	0.04	0.04	0.05	0.06	0.06	0.08
			Ratio 1st/2nd	1.10	1.11	1.12	1.14	1.19	1.22	1.30
		65°C	1st	0.04	0.04	0.05	0.06	0.07	0.08	0.11
			2nd	0.04	0.04	0.04	0.05	0.06	0.07	0.09
			Ratio 1st/2nd	1.12	1.13	1.14	1.16	1.21	1.24	1.32
		55°C	1st	0.03	0.04	0.04	0.05	0.06	0.07	0.10
			2nd	0.03	0.04	0.04	0.05	0.06	0.07	0.08
			Ratio 1st/2nd	0.98	0.99	1.00	1.02	1.06	1.09	1.16
	log(|G*(T, f=0.278 Hz)|)	85°C	1st	0.03	0.04	0.04	0.05	0.06	0.07	0.10
			2nd	0.03	0.03	0.04	0.04	0.05	0.06	0.08
			Ratio 1st/2nd	1.01	1.02	1.03	1.05	1.09	1.12	1.19
		75°C	1st	0.04	0.04	0.05	0.05	0.07	0.08	0.10
			2nd	0.03	0.04	0.04	0.05	0.06	0.06	0.08
			Ratio 1st/2nd	1.10	1.11	1.12	1.14	1.18	1.21	1.29
		65°C	1st	0.04	0.04	0.05	0.06	0.07	0.08	0.11
			2nd	0.03	0.04	0.04	0.05	0.06	0.07	0.08
			Ratio 1st/2nd	1.12	1.14	1.15	1.17	1.21	1.24	1.33
		55°C	1st	0.03	0.04	0.04	0.05	0.06	0.07	0.09
			2nd	0.03	0.04	0.04	0.05	0.06	0.07	0.08
			Ratio 1st/2nd	0.95	0.96	0.97	0.98	1.02	1.05	1.12

Table A1.2. Confidence interval half-width values ε – norm of complex shear modulus for frequencies: 0.464 Hz, 0.774 Hz and 2.15 Hz.

		Temp.	Estimation method	Confidence level α						
				90 %	93%	95%	97%	99%	99.5 %	99.9 %
confidence interval half-width ε	***log(|G*(T, f=0.464 Hz)|)***	85°C	1st	0.03	0.04	0.04	0.05	0.06	0.07	0.10
			2nd	0.03	0.04	0.04	0.04	0.05	0.06	0.08
			Ratio 1st/2nd	1.01	1.02	1.03	1.05	1.09	1.12	1.19
		75°C	1st	0.04	0.04	0.05	0.05	0.07	0.08	0.10
			2nd	0.03	0.04	0.04	0.05	0.06	0.06	0.08
			Ratio 1st/2nd	1.09	1.10	1.12	1.13	1.18	1.21	1.29
		65°C	1st	0.04	0.04	0.05	0.06	0.07	0.08	0.11
			2nd	0.03	0.04	0.04	0.05	0.06	0.07	0.08
			Ratio 1st/2nd	1.13	1.14	1.15	1.17	1.22	1.25	1.33
		55°C	1st	0.03	0.04	0.04	0.05	0.06	0.07	0.09
			2nd	0.04	0.04	0.04	0.05	0.06	0.07	0.09
			Ratio 1st/2nd	0.91	0.92	0.93	0.94	0.98	1.00	1.07
	log(|G*(T, f=0.774 Hz)|)	85°C	1st	0.03	0.04	0.04	0.05	0.06	0.07	0.09
			2nd	0.03	0.04	0.04	0.04	0.06	0.06	0.08
			Ratio 1st/2nd	1.01	1.02	1.03	1.05	1.09	1.12	1.19
		75°C	1st	0.04	0.04	0.04	0.05	0.07	0.08	0.10
			2nd	0.03	0.04	0.04	0.05	0.06	0.06	0.08
			Ratio 1st/2nd	1.09	1.10	1.11	1.13	1.17	1.21	1.28
		65°C	1st	0.04	0.04	0.05	0.05	0.07	0.08	0.11
			2nd	0.03	0.04	0.04	0.05	0.06	0.06	0.08
			Ratio 1st/2nd	1.13	1.15	1.16	1.18	1.22	1.25	1.34
		55°C	1st	0.03	0.04	0.04	0.04	0.06	0.07	0.09
			2nd	0.04	0.04	0.04	0.05	0.06	0.07	0.09
			Ratio 1st/2nd	0.87	0.87	0.88	0.90	0.93	0.96	1.02
	log(|G*(T, f=2.15 Hz)|)	85°C	1st	0.03	0.04	0.04	0.05	0.06	0.07	0.09
			2nd	0.03	0.04	0.04	0.05	0.06	0.06	0.08
			Ratio 1st/2nd	1.01	1.02	1.03	1.05	1.09	1.12	1.19
		75°C	1st	0.03	0.04	0.04	0.05	0.06	0.07	0.10
			2nd	0.03	0.04	0.04	0.04	0.06	0.06	0.08
			Ratio 1st/2nd	1.08	1.10	1.11	1.13	1.17	1.20	1.28
		65°C	1st	0.04	0.04	0.05	0.05	0.07	0.08	0.11
			2nd	0.03	0.04	0.04	0.04	0.06	0.06	0.08
			Ratio 1st/2nd	1.14	1.15	1.17	1.19	1.23	1.26	1.35
		55°C	1st	0.03	0.03	0.04	0.04	0.05	0.06	0.08
			2nd	0.04	0.04	0.05	0.05	0.06	0.07	0.09
			Ratio 1st/2nd	0.78	0.79	0.80	0.81	0.84	0.86	0.92

Table A1.3. Confidence interval half-width values ε – norm of complex shear modulus for frequencies: 3.59 Hz, 5.99 Hz and 10 Hz.

		Temp.	Estimation method	Confidence level α						
				90%	93%	95%	97%	99%	99.5 %	99.9 %
confidence interval half-width ε	***log(|G*(T, f=3.59 Hz)|)***	85°C	1st	0.03	0.04	0.04	0.05	0.06	0.07	0.09
			2nd	0.03	0.04	0.04	0.05	0.06	0.07	0.08
			Ratio 1st/2nd	1.01	1.02	1.03	1.05	1.09	1.11	1.19
		75°C	1st	0.03	0.04	0.04	0.05	0.06	0.07	0.10
			2nd	0.03	0.04	0.04	0.04	0.05	0.06	0.08
			Ratio 1st/2nd	1.08	1.09	1.10	1.12	1.16	1.19	1.27
		65°C	1st	0.04	0.04	0.05	0.05	0.07	0.08	0.10
			2nd	0.03	0.04	0.04	0.04	0.05	0.06	0.08
			Ratio 1st/2nd	1.15	1.16	1.17	1.19	1.23	1.27	1.35
		55°C	1st	0.03	0.03	0.04	0.04	0.05	0.06	0.08
			2nd	0.04	0.04	0.05	0.05	0.07	0.07	0.09
			Ratio 1st/2nd	0.74	0.75	0.76	0.77	0.80	0.82	0.88
	log(|G*(T, f=5.99 Hz)|)	85°C	1st	0.03	0.04	0.04	0.05	0.06	0.07	0.09
			2nd	0.04	0.04	0.04	0.05	0.06	0.07	0.09
			Ratio 1st/2nd	1.00	1.01	1.02	1.04	1.08	1.11	1.18
		75°C	1st	0.03	0.04	0.04	0.05	0.06	0.07	0.10
			2nd	0.03	0.04	0.04	0.04	0.05	0.06	0.08
			Ratio 1st/2nd	1.07	1.08	1.09	1.11	1.15	1.18	1.26
		65°C	1st	0.04	0.04	0.04	0.05	0.07	0.08	0.10
			2nd	0.03	0.03	0.04	0.04	0.05	0.06	0.08
			Ratio 1st/2nd	1.15	1.16	1.17	1.19	1.24	1.27	1.35
		55°C	1st	0.03	0.03	0.04	0.04	0.05	0.06	0.08
			2nd	0.04	0.04	0.05	0.05	0.07	0.08	0.10
			Ratio 1st/2nd	0.72	0.72	0.73	0.74	0.77	0.79	0.85
	log(|G*(T, f=10 Hz)|)	85°C	1st	0.03	0.04	0.04	0.05	0.06	0.07	0.09
			2nd	0.04	0.04	0.05	0.05	0.06	0.07	0.09
			Ratio 1st/2nd	0.99	1.00	1.01	1.03	1.07	1.09	1.17
		75°C	1st	0.03	0.04	0.04	0.05	0.06	0.07	0.10
			2nd	0.03	0.04	0.04	0.04	0.05	0.06	0.08
			Ratio 1st/2nd	1.06	1.07	1.08	1.10	1.14	1.17	1.24
		65°C	1st	0.04	0.04	0.04	0.05	0.07	0.08	0.10
			2nd	0.03	0.03	0.04	0.04	0.05	0.06	0.07
			Ratio 1st/2nd	1.16	1.17	1.18	1.20	1.25	1.28	1.36
		55°C	1st	0.03	0.03	0.03	0.04	0.05	0.06	0.08
			2nd	0.04	0.04	0.05	0.06	0.07	0.08	0.10
			Ratio 1st/2nd	0.70	0.71	0.72	0.73	0.76	0.77	0.83

Table A1.4. Confidence interval half-width values ε / maximum variation Δ ratios – norm of complex shear modulus for frequencies: 0.10 Hz, 0.167 Hz, 0.278 Hz, 0.464 Hz, 0.774 Hz, 2.15 Hz.

ε / Δ		Temp.	Est. meth.	Confidence level α						
				90%	93%	95%	97%	99%	99.5%	99.9%
	log(|G*(T,f=0.1 Hz)|)	85°C	1st	4.0%	4.5%	5.0%	5.7%	7.3%	8.4%	11.3%
			2nd	3.2%	3.6%	4.0%	4.5%	5.6%	6.2%	7.9%
		75°C	1st	3.8%	4.3%	4.7%	5.4%	7.0%	8.1%	10.8%
			2nd	3.2%	3.6%	4.0%	4.5%	5.6%	6.3%	7.9%
		65°C	1st	3.7%	4.2%	4.6%	5.3%	6.9%	7.9%	10.6%
			2nd	3.1%	3.5%	3.8%	4.3%	5.4%	6.0%	7.6%
		55°C	1st	2.9%	3.3%	3.6%	4.2%	5.4%	6.2%	8.3%
			2nd	2.7%	3.0%	3.2%	3.7%	4.5%	5.1%	6.4%
	log(|G*(T, f=0.167 Hz)|)	85°C	1st	3.9%	4.4%	4.9%	5.6%	7.2%	8.3%	11.1%
			2nd	3.3%	3.6%	4.0%	4.5%	5.6%	6.3%	7.9%
		75°C	1st	3.8%	4.3%	4.7%	5.4%	7.0%	8.0%	10.8%
			2nd	3.3%	3.6%	4.0%	4.5%	5.6%	6.3%	7.9%
		65°C	1st	3.7%	4.2%	4.6%	5.3%	6.9%	7.9%	10.6%
			2nd	3.1%	3.5%	3.8%	4.3%	5.3%	6.0%	7.5%
		55°C	1st	2.9%	3.3%	3.6%	4.2%	5.4%	6.2%	8.3%
			2nd	2.7%	3.1%	3.3%	3.8%	4.7%	5.3%	6.6%
	log(|G*(T, f=0.278 Hz)|)	85°C	1st	3.9%	4.4%	4.8%	5.5%	7.1%	8.2%	11.0%
			2nd	3.3%	3.7%	4.1%	4.6%	5.7%	6.4%	8.0%
		75°C	1st	3.8%	4.3%	4.7%	5.4%	7.0%	8.0%	10.8%
			2nd	3.3%	3.6%	4.0%	4.5%	5.6%	6.3%	7.9%
		65°C	1st	3.7%	4.2%	4.7%	5.4%	6.9%	7.9%	10.7%
			2nd	3.1%	3.5%	3.8%	4.3%	5.3%	6.0%	7.5%
		55°C	1st	2.9%	3.3%	3.7%	4.2%	5.4%	6.2%	8.4%
			2nd	2.8%	3.2%	3.5%	3.9%	4.9%	5.5%	6.9%
	log(|G*(T,f=0, 464 Hz)|)	85°C	1st	3.9%	4.3%	4.8%	5.5%	7.1%	8.2%	11.0%
			2nd	3.4%	3.8%	4.2%	4.7%	5.8%	6.5%	8.2%
		75°C	1st	3.8%	4.3%	4.7%	5.4%	7.0%	8.0%	10.8%
			2nd	3.3%	3.7%	4.0%	4.5%	5.6%	6.3%	7.9%
		65°C	1st	3.8%	4.2%	4.7%	5.4%	6.9%	8.0%	10.7%
			2nd	3.1%	3.4%	3.8%	4.3%	5.3%	5.9%	7.5%
		55°C	1st	3.0%	3.3%	3.7%	4.2%	5.5%	6.3%	8.4%
			2nd	3.0%	3.3%	3.6%	4.1%	5.1%	5.7%	7.2%
	log(|G*(T, f=0.774 Hz)|)	85°C	1st	3.8%	4.3%	4.8%	5.5%	7.1%	8.2%	11.0%
			2nd	3.5%	3.9%	4.3%	4.8%	6.0%	6.7%	8.4%
		75°C	1st	3.8%	4.3%	4.7%	5.4%	7.0%	8.1%	10.8%
			2nd	3.3%	3.7%	4.0%	4.5%	5.6%	6.3%	8.0%
		65°C	1st	3.8%	4.3%	4.7%	5.4%	7.0%	8.0%	10.8%
			2nd	3.1%	3.4%	3.8%	4.3%	5.3%	5.9%	7.5%
		55°C	1st	3.0%	3.3%	3.7%	4.2%	5.5%	6.3%	8.5%
			2nd	3.1%	3.5%	3.8%	4.3%	5.4%	6.0%	7.6%
	log(|G*(T, f=2.15 Hz)|)	85°C	1st	3.9%	4.4%	4.8%	5.5%	7.1%	8.2%	11.0%
			2nd	3.7%	4.1%	4.5%	5.1%	6.3%	7.1%	8.9%
		75°C	1st	3.8%	4.3%	4.8%	5.5%	7.1%	8.2%	10.9%
			2nd	3.3%	3.7%	4.0%	4.6%	5.7%	6.4%	8.0%
		65°C	1st	3.9%	4.4%	4.8%	5.6%	7.2%	8.2%	11.1%
			2nd	3.1%	3.5%	3.8%	4.3%	5.3%	5.9%	7.5%
		55°C	1st	3.0%	3.4%	3.7%	4.3%	5.5%	6.4%	8.6%
			2nd	3.5%	3.9%	4.2%	4.8%	5.9%	6.7%	8.4%

Table A1.5. Confidence interval half-width values ε / maximum variation Δ ratios – norm of complex shear modulus for frequencies: 3.59 Hz, 5.99 Hz, 10 Hz.

		Temp.	Est. meth.	Confidence level α						
				90%	93%	95%	97%	99%	99.5%	99.9%
ε / Δ	log(|G*(T, f=3.59 Hz)|)	85°C	1st	3.9%	4.4%	4.8%	5.6%	7.2%	8.2%	11.1%
			2nd	3.8%	4.3%	4.7%	5.3%	6.6%	7.4%	9.3%
		75°C	1st	3.9%	4.4%	4.8%	5.5%	7.1%	8.2%	11.0%
			2nd	3.3%	3.7%	4.1%	4.6%	5.7%	6.4%	8.1%
		65°C	1st	3.9%	4.4%	4.9%	5.6%	7.3%	8.4%	11.2%
			2nd	3.1%	3.5%	3.8%	4.3%	5.3%	6.0%	7.5%
		55°C	1st	3.0%	3.4%	3.8%	4.4%	5.6%	6.5%	8.7%
			2nd	3.7%	4.1%	4.5%	5.0%	6.3%	7.0%	8.8%
	log(|G*(T, f=5.99 Hz)|)	85°C	1st	3.9%	4.4%	4.9%	5.6%	7.2%	8.3%	11.1%
			2nd	4.0%	4.4%	4.9%	5.5%	6.8%	7.7%	9.7%
		75°C	1st	3.9%	4.4%	4.9%	5.6%	7.2%	8.3%	11.2%
			2nd	3.4%	3.8%	4.2%	4.7%	5.8%	6.5%	8.2%
		65°C	1st	4.0%	4.5%	5.0%	5.7%	7.4%	8.5%	11.4%
			2nd	3.1%	3.5%	3.8%	4.3%	5.4%	6.0%	7.6%
		55°C	1st	3.1%	3.5%	3.9%	4.4%	5.7%	6.6%	8.9%
			2nd	3.8%	4.3%	4.7%	5.3%	6.6%	7.4%	9.3%
	log(|G*(T, f=10 Hz)|)	85°C	1st	3.9%	4.4%	4.9%	5.6%	7.3%	8.4%	11.2%
			2nd	4.2%	4.7%	5.1%	5.8%	7.2%	8.1%	10.2%
		75°C	1st	4.0%	4.5%	4.9%	5.7%	7.3%	8.4%	11.3%
			2nd	3.5%	3.9%	4.3%	4.8%	6.0%	6.7%	8.4%
		65°C	1st	4.1%	4.6%	5.1%	5.9%	7.6%	8.7%	11.7%
			2nd	3.2%	3.5%	3.9%	4.4%	5.4%	6.1%	7.7%
		55°C	1st	3.2%	3.6%	4.0%	4.6%	5.9%	6.8%	9.1%
			2nd	4.0%	4.5%	4.9%	5.5%	6.9%	7.7%	9.7%

Table A1.6. Maximum variations *Δ* of measured values of norm of complex shear modulus for frequencies: 0.10 Hz, 0.167 Hz, 0.278 Hz, 0.464 Hz, 0.774 Hz, 2.15 Hz for all binder blends according to the 1st or 2nd estimation method.

Parameter	Temp.	Est. method	***Δ***
log(|G*(T, f=0.10 Hz)|)	85°C	1st 2nd	0.87 0.94
	75°C	1st 2nd	0.98 1.03
	65°C	1st 2nd	1.07 1.14
	55°C	1st 2nd	1.16 1.26
log(|G*(T, f=0.167 Hz)|)	85°C	1st 2nd	0.87 0.94
	75°C	1st 2nd	0.97 1.02
	65°C	1st 2nd	1.06 1.13
	55°C	1st 2nd	1.14 1.24
log(|G*(T, f=0.278 Hz)|)	85°C	1st 2nd	0.87 0.93
	75°C	1st 2nd	0.96 1.02
	65°C	1st 2nd	1.04 1.12
	55°C	1st 2nd	1.11 1.21
log(|G*(T, f=0.464 Hz)|)	85°C	1st 2nd	0.87 0.93
	75°C	1st 2nd	0.95 1.01
	65°C	1st 2nd	1.02 1.10
	55°C	1st 2nd	1.08 1.18
log(|G*(T, f=0.774 Hz)|)	85°C	1st 2nd	0.86 0.92
	75°C	1st 2nd	0.94 1.00
	65°C	1st 2nd	1.00 1.08
	55°C	1st 2nd	1.05 1.15
log(|G*(T, f=2.15 Hz)|)	85°C	1st 2nd	0.84 0.91
	75°C	1st 2nd	0.91 0.97
	65°C	1st 2nd	0.95 1.04
	55°C	1st 2nd	0.98 1.09

Table A1.7. Maximum variations *Δ* of measured values of norm of complex shear modulus for frequencies: 3.59 Hz, 5.99 Hz, 10 Hz for all binder blends according to the 1st or 2nd estimation method.

Parameter	Temp.	Est. method	***Δ***
log(|G*(T, f=3.59 Hz)|)	85°C	1st 2nd	0.83 0.90
	75°C	1st 2nd	0.89 0.96
	65°C	1st 2nd	0.93 1.02
	55°C	1st 2nd	0.95 1.06
log(|G*(T, f=5.99 Hz)|)	85°C	1st 2nd	0.82 0.89
	75°C	1st 2nd	0.87 0.94
	65°C	1st 2nd	0.90 1.00
	55°C	1st 2nd	0.91 1.03
log(|G*(T, f=10 Hz)|)	85°C	1st 2nd	0.81 0.88
	75°C	1st 2nd	0.85 0.92
	65°C	1st 2nd	0.87 0.97
	55°C	1st 2nd	0.87 0.99

Table A1.8. Confidence levels corresponding to 5% ε/Δ ratios of norm of complex shear modulus for frequencies: 0.10 Hz, 0.167 Hz, 0.278 Hz, 0.464 Hz, 0.774 Hz, 2.15 Hz for all binder blends according to the 1st or 2nd estimation method.

Parameter	Temp.	Est. method	**confidence level corresp. to 5% ε/Δ**
log(|G*(T, f=0.10 Hz)|)	85°C	1st 2nd	95.00% 98.20%
	75°C	1st 2nd	95.80% 98.20%
	65°C	1st 2nd	96.10% 98.50%
	55°C	1st 2nd	98.60% 99.40%
log(|G*(T, f=0.167 Hz)|)	85°C	1st 2nd	95.40% 98.10%
	75°C	1st 2nd	95.80% 98.10%
	65°C	1st 2nd	96.10% 98.50%
	55°C	1st 2nd	98.60% 99.30%
log(|G*(T, f=0.278 Hz)|)	85°C	1st 2nd	95.50% 98.00%
	75°C	1st 2nd	95.80% 98.10%
	65°C	1st 2nd	96.00% 98.60%
	55°C	1st 2nd	98.50% 99.10%
log(|G*(T, f=0.464 Hz)|)	85°C	1st 2nd	95.50% 97.70%
	75°C	1st 2nd	95.80% 98.10%
	65°C	1st 2nd	95.90% 98.60%
	55°C	1st 2nd	98.50% 98.90%
log(|G*(T, f=0.774 Hz)|)	85°C	1st 2nd	95.60% 97.40%
	75°C	1st 2nd	95.80% 98.10%
	65°C	1st 2nd	95.80% 98.60%
	55°C	1st 2nd	98.50% 98.50%
log(|G*(T, f=2.15 Hz)|)	85°C	1st 2nd	95.50% 96.60%
	75°C	1st 2nd	95.60% 98.00%
	65°C	1st 2nd	95.40% 98.60%
	55°C	1st 2nd	98.40% 97.50%

Table A1.9. Confidence levels corresponding to 5% ε/Δ ratios of norm of complex shear modulus for frequencies: 3.59 Hz, 5.99 Hz, 10 Hz for all binder blends according to the 1st or 2nd estimation method.

Parameter	Temp.	Est. method	**confidence level corresp. to 5% ε/Δ**
log(|G*(T, f=3.59 Hz)|)	85°C	1st 2nd	95.40% 96.20%
	75°C	1st 2nd	95.50% 97.90%
	65°C	1st 2nd	95.20% 98.50%
	55°C	1st 2nd	98.30% 97.00%
log(|G*(T, f=5.99 Hz)|)	85°C	1st 2nd	95.30% 95.30%
	75°C	1st 2nd	95.30% 97.70%
	65°C	1st 2nd	95.00% 98.50%
	55°C	1st 2nd	98.10% 96.00%
log(|G*(T, f=10 Hz)|)	85°C	1st 2nd	95.20% 94.30%
	75°C	1st 2nd	95.10% 97.50%
	65°C	1st 2nd	94.80% 98.40%
	55°C	1st 2nd	97.90% 95.20%

Appendix 2

-Bituminous mixtures-

A.2.1. Measured and adjusted stiffness modulus

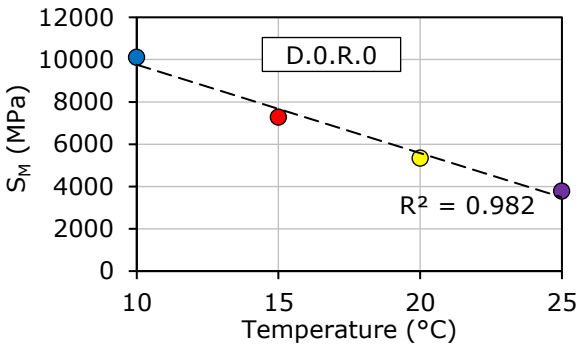

Figure A2.1. Measured stiffness modulus as a function of the test temperature for the bituminous mixture: D.0.R.0.

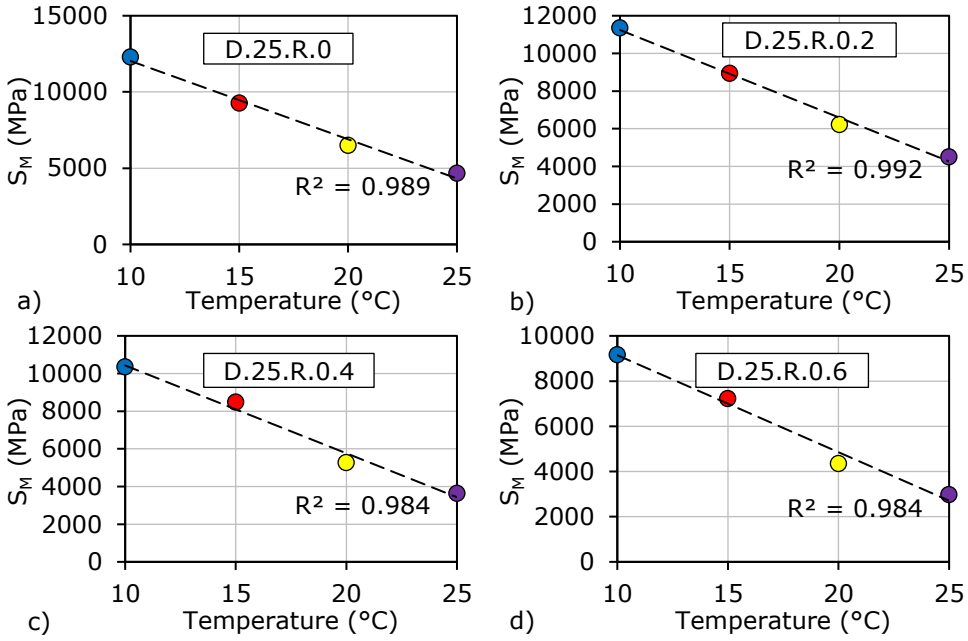

Figure A2.2. Measured stiffness modulus as a function of the test temperature for the bituminous mixtures: (a) D.25.R.0; (b) D.25.R.0.2; (c) D.25.R.0.4; (d) D.25.R.0.6.

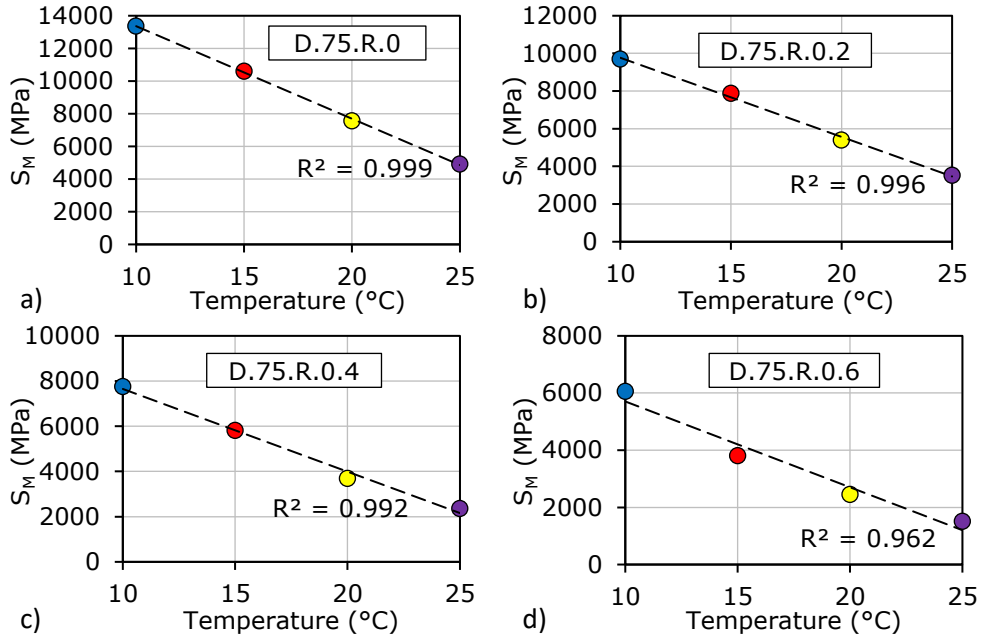

Figure A2.3. Measured stiffness modulus as a function of the test temperature for the bituminous mixtures: (a) D.75.R.0; (b) D.75.R.0.2; (c) D.75.R.0.4; (d) D.75.R.0.6.

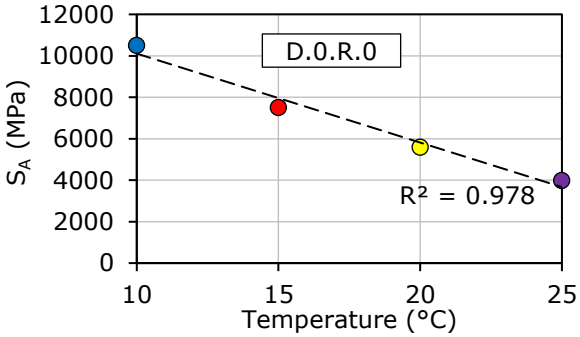

Figure A2.4. Adjusted stiffness modulus as a function of the test temperature for the bituminous mixture: D.0.R.0.

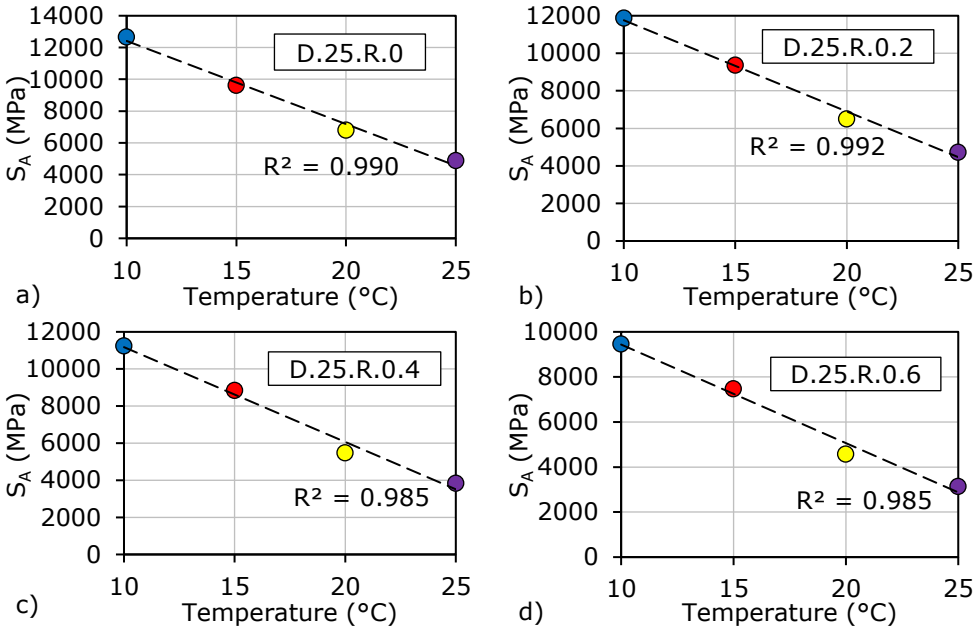

Figure A2.5. Adjusted stiffness modulus as a function of the test temperature for the bituminous mixtures: (a) D.25.R.0; (b) D.25.R.0.2; (c) D.25.R.0.4; (d) D.25.R.0.6.

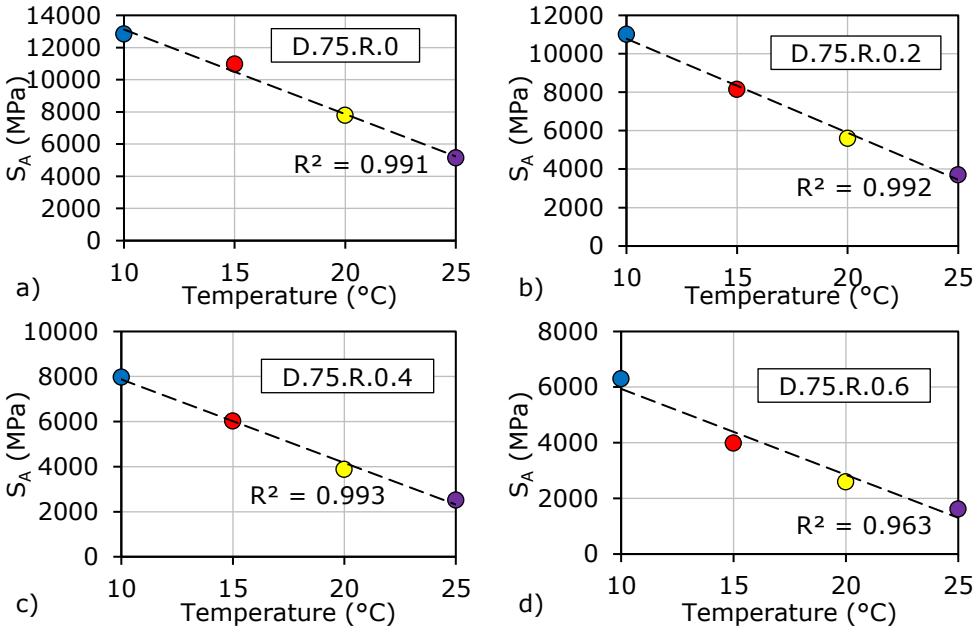

Figure A2.6. Adjusted stiffness modulus as a function of the test temperature for the bituminous mixtures: (a) D.75.R.0; (b) D.75.R.0.2; (c) D.75.R.0.4; (d) D.75.R.0.6.

A.2.2. 2S2P1D model fitting of complex modulus test results

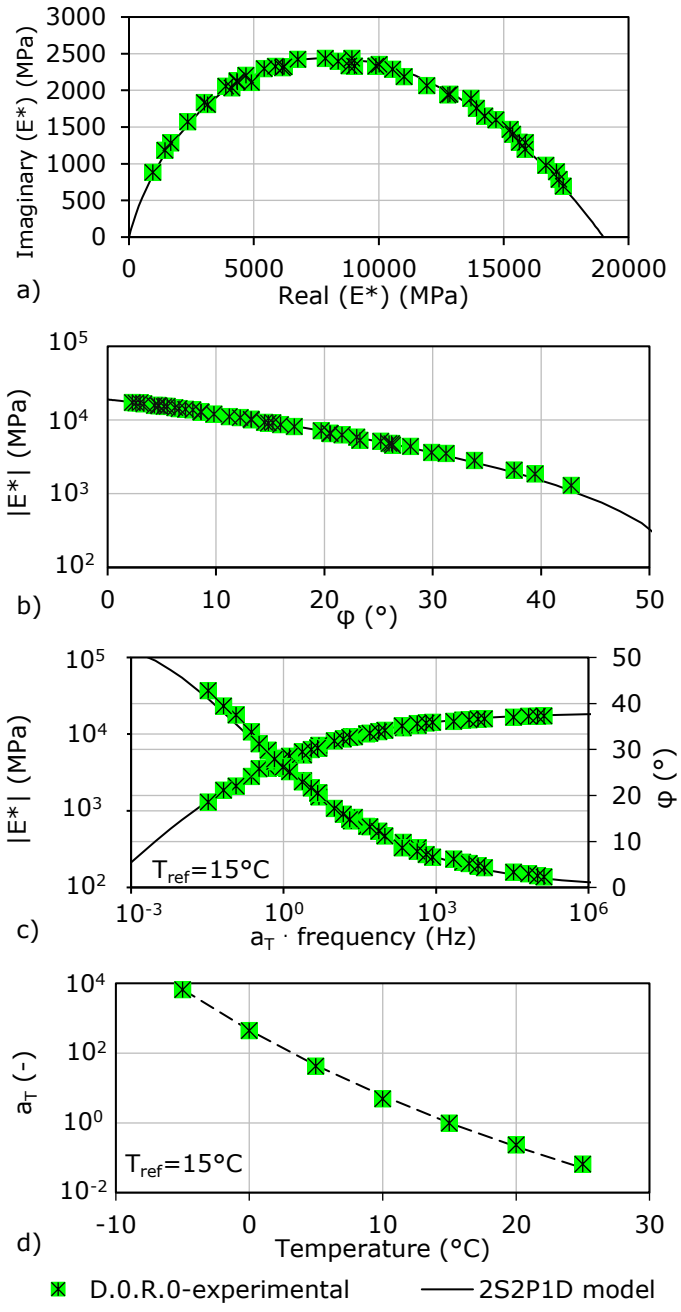

Figure A2.7. 2S2P1D model fitting of complex modulus test results for mixture D.0.R.0: (a) Cole-Cole curve; (b) Black curve; (c) master curves of the norm of complex modulus and phase angle; (d) a_T shift factors and WLF versus temperature.

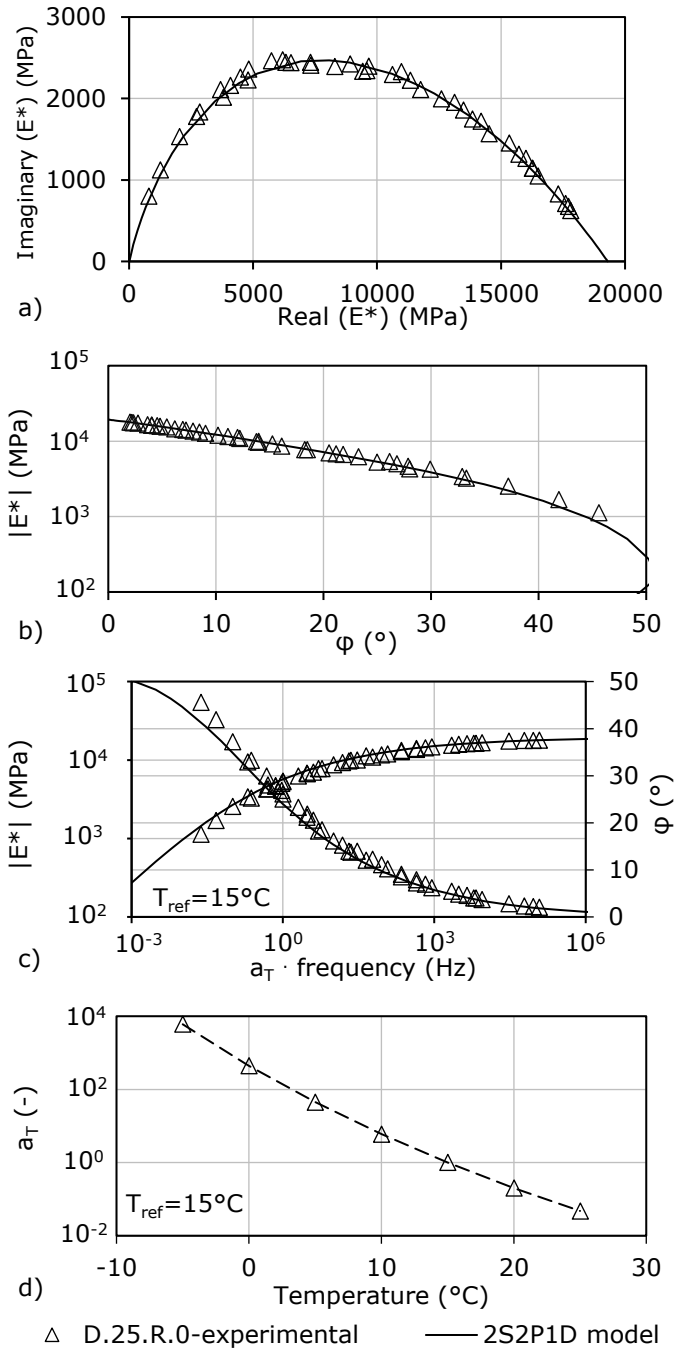

Figure A2.8. 2S2P1D model fitting of complex modulus test results for mixture D.25.R.0: (a) Cole-Cole curve; (b) Black curve; (c) master curves of the norm of complex modulus and phase angle; (d) a_T shift factors and WLF versus temperature.

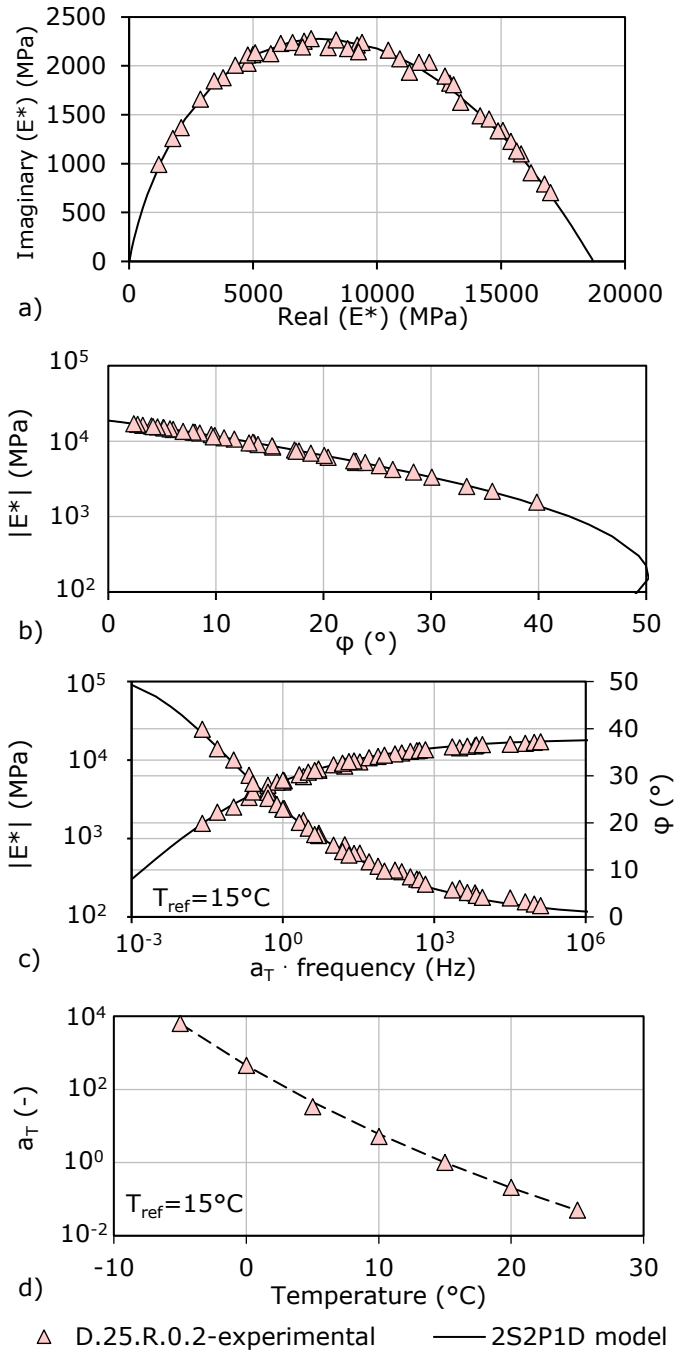

Figure A2.9. 2S2P1D model fitting of complex modulus test results for mixture D.25.R.0.2: (a) Cole-Cole curve; (b) Black curve; (c) master curves of the norm of complex modulus and phase angle; (d) a_T shift factors and WLF versus temperature.

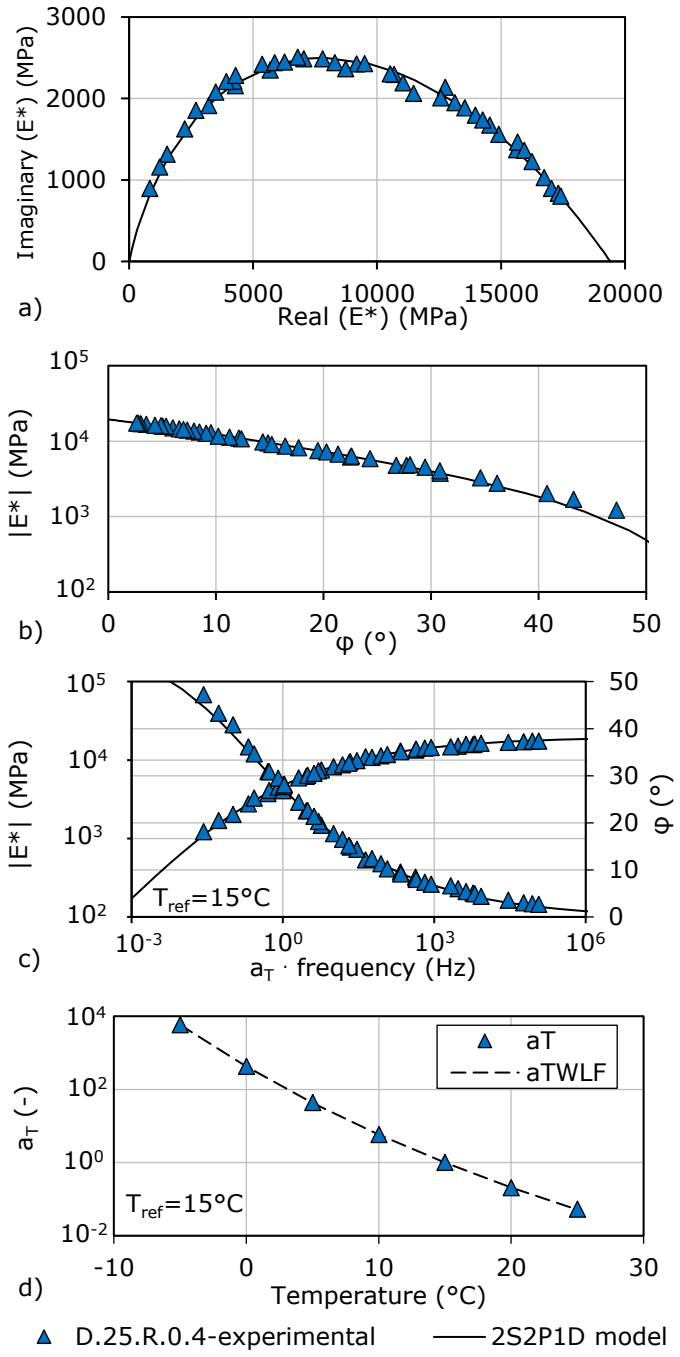

Figure A2.10. 2S2P1D model fitting of complex modulus test results for mixture D.25.R.0.4: (a) Cole-Cole curve; (b) Black curve; (c) master curves of the norm of complex modulus and phase angle; (d) a_T shift factors and WLF versus temperature.

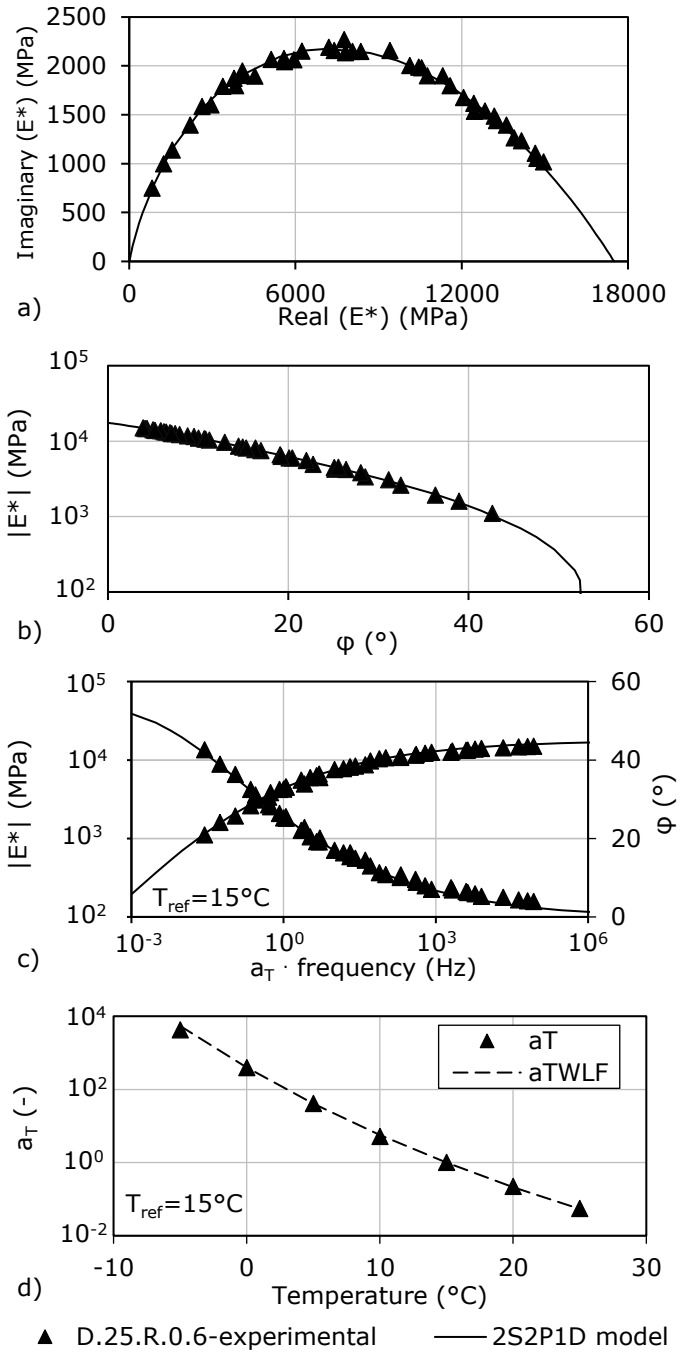

Figure A2.11. 2S2P1D model fitting of complex modulus test results for mixture D.25.R.0.6: (a) Cole-Cole curve; (b) Black curve; (c) master curves of the norm of complex modulus and phase angle; (d) a_T shift factors and WLF versus temperature.

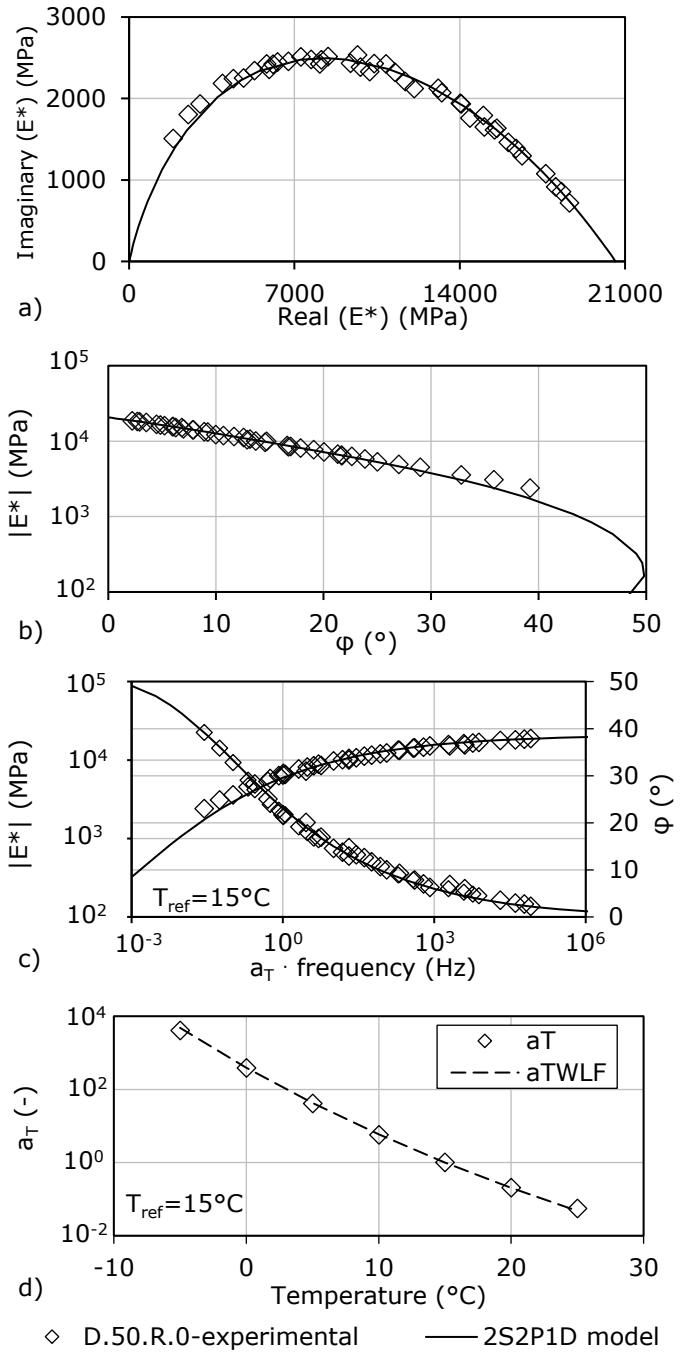

Figure A2.12. 2S2P1D model fitting of complex modulus test results for mixture D.50.R.0: (a) Cole-Cole curve; (b) Black curve; (c) master curves of the norm of complex modulus and phase angle; (d) a_T shift factors and WLF versus temperature.

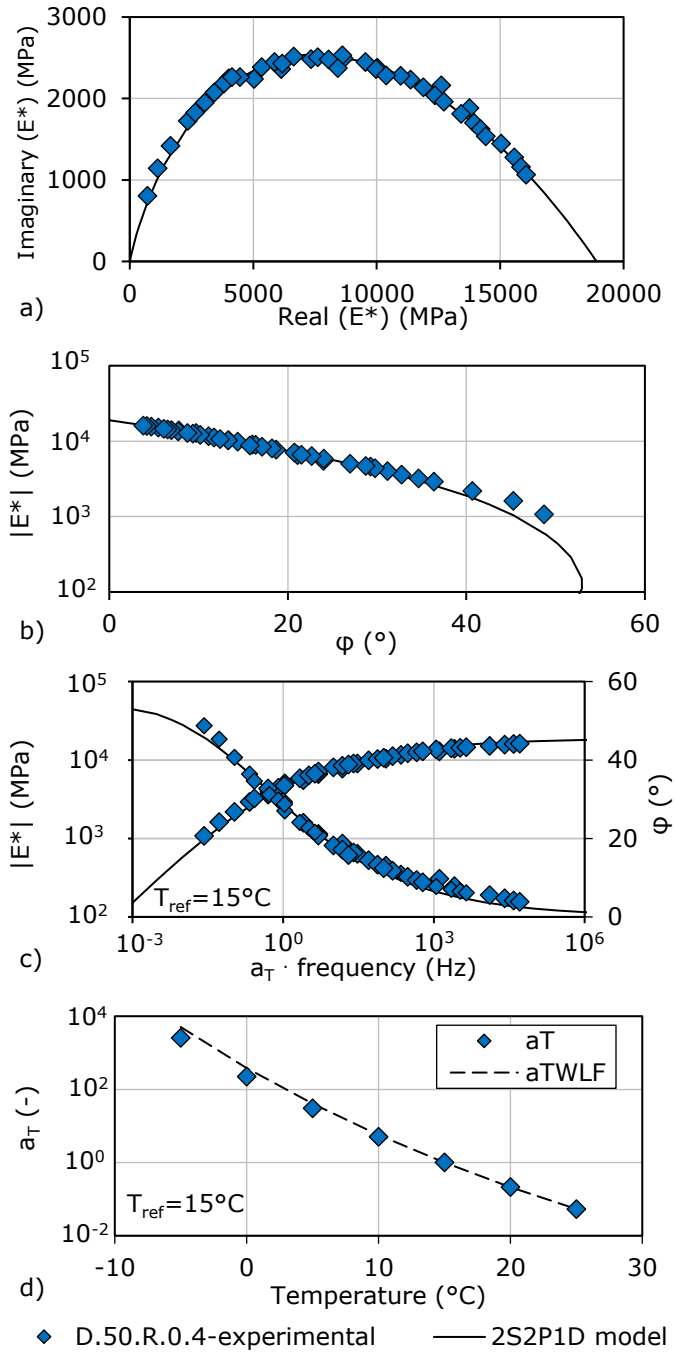

Figure A2.13. 2S2P1D model fitting of complex modulus test results for mixture D.50.R.0.4: (a) Cole-Cole curve; (b) Black curve; (c) master curves of the norm of complex modulus and phase angle; (d) a_T shift factors and WLF versus temperature.

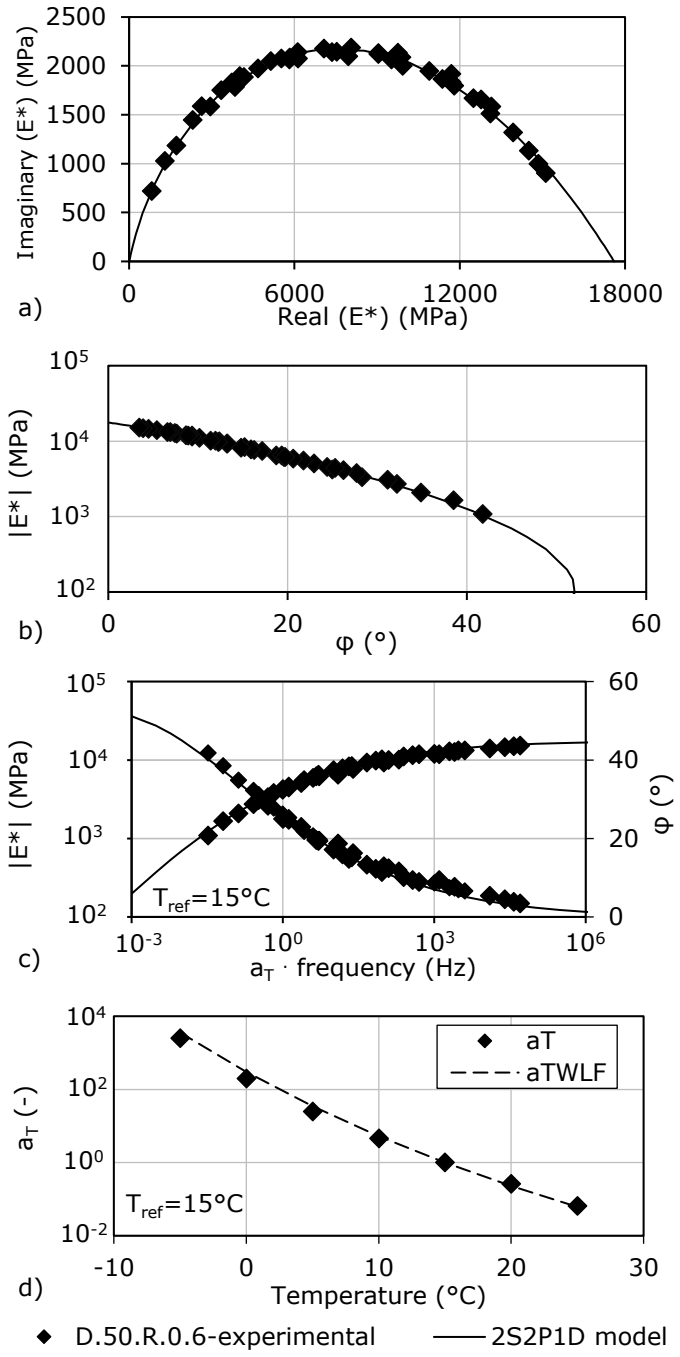

Figure A2.14. 2S2P1D model fitting of complex modulus test results for mixture D.50.R.0.6: (a) Cole-Cole curve; (b) Black curve; (c) master curves of the norm of complex modulus and phase angle; (d) a_T shift factors and WLF versus temperature.

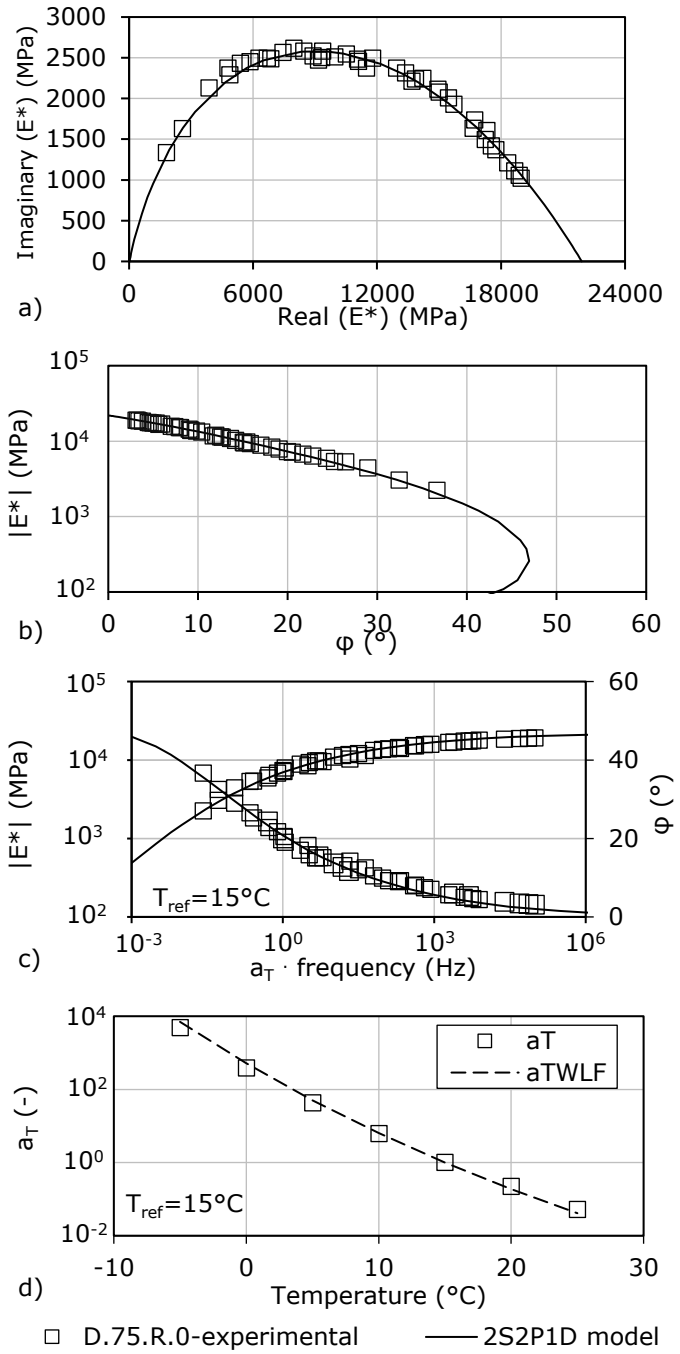

Figure A2.15. 2S2P1D model fitting of complex modulus test results for mixture D.75.R.0: (a) Cole-Cole curve; (b) Black curve; (c) master curves of the norm of complex modulus and phase angle; (d) a_T shift factors and WLF versus temperature.

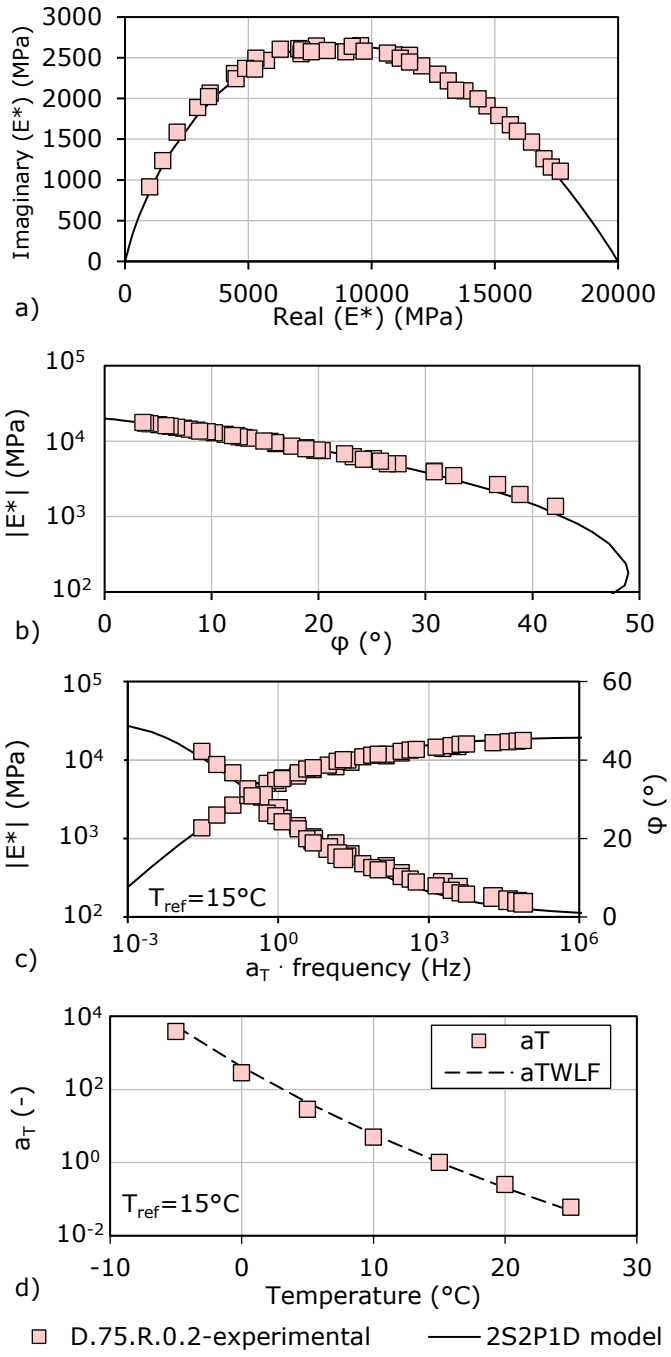

Figure A2.16. 2S2P1D model fitting of complex modulus test results for mixture D.75.R.0.2: (a) Cole-Cole curve; (b) Black curve; (c) master curves of the norm of complex modulus and phase angle; (d) a_T shift factors and WLF versus temperature.

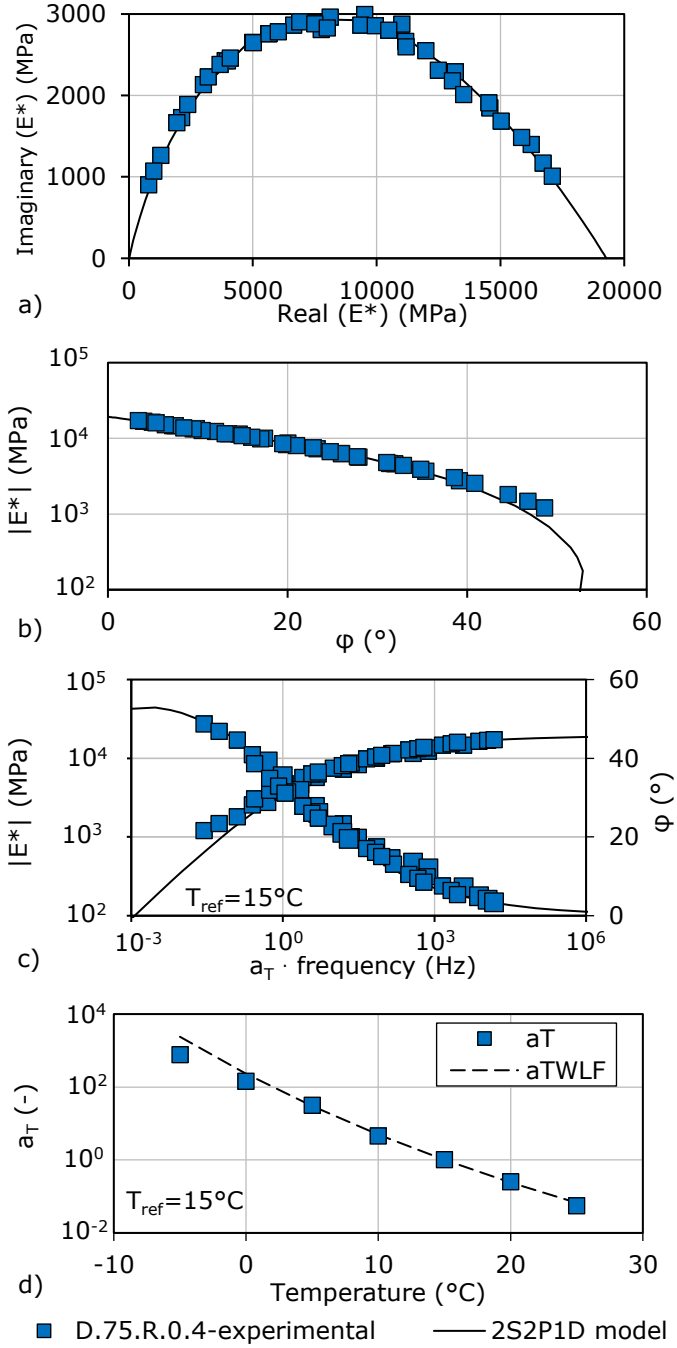

Figure A2.17. 2S2P1D model fitting of complex modulus test results for mixture D.75.R.0.4: (a) Cole-Cole curve; (b) Black curve; (c) master curves of the norm of complex modulus and phase angle; (d) a_T shift factors and WLF versus temperature.

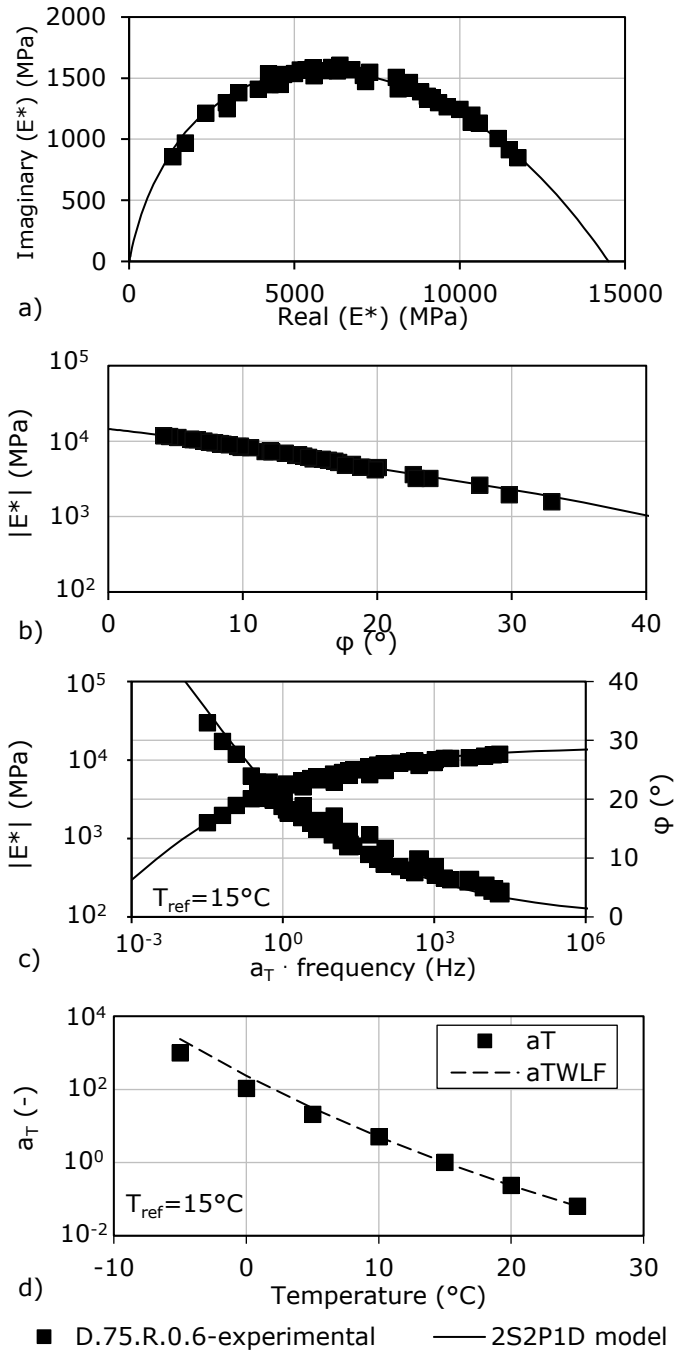

Figure A2.18. 2S2P1D model fitting of complex modulus test results for mixture D.75.R.0.6: (a) Cole-Cole curve; (b) Black curve; (c) master curves of the norm of complex modulus and phase angle; (d) a_T shift factors and WLF versus temperature.

A.2.3. SHStS transformation

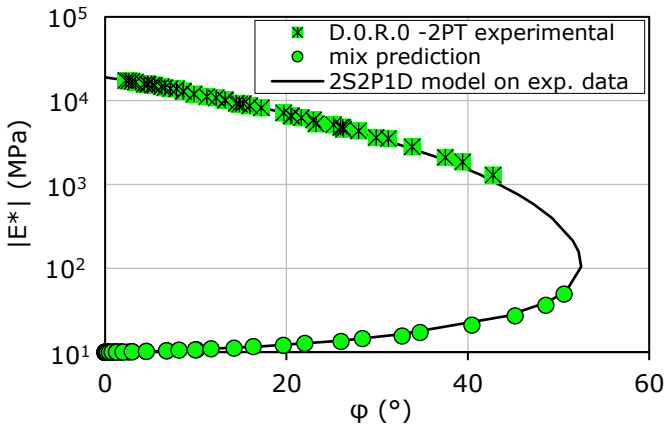

Figure A2.19. Simulation of LVE behaviour from DSR tests on binder blend 50/70 for mixture D.0.R.0 by using SHStS transformation: Black curves.

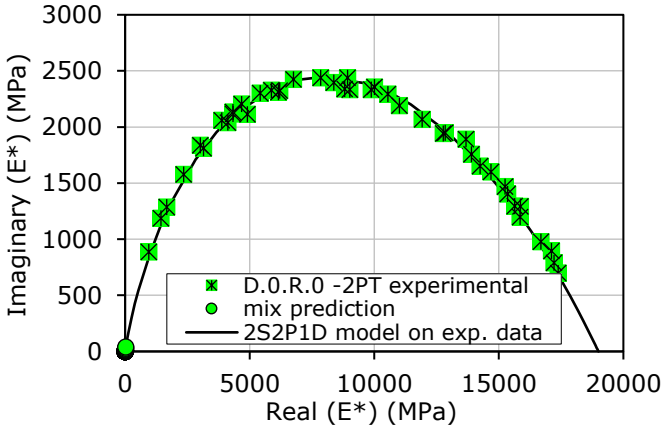

Figure A2.20. Simulation of LVE behaviour from DSR tests on binder blend 50/70 for mixture D.0.R.0 by using SHStS transformation: Cole-Cole curves.

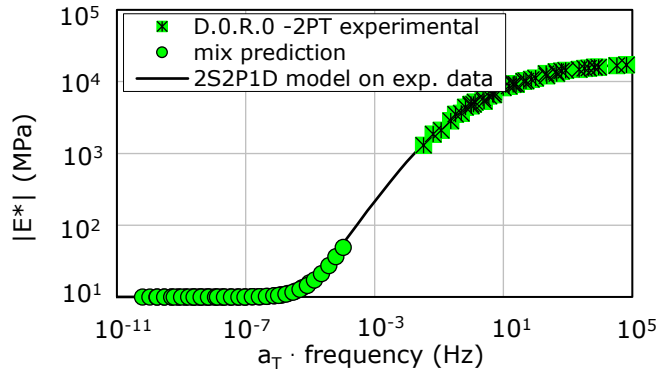

Figure A2.21. Simulation of LVE behaviour from DSR tests on binder blend 50/70 for mixture D.0.R.0 by using SHStS transformation: $|E^*|$ master curves at $T_{ref} = 15°C$.

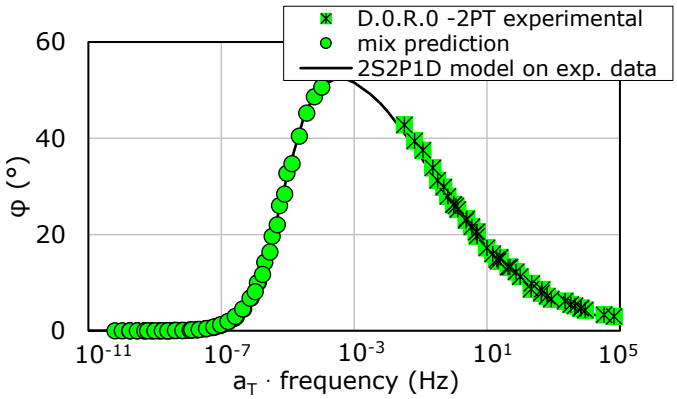

Figure A2.22. Simulation of LVE behaviour from DSR tests on binder blend 50/70 for mixture D.0.R.0 by using SHStS transformation: φ master curves at $T_{ref} = 15°C$.

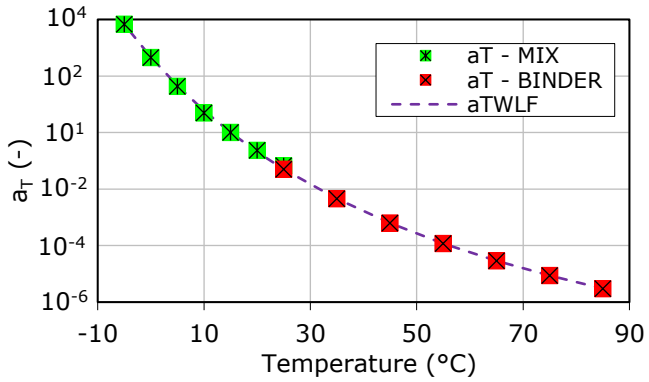

Figure A2.23. Temperature shift factors and WLF curves for the binder 50/70 and mixture D.0.R.0.

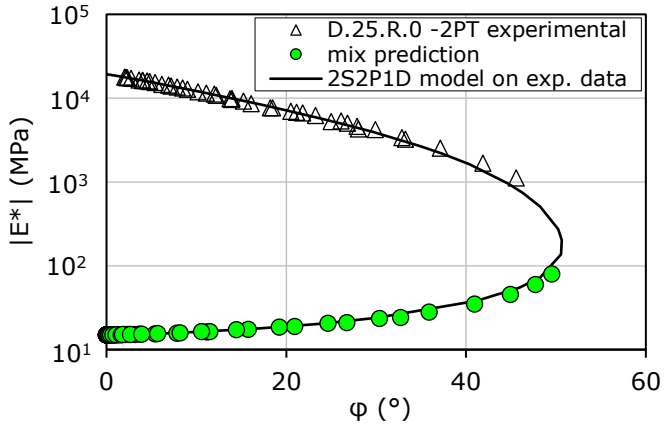

Figure A2.24. Simulation of LVE behaviour from DSR tests on binder blend 50/70+25%RAP for mixture D.25.R.0 by using SHStS transformation: Black curves.

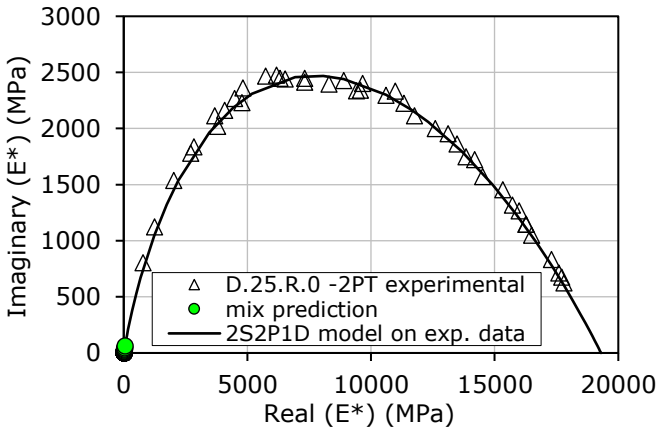

Figure A2.25. Simulation of LVE behaviour from DSR tests on binder blend 50/70+25%RAP for mixture D.25.R.0 by using SHStS transformation: Cole-Cole curves.

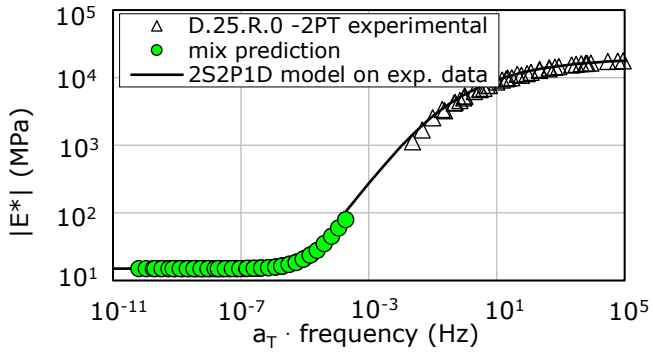

Figure A2.26. Simulation of LVE behaviour from DSR tests on binder blend 50/70+25%RAP for mixture D.25.R.0 by using SHStS transformation: $|E^*|$ master curves at $T_{ref} = 15°C$.

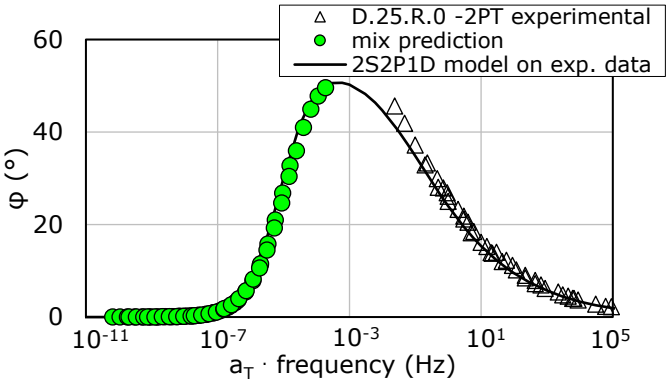

Figure A2.27. Simulation of LVE behaviour from DSR tests on binder blend 50/70+25%RAP for mixture D.25.R.0 by using SHStS transformation: φ master curves at $T_{ref} = 15°C$.

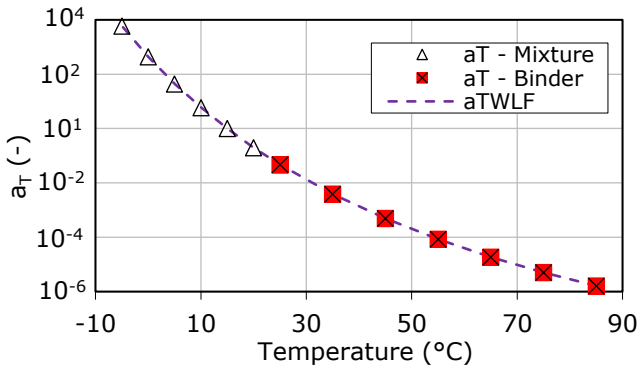

Figure A2.28. Temperature shift factors and WLF curves for the binder 50/70+ 25%RAP and mixture D.25.R.0.

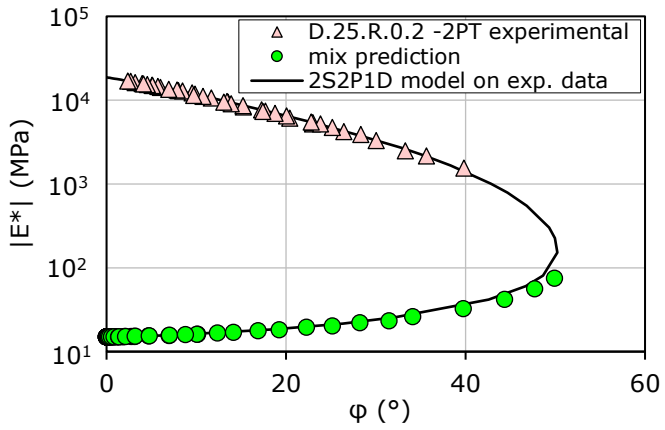

Figure A2.29. Simulation of LVE behaviour from DSR tests on binder blend 50/70+ 25%RAP+5%Rej for mixture D.25.R.0.2 by using SHStS transformation: Black curves.

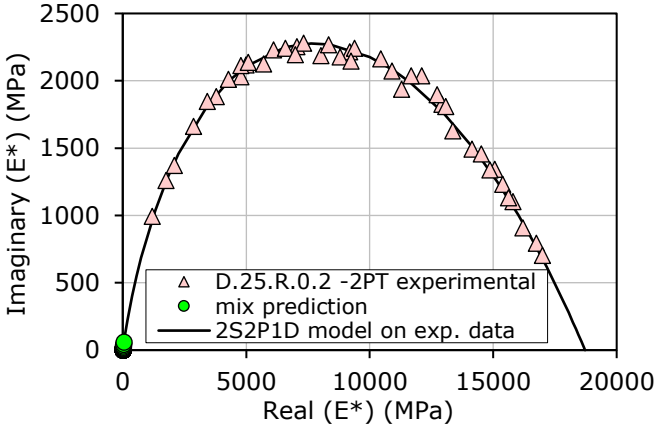

Figure A2.30. Simulation of LVE behaviour from DSR tests on binder blend 50/70+ 25%RAP+5%Rej for mixture D.25.R.0.2 by using SHStS transformation: Cole-Cole curves.

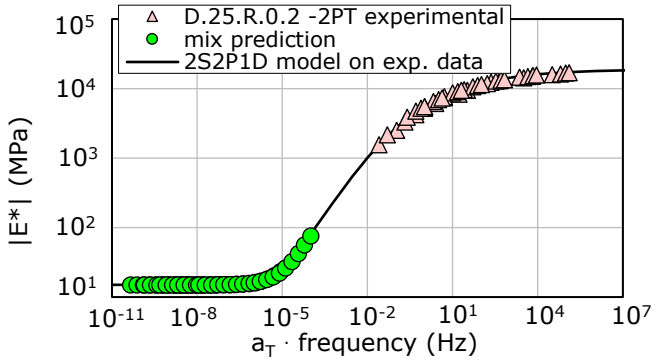

Figure A2.31. Simulation of LVE behaviour from DSR tests on binder blend 50/70+ 25%RAP+5%Rej for mixture D.25.R.0.2 by using SHStS transformation: $|E^*|$ master curves at $T_{ref} = 15°C$.

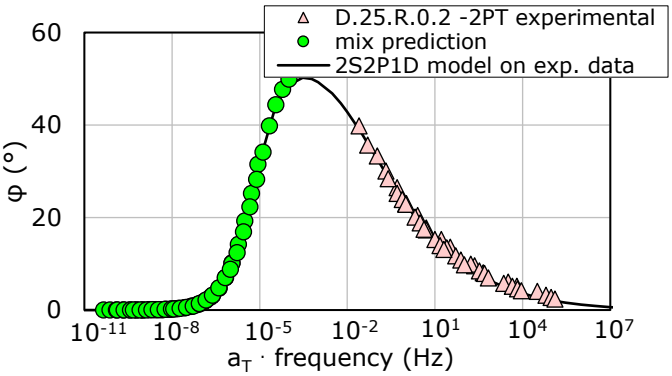

Figure A2.32. Simulation of LVE behaviour from DSR tests on binder blend 50/70+ 25%RAP+5%Rej for mixture D.25.R.0.2 by using SHStS transformation: φ master curves at $T_{ref} = 15°C$.

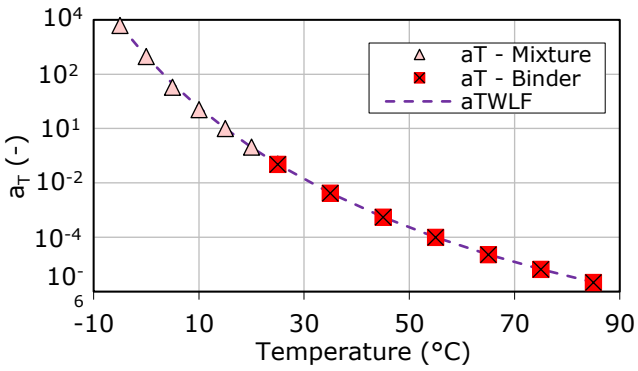

Figure A2.33. Temperature shift factors and WLF curves for the binder 50/70+ 25%RAP+5%Rej and mixture D.25.R.0.2.

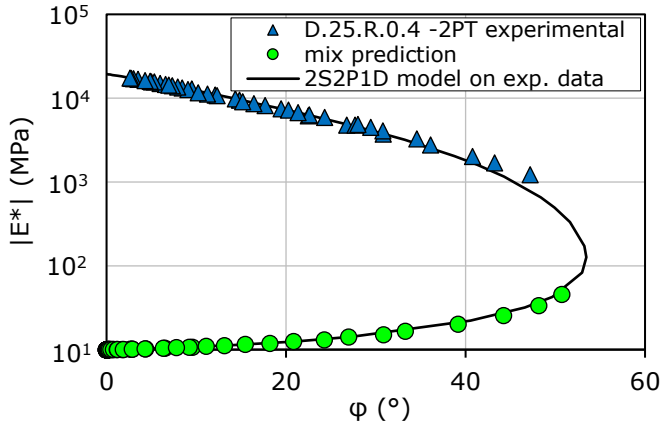

Figure A2.34. Simulation of LVE behaviour from DSR tests on binder blend 50/70+ 25%RAP+10%Rej for mixture D.25.R.0.4 by using SHStS transformation: Black curves.

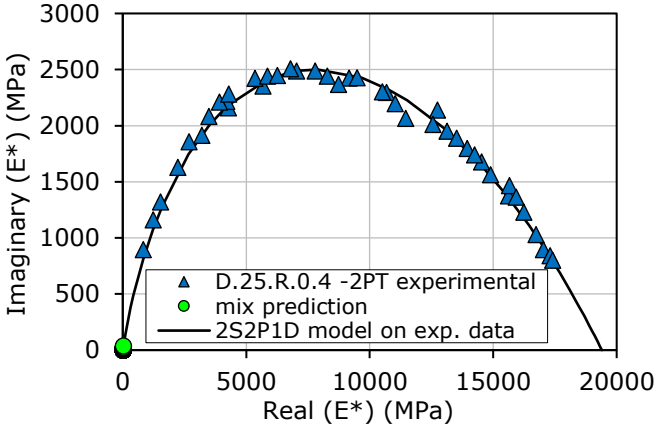

Figure A2.35. Simulation of LVE behaviour from DSR tests on binder blend 50/70+ 25%RAP+10%Rej for mixture D.25.R.0.4 by using SHStS transformation: Cole-Cole curves.

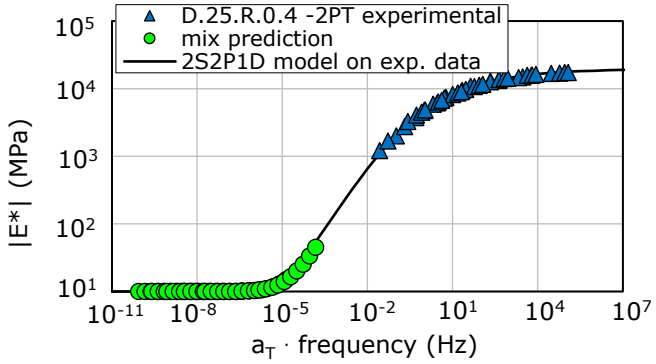

Figure A2.36. Simulation of LVE behaviour from DSR tests on binder blend 50/70+ 25%RAP+10%Rej for mixture D.25.R.0.4 by using SHStS transformation: $|E^*|$ master curves at $T_{ref} = 15°C$.

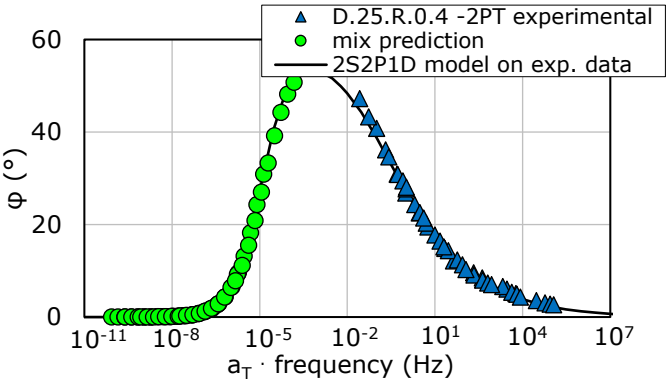

Figure A2.37. Simulation of LVE behaviour from DSR tests on binder blend 50/70+ 25%RAP+10%Rej for mixture D.25.R.0.4 by using SHStS transformation: φ master curves at $T_{ref} = 15°C$.

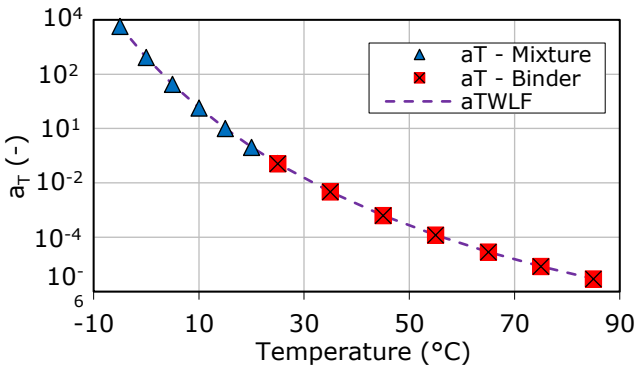

Figure A2.38. Temperature shift factors and WLF curves for the binder 50/70+ 25%RAP+10%Rej and mixture D.25.R.0.4.

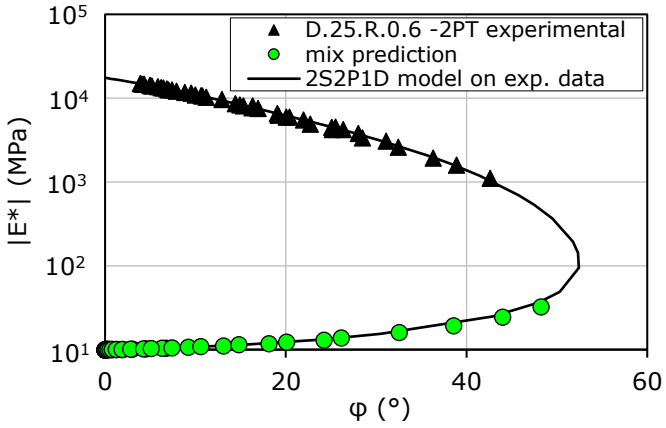

Figure A2.39. Simulation of LVE behaviour from DSR tests on binder blend 50/70+ 25%RAP+15%Rej for mixture D.25.R.0.6 by using SHStS transformation: Black curves.

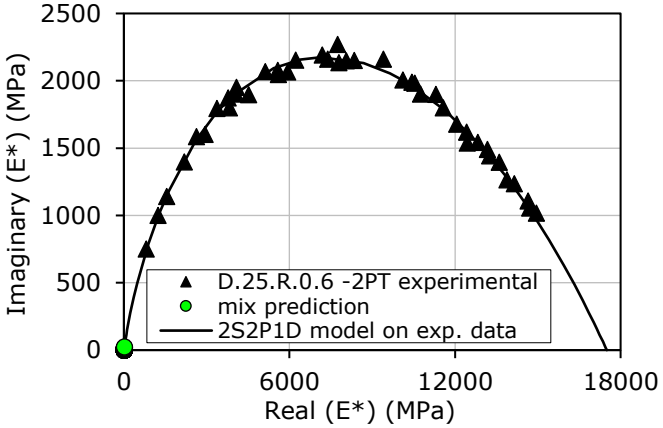

Figure A2.40. Simulation of LVE behaviour from DSR tests on binder blend 50/70+ 25%RAP+15%Rej for mixture D.25.R.0.6 by using SHStS transformation: Cole-Cole curves.

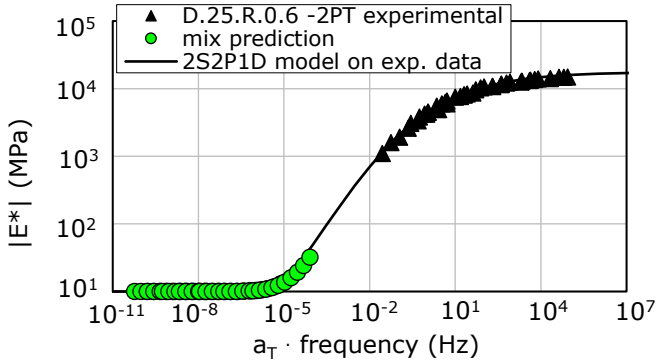

Figure A2.41. Simulation of LVE behaviour from DSR tests on binder blend 50/70+ 25%RAP+15%Rej for mixture D.25.R.0.6 by using SHStS transformation: $|E^*|$ master curves at $T_{ref} = 15°C$.

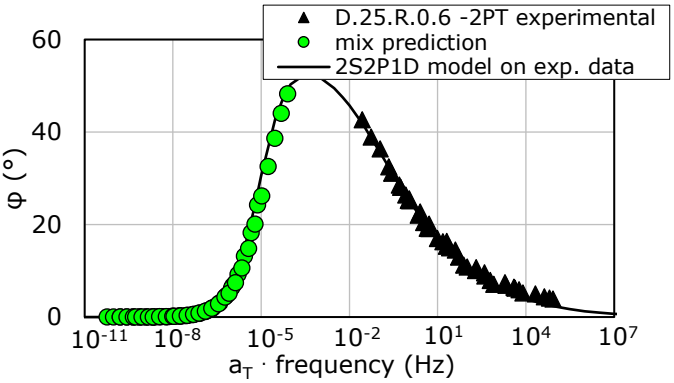

Figure A2.42. Simulation of LVE behaviour from DSR tests on binder blend 50/70+ 25%RAP+15%Rej for mixture D.25.R.0.6 by using SHStS transformation: φ master curves at $T_{ref} = 15°C$.

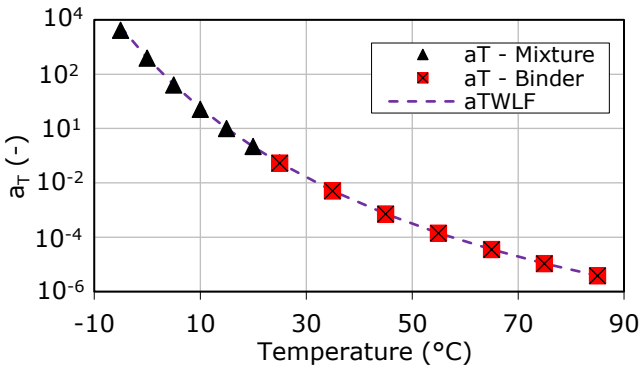

Figure A2.43. Temperature shift factors and WLF curves for the binder 50/70+ 25%RAP+15%Rej and mixture D.25.R.0.6.

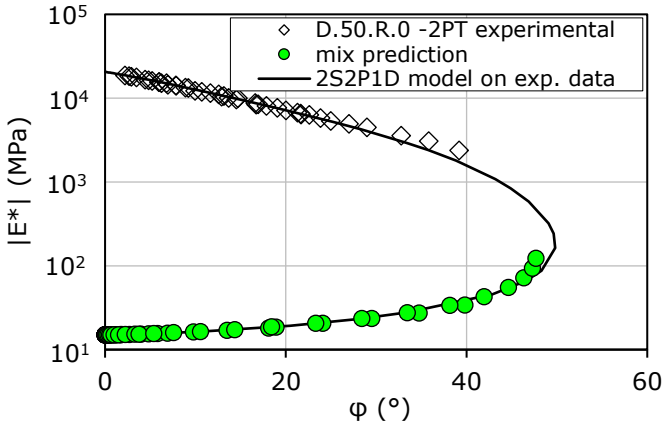

Figure A2.44. Simulation of LVE behaviour from DSR tests on binder blend 50/70+ 50%RAP for mixture D.50.R.0 by using SHStS transformation: Black curves.

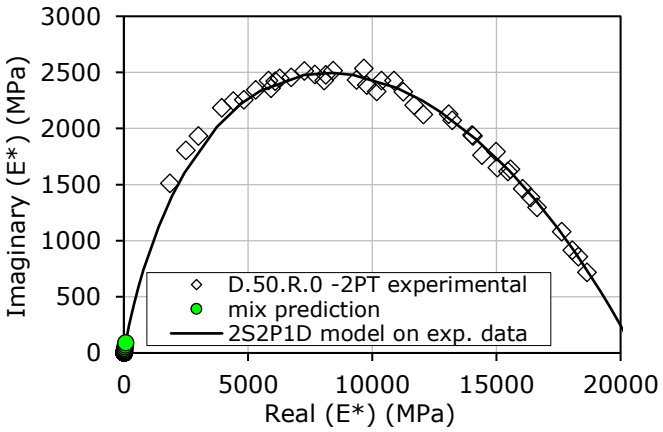

Figure A2.45. Simulation of LVE behaviour from DSR tests on binder blend 50/70+ 50%RAP for mixture D.50.R.0 by using SHStS transformation: Cole-Cole curves.

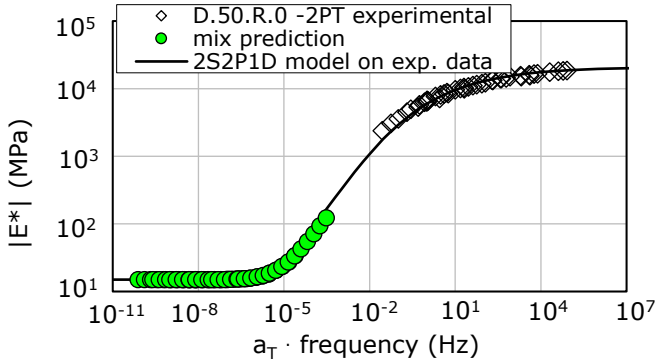

Figure A2.46. Simulation of LVE behaviour from DSR tests on binder blend 50/70+ 50%RAP for mixture D.50.R.0 by using SHStS transformation: $|E^*|$ master curves at $T_{ref} = 15°C$.

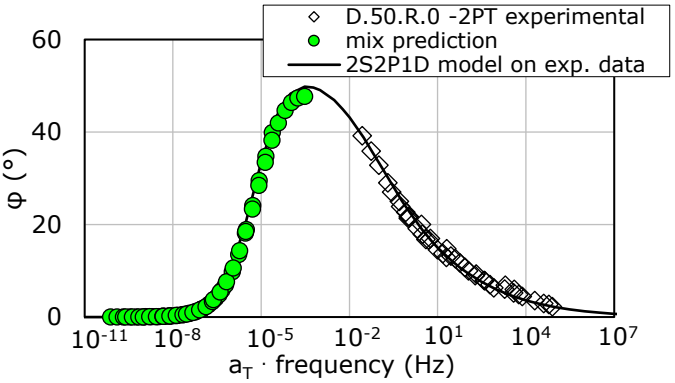

Figure A2.47. Simulation of LVE behaviour from DSR tests on binder blend 50/70+ 50%RAP for mixture D.50.R.0 by using SHStS transformation: φ master curves at $T_{ref} = 15°C$.

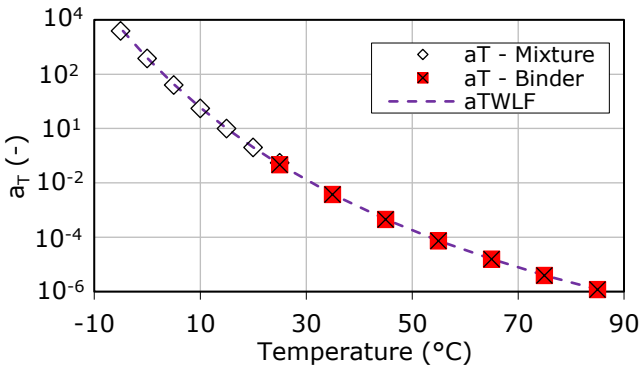

Figure A2.48. Temperature shift factors and WLF curves for the binder 50/70+ 50%RAP and mixture D.50.R.0.

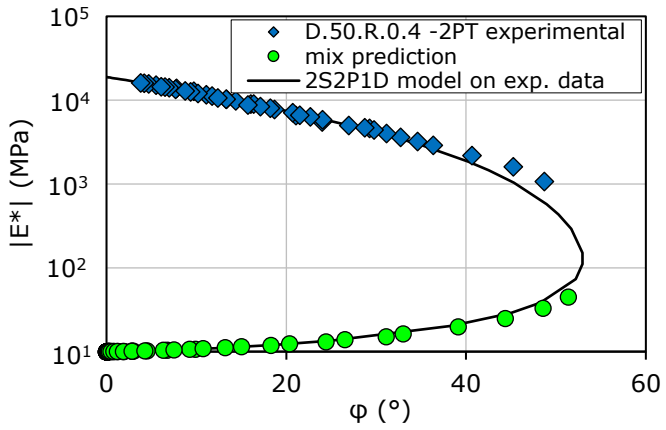

Figure A2.49. Simulation of LVE behaviour from DSR tests on binder blend 50/70+ 50%RAP+10%Rej for mixture D.50.R.0.4 by using SHStS transformation: Black curves.

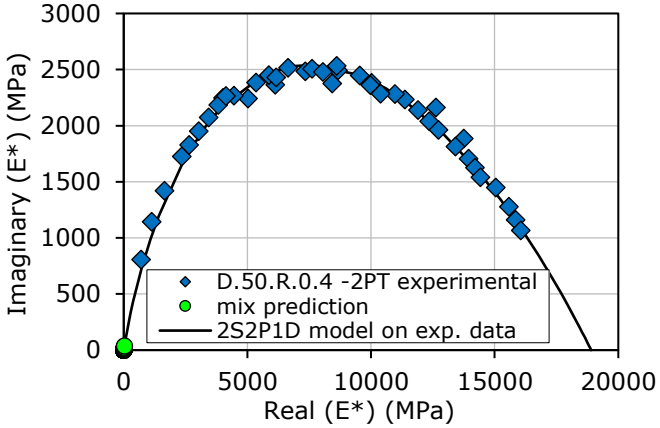

Figure A2.50. Simulation of LVE behaviour from DSR tests on binder blend 50/70+ 50%RAP+10%Rej for mixture D.50.R.0.4 by using SHStS transformation: Cole-Cole curves.

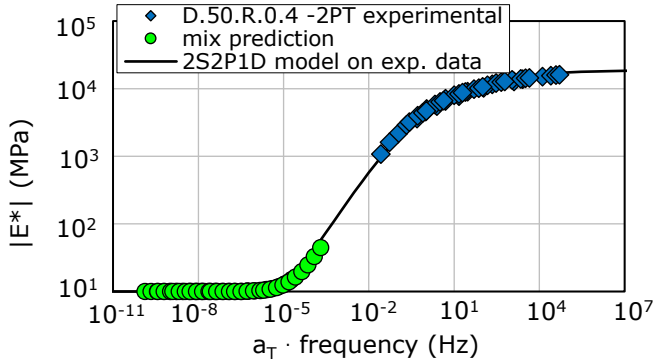

Figure A2.51. Simulation of LVE behaviour from DSR tests on binder blend 50/70+ 50%RAP+10%Rej for mixture D.50.R.0.4 by using SHStS transformation: $|E^*|$ master curves at $T_{ref} = 15°C$.

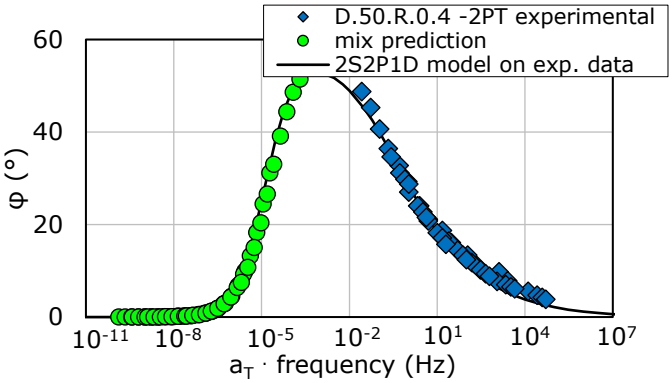

Figure A2.52. Simulation of LVE behaviour from DSR tests on binder blend 50/70+ 50%RAP+10%Rej for mixture D.50.R.0.4 by using SHStS transformation: φ master curves at $T_{ref} = 15°C$.

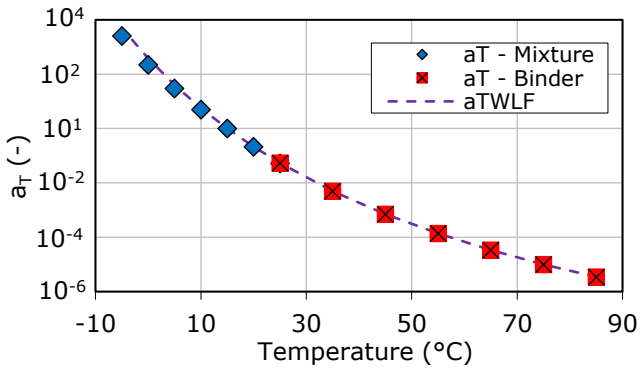

Figure A2.53. Temperature shift factors and WLF curves for the binder 50/70+ 50%RAP+10%Rej and mixture D.50.R.0.4.

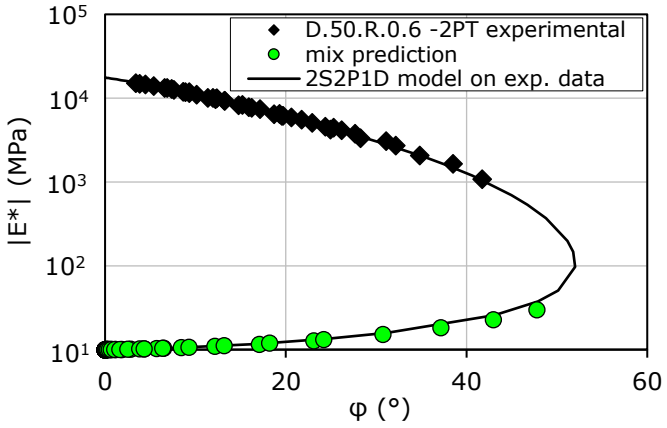

Figure A2.54. Simulation of LVE behaviour from DSR tests on binder blend 50/70+ 50%RAP+15%Rej for mixture D.50.R.0.6 by using SHStS transformation: Black curves.

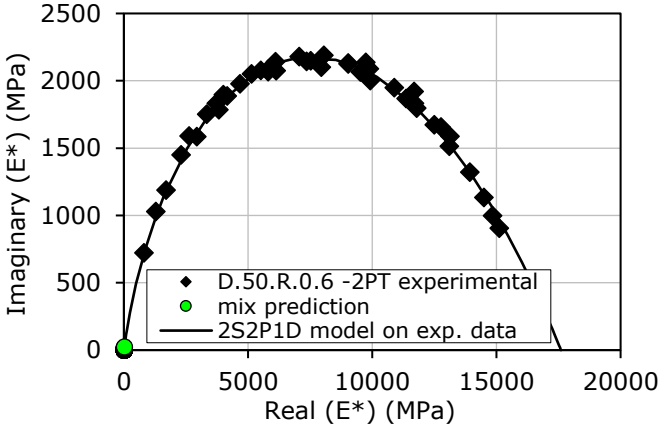

Figure A2.55. Simulation of LVE behaviour from DSR tests on binder blend 50/70+ 50%RAP+15%Rej for mixture D.50.R.0.6 by using SHStS transformation: Cole-Cole curves.

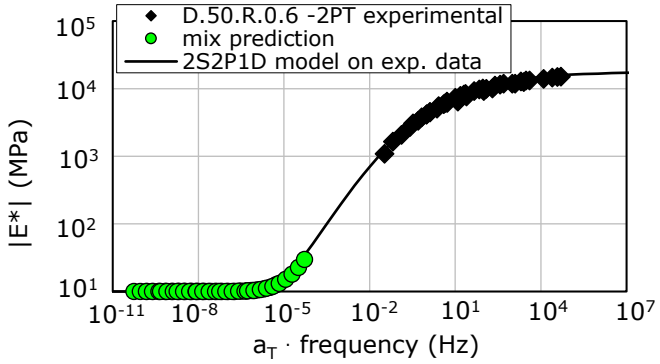

Figure A2.56. Simulation of LVE behaviour from DSR tests on binder blend 50/70+ 50%RAP+15%Rej for mixture D.50.R.0.6 by using SHStS transformation: $|E^*|$ master curves at $T_{ref} = 15°C$.

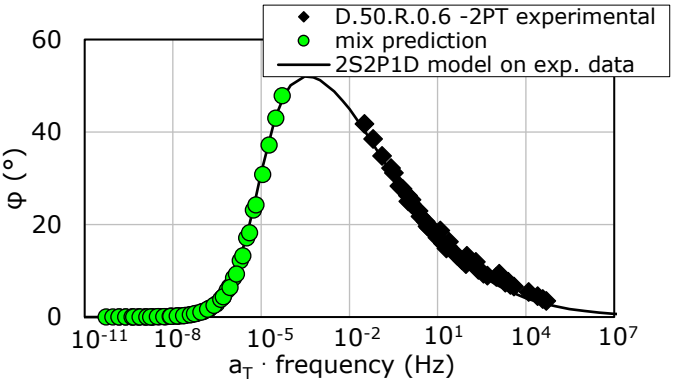

Figure A2.57. Simulation of LVE behaviour from DSR tests on binder blend 50/70+ 50%RAP+15%Rej for mixture D.50.R.0.6 by using SHStS transformation: φ master curves at $T_{ref} = 15°C$.

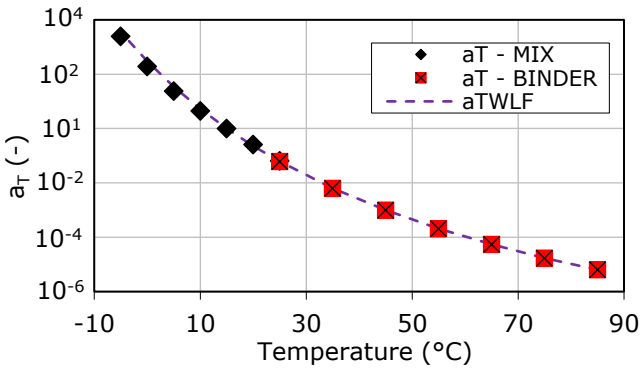

Figure A2.58. Temperature shift factors and WLF curves for the binder 50/70+ 50%RAP+15%Rej and mixture D.50.R.0.6.

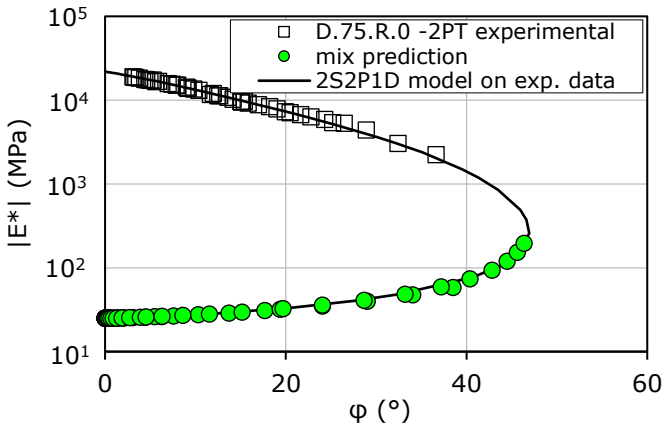

Figure A2.59. Simulation of LVE behaviour from DSR tests on binder blend 50/70+ 75%RAP for mixture D.75.R.0 by using SHStS transformation: Black curves.

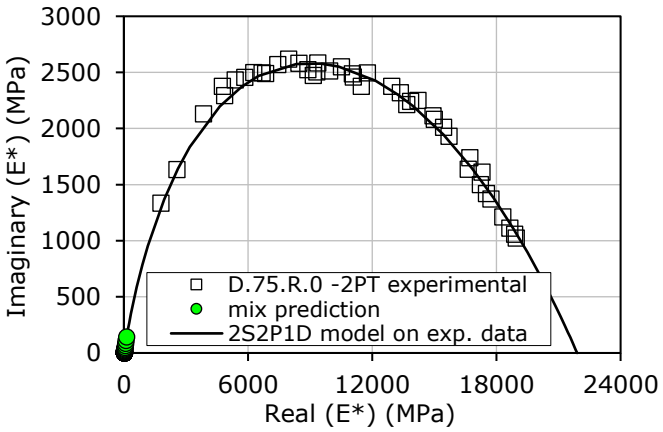

Figure A2.60. Simulation of LVE behaviour from DSR tests on binder blend 50/70+ 75%RAP for mixture D.75.R.0 by using SHStS transformation: Cole-Cole curves.

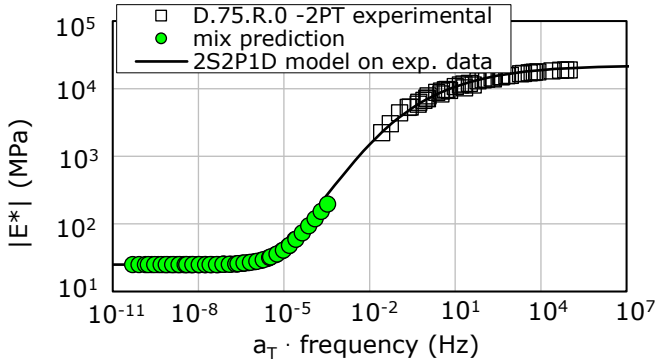

Figure A2.61. Simulation of LVE behaviour from DSR tests on binder blend 50/70+ 75%RAP for mixture D.75.R.0 by using SHStS transformation: $|E^*|$ master curves at $T_{ref} = 15°C$.

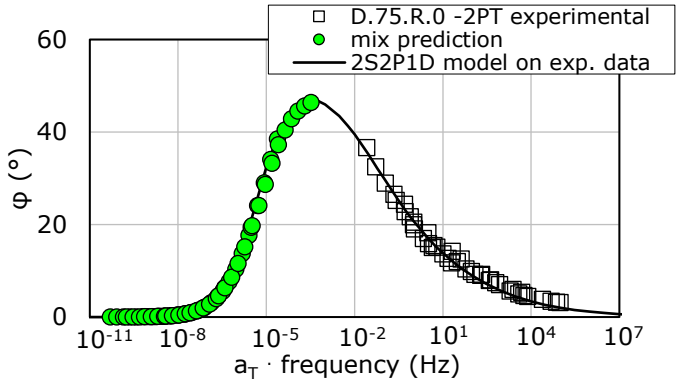

Figure A2.62. Simulation of LVE behaviour from DSR tests on binder blend 50/70+ 75%RAP for mixture D.75.R.0 by using SHStS transformation: φ master curves at $T_{ref} = 15°C$.

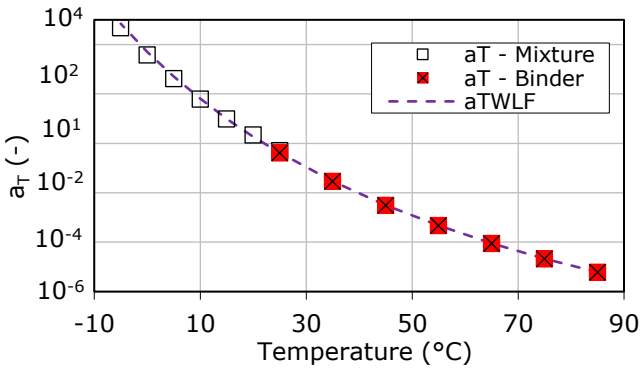

Figure A2.63. Temperature shift factors and WLF curves for the binder 50/70+ 75%RAP and mixture D.75.R.0.

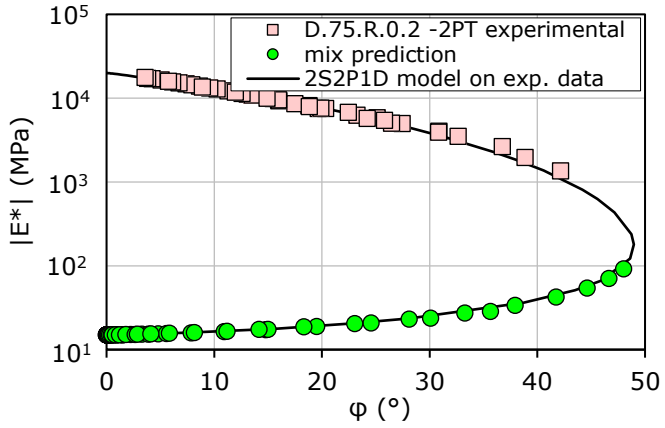

Figure A2.64. Simulation of LVE behaviour from DSR tests on binder blend 50/70+ 75%RAP+5%Rej for mixture D.75.R.0.2 by using SHStS transformation: Black curves.

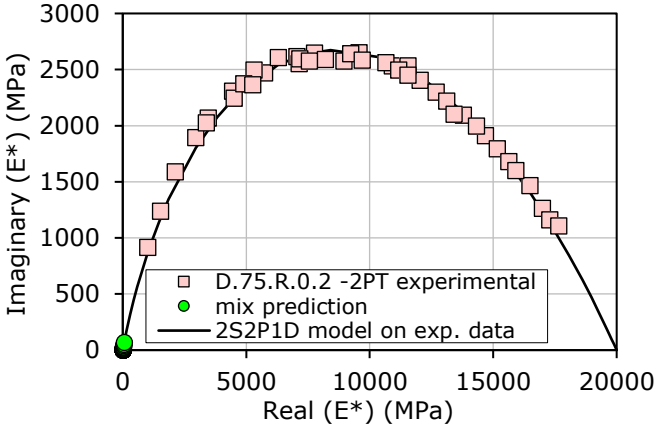

Figure A2.65. Simulation of LVE behaviour from DSR tests on binder blend 50/70+ 75%RAP+5%Rej for mixture D.75.R.0.2 by using SHStS transformation: Cole-Cole curves.

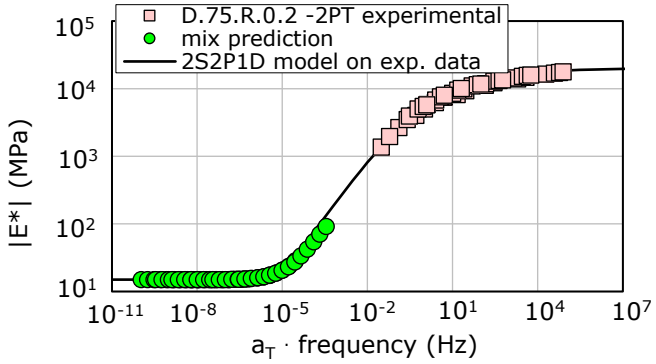

Figure A2.66. Simulation of LVE behaviour from DSR tests on binder blend 50/70+ 75%RAP+5%Rej for mixture D.75.R.0.2 by using SHStS transformation: $|E^*|$ master curves at $T_{ref} = 15°C$.

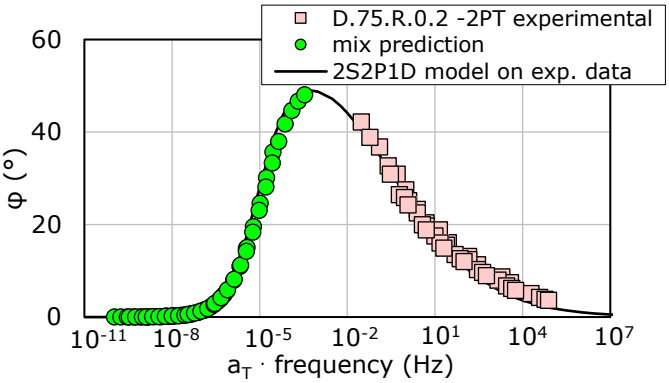

Figure A2.67. Simulation of LVE behaviour from DSR tests on binder blend 50/70+ 75%RAP+5%Rej for mixture D.75.R.0.2 by using SHStS transformation: φ master curves at $T_{ref} = 15°C$.

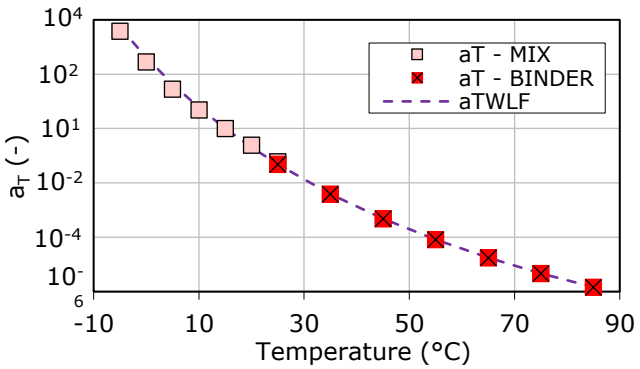

Figure A2.68. Temperature shift factors and WLF curves for the binder 50/70+ 75%RAP+5%Rej and mixture D.75.R.0.2.

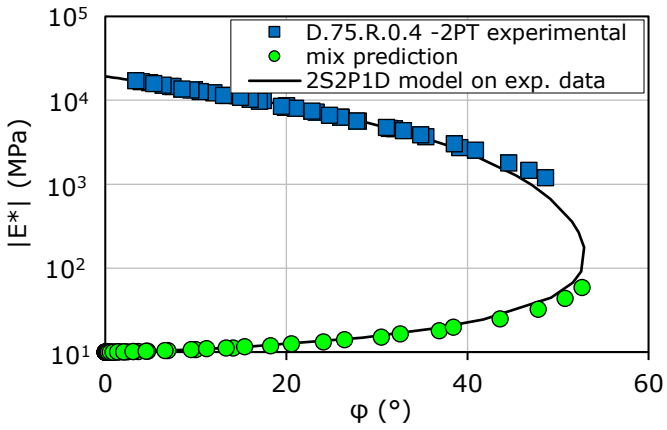

Figure A2.69. Simulation of LVE behaviour from DSR tests on binder blend 50/70+ 75%RAP+10%Rej for mixture D.75.R.0.4 by using SHStS transformation: Black curves.

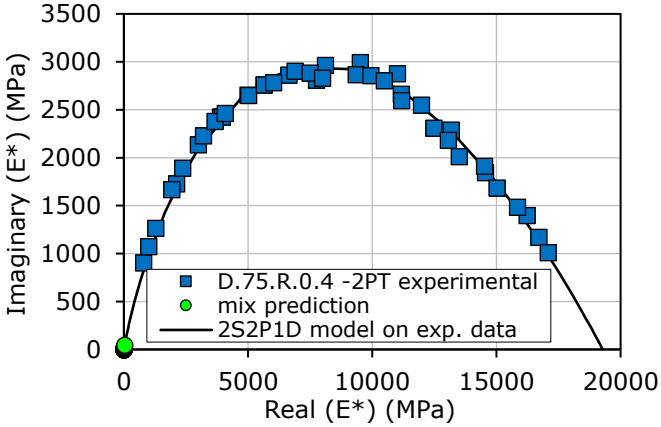

Figure A2.70. Simulation of LVE behaviour from DSR tests on binder blend 50/70+ 75%RAP+10%Rej for mixture D.75.R.0.4 by using SHStS transformation: Cole-Cole curves.

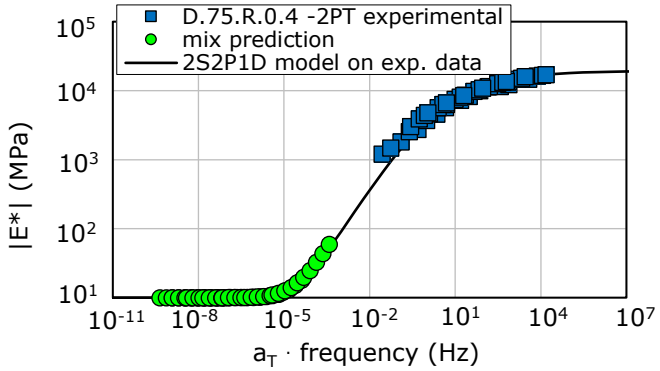

Figure A2.71. Simulation of LVE behaviour from DSR tests on binder blend 50/70+ 75%RAP+10%Rej for mixture D.75.R.0.4 by using SHStS transformation: $|E^*|$ master curves at $T_{ref} = 15°C$.

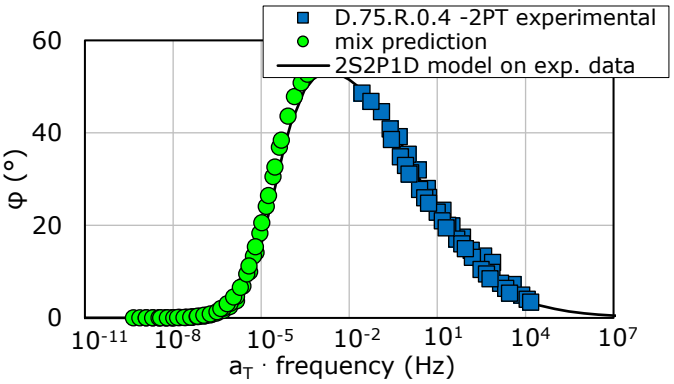

Figure A2.72. Simulation of LVE behaviour from DSR tests on binder blend 50/70+ 75%RAP+10%Rej for mixture D.75.R.0.4 by using SHStS transformation: φ master curves at $T_{ref} = 15°C$.

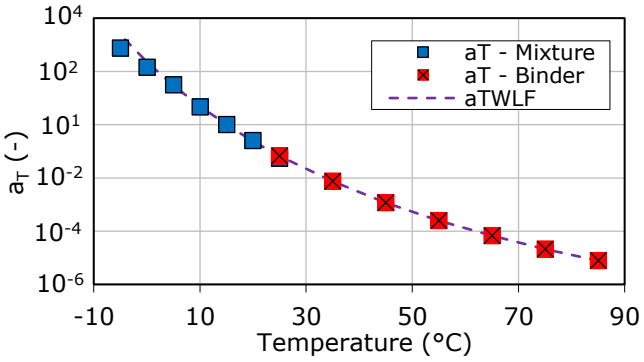

Figure A2.73. Temperature shift factors and WLF curves for the binder 50/70+ 75%RAP+10%Rej and mixture D.75.R.0.4.

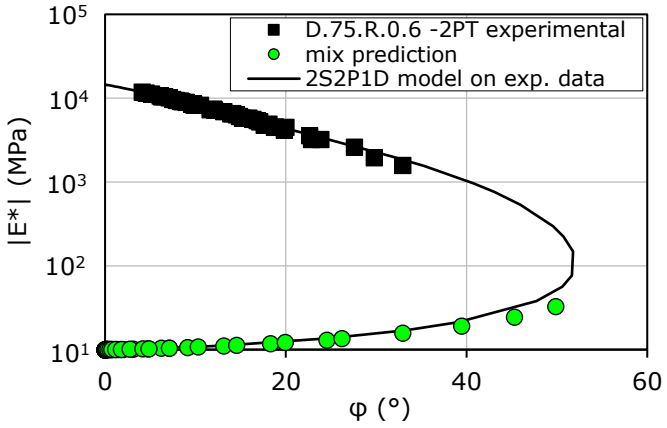

Figure A2.74. Simulation of LVE behaviour from DSR tests on binder blend 50/70+ 75%RAP+15%Rej for mixture D.75.R.0.6 by using SHStS transformation: Black curves.

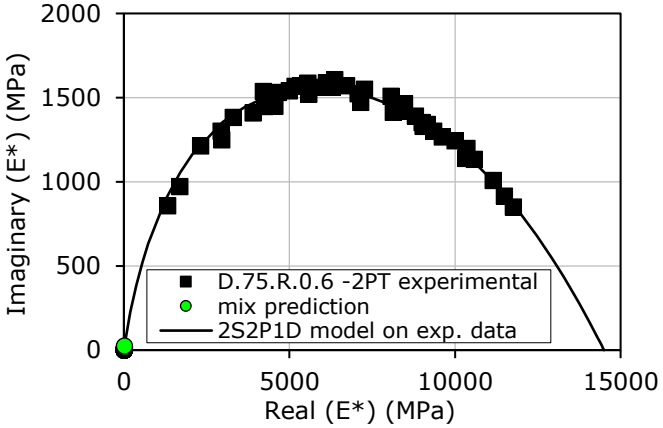

Figure A2.75. Simulation of LVE behaviour from DSR tests on binder blend 50/70+ 75%RAP+15%Rej for mixture D.75.R.0.6 by using SHStS transformation: Cole-Cole curves.

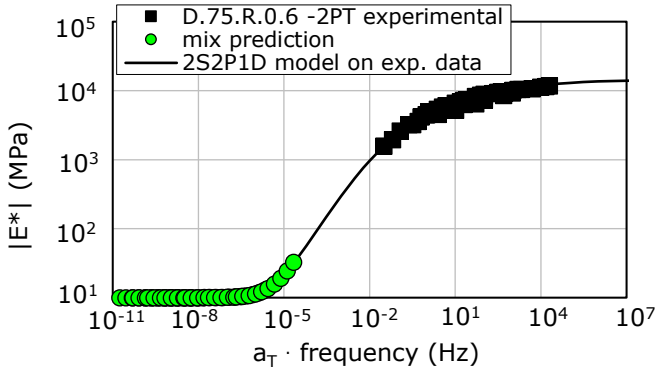

Figure A2.76. Simulation of LVE behaviour from DSR tests on binder blend 50/70+ 75%RAP+15%Rej for mixture D.75.R.0.6 by using SHStS transformation: $|E^*|$ master curves at $T_{ref} = 15°C$.

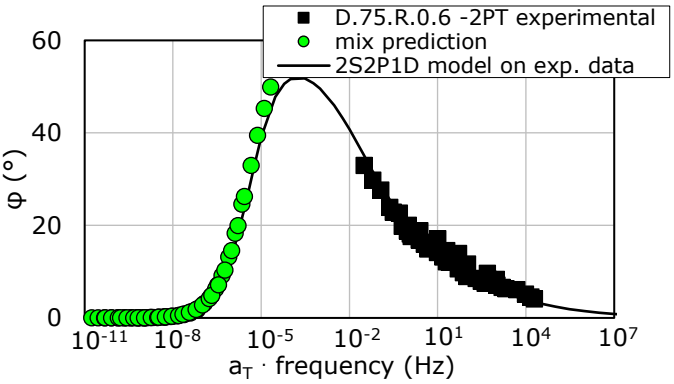

Figure A2.77. Simulation of LVE behaviour from DSR tests on binder blend 50/70+ 75%RAP+15%Rej for mixture D.75.R.0.6 by using SHStS transformation: φ master curves at $T_{ref} = 15°C$.

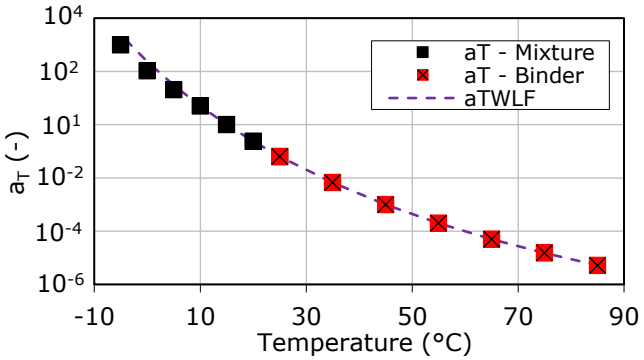

Figure A2.78. Temperature shift factors and WLF curves for the binder 50/70+ 75%RAP+15%Rej and mixture D.75.R.0.6.

Appendix 3

- Environmental Impact Assessment (E.I.A.) -

A.3.1. E.I. indicators (EN 15804+A1) stage A1, A2 and A3

Table A3.1. Environmental impact indicators obtained for stages A1, A2 and A3, per declared unit for the reference HMA (D.0.R.0), according to EN 15804+A1.

Potential environmental impact			D.0.R.0		
Environmental impact indicators	Parameter	Unit	A1	A2	A3
	Global warming potential (GWP)	kg CO2 eq.	41.02	14.62	16.90
	Ozone Depletion Potential(ODP)	kg R11 eq.	1.62E-13	3.96E-15	6.61E-16
	Acidification potential (AP)	kg SO2 eq.	7.94E-02	4.98E-02	9.46E-03
	Eutrophication potential (EP)	kg Phosphate eq.	9.11E-03	1.23E-02	2.22E-03
	Photochemical Ozone Creation Potential (POCP)	kg Ethene eq.	1.63E-02	-1.64E-02	1.34E-03
	Abiotic depletion potential for non-fossil resources (ADPE)	kg Sb eq.	8.35E-06	1.33E-06	2.17E-06
	Abiotic depletion potential for fossil resources (ADPF)	MJ	2.74E+03	1.98E+02	2.83E+02

Table A3.2. Environmental impact indicators obtained for stages A1, A2 and A3, per declared unit for the bituminous mixture D.25.R.0, according to EN 15804+A1.

Potential environmental impact			D.25.R.0		
Environmental impact indicators	Parameter	Unit	A1	A2	A3
	Global warming potential (GWP)	kg CO2 eq.	32.01	10.90	13.70
	Ozone Depletion Potential(ODP)	kg R11 eq.	1.22E-13	2.95E-15	5.36E-16
	Acidification potential (AP)	kg SO2 eq.	6.39E-02	3.80E-02	7.67E-03
	Eutrophication potential (EP)	kg Phosphate eq.	7.20E-03	9.40E-03	1.80E-03
	Photochemical Ozone Creation Potential (POCP)	kg Ethene eq.	1.33E-02	-1.28E-02	1.08E-03
	Abiotic depletion potential for non-fossil resources (ADPE)	kg Sb eq.	6.66E-06	9.95E-07	1.76E-06
	Abiotic depletion potential for fossil resources (ADPF)	MJ	2.23E+03	1.48E+02	2.30E+02

Table A3.3. Environmental impact indicators obtained for stages A1, A2 and A3, per declared unit for the bituminous mixture D.25.R.0.2, according to EN 15804+A1.

Potential environmental impact			D.25.R.0.2		
Environmental impact indicators	Parameter	Unit	A1	A2	A3
	Global warming potential(GWP)	kg CO2 eq.	31.31	10.92	13.70
	Ozone Depletion Potential(ODP)	kg R11 eq.	4.94E-07	2.95E-15	5.36E-16
	Acidification potential (AP)	kg SO2 eq.	6.65E-02	3.80E-02	7.67E-03
	Eutrophication potential (EP)	kg Phosphate eq.	7.76E-03	9.41E-03	1.80E-03
	Photochemical Ozone Creation Potential (POCP)	kg Ethene eq.	1.46E-02	-1.28E-02	1.08E-03
	Abiotic depletion potential for non-fossil resources (ADPE)	kg Sb eq.	6.67E-06	9.96E-07	1.76E-06
	Abiotic depletion potential for fossil resources (ADPF)	MJ	2.22E+03	1.48E+02	2.30E+02

Table A3.4. Environmental impact indicators obtained for stages A1, A2 and A3, per declared unit for the bituminous mixture D.25.R.0.6, according to EN 15804+A1.

Potential environmental impact			D.25.R.0.6		
Environmental impact indicators	**Parameter**	**Unit**	**A1**	**A2**	**A3**
	Global warming potential (GWP)	kg CO2 eq.	29.99	10.94	13.70
	Ozone Depletion Potential (ODP)	kg R11 eq.	1.48E-06	2.96E-15	5.36E-16
	Acidification potential (AP)	kg SO2 eq.	7.19E-02	3.81E-02	7.67E-03
	Eutrophication potential (EP)	kg Phosphate eq.	8.91E-03	9.43E-03	1.80E-03
	Photochemical Ozone Creation Potential (POCP)	kg Ethene eq.	1.72E-02	-1.28E-02	1.08E-03
	Abiotic depletion potential for non-fossil resources (ADPE)	kg Sb eq.	6.71E-06	9.99E-07	1.76E-06
	Abiotic depletion potential for fossil resources (ADPF)	MJ	2.23E+03	1.48E+02	2.30E+02

Table A3.5. Environmental impact indicators obtained for stages A1, A2 and A3, per declared unit for the bituminous mixture D.50.R.0, according to EN 15804+A1.

Potential environmental impact			D.50.R.0		
Environmental impact indicators	**Parameter**	**Unit**	**A1**	**A2**	**A3**
	Global warming potential (GWP)	kg CO2 eq.	23.08	7.33	10.56
	Ozone Depletion Potential (ODP)	kg R11 eq.	8.05E-14	1.98E-15	4.13E-16
	Acidification potential (AP)	kg SO2 eq.	4.84E-02	2.66E-02	5.91E-03
	Eutrophication potential (EP)	kg Phosphate eq.	5.29E-03	6.59E-03	1.39E-03
	Photochemical Ozone Creation Potential (POCP)	kg Ethene eq.	1.03E-02	-9.30E-03	8.36E-04
	Abiotic depletion potential for non-fossil resources (ADPE)	kg Sb eq.	4.96E-06	6.69E-07	1.35E-06
	Abiotic depletion potential for fossil resources (ADPF)	MJ	1.71E+03	9.93E+01	1.77E+02

Table A3.6. Environmental impact indicators obtained for stages A1, A2 and A3, per declared unit for the bituminous mixture D.50.R.0.2, according to EN 15804+A1.

Potential environmental impact			D.50.R.0.2		
Environmental impact indicators	**Parameter**	**Unit**	**A1**	**A2**	**A3**
	Global warming potential (GWP)	kg CO2 eq.	21.76	7.36	10.56
	Ozone Depletion Potential (ODP)	kg R11 eq.	9.88E-07	1.99E-15	4.13E-16
	Acidification potential (AP)	kg SO2 eq.	5.38E-02	2.67E-02	5.91E-03
	Eutrophication potential (EP)	kg Phosphate eq.	6.43E-03	6.61E-03	1.39E-03
	Photochemical Ozone Creation Potential (POCP)	kg Ethene eq.	1.29E-02	-9.32E-03	8.36E-04
	Abiotic depletion potential for non-fossil resources (ADPE)	kg Sb eq.	5.00E-06	6.72E-07	1.35E-06
	Abiotic depletion potential for fossil resources (ADPF)	MJ	1.71E+03	9.97E+01	1.77E+02

Table A3.7. Environmental impact indicators obtained for stages A1, A2 and A3, per declared unit for the bituminous mixture D.50.R.0.4, according to EN 15804+A1.

Potential environmental impact			D.50.R.0.4		
	Parameter	Unit	A1	A2	A3
Environmental impact indicators	Global warming potential (GWP)	kg CO2 eq.	20.41	7.39	10.56
	Ozone Depletion Potential (ODP)	kg R11 eq.	1.98E-06	2.00E-15	4.13E-16
	Acidification potential (AP)	kg SO2 eq.	5.90E-02	2.68E-02	5.91E-03
	Eutrophication potential (EP)	kg Phosphate eq.	7.57E-03	6.64E-03	1.39E-03
	Photochemical Ozone Creation Potential (POCP)	kg Ethene eq.	1.55E-02	-9.34E-03	8.36E-04
	Abiotic depletion potential for non-fossil resources (ADPE)	kg Sb eq.	5.03E-06	6.75E-07	1.35E-06
	Abiotic depletion potential for fossil resources (ADPF)	MJ	1.71E+03	1.00E+02	1.77E+02

Table A3.8. Environmental impact indicators obtained for stages A1, A2 and A3, per declared unit for the bituminous mixture D.50.R.0.6, according to EN 15804+A1.

Potential environmental impact			D.50.R.0.6		
	Parameter	Unit	A1	A2	A3
Environmental impact indicators	Global warming potential (GWP)	kg CO2 eq.	19.09	7.43	10.56
	Ozone Depletion Potential (ODP)	kg R11 eq.	2.96E-06	2.01E-15	4.13E-16
	Acidification potential (AP)	kg SO2 eq.	6.44E-02	2.69E-02	5.91E-03
	Eutrophication potential (EP)	kg Phosphate eq.	8.71E-03	6.66E-03	1.39E-03
	Photochemical Ozone Creation Potential (POCP)	kg Ethene eq.	1.80E-02	-9.37E-03	8.36E-04
	Abiotic depletion potential for non-fossil resources (ADPE)	kg Sb eq.	5.06E-06	6.78E-07	1.35E-06
	Abiotic depletion potential for fossil resources (ADPF)	MJ	1.72E+03	1.01E+02	1.77E+02

Table A3.9. Environmental impact indicators obtained for stages A1, A2 and A3, per declared unit for the bituminous mixture D.75.R.0, according to EN 15804+A1.

Potential environmental impact			D.75.R.0		
	Parameter	Unit	A1	A2	A3
Environmental impact indicators	Global warming potential (GWP)	kg CO2 eq.	14.08	4.46	7.42
	Ozone Depletion Potential (ODP)	kg R11 eq.	3.84E-14	1.21E-15	2.90E-16
	Acidification potential (AP)	kg SO2 eq.	3.28E-02	1.71E-02	4.15E-03
	Eutrophication potential (EP)	kg Phosphate eq.	3.36E-03	4.26E-03	9.74E-04
	Photochemical Ozone Creation Potential (POCP)	kg Ethene eq.	7.33E-03	-6.28E-03	5.88E-04
	Abiotic depletion potential for non-fossil resources (ADPE)	kg Sb eq.	3.26E-06	4.07E-07	9.52E-07
	Abiotic depletion potential for fossil resources (ADPF)	MJ	1.19E+03	6.05E+01	1.25E+02

Table A3.10. Environmental impact indicators obtained for stages A1, A2 and A3, per declared unit for the bituminous mixture D.75.R.0.2, according to EN 15804+A1.

Potential environmental impact			D.75.R.0.2		
	Parameter	**Unit**	**A1**	**A2**	**A3**
Environmental impact indicators	Global warming potential (GWP)	kg CO2 eq.	12.08	4.52	7.42
	Ozone Depletion Potential (ODP)	kg R11 eq.	1.48E-06	1.22E-15	2.90E-16
	Acidification potential (AP)	kg SO2 eq.	4.08E-02	1.73E-02	4.15E-03
	Eutrophication potential (EP)	kg Phosphate eq.	5.07E-03	4.30E-03	9.74E-04
	Photochemical Ozone Creation Potential (POCP)	kg Ethene eq.	1.12E-02	-6.32E-03	5.88E-04
	Abiotic depletion potential for non-fossil resources (ADPE)	kg Sb eq.	3.30E-06	4.13E-07	9.52E-07
	Abiotic depletion potential for fossil resources (ADPF)	MJ	1.20E+03	6.13E+01	1.25E+02

Table A3.11. Environmental impact indicators obtained for stages A1, A2 and A3, per declared unit for the bituminous mixture D.75.R.0.4, according to EN 15804+A1.

Potential environmental impact			D.75.R.0.4		
	Parameter	**Unit**	**A1**	**A2**	**A3**
Environmental impact indicators	Global warming potential (GWP)	kg CO2 eq.	10.11	4.58	7.42
	Ozone Depletion Potential (ODP)	kg R11 eq.	2.96E-06	1.24E-15	2.90E-16
	Acidification potential (AP)	kg SO2 eq.	4.88E-02	1.75E-02	4.15E-03
	Eutrophication potential (EP)	kg Phosphate eq.	6.79E-03	4.34E-03	9.74E-04
	Photochemical Ozone Creation Potential (POCP)	kg Ethene eq.	1.50E-02	-6.36E-03	5.88E-04
	Abiotic depletion potential for non-fossil resources (ADPE)	kg Sb eq.	3.36E-06	4.18E-07	9.52E-07
	Abiotic depletion potential for fossil resources (ADPF)	MJ	1.20E+03	6.21E+01	1.25E+02

Table A3.12. Environmental impact indicators obtained for stages A1, A2 and A3, per declared unit for the bituminous mixture D.75.R.0.6, according to EN 15804+A1.

Potential environmental impact			D.75.R.0.6		
	Parameter	**Unit**	**A1**	**A2**	**A3**
Environmental impact indicators	Global warming potential (GWP)	kg CO2 eq.	8.14	4.64	7.42
	Ozone Depletion Potential (ODP)	kg R11 eq.	4.45E-06	1.25E-15	2.90E-16
	Acidification potential (AP)	kg SO2 eq.	5.69E-02	1.76E-02	4.15E-03
	Eutrophication potential (EP)	kg Phosphate eq.	8.50E-03	4.38E-03	9.74E-04
	Photochemical Ozone Creation Potential (POCP)	kg Ethene eq.	1.89E-02	-6.41E-03	5.88E-04
	Abiotic depletion potential for non-fossil resources (ADPE)	kg Sb eq.	3.41E-06	4.23E-07	9.52E-07
	Abiotic depletion potential for fossil resources (ADPF)	MJ	1.21E+03	6.28E+01	1.25E+02

A.3.2. E.I. impact indicators (EN 15804+A2) stage A1, A2 and A3

Table A3.13. Environmental impact indicators obtained for stages A1, A2 and A3, per declared unit for the bituminous mixture D.0.R.0.

Potential environmental impact			D.0.R.0		
	Parameter	Unit	A1	A2	A3
Environmental impact indicators	Climate Change	kg CO_2 eq.	44.30	14.99	17.15
	Climate Change (fossil)	kg CO_2 eq.	43.95	14.88	17.15
	Climate Change (biogenic)	kg CO_2 eq.	3.25E-01	-1.79E-02	6.95E-03
	Climate Change (land use change)	kg CO_2 eq.	3.02E-02	1.23E-01	8.90E-04
	Ozone depletion	kg CFC-11 eq.	1.21E-13	2.97E-15	4.95E-16
	Acidification terrestrial and freshwater	Mole of H+ eq.	9.92E-02	7.27E-02	1.36E-02
	Eutrophication freshwater	kg P eq.	4.56E-05	4.46E-05	5.91E-07
	Eutrophication marine	kg N eq.	2.37E-02	3.49E-02	6.50E-03
	Eutrophication terrestrial	Mole of N eq.	2.64E-01	3.87E-01	7.17E-02
	Photochemical ozone formation - human health	kg NMVOC eq.	9.53E-02	6.99E-02	1.83E-02
	Resource use, mineral and metals	kg Sb eq.	8.28E-06	1.33E-06	2.17E-06
	Resource use, energy carriers	MJ	2775.80	200.12	283.56
	Water scarcity	m^3 world equiv.	2.77E+00	1.39E-01	6.86E-03

Table A3.14. Environmental impact indicators obtained for stages A1, A2 and A3, per declared unit for the bituminous mixture D.25.R.0.

Potential environmental impact			D.25.R.0		
	Parameter	Unit	A1	A2	A3
Environmental impact indicators	Climate Change	kg CO_2 eq.	34.66	11.17	13.91
	Climate Change (fossil)	kg CO_2 eq.	34.38	11.10	13.90
	Climate Change (biogenic)	kg CO_2 eq.	2.61E-01	-1.33E-02	5.64E-03
	Climate Change (land use change)	kg CO_2 eq.	2.30E-02	9.16E-02	7.22E-04
	Ozone depletion	kg CFC-11 eq.	9.14E-14	2.21E-15	4.02E-16
	Acidification terrestrial and freshwater	Mole of H+ eq.	7.96E-02	5.55E-02	1.10E-02
	Eutrophication freshwater	kg P eq.	3.59E-05	3.33E-05	4.79E-07
	Eutrophication marine	kg N eq.	1.88E-02	2.67E-02	5.27E-03
	Eutrophication terrestrial	Mole of N eq.	2.08E-01	2.96E-01	5.81E-02
	Photochemical ozone formation - human health	kg NMVOC eq.	7.63E-02	5.31E-02	1.48E-02
	Resource use, mineral and metals	kg Sb eq.	6.61E-06	9.93E-07	1.76E-06
	Resource use, energy carriers	MJ	2251.86	149.22	229.88
	Water scarcity	m^3 world equiv.	2.10E+00	1.04E-01	5.56E-03

Table A3.15. Environmental impact indicators obtained for stages A1, A2 and A3, per declared unit for the bituminous mixture D.25.R.0.2.

Potential environmental impact			D.25.R.0.2		
	Parameter	Unit	A1	A2	A3
Environmental impact indicators	Climate Change	kg CO_2 eq.	36.34	11.19	13.91
	Climate Change (fossil)	kg CO_2 eq.	35.26	11.11	13.90
	Climate Change (biogenic)	kg CO_2 eq.	-1.1E+00	-1.34E-02	5.64E-03
	Climate Change (land use change)	kg CO_2 eq.	2.15E+00	9.17E-02	7.22E-04
	Ozone depletion	kg CFC-11 eq.	3.71E-07	2.22E-15	4.02E-16
	Acidification terrestrial and freshwater	Mole of H+ eq.	8.36E-02	5.56E-02	1.10E-02
	Eutrophication freshwater	kg P eq.	5.58E-05	3.33E-05	4.79E-07
	Eutrophication marine	kg N eq.	1.95E-02	2.67E-02	5.27E-03
	Eutrophication terrestrial	Mole of N eq.	2.25E-01	2.96E-01	5.81E-02
	Photochemical ozone formation - human health	kg NMVOC eq.	8.08E-02	5.32E-02	1.48E-02
	Resource use, mineral and metals	kg Sb eq.	6.62E-06	9.95E-07	1.76E-06
	Resource use, energy carriers	MJ	2249.26	149.45	229.88
	Water scarcity	m^3 world equiv.	2.57E+00	1.04E-01	5.56E-03

Table A3.16. Environmental impact indicators obtained for stages A1, A2 and A3, per declared unit for the bituminous mixture D.25.R.0.6.

Potential environmental impact			D.25.R.0.6		
	Parameter	Unit	A1	A2	A3
Environmental impact indicators	Climate Change	kg CO_2 eq.	39.76	11.22	13.91
	Climate Change (fossil)	kg CO_2 eq.	37.10	11.14	13.90
	Climate Change (biogenic)	kg CO_2 eq.	-3.7E+00	-1.34E-02	5.64E-03
	Climate Change (land use change)	kg CO_2 eq.	6.41E+00	9.19E-02	7.22E-04
	Ozone depletion	kg CFC-11 eq.	1.11E-06	2.22E-15	4.02E-16
	Acidification terrestrial and freshwater	Mole of H+ eq.	9.17E-02	5.57E-02	1.10E-02
	Eutrophication freshwater	kg P eq.	9.56E-05	3.34E-05	4.79E-07
	Eutrophication marine	kg N eq.	2.11E-02	2.68E-02	5.27E-03
	Eutrophication terrestrial	Mole of N eq.	2.60E-01	2.97E-01	5.81E-02
	Photochemical ozone formation - human health	kg NMVOC eq.	9.01E-02	5.33E-02	1.48E-02
	Resource use, mineral and metals	kg Sb eq.	6.65E-06	9.97E-07	1.76E-06
	Resource use, energy carriers	MJ	2252.61	149.84	229.88
	Water scarcity	m^3 world equiv.	3.53E+00	1.04E-01	5.56E-03

Table A3.17. Environmental impact indicators obtained for stages A1, A2 and A3, per declared unit for the bituminous mixture D.50.R.0.

Potential environmental impact			D.50.R.0		
	Parameter	Unit	A1	A2	A3
Environmental impact indicators	Climate Change	kg CO_2 eq.	25.12	7.51	10.72
	Climate Change (fossil)	kg CO_2 eq.	24.91	7.46	10.72
	Climate Change (biogenic)	kg CO_2 eq.	1.96E-01	-8.97E-03	4.35E-03
	Climate Change (land use change)	kg CO_2 eq.	1.56E-02	6.16E-02	5.56E-04
	Ozone depletion	kg CFC-11 eq.	6.04E-14	1.49E-15	3.10E-16
	Acidification terrestrial and freshwater	Mole of H+ eq.	6.00E-02	3.89E-02	8.51E-03
	Eutrophication freshwater	kg P eq.	2.61E-05	2.24E-05	3.69E-07
	Eutrophication marine	kg N eq.	1.38E-02	1.88E-02	4.06E-03
	Eutrophication terrestrial	Mole of N eq.	1.53E-01	2.08E-01	4.48E-02
	Photochemical ozone formation - human health	kg NMVOC eq.	5.73E-02	3.70E-02	1.14E-02
	Resource use, mineral and metals	kg Sb eq.	4.93E-06	6.68E-07	1.35E-06
	Resource use, energy carriers	MJ	1729.56	100.34	177.22
	Water scarcity	m^3 world equiv.	1.42E+00	6.99E-02	4.28E-03

Table A3.18. Environmental impact indicators obtained for stages A1, A2 and A3, per declared unit for the bituminous mixture D.50.R.0.2.

Potential environmental impact			D.50.R.0.2		
	Parameter	Unit	A1	A2	A3
Environmental impact indicators	Climate Change	kg CO_2 eq.	28.55	7.54	10.72
	Climate Change (fossil)	kg CO_2 eq.	26.75	7.49	10.72
	Climate Change (biogenic)	kg CO_2 eq.	-2.5E+00	-9.01E-03	4.35E-03
	Climate Change (land use change)	kg CO_2 eq.	4.27E+00	6.18E-02	5.56E-04
	Ozone depletion	kg CFC-11 eq.	7.41E-07	1.49E-15	3.10E-16
	Acidification terrestrial and freshwater	Mole of H+ eq.	6.82E-02	3.90E-02	8.51E-03
	Eutrophication freshwater	kg P eq.	6.59E-05	2.25E-05	3.69E-07
	Eutrophication marine	kg N eq.	1.53E-02	1.88E-02	4.06E-03
	Eutrophication terrestrial	Mole of N eq.	1.88E-01	2.09E-01	4.48E-02
	Photochemical ozone formation - human health	kg NMVOC eq.	6.66E-02	3.71E-02	1.14E-02
	Resource use, mineral and metals	kg Sb eq.	4.96E-06	6.70E-07	1.35E-06
	Resource use, energy carriers	MJ	1733.00	100.74	177.22
	Water scarcity	m^3 world equiv.	2.38E+00	7.02E-02	4.28E-03

Table A3.19. Environmental impact indicators obtained for stages A1, A2 and A3, per declared unit for the bituminous mixture D.50.R.0.4.

Potential environmental impact			D.50.R.0.4		
	Parameter	**Unit**	**A1**	**A2**	**A3**
Environmental impact indicators	Climate Change	kg CO_2 eq.	31.94	7.58	10.72
	Climate Change (fossil)	kg CO_2 eq.	28.55	7.53	10.72
	Climate Change (biogenic)	kg CO_2 eq.	-5.1E+00	-9.05E-03	4.35E-03
	Climate Change (land use change)	kg CO_2 eq.	8.53E+00	6.21E-02	5.56E-04
	Ozone depletion	kg CFC-11 eq.	1.48E-06	1.50E-15	3.10E-16
	Acidification terrestrial and freshwater	Mole of H+ eq.	7.63E-02	3.91E-02	8.51E-03
	Eutrophication freshwater	kg P eq.	1.06E-04	2.26E-05	3.69E-07
	Eutrophication marine	kg N eq.	1.69E-02	1.89E-02	4.06E-03
	Eutrophication terrestrial	Mole of N eq.	2.23E-01	2.09E-01	4.48E-02
	Photochemical ozone formation - human health	kg NMVOC eq.	7.58E-02	3.73E-02	1.14E-02
	Resource use, mineral and metals	kg Sb eq.	4.99E-06	6.74E-07	1.35E-06
	Resource use, energy carriers	MJ	1732.17	101.23	177.22
	Water scarcity	m^3 world equiv.	3.33E+00	7.05E-02	4.28E-03

Table A3.20. Environmental impact indicators obtained for stages A1, A2 and A3, per declared unit for the bituminous mixture D.50.R.0.6.

Potential environmental impact			D.50.R.0.6		
	Parameter	**Unit**	**A1**	**A2**	**A3**
Environmental impact indicators	Climate Change	kg CO_2 eq.	35.36	7.62	10.72
	Climate Change (fossil)	kg CO_2 eq.	30.39	7.57	10.72
	Climate Change (biogenic)	kg CO_2 eq.	-7.8E+00	-9.10E-03	4.35E-03
	Climate Change (land use change)	kg CO_2 eq.	1.28E+01	6.24E-02	5.56E-04
	Ozone depletion	kg CFC-11 eq.	2.22E-06	1.51E-15	3.10E-16
	Acidification terrestrial and freshwater	Mole of H+ eq.	8.44E-02	3.93E-02	8.51E-03
	Eutrophication freshwater	kg P eq.	1.46E-04	2.27E-05	3.69E-07
	Eutrophication marine	kg N eq.	1.84E-02	1.90E-02	4.06E-03
	Eutrophication terrestrial	Mole of N eq.	2.58E-01	2.10E-01	4.48E-02
	Photochemical ozone formation - human health	kg NMVOC eq.	8.50E-02	3.74E-02	1.14E-02
	Resource use, mineral and metals	kg Sb eq.	5.02E-06	6.77E-07	1.35E-06
	Resource use, energy carriers	MJ	1735.57	101.75	177.22
	Water scarcity	m^3 world equiv.	4.29E+00	7.09E-02	4.28E-03

Table A3.21. Environmental impact indicators obtained for stages A1, A2 and A3, per declared unit for the bituminous mixture D.75.R.0.

Potential environmental impact			D.75.R.0		
	Parameter	**Unit**	**A1**	**A2**	**A3**
Environmental impact indicators	Climate Change	kg CO_2 eq.	15.50	4.58	7.54
	Climate Change (fossil)	kg CO_2 eq.	15.36	4.54	7.53
	Climate Change (biogenic)	kg CO_2 eq.	1.32E-01	-5.46E-03	3.05E-03
	Climate Change (land use change)	kg CO_2 eq.	8.01E-03	3.75E-02	3.91E-04
	Ozone depletion	kg CFC-11 eq.	2.88E-14	9.06E-16	2.18E-16
	Acidification terrestrial and freshwater	Mole of H+ eq.	4.04E-02	2.51E-02	5.98E-03
	Eutrophication freshwater	kg P eq.	1.62E-05	1.36E-05	2.59E-07
	Eutrophication marine	kg N eq.	8.78E-03	1.22E-02	2.86E-03
	Eutrophication terrestrial	Mole of N eq.	9.71E-02	1.35E-01	3.15E-02
	Photochemical ozone formation - human health	kg NMVOC eq.	3.83E-02	2.37E-02	8.02E-03
	Resource use, mineral and metals	kg Sb eq.	3.24E-06	4.07E-07	9.52E-07
	Resource use, energy carriers	MJ	1206.04	61.11	124.56
	Water scarcity	m^3 world equiv.	7.45E-01	4.26E-02	3.01E-03

Table A3.22. Environmental impact indicators obtained for stages A1, A2 and A3, per declared unit for the bituminous mixture D.75.R.0.2.

Potential environmental impact			D.75.R.0.2		
	Parameter	**Unit**	**A1**	**A2**	**A3**
Environmental impact indicators	Climate Change	kg CO_2 eq.	20.61	4.63	7.54
	Climate Change (fossil)	kg CO_2 eq.	18.09	4.60	7.53
	Climate Change (biogenic)	kg CO_2 eq.	-3.9E+00	-5.53E-03	3.05E-03
	Climate Change (land use change)	kg CO_2 eq.	6.39E+00	3.80E-02	3.91E-04
	Ozone depletion	kg CFC-11 eq.	1.11E-06	9.17E-16	2.18E-16
	Acidification terrestrial and freshwater	Mole of H+ eq.	5.25E-02	2.53E-02	5.98E-03
	Eutrophication freshwater	kg P eq.	7.59E-05	1.38E-05	2.59E-07
	Eutrophication marine	kg N eq.	1.11E-02	1.23E-02	2.86E-03
	Eutrophication terrestrial	Mole of N eq.	1.49E-01	1.36E-01	3.15E-02
	Photochemical ozone formation - human health	kg NMVOC eq.	5.21E-02	2.39E-02	8.02E-03
	Resource use, mineral and metals	kg Sb eq.	3.28E-06	4.12E-07	9.52E-07
	Resource use, energy carriers	MJ	1207.05	61.89	124.56
	Water scarcity	m^3 world equiv.	2.18E+00	4.31E-02	3.01E-03

Table A3.23. Environmental impact indicators obtained for stages A1, A2 and A3, per declared unit for the bituminous mixture D.75.R.0.4.

Potential environmental impact			D.75.R.0.4		
	Parameter	**Unit**	**A1**	**A2**	**A3**
Environmental impact indicators	Climate Change	kg CO_2 eq.	25.76	4.69	7.54
	Climate Change (fossil)	kg CO_2 eq.	20.86	4.66	7.53
	Climate Change (biogenic)	kg CO_2 eq.	-7.9E+00	-5.61E-03	3.05E-03
	Climate Change (land use change)	kg CO_2 eq.	1.28E+01	3.85E-02	3.91E-04
	Ozone depletion	kg CFC-11 eq.	2.22E-06	9.29E-16	2.18E-16
	Acidification terrestrial and freshwater	Mole of H+ eq.	6.48E-02	2.56E-02	5.98E-03
	Eutrophication freshwater	kg P eq.	1.36E-04	1.40E-05	2.59E-07
	Eutrophication marine	kg N eq.	1.34E-02	1.24E-02	2.86E-03
	Eutrophication terrestrial	Mole of N eq.	2.02E-01	1.37E-01	3.15E-02
	Photochemical ozone formation - human health	kg NMVOC eq.	6.60E-02	2.42E-02	8.02E-03
	Resource use, mineral and metals	kg Sb eq.	3.33E-06	4.17E-07	9.52E-07
	Resource use, energy carriers	MJ	1212.31	62.69	124.56
	Water scarcity	m^3 world equiv.	3.61E+00	4.37E-02	3.01E-03

Table A3.24. Environmental impact indicators obtained for stages A1, A2 and A3, per declared unit for the bituminous mixture D.75.R.0.6.

Potential environmental impact			D.75.R.0.6		
	Parameter	**Unit**	**A1**	**A2**	**A3**
Environmental impact indicators	Climate Change	kg CO_2 eq.	30.91	4.75	7.54
	Climate Change (fossil)	kg CO_2 eq.	23.63	4.72	7.53
	Climate Change (biogenic)	kg CO_2 eq.	-1.2E+01	-5.68E-03	3.05E-03
	Climate Change (land use change)	kg CO_2 eq.	1.92E+01	3.90E-02	3.91E-04
	Ozone depletion	kg CFC-11 eq.	3.33E-06	9.41E-16	2.18E-16
	Acidification terrestrial and freshwater	Mole of H+ eq.	7.71E-02	2.58E-02	5.98E-03
	Eutrophication freshwater	kg P eq.	1.95E-04	1.42E-05	2.59E-07
	Eutrophication marine	kg N eq.	1.58E-02	1.25E-02	2.86E-03
	Eutrophication terrestrial	Mole of N eq.	2.55E-01	1.39E-01	3.15E-02
	Photochemical ozone formation - human health	kg NMVOC eq.	7.99E-02	2.44E-02	8.02E-03
	Resource use, mineral and metals	kg Sb eq.	3.39E-06	4.22E-07	9.52E-07
	Resource use, energy carriers	MJ	1217.61	63.49	124.56
	Water scarcity	m^3 world equiv.	5.04E+00	4.42E-02	3.01E-03